ВЕСТНИК ТРАНСПЛАНТОЛОГИИ И ИСКУССТВЕННЫХ ОРГАНОВ

VESTNIK TRANSPLANTOLOGII I ISKUSSTVENNYKH ORGANOV

RUSSIAN JOURNAL OF TRANSPLANTOLOGY AND ARTIFICIAL ORGANS

УЧРЕДИТЕЛЬ: ОБЩЕРОССИЙСКАЯ ОБЩЕСТВЕННАЯ ОРГАНИЗАЦИЯ ТРАНСПЛАНТОЛОГОВ «РОССИЙСКОЕ ТРАНСПЛАНТОЛОГИЧЕСКОЕ ОБЩЕСТВО»

THE OFFICIAL JOURNAL OF ALL-RUSSIAN PUBLIC ORGANIZATION OF TRANSPLANTOLOGISTS "RUSSIAN TRANSPLANT SOCIETY"

2025. Том XXVII. № 2

2025. Vol. XXVII. № 2

Научно-практический журнал основан в 1999 г.
Регистр. № 018616

Scientific and Practical Journal was founded in 1999
Reg. № 018616

Журнал «Вестник трансплантологии и искусственных органов» включен ВАК РФ в перечень российских рецензируемых научных изданий, в которых должны быть опубликованы результаты диссертационных работ

Журнал «Вестник трансплантологии и искусственных органов» включен ФГБУ «НМИЦ ТИО им. ак. В.И. Шумакова» Минздрава России в перечень российских рецензируемых научных изданий, в которых должны быть опубликованы основные результаты исследований в рамках диссертаций, представляемых к защите в диссертационный совет ФГБУ «НМИЦ ТИО им. ак. В.И. Шумакова» Минздрава России

Журнал «Вестник трансплантологии и искусственных органов» индексируется в Scopus и размещен на платформе Web of Science Core Collection: Emerging Science Citation Index

"Russian Journal of Transplantology and Artificial Organs" is included in the list of leading peer-reviewed scientific publication editions, produced in the Russian Federation and is recommended for publication of primary results of dissertation research

"Russian Journal of transplantology and artificial organs" is included by the Federal State Budgetary Institution "Shumakov National Medical Research Center of Transplantology and Artificial Organs" of the Ministry of Health of Russia in the list of Russian peer-reviewed scientific publications in which the main results of research should be published within the framework of dissertations submitted for defense to the dissertation council of Shumakov National Medical Research Center of Transplantology and Artificial Organs

"Russian Journal of Transplantology and Artificial Organs" is indexed in Scopus and in the Emerging Science Citation Index of the Web of Science Core Collection

ISSN 1995-1191

Адрес для корреспонденции:

Россия, 123182, Москва, ул. Щукинская, 1
Тел./факс +7 (499) 193 87 62
E-mail: vestniktranspl@gmail.com
Интернет-сайт журнала: http://journal.transpl.ru
Научная электронная библиотека: http://elibrary.ru

Address for correspondence:

1, Shchukinskaya st., Moscow 123182, Russia
Tel./Fax +7 (499) 193 87 62
E-mail: vestniktranspl@gmail.com
Journal's web site: http://journal.transpl.ru
Scientific eLibrary: http://elibrary.ru

Подписной индекс в каталоге почты России – ПН380

СОДЕРЖАНИЕ

СТРАНИЦА ГЛАВНОГО РЕДАКТОРА

КЛИНИЧЕСКАЯ ТРАНСПЛАНТОЛОГИЯ

CONTENTS

EDITORIAL

CLINICAL TRANSPLANTOLOGY

ТРАНСПЛАНТАЦИЯ СЕРДЦА И ВСПОМОГАТЕЛЬНОЕ КРОВООБРАЩЕНИЕ

РЕГЕНЕРАТИВНАЯ МЕДИЦИНА И КЛЕТОЧНЫЕ ТЕХНОЛОГИИ

HEART TRANSPLANTATION AND ASSISTED CIRCULATION

REGENERATIVE MEDICINE AND CELL TECHNOLOGIES

ВЕКТОРЫ ОТЕЧЕСТВЕННОЙ ТРАНСПЛАНТОЛОГИИ: РАЗВИТИЕ ТЕХНОЛОГИЙ, ТРАНСЛЯЦИЯ В РЕГИОНЫ

ADVANCING TRANSPLANTOLOGY IN RUSSIA: INNOVATION PATHWAYS AND REGIONAL DEPLOYMENT

Глубокоуважаемые коллеги!

3 июня в г. Волжский Волгоградской области состоялась Всероссийская научно-практическая конференция «Опыт первой пятилетки», посвященная 5-летию Филиала Национального медицинского исследовательского центра трансплантологии и искусственных органов имени академика В.И. Шумакова. Это знаковое и значимое событие не только для коллектива Центра Шумакова и его филиала, но для всей отечественной трансплантологии, и пожалуй, всего отечественного здравоохранения.

Участников конференции приветствовали Министр здравоохранения РФ М.А. Мурашко, руководители органов государственной власти и медицинской общественности региона. Среди участников – специалисты из многих регионов нашей страны. В программе конференции – концептуальное заседание «Трансплантация органов: векторы развития», вопросы организации и реализации программ трансплантации почки, печени, сердца, легких, донорства органов, педиатрической трансплантации.

В июне 2020 года в день медицинского работника в Южном федеральном округе, на левом берегу реки Ахтубы – притока Волги, был торжественно открыт филиал Центра Шумакова. На открытие специально приехали Министр здравоохранения РФ М.А. Мурашко, губернатор Волгоградской области, Герой России А.И. Бочаров, и что особенно знаменательно, по ВКС коллектив приветствовал Президент России В.В. Путин. Филиал Центра Шумакова – это современное многофункциональное медицинское учреждение, и сегодня уже есть возможность подвести некоторые итоги работы за прошедшую пятилетку.

Многолетний опыт работы НМИЦ ТИО имени академика В.И. Шумакова по продвижению идей и возможностей трансплантологии в регионы страны

Dear colleagues,

On June 3, the National Research and Development Conference titled "Experience of the First Five-Year Plan" was held in Volzhsky, Volgograd Oblast. This marked the 5th anniversary of the Volzhsky Branch of Shumakov National Medical Research Center of Transplantology and Artificial Organs. The event stands as a landmark not only for the staff of the Shumakov Center and its regional branch, but also for the entire field of national transplantology – and perhaps, for the broader Russian healthcare system.

The Conference was opened with welcoming remarks from the Minister of Health of the Russian Federation, Mikhail Murashko, along with authorities from the regional government and the medical community. The event brought together specialists from numerous regions across the country. The conference program featured a conceptual session titled "Organ Transplantation: Vectors of Development", which addressed key issues including the organization and implementation of kidney, liver, heart, and lung transplant programs, organ donation strategies, and advances in pediatric transplantation.

In June 2020, on Medical Workers Day in Russia's Southern Federal District, a branch of the Shumakov Center was inaugurated on the left bank of the Akhtuba River, a tributary of the Volga River. The ceremony was attended by the Minister of Health of the Russian Federation Mikhail Murashko, the Governor of Volgograd Oblast Andrey Bocharov, a Hero of the Russian Federation. In a significant gesture, the staff was greeted by the President of Russia Vladimir Putin via a video-conference. The Shumakov Center branch is a modern multifunctional medical facility. Now, five years since its opening, we can reflect on its achievements and the impact it has had on regional and national transplantology.

The solid experience garnered by the Shumakov National Medical Research Center of Transplantology and Artificial Organs in advancing the principles and oppor-

позволил в короткие сроки мобилизовать донорский ресурс Волгоградской области в тесном контакте с руководством и медицинской общественностью региона.

Оснащенность Филиала современной аппаратурой, высокий профессионализм работающих специалистов позволили уже выполнить около 11 тысяч операций, включая сложнейшие и даже уникальные, в том числе проведено более 300 операций по трансплантации жизненно важных органов – почки, печени, сердца – взрослым и детям.

Отечественная трансплантология сегодня – это и вид высокотехнологичной медицинской помощи, доступный населению нашей страны, и направление мультидисциплинарных исследований, реализующее научные достижения в клинику, и область технологических разработок с созданием медицинских изделий и аппаратов, предназначенных для замещения функций поврежденных органов.

Деятельность НМИЦ ТИО имени академика В.И. Шумакова – яркий пример реализации задач Минздрава России в рамках федерального проекта «Развитие сети национальных медицинских исследовательских центров и внедрение инновационных медицинских технологий» национального проекта «Здравоохранение», направленных на продвижение высокотехнологичной медицинской помощи и трансляцию достижений современной медицины в субъекты Российской Федерации.

tunities of transplantology has played a crucial role in expanding these practices across Russia. This expertise enabled the successful mobilization of donor resources in Volgograd Oblast within a short period, achieved through close collaboration with regional authorities and the medical community.

Thanks to modern medical equipment and high professionalism among specialists, the branch has performed about 11,000 surgical procedures to date. These include some of the most complex and even unique operations, with over 300 life-saving organ transplants – kidney, liver, and heart – carried out on both adult and pediatric patients.

Today, our national transplantology is a high-tech health care that is accessible to the population across Russia. It is also a multidisciplinary field of research that translates scientific advances into clinical practice, while simultaneously driving technological innovation through development of medical devices and systems designed to replace or restore the function of damaged organs.

The activity of Shumakov Center serves as a compelling example of the implementation of the Russian Ministry of Health's objectives under the federal project "Development of the Network of National Medical Research Centers and Introduction of Innovative Medical Technologies", part of the national project "Healthcare". This initiative is focused on expanding access to high-tech medical care and facilitating the transfer of cutting-edge medical advancements to the regions of the Russian Federation.

С уважением,
главный редактор
академик РАН С.В. Готье

Sincerely,

Sergey Gautier,
Fellow, Russian Academy of Sciences
Editor-in-chief, Russian Journal
of Transplantology and Artificial Organs

DOI: 10.15825/1995-1191-2025-2-8-22

COMBINED SEQUENTIAL HYPOTHERMIC OXYGENATED AND NORMOTHERMIC MACHINE PERFUSION FOR LIVER TRANSPLANT FROM AN EXPANDED CRITERIA DONOR: FIRST CLINICAL APPLICATION IN RUSSIA

S.V. Gautier[1, 2], N.V. Grudinin[1], A.R. Monakhov[1, 2], M.A. Boldyrev[1], V.K. Bogdanov[1], D.M. Bondarenko[1], S.I. Zubenko[1], N.P. Mozheiko[1], M.G. Minina[1, 3], O.M. Tsirulnikova[1, 2]

[1] Shumakov National Medical Research Center of Transplantology and Artificial Organs, Moscow, Russian Federation

[2] Sechenov University, Moscow, Russian Federation

[3] Botkin Hospital, Moscow, Russian Federation

Objective: to analyze a clinical case series and evaluate the safety and efficacy of a sequential machine perfusion protocol combining dual hypothermic oxygenated perfusion (D-HOPE) and normothermic machine perfusion (NMP) for conditioning and viability assessment of liver grafts retrieved from expanded criteria donors (ECD) in routine clinical practice. **Materials and methods.** Between November and December 2024, two sessions of combined D-HOPE followed by NMP were conducted at Shumakov National Medical Research Center of Transplantology and Artificial Organs ("Shumakov Research Center") using liver allografts obtained from ECD after brain death. Following an initial period of static cold storage (SCS), machine perfusion was initiated using a circulatory assist device. A histidine-tryptophan-ketoglutarate (HTK)-based perfusate was used during the D-HOPE phase, while a red blood cell (RBC) suspension was used during the NMP stage. Throughout perfusion, temperature and hemodynamic parameters were continuously monitored and maintained. Laboratory parameters were assessed at designated intervals, in accordance with the institutional protocol developed at Shumakov Research Center. **Results.** Allograft #1 was deemed non-viable due to elevated lactate levels after 3 hours of perfusion and lack of glucose metabolism. The preservation times were as follows: SCS – 424 minutes, D-HOPE – 120 minutes, NMP – 300 minutes, totaling 844 minutes. Allograft #2 met the viability criteria and was successfully transplanted. Preservation times were: SCS – 260 minutes, D-HOPE – 124 minutes, NMP – 480 minutes, with a total preservation time of 884 minutes. Post-transplant peak levels of AST, ALT, and total bilirubin in the recipient were 922.5 U/L, 613 U/L, and 63.3 μmol/L, respectively. The only postoperative complication was acute kidney injury, managed with two sessions of hemodialysis. The patient was discharged after 14 days of hospitalization without need for readmission. At the time of writing, the patient is alive and complication-free, with a follow-up period of 3 months. **Conclusions.** Combined machine perfusion of liver grafts appears to be a safe and effective strategy to mitigate ischemia-reperfusion and preservation-related injury in liver transplantation. It also facilitates viability assessment of marginal liver grafts, reduces potential recipient complications, and expands the donor pool through the use of allografts from ECD.

Keywords: ex vivo perfusion, liver transplantation, machine perfusion.

INTRODUCTION

One of the most pressing and unresolved challenges in modern clinical transplantology is the significant mismatch between the number of patients on waiting lists and the availability of donor organs [1–3]. According to the Scientific Registry of Transplant Recipients (SRTR), at the end of 2022, there were 10,548 patients awaiting a liver transplant (LT) in the United States. During the same period, 12,862 patients were added to the waiting list, 13,638 were removed, and a total of 9,527 LTs were performed [3]. One of the primary strategies to expand the donor pool under these circumstances is the broader acceptance of organs from expanded criteria donors (ECDs), including those with significant steatosis, older donors, hemodynamically unstable donors, those in intensive care units for prolonged periods, and donors after circulatory death [4, 5]. However, such "marginal" organs have historically been associated with less favorable outcomes, including poorer recipient and graft survival rates [6–8, 26]. For example, severe macrovesicular steatosis of the allograft (>60%) has been shown to significantly increase the risk of primary nonfunction

Corresponding author: Mikhail Boldyrev. Address: 1, Shchukinskaya str., Moscow, 123182, Russian Federation. Phone: (961) 974-59-55. E-mail: comex.ksb@gmail.com

(p = 0.002), acute kidney injury (p = 0.040), and the need for retransplantation (p = 0.012) [9]. The risk of graft loss (HR 2.3, 95% CI 1.7–3.0) and recipient death (HR 2.0, 95% CI 1.4–2.8) is approximately twice as high following transplantation of an organ from a donor after circulatory death (DCD), with biliary causes of graft loss occurring more frequently in the DCD group compared to the standard group (6% *vs* 1%, p = 0.04) [10]. It is increasingly clear that static cold storage (SCS), which has been the gold standard for donor organ preservation for over three decades, is no longer sufficient in the era of expanded donor eligibility. It does not provide an adequate level of protection against preservation-related injury for marginal allografts. For instance, one of the few randomized controlled trials on machine perfusion (MP) demonstrated that MP, compared to SCS, reduced the incidence of early allograft dysfunction by 14% (26% *vs* 40%; OR 0.61, 95% CI 0.39–0.96) and significantly decreased the occurrence of non-anastomotic biliary strictures by 12% (OR 0.36; 95% CI 0.14–0.94; p = 0.03) [14]. Dynamic or machine perfusion preservation not only protects marginal liver allografts from the deleterious effects of ischemia-reperfusion-preservation injury (IRPI) but also enables outcomes comparable to those achieved with standard donor organs, potentially increasing the number of usable organs for transplantation by 20% or more [11–14, 52].

Combined sequential machine perfusion is an actively developing method of perfusion conditioning for liver allografts [11, 23, 24]. This approach leverages hypothermic oxygenated machine perfusion (HOPE) to restore cellular ATP stores and minimize energy demands under hypothermic conditions, while clearing anaerobic metabolic byproducts such as succinate and NADH+. Following this, controlled oxygenated rewarming (COR) provides gradual, stepwise warming of the allograft under continuous oxygenated perfusion, further optimizing graft condition before proceeding to direct viability assessment during normothermic machine perfusion (NMP) [18, 11, 23]. Although the current evidence base remains limited, combined sequential perfusion is increasingly viewed as a highly promising development in machine perfusion and is steadily gaining a firm place in clinical transplantation practice.

The program for machine perfusion of liver transplants from ECDs has been actively developed at Shumakov National Medical Research Center of Transplantology and Artificial Organs since 2024. In this article, we present the first Russian clinical experience with the use of NMP as part of a combined HOPE-NMP protocol. In the first case, it was decided to abandon the use of the organ due to failure to meet viability criteria, while in the second case, the organ, having successfully met viability criteria, was transplanted into the recipient.

MATERIALS AND METHODS

Liver transplant

In all cases, liver allografts were used from ECDs as defined by Eurotransplant [25], with modifications by Shumakov National Medical Research Center of Transplantology and Artificial Organs (requiring the presence of one or more criteria):

- Donor age ≥65 years;
- Non-heart-beating donation (donation after circulatory death, DCD);
- Macrovesicular steatosis ≥40% (based on biopsy or visual assessment);
- Body mass index (BMI) ≥30;
- Donor blood sodium level ≥165 mmol/L;
- Intensive care unit (ICU) stay or mechanical ventilation (MV) duration >7 days;
- Predicted cold ischemia time ≥13 hours;
- AST >99 U/L;
- ALT >105 U/L;
- Total bilirubin >51 mmol/L;
- Need for adrenaline;
- Massive vasopressor support (norepinephrine >500 ng/kg/min);
- Periods of hypotension (mean arterial pressure <60 mmHg for 10 minutes or more);
- History of alcohol abuse or admission to ICU under the influence of alcohol;
- Donor risk index (DRI) >1.7 [26];
- Balance of Risk (BAR) score >18 [27].

Transplants from brain-dead donors were used in all cases. Multi-organ liver explantation from the donor was performed according to the standard technique in the Russian Federation [28]. No violations were identified during organ retrieval, transportation, or subsequent storage.

Pre-transplant preparation of the allograft was carried out according to a modified protocol. Initially, the portal vein was isolated, ligated, and cannulated using a 26 Fr cannula. Following portal vein cannulation, HOPE was initiated.

Given the requirement for subsequent NMP – which necessitates cannulation of both the portal vein and hepatic artery – HOPE was performed in dual mode (D-HOPE), perfusing through both vessels. It is important to note that while the immediate protective advantage of D-HOPE over standard HOPE at the hypothermic stage remains under investigation, we opted for dual cannulation to ensure readiness for NMP, which mandates both arterial and portal perfusion [29, 30].

The hepatic artery of the graft was isolated and cannulated with a 10 Fr cannula. Perfusion through the hepatic artery was initiated. Upon completion of the HOPE session, the graft was placed in a separate basin with ice chips and perfusion solution until it was ready for connection to the NMP. During this time, cannulation of

the biliary tract was performed using a 6 Fr probe, and the subhepatic section of the inferior vena cava (IVC) was cannulated with a 32 Fr cannula. The suprahepatic portion of the IVC was either clamped or tightly sutured.

All allografts exhibited standard vascular anatomy; however, in cases where an aberrant hepatic artery was present, a temporary or permanent anastomosis was created with the main artery to ensure adequate perfusion.

The grafts were weighed before perfusion, after completing the HOPE phase, and again after completing the NMP phase. Biopsies were taken before perfusion, after HOPE session, after the NMP session, and at the end of surgery.

Combined perfusion preservation

It should be noted that, at present, there is no universally accepted, validated algorithm for selecting the optimal method of perfusion preservation for liver allografts [31].

For perfusion, a standard set of consumables and equipment typically used for cardiopulmonary bypass during cardiac surgery was used. The material and technical support included the following: heart-lung machine Sorin Stockert S5 (LivaNova, UK), thermostatic regulating device Stockert 3T (LivaNova, UK), oxygenator Affinity NT (Medtronic, USA), thermoregulation and trunk line set.

The design of the perfusion circuit for "seamless" machine perfusion – meaning it does not require replacement of the tubing set when transitioning from D-HOPE to NMP – is an in-house development by Shumakov National Medical Research Center of Transplantology and Artificial Organs.

The circuit includes lines for perfusate supply to the portal vein and hepatic artery, a perfusate drainage line from the IVC of the graft, A drainage line from the organ container, and a cardiotomy reservoir.

During both stages, perfusion was conducted with flow adjustments to maintain appropriate perfusion pressures.

The first stage of combined machine perfusion consisted of a 2-hour D-HOPE session. The perfusate comprised 3 liters of HTK solution, supplemented with 150 mL of 25% human albumin to ensure adequate colloid osmotic pressure, and 2100 mg of the antioxidant acetylcysteine. Continuous recirculation of the perfusate was maintained at a flow rate of 1 liter per minute. Perfusate acid-base status (pH, pCO_2, pO_2, bicarbonate) was monitored every 30 minutes. Standard biochemical analysis of the perfusate was also performed at 30-minute intervals. A general view of the allograft during D-HOPE is presented in Fig. 1.

After the D-HOPE session, the allograft was disconnected from the perfusion circuit. The perfusion lines were then flushed with a 5% dextrose solution to remove residual perfusate. Following drainage of the dextrose solution, the circuit was refilled with the perfusate prepared for the NMP session. Recommended perfusion parameters are shown in Table.

After initiation of perfusate recirculation and achievement of the target temperature within the circuit, perfusate composition was adjusted based on the results of the initial acid-base analysis. Following this adjustment, the NMP session was commenced with a planned duration of at least 4 hours. Continuous infusion of heparin (1000 units/hour) and alprostadil (5–10 μg/hour) was maintained throughout the NMP session. The general appearance of the liver allograft during NMP is shown in Fig. 2, and bile secretion during NMP is illustrated in Fig. 3.

Thereafter, the acid-base sample was performed every 30 minutes throughout the perfusion. Standard biochemical analysis of the perfusate and acid-base analysis of bile were conducted 30 minutes after the start of perfusion

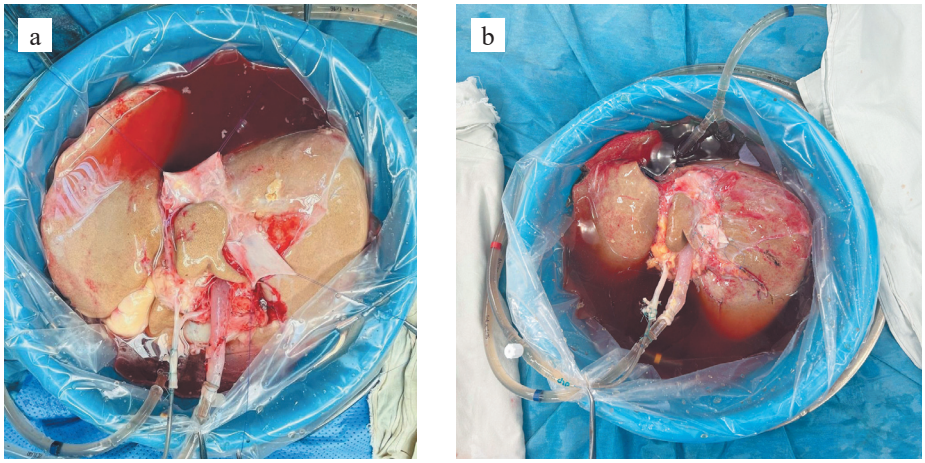

Fig. 1. Liver allografts during hypothermic oxygenated machine perfusion: (a) Case #1 – non-viable and subsequently rejected; (b) Case #2 – met viability criteria and was successfully transplanted

and subsequently every hour. Perfusion parameters – including flow rates, pressures, pump revolutions per minute, allograft temperature, graft consistency, perfusion homogeneity, oxygenation levels, and volume and characteristics of bile output – were continuously monitored, with data recorded every 30 minutes. All perfusion data were systematically entered into the perfusion protocol card developed at Shumakov National Medical Research Center of Transplantology and Artificial Organs.

Table

Recommended perfusion parameters for hypothermic oxygenated and normothermic machine perfusion of liver allografts

Parameter	HOPE [20, 63, 40]	NMP [23, 28, 40]
Perfusate temperature (°C)	8–10	36–38
Oxygenation level (pO_2, mmHg)	400–600	90–200
Flow, hepatic artery (mL/min)	40–70	>150–300
Flow, portal vein (mL/min)	300–400 (up to 500)	>500
Pressure, hepatic artery (mmHg)	20–25	60–70
Pressure, portal vein (mmHg)	3–5	10–13

Viability criteria

Assessment of liver allograft viability during the D-HOPE phase was not performed, as the determination of flavin mononucleotide (FMN) in the perfusate remains a promising but still investigational area requiring further precision studies [32, 33, 34]. The use of classical metabolic indicators (such as lactate, glucose, and pH) and markers of organ injury (LDH, AST, ALT) during hypothermic perfusion also remains under investigation and is not currently recognized as a validated method for viability assessment [34].

It should be emphasized that no universally accepted and validated criteria for viability assessment during NMP exist at present. Consequently, each group either develops their own criteria or relies on previously proposed standards [35, 36]. After a thorough review of the available literature, we adopted the VITTAL criteria developed and validated in the VITTAL study (Birmingham, UK) [20]. These criteria were modified to include mandatory qualitative bile analysis, based on the work of van Leeuwen and Matton [11, 37].

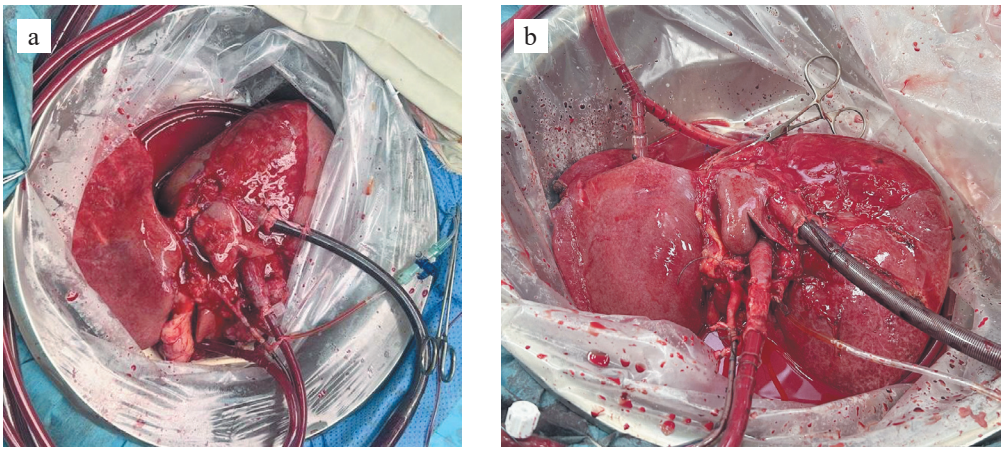

Fig. 2. Liver allografts during normothermic machine perfusion: (a) Case #1 – non-viable and subsequently rejected; (b) Case #2 – met viability criteria and was successfully transplanted

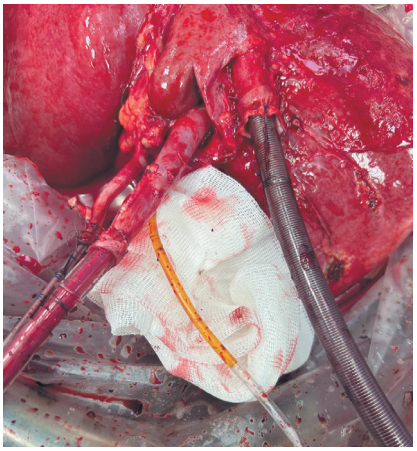

Fig. 3. Bile secretion by allograft in Case #1 during normothermic machine perfusion

Assessment of hepatocellular allograft link

Mandatory criterion: perfusate lactate level <2.5 mmol/L after 4 hours of perfusion; alternatively, a stable decrease in lactate was acceptable (lactate <2.5 mmol/L after 5 hours or <2.0 mmol/L after 6 hours).

Presence of *two or more* of the following additional criteria:

– Bile production totaling at least 5 mL, with 4 mL or more produced during the final hour of perfusion, and ideally exceeding 10 mL per hour;

– Perfusate pH >7.3 without the need for continuous infusion or boluses of sodium bicarbonate;
– Evidence of glucose metabolism (progressive reduction in glucose concentration, response to glucose boluses, and insulin infusion);
– Stable portal and arterial flow rates (>500 mL/min and >150 mL/min, respectively);
– Uniform parenchymal perfusion with soft organ consistency.

Evaluation of the cholangiocellular link of the allograft

Viability assessment of the cholangiocellular link was based on the presence of two or more of the following criteria:

– Bile pH >7.48, with a pH difference between bile and perfusate >0.05;
– Bicarbonate (HCO_3^-) concentration in bile >18 mmol/L, with a HCO_3^- difference between bile and perfusate >3.0 mmol/L;
– Glucose concentration in bile <16 mmol/L, with a glucose difference between bile and perfusate <–3.0 mmol/L, or a bile-to-perfusate glucose ratio <0.67;

If the allograft failed to meet the viability criteria, perfusion was discontinued and the organ was used for research or discarded. If viability criteria were achieved, perfusion was continued with ongoing monitoring of all parameters. In parallel, the recipient was prepared and brought to the operating room, where standard anesthetic management was provided, followed by hepatectomy. Upon retrieval of the recipient's native liver, perfusion of the donor graft was stopped, the graft was cooled with ice chips, and flushed with Custodiol solution through the portal vein and hepatic artery (3 and 2 liters, respectively), after which it was transferred for implantation.

Liver transplantation and postoperative period

Liver transplantation was performed using the technique of hepatectomy with either preservation or replacement of the recipient's own IVC, depending on intraoperative and anatomical considerations. The postoperative period included a 1-day stay in the ICU, followed by transfer to a specialized transplant ward.

Induction immunosuppression was initiated with a pulse dose of methylprednisolone, followed by rapid tapering over the next 4 days. Tacrolimus, as the main component of maintenance immunosuppression, was started on postoperative days 2–3, with a target blood level of 7–8 ng/mL. Mycophenolic acid or mycophenolate mofetil was introduced after normalization of the complete blood count.

Comprehensive laboratory and instrumental monitoring was conducted daily during the first 7 postoperative days, and then every other day during the second week after transplantation.

Acute graft rejection was suspected based on laboratory abnormalities (elevations in total bilirubin, aminotransferases, and cholestasis markers) after excluding other causes (including vascular complications) and was confirmed by percutaneous liver biopsy.

Acute kidney injury (AKI) was diagnosed according to the following KDIGO criteria [39].

1. Rise in serum creatinine of ≥0.3 mg/dL within 48 hours;
2. Rise in serum creatinine to ≥1.5 times (≥50%) the baseline, which is known or presumed to have occurred within the prior 7 days;
3. Urine output <0.5 mL/kg/hour for 6 hours.

Early allograft dysfunction (EAD) was recorded according to the criteria proposed by K. Olthoff et al. [38]:

1. Total bilirubin >171 μmol/L on postoperative day 7;
2. International normalized ratio (INR) >1.6 on postoperative day 7;
3. AST or ALT >2000 U/L within the first 7 postoperative days.

Primary nonfunction (PNF) was diagnosed according to the UNOS criteria [40]:

Death or retransplantation within the first 7 postoperative days, associated with AST >3000 U/L and at least one of the following:

1. INR >2.5;
2. Acidosis (arterial pH <7.30, venous pH <7.25) or lactate >4 mmol/L.

The diagnosis of ischemic non-anastomotic cholangiopathy (NAC) of the liver graft was established using a combination of clinical, laboratory, and instrumental evaluation methods. Clinical signs included pruritus and jaundice, while laboratory indicators focused on elevated markers of cholestasis, specifically gamma-glutamyl transpeptidase (GGT) and alkaline phosphatase (ALP).

In patients presenting with clinical or laboratory abnormalities suggestive of NAC, magnetic resonance cholangiopancreatography (MRCP) was performed to confirm or exclude the diagnosis.

In cases where MRCP findings indicated NAC without corresponding clinical or laboratory signs, the condition was classified as asymptomatic NAC.

Donors

Liver allografts from ECDs who were brain-dead were used. These organs had been previously declined by all transplant centers and were subsequently included in the machine perfusion preservation program. A brief description of the donors is provided below.

Case #1. Donor G. Male, 58 years old. BMI 34.3. Cause of death: hemorrhagic stroke (subarachnoid hemorrhage). Time in hospital and ICU: 1 day. Laboratory parameters: creatinine: 102 mmol/L, AST: 60 U/L, ALT:

45 U/L, total bilirubin: 20 μmol/L, plasma sodium level: 139 mEq/L. The liver allograft exhibited dense consistency and pronounced steatosis, with visual assessment indicating more than 60% involvement. Histological examination confirmed macrovesicular steatosis ranging between 65–70%. The weight of the liver allograft prior to perfusion was 3090 grams. Static cold preservation time upon arrival at Shumakov National Medical Research Center of Transplantology and Artificial Organs was 424 minutes.

Case #2. Donor N., female, 59 years old, BMI 45.8. Cause of death: hemorrhagic stroke (subarachnoid hemorrhage). Effective circulatory arrest lasted 15 minutes at the prehospital stage. Time in hospital and ICU: 3 days. Laboratory parameters: creatinine 90 μmol/L, AST 26 U/L, ALT 28 U/L, total bilirubin 9.9 μmol/L, plasma sodium level 136 mEq/L. The liver allograft demonstrated dense consistency and moderate steatosis upon visual inspection, with steatosis estimated at more than 30%. However, pathomorphological evaluation revealed a discrepancy: macrovesicular steatosis was 5–10%, while microvesicular steatosis was 55–60%. Weight of liver allograft prior to perfusion was 1910 grams. Static cold storage time at the moment of organ admission to the clinic was 260 minutes.

Recipient

In Case #2, the graft was transplanted to a recipient with an identical ABO blood group and compatible anthropometric indices. The recipient was a 53-year-old patient suffering from liver cirrhosis due to chronic HBV and HDV infection, with a MELD 3.0 score of 21 points. It is important to note that the patient experienced recurrent diuretic-resistant hydrothorax and ascites, requiring intensive diuretic therapy (spironolactone 300 mg/day, torasemide 40 mg/day) and frequent hospitalizations at Shumakov National Medical Research Center of Transplantology and Artificial Organs for laparocentesis and thoracocentesis procedures.

Perfusion parameters and viability assessment

Viability assessment of the liver allograft at the D-HOPE phase was not performed. NMP parameters are presented in Fig. 4.

Case #1. During the D-HOPE session, significant cytolysis was observed at 30 minutes into perfusion (ALT: 1500 U/L, AST: 1600 U/L) and further increased at 60 minutes (ALT: 3260 U/L, AST: 6440 U/L). Perfusate lactate at 60 minutes was 3.8 mmol/L, while perfusate glucose was 9.6 mmol/L. The pO_2 difference between inflow and outflow was 269 mmHg (inflow pO_2: 448 mmHg; outflow pO_2: 179 mmHg). It should be noted that these data were collected purely for subsequent retrospective analysis and did not influence real-time management decisions.

During the NMP phase, although a decrease in perfusate lactate was initially observed – reaching a minimum of 2.1 mmol/L at 180 minutes – a subsequent rise to 4.4 mmol/L occurred at 4 hours of perfusion. In addition, despite continuous infusion and periodic boluses of insulin, perfusate glucose level remained high, indicating impaired glucose metabolism and poor hormonal responsiveness in the allograft – a recognized indicator of non-viability [41, 42].

Bile production peaked early at 30 minutes of perfusion (4 mL) but subsequently declined and failed to meet the target values. Other hepatocellular viability parameters remained within normal limits. However, persistent high levels of cytolysis enzymes (max AST: 4650 U/L, ALT: 1950 U/L) – a factor considered in viability assessment by several groups [43] – raised additional concerns. Notably, the cholangiocellular viability parameters remained within normal limits.

The weight of the organ at the end of perfusion was practically unchanged, measuring 3067 g (compared to 3090 g pre-perfusion).

So, based on comprehensive assessment using the viability criteria of Shumakov National Medical Research Center of Transplantology and Artificial Organs, it was decided to abandon the use of the organ.

The D-HOPE and NMP time was 120 minutes and 300 minutes, respectively. Total machine perfusion time was 420 minutes, while total organ preservation time measured 844 minutes.

Case #2. The D-HOPE session demonstrated moderate cytolysis at 30 minutes (ALT: 645 U/L, AST: 890 U/L) and at 60 minutes (ALT: 799 U/L, AST: 1095 U/L). Perfusate lactate at 60 minutes measured 2.3 mmol/L, perfusate glucose was 8.2 mmol/L, and the pO_2 difference between inflow and outflow was 207 mmHg (inflow pO_2: 452 mmHg; outflow pO_2: 245 mmHg).

During the NMP phase, a slower pH normalization was noted compared to Case #1, although this did not require sodium bicarbonate boluses. Following an initial episode of hyperglycemia, glucose metabolism improved, with perfusate glucose levels stabilizing near physiologic values (8–12 mmol/L).

Lactate levels remained relatively elevated initially but showed a sharp decline at 4 hours of perfusion, reaching 2.6 mmol/L. Per protocol, due to the positive trend in lactate clearance, observation was continued. At 6 hours, lactate level further decreased to 2.3 mmol/L, and by 8 hours, it had reached 0.5 mmol/L, meeting viability criteria.

A consistently low level of cytolysis was also noted. Other hepatocellular and cholangiocellular viability parameters remained within normal limits throughout perfusion. Allograft weight after perfusion was 2000 g,

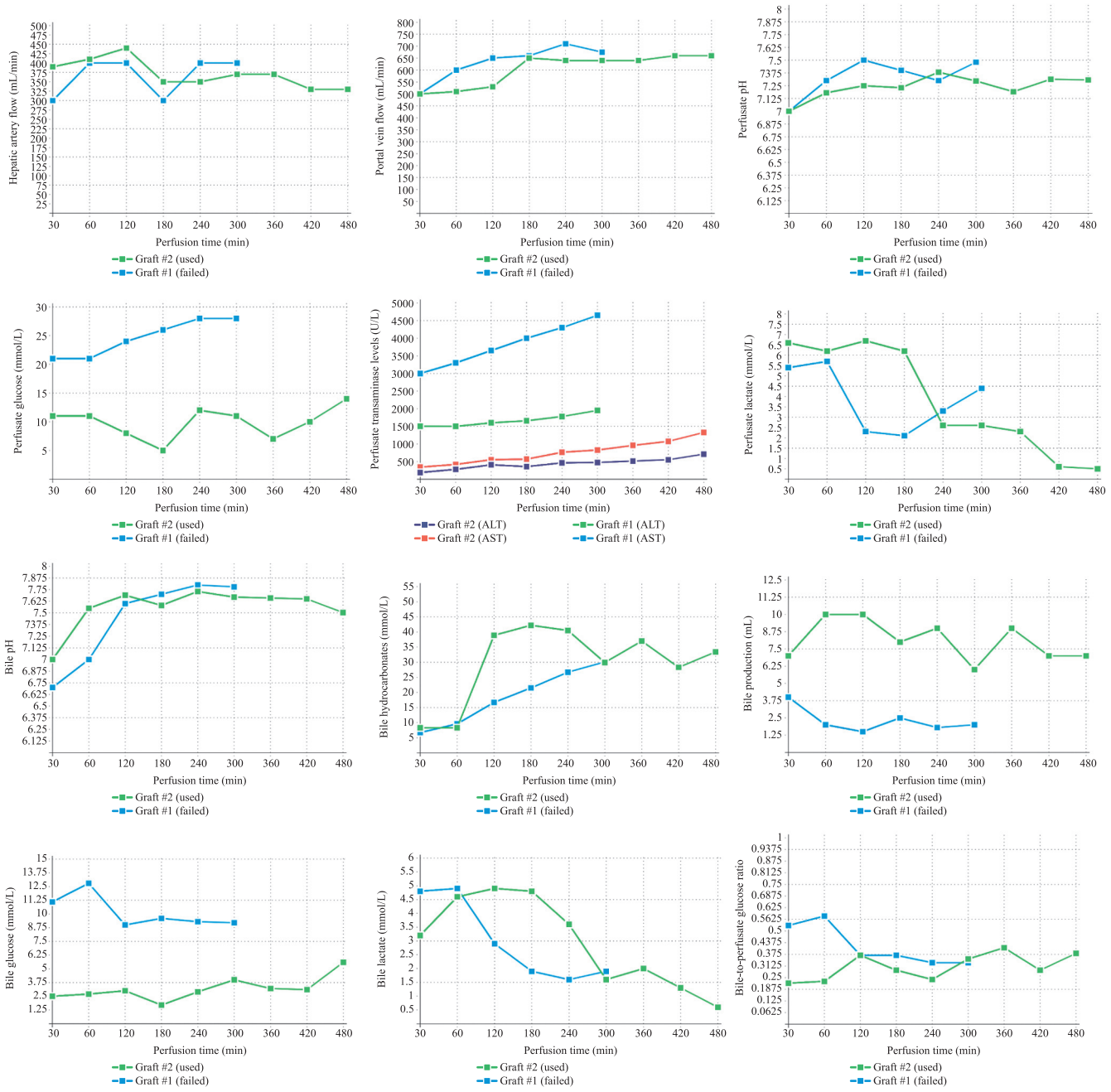

Fig. 4. Perfusion parameters of liver allografts in Case #1 (non-viable) and Case #2 (transplanted)

virtually unchanged from the pre-perfusion weight of 1910 g.

Based on these findings, the liver allograft was deemed viable. The D-HOPE time was 124 minutes, and the NMP time was 480 minutes. Total machine perfusion time was 604 minutes.

Liver transplantation

In Case #2, the LT operation lasted 290 minutes. Secondary warm ischemia time measured 20 minutes. Biliary ischemia time was 40 minutes, while total organ preservation time 884 minutes. After venous reperfusion of the graft, postreperfusion syndrome [44] did not develop. Moreover, there was no hemodynamic reaction to initiation of venous blood flow. Intraoperative blood loss was 200 mL, and transfusion included one unit of red blood cell mass.

Postoperative period

A schematic representation of the laboratory parameter dynamics during the postoperative period is shown in Fig. 5.

The peak AST level (922.5 U/mL) and ALT level (613 U/mL) were observed on postoperative day 1. The highest INR value (1.68) and total bilirubin level (63.3 μmol/L) were also recorded on postoperative day 1, followed by steady improvement. AKI developed on postoperative days 2–3, with peak creatinine of

400 μmol/L and urea of 29.2 μmol/L, requiring renal replacement therapy (RRT) via hemodialysis (two sessions). Following treatment, renal function fully recovered.

The total legnth of hospital stay was 14 days. During this period, due to the development of significant hydrothorax, pleural puncture and drainage were performed on the right side (postoperative day 1) and the left side (postoperative day 2). After adjustment of diuretic therapy, the hydrothorax regressed.

At the time of writing, the follow-up period was 3 months. The patient remains alive, has not been rehospitalized, and shows normal laboratory and instrumental parameters. It is noteworthy that IRPI was mild, and there were no signs of EAD, PNF, vascular or biliary complications.

Pathomorphologic study of liver allografts

In all cases, microscopic (using light microscopy) examination of allograft biopsies was mandatory at three stages: before perfusion, after completion of NMP, and before closure of the recipient's postoperative wound. Biopsies were obtained via an incisional method from the edge of both liver lobes, fixed in buffered 10% formalin, and submitted for pathomorphologic analysis.

– In *case #1*, the preperfusion (a) biopsy revealed, as previously noted, macrovesicular steatosis involving 65–70% of hepatocytes, hepatic fibrosis (stage F1 on the METAVIR scale), and diffuse, focal, moderate granular protein dystrophy of hepatocytes. The *postperfusion* (b) biopsy showed severe ischemia-reperfusion injury (IRI), characterized by diffuse focal hepatocyte necrosis within the parenchyma, predominantly in zones 1 and 3 of the hepatic acinus, accompanied by hemorrhages. Representative microphotographs are shown in Fig. 6.
– In *case #2*, the *preperfusion* (a) biopsy demonstrated diffuse focal large-droplet fatty degeneration of hepatocytes involving 5–10%, diffuse focal moderate granular protein dystrophy of hepatocytes, and hepatic fibrosis corresponding to stage F1–F2 on the METAVIR scale. The *postperfusion* (b) biopsy revealed moderate IRI of the liver. Similarly, the postreperfusion (c) biopsy pattern was consistent with moderate IRI, featuring subcapsular hepatocyte necrosis, most likely of compressive origin. Representative microphotographs are presented in Fig. 7.

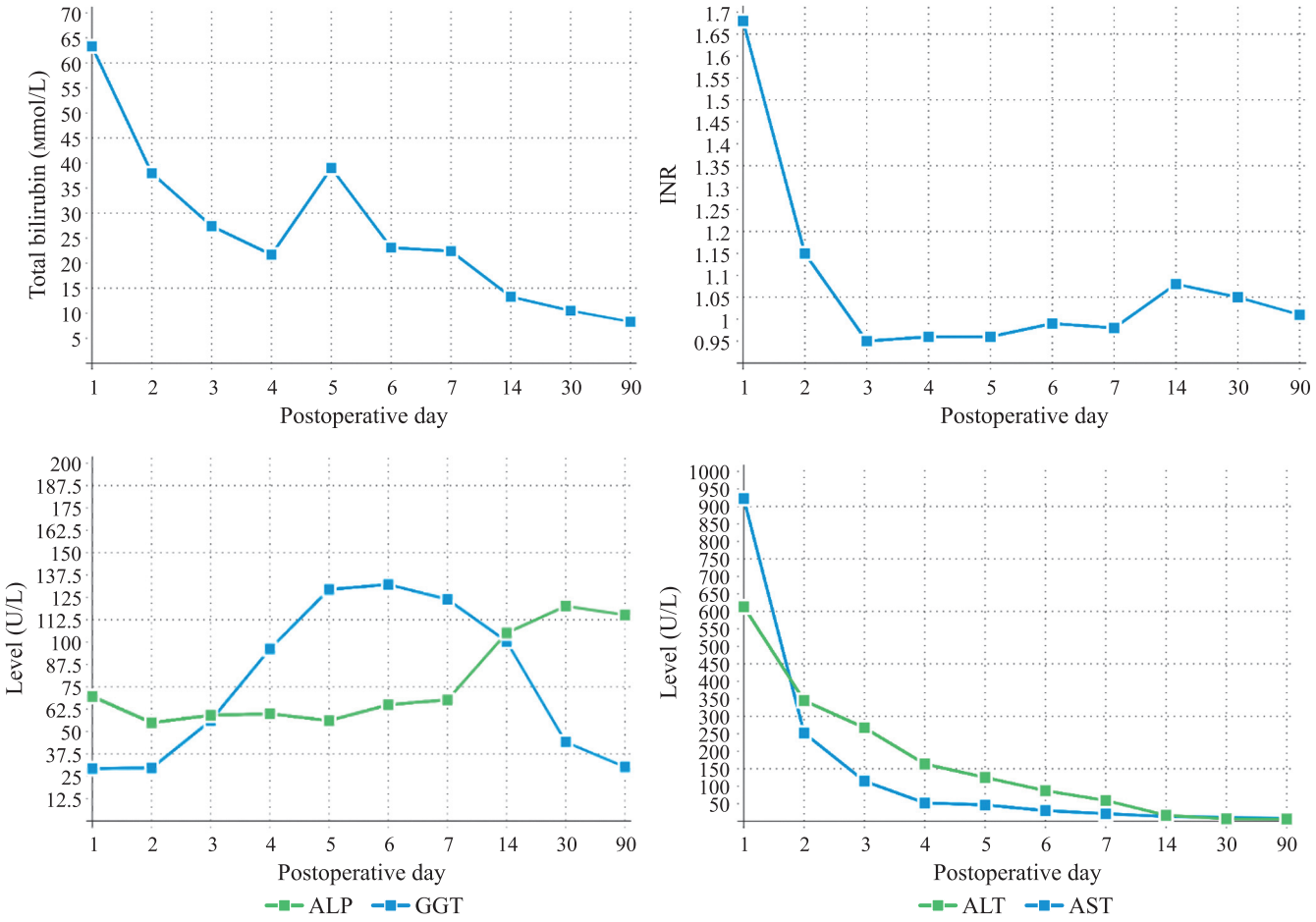

Fig. 5. Laboratory dynamics during the postoperative period in the liver recipient (Case #2)

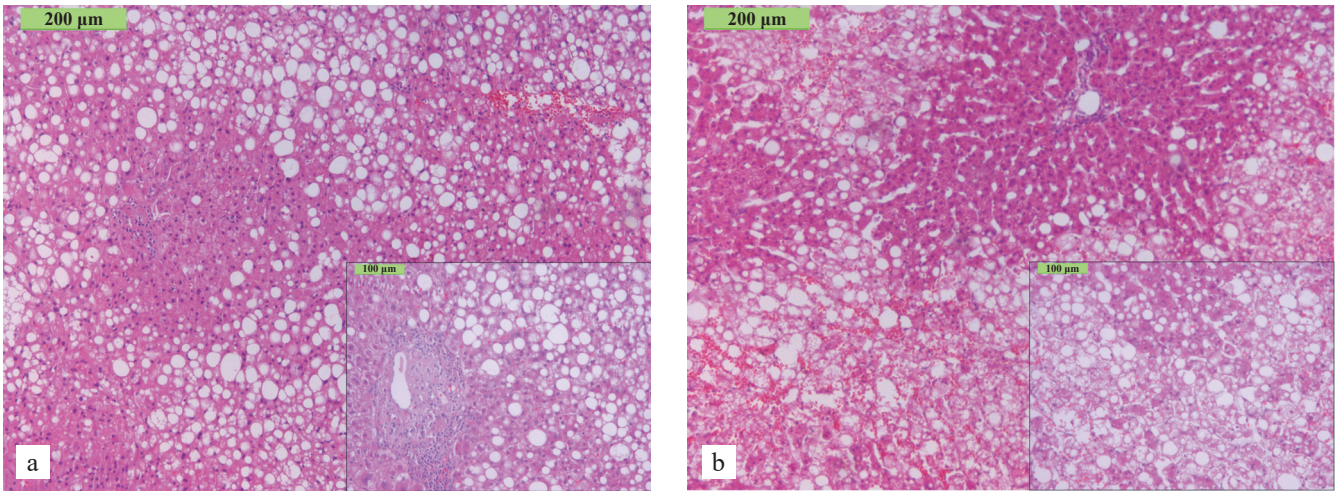

Fig. 6. Microphotographs of liver allograft biopsy in Case #1: (a) before machine perfusion, and (b) after perfusion. Histological description provided in the main text

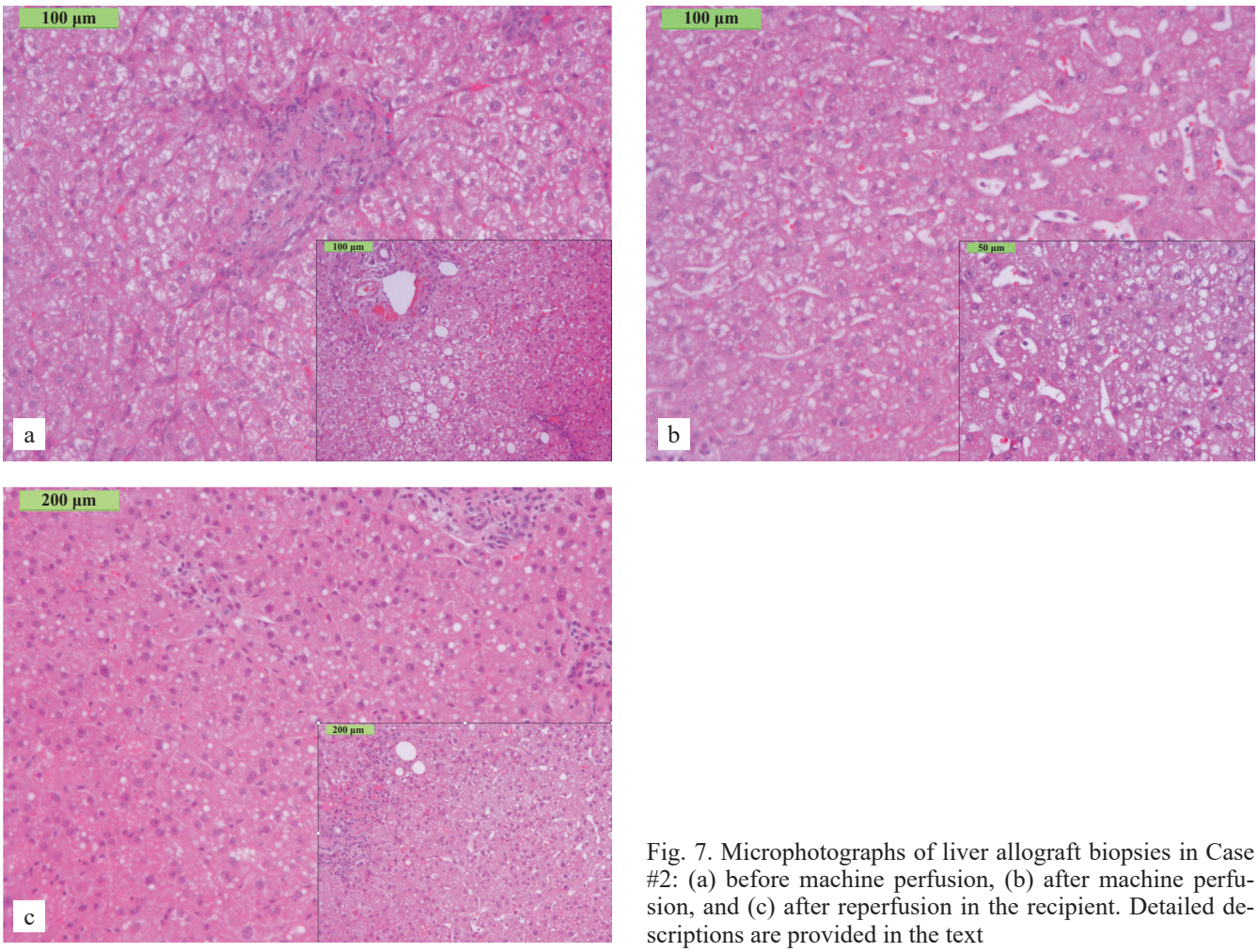

Fig. 7. Microphotographs of liver allograft biopsies in Case #2: (a) before machine perfusion, (b) after machine perfusion, and (c) after reperfusion in the recipient. Detailed descriptions are provided in the text

DISCUSSION

Machine perfusion is gaining prominence as a new gold standard for preserving liver allografts, especially those from ECDs. However, the isolated use of the main liver machine perfusion techniques – HOPE and NMP – despite their individual advantages, still presents a number of limitations [13–16]. For instance, assessment of liver graft viability during HOPE is restricted primarily to the measurement of a single validated marker, the concentration of FMN in the perfusate [17]. Moreover, the technical complexity of HOPE and the need for specialized equipment limit its availability to many centers,

thereby hindering broader adoption. While NMP offers extensive opportunities for comprehensive viability assessment, it does not fully eliminate IRPI due to normothermic reperfusion, although the injury is milder in an *ex vivo* setting [18–20].

Combined perfusion is a promising new direction in the development of liver allograft preservation, offering the opportunity to integrate the advantages of several machine perfusion techniques [11, 18, 23]. For instance, van Leeuwen et al., in a study involving combined perfusion of 54 allografts from high-risk donors (mean DRI 2.84, IQR 2.52–3.11), reported successful transplantation of 63% of organs, with 1-year graft and recipient survival rates of 94% and 100%, respectively. No cases of PNF were observed, and non-anastomotic biliary strictures developed in only one patient (3%). Two retransplantations were required due to chronic rejection (3%) and venous obstruction (3%) [11].

A sudden change in graft temperature from hypothermic (~4 °C) to normothermic (37 °C) conditions can induce "rewarming injury" or thermal injury, leading to further damage to the allograft [18, 21, 22]. To address this, the COR technique has been increasingly incorporated into combined perfusion protocols and has shown effectiveness when used as a standalone approach [21]. D. Hoyer, for example, reported a 50% reduction in peak AST levels (a surrogate marker for graft injury) in the COR group compared to the SCS group (AST 563.5 U/L *vs* 1204 U/L, P = 0.023) [22]. Nevertheless, there are no precise data on the efficacy of COR as part of combined protocols. Therefore, in the present cases, the combined perfusion protocol included only the "classical" HOPE and NMP stages.

At present, there is no universally accepted and validated algorithm for choosing the best perfusion strategy (isolated or combined, with various combinations) for each specific liver allograft [31]. This issue appears to be particularly pressing, as the routine application of "advanced" dynamic preservation techniques, including normothermic perfusion, to all organs meeting even a single expanded criteria donor (ECD) factor would be redundant and economically inefficient. On the other hand, the isolated use of hypothermic oxygenated perfusion for high-risk allografts (those presenting multiple risk factors) may be insufficient and could naturally lead to a higher incidence of complications. At Shumakov National Medical Research Center of Transplantology and Artificial Organs, the choice of perfusion method is made individually for each case, based on a comprehensive analysis of both donor and recipient factors. Continued experience accumulation and strengthened intercenter collaboration are expected to facilitate the development of more precise and standardized strategies for perfusion method selection in the future.

Assessment of liver graft viability remains a critical focus of contemporary research. In our work, we employed one of the most widely recognized viability assessment protocols, which demonstrated its effectiveness in the large VITTAL study [12, 20]. It is important to note that excessively stringent criteria may reduce the ability to identify potentially viable grafts, whereas overly liberal criteria increase the risk of post-transplant complications [35, 36]. For example, Panconesi et al. showed that using lactate clearance assessment at the sixth hour of NMP, only 13 (6.1%) of 213 allografts were classified as non-viable. In contrast, applying the Groningen or Brisbane criteria would have resulted in higher non-viability rates – 14.6% and 11.2%, respectively. The authors also highlighted that outcomes with so-called "lactate-high" allografts were comparable to those with lower lactate levels [51].

At the same time, as previously mentioned, studies by Mergental et al. revealed that the absence of mandatory qualitative bile assessment during viability evaluation led to ischemic cholangiopathy in four recipients [12, 20]. Retrospective analysis showed that, in three cases, non-anastomotic biliary strictures developed in recipients of DCD livers, where the bile produced during perfusion had low pH (<7.65) and low bicarbonate concentrations (<25 mmol/L) [12].

Based on these findings and a comprehensive review of the available literature, we modified the basic VITTAL protocol by incorporating mandatory assessment of biliary tree viability. It should be emphasized that, to date, there are no universally accepted criteria for liver graft viability assessment, and this remains an important area for further research and standardization.

We presented the machine perfusion of two liver grafts that had been rejected by all transplant centers due to their high degree of "marginality". Despite ex-vivo viability testing, the first allograft was ultimately deemed unsuitable for transplantation. The second graft met the viability criteria established by our center and was successfully transplanted into the recipient. This experience highlights the subjective nature of donor liver evaluation when based solely on initial clinical data.

The recipient's postoperative period was uneventful overall, despite the development of AKI, which may have been partially attributable to the patient's initially compromised condition and the use of high-dose diuretics prior to transplantation. Nevertheless, AKI resolved following two RRT sessions, and the total length of stay in the hospital was 14 days, which is consistent with the average in our center.

According to available data, the combined perfusion approach described here – particularly the application of the normothermic phase – is the first such experience in clinical practice in Russia. Thus, our observations demonstrate the high efficacy, safety, and reproducibili-

ty of the combined machine perfusion method for liver allografts obtained from ECDs.

The authors declare no conflict of interest.

REFERENCES

1. *Lewis A, Koukoura A, Tsianos GI, Gargavanis AA, Nielsen AA, Vassiliadis E.* Organ donation in the US and Europe: The supply *vs* demand imbalance. *Transplant Rev (Orlando)*. 2021 Apr; 35 (2): 100585. doi: 10.1016/j.trre.2020.100585. Epub 2020 Oct 11. PMID: 33071161.
2. *Langone AJ, Helderman JH.* Disparity between solid-organ supply and demand. *N Engl J Med*. 2003 Aug 14; 349 (7): 704–706. doi: 10.1056/NEJMe038117. PMID: 12917309.
3. *Kwong AJ, Kim WR, Lake JR, Schladt DP, Schnellinger EM, Gauntt K et al.* OPTN/SRTR 2022 Annual Data Report: Liver. *Am J Transplant*. 2024 Feb; 24 (2S1): S176–S265. doi: 10.1016/j.ajt.2024.01.014. PMID: 38431359.
4. *Goldaracena N, Cullen JM, Kim DS, Ekser B, Halazun KJ.* Expanding the donor pool for liver transplantation with marginal donors. *Int J Surg*. 2020 Oct; 82S: 30–35. doi: 10.1016/j.ijsu.2020.05.024. Epub 2020 May 15. PMID: 32422385.
5. *Moein M, Bahreini A, Razavi A, Badie S, Coyle S, Abedini M et al*. A Review of Long-Term Outcomes of Liver Transplantation Using Extended Criteria Donors in the United States. *J Surg Res*. 2025 Feb; 306: 561–569. doi: 10.1016/j.jss.2024.12.055. Epub 2025 Jan 31. PMID: 39892300.
6. *Zhang T, Dunson J, Kanwal F, Galvan NTN, Vierling JM, O'Mahony C et al*. Trends in Outcomes for Marginal Allografts in Liver Transplant. *JAMA Surg*. 2020 Aug 5; 155 (10): 926–32. doi: 10.1001/jamasurg.2020.2484. Epub ahead of print. Erratum in: *JAMA Surg*. 2020 Oct 1; 155 (10): 1002. doi: 10.1001/jamasurg.2020.4315. PMID: 32777009; PMCID: PMC7407315.
7. *Clavien PA, Harvey PR, Strasberg SM.* Preservation and reperfusion injuries in liver allografts. An overview and synthesis of current studies. *Transplantation*. 1992 May; 53 (5): 957–978. doi: 10.1097/00007890-199205000-00001. PMID: 1585489.
8. *Lozanovski VJ, Probst P, Arefidoust A, Ramouz A, Aminizadeh E, Nikdad M et al*. Prognostic role of the Donor Risk Index, the Eurotransplant Donor Risk Index, and the Balance of Risk score on graft loss after liver transplantation. *Transpl Int*. 2021 May; 34 (5): 778–800. doi: 10.1111/tri.13861. Epub 2021 May 1. PMID: 33728724.
9. *De Graaf EL, Kench J, Dilworth P, Shackel NA, Strasser SI, Joseph D et al*. Grade of deceased donor liver macrovesicular steatosis impacts graft and recipient outcomes more than the Donor Risk Index. *J Gastroenterol Hepatol*. 2012 Mar; 27 (3): 540–546. doi: 10.1111/j.1440-1746.2011.06844.x. PMID: 21777274.
10. *Callaghan CJ, Charman SC, Muiesan P, Powell JJ, Gimson AE, van der Meulen JH; UK Liver Transplant Audit.* Outcomes of transplantation of livers from donation after circulatory death donors in the UK: a cohort study. *BMJ Open*. 2013 Sep 3; 3 (9): e003287. doi: 10.1136/bmjopen-2013-003287. PMID: 24002984; PMCID: PMC3773642.
11. *Van Leeuwen OB, Bodewes SB, Lantinga VA, Haring MPD, Thorne AM, Brüggenwirth IMA et al*. Sequential hypothermic and normothermic machine perfusion enables safe transplantation of high-risk donor livers. *Am J Transplant*. 2022 Jun; 22 (6): 1658–1670. doi: 10.1111/ajt.17022. Epub 2022 Apr 18. PMID: 35286759; PMCID: PMC9325426.
12. *Mergental H, Laing RW, Kirkham AJ, Clarke G, Boteon YL, Barton D et al*. Discarded livers tested by normothermic machine perfusion in the VITTAL trial: Secondary end points and 5-year outcomes. *Liver Transpl*. 2024 Jan 1; 30 (1): 30–45. doi: 10.1097/LVT.0000000000000270. Epub 2023 Dec 15. PMID: 38109282.
13. *Dutkowski P, Polak WG, Muiesan P, Schlegel A, Verhoeven CJ, Scalera I et al*. First Comparison of Hypothermic Oxygenated PErfusion Versus Static Cold Storage of Human Donation After Cardiac Death Liver Transplants: An International-matched Case Analysis. *Ann Surg*. 2015 Nov; 262 (5): 764–770; discussion 770–771. doi: 10.1097/SLA.0000000000001473. PMID: 26583664.
14. *Van Rijn R, Schurink IJ, de Vries Y, van den Berg AP, Cortes Cerisuelo M, Darwish Murad S et al*. Hypothermic Machine Perfusion in Liver Transplantation – A Randomized Trial. *N Engl J Med*. 2021 Apr 15; 384 (15): 1391–1401. doi: 10.1056/NEJMoa2031532. Epub 2021 Feb 24. PMID: 33626248.
15. *Nasralla D, Coussios CC, Mergental H, Akhtar MZ, Butler AJ, Ceresa CDL et al*. A randomized trial of normothermic preservation in liver transplantation. *Nature*. 2018 May; 557 (7703): 50–56. doi: 10.1038/s41586-018-0047-9. Epub 2018 Apr 18. PMID: 29670285.
16. *Markmann JF, Vagefi PA, MacConmara MP*. Normothermic Machine Perfusion Increases Donor Liver Use. *JAMA Surg*. 2022 Aug 1; 157 (8): 742–743. doi: 10.1001/jamasurg.2022.1424. PMID: 35507357.
17. *Eden J, Thorne AM, Bodewes SB, Patrono D, Roggio D, Breuer E et al*. Assessment of liver graft quality during hypothermic oxygenated perfusion: The first international validation study. *J Hepatol*. 2025 Mar; 82 (3): 523–534. doi: 10.1016/j.jhep.2024.08.030. Epub 2024 Sep 7. PMID: 39251091; PMCID: PMC11830552.
18. *Van Leeuwen OB, Lantinga VA, Lascaris B, Thorne AM, Bodewes SB, Nijsten MW et al.* 'Back-to-base' combined hypothermic and normothermic machine perfusion of human donor livers. *Nat Protoc.* 2025. https://doi.org/10.1038/s41596-024-01130-8.
19. *Watson CJE, Kosmoliaptsis V, Randle LV, Gimson AE, Brais R, Klinck JR et al*. Normothermic Perfusion in the Assessment and Preservation of Declined Livers Before Transplantation: Hyperoxia and Vasoplegia-Important Lessons From the First 12 Cases. *Transplantation*. 2017 May; 101 (5): 1084–1098. doi: 10.1097/TP.0000000000001661. PMID: 28437389; PMCID: PMC5642347.

20. *Mergental H, Laing RW, Kirkham AJ, Perera MTPR, Boteon YL, Attard J et al*. Transplantation of discarded livers following viability testing with normothermic machine perfusion. *Nat Commun*. 2020 Jun 16; 11 (1): 2939. doi: 10.1038/s41467-020-16251-3. PMID: 32546694; PMCID: PMC7298000.
21. *Minor T, von Horn C, Zlatev H, Saner F, Grawe M, Lüer B et al*. Controlled oxygenated rewarming as novel end-ischemic therapy for cold stored liver grafts. A randomized controlled trial. *Clin Transl Sci*. 2022 Dec; 15 (12): 2918–2927. doi: 10.1111/cts.13409. Epub 2022 Oct 17. PMID: 36251938; PMCID: PMC9747115.
22. *Hoyer DP, Mathé Z, Gallinat A, Canbay AC, Treckmann JW, Rauen U et al*. Controlled Oxygenated Rewarming of Cold Stored Livers Prior to Transplantation: First Clinical Application of a New Concept. *Transplantation*. 2016 Jan; 100 (1): 147–152. doi: 10.1097/TP.0000000000000915. PMID: 26479280.
23. *Liu Q, Del Prete L, Ali K, Grady P, Bilancini M, Etterling J et al*. Sequential hypothermic and normothermic perfusion preservation and transplantation of expanded criteria donor livers. *Surgery*. 2023 Mar; 173 (3): 846–854. doi: 10.1016/j.surg.2022.07.035. Epub 2022 Oct 24. PMID: 36302699.
24. *De Vries Y, Matton APM, Nijsten MWN, Werner MJM, van den Berg AP, de Boer MT et al*. Pretransplant sequential hypo- and normothermic machine perfusion of suboptimal livers donated after circulatory death using a hemoglobin-based oxygen carrier perfusion solution. *Am J Transplant*. 2019 Apr; 19 (4): 1202–1211. doi: 10.1111/ajt.15228. Epub 2019 Jan 23. PMID: 30588774; PMCID: PMC6590255.
25. *Oosterlee A, Rahmel A.* Eurotransplant International Foundation Annual Report 2008. 2011.
26. *Feng S, Goodrich NP, Bragg-Gresham JL, Dykstra DM, Punch JD, DebRoy MA et al*. Characteristics associated with liver graft failure: the concept of a donor risk index. *Am J Transplant*. 2006 Apr; 6 (4): 783–790. doi: 10.1111/j.1600-6143.2006.01242.x. Erratum in: *Am J Transplant*. 2018 Dec; 18 (12): 3085. doi: 10.1111/ajt.15155. PMID: 16539636.
27. *Martínez JA, Pacheco S, Bachler JP, Jarufe N, Briceño E, Guerra JF et al*. Accuracy of the BAR score in the prediction of survival after liver transplantation. *Ann Hepatol*. 2019 Mar-Apr; 18 (2): 386–392. doi: 10.1016/j.aohep.2019.01.002. Epub 2019 Apr 17. PMID: 31036493.
28. *Pogrebnichenko IV.* Effektivnoe ispol'zovanie pecheni mul'tiorgannogo donora dlya transplantatsii: dis. … kand. med. nauk. M., 2014; 143.
29. *Koch DT, Tamai M, Schirren M, Drefs M, Jacobi S, Lange CM et al*. Mono-HOPE Versus Dual-HOPE in Liver Transplantation: A Propensity Score-Matched Evaluation of Early Graft Outcome. *Transpl Int*. 2025 Feb 5; 38: 13891. doi: 10.3389/ti.2025.13891. PMID: 39974599; PMCID: PMC11835512.
30. *De Vries Y, Brüggenwirth IMA, Karangwa SA, von Meijenfeldt FA, van Leeuwen OB, Burlage LC et al*. Dual Versus Single Oxygenated Hypothermic Machine Perfusion of Porcine Livers: Impact on Hepatobiliary and Endothelial Cell Injury. *Transplant Direct*. 2021 Aug 5; 7 (9): e741. doi: 10.1097/TXD.0000000000001184. PMID: 34386578; PMCID: PMC8354629.
31. *Sousa Da Silva RX, Weber A, Dutkowski P, Clavien PA*. Machine perfusion in liver transplantation. *Hepatology*. 2022 Nov; 76 (5): 1531–1549. doi: 10.1002/hep.32546. Epub 2022 May 17. PMID: 35488496.
32. *Schlegel A, Muller X, Mueller M, Stepanova A, Kron P, de Rougemont O et al*. Hypothermic oxygenated perfusion protects from mitochondrial injury before liver transplantation. *EBioMedicine*. 2020 Oct; 60: 103014. doi: 10.1016/j.ebiom.2020.103014. Epub 2020 Sep 24. PMID: 32979838; PMCID: PMC7519249.
33. *Eden J, Breuer E, Birrer D, Müller M, Pfister M, Mayr H et al*. Screening for mitochondrial function before use-routine liver assessment during hypothermic oxygenated perfusion impacts liver utilization. *EBioMedicine*. 2023 Dec; 98: 104857. doi: 10.1016/j.ebiom.2023.104857. Epub 2023 Oct 31. PMID: 37918219; PMCID: PMC10641151.
34. *Patrono D, Catalano G, Rizza G, Lavorato N, Berchialla P, Gambella A et al*. Perfusate Analysis During Dual Hypothermic Oxygenated Machine Perfusion of Liver Grafts: Correlations With Donor Factors and Early Outcomes. *Transplantation*. 2020 Sep; 104 (9): 1929–1942. doi: 10.1097/TP.0000000000003398. PMID: 32769628.
35. *Groen PC, van Leeuwen OB, de Jonge J, Porte RJ.* Viability assessment of the liver during *ex situ* machine perfusion prior to transplantation. *Curr Opin Organ Transplant*. 2024 Aug 1; 29 (4): 239–247. doi: 10.1097/MOT.0000000000001152. Epub 2024 May 17. PMID: 38764406; PMCID: PMC11224566.
36. *Jeddou H, Tzedakis S, Chaouch MA, Sulpice L, Samson M, Boudjema K*. Viability Assessment During Normothermic Machine Liver Perfusion: A Literature Review. *Liver Int*. 2025 Feb; 45 (2): e16244. doi: 10.1111/liv.16244. PMID: 39821671; PMCID: PMC11740183.
37. *Matton APM, de Vries Y, Burlage LC, van Rijn R, Fujiyoshi M, de Meijer VE et al*. Biliary Bicarbonate, pH, and Glucose Are Suitable Biomarkers of Biliary Viability During *Ex Situ* Normothermic Machine Perfusion of Human Donor Livers. *Transplantation*. 2019 Jul; 103 (7): 1405–1413. doi: 10.1097/TP.0000000000002500. PMID: 30395120; PMCID: PMC6613725.
38. *Olthoff KM, Kulik L, Samstein B, Kaminski M, Abecassis M, Emond J et al*. Validation of a current definition of early allograft dysfunction in liver transplant recipients and analysis of risk factors. *Liver Transpl*. 2010 Aug; 16 (8): 943–949. doi: 10.1002/lt.22091. PMID: 20677285.
39. *Khwaja A.* KDIGO clinical practice guidelines for acute kidney injury. *Nephron Clin Pract*. 2012; 120 (4): c179–c184. doi: 10.1159/000339789. Epub 2012 Aug 7. PMID: 22890468.
40. *Al-Freah MAB, McPhail MJW, Dionigi E, Foxton MR, Auzinger G, Rela M et al*. Improving the Diagnostic Criteria for Primary Liver Graft Nonfunction in Adults Utilizing Standard and Transportable Laboratory Parameters: An Outcome-Based Analysis. *Am J Transplant*.

2017 May; 17 (5): 1255–1266. doi: 10.1111/ajt.14230. Epub 2017 Apr 5. PMID: 28199762.

41. *Eshmuminov D, Becker D, Bautista Borrego L, Hefti M, Schuler MJ, Hagedorn C et al*. An integrated perfusion machine preserves injured human livers for 1 week. *Nat Biotechnol*. 2020 Feb; 38 (2): 189–198. doi: 10.1038/s41587-019-0374-x. Epub 2020 Jan 13. PMID: 31932726; PMCID: PMC7008032.
42. *Schurink IJ, Willemse J, Verstegen MMA, van der Laan LJW, de Jonge J*. Long-Term Perfusion of the Liver Outside the Body: Warming Up for *Ex vivo* Therapies? *Hepatology*. 2020 Oct; 72 (4): 1485–1487. doi: 10.1002/hep.31474. PMID: 33464565; PMCID: PMC7702161.
43. *Olumba FC, Zhou F, Park Y, Chapman WC; RESTORE Investigators Group.* Normothermic Machine Perfusion for Declined Livers: A Strategy to Rescue Marginal Livers for Transplantation. *J Am Coll Surg*. 2023 Apr 1; 236 (4): 614–625. doi: 10.1097/XCS.0000000000000555. Epub 2023 Jan 11. PMID: 36728302.
44. *Siniscalchi A, Gamberini L, Laici C, Bardi T, Ercolani G, Lorenzini L, Faenza S*. Post reperfusion syndrome during liver transplantation: From pathophysiology to therapy and preventive strategies. *World J Gastroenterol*. 2016 Jan 28; 22 (4): 1551–1569. doi: 10.3748/wjg.v22.i4.1551. PMID: 26819522; PMCID: PMC4721988.
45. *Parente A, Tirotta F, Pini A, Eden J, Dondossola D, Manzia TM Dutkowski P, Schlegel A*. Machine perfusion techniques for liver transplantation – A meta-analysis of the first seven randomized-controlled trials. *J Hepatol*. 2023 Nov; 79 (5): 1201–1213. doi: 10.1016/j.jhep.2023.05.027. Epub 2023 Jun 9. PMID: 37302578.
46. *Tingle SJ, Dobbins JJ, Thompson ER, Figueiredo RS, Mahendran B, Pandanaboyana S, Wilson C*. Machine perfusion in liver transplantation. *Cochrane Database Syst Rev*. 2023 Sep 12; 9 (9): CD014685. doi: 10.1002/14651858.CD014685.pub2. PMID: 37698189; PMCID: PMC10496129.
47. *Banker A, Bhatt N, Rao PS, Agrawal P, Shah M, Nayak M, Mohanka R.* A Review of Machine Perfusion Strategies in Liver Transplantation. *J Clin Exp Hepatol*. 2023 Mar-Apr; 13 (2): 335–349. doi: 10.1016/j.jceh.2022.08.001. Epub 2022 Aug 10. PMID: 36950485; PMCID: PMC10025749.
48. *Boteon YL, Laing RW, Schlegel A, Wallace L, Smith A, Attard J et al*. Combined Hypothermic and Normothermic Machine Perfusion Improves Functional Recovery of Extended Criteria Donor Livers. *Liver Transpl*. 2018 Dec; 24 (12): 1699–1715. doi: 10.1002/lt.25315. PMID: 30058119; PMCID: PMC6588092.
49. *Chen Z, Hong X, Huang S, Wang T, Ma Y, Guo Y et al*. Continuous Normothermic Machine Perfusion for Renovation of Extended Criteria Donor Livers Without Recooling in Liver Transplantation: A Pilot Experience. *Front Surg*. 2021 May 24; 8: 638090. doi: 10.3389/fsurg.2021.638090. PMID: 34109206; PMCID: PMC8180843.
50. *Chen Z, Wang T, Chen C, Zhao Q, Ma Y, Guo Y et al*. Transplantation of Extended Criteria Donor Livers Following Continuous Normothermic Machine Perfusion Without Recooling. *Transplantation*. 2022 Jun 1; 106 (6): 1193–1200. doi: 10.1097/TP.0000000000003945. Epub 2022 Sep 7. PMID: 34495016; PMCID: PMC9128617.
51. *Panconesi R, Shanmugarajah K, Satish S, Zhang M, Wehrle C, Jiao C et al*. Rethinking Lactate's Role as a Post-Transplant Outcome Predictor During Normothermic Machine Perfusion: Science or Speculation? *Am J Transplant*. 2025 Jan; 25 (1 Suppl 1): S126.
52. *Van Leeuwen OB, de Vries Y, Fujiyoshi M, Nijsten MWN, Ubbink R, Pelgrim GJ et al*. Transplantation of High-risk Donor Livers After *Ex Situ* Resuscitation and Assessment Using Combined Hypo- and Normothermic Machine Perfusion: A Prospective Clinical Trial. *Ann Surg*. 2019 Nov; 270 (5): 906–914. doi: 10.1097/SLA.0000000000003540. PMID: 31633615.

The article was submitted to the journal on 9.04.2025

DOI: 10.15825/1995-1191-2025-2-23-30

KIDNEY TRANSPLANTATION IN PATIENTS WITH AUTOSOMAL DOMINANT POLYCYSTIC KIDNEY DISEASE: SURGICAL TACTICS, IMMEDIATE AND LONG-TERM OUTCOMES

V.S. Daineko[1, 3], D.D. Fedotova[2], A.N. Ananiev[1, 2], I.V. Uliankina[1, 2], I.V. Loginov[1], D.V. Fitro[1], A.A. Kutenkov[1, 2], D.O. Kuzmin[1, 2], M.E. Malyshev[1], V.N. Kravchuk[3], O.N. Reznik[1, 2], D.V. Kandyba[1, 3], S.F. Bagnenko[2], V.A. Manukovsky[1, 3]

[1] St. Petersburg Research Institute of Emergency Medicine, St. Petersburg, Russian Federation
[2] Pavlov University, St. Petersburg, Russian Federation
[3] North-Western State Medical University, St. Petersburg, Russian Federation

Introduction. Treatment and kidney transplantation (KT) for patients with autosomal dominant polycystic kidney disease (ADPKD) are associated with increased risks, particularly due to the potential for infection of polycystic kidney (PK) cysts. Currently, no standardized guidelines exist for the surgical management and pre-transplant preparation of these patients. **Objective:** to analyze the 15-year experience at a transplant center managing KT recipients with end-stage chronic kidney disease (eCKD) due to ADPKD. **Materials and methods.** A retrospective and prospective analysis was conducted on 132 ADPKD patients who underwent staged surgical treatment between 2008 and 2023. In the first stage, outcomes of 155 PK nephrectomies performed via laparoscopic and open approaches were evaluated. In the second stage, KT outcomes were assessed in 63 ADPKD recipients, comparing those with preserved native kidneys to those who had undergone nephrectomy. Additionally, as a control group, KT outcomes in 129 patients with eCKD of other etiologies from 2013 to 2023 were analyzed. **Results.** The study revealed significant advantages of laparoscopic access for PK nephrectomy, including a shorter length of stay in both intensive care and the hospital, as well as a lower complication rate (47.8% for laparotomy and lumbotomy approaches, and 12.8% for laparoscopic access). However, patients who underwent KT with preserved PK exhibited a higher incidence of infectious complications (26.9%), primarily due to cyst infections and resistance to standard antibiotic prophylaxis. Long-term graft survival was notably lower in this group, with a ten-year survival rate of 46.2%, compared to 73.1% in patients who had undergone nephrectomy and 74.1% in the comparison group. **Conclusion.** The integration of laparoscopic surgery for polycystic kidney disease into clinical practice has the potential to significantly reduce surgical complications and broaden the indications for PK nephrectomy. Among ADPKD patients who underwent nephrectomy, the post-transplant period was more favorable, with outcomes comparable to those of KT recipients with eCKD of other etiologies.

Keywords: autosomal dominant polycystic kidney disease, kidney transplantation, polycystic kidneys, laparoscopic access, nephrectomy.

INTRODUCTION

Autosomal dominant polycystic kidney disease (ADPKD) is a progressive disorder characterized by multiple bilateral cysts within the renal parenchyma, ultimately leading to impaired kidney function and, in many cases, the need for renal replacement therapy (RRT) [1–3]. By age 60, a significant portion of individuals with ADPKD experience end-stage chronic kidney disease (eCKD), and approximately 10–15% of those receiving maintenance dialysis via peritoneal dialysis fall into this category [2, 5].

In approximately 20% of individuals with polycystic kidney disease (PKD), kidney removal (nephrectomy) is considered due to clinical manifestations and complications. Due to the large size of polycystic kidneys (PK), many centers perform nephrectomy using laparotomy or lumbotomy approaches. These surgical interventions are associated with a high complication rate (up to 38%) and a mortality rate of up to 3% [1, 6].

Cyst infection is a serious complication of ADPKD, accounting for approximately 11% of hospitalizations in patients with this condition. In ADPKD patients, 30–50% experience kidney infections during their lifetime, and over 50% report one or more symptomatic infection episodes [7–9].

Laparoscopic nephrectomy for PKD was first performed in 1996, and is now widely used, offering the benefits associated with a minimally invasive procedure [2, 10].

Corresponding author: Vasily Daineko. Address: 3, Budapestskaya str., St.-Petersburg, 192242, Russian Federation. Phone: (911) 027-48-44. E-mail: vsdaineko@yandex.ru

We have previously demonstrated that PKD has a high infection rate of 80%. The asymptomatic nature of ADPKD does not preclude the presence of infected small-diameter cysts [11]. The diagnostic capabilities of standard imaging modalities, such as spiral computed tomography and ultrasound remain limited in this context. Infection of renal cysts in PKD patients can worsen the prognosis of future kidney transplantation (KT). The presence of a non-sanitized focus of infection, combined with modern immunosuppressive therapy regimens, can lead to the development of a systemic inflammatory response and sepsis. Removal of polycystic kidneys to sanitize an active infection focus carries a high risk of complications and mortality [11–12].

To date, there are various approaches to the need for pre-transplant nephrectomy [13–19]. Our center uses a previously developed diagnostic and surgical preparation algorithm for KT in patients with ADPKD (Fig. 1), which is based on clinical presentation and comprehensive patient evaluation [20].

MATERIALS AND METHODS

The study is based on the results of the analysis of staged surgical treatment of 132 patients with PKD in the period from 2008 to 2023. The 15-year experience of the Center's work with this patient cohort was summarized and analyzed. Surgical preparation for transplantation from 2013 was performed according to the previously

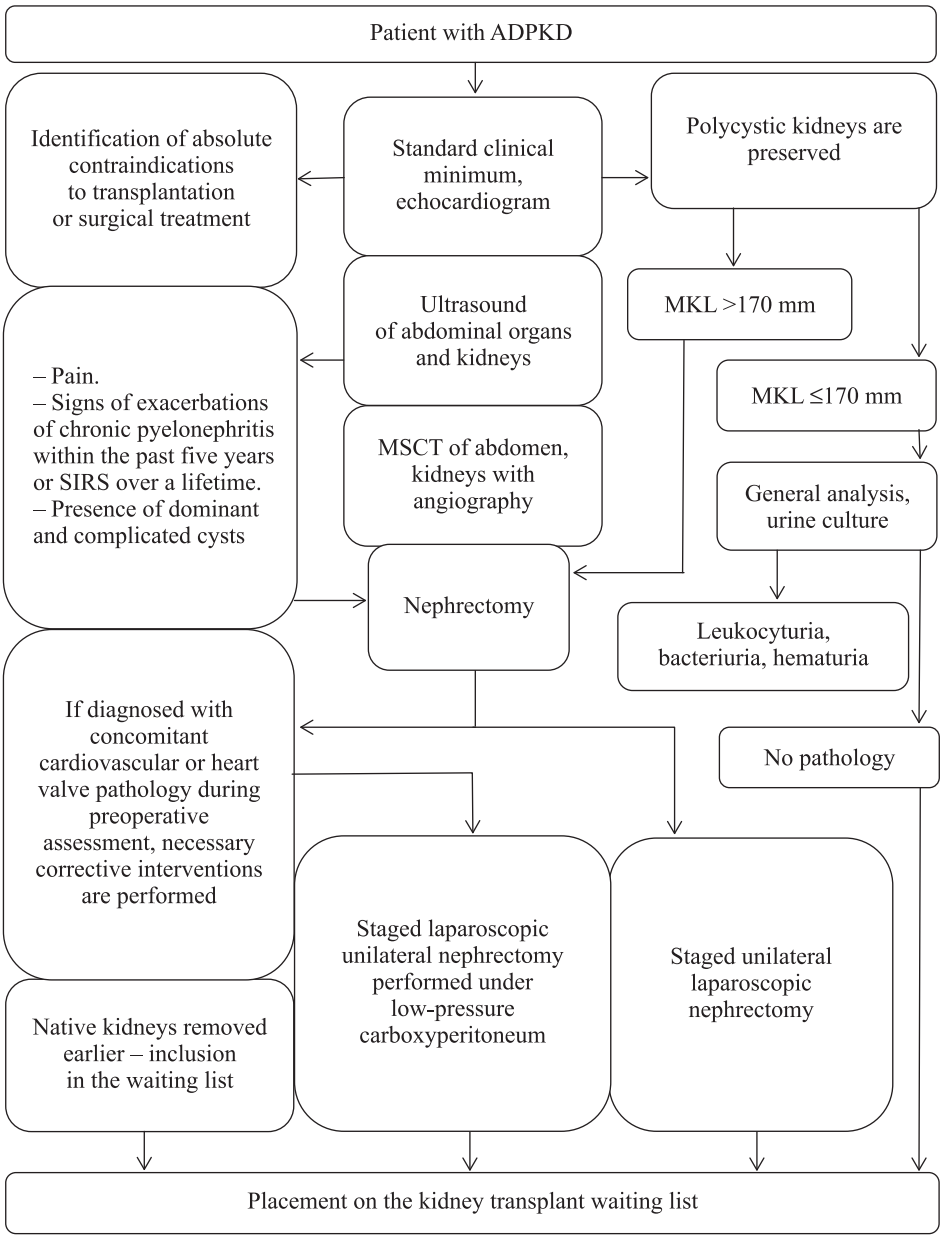

Fig. 1. Algorithm for inclusion in the kidney transplant waiting list for an ADPKD patient [21]. ADPKD, autosomal dominant polycystic kidney disease; SIRS, systemic inflammatory response syndrome; MSCT, multislice computed tomography; MKL, maximum kidney length

developed algorithm based assessment of clinical picture and maximum PKD size (Fig. 1).

For comparison, we analyzed KT outcomes in a control group of 129 patients with eCKD of other etiologies, treated between 2013 and 2023. Given the high risk of specific complications, patients with diabetes mellitus, repeat transplants, or rare genetic disorders were excluded from the study.

Between 2008 and 2023, a total of 155 nephrectomies were performed in 106 individuals as part of pre-transplant preparation or for clinical indications. Of these, 46 surgeries were carried out in 39 patients using either lumbotomy (for unilateral nephrectomy) or laparotomy (for bilateral nephrectomy). The remaining 67 patients underwent laparoscopic procedures, accounting for 109 nephrectomies in total. All laparoscopic interventions were unilateral.

Laparoscopic nephrectomies have been routinely performed since 2013, while the majority of open surgeries occurred prior to this period, due to their well-documented advantages. Surgical indications included preparation for KT and management of clinical symptoms of PKD such as hematuria, frequent recurrent pyelonephritis, and chronic pain.

The clinical characteristics of the patient cohorts and the outcomes of surgical treatment are presented in Table 1.

Between 2008 and 2023, 63 ADPKD patients underwent KT. Depending on whether native kidneys were preserved or removed, two groups of patients were distinguished:

– Group 1 (n = 26), patients who had preserved PKD at the time of transplantation.
– Group 2 (n = 37), patients who underwent nephrectomy before transplantation.

As a comparison group, we analyzed kidney transplant outcomes between 2013 and 2023 in 129 patients with eCKD of non-ADPKD etiology. All transplants were performed using immunologically compatible kidneys from brain-dead donors, following standard matching criteria. Baseline characteristics between the ADPKD and comparison groups showed no statistically significant differences (Table 2).

RESULTS

The outcomes of nephrectomy in patients with polycystic kidney disease are presented in Table 1. Notably, the laparoscopic approach was associated with a more favorable perioperative course. Although laparoscopic surgeries had a longer operative time, both intensive care

Table 1

Outcomes of polycystic kidney nephrectomy

Indicator	Nephrectomy (laparotomy, lumbotomy), n = 46	Laparoscopic nephrectomy, n = 109	P
Mean patient age (years)	53.2 ± 8.7	54.5 ± 8.1	p = 0.41
Patient gender – Male – Female	n = 39 21 (53.8%) 18 (46.2%)	n = 67 35 (52.2%) 32 (47.8%)	p > 0.05
Mean time to receive RRT by hemodialysis before surgery (months)	30.6 ± 19.3	38.5 ± 33.7	p = 0.141
Indications for surgical treatment – Clinical indications – Pre-transplant preparation	 31 (67.4%) 15 (32.6%)	 44 (40.4%) 65 (59.6%)	**p = 0.003**
Average surgery time (minutes)	118 ± 36.8	147.5 ± 57.5	**p = 0.003**
ICU length of stay (days)	2–3 days (2.9 ± 1.4)	1–2 days (1.1 ± 0.47)	**p = 0.001**
Bed-days spent in hospital (days)	14–16 (14.2 ± 5.7)	7–8 (8.5 ± 7.9)	**p < 0.001**
Surgical complication rate	47.8% (22)	12.8% (14)	**p < 0.001**
Arteriovenous fistula thrombosis	4.3% (2)	3.6% (4)	p = 1.000
SIRS, sepsis	10.8% (5)	3.6% (4)	p = 0.126
Intestinal paresis	10.8% (5)	–	**p = 0.002**
Wound suppuration	8.6% (4)	1.8% (2)	p = 0.064
Bleeding with hematoma formation in the postoperative wound and retroperitoneal space	8.6% (4)	2.7% (3)	p = 0.196
Additional surgical interventions	10.8% (5)	3.6% (4)	p = 0.126
Mesenteric thrombosis	0.0%	0.9% (1)	p = 1.000
Eventration	4.3% (2)	0.0%	p = 0.086
Access conversion	–	5.5% (6)	
Mortality	8.6% (4)	1.83% (2)	p = 0.064

Note: RRT, renal replacement therapy; ICU, intensive care unit; SIRS, systemic inflammatory response syndrome.

Table 2

Main characteristics and outcomes of kidney transplantation

Indicator	Group 1, n = 26	Group 2, n = 37	Comparison group, n = 129	P
Mean patient age (years)	49.8 ± 9.2	51.2 ± 10.5	47.8 ± 9.8	p > 0.05
Patient gender – Male – Female	 15 (57.7%) 11 (42.3%)	 21 (56.8%) 16 (43.2%)	 61 (47.3%) 68 (52.7%)	p > 0.05
Mean time to receive RRT by hemodialysis before surgery (months)	31.8 ± 27.6	41.8 ± 31.6	35.3 ± 28.4	p > 0.05
Donor characteristics				
Average age	51.2 ± 9.7	52.4 ± 10.1	49.4 ± 9.2	p > 0.05
Average creatinine level (μmol/L)	96.3 ± 12.1	103.5 ± 11.3	98.7 ± 9.4	p > 0.05
Average number of HLA matches	4.1 ± 1.2	4.3 ± 0.9	3.9 ± 1.1	p > 0.05
Kidney transplant outcomes				
Graft function: – Immediate – Delayed	 14 (53.8%) 12 (46.2%)	 22 (59.4%) 15 (40.6%)	 76 (58.9%) 53 (41.1%)	p > 0.05
Early complications (within 1 month of transplantation)				
Primary non-function	1 (3.8%)	0.0%	3 (2.3%)	p > 0.05
Acute transplant rejection	1 (3.8%)	1 (2.7%)	3 (2.3%)	p > 0.05
Infectious complications of various localizations	7 (26.9%)	2 (5.4%)	8 (6.2%)	**p < 0.05**
Nephrectomy due to infected cysts	2 (7.6%)	–	–	–
Late complications				
Transplant rejection	2 (7.6%)	3 (8.1%)	9 (6.9%)	p > 0.05
Pyelonephritis, episodes of hematuria, leukocyturia (number of cases per year)	1.9 ± 0.71	0.21 ± 0.11	0.23 ± 0.15	**p < 0.05**
Post-transplant nephrectomy according to clinical indications	4 (15.4%)	–	–	

Note: RRT, renal replacement therapy.

unit (ICU) and overall hospital stays were significantly shorter compared to open surgery. The incidence of postoperative complications in the laparoscopic group remained low, not exceeding 13%.

Transplant outcomes in the analyzed groups are presented in Table 2.

Infectious complications of various localizations included pneumonia, sepsis, graft pyelonephritis, postoperative wound suppuration, and infection of cysts in preserved native kidneys. A notable increase in the frequency of complications was observed in patients with preserved polycystic kidneys (PK), primarily due to cyst infections and the presence of pathogens resistant to standard antibiotic prophylaxis. For group 1, the incidence of infectious complications was 26.9%, p = 0.028 when comparing group 1 and group 2, and p = 0.004 when comparing group 1 and comparison group. Additionally, Group 1 showed a significantly higher frequency of leukocyturia (more than 20 leukocytes per field of view) and hematuria (more than 20 red blood cells per field of view). In seven cases, nephrectomy of native kidneys was required post-transplant due to PKD-related complications. Overall, among all ADPKD patients who underwent KT, the native kidney was removed in 69.8% (44 cases), predominantly due to infectious complications.

Ten-year kidney graft and recipient survival rates are shown in Figs. 2 and 3. Notably, 10-year graft survival was 46.2% in group 1, compared to 73.1% and 74.1% in group 2 and comparison group, respectively.

DISCUSSION

The high infection rate of 80% in PKD does warrant the expansion of indications for nephrectomy during the pre-transplantation preparation stage [11]. Effective treatment of non-sanitized infections during pre-transplant preparation is challenging. This makes managing infections both before and after transplantation more difficult. Simultaneous nephrectomy with kidney transplantation for PKD patients is a common procedure today. In our opinion, this practice is doubtful, as the large volume of surgery and high risk of infectious complications jeopardize the fate of the graft and the life of the recipient [21–23].

The use of laparoscopic technologies in PKD surgery has significantly broadened the indications for pre-transplant nephrectomy by reducing the risks associated with surgical intervention. Native kidney removal is required in 69.8% of ADPKD patients for various clinical reasons. In 21.7% of cases, nephrectomy became necessary after transplantation due to PKD-related complications that developed under immunosuppressive therapy.

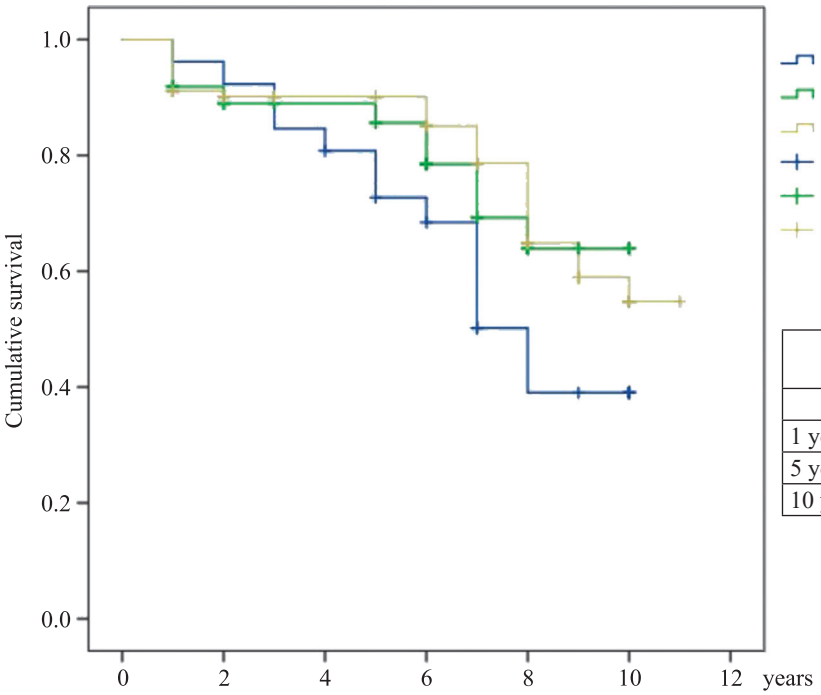

	Group 1	Group 2	Comparison group
Graft survival (%)			
1 year	92.3	94.5	96.3
5 years	76.9	81.1	83.2
10 years	462	73.1	74.1

Fig. 2. Cumulative kidney graft survival (p = 0,063)

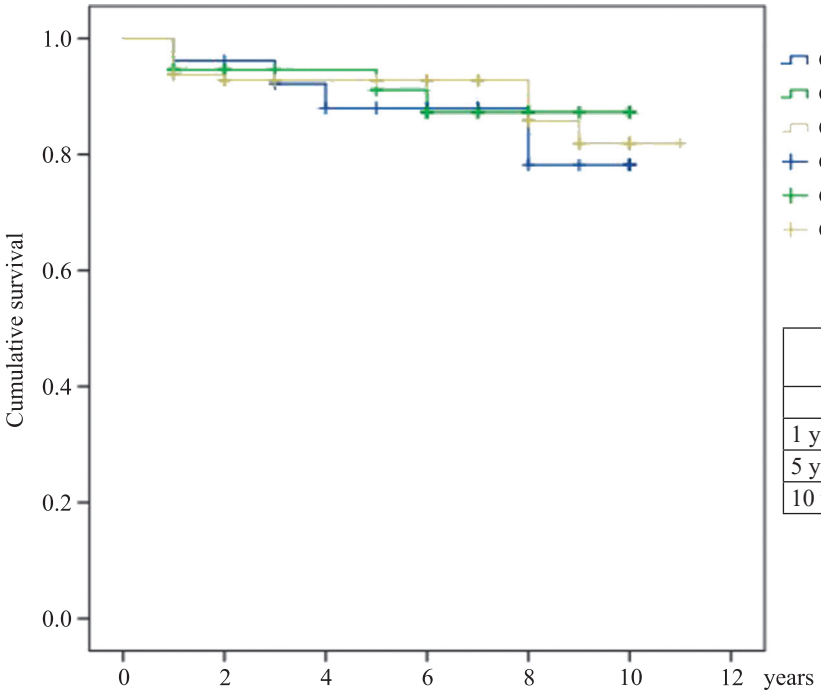

	Group 1	Group 2	Comparison group
Recipient survival (%)			
1 year	92.3	97.2	96.4
5 years	88.5	91.8	92.8
10 years	84.6	89.2	88.3

Fig. 3. Cumulative survival of kidney transplant recipients (p = 0.531)

The use of laparoscopic techniques for polycystic kidneys in ADPKD has allowed for safer pre-transplant nephrectomies by minimizing the risks of surgical intervention. Removal of native kidneys for various reasons was required in 69.8% of patients with ADPKD. In 21.7% of cases, nephrectomy was performed post-transplantation due to PKD-related complications while the patients were on immunosuppressive therapy.

Bilateral nephrectomy should be considered in select cases. At our center, conversion to an alternative surgical approach was necessary in cases involving a horseshoe kidney or insufficient "working space" in the abdominal cavity due to the giant size of the kidneys.

Patients with ADPKD have a significantly higher frequency of various cardiovascular pathologies compared to the general population of patients with eCKD. Preparation of each patient in this group should include

a comprehensive cardiological examination. In cases where concomitant cardiovascular pathology is detected, nephrectomy under low-pressure carboxyperitoneum is available [24].

Notably, after 10 years, only 46.2% of grafts in patients with preserved PKD remained functional, and the mortality rate in this group reached 15.4%. In contrast, PKD patients who underwent pre-transplant nephrectomy had a more favorable postoperative course, with significantly lower rates of leukocyturia, bacteriuria, and hematuria.

At the same time, total native nephrectomy of all kidneys with cystic changes should be excluded. Maximum kidney length (MKL) measured by spiral computed tomography (SCT) serves as a reliable threshold. Mathematically, this parameter is a strong predictor of complications and the need for nephrectomy, offering a straightforward and easily calculable metric via SCT. According to earlier studies, an MKL of 170 mm is considered the optimal threshold for nephrectomy in cases of asymptomatic disease progression [25]. At the same time, in the presence of pain syndrome or signs of kidney and urinary tract infection, PKD size is not a determining factor, and laparoscopic nephrectomy is indicated [25].

CONCLUSION

Laparoscopic techniques can broaden indications and minimize surgical risks in the treatment and pre-transplant preparation of ADPKD patients on the KT waiting list. KT outcomes in ADPKD patients are comparable to those in patients with eCKD from non-ADPKD causes. Patients who had polycystic kidney removed had a more favorable post-transplant period due to a lower incidence of infectious complications. Given the necessity of renoprivation in ADPKD patients, they should be prioritized in the selection of KT recipients.

The authors declare no conflict of interest.

REFERENCES

1. *Grantham JJ.* Clinical practice. Autosomal dominant polycystic kidney disease. *N Engl J Med*. 2008 Oct 2; 359 (14): 1477–1485.
2. *Thomas MN, Datta RR, Wahba R, Buchner D, Chiapponi C, Kurschat C et al.* Introduction of laparoscopic nephrectomy for autosomal dominant polycystic kidney disease as the standard procedure. *Langenbecks Arch Surg*. 2023 Jan 5; 408 (1): 8.
3. *Torres VE, Harris PC, Pirson Y.* Autosomal dominant polycystic kidney disease. *Lancet*. 2007 Apr 14; 369 (9569): 1287–1301.
4. *Furlano M, Loscos I, Martí T, Bullich G, Ayasreh N, Rius A et al.* Autosomal dominant polycystic kidney disease: clinical assessment of rapid progression. *Am J Nephrol*. 2018; 48 (4): 308–317.
5. *Badani KK, Hemal AK, Menon M.* Autosomal dominant polycystic kidney disease and pain – a review of the disease from a etiology, evaluation, past surgical treatment options to current practice. *J Postgrad Med*. 2004 Jul-Sep; 50 (3): 222–226.
6. *Guo P, Xu W, Li H, Ren T, Ni S, Ren M.* Laparoscopic Nephrectomy versus Open Nephrectomy for Patients with Autosomal Dominant Polycystic Kidney Disease: A Systematic Review and Meta-Analysis. *PLoS One*. 2015; 10 (6): e0129317.
7. *Ars E, Bernis C, Fraga G, Martínez V, Martins J, Ortiz A et al*. Spanish guidelines for the management of autosomal dominant polycystic kidney disease. *Nephrol Dial Transplant*. 2014 Sep; 29 Suppl 4: iv95–105.
8. *Pijl JP, Kwee TC, Slart RHJA, Glaudemans AWJM*. FDG-PET/CT for diagnosis of cyst infection in autosomal dominant polycystic kidney disease. *Clin Transl Imaging*. 2018; 6 (1): 61–67.
9. *Kim H, Oh YK, Park HC, Park S, Lee S, Lee HY et al.* Clinical experience with white blood cell-PET/CT in autosomal dominant polycystic kidney disease patients with suspected cyst infection: A prospective case series. *Nephrology (Carlton)*. 2018 Jul; 23 (7): 661–668.
10. *Elashry OM, Nakada SY, Wolf JS Jr, McDougall EM, Clayman RV.* Laparoscopy for adult polycystic kidney disease: a promising alternative. *Am J Kidney Dis*. 1996 Feb; 27 (2): 224–233.
11. *Daineko VS, Ananiev AN, Nevirovich ES, Naser NR, Manukovskiy VA, Reznik ON.* The structure and incidence of infection in the cysts in patients with autosom al dominant polycystic kidney disease on the waiting list of kidney transplantation. *Russian Journal of Transplantology and Artificial Organs*. 2018; 20 (3): 20–25. [In Russ. English abstract]. doi: 10.15825/1995-1191-2018-3-20-25.
12. *Akoh J.* Current management of autosomal dominant polycystic kidney disease. *World J Nephrol*. 2015 Sep; 4 (4): 468–479.
13. *Budhram B, Akbari A, Brown P, Biyani M, Knoll G, Zimmerman D et al.* End-Stage Kidney Disease in Patients With Autosomal Dominant Polycystic Kidney Disease: A 12-Year Study Based on the Canadian Organ Replacement Registry. *Can J Kidney Health Dis*. 2018 Jun 11; 5: 2054358118778568.
14. *Jankowska M, Kuźmiuk-Glembin I, Skonieczny P, Dębska-Ślizień A.* Native Nephrectomy in Renal Transplant Recipients With Autosomal Dominant Polycystic Kidney Disease. *Transplant Proc*. 2018 Jul-Aug; 50 (6): 1863–1867.
15. *Patel P, Horsfield C, Compton F, Taylor J, Koffman G, Olsburgh J.* Native nephrectomy in transplant patients with autosomal dominant polycystic kidney disease. *Ann R Coll Surg Engl*. 2011 Jul; 93 (5): 391–395.
16. *Karam, G, Kälble T, Alcaraz A, Aki FT, Budde K, Humke U et al*. Guidelines on renal transplantation. European Association of Urology, 2014: 23.
17. *Bennett W.* Peritransplant management of retained native kidneys in autosomal dominant polycystic kidney disease. *Nephrol Dial Transplant*. 2013 Feb; 28 (2): 245–246.
18. *Chebib FT, Prieto M, Jung Y, Irazabal MV, Kremers WK, Dean PG et al.* Native Nephrectomy in Renal Transplant

Recipients with Autosomal Dominant Polycystic Kidney Disease. *Transplant Direct*. 2015 Nov 1; 1 (10): e43.
19. *Jean RA, Alexandre M, Yoo PS.* Kidney Transplantation With and Without Native Nephrectomy for Polycystic Kidney Disease: Results of the National Inpatient Sample and the Rationale for a 2-Staged Procedure. *J Am Coll Surg*. 2018 Jun; 226 (6): 1079–1084.
20. *Daineko VS.* Optimizaciya taktiki hirurgicheskogo lecheniya i podgotovki k transplantacii pacientov s terminal'noj pochechnoj nedostatochnost'yu, obuslovlennoj autosomno-dominantnym polikistozom pochek. [Dissertation]. M., 2019; 123.
21. *Neeff HP, Pisarski P, Tittelbach-Helmrich D, Karajanev K, Neumann HP, Hopt UT, Drognitz O*. One hundred consecutive kidney transplantations with simultaneous ipsilateral nephrectomy in patients with autosomal dominant polycystic kidney disease. *Nephrol Dial Transplant*. 2013 Feb; 28 (2): 466–471.
22. *Grodstein EI, Baggett N, Wayne S, Leverson G, D'Alessandro AM, Fernandez LA et al*. An Evaluation of the Safety and Efficacy of Simultaneous Bilateral Nephrectomy and Renal Transplantation for Polycystic Kidney Disease: A 20-Year Experience. *Transplantation*. 2017 Nov; 101 (11): 2774–2779.
23. *Gill IS, Kaouk JH, Hobart MG, Sung GT, Schweizer DK, Braun WE*. Laparoscopic bilateral synchronous nephrectomy for autosomal dominant polycystic kidney disease: the initial experience. *J Urol*. 2001 Apr; 165 (4): 1093–1098.
24. *Daineko VS, Nevirovich ES, Ananiev AN, Uliyankina IV, Reznik ON.* Gasless laparoscopic nephrectomy in patients with autosomal dominant polycystic kidney disease. *Urologicheskie vedomosti*. 2019; 9 (1): 17–22. doi: 10.17816/uroved9117-22.
25. *Daineko VS, Ananiev AN, Nevirovich ES, Skvorcov AE, Budylev SA, Selivanov AN et al*. Results of kidney transplantation in patients with end-stage renal failure caused by autosomal dominant polycystic kidney disease. *Russian Journal of Transplantology and Artificial Organs*. 2019; 21 (2): 39–48. [In Russ. English abstract]. doi: 10.15825/1995-1191-2019-2-39-48.

The article was submitted to the journal on 25.09.2024

DOI: 10.15825/1995-1191-2025-2-31-38

INDOCYANINE GREEN FLUORESCENCE IMAGING OF THE COMMON BILE DUCT BLOOD SUPPLY IN THE PREVENTION OF BILIARY COMPLICATIONS IN LIVER TRANSPLANTATION: RATIONALE AND RESULTS

A.V. Shabunin[1, 2], P.A. Drozdov[1, 2], Z.A. Bagateliya[1, 2], D.A. Makeev[1], S.A. Astapovich[1], E.A. Lidjieva[2]

[1] Botkin Hospital, Moscow, Russian Federation
[2] Russian Medical Academy of Continuous Professional Education, Moscow, Russian Federation

Objective: to enhance liver transplant (LT) outcomes by developing and implementing intraoperative fluorescence imaging of common bile duct (CBD) blood supply using indocyanine green (ICG). **Material and methods.** The study analyzed treatment outcomes in 203 recipients who received a whole liver from deceased donors. In the first stage, the incidence and potential risk factors of biliary complications were assessed in Group I, comprising 138 patients. The median follow-up period was 35.6 months (IQR: 25–68 months). Group II consisted of 65 cases, with a median follow-up of 7.2 months (IQR: 6.5–13). In this group, intraoperative ICG fluorescence imaging was employed to assess CBD blood supply. Following cholecystectomy, a 5 mL intravenous injection of ICG solution (2.5 mg/mL) was administered. Near-infrared fluorescence imaging was then performed by overlaying near-infrared light onto white light to visualize ICG fluorescence in CBD tissues. In cases where fluorescence imaging indicated hypoperfusion of the distal part of the graft's CBD, the affected segment was excised within the boundaries of well-perfused tissue. In all cases, the resected CBD portions were sent for histological examination. **Results.** In Group I, biliary anastomosis complications were recorded in 13 out of 138 cases (9.4%), all of which were strictures. Analysis of potential risk factors on both the recipient and donor sides did not reveal any statistically significant associations ($p > 0.05$). Comparison of intraoperative fluorescence imaging results with postoperative histological examination demonstrated a sensitivity of 87% and a specificity of 92% for detecting ischemic changes in CBD. In groups with comparable baseline characteristics ($p > 0.05$), the incidence of biliary anastomotic strictures (BAS) was significantly lower in the ICG imaging group: 9.4% in Group I versus 1.5% in Group II ($p = 0.04$). **Conclusion.** The use of fluorescence imaging to assess the blood supply of the CBD in LT is an effective method for preventing biliary complications. This technique enables the formation of biliary anastomosis within a well-perfused tissue, significantly reducing the risk of BAS.

Keywords: common bile duct, biliary complications, liver transplantation, fluorescence.

INTRODUCTION

Biliary complications have long been regarded as the "Achilles' heel" of liver transplantation (LT). These include biliary anastomotic failure, anastomotic strictures (AS), and non-anastomotic strictures (NAS) of the bile ducts. NAS typically encompasses ischemic cholangiopathy resulting from inadequate arterial blood supply to the bile ducts, post-transplant cholangiopathy caused by severe ischemia-reperfusion injury to the graft and its biliary system, and recurrent autoimmune diseases affecting the bile ducts in the transplanted liver [1–2]. In most cases, complications arising from the choledochal anastomosis are primarily attributed to technical peculiarities of biliary reconstruction.

Biliary anastomotic failure typically occurs in the early postoperative period with a 5–10% incidence. The primary contributing factors are conditions that predispose the anastomosis to ischemia, including excessive tension, suture line compromise, and over-reliance on electrocoagulation to control bleeding from the donor and recipient bile duct stumps. Hepatic artery thrombosis is a serious complication that can lead to necrosis of the donor bile duct segment.

An anastomotic stricture (AS) is a localized narrowing at the site of a biliary anastomosis, typically solitary and short, often diagnosed within the first year after LT [3–4]. AS occurs in 7–12% of patients and accounts for up to 86% of all post-transplant biliary strictures. Ischemia and subsequent fibrosis of the bile ducts, often resulting from suboptimal surgical technique or early postoperative complications, are considered primary contributors to AS pathogenesis [5]. Key predisposing factors include small bile duct diameter, prolonged biliary ischemia,

Corresponding author: Elza Lidjieva. Address: 10/2, Samarkandskiy Bul'var, apt. 44, Moscow, 109444, Russian Federation. Phone: (963) 648-16-59. E-mail: lidjieva99@mail.ru

donor-recipient duct size mismatch, inappropriate suture material, excessive anastomotic tension, redundant donor duct, and overuse of electrocoagulation. Studies have linked prolonged cold ischemia time, cytomegalovirus (CMV) and Epstein-Barr virus (EBV) infections, and acute and chronic cellular rejection to the development of complications [6].

According to current literature, local ischemia plays a key role in the development of biliary anastomotic complications. Due to the bile duct's blood supply anatomy, the distal segment of the donor common bile duct is particularly vulnerable to inadequate perfusion. Numerous studies in abdominal surgery have demonstrated the efficacy of indocyanine green (ICG) fluorescence imaging in assessing tissue perfusion; however, its application in LT remains limited. In this study, we present preliminary results on the use of ICG fluorescence imaging to evaluate blood supply in the donor segment of the ductus hepaticocholedochus (bile duct), with the aim of preventing biliary anastomosis-related complications.

MATERIALS AND METHODS

This retrospective study analyzed the treatment outcomes of 203 recipients who underwent whole LT from deceased donors at Botkin Hospital between 2018 and 2023. Recipients who died or required retransplantation within 1 year post-transplant were excluded from the analysis. In all cases, duct-to-duct anastomosis was performed using a knotted PDS 6-0 suture.

In the first phase of the study, we analyzed the incidence and potential risk factors associated with the development of anastomotic biliary complications in 138 patients operated on between 2018 and 2022 (Group I, control). The cohort included 82 males (59.4%) and 56 females (40.6%). The median recipient age was 48 years (IQR: 36–58), with a median BMI of 26 kg/m^2 (IQR: 22–27) and a median MELD score of 16 (IQR: 12–18). The median donor age was 48 years (IQR: 40–55), with a median BMI of 25.5 kg/m^2 (IQR: 23.0–29.5). Donors met extended criteria in 34 cases (24.6%), while the remaining donors were classified as standard. Median cold ischemia time was 5.6 hours (IQR: 5.2–7.4), and secondary warm ischemia time was 35 minutes (IQR: 35–45). Surgery lasted for 7.4 hours (IQR: 5.5–8.5), with a biliary ischemia time of 40 minutes (IQR: 45–50). Median intraoperative blood loss was 1,400 mL (IQR: 1,000–4,200). The recipients were followed up for a median duration of 35.6 months (IQR: 25–68). Detailed characteristics of Group I are presented in Table 3.

Group II included 65 recipients who underwent LT between 2022 and 2023 with the use of ICG fluorescence imaging. The group comprised 35 males (53.8%) and 30 females (46.2%). The median recipient age was 47 years (IQR: 35–62), with a median BMI of 25 kg/m^2 (IQR: 21–29) and a MELD score of 18 (IQR: 13–25). Donor characteristics included a median age of 52 years (IQR: 32–64) and a median BMI of 27.2 kg/m^2 (IQR: 23.0–32.0). Donors met extended criteria in 21 cases (32.3%), while the remaining observations were standard. Median cold ischemia time was 5.7 hours (IQR: 4.5–6.5), and the median secondary warm ischemia time was 35 minutes (IQR: 30–45). Median operative time was 6.5 hours (IQR: 5.0–7.5), with a biliary ischemia time of 35 minutes (IQR: 35–45). Intraoperative blood loss was 1,250 mL (IQR: 1,000–3,200). The recipients were followed up for a median duration of 7.2 months (IQR: 3.5–11). Detailed characteristics of Group II are presented in Table 3.

Methodology of ICG fluorescence imaging for assessment of ductus hepaticocholedochus perfusion in liver transplantation

Following cholecystectomy and during the preparation of the graft choledochus for biliary reconstruction, 5 mL of ICG solution was administered intravenously by an anesthesiologist at a concentration of 2.5 mg/mL. Fluorescence imaging was then performed using the Karl Storz visualization system, which superimposes near-infrared light on white light to detect ICG fluorescence in the bile duct tissues (Fig. 1).

In cases where uniform fluorescence of the entire length of the donor ductus hepaticocholedochus was observed (interpreted as a negative result indicating good perfusion, Fig. 1), the excess length of the graft bile duct was excised, and a standard end-to-end anastomosis was created with the recipient's bile duct. A positive result (Fig. 2) was defined as the presence of hypoperfusion in the distal portion of the donor choledochus. In these cases, the bile duct was transected within the boundaries of adequately perfused tissue.

If the residual length of the donor choledochus was insufficient to create a tension-free anastomosis, the recipient's bile duct was mobilized from surrounding tissues – carefully avoiding skeletonization. Perfusion

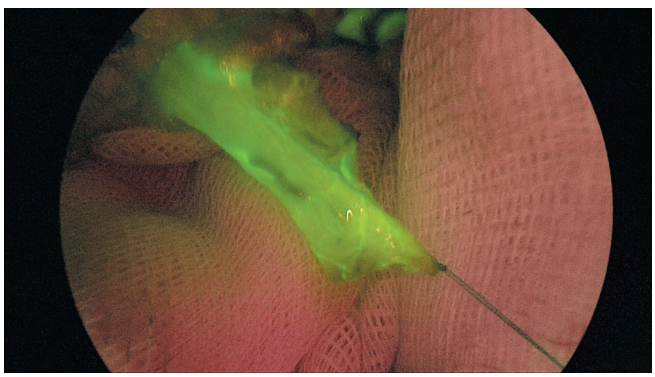

Fig. 1. Intraoperative indocyanine green fluorescence imaging of blood supply of a donor common bile duct (CBD). Satisfactory perfusion of the CBD throughout the whole length

of the recipient's choledochus was also confirmed using ICG fluorescence imaging.

In two cases, additional mobilization of the duodenum was performed using the Kocher maneuver to increase the mobility of the recipient's bile duct and facilitate a tension-free end-to-end anastomosis.

Resected sections of the donor common bile ducts from all cases were submitted for histological examination to assess the severity of ischemic changes in both the proximal and distal segments. To evaluate the diagnostic performance of the fluorescence imaging technique in identifying choledochal ischemia, a comparative analysis was conducted between the intraoperative fluorescence findings and histopathological assessment results.

Statistical analysis

Statistical analysis was performed using SPSS Statistics for Windows, Version 26.0 (IBM Corp., USA). Due to the relatively small sample size, the Mann-Whitney U test was used to compare two groups of quantitative variables, irrespective of distribution. Categorical variables were compared using Pearson's chi-squared test or Fisher's exact test, as appropriate. Differences were considered statistically significant at $p < 0.05$.

RESULTS

Analysis of the frequency and risk factors of anastomotic biliary complications

In the cohort of 138 recipients, biliary anastomotic complications were observed in 13 cases (9.4%), all of which presented as bile duct strictures. The median time from transplantation to the onset of complications was 6.5 months (IQR: 1.0–12.5). Additionally, two cases of non-anastomotic biliary strictures were recorded; one of these was associated with hepatic artery stenosis.

The occurrence of anastomotic biliary strictures (ABS) showed no statistically significant association with early liver graft dysfunction. The incidence among patients with early graft dysfunction was 4 out of 45 (8.9%), compared to 9 out of 93 (9.7%) among recipients with initially satisfactory graft function ($p = 0.415$). Recipient-related variables, including age, sex, BMI, and MELD score, did not demonstrate a statistically significant correlation with ABS ($p > 0.05$). Similarly, donor characteristics and perioperative parameters were not significantly associated with stricture formation ($p > 0.05$). Detailed results are presented in Table 1.

Results of the study on the sensitivity and specificity of ICG fluorescence Imaging for detecting ischemia in the distal donor choledochus

ICG fluorescence imaging was performed intraoperatively during biliary reconstruction in all recipients from the prospective group II ($n = 65$). A positive fluorescence result – indicating hypoperfusion of the distal portion of the donor choledochus – was recorded in 39 cases (60%). In the remaining observations, perfusion was deemed satisfactory along the entire length of the bile duct.

Histological analysis confirmed more pronounced ischemic changes in the distal part of the donor choledochus compared to the proximal part in 36 cases (55.3%). An example of histological preparation comparing the proximal and distal segments of the bile duct graft is presented in Fig. 3.

The sensitivity and specificity of the method for detecting ischemia, as confirmed by histological examination, were 87% and 92%, respectively. The positive predictive value was 88.1%, and the negative predictive value was 98.1% (Table 2).

Clinical outcomes of ICG fluorescence imaging in the assessment of ductus hepaticocholedochus blood supply

Comparison of recipient characteristics between the two study groups revealed no statistically significant

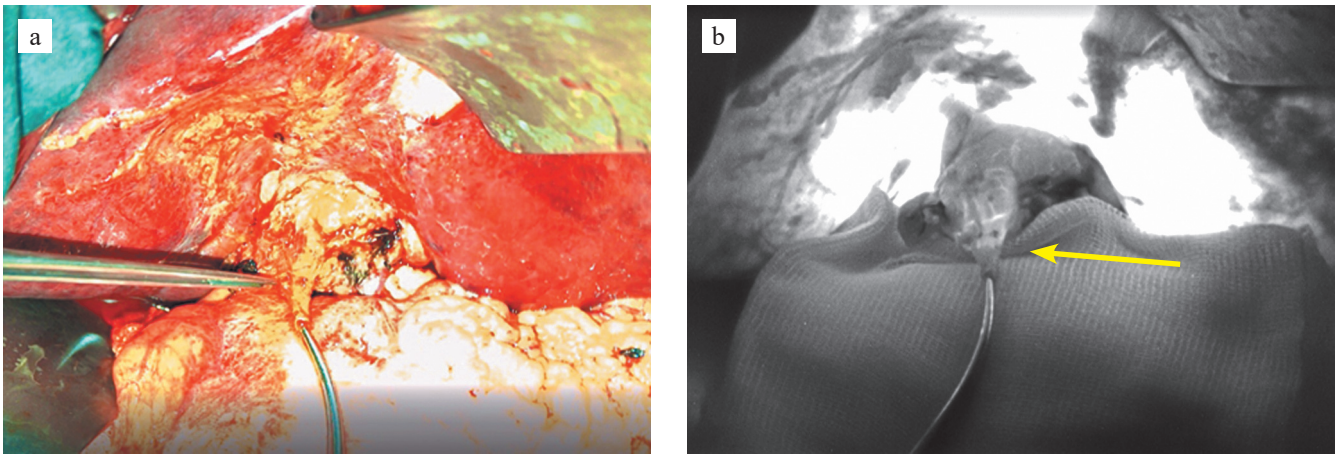

Fig. 2. Intraoperative indocyanine green fluorescence imaging of blood supply of a donor common bile duct (CBD). Poor perfusion of the distal part of the donor CBD (yellow arrow): a, standard mode; b, near infrared light overlay mode

Table 1

Risk factors for biliary anastomotic strictures

Indicator	AS-free, n = 125	AS, n = 13	Significance point (p value)
Recipient risk factors			
Recipient age (years)	43 (IQR: 35–51)	45 (IQR: 32–58)	0.23
Recipient male gender	75 (60%)	7 (53.8%)	0.77
Recipient BMI (kg/m^2)	25 (IQR: 22–27)	25 (IQR: 23–29)	0.52
MELD	16 (IQR: 14–23)	18 (IQR: 15–26)	0.18
Donor risk factors			
Donor age (years)	46 (IQR: 39–56)	44 (IQR: 32–66)	0.4
Donor BMI (kg/m^2)	26 (IQR: 23–29)	27 (IQR: 22–32)	0.48
Macrosteatosis >40%	22 (17.6%)	4 (30.8%)	0.27
Norepinephrine dose >1000 ng/kg/mL or presence of two vasopressors	16 (12.8%)	3 (23.1%)	0.39
Duration of donor's stay in intensive care (hours)	48 (IQR: 41–56)	48 (IQR: 24–72)	0.36
Expanded criteria donor (as defined by Eurotransplant)	27 (21.6%)	4 (30.8%)	0.49
Perioperative risk factors			
Static cold preservation time (hours)	5.5 (IQR: 4.5–6.5)	6.0 (IQR: 4.0–7.0)	0.62
Secondary warm ischemia time (minutes)	40 (IQR: 35–40)	40 (IQR: 35–40)	0.83
Biliary ischemia time (minutes)	40 (IQR: 40–50)	45 (IQR: 40–55)	0.24
Intraoperative blood loss (mL)	1500 (IQR: 800–2500)	1600 (IQR: 1000–2500)	0.6
Cell saver blood reinfusion (mL)	300 (IQR: 250–400)	350 (IQR: 150–550)	0.53
Fresh frozen plasma transfusion (doses)	2 (IQR: 1–3)	2 (IQR: 1–5)	0.1
Erythrocyte suspension transfusion (doses)	1 (IQR: 0–2)	1 (IQR: 0–4)	0.38

Note: AS, anastomotic stricture.

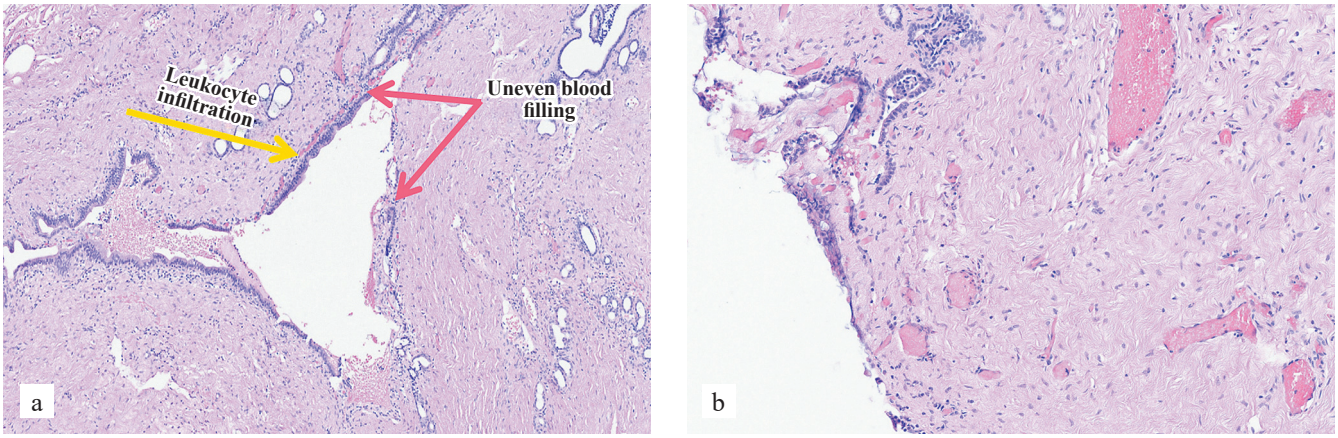

Fig. 3. Morphological examination of the proximal and distal sections of the donor's common bile duct: a, distal section (positive result) – more pronounced inflammation, fibrosis, vascular paresis, irregular blood flow, edema, leukostasis are noted; b, proximal section (negative result): less pronounced inflammation, more pronounced vascular congestion with perivascular hemorrhages

Table 2

Sensitivity and specificity of ICG fluorescence imaging of common bile duct blood supply in relation to ischemia

Histological examination	ICG imaging		Se, %	Sp, %	PPV, %	NPV, %
	Positive	Negative				
Positive	34	2	87	92	88.1	98.1
Negative	5	24				
Total	39	26				

differences in age, sex, BMI, or MELD score ($p = 0.25$, $p = 0.453$, $p = 0.36$, and $p = 0.091$, respectively). Donor characteristics and perioperative parameters were also comparable between the groups ($p > 0.05$). The median follow-up was significantly longer in group I ($p < 0.001$). No significant difference was observed in recipient length of stay in the ICU ($p = 0.921$); however, the total length of stay in the hospital was significantly shorter in group II (fluorescence-guided group) ($p = 0.012$). The incidence

Table 3

Comparative characteristics of the groups and clinical results

Indicator	Group I (Without ICG imaging), n = 138	Group II (ICG imaging), n = 65	Significance point (p-value)
Recipient characteristics			
Recipient age (years)	48 (IQR: 36–58)	47 (IQR: 35–62)	0.25
Recipient male gender	82 (59.4%)	35 (53.8%)	0.453
Recipient BMI (kg/m^2)	26 (IQR: 22–27)	25 (IQR: 21–29)	0.36
MELD	16 (IQR: 12–18)	18 (IQR: 13–25)	0.091
Donor characteristics			
Donor age (years)	48 (IQR: 40–55)	52 (IQR: 32–64)	0.39
Duration of donor's stay in intensive care (hours)	52 (IQR: 36.0–70.0)	58 (IQR: 36.0–72.0)	0.052
Donor BMI (kg/m^2)	25.5 (IQR: 23.0–29.5)	27.2 (IQR: 23–32.0)	0.08
Norepinephrine dose >1000 ng/kg/mL or two vasopressors (%)	19 (13.7%)	11 (16.9%)	0.534
Na (mmol/L)	143 (IQR: 136–146)	145 (IQR: 134–156)	0.823
AST (U/L)	31.0 (IQR: 22.0–45.0)	37.5 (IQR: 28.0–58.0)	0.061
ALT (U/L)	33.0 (IQR: 26.0–51.5)	28.0 (IQR: 25.0–57.5)	0.236
Macrosteatosis >40%	26 (18.8%)	17 (26.2%)	0.234
Expanded criteria donor (n, %)	34 (24.6%)	21 (32.3%)	0.251
Perioperative risk factors			
Static cold preservation time (hours)	5.6 (IQR: 5.2–7.4)	5.7 (IQR: 4.5–6.5)	0.842
Operation time (minutes)	7.4 (IQR: 5.5–8.5)	6.5 (IQR: 5.0–7.5)	0.063
Secondary warm ischemia time (minutes)	35 (IQR: 35–45)	35 (IQR: 30–45)	0.92
Biliary ischemia time (minutes)	40 (IQR: 45–50)	35 (IQR: 35–45)	0.32
Blood loss (mL)	1400 (IQR: 1000–4200)	1250 (IQR: 1000–3200)	0.12
Reinfusion (mL)	350 (IQR: 50–1000)	200 (IQR: 50–700)	0.461
Fresh frozen plasma transfusion (doses)	2 (IQR: 2–6)	3 (IQR: 2–4)	0.61
Erythrocyte suspension transfusion (doses)	1 (IQR: 0–3)	0 (IQR: 0–2)	0.74
Results			
Length of stay in intensive care unit (days)	3 (IQR: 1–4)	3 (IQR: 1–4)	0.921
Length of stay in the hospital (days)	18 (IQR: 15–34)	13 (IQR: 9–25)	0.012
Early allograft dysfunction (n, %)	45 (32.6%)	16 (24.6%)	0.246
Median follow-up of recipients (months)	35.6 (IQR: 25–68)	7.2 (IQR: 6.5–13)	<0.001
Biliary anastomotic stricture (n, %)	13 (9.4%)	1 (1.5%)	0.04

of early graft dysfunction did not differ significantly between the groups – 45 cases (32.6%) in group I versus 16 cases (24.6%) in group II (p = 0.246).

Importantly, no cases of biliary anastomosis failure were recorded in either group (p = 1). The incidence of biliary anastomotic strictures was significantly lower in the fluorescence imaging group – 1 case (1.5%) versus 13 cases (9.4%) in the control group (p = 0.04).

No adverse events were associated with the administration of ICG in any of the patients. Detailed clinical outcomes are summarized in Table 3.

DISCUSSION

LT remains the only definitive and highly effective treatment for end-stage liver disease, offering excellent long-term survival outcomes. However, it is associated with a range of specific complications, particularly involving the biliary anastomosis, which can lead to repeated hospitalizations and increased treatment costs. While advancements in surgery and suture materials have significantly decreased biliary anastomotic failure risk, challenges persist. In our series of 203 liver transplantations, no cases of anastomotic failure were observed. Nonetheless, the incidence of biliary anastomotic strictures (BAS) remained relatively high (9.4%), prompting an in-depth analysis of associated risk factors and the development of strategies for their prevention.

Most authors emphasize that technical challenges during biliary reconstruction are a central cause and risk factor for BAS. These challenges can lead to localized disruption of the bile duct's blood supply and subsequent scar formation at the anastomotic site. In our study, none of the analyzed recipient, donor, or perioperative parameters showed a statistically significant association with the occurrence of this complication (p > 0.05), which indirectly supports the predominant influence of surgical technique. Accordingly, the most effective strategy for preventing anastomotic strictures is the precision cons-

truction of the biliary anastomosis within well-perfused tissue of the ductus hepaticocholedochus. Traditionally, assessment of blood supply to the graft bile duct relies on the surgeon's subjective evaluation of the intensity of bleeding from the duct stump, a method that lacks precision. Fig. 2, a, illustrates an intraoperative view in which visual inspection suggests uniform perfusion of both proximal and distal segments of the choledochus. However, as demonstrated in Fig. 2, b, intraoperative ICG fluorescence imaging reveals a clear hypoperfusion area in the distal segment, which should be excised before forming a biliary anastomosis.

Intraoperative use of ICG fluorescence imaging for assessing tissue perfusion is well-established and used in various abdominal surgerie [7]; however, its application in LT remains limited. To date, we have identified only two published studies specifically addressing the use of this technique for evaluating bile duct perfusion during LT. The first report, by Coubeau Laurent et al. (2017) from a clinical university in Belgium, described a successful case of ICG fluorescence imaging in a liver transplant from a donor after cardiac arrest. Despite the macroscopic appearance suggesting adequate perfusion of the distal bile duct, intraoperative fluorescence imaging revealed hypoperfusion at the distal segment of the donor choledochus. Histological analysis of the resected portion confirmed ischemic injury, including epithelial destruction and separation of epithelial and subepithelial layers. The patient remained free of biliary complications during a 10-month follow-up. The second study, conducted by Panaro et al. (2018) at the University of Montpellier in France, included six clinical cases, although donor type was not specified. In two of these cases, fluorescence imaging prompted the resection of non-perfused segments that were initially deemed viable by visual inspection alone. During a 12-month follow-up, none of the patients developed BAS.

In our larger cohort of 65 recipients, the use of intraoperative fluorescence imaging proved to be an effective method for detecting choledochal ischemia, as confirmed by histological analysis. The technique demonstrated a sensitivity of 87% and a specificity of 92% in identifying ischemic segments. Formation of biliary anastomosis within well-perfused tissue significantly reduced the incidence of anastomotic strictures from 9.3% to 1.5% in groups matched for key clinical characteristics ($p = 0.04$).

Limitations

The main limitations of this study include its retrospective nature and relatively small sample size. It is possible that some contributing factors to biliary complications were not fully accounted for in the analysis. In assition, the median follow-up period in Group II was significantly shorter than that of the control group. However, since the median time to detection of anastomotic stricture identified in the first phase of the study was relatively short, we believe the differences in follow-up duration are not clinically significant.

CONCLUSION

The use of fluorescence imaging to assess bile duct blood supply during LT is a safe and effective method for preventing biliary complications. By ensuring biliary anastomoses occur in well-perfused tissue, this technique significantly reduced anastomotic strictures across key clinical parameters, as demonstrated by statistically significant results in comparable patient groups.

The authors declare no conflict of interest.

REFERENCES

1. *Magro B, Tacelli M, Mazzola A, Conti F, Celsa C.* Biliary complications after liver transplantation: current perspectives and future strategies. *Hepatobiliary Surg Nutr.* 2021 Jan; 10 (1): 76–92. https://doi.org/10.21037%2Fhbsn.2019.09.01.
2. *Boeva I, Karagyozov PI, Tishkov I.* Post-liver transplant biliary complications: Current knowledge and therapeutic advances. *World J Hepatol.* 2021 Jan 27; 13 (1): 66–79. https://doi.org/10.4254/wjh.v13.i1.66.
3. *Karakoyun R, Ericzon BG, Kar I, Nowak G.* Risk Factors for Development of Biliary Stricture After Liver Transplant in Adult Patients: A Single-Center Retrospective Study. *Transplant Proc.* 2021 Dec; 53 (10): 3007–3015. https://doi.org/10.1016/j.transproceed.2021.09.023.
4. *Dumortier J, Chambon-Augoyard C, Guillaud O, Pioche M, Rivory J, Valette PJ et al.* Anastomotic biliobiliary stricture after adult liver transplantation: A retrospective study over 20 years in a single center. *Clin Res Hepatol Gastroenterol.* 2020 Sep; 44 (4): 564–571. https://doi.org/10.1016/j.clinre.2019.08.008.
5. *Jarlot-Gas C, Muscari F, Mokrane FZ, Del Bello A, Culetto A, Buscail E et al.* Management of anastomotic biliary stricture after liver transplantation and impact on survival. *HPB (Oxford).* 2021 Aug; 23 (8): 1259–1268. https://doi.org/10.1016/j.hpb.2020.12.008.
6. *Moy BT, Birk JW.* A Review on the Management of Biliary Complications after Orthotopic Liver Transplantation. *J Clin Transl Hepatol.* 2019 Mar 28; 7 (1): 61–71. https://doi.org/10.14218/JCTH.2018.00028.
7. *Titov KS, Lebedinskiy IN, Kuts IN, Dzhamilov ShR, Sukhotko AS, Lorie ZV et al.* Fluorescent signal lymph node mapping using indocyanine green in early breast cancer patients (Botkin Hospital experience). *Tumors of female reproductive system*. 2024; 20 (1): 52–58. (In Russ.). https://doi.org/10.17650/1994-4098-2024-20-1-52-58.

The article was submitted to the journal on 7.10.2024

DOI: 10.15825/1995-1191-2025-2-39-45

SUCCESSFUL LIVER TRANSPLANTATION IN A CRITICALLY UNDERWEIGHT PATIENT: A CASE REPORT

K.O. Semash[1], T.A. Dzhanbekov[1], R.A. Ibadov[2]

[1] National Children's Medical Center, Tashkent, Republic of Uzbekistan

[2] Republican Specialized Surgical Scientific and Practical Medical Center, Tashkent, Republic of Uzbekistan

Introduction. Living-donor liver transplantation (LT) is a viable and effective treatment option for patients with end-stage liver disease. Cachexia is widely recognized in medical literature as a risk factor affecting patient survival after LT. However, there are relatively few reports on LT in adult patients with critically low body weight. **Materials and methods.** The clinical case of successful LT in a critically underweight patient (BMI 12.9 kg/m^2) is presented. **Results.** The patient's pre-transplant preparation included intensified enteral and parenteral nutrition, albumin and fresh frozen plasma transfusions, diuretic therapy, multivitamins, symptomatic treatment, and structured exercise. At the time of transplantation, the recipient's MELD (Model for End-Stage Liver Disease) score was 22. In the postoperative period, the patient had multiple complications, reflected by a comprehensive complication index (Comprehensive Comprehensive) score of 99. Multicomponent rehabilitation was implemented. The patient was discharged 30 days after LT. During a 17-month follow-up, graft function remained satisfactory. **Conclusion.** Our experience, supported by literature data, indicates that cachexia in liver transplant recipients is associated with a higher overall complication rate after LT. Patients with low body weight require careful pre-transplant preparation, including intensive nutritional support and exercise programs. Successful treatment of such patients is feasible only in a multidisciplinary hospital or a transplant center with extensive expertise in managing complex cases.

Keywords: liver transplantation, related liver transplantation, underweight, cachexia, complications, rehabilitation.

INTRODUCTION

Living-donor liver transplantation (LT) is an effective treatment method for end-stage liver disease. Patients with liver cirrhosis are known to often develop metabolic complications [1]. Studies suggest that body mass index (BMI) can impact survival rates after LT [2–6]. At the same time, the majority of works on this topic are devoted to obese patients, and only a small part – to underweight and/or cachexic patients [7–9]. A low BMI (less than 18.5 kg/m^2) is generally associated with poorer surgical outcomes, and emaciated patients should be carefully prepared for upcoming surgical intervention [10]. LT is characterized by prolonged operative duration, significant surgical and anesthetic risks, and extensive surgical trauma, all of which significantly impact the course of the postoperative period in patients [11]. Below we present a clinical case of a successful LT in a critically underweight patient (with a body mass index of 12.9 kg/m^2): the peculiarities of the patient's pre-transplant preparation, as well as the peculiarities of the postoperative course and treatment of complications in this patient.

CLINICAL CASE

Patient H., 55 years old (Case No. 6729/2022), presented to our center on September 15, 2022, with complaints of jaundice, abdominal distension, lower extremity edema, severe weakness, and a 30-kg weight loss over the past year. He was unable to move independently or care for himself.

On initial examination, his height was 189 cm and weight 51 kg, corresponding to a BMI of 14.3 kg/m^2 (see Fig. 1). Diagnostic evaluation – including ultrasound, whole-body CT with intravenous contrast, and serologic testing – revealed decompensated liver cirrhosis, classified as Child–Pugh Class C with a MELD-Na score of 25. The cirrhosis was attributed to chronic hepatitis B and D coinfection in the active replication phase (HBV 8×10^8 copies/mL, HDV 3×10^7 copies/mL, confirmed by PCR). No signs of malignancy were detected.

The patient underwent a comprehensive work-up in accordance with the center's standard protocol [12, 13], which confirmed portal hypertension syndrome and associated complications, including ascites, splenomegaly, grade 2 esophageal varices, and thrombocytopenia (platelets 37×10^9/L).

Corresponding author: Konstantin Semash. Address: 10, Kichik Khalka Yuli str., Tashkent, 100096, Uzbekistan. Phone: +998 (94) 090-89-05. Email: mail@doctorsemash.com

Initial treatment involved antiviral therapy with tenofovir 25 mg daily for HBV. A stable virologic response was achieved after 35 days of therapy.

The patient was admitted to our center to prepare for LT. At the time of admission, the MELD-Na score was 26. In addition to ongoing antiviral therapy, pre-transplant management included transfusions of albumin and fresh frozen plasma (FFP), diuretics, ursodeoxycholic acid, gastroprotective therapy (esomeprazole and a combination of algeldrate with magnesium hydroxide), and vitamin supplementation.

Nutritional support consisted of a high-protein, high-carbohydrate diet, along with parenteral nutrition comprising amino acids, fats, carbohydrates, and electrolytes (total volume: 1920 mL/day), providing an estimated caloric intake of approximately 3,500 kcal/day. The patient also received supervised rehabilitation therapy, including therapeutic physical exercises.

As a result of comprehensive treatment, ascites resolved completely and lower limb edema subsided. However, due to fluid loss, the patient's weight decreased to 46 kg after one month (BMI 12.9 kg/m^2). Despite the weight loss, the patient reported increased energy, regained independent mobility, and was able to participate in physical therapy. At the time of transplantation, the MELD-Na score had improved to 22.

In parallel, following the standard protocol at our ward [12], the patient's 35-year-old son was evaluated as a living related donor of the right liver lobe. No absolute contraindications to liver donation were identified.

On November 23, 2022, the patient underwent a right lobe LT from his son. The graft weighed 900 grams, resulting in a graft-to-recipient weight ratio (GRWR) of 2.0%. Surgical technique details have been described in previous publications [13, 14].

Intraoperatively, hepatectomy was technically uneventful; however, blood loss occurred during inferior vena cava mobilization, necessitating intraoperative autologous blood reinfusion. Cold ischemia time was 93 minutes. The right lobe graft included an additional substantial inferior right hepatic vein (11 mm in diameter), requiring a second caval anastomosis. Warm ischemia time was 31 minutes.

Induction immunosuppression consisted of methylprednisolone 500 mg and basiliximab 20 mg. Arterial anastomosis was performed using interrupted sutures. The splenic artery was ligated to modulate portal blood flow and prevent steal syndrome [14, 15].

Biliary reconstruction presented technical challenges due to the patient's anthropometric features. Although the graft had a single bile duct, its deep location in the right subdiaphragmatic space precluded biliary-biliary anastomosis. Additionally, the short jejunal mesentery created tension during construction of the biliodigestive anastomosis. Nonetheless, stent placement and bile duct drainage were successfully completed.

The total operation time was 570 minutes, with an estimated blood loss of 1300 mL. Intraoperative Doppler sonography confirmed satisfactory vascular anastomoses with no abnormalities detected.

Fig. 1. Patient's appearance: a, on first examination: BMI was 14.3 kg/m^2; b, on day 17 after liver transplantation: BMI was 12.9 kg/m^2; c, 10 months after transplantation: BMI was 21.8 kg/m^2

The recipient was initially managed in the intensive care unit (ICU), where extubation was performed uneventfully 12 hours after surgery. The standard immunosuppressive regimen included low-dose methylprednisolone and tacrolimus. On postoperative day 3, the patient developed febrile fever (up to 39 °C). In response, the antibacterial therapy was adjusted, and immunosuppressive treatment was temporarily discontinued. Ultrasound on postoperative day 4 revealed fluid accumulation in the right subdiaphragmatic region; diagnostic puncture confirmed the presence of bile, indicating a biloma.

Despite percutaneous drainage, adequate cavity sanitation could not be achieved. The patient continued to experience febrile episodes, and inflammatory markers rose sharply (C-reactive protein: 152 mg/L; procalcitonin: 20 ng/mL). This clinical deterioration necessitated relaparotomy with abdominal cavity sanitation and redrainage on postoperative day 6.

Following surgery, the patient demonstrated clinical improvement, marked by a decline in inflammatory markers. He was transferred from the ICU to the surgical ward on postoperative day 9 (day 3 after relaparotomy).

On postoperative day 10, in the evening, the patient vomited the food he had eaten and and subsequently aspirated during sleep, leading to a sharp drop in oxygen saturation to 30%. No circulatory arrest occurred. The patient was urgently transferred to the ICU, where he was intubated and placed on mechanical ventilation.

Emergency fibrobronchoscopy revealed and cleared a substantial amount of aspirated food material (porridge) from both lungs. Due to the severity of the aspiration event, the patient required prolonged ventilatory support. Daily sanitation fibrobronchoscopies were performed twice daily.

He received comprehensive care, including broad-spectrum antibacterial and antiviral therapy, gastroprotective agents, albumin and FFP transfusions, inhalation therapy, and symptomatic treatment. In light of ongoing aspiration pneumonia, persistent subfebrile and febrile episodes, and elevated inflammatory markers, immunosuppressive therapy was withheld. Despite the complications, liver graft function remained stable throughout, as shown in Fig. 2.

The patient also developed recurrent bilateral pleurisy, necessitating repeated thoracenteses and eventual pleural drainage. Given his severe malnutrition and cachexia, a naso-intestinal feeding tube was placed endoscopically. Nutritional support included both enteral feeding and parenteral nutrition with amino acid, fat, carbohydrate, and electrolyte solutions.

Importantly, the patient was not sedated during the extended period of ventilation. He was maintained in a sitting position and engaged in twice-daily physical therapy sessions under the supervision of a physiotherapist.

Against the background of comprehensive therapy, the patient showed positive clinical progress. The septic condition resolved, and extubation was successfully per-

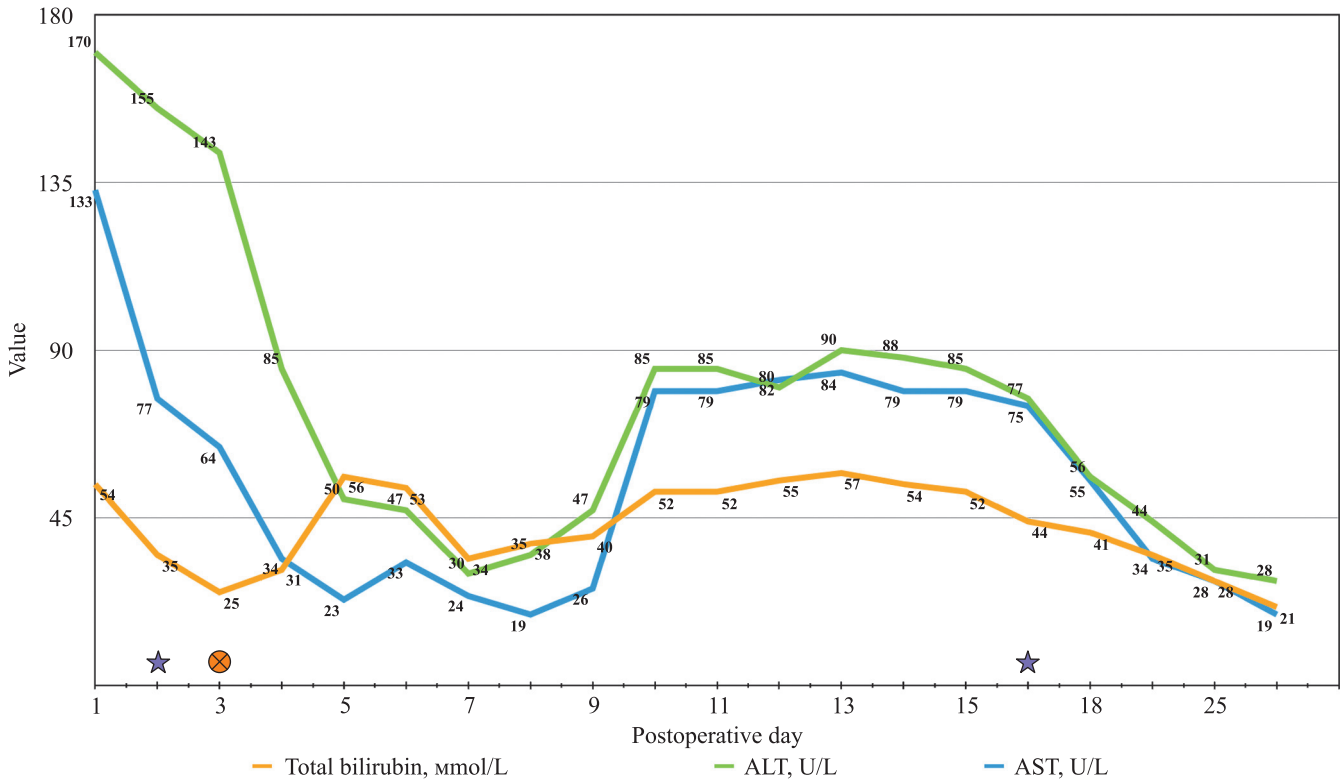

Fig. 2. Laboratory dynamics of liver graft function. Asterisk indicates days when tacrolimus was administered. Cross indicates the days when immunosuppressive therapy was completely discontinued

Table

Complications in the patient

Complication	Clavien–Dindo grade
Need for parenteral nutrition	2
Biloma (puncture)	3a
Right-sided pleurisy, puncture	3a
Left-sided pleurisy, puncture	3a
Right-sided pleurisy, drainage (×2)	3a
Left-sided pleurisy, drainage	3a
Malnutrition, insertion of nasointestinal tube	3a
Aspiration pneumonia, need for daily bronchoscopies (×11)	3a
Peritonitis (relaparotomy)	3b
Aspiration	4a
Sepsis	4a
Calculation of Comprehensive Complication Index (CCI) score	99

formed on postoperative day 17 (day 7 after aspiration). The patient was subsequently transferred to the surgical ward for continued care.

Immunosuppression was maintained with tacrolimus monotherapy, targeting serum levels of 6–9 ng/mL. In addition to ongoing medical management, the patient received daily massage therapy and continued rehabilitation with physiotherapists. Liver graft function fully normalized.

The enteral feeding tube was removed on postoperative day 24, coinciding with the discontinuation of parenteral nutrition. The patient was successfully transitioned to full oral nutrition.

Spontaneous resolution of bile leakage occurred by postoperative day 26, and the safety drain from the bile leak site, placed earlier, had already been removed on postoperative day 2. A summary of the patient's complications is presented in Table.

The patient was discharged in satisfactory condition on postoperative day 30, with stable graft function. He continues to be followed on an outpatient basis and remains alive 17 months post-transplant, with consistently stable liver graft function. His weight increased to 78 kg, corresponding to a BMI of 21.8 kg/m^2 (Fig. 1).

DISCUSSION

Sarcopenia is a well-documented complication of cirrhosis [1, 3]. Nevertheless, according to literature review, there are significantly more overweight patients (BMI >30 kg/m^2) who are LT candidates than critically underweight patients [2]. In addition, most studies have focused on managing obese liver recipients [4–6]. For example, according to an analysis of the UNOS database over a 22-year period, among 73,538 adult liver transplant recipients, less than 1% of patients had a BMI of less than 18.5 kg/m^2 [7]. Meanwhile, the impact of cachexia on the survival of LT recipients has been extensively studied. Underweight status in LT recipients has been identified as an independent risk factor that significantly impairs post-transplant survival. Analyses conducted across different decades consistently show that low BMI is a significant predictor of reduced survival. Specifically, the three-year survival rate for patients with a BMI below 18.5 kg/m^2 was 68%.

Also, according to other studies, an interesting correlation was obtained when low BMI in recipients was adjusted for MELD [8, 9]. Patients with low body weight and a MELD score of either <20 or >26 had increased mortality rates. However, the authors failed to show any significant relationships between other patient factors (e.g., comorbidities), donor factors (graft quality) and post-transplant mortality in patients with low BMI and MELD score.

Notably, liver recipients with critically low body weight face a markedly increased risk of infectious complications. Compared to individuals with normal or slightly elevated BMI, those with a BMI under 16 kg/m^2 had a tenfold higher risk of developing severe infections, including pneumonia, abscesses, intra-abdominal infections, and sepsis [4]. Interestingly, despite this heightened vulnerability to systemic infections, cachectic patients were found to have a lower incidence of wound infections than their normal or overweight counterparts.

Our clinical case reinforces the above findings. A critically underweight patient with decompensated cirrhosis (Child–Pugh class C) required specific preparation for LT. In addition to antiviral therapy and management of cirrhosis-related complications, particular emphasis was placed on comprehensive nutritional support [10, 16]. Malnutrition in patients with cirrhosis is a known factor associated with poorer survival outcomes – not only compared to individuals with normal weight but also to those with obesity. A large cohort study investigated whether optimizing nutritional status prior to LT could improve outcomes. The authors demonstrated that each unit increase in BMI resulted in a 2% decrease in mortality rate [16]. However, this study did not account for the patient's dry weight in the calculations. In our case, des-

pite comprehensive therapy for cirrhosis complications and adequate nutritional support through enteral and parenteral methods, the patient's body weight decreased due to removal of excess fluid, ultimately achieving the patient's dry weight. Nevertheless, this reduction was accompanied by an improvement in the patient's overall condition, allowing for independent movement, partial self-care, and engagement in physical exercises.

Postoperative complications were assessed using the Clavien–Dindo classification. However, this system does not account for the cumulative burden of multiple complications in a single patient. Therefore, we also utilized the Comprehensive Complication Index (CCI), which offers a more nuanced evaluation by integrating all postoperative complications into a single score. In this case, the patient's CCI was 99 – approaching the maximum score of 100, which corresponds to patient death – indicating the extreme severity of the postoperative course [17].

Regarding the postoperative complications observed in our recipient, we believe cachexia was a significant contributing factor. The development of bile leakage was primarily influenced by the patient's anthropometric characteristics, which created technical challenges in the formation of the biliodigestive anastomosis. Biliary stenting subsequently necessitated percutaneous drainage of the resulting biloma and ultimately led to relaparotomy. Aspiration pneumonia, followed by sepsis, further complicated the clinical course.

Cachexia is known to be an independent risk factor for aspiration and aspiration-related complications [18]. In this case, daily tracheobronchial drainage and comprehensive antibacterial therapy facilitated resolution of the pneumonia and a return to spontaneous breathing.

Despite intensified nutritional support and albumin supplementation, ongoing protein-energy malnutrition, combined with multiple infectious complications, resulted in the development of bilateral pleural effusions, which required thoracentesis and subsequent pleural drainage.

A key component of successful rehabilitation in such patients, in addition to nutritional support, is early and sustained physical activation [10]. Notably, the patient was not sedated even during prolonged mechanical ventilation and engaged in passive and active physical exercises in lying and sitting positions. Physical therapists and massage specialists were actively involved in the rehabilitation process. It was only through this comprehensive, multidisciplinary approach that we were able to save the patient and discharge him in satisfactory condition.

CONCLUSION

Our experience, supported by literature data, indicates that cachexia in liver transplant recipients is associated with a higher overall complication rate after LT. Patients with low body weight require careful pre-transplant preparation, including intensive nutritional support and exercise programs. Successful treatment of such patients is feasible only in a multidisciplinary hospital or a transplant center with extensive expertise in managing complex cases.

The authors declare no conflict of interest.

REFERENCES

1. *Salimov UR, Stoma IO, Fedoruk DA, Kovalev AA, Scherba AE, Rummo OO*. Sarcopenia in chronic liver disease, can we predict complications? *Transplantologiya. The Russian Journal of Transplantation*. 2022; 14 (4): 408–420. https://doi.org/10.23873/2074-0506-2022-14-4-408-420.
2. *Pelletier SJ, Schaubel DE, Wei G, Englesbe MJ, Punch JD, Wolfe RA et al*. Effect of body mass index on the survival benefit of liver transplantation. *Liver Transpl*. 2007; 13 (12): 1678–1683. https://doi.org/10.1002/lt.21183.
3. *Salimov U, Kovalev A, Stoma I, Fedoruk A, Rummo O*. Evaluation of Factors Affecting Long-Term Survival after Liver Transplantation. *Surgery. Eastern Europe*. 2023; 12 (3): 238–247. https://doi.org/10.34883/PI.2023.12.3.016.
4. *Diaz-Nieto R, Lykoudis PM, Davidson BR.* Recipient body mass index and infectious complications following liver transplantation. *HPB (Oxford)*. 2019 Aug; 21 (8): 1032–1038. https://doi.org/10.1016/j.hpb.2019.01.002.
5. *Van Son J, Stam SP, Gomes-Neto AW, Osté MCJ, Blokzijl H, van den Berg AP et al.* Post-transplant obesity impacts long-term survival after liver transplantation. *Metabolism*. 2020 May; 106: 154204. https://doi.org/10.1016/j.metabol.2020.154204.
6. *García-Fernández N, Cepeda-Franco C, Beltrán-Miranda P, García-Muñoz P, Álamo-Martínez JM, Padillo-Ruiz FJ, Gómez-Bravo MÁ*. Body Mass Index as a Prognostic Factor in Liver Transplantation. *Transplant Proc*. 2020 Jun; 52 (5): 1493–1495. https://doi.org/10.1016/j.transproceed.2020.03.008.
7. *Dick AA, Spitzer AL, Seifert CF, Deckert A, Carithers RL Jr, Reyes JD, Perkins JD*. Liver transplantation at the extremes of the body mass index. *Liver Transpl*. 2009 Aug; 15 (8): 968–977. https://doi.org/10.1002/lt.21785.
8. *Bambha KM, Dodge JL, Gralla J, Sprague D, Biggins SW.* Low, rather than high, body mass index confers increased risk for post-liver transplant death and graft loss: Risk modulated by model for end-stage liver disease. *Liver Transpl*. 2015 Oct; 21 (10): 1286–1294. https://doi.org/10.1002/lt.24188.
9. *Bari K, Sharma P.* Impact of body mass index on post-transplant outcomes reexamined. *Liver Transpl*. 2015 Oct; 21 (10): 1238–1240. https://doi.org/10.1002/lt.24227.
10. *Joliat GR, Kobayashi K, Hasegawa K, Thomson JE, Padbury R, Scott M et al.* Guidelines for Perioperative Care for Liver Surgery: Enhanced Recovery After Surgery (ERAS) Society Recommendations 2022. *World J*

Surg. 2023 Jan; 47 (1): 11–34. https://doi.org/10.1007/s00268-022-06732-5.

11. *Lee DD, Li J, Wang G, Croome KP, Burns JM, Perry DK, Nguyen JH et al.* Looking inward: The impact of operative time on graft survival after liver transplantation. *Surgery*. 2017 Oct; 162 (4): 937–949. https://doi.org/10.1016/j.surg.2017.05.010.
12. *Semash K, Janbekov T, Akbarov M, Usmonov A, Gaibullaev T*. Stages of preparation and examination of related liver donors and their perioperative management. *Coloproc*. 2023; 15 (1): 41–54. https://doi.org/10.56121/2181-4260-2023-1-41-54.
13. *Semash K, Dzhanbekov T, Akbarov M, Mirolimov M, Usmonov A, Razzokov N et al.* Implementation of Living Donor Liver Transplantation Program in the Republic of Uzbekistan – Report of First 40 cases. *Clin Transplant Res*. 2024 Jun 30; 38 (2): 116–127. https://doi.org/10.4285/ctr.24.0013.
14. *Semash KO, Dzhanbekov TA, Gaybullaev TZ*. Single center experience of intraoperative ligation of the splenic artery for prevention of splenic artery steal syndrome in patients after living donor liver transplant. *Transplantologiya. The Russian Journal of Transplantation.* 2024; 16 (2): 230–243. https://doi.org/10.23873/2074-0506-2024-16-2-230-243.
15. *Semash KO, Dzhanbekov TA, Akbarov MM*. Vascular complications after liver transplantation: contemporary approaches to detection and treatment. A literature review. *Russian Journal of Transplantology and Artificial Organs*. 2023; 25 (4): 46–72. (In Russ.). http://doi.org/10.15825/1995-1191-2023-4-46-72.
16. *Orci LA, Majno PE, Berney T, Morel P, Mentha G, Toso C*. The impact of wait list body mass index changes on the outcome after liver transplantation. *Transpl Int*. 2013 Feb; 26 (2): 170–176. https://doi.org/10.1111/tri.12017.
17. *Lai Q, Melandro F, Nowak G, Nicolini D, Iesari S, Fasolo E et al.* The role of the comprehensive complication index for the prediction of survival after liver transplantation. *Updates Surg*. 2021 Feb; 73 (1): 209–221. https://doi.org/10.1007/s13304-020-00878-4.
18. *Niederman MS, Cilloniz C*. Aspiration pneumonia. *Rev Esp Quimioter*. 2022 Apr; 35 Suppl 1 (Suppl 1): 73–77. https://doi.org/10.37201/req/s01.17.2022.

The article was submitted to the journal on 25.06.2024

DOI: 10.15825/1995-1191-2025-2-46-53

KIDNEY TRANSPLANT PROGRAM IN IRKUTSK REGION

A.V. Novozhilov[1, 2], S.E. Grigoriev[1, 2], O.Yu. Yakovleva[1], S.A. Yezhikeev[1]

[1] Irkutsk Regional Clinical Hospital, Irkutsk, Russian Federation
[2] Irkutsk State Medical University, Irkutsk, Russian Federation

Introduction. Kidney transplantation (KT) is often considered the best option for renal replacement therapy (RRT), significantly improving patient outcomes. Post-transplant, life expectancy doubles, and mortality decreases more than 4-fold compared to other RRT modalities. This article presents KT outcomes in Irkutsk Region from 2018 to 2023. All procedures were performed at a single center – the Irkutsk Regional Clinical Hospital. **Objective:** to analyze the immediate and long-term outcomes of KT in Irkutsk Region. **Material and methods.** A retrospective analysis was conducted on the treatment outcomes of 125 patients with kidney failure (KF). Among them, 74 were men with a median age of 42 (35–49) years, and 51 were women with a median age of 46 (37–55) years. The median transplant waitlist time was 15.5 (range: 6–32) months. The leading cause of KF was chronic glomerulonephritis, observed in 60 patients (48%). There were no HLA matches in 36 patients (28.8%), while 38 patients (30.4%) had one match. Arterial anastomosis was primarily performed end-to-end with the external iliac artery in 121 cases (96.8%), while in 3 cases (2.4%), the internal iliac artery was used due to external iliac artery spasm. Cold ischemia time was 222 minutes (range: 162–360), and warm ischemia time was 39 minutes (range: 30–46). **Results.** Length of hospital stay was 16 (range: 13–25) bed days. Primary renal function was achieved in 95 patients (77%), while 25 patients (20%) experienced delayed graft function. Blood tacrolimus reached target levels by postoperative days 9–12. Creatinine level at discharge was 120 μmol/L (range: 97–165). Surgical complications occurred in 24 patients (19.2%), while urinary tract infections were observed in 36 patients (28.8%), with 17 cases (13.6%) presenting clinical symptoms. Immunosuppressive therapy was initiated in 124 patients (99.2%) using a standard triple-drug regimen (calcineurin inhibitors, mycophenolates, and glucocorticoids). One patient (0.8%) succumbed to complications from COVID-19. One-year graft survival was 94.1%. **Conclusion.** The immediate outcomes align with national averages. There is a consistent upward trend in the number of kidney transplants performed. Further development of the regional transplant program will enhance access to this high-tech medical service, meeting the needs of the local population.

Keywords: chronic kidney disease, kidney transplantation, donor resource, kidney transplant complications, Irkutsk Oblast.

INTRODUCTION

Transplantation of human organs and tissues is a rapidly advancing, high-tech, and resource-intensive clinical field aimed at saving lives and restoring health in patients at the end stages of certain diseases [1, 2]. Kidney transplantation (KT) is considered the most favorable form of renal replacement therapy (RRT). In contrast, chronic hemodialysis (or peritoneal dialysis) should be regarded as a temporary bridge to transplantation, as KT has been shown to double life expectancy and reduce mortality by more than four times compared to other RRT modalities. Moreover, transplantation enables optimal social rehabilitation, evidenced by a significant improvement in quality of life and a marked increase in the recipient's ability to work within a relatively short period after surgery [3–6].

The average annual cost of post-transplant medical care per patient is about four times lower than that of chronic hemodialysis. However, the primary hurdle to expanding KT for end-stage chronic kidney disease (CKD) is the shortage and inefficient use of available donor organs [7, 8].

Irkutsk Oblast is the second-largest region in Siberian Federal District by area but has a low population density (3.03 people per square kilometer). As of 2024, the total population is 2,330,537, with approximately 1.804 million residing in large cities. The Irkutsk agglomeration, defined by a 2–3-hour transport radius, includes around 1.082 million people [9].

In 2024, 1,024 patients in the region received maintenance hemodialysis. Each year, about 50 individuals are placed on the waiting list for deceased-donor KT, while the estimated annual need is about 60 transplant procedures.

The KT program in Irkutsk Oblast began in 2003 at Irkutsk Regional Clinical Hospital (IOCH), with the region's first living-related transplant. In 2008, the region developed and implemented protocols for brain death certification. However, over the following decade, kidney transplant procedures remained sporadic and limited

Corresponding author: Sergey Grigoriev. Address: 1, Krasnogo Vosstaniya, Irkutsk, 664003, Russian Federation. Phone: (902) 176-71-06. E-mail: grigorievse@gmail.com

in number, highlighting the urgent need to reorganize the regional donation and transplantation system.

To address this, a collaboration agreement was signed in 2018 between Shumakov National Medical Research Center of Transplantology and Artificial Organs, the region's Ministry of Health, and IOCH. As part of this initiative, a roadmap for the development of organ donation and transplantation in Irkutsk Oblast was established. This included updates to regulatory and legal frameworks, creation of an independent structural unit within IOCB – the Organ Donation Coordination Department – and implementation of specialized personnel training.

These measures significantly increased the number of effective donors and the total number of transplant procedures, particularly kidney transplants.

Over the past 20 years, over 263 transplantations, including procedures for patients with diabetic nephropathy, have been performed. Additionally, one simultaneous liver–kidney transplantation was carried out (Fig. 1).

Since 2019, the number of transplantations has increased, primarily due to improved organization of the regional organ donation coordination service (Fig. 2). However, the number of procedures remains below target levels, reaching only 16.9 per 1 million population in 2023.

The **objective** of this study is to analyze both the immediate and long-term outcomes of KT in Irkutsk Oblast.

MATERIALS AND METHODS

A retrospective analysis was conducted using medical records of patients who received inpatient care at IRCH between 2018 and 2023. A total of 125 recipients – 74 men and 51 women – with end-stage CKD underwent KT during this period.

Statistical data processing

Statistical analysis was performed using the software package Statistica for Windows, version 10.0. Numerical data are presented as medians (Me) with interquartile ranges (25%–75%).

The overall median age of recipients was 44 years (35–51); 46 years (37–55) for women, and 42 years (35–49) for men (Table 1). The median time on the KT waiting list was 15.5 months (6–32).

The underlying causes of CKD were as follows: glomerulonephritis in 60 patients (48%), tubulointerstitial nephritis in 4 (3.2%), hypertension in 7 (5.6%), congenital anomalies of the kidney and urinary tract in 12 (9.6%), diabetes mellitus in 10 (8%), polycystic kidney disease in 5 (4%), other causes in 16 (12.8%), and unspecified etiology in 11 patients (8.8%).

Table 1

Patient distribution by age

Age (years)	Number	%
20–29	18	14.4
30–39	33	26.4
40–49	42	33.6
50–59	26	20.8
60–69	6	4.8

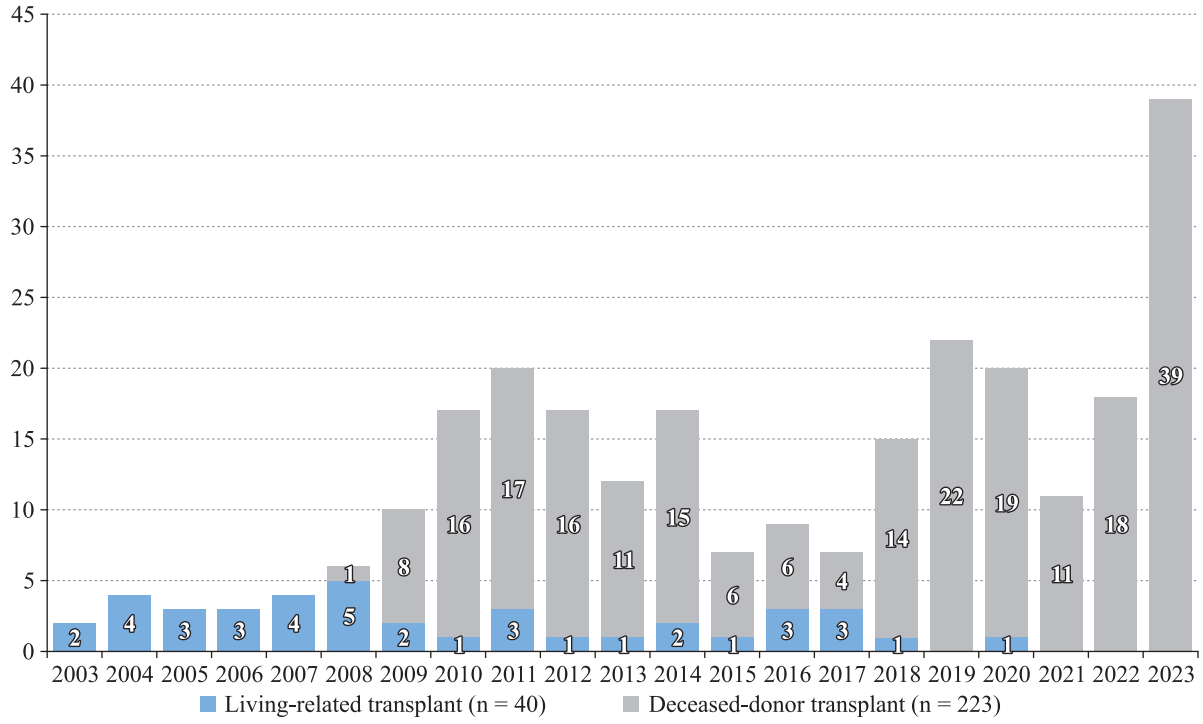

Fig. 1. Trends in the total number of kidney transplants (2003–2023)

Comorbid conditions included anemia in 80 patients (64%), hypoparathyroidism in 14 (11.2%), hyperparathyroidism in 13 (10.4%), type 2 diabetes mellitus in 2 (1.6%), hepatitis C in 3 (2.4%), and epilepsy in 1 patient (0.8%). Nine patients (7.2%) were on peritoneal dialysis at the time of transplantation.

A total of 114 kidneys were transplanted from 57 deceased donors, with each donor contributing two kidneys. In 7 cases, only one kidney was retrieved. Three transplants were performed using organs from living related donors. The median age of deceased donors was 50 years (interquartile range: 41–59), with the youngest donor aged 22 and the oldest aged 71. Data on HLA (human leukocyte antigen) matching are presented in Table 2.

Cold ischemia time was 222 minutes (IQR: 162–360), which can be attributed to the fact that, in most cases, organ retrieval was performed at IRCH in an operating room adjacent to the transplant suite. Warm ischemia time was 39 minutes (30–46). Intraoperative blood loss was minimal – 100 ml (20–100).

The graft was most frequently implanted in the right iliac fossa. Arterial anastomosis was performed predominantly end-to-side with the external iliac artery (EIA) in 121 cases (96.8%). In three cases (2.4%), anastomosis was performed with the internal iliac artery due to EIA spasm. One case (0.8%) involved anastomosis with the common iliac artery following two previous failed transplant attempts in the iliac fossa, necessitating kidney implantation into the abdominal cavity.

A single arterial anastomosis was performed in 122 patients (97.6%), while two were required in 3 cases (2.4%). Venous anastomosis was performed once in

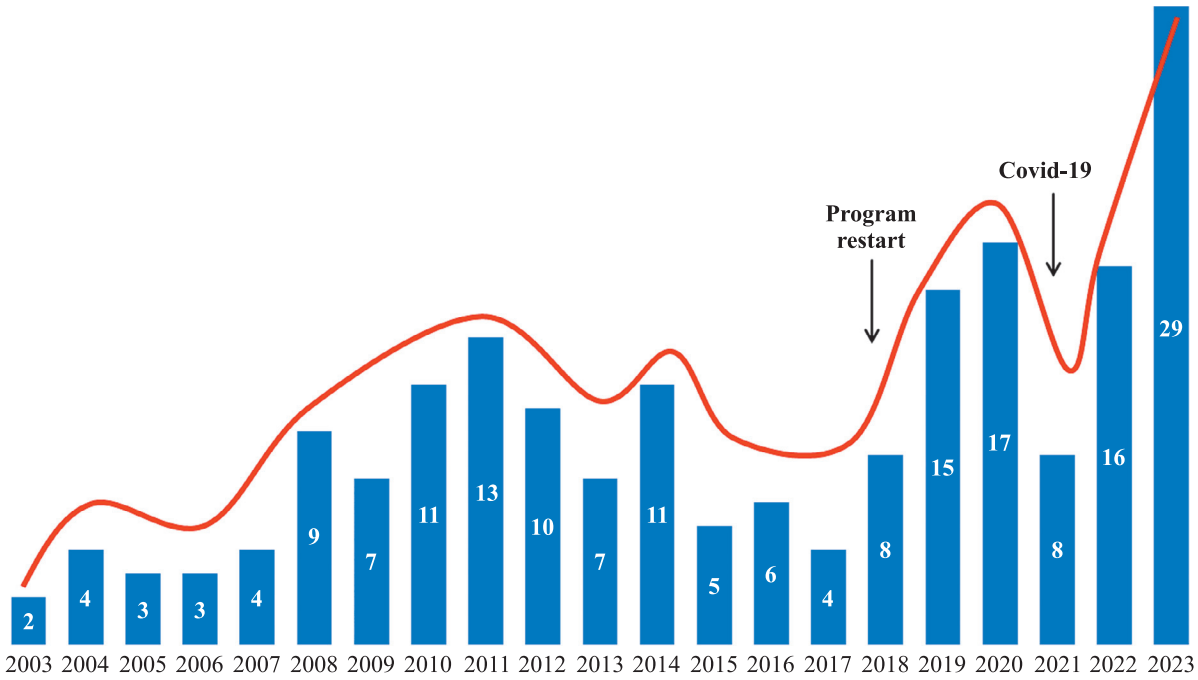

Fig. 2. Trends in the total number of effective donors (2003–2023)

Table 2

Number of HLA matches

HLA match	Number
0	36 (28.8%)
1	38 (30.4%)
2	24 (19.2%)
≥3	27 (21.6%)

Table 3

Postoperative hemodialysis

Number of sessions	Number of patients
1	4
2–3	14
>3	19

124 patients (99.2%) and twice in 1 case (0.8%). To minimize the number of anastomoses, standard angiosurgical techniques such as single-site suturing and side-to-side angioplasty were used.

RESULTS

Hospitalization lasted for 16 days (IQR: 13–25), including 3 days (IQR: 1–4) spent in the intensive care unit (ICU). Surgical drainages were typically removed on day 5 (IQR: 4–8), and urethral catheter on day 7 (IQR: 6–8).

Primary renal function was observed in 83 patients (66.4%). In 37 cases (29.6%), RRT was initially required, followed by recovery of graft function (Table 3) [there was a mistake]. Graft removal was necessary in 4 patients (3%) during the early postoperative period. One

patient (0.8%) experienced primary non-function of the graft, which did not necessitate nephrectomy.

Target blood tacrolimus levels were achieved between postoperative days 9 and 12 (Fig. 3).

Serum creatinine levels decreased significantly by day 10, reaching 120 μmol/L (IQR: 97–165) at the time of discharge (Fig. 4).

The dynamics of serum urea reduction during the postoperative period are illustrated in Fig. 5.

Surgical complications occurred in 24 patients (19.2%). In 4 cases (3.2%), graft removal was required due to the following causes: renal vein thrombosis (1 patient, 0.8%), postoperative infection (1 patient, 0.8%), non-functional arterial anastomosis (initial pathology of the vessel wall, graft removal during the first operation) (1 patient, 0.8%), and graft rupture due to superacute rejection (1 patient, 0.8%).

Repeat surgery was performed in 8 patients (6.4%) due to bleeding in 5 cases (4%), vesicoureteral anastomosis failure in 2 cases (1.6%), and paranephric hematoma in 1 case (0.8%).

Complications requiring minimally invasive intervention occurred in 8 patients (6.4%). X-ray endovascular stenting for arterial anastomosis stenosis was performed in 4 (3.2%) observations, ultrasound-guided lymphocele drainage in 3 cases (2.4%), and nephrostomy due to ureteral anastomosis stricture in 1 case (0.8%).

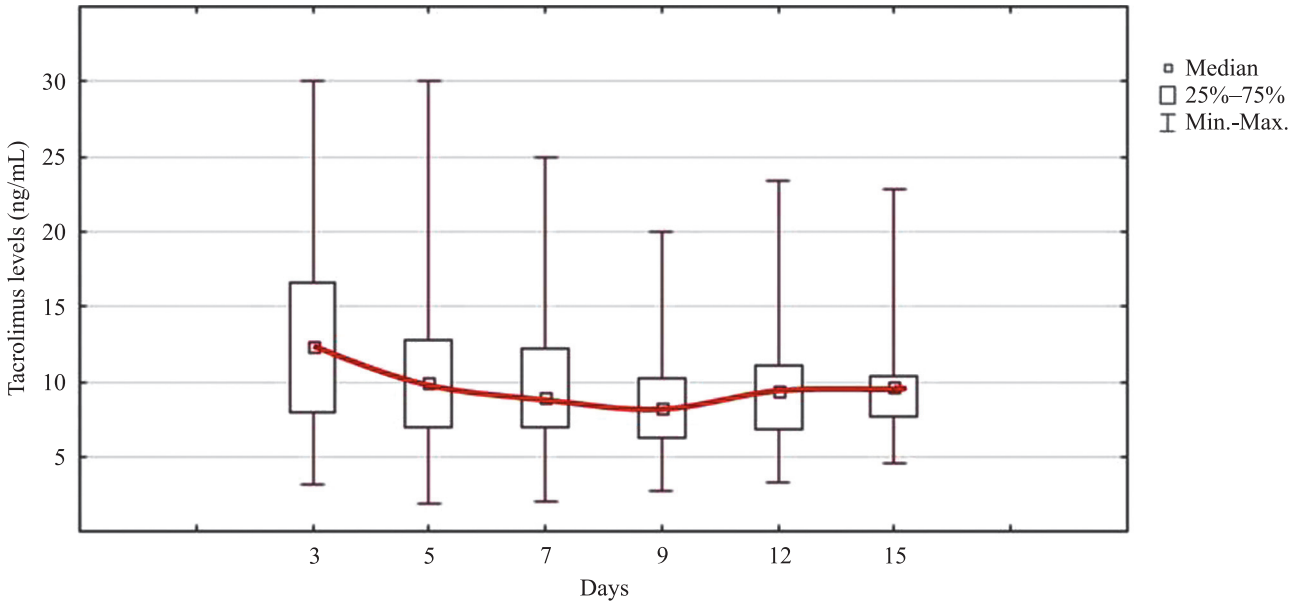

Fig. 3. Tacrolimus blood levels

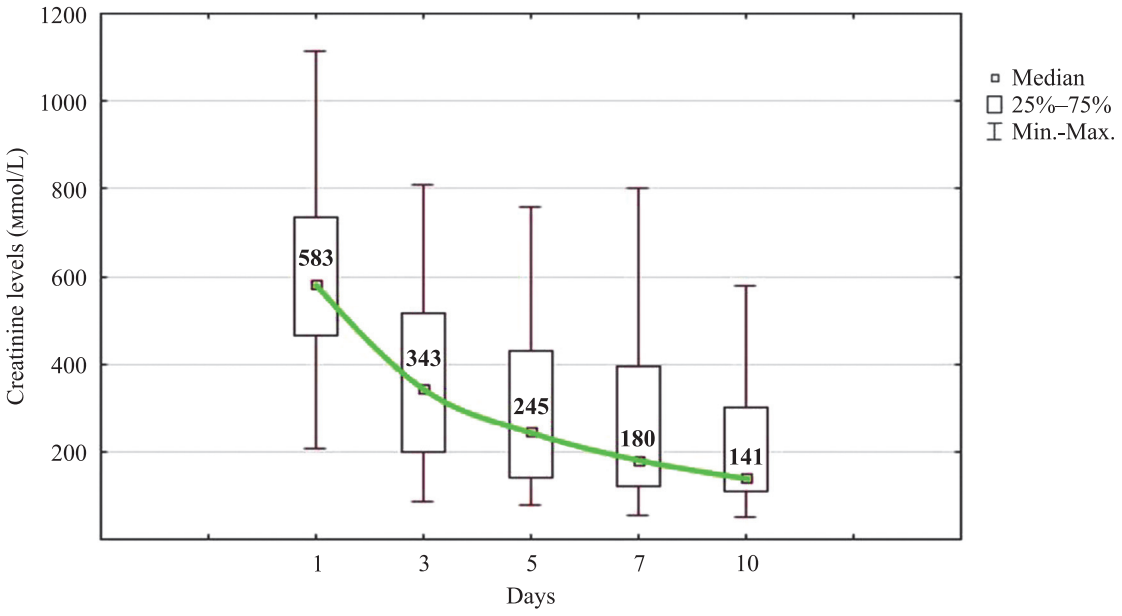

Fig. 4. Creatinine levels

Ischemia of the graft pole, confirmed by Doppler ultrasound and angiography, was identified in 2 patients (1.6%) (Fig. 6). However, no surgical or interventional correction was necessary in these cases.

One patient (0.8%) died as a result of COVID-19. Urinary tract infections were diagnosed in 36 patients (28.8%), of which 17 (13.6%) presented with clinical symptoms and 19 (15.2%) were asymptomatic. The primary causative agents are illustrated in Fig. 7.

Immunosuppressive therapy was initiated using a standard triple-drug regimen – calcineurin inhibitors, mycophenolates, and glucocorticoids – in 124 patients (99.2%). One patient (0.8%) received azathioprine instead of tacrolimus due to drug intolerance.

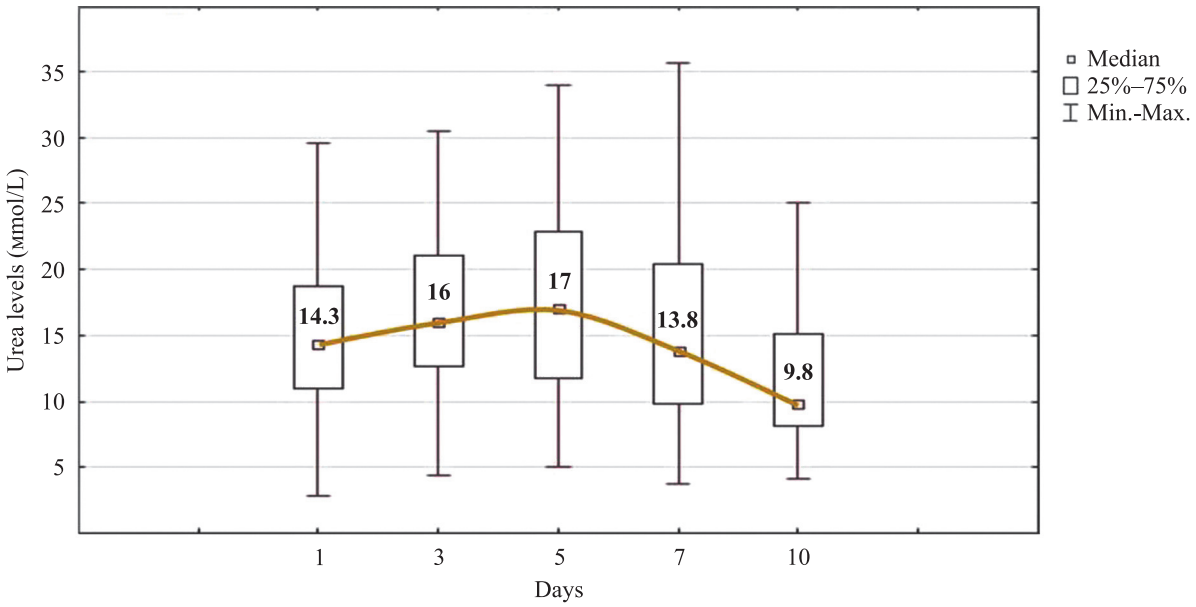

Fig. 5. Blood urea levels

Fig. 6. Selective angiogram of the graft showing the ischemic zone

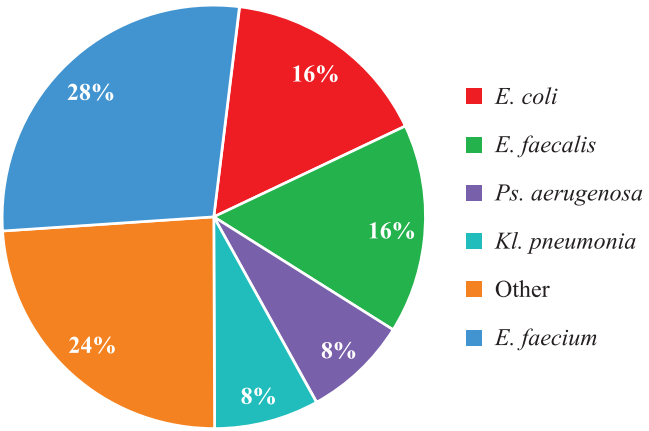

Fig. 7. Urinary tract infection pathogens

Acute humoral rejection occurred in 4 patients (3.2%), necessitating graft removal in 2 of these cases (1.6%). Acute cellular rejection, managed successfully with conservative treatment, was observed in 3 patients (2.4%).

The one-year graft survival rate was 94.1%.

DISCUSSION

KT outcomes depend on many factors, one of the most critical being organ preservation time. In our series,

the median cold ischemia time was about 220 minutes. This relatively short duration was achieved due to the organizational structure of the transplantation process: the majority of donor organ retrievals and subsequent transplantations were performed within a single institution – IRCH. This logistical advantage significantly minimized anoxic time and contributed to improved immediate postoperative outcomes.

Primary graft function was observed in 66.4% of recipients, while delayed graft function was seen in others and typically resolved after 2–3 sessions of hemodialysis.

Most postoperative complications were addressed promptly. Graft removal was necessary in 6 cases (4.8%), including 2 due to vascular complications (1.6%), 3 due to immune-mediated rejection (2.4%), and 1 due to postoperative infection (0.8%). One graft was removed intraoperatively during the initial transplant procedure and was therefore excluded from the graft survival analysis.

Interestingly, in two cases, ischemia affecting a segment of the graft – confirmed via imaging – did not lead to functional impairment and did not require any corrective intervention.

In most urinary infection cases, asymptomatic bacteriuria was detected and managed with targeted antibacterial therapy. These findings underscore the critical importance of rigorous infection surveillance, particularly in the early postoperative period.

One patient (0.8%) died; however, this was unrelated to the surgical procedure; it was attributed to COVID-19.

The timely prevention and management of both early and late post-transplant complications play a decisive role in graft function and long-term survival. Therefore, continuous monitoring of the recipient's clinical status and graft function is essential – not only during the inpatient period but also throughout the outpatient follow-up.

CONCLUSION

Thus, the current need for KT in Irkutsk Oblast is only partially met, primarily due to inefficient use of available donor pool and the absence of a well-structured system for forming and managing the waiting list.

The immediate KT outcomes in the region align with national averages. There is a steady upward trend in transplant numbers. Continued development of the regional transplant program will will enable the healthcare system to better meet the growing demand for this high-tech medical service in the region.

The authors declare no conflict of interest.

REFERENCES

1. *Gautier SV.* Clinical transplantology in the Russian Federation: from innovative phenomenology to accessible medical care. *Russian Journal of Transplantology and Artificial Organs*. 2022; 24 (4): 5–6. [In Russ, English abstract].
2. *Karakulina EV, Khomyakov SM, Aleksandrova OA, Lysikov IV, Shedenko SV, Gautier SV.* Ways of improving the legal regulation of human organ and tissue transplantation in the Russian Federation. *Russian Journal of Transplantology and Artificial Organs*. 2022; 24 (2): 108–118. [In Russ, English abstract]. doi: 10.15825/1995-1191-2022-2-108-118.
3. *Lakman IA, Khalikova AA, Korzhenevskiy AA.* The evaluation of effect of various outcomes of kidney transplantation surgery on economic costs under treatment of kidneys chronic disease. *Zdravookhranenie Rossiiskoi Federatsii (Health Care of the Russian Federation Russian journal*). 2018; 62 (2): 60–67. [In Russ, English abstract]. doi: 10.18821/0044-197X-2018-62-2-60-67.
4. *Smirnova VV, Shmarina NV, Dmitriev IV, Balkarov AG, Zagorodnikova NV, Vinogradov VE, Minina MG.* Early and long-term outcomes of deceased-donor kidney transplant in recipients 70 years of age and older. *Russian Journal of Transplantology and Artificial Organs*. 2024; 26 (3): 111–116. [In Russ, English abstract]. doi: 10.15825/1995-1191-2024-3-111-116.
5. *Khubutiya MSh, Pinchuk AV, Shmarina NV, Dmitriev IV, Vinogradov VE, Kazantsev AI, Balkarov AG.* Patient and kidney graft survival rates after first and second kidney transplantation. *Transplantologiya (The Russian Journal of Transplantation)*. 2021; 13 (2): 130–140. [In Russ, English abstract]. doi: 10.23873/2074-0506-2021-13-2-130-140.
6. *Aleksandrova VO, Dmitriev IV, Borovkova NV, Balkarov AG, Mushta NA, Shmarina NV et al.* Diagnostic value of anti-HLA antibody monitoring in the diagnosis of immunological complications following kidney transplantation. *Russian Journal of Transplantology and Artificial Organs.* 2024; 26 (3): 91–98. [In Russ, English abstract]. doi: 10.15825/1995-1191-2024-3-91-98.
7. *Pirov BS, Odinaev OM, Izatshoev AA, Samadov AH, Nazarov PH.* Results of kidneys transplantation in the regional department of human organs and tissues transplantation. *Vestnik poslediplomnogo obrazovaniya v sfere zdravoohraneniya* (*Bulletin of Postgraduate Education in Healthcare)*. 2018; 4: 86–91. [In Russ, English abstract].
8. *Minina MG, Sevostyanov VM, Tenchurina EA.* 30 donors per million population in Moscow. Impact on the effectiveness of transplant care. *Russian Journal of Transplantology and Artificial Organs* [In Russ]. 2024; 26 (S): 5. doi: 10.15825/1995-1191-2024-S-5.
9. Information on the population number and demographic characteristics of the Irkutsk region [Internet]. The official portal of the Irkutsk region [website]. Cited 2025 Jan 19. Available from: https://irkobl.ru/region/demografy.

The article was submitted to the journal on 31.01.2025

DOI: 10.15825/1995-1191-2025-2-54-59

ASSESSMENT OF LIVER GRAFT HYPOXIA VIA ^{18}F-FMISO PET-CT IMAGING

I.I. Tileubergenov, A.A. Ivanova, A.L. Dolbov, O.A. Gerasimova, A.R. Sheraliev, V.N. Zhuykov, D.A. Granov

Russian Research Center of Radiology and Surgical Technologies, St. Petersburg, Russian Federation

Objective: drawing on existing literature and the clinical use of radiopharmaceutical (RFP) ^{18}F-FMISO in oncology, this pilot study aims to assess the feasibility of using non-invasive PET-CT imaging to detect hypoxia in liver grafts resulting from ischemia-reperfusion injury. **Materials and methods.** ^{18}F-FMISO uptake in tumors, as visualized by PET-CT, enables the generation of quantitative maps of tissue hypoxia, a technique that is increasingly being explored to guide radiation therapy planning. As part of refining the study methodology, the research team successfully obtained the first PET-CT images demonstrating ^{18}F-FMISO uptake in the liver of a patient at a late postoperative stage following liver transplantation. **Results.** A positive indication of transplant hypoxia was defined as an increase in both the mean and maximum standardized uptake values (SUVs) when measured at 180 minutes post-intravenous injection of the radiopharmaceutical, compared to measurements at 90 minutes. Two imaging series – CT and PET – were acquired. Diffuse uptake of the radiopharmaceutical was observed in the liver, with greater tracer retention relative to background at 180 minutes compared to 90 minutes post-injection. **Conclusion.** The findings suggest the presence of transplant hypoxia despite the absence of biochemical abnormalities. This technique shows promise as a non-invasive diagnostic tool for detecting hypoxic changes in liver grafts. However, further optimization and validation of the technique are necessary.

Keywords: ^{18}F-FMISO, radiopharmaceutical, liver transplant, PET-CT, ischemia-reperfusion injury.

INTRODUCTION

Ischemia-reperfusion injury (IRI) after liver transplantation (LT) is a significant complication, contributing to the development of biliary complications and graft fibrosis. IRI is mediated by multiple mechanisms, including activation of toll-like receptor (TLR) signaling pathways, changes in microRNA expression, production of reactive oxygen species (ROS), modulation of autophagy, and activation of hypoxia-inducible factors. These processes involve a variety of cell types such as sinusoidal endothelial cells, hepatocytes, Kupffer cells, neutrophils, and platelets. Recognized risk factors for IRI in LT include donor liver steatosis, prolonged ischemic time, advanced donor age, and coagulopathies in both the donor and recipient [1].

Liver ischemia-reperfusion injury (IRI) is initiated by hemodynamic alterations and begins during the early stages of organ retrieval and preservation. During warm and cold ischemia, hypoxia-induced metabolic dysfunction develops, leading to damage of hepatocytes, cholangiocytes, and sinusoidal endothelial cells [2]. Restoration of blood flow (reperfusion) exacerbates this injury through transient portal hypertension and hyperdynamic stress. Transient portal hypertension serves as the primary event triggering endothelial damage. Following reperfusion, portal vein pressure can rise sharply from 30–35 cm H_2O to 60–70 cm H_2O [3]. The abrupt surge in blood volume causes direct injury to sinusoidal endothelial cells and exposes the vessel walls to circulating platelets and leukocytes. Platelet aggregation subsequently narrows the venules, and the activated platelets release large amounts of cytokines, chemokines, and vasoactive molecules [4, 5].

The imbalance between vasoconstrictive and vasodilatory factors further aggravates microcirculatory disorders. Levels of the vasoconstrictor peptide endothelin-1 were found to increase 1.6-fold, whereas endothelial nitric oxide synthase, which produces nitric oxide, was found to decrease by 17.4 μmol/L [3]. Disruption of microcirculation exacerbates hyperdynamic stress, which may lead to sinusoidal occlusion and collapse of the space of Disse between endothelial cells and hepatocytes, thereby prolonging tissue hypoxia. Reperfusion injury becomes more devastating due to the massive production of reactive oxygen species, primarily generated by intrahepatic neutrophils and Kupffer cells. In neointimal grafts, mitochondrial dysfunction is more pronounced and multifactorial in nature. Oxidative stress reaches its peak approximately 2–6 hours after reperfusion. As a result of extensive cellular damage, molecular structures are released into the circulation, further activating the innate immune response [6].

Corresponding author: Olga Gerasimova. Address: 70, Leningradskaya str., St. Petersburg, 197758, Russian Federation. Phone: (812) 439-66-40. E-mail: ren321@mail.ru

Unfortunately, IRI remains an inevitable consequence of LT and continues to pose a significant challenge due to the associated risks of early graft dysfunction and graft loss. Although the molecular mechanisms underlying IRI are gradually being elucidated, effective preventive and therapeutic strategies are still lacking. Early injury to the graft is driven by disruptions in microcirculatory regulation, impaired redox homeostasis, and mitochondrial dysfunction, which collectively initiate the immune cascade. Both innate and adaptive immune responses contribute to the progression of graft injury through adhesion and recruitment of macrophages, neutrophils, and dendritic cells, as well as activation of lymphoid cells, natural killer cells, and cytotoxic T lymphocytes.

Recent studies have identified several new biomarkers that may better predict early graft injury following LT. One such biomarker is lactate. Elevated lactate levels in the liver and systemic circulation are observed during IRI as a result of increased glycolysis following impaired microcirculation and prolonged hypoxia. Given that hepatocytes are responsible for metabolizing more than 70% of circulating lactate, an increase in blood or graft lactate levels, or a decrease in lactate clearance, likely reflects graft dysfunction. An arterial blood lactate level greater than 5 mmol/L has been proposed as an IRI biomarker, with a positive predictive value of 35.5% [7]. The reported sensitivity and specificity were 0.39 and 0.83, respectively. However, because lactate levels are highly dynamic and lactate can be produced by any tissue experiencing hypoperfusion, relying solely on arterial lactate as a biomarker may be insufficient for accurately predicting early IRI.

In the later postoperative period, persistent graft ischemia may be maintained by inadequate perfusion and redistribution of hepatic blood flow. Prolonged ischemia can contribute to the formation of non-anastomotic biliary strictures and the development of secondary biliary cirrhosis.

An angiographic study combined with fluorometry is currently required to diagnose hypoperfusion of the liver transplant, as noninvasive diagnostic methods such as ultrasound and multislice computed tomography may not reliably detect perfusion disorders [8]. However, angiographic studies are invasive, performed in hospital settings, and carry a risk of complications. The search for noninvasive diagnostic alternatives has led researchers to explore the use of positron emission tomography-computed tomography (PET-CT) in outpatient settings with the injection of the isotope ^{18}F-fluoromisonidazole (^{18}F-FMISO). Given the isotope's mechanism of marking hypoxic areas, it is hypothesized that ^{18}F-FMISO PET-CT may be applicable for assessing both early ischemia-reperfusion complications and ineffective arterial blood supply in the later stages after LT. To date, such studies have not been conducted in the Russian Federation. A prospective study is planned to evaluate patients with liver transplant perfusion disorders at different postoperative periods.

^{18}F-FMISO marks hypoxia in solid tumor tissues, and considerable experience has been accumulated regarding its application in oncology. The radiopharmaceutical contains a nitroimidazole molecule labeled with fluorine-18 [9, 10]. After administration, the nitroimidazole enters cells via the bloodstream and can undergo oxidation-reduction reactions mediated by xanthine oxidase. In normoxic (oxygenated) cells, the reduced nitro group can be reoxidized to its original form by molecular oxygen (O_2), enabling the radiopharmaceutical to exit the cells. In contrast, in hypoxic cells, the reduced nitro group cannot be reoxidized due to the lack of oxygen, resulting in stable binding of the radiopharmaceutical to the cells.

The accumulation of ^{18}F-FMISO in tissues is inversely proportional to the local oxygen levels. The distribution of hypoxic tissue can then be quantitatively visualized using PET [11, 12]. In oncology, ^{18}F-FMISO uptake provides a quantitative hypoxia map that can guide strategies such as radiation dose escalation. Several methods have been developed for quantifying and delineating hypoxic tumor volumes, including the tumor-to-blood ratio (TBR), tumor-to-normal ratio (TNR), and compartmental modeling approaches [13].

Large-scale clinical trials using ^{18}F-FMISO have not yet been conducted; however, evidence from small, early imaging studies suggests that FMISO-based hypoxia assessment may predict survival outcomes and certain locoregional parameters in patients with head and neck cancer and other malignancies. The use of hypoxia imaging to guide radiotherapy remains an area of active investigation [14].

Despite its ability to detect hypoxic regions in tumor tissues, the specificity and sensitivity of ^{18}F-FMISO imaging remain subjects of ongoing debate [15]. In addition to oncological applications, there is growing scientific interest in using FMISO for cardiac hypoxia imaging. However, experience in this field is limited, partly due to the minimal contrast between target and background, as well as delayed imaging times required because of the radiotracer's slow blood clearance [16].

We present a clinical case demonstrating the diagnostic potential of PET-CT with ^{18}F-FMISO for detecting ischemic injury in a liver transplant. This experience was obtained for the first time during the refinement of liver imaging techniques using this method.

CLINICAL CASE

Patient O., born in 1962, underwent LT on May 6, 2022, at the Russian Research Center of Radiology and

Surgical Technologies in St. Petersburg. The indication for LT was a combination of primary biliary cholangitis and primary sclerosing cholangitis, resulting in decompensated biliary cirrhosis (MELD-Na score of 20).

In the early postoperative period, on postoperative day 13, hemodynamically significant stenosis of the inferior vena cava (IVC) was identified, requiring endovascular stenting. Despite this intervention, angiography revealed persistent signs of hepatic artery stenosis. On postoperative day 20, splenic artery embolization was performed to optimize hepatic arterial blood flow. Post-embolization, the patient developed fever and systemic inflammatory response due to splenic infarcts, necessitating intensive infusion and antibacterial therapy.

The patient was discharged on postoperative day 38 with a functioning liver graft for outpatient follow-up. During the long-term postoperative period, complications arose, including the development of common bile duct (CBD) stricture, requiring multiple hospitalizations for interventional procedures such as drainage, balloon plasty, and CBD stenting.

A control angiogram detected no IVC stenosis. However, the patient continued to experience recurrent episodes of cholangitis, requiring periodic courses of antibacterial therapy. Immunosuppressive therapy consisted of a two-drug regimen: prolonged-release tacrolimus and mycophenolic acid.

At the time of PET-CT with ^{18}F-FMISO (27 months after LT), laboratory parameters reflecting liver function remained within normal ranges. No special preparation was required prior to the study. The radiopharmaceutical ^{18}F-FMISO was administered intravenously at a dose of 3.7 MBq per kilogram of body weight.

Imaging was performed using a Siemens mCT40 PET/CT scanner (Siemens, Germany). Two sequential scans were conducted: 90 and 180 min after administration of the radiopharmaceutical. The first scan covered the region from the top of the head to the thighs (whole-body protocol), while the second scan focused solely on the abdominal region. Each scan included a topogram, a non-contrast-enhanced CT performed during free breathing, and PET acquisition. The first scan required approximately 20 minutes, while the second scan took about 10 minutes.

Image processing was performed using an AW Volume Share 7 workstation (GE Healthcare, USA).

Each series of images was reconstructed in three anatomical planes: axial, coronal, and sagittal, as well as in a three-dimensional (3D) format. In addition, PET and CT image series were fused (Figs. 1–3).

^{18}F-FMISO uptake in the liver was assessed in both studies using visual analysis and a semi-quantitative method based on the standardized uptake value (SUV). For each PET series, the maximum and mean SUV values across the entire liver volume were measured.

An increase in mean and maximum SUV at 180 minutes compared to 90 minutes was interpreted as a positive result, indicating the presence of graft hypoxia. Each imaging session generated two series: CT and PET.

Since such a study had not been previously performed, interpretation of the results posed a significant challenge. Nevertheless, given the patient's clinical history, there was sufficient reason to suspect ongoing hypoxia in the graft despite satisfactory liver function tests.

As shown in the presented images (Figs. 1–3), there was a noticeable increase in the uptake of the radiophar-

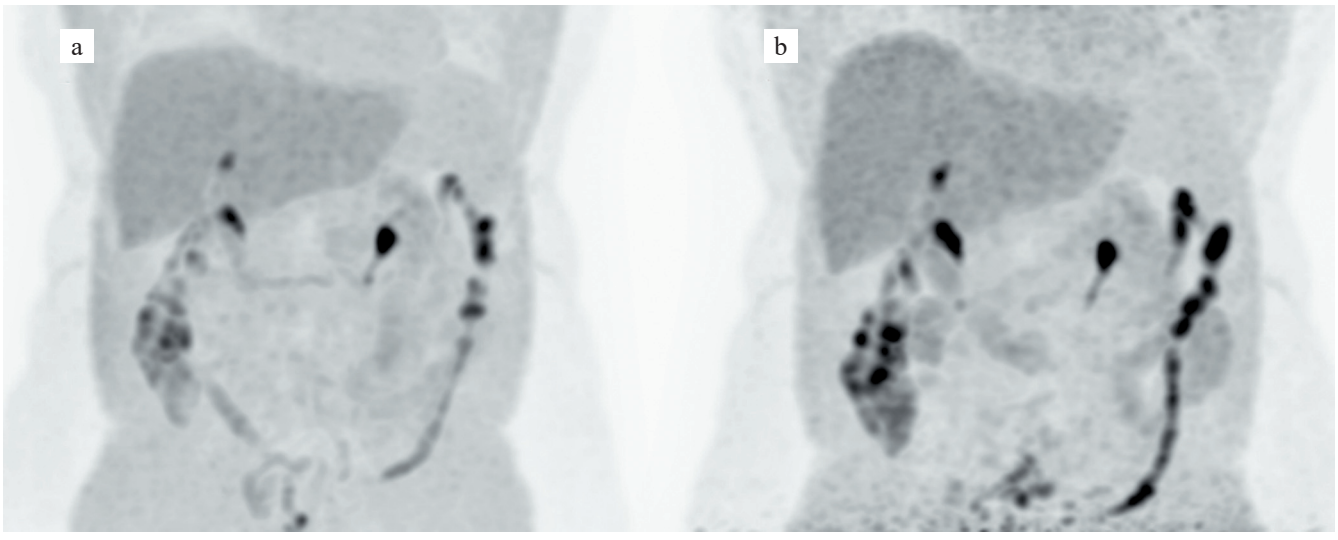

Fig. 1. 3D PET images (maximum intensity projection) with ^{18}F-FMISO: (a) at 90 minutes post-injection; (b) at 180 minutes post-injection. Diffuse tracer uptake is evident in the liver, with higher tracer retention relative to background at 180 minutes compared to 90 minutes. Physiological uptake of ^{18}F-FMISO is also noted in the renal pelvis and calyces, along the colon

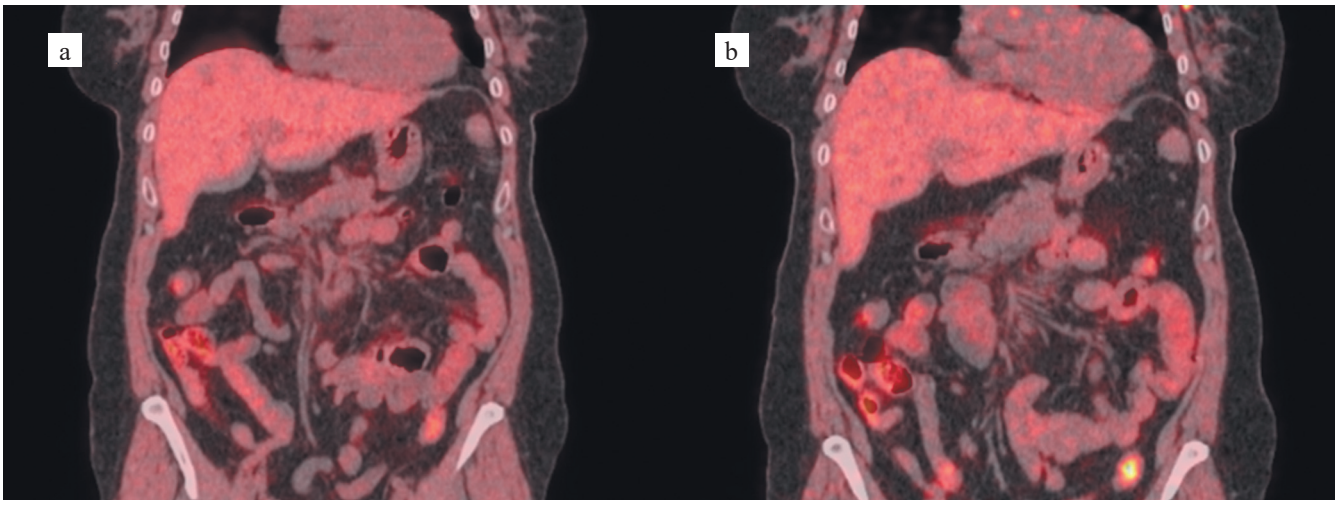

Fig. 2. Coronal fused PET/CT images with ^{18}F-FMISO (native CT): (a) at 90 minutes post-injection; (b) at 180 minutes post-injection. Diffuse tracer uptake is evident in the liver, with higher tracer retention relative to background at 180 minutes compared to 90 minutes. Physiological uptake of ^{18}F-FMISO along the colon is also observed

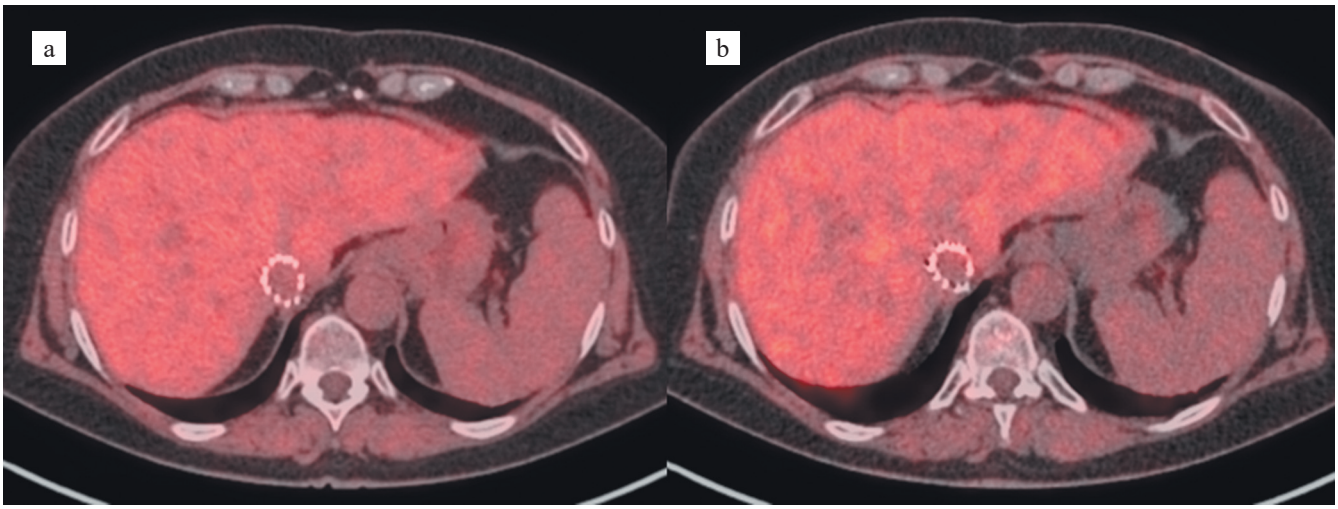

Fig. 3. Axial fused PET/CT images with ^{18}F-FMISO (native CT): (a) at 90 minutes post-injection; (b) at 180 minutes post-injection. Diffuse tracer uptake is evident in the liver, with higher tracer retention relative to background at 180 minutes compared to 90 minutes

maceutical at 180 minutes after injection compared to 90 minutes, supporting the presence of hypoxic changes in the liver graft.

CONCLUSION

Based on the obtained data confirming the presence of hypoxia in the liver graft 27 months after transplantation, the authors consider this method promising for the diagnosis of perfusion-related changes in the liver transplant leading to hypoxia. However, further refinement of the technique and accumulation of additional clinical cases are necessary to validate its effectiveness, both in the early and late post-transplant periods.

The authors declare no conflict of interest.

REFERENCES

1. *Dar WA, Sullivan E, Bynon JS, Eltzschig H, Ju C.* Ischaemia reperfusion injury in liver transplantation: Cellular and molecular mechanisms. *Liver Int*. 2019 May; 39 (5): 788–801. doi: 10.1111/liv.14091.
2. *Zhai Y, Petrowsky H, Hong JC, Busuttil RW, Kupiec-Weglinski JW.* Ischaemia-reperfusion injury in liver transplantation – from bench to bedside. *Nat Rev Gastroenterol Hepatol.* 2013 Feb; 10 (2): 79–89. doi: 10.1038/nrgastro.2012.225.
3. *Man K, Fan ST, Lo CM, Liu CL, Fung PC, Liang TB et al.* Graft injury in relation to graft size in right lobe live donor liver transplantation: a study of hepatic sinusoidal injury in correlation with portal hemodynamics and intragraft gene expression. *Ann Surg.* 2003 Feb; 237 (2): 256–264. doi: 10.1097/01.SLA.0000048976.11824.67.

4. *Esch JS, Jurk K, Knoefel WT, Roeder G, Voss H, Tustas RY et al.* Platelet activation and increased tissue factor expression on monocytes in reperfusion injury following orthotopic liver transplantation. *Platelets.* 2010; 21 (5): 348–359. doi: 10.3109/09537101003739897.
5. *Miyashita T, Nakanuma S, Ahmed AK, Makino I, Hayashi H, Oyama K et al.* Ischemia reperfusion-facilitated sinusoidal endothelial cell injury in liver transplantation and the resulting impact of extravasated platelet aggregation. *Eur Surg.* 2016; 48: 92–98. doi: 10.1007/s10353-015-0363-3.
6. *Liu J, Man K.* Mechanistic Insight and Clinical Implications of Ischemia/Reperfusion Injury Post Liver Transplantation. *Cell Mol Gastroenterol Hepatol.* 2023; 15 (6): 1463–1474. doi: 10.1016/j.jcmgh.2023.03.003.
7. *Golse N, Guglielmo N, El Metni A, Frosio F, Cosse C, Naili S et al.* Arterial Lactate Concentration at the End of Liver Transplantation Is an Early Predictor of Primary Graft Dysfunction. *Ann Surg.* 2019 Jul; 270 (1): 131–138. doi: 10.1097/SLA.0000000000002726.
8. *Moiseenko AV, Polikarpov AA, Tarazov PG, Granov DA.* Initial experience in direct graft perfusion assessment following orthotopic liver transplant. *Russian Journal of Transplantology and Artificial Organs.* 2020; 22 (3): 99–106. https://doi.org/10.15825/1995-1191-2020-3-99-106.
9. *Rajendran JG, Mankoff DA, O'Sullivan F, Peterson LM, Schwartz DL, Conrad EU et al.* Hypoxia and glucose metabolism in malignant tumors: evaluation by [18F]fluoromisonidazole and [18F]fluorodeoxyglucose positron emission tomography imaging. *Clin Cancer Res*. 2004 Apr 1; 10 (7): 2245–2252. doi: 10.1158/1078-0432.ccr-0688-3.
10. *Zschaeck S, Steinbach J, Troost EG.* FMISO as a Biomarker for Clinical Radiation Oncology. *Recent Results Cancer Res.* 2016; 198: 189–201. doi: 10.1007/978-3-662-49651-0_10.
11. *Masaki Y, Shimizu Y, Yoshioka T, Tanaka Y, Nishijima K, Zhao S et al.* The accumulation mechanism of the hypoxia-imaging probe "FMISO" by imaging mass spectrometry: possible involvement of low-molecular metabolites. *Sci Rep.* 2015 Nov 19; 5: 16802. doi: 10.1038/srep16802.
12. *Sorace AG, Elkassem AA, Galgano SJ, Lapi SE, Larimer BM, Partridge SC et al.* Imaging for Response Assessment in Cancer Clinical Trials. *Semin Nucl Med.* 2020 Nov; 50 (6): 488–504. doi: 10.1053/j.semnuclmed.2020.05.001.
13. *Abdo R-alla, Lamare F, Allard M, Fernandez P, Bentourkia M.* Delineation techniques of tumor hypoxia volume with ^{18}F-FMISO PET imaging. *IEEE Nuclear Science Symposium and Medical Imaging Conference Proceedings (NSS/MIC)*. 2018: 1–5. doi: 10.1109/NSSMIC.2018.8824757.
14. *Lopes S, Ferreira S, Caetano M.* PET/CT in the Evaluation of Hypoxia for Radiotherapy Planning in Head and Neck Tumors: Systematic Literature Review. *J Nucl Med Technol*. 2021 Jun; 49 (2): 107–113. doi: 10.2967/jnmt.120.249540.
15. *Wray R, Mauguen A, Michaud L, Leithner D, Yeh R, Riaz N et al*. Development of ^{18}F-Fluoromisonidazole Hypoxia PET/CT Diagnostic Interpretation Criteria and Validation of Interreader Reliability, Reproducibility, and Performance. *J Nucl Med*. 2024 Oct 1; 65 (10): 1526–1532. doi: 10.2967/jnumed.124.267775. PMID: 39266287; PMCID: PMC11448606.
16. *Jagtap R, Asopa RV, Basu S*. Evaluating cardiac hypoxia in hibernating myocardium: Comparison of ^{99m}Tc-MIBI/^{18}F-fluorodeoxyglucose and ^{18}F-fluoromisonidazole positron emission tomography-computed tomography in relation to normal, hibernating, and infarct myocardium. *World J Nucl Med*. 2019 Jan-Mar; 18 (1): 30–35. doi: 10.4103/wjnm.WJNM_16_18. PMID: 30774543; PMCID: PMC6357711.

The article was submitted to the journal on 28.09.2024

DOI: 10.15825/1995-1191-2025-2-60-68

PEDIATRIC HEART TRANSPLANTATION AFTER A FONTAN PROCEDURE

D.V. Ryabtsev[1], A.S. Ivanov[1], M.T. Bekov[1], E.A. Spirina[1], V.N. Poptsov[1], E.S. Kavardakova[1], A.C. Chartaev[1], S.V. Gautier[1, 2]

[1] Shumakov National Medical Research Center of Transplantology and Artificial Organs, Moscow, Russian Federation

[2] Sechenov University, Moscow, Russian Federation

The Fontan procedure is a surgical technique used for hemodynamic correction of complex congenital heart defects (CHDs), and is used when radical correction of CHDs is anatomically impossible. In the long term – from 10 to 20 years – Fontan circulation can lead to "failing Fontan" characterized by heart failure symptoms, requiring adjustments to medical treatment and potentially surgical interventions, including heart transplantation (HT). Foreign studies indicate that HT is an effective method for prolonging life in patients with failing Fontan circulation. It stabilizes the patient's condition. This paper presents the first documented case of HT in a child following a Fontan procedure in the Russian Federation.

Keywords: heart transplantation, Fontan procedure, protein-losing enteropathy.

INTRODUCTION

The Fontan procedure is a hemodynamic, palliative surgical procedure designed to direct systemic venous blood flow to the pulmonary arteries bypassing the ventricle. It is typically performed for a range of complex congenital heart defects [1]. While the procedure often yields satisfactory medium- and long-term outcomes, it remains inherently palliative [2, 3]. Establishing univentricular circulation can significantly extend life expectancy; however, patients remain at lifelong risk for serious complications, including systemic ventricular dysfunction, arrhythmias, chronic hypoxia, thromboembolic events, protein-losing enteropathy (PLE), and plastic bronchitis. These complications can impair central hemodynamics, culminating in the development of the so-called "Failing Fontan" syndrome [4, 5]. According to published data, the incidence of heart failure after a Fontan procedure is 7% at 20 years, rising to 38% by the age of 40 [6].

Treatment strategies vary and include pharmacological management, endovascular interventions, and surgical procedures [7, 8]. Among the most advanced surgical options are left ventricular assist device implantation as a bridge to transplantation and orthotopic heart transplantation (HT). With improvements in surgical techniques for congenital heart defects, the number of people living with Fontan physiology has steadily increased, making the issue of failing Fontan increasingly relevant and urgent [9, 10].

However, HT in this patient population poses unique technical and clinical challenges, largely due to the complex surgical interventions performed before Fontan hemodynamic correction. Despite these complexities, numerous case series and observational studies in the international literature report encouraging outcomes in such patients. A meta-analysis of 426 Fontan patients who underwent HT revealed 1- and 5-year post-HT survival rates of 79.9% and 76.7%, respectively. The analysis encompassed studies conducted over a 22-year period, indicating that HT is a viable and effective treatment for this patient cohort, offering acceptable risk profiles and survival outcomes [11].

To date, no cases of HT for failing Fontan have been registered in Russia. Therefore, the present clinical case represents the first documented experience in the country.

OBJECTIVE

To present the first documented case of HT following a previously performed Fontan procedure in the Russian Federation.

CLINICAL REVIEW

Patient background

Patient P., a 14-year-old male, has been seen by a cardiologist at his place of residence since birth. He was initially evaluated and followed at Bakulev National Medical Research Center for Cardiovascular Surgery in Moscow for congenital heart disease: common atrioventricular canal, double outlet right ventricle, hypoplastic left heart syndrome, ventricular septal defect, and left pulmonary artery hypoplasia (Fig. 1).

Corresponding author: Abulmuslim Chartaev. Address: 1, Shchukinskaya str., Moscow, 123182, Russian Federation. Phone: (926) 857-38-69. E-mail: vps-kho2@mail.ru

Beginning in 2010, the patient underwent multiple staged palliative surgical interventions, including: modified Blalock–Taussig subclavian-to-pulmonary anastomosis on the left using a PTFE (polytetrafluoroethylene) graft; bidirectional cavopulmonary anastomosis on the right side; pulmonary artery branch plasty and ligation of the main pulmonary artery under cardiopulmonary bypass (CPB); transluminal balloon angioplasty of the left pulmonary artery; embolization of major aortopulmonary collaterals (MAPCAs); left pulmonary artery stenting (Fig. 2); MAPCAs embolization. The Fontan procedure, representing the final stage of this palliative strategy, was performed subsequently. In February 2019, the patient underwent cardiac catheterization with intravascular ultrasound of the stent in the left pulmonary artery.

A decision was made to perform a hybrid surgical intervention under intensive care unit (ICU) conditions: Fontan procedure with extracardiac conduit modification, combined with transluminal balloon angioplasty of the left pulmonary artery stent.

In the early postoperative period, the patient developed signs of cardiopulmonary insufficiency, as well as prolonged transudation through the drainage systems, which required intensive pharmacological support.

Following discharge, the child remained under close surveillance by local cardiologists and specialists at Bakulev National Medical Research Center for Cardiovascular Surgery.

About 3 years after the Fontan procedure, the patient began to exhibit signs consistent with the failing Fontan syndrome, including: frequent watery stools (3–4 times daily for over one month), abdominal pain, and intermittent episodes of vomiting. The patient was hospitalized at the Russian Children's Clinical Hospital in response to these symptoms. Physical examination and diagnostic workup revealed: hepatomegaly (+2 cm below the costal margin), peripheral edema (notably in the shin), Signs of ascites, laboratory PLE (total serum protein – 42 g/L, serum albumin – 23 g/L), elevated fecal alpha-1-antitrypsin – >2250 mg/L, fecal calprotectin – 789 mg/kg (Fig. 3). Symptomatic therapy was administered. Due to

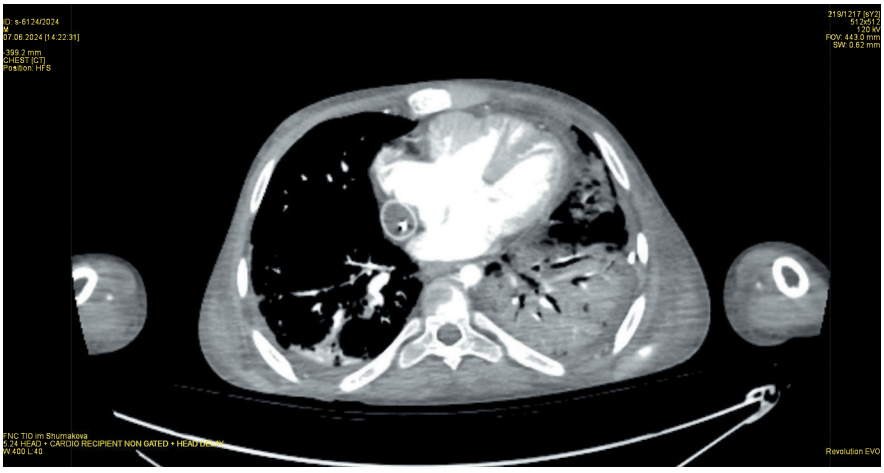

Fig. 1. Assessment of anatomy at the time of admission at Shumakov National Medical Research Center of Transplantology and Artificial Organs

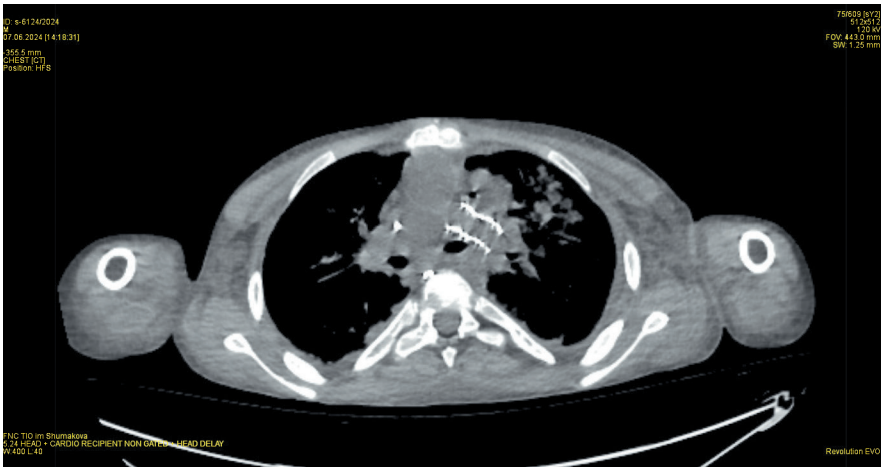

Fig. 2. Stent in the left pulmonary artery

the progressive accumulation of ascitic fluid, the patient underwent laparocentesis.

During inpatient treatment, two episodes of gastrointestinal bleeding were observed. These were attributed to hemostatic dysfunction, likely secondary to PLE. The bleeding episodes led to a critical drop in hemoglobin levels to 29 g/l. Management included multiple transfusions of erythrocyte suspensions, which contributed to clinical stabilization. Following improvement, the patient was discharged home, but recurrent symptoms necessitated readmission at Sukhanov Federal Center for Cardiovascular Surgery in Perm. There, cardiac catheterization was performed to assess Fontan circuit function. Based on the findings, it was decided to perform the following: stenting of the Fontan fenestration, and transluminal balloon angioplasty of the previously placed left pulmonary artery stent. The intervention was successful, and the patient was discharged in stable condition with positive clinical dynamics.

About six months later, the patient's condition deteriorated, with increasing weakness and dyspnea. He was hospitalized in Rostov-on-Don due to signs of worsening cardiovascular insufficiency. Clinical evaluation revealed severe hypoproteinemia and hypoalbuminemia, hemostatic abnormalities, and acid-base and electrolyte imbalance.

Due to unstable hemodynamics, arterial hypotension, and progressive edematous syndrome, the patient was transferred to the ICU, where cardiotonic therapy was initiated. Given the absence of viable options for further surgical correction, a decision was made to transfer the child to Shumakov National Medical Research Center of Transplantology and Artificial Organs. Upon admission to the ICU at Shumakov Center, the following diagnosis was confirmed: PLE following Fontan surgery with signs of decompensation, consistent with the failing Fontan clinical syndrome.

Echocardiographic findings on admission revealed moderately reduced ejection fraction (35–40%) of the single functioning ventricle, despite ongoing inotropic support.

A multidisciplinary council concluded that due to the prolonged course of PLE with signs of progressive decompensation and refractoriness to medical management, the patient was indicated for HT. He was subsequently placed on the emergency HT waiting list.

Heart transplantation and postoperative period

On June 8, 2024, the patient (initial weight: 40 kg, height: 160 cm) underwent orthotopic HT using the bicaval technique. The donor was a 27-year-old male with a weight of 90 kg. The cause of brain death was hemorrhagic stroke. The optimal donor was identified on day 3 following inclusion on the emergency transplant waiting list.

Graft ischemia time was 252 minutes, while CPB lasted for 177 minutes. Preoperative imaging and examination revealed two potential risk factors for perioperative and postoperative complications: tight adhesion of the aorta to the posterior surface of the sternum and narrowing of the left main bronchus, secondary to the presence of a stent in the pulmonary artery, respectively (see Fig. 4, Fig. 5, Fig. 6).

Despite the posterior position of the aorta, resternotomy proceeded without complications. However, pronounced adhesions in the mediastinum made surgical dissection challenging. The left innominate vein, in particular, was firmly adherent to the posterior sternal wall, making it difficult to isolate. Due to elevated venous pressure and thinning of the vessel wall, even minor trauma to the vein resulted in significant bleeding. One such major injury led to profuse hemorrhage, which was successfully controlled without the need for peripheral CPB initiation.

After prolonged cardiolysis, cannulation of the aorta, superior vena cava, and inferior vena cava was achieved, and CPB was initiated. Further cardiolysis in the region of the pulmonary artery branches and aorta was performed after establishing CPB.

Once aortic clamping was feasible, the recipient heart was explanted. Despite a history of MAPCA closure and no significant recanalization or MAPCA development

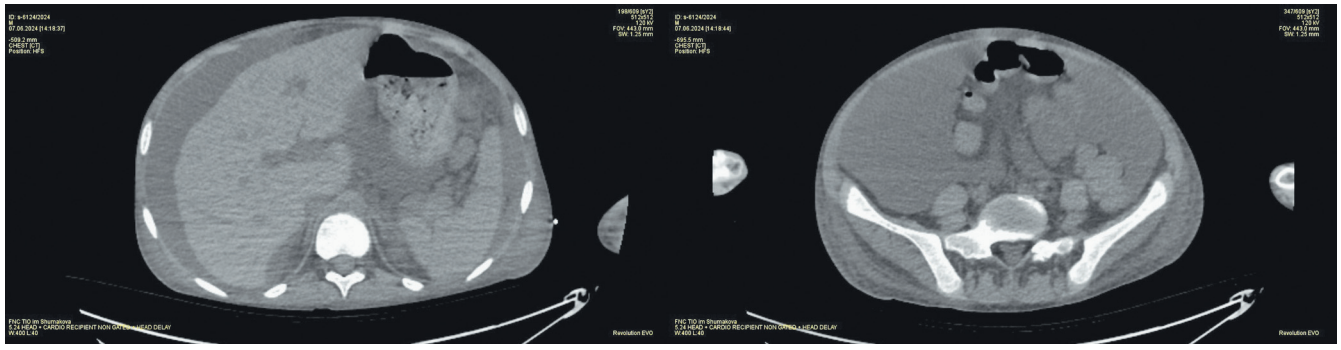

Fig. 3. Severe ascites

on preoperative CT, there was substantial pulmonary venous return, which complicated cardiac excision. The extracardiac conduit was then severed from the inferior surface of the right pulmonary artery, and the superior cavopulmonary anastomosis was also divided.

The resulting defects were combined into a single defect, which was then repaired using a xenopericardial patch. This stage was further complicated by pronounced blood return from the pulmonary arteries. Given the prolonged ischemia time and the stable, optimal positioning of the stent in the left pulmonary artery, the decision was made not to explant the stent, despite the potential for postoperative compression of the left main bronchus.

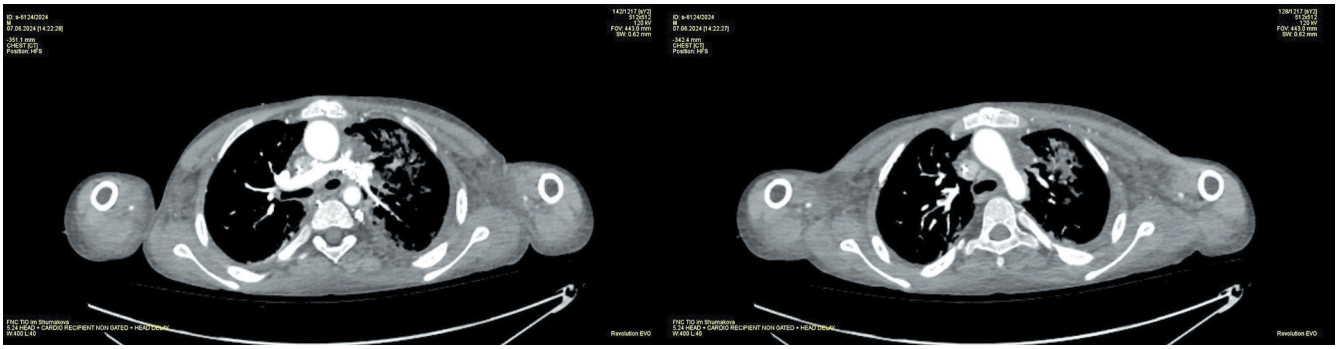

Fig. 4. Retrosternal location of the aorta

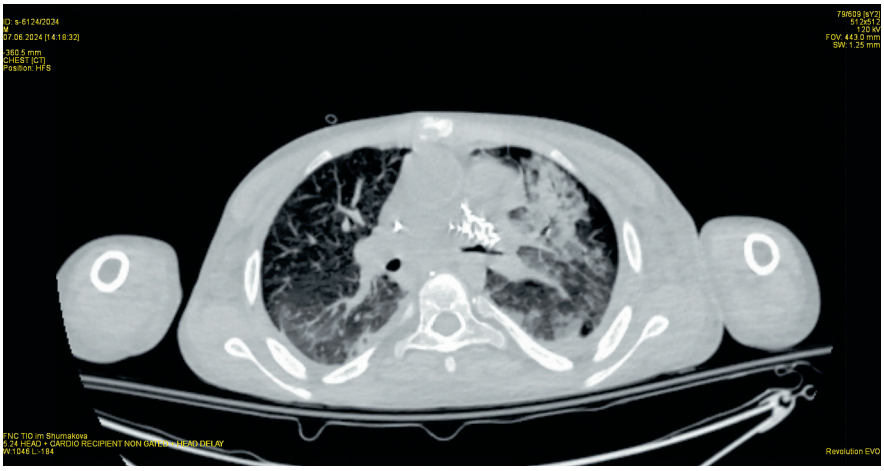

Fig. 5. Narrowing of the left main bronchus due to a neighbouring stent in the left pulmonary artery, before transplantation

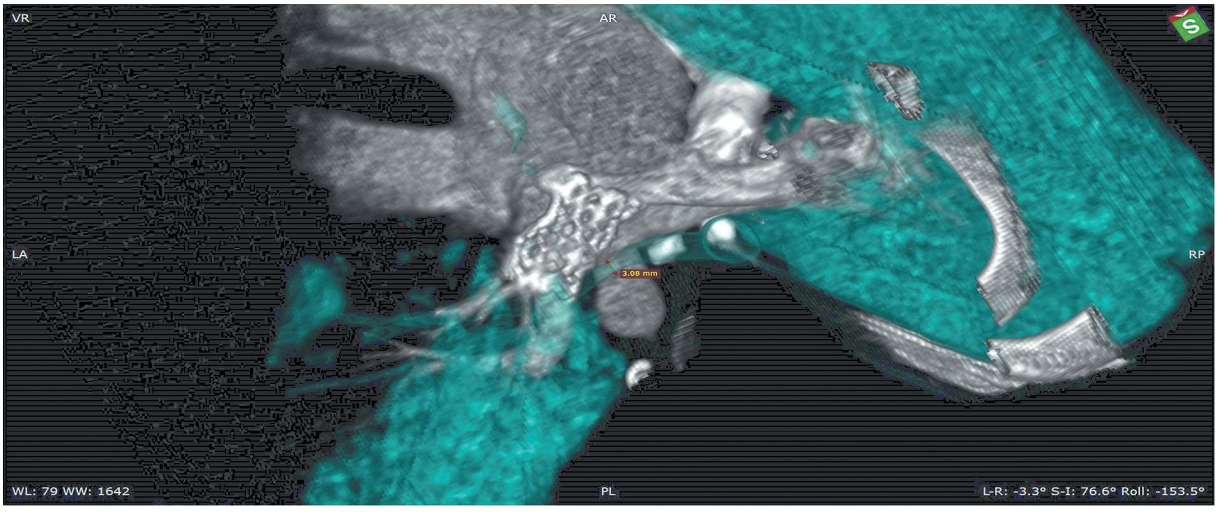

Fig. 6. 3D model of left main bronchus stenosis before transplantation

Graft implantation proceeded in the following sequence: left atrium, pulmonary artery, inferior vena cava, superior vena cava, and aorta. After aortic clamp removal, transesophageal echocardiography confirmed good graft function. The sternum was sutured immediately. The total duration from skin incision to skin closure was 6 hours.

In the immediate postoperative period, inotropic support with dobutamine was initiated at 2 mcg/kg/min, with gradual tapering as myocardial function stabilized and signs of graft insufficiency resolved. Basiliximab was administered as induction therapy in accordance with current guidelines for the management of patients following HT.

Given the presence of preoperative risk factors, the patient underwent fibrobronchoscopy prior to tracheal extubation, which revealed narrowing of the left main bronchus with a pulsating structure along the anterior bronchial wall (Fig. 7). The most likely cause of this finding was the presence of a stent in the left pulmonary artery. The total duration of mechanical ventilation was 26 hours. Following extubation, the patient developed dyspnea and worsening respiratory insufficiency, particularly in the supine position (Fig. 8).

Due to the clinical signs of respiratory failure, the radiographic evidence of atelectasis, and the bronchoscopic confirmation of bronchial narrowing, a CT scan was performed to assess the extent of bronchial stenosis and determine the feasibility of stent placement in the left main bronchus (Fig. 9).

Following the imaging assessment, endoscopic stenting of the left main bronchus was successfully performed using a nitinol stent with an 8 mm diameter (Fig. 10). The patient was transferred to the cardiothoracic department on postoperative day 10 for continued monitoring and treatment.

At the time of transfer, echocardiography revealed satisfactory global systolic function of the left ventricle,

Fig. 7. Fibrobronchoscopy before extubation showing compression of the left main bronchus along the anterior wall

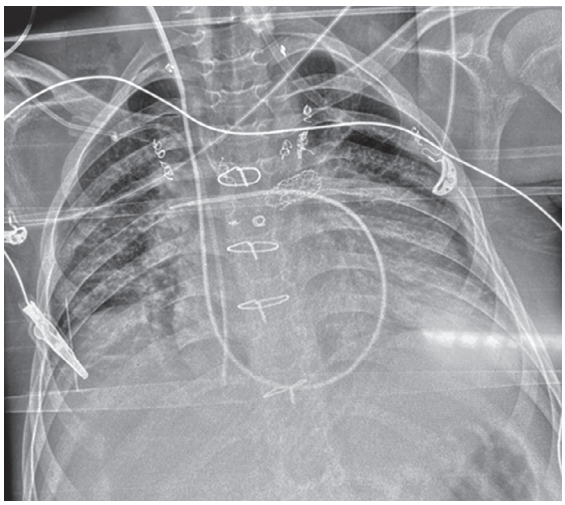

Fig. 8. Pneumonography immediately after extubation

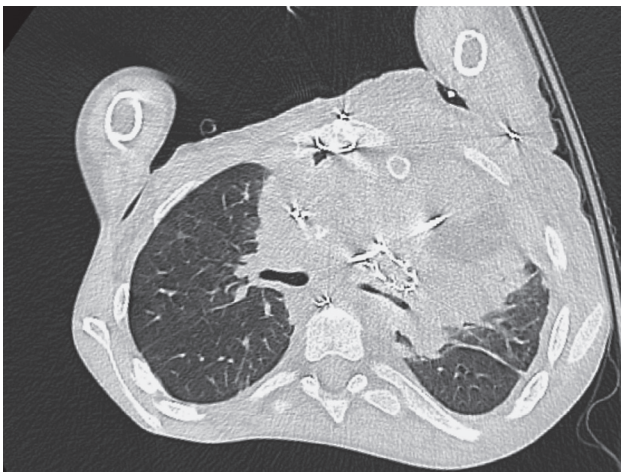

Fig. 9. Computed tomography assessing bronchial narrowing and feasibility of stenting

with a left ventricular ejection fraction (LVEF) of 64%. Dobutamine inotropic support was discontinued on postoperative day 5 in the ICU.

A triple-drug immunosuppressive maintenance regimen was initiated, consisting of a calcineurin inhibitor (tacrolimus), an antimetabolite (mycophenolate mofetil), and corticosteroids (methylprednisolone).

To monitor for cardiac graft rejection and evaluate for donor-transmitted coronary artery disease, both coronary angiography and endomyocardial biopsy were performed. It revealed no signs of acute cellular or antibody-mediated rejection of the cardiac graft. Additionally, coronary angiography showed no stenotic lesions in the coronary arteries of the transplanted heart.

During postoperative week 1, serum levels of total protein and albumin normalized, and diarrheal episodes resolved. However, 10 days after transfer to the general ward, there was a decline in total protein and albumin levels (to 34 g/L and 19 g/L, respectively), along with reappearance of loose stools. This clinical presentation was regarded as recurrent PLE.

A comprehensive evaluation was conducted to exclude alternative causes of the recurrent PLE. Symptomatic therapy and a fat-free diet were initiated. During hospitalization, serial assessments were performed to monitor the bronchial stent position and presence of granulations in the left main bronchus.

At three months post-stenting, a scheduled removal of the stent from the left main bronchus was successfully

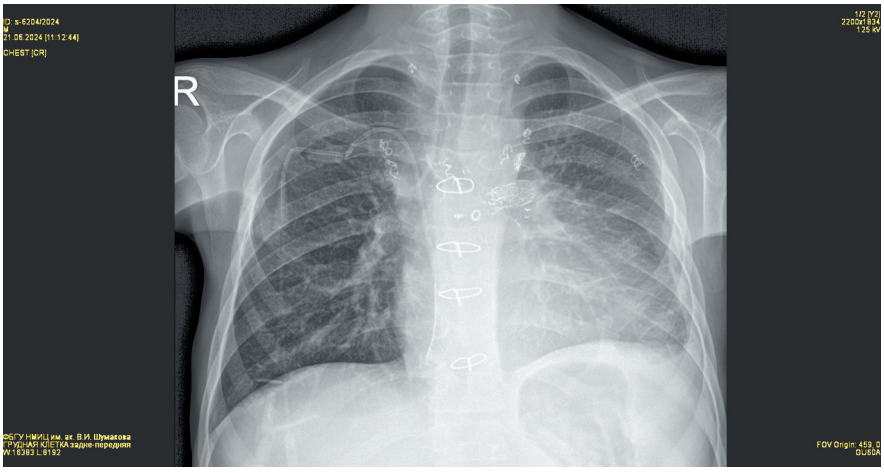

Fig. 10. Pneumonography after stenting of the left main bronchus

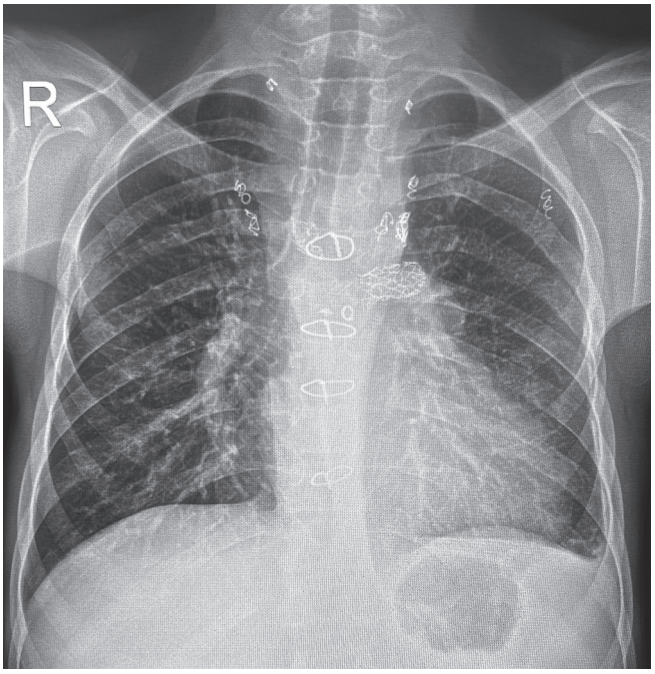

Fig. 11. Pneumonography after stent retrieval from the left main bronchus

performed (Fig. 11). Postoperative bronchoscopy revealed that the structural patency of the left main bronchus was preserved. In the context of ongoing therapy for PLE and adherence to a fat-free diet, albumin infusions were discontinued on day 174 post-transplant due to stable laboratory values of total protein and albumin. However, subsequent monitoring showed a moderate decline in these parameters.

At the time of discharge (on day 201 post-transplant) from Shumakov National Medical Research Center of Transplantology and Artificial Organs, the patient demonstrated no clinical or echocardiographic evidence of cardiac graft dysfunction. Final laboratory values at discharge were: total protein – 57.2 g/L, and albumin – 35.5 g/L.

DISCUSSION

Patients with failing Fontan can be broadly categorized into two groups based on the underlying cause: reduced ventricular function (RVF), and impaired Fontan hemodynamics (IFH). RVF is typically defined as a single ventricular ejection fraction less than 30%. On the

other hand, IFH refers to a constellation of clinical and hemodynamic abnormalities despite preserved ventricular function. Conditions that suggest IFH include severe growth retardation, impaired systolic function with evidence of low cardiac output, PLE, plastic bronchitis; Fontan-associated liver disease, and pulmonary arteriovenous malformations [12, 13]. PLE is specifically defined as hypoalbuminemia (albumin <30 g/L) lasting more than 3 months, accompanied by clinical signs or symptoms like ascites, pleural effusion, edema, diarrhea, or abdominal pain, persisting for more than 3 months [14]. In our case, the primary indication for HT was the development of severe PLE. The interval between the Fontan procedure and the onset of PLE was 3 years, 6 months, and 5 days.

A review of several multicenter studies involving patients with failing Fontan who underwent HT revealed in-hospital and early mortality rates ranging from 15% to 23% in cohorts of over 70 patients [15–18]. However, our single case report does not permit definitive conclusions regarding these outcomes.

According to a 2006 multicenter study, more than 60% of patients with failing Fontan underwent HT within 6 months of clinical deterioration. In our observation, the waiting list duration was only 3 days. Following transplantation, albumin levels normalized within 30 days, consistent with previous findings in PLE patients [16].

In our observation, normalization of total protein and albumin levels, as well as cessation of diarrhea, occurred during the first week following HT. However, 10 days after transfer to the ward, there was a decline in total protein and albumin levels (to 34 g/L and 19 g/L, respectively), accompanied by reappearance of liquid stools. This clinical presentation was regarded as a recurrent PLE.

According to a study involving 7 individuals who experienced recurrent PLE after HT, the primary causes identified included acute or chronic rejection, graft dysfunction, anastomotic site stenosis, vascular thrombosis, infectious complications (including cytomegalovirus enteritis), and post-transplant lymphoproliferative disorders [19]. All possible causes of the recurrent PLE were excluded. Symptomatic therapy and a fat-free diet were initiated. At present, the patient demonstrates positive clinical dynamics, evidenced by a gradual increase in total protein and albumin levels.

Some studies have reported an association between shorter waiting list times and more rapid normalization of protein and albumin levels, suggesting that a shorter time on the transplant waiting list may be linked to faster recovery of these parameters post-transplant [14]. In our case, however, despite the exceptionally short waiting period (3 days), normalization of protein and albumin levels after relapse required more than 6 months, indicating a prolonged recovery.

It is important to note that this patient cohort – although quite common – often lacks early diagnosis, which can delay listing for transplantation. In our observation, about 5 months after transplantation, echocardiography confirmed satisfactory graft function, with an LVEF of 64%, and no episodes of pulmonary hypertension were observed. No episodes of rejection were recorded in the patient during the 7-month follow-up period.

Two studies assessing 1- and 5-year survival rates after HT in patients with failing Fontan were reviewed. The first study, covering the period from 1990 to 2002, demonstrated lower survival rates in the Fontan group compared to those without prior Fontan surgery: 1-year survival was 71% in the Fontan group versus 83% in the non-Fontan group, while 5-year survival was 60% versus 74%, respectively. In contrast, a more recent study spanning 22 years reported improved outcomes, with 1-year and 5-year survival rates of 79.9% and 76.7%, respectively, in patients who underwent HT for a failing Fontan [11, 15]. These data suggest that careful patient selection, early referral for surgical intervention prior to the onset of irreversible target organ damage, and the use of lower-intensity initial immunosuppressive regimens may significantly enhance post-transplant survival in this high-risk population [11, 14, 15, 20].

CONCLUSION

Our clinical case shows the feasibility and potential success of HT in patients with a failing Fontan, even in the presence of significant technical challenges and frequent preoperative decompensation. However, it is important to recognize that the resolution of associated complications, such as PLE, may be prolonged – even in the absence of identifiable precipitating factors.

The authors declare no conflict of interest.

REFERENCES

1. *Fredenburg TB, Johnson TR, Cohen MD.* The Fontan procedure: anatomy, complications, and manifestations of failure. *Radiographics*. 2011 Mar-Apr; 31 (2): 453–463. doi: 10.1148/rg.312105027.
2. *d'Udekem Y, Iyengar AJ, Galati JC, Forsdick V, Weintraub RG, Wheaton GR et al.* Redefining expectations of long-term survival after the Fontan procedure: twenty-five years of follow-up from the entire population of Australia and New Zealand. *Circulation* 2014 Sep 9; 130 (11 Suppl 1): S32–S38.
3. *Pundi KN, Johnson JN, Dearani JA, Pundi KN, Li Z, Hinck CA et al.* 40-year follow-up after the Fontan operation: long-term outcomes of 1,052 patients. *J Am Coll Cardiol*. 2015 Oct 13; 66 (15): 1700–1710.
4. *Gewillig M, Brown SC, van de Bruaene A, Rychik J.* Providing a framework of principles for conceptualising the Fontan circulation. *Acta Paediatr*. 2020 Apr; 109 (4): 651–658.

5. *Goldberg DJ, Shaddy RE, Ravishankar C, Rychik J.* The failing Fontan: etiology, diagnosis and management. *Expert Rev Cardiovasc Ther*. 2011 Jun; 9 (6): 785–793.
6. *Ghanayem NS, Berger S, Tweddell JS.* Medical management of the failing Fontan. *Pediatr Cardiol*. 2007 Nov-Dec; 28 (6): 465–471.
7. *Book WM, Gerardin J, Saraf A, Marie Valente A, Rodriguez F 3rd.* Clinical phenotypes of Fontan failure: implications for management. *Congenit Heart Dis*. 2016 Jul; 11 (4): 296–308.
8. *Gierlinger G, Sames-Dolzer E, Kreuzer M, Mair R, Nawrozi MP, Tulzer A et al.* Surgical and interventional rescue strategies for Fontan failure. *Interact Cardiovasc Thorac Surg*. 2022 Aug 3; 35 (3): ivac098.
9. *Van Melle JP, Wolff D, Hörer J, Belli E, Meyns B, Padalino M et al.* Surgical options after Fontan failure. *Heart*. 2016 Jul 15; 102 (14): 1127–1133.
10. *Schilling C, Dalziel K, Nunn R, Du Plessis K, Shi WY, Celermajer D et al.* The Fontan epidemic: population projections from the Australia and New Zealand Fontan registry. *Int J Cardiol*. 2016 Sep 15; 219: 14–19.
11. *Hassan W, Kotak S, Khatri M, Ahmed A, Ahmed J, Ali SS, Khan T.* Efficacy of heart transplantation in patients with a failing Fontan: a systematic review and meta-analysis. *Cardiothorac Surg*. 2021; 29 (1). doi: 10.1186/s43057-021-00043-6.
12. *Griffiths ER, Kaza AK, Wyler von Ballmoos MC, Loyola H, Valente AM, Blume ED, del Nido P.* Evaluating failing Fontans for heart transplantation: predictors of death. *Ann Thorac Surg*. 2009 Aug; 88 (2): 558–563.
13. *Jayakumar KA, Addonizio LJ, Kichuk-Chrisant MR, Galantowicz ME, Lamour JM, Quaegebeur JM, Hsu DT.* Cardiac transplantation after the Fontan or Glenn procedure. *J Am Coll Cardiol*. 2004 Nov 16; 44 (10): 2065–2072.
14. *Lin SN, Huang SC, Chen YS, Chih NH, Wang CH, Chou NK et al*. Case Series: Heart Transplantation After Fontan Operation-Single-Center Experience. *Transplant Proc*. 2016 Apr; 48 (3): 959–964. doi: 10.1016/j.transproceed.2016.01.037.
15. *Lamour JM, Kanter KR, Naftel DC, Chrisant MR, Morrow WR, Clemson BS et al.* The effect of age, diagnosis, and previous surgery in children and adults undergoing heart transplantation for congenital heart disease. *J Am Coll Cardiol*. 2009 Jul 7; 54 (2): 160–165.
16. *Bernstein D, Naftel D, Chin C, Addonizio LJ, Gamberg P, Blume ED et al.* Outcome of listing for cardiac transplantation for failed Fontan: a multi-institutional study. *Circulation*. 2006 Jul 25; 114 (4): 273–280.
17. *Kovach JR, Naftel DC, Pearce FB, Tresler MA, Edens RE, Shuhaiber JH et al.* Comparison of risk factors and outcomes for pediatric patients listed for heart trans plantation after bidirectional Glenn and after Fontan: an analysis from the Pediatric Heart Transplant Study. *J Heart Lung Transplant*. 2012 Feb; 31 (2): 133–139.
18. *Karamlou T, Diggs BS, Welke K, Tibayan F, Gelow J, Guyton SW et al.* Impact of single ventricle physiology on death after heart transplantation in adults with congenital heart disease. *Ann Thorac Surg*. 2012 Oct; 94 (4): 1281–1287.
19. *Sagray E, Johnson JN, Schumacher KR, West S, Lowery RE, Simpson K.* Protein-losing enteropathy recurrence after pediatric heart transplantation: Multicenter case series. *Pediatr Transplant*. 2022 Aug; 26 (5): e14295. doi: 10.1111/petr.14295.
20. *Backer CL, Russell HM, Pahl E, Mongé MC, Gambetta K, Kindel SJ et al.* Heart Transplantation for the Failing Fontan. *Ann Thorac Surg*. 2013 Oct; 96 (4): 1413–1419. doi: 10.1016/j.athoracsur.2013.05.087.

The article was submitted to the journal on 9.01.2025

DOI: 10.15825/1995-1191-2025-2-69-80

IMPACT OF MHC MISMATCHES ON THE DEVELOPMENT OF EARLY POSTTRANSPLANT ACUTE HEART REJECTION

S.V. Spiridonov[1], A.I. Tsyrkunov[2], M.H. Koliadko[1], I.S. Sivets[3], Yu.P. Ostrovsky[1]

[1] Republican Scientific and Practical Center "Cardiology", Minsk, Republic of Belarus
[2] Belarusian State Medical University, Minsk, Republic of Belarus
[3] Republican Scientific and Practical Center of Transfusiology and Medical Biotechnology, Minsk, Republic of Belarus

Objective: to analyze the impact of MHC mismatches, considering recipient nationality and age, on the development of rejection crisis. **Material and methods.** A retrospective study was conducted, including 264 recipients and their 264 matched donors. HLA typing was performed by serological and molecular genetic (SSP) methods. Mismatches in the following MHC class I and II genes were assessed: HLA-A, HLA-B, HLA-DRB1, HLA-DQB1. Recipient age and nationality were also considered in the analysis. **Results.** MHC Class I mismatches (HLA-A, HLA-B) did not significantly impact the occurrence of acute rejection crises. MHC Class II mismatches (HLA-DRB1, HLA-DQB1) significantly increased the risk of acute rejection ($\chi^2 = 6.790$; df = 1; p = 0.009), with an odds ratio (OR) of 5.69 (95% CI: 1.32–24.50). Recipient age had a significant effect on acute rejection ($\chi^2 = 8.200$; df = 1; p = 0.004). Recipients under 45 years experienced rejection in 34.8% of cases, 18.9% more than those aged 45 and older, with an OR of 2.30 (95% CI: 1.29–4.10). Donor-recipient nationality mismatch significantly influenced acute rejection ($\chi^2 = 4.660$; df = 1; p = 0.031), with an OR of 2.00 (95% CI: 1.06–3.79). The analysis, considering all three above-mentioned factors, confirmed that MHC mismatches significantly influence the development of acute graft rejection in Belarusian recipients under 45 years old ($\chi^2 = 4.068$; df = 1; p = 0.044) and in recipients of other nationalities (Russians, Israelis, Georgians, Armenians, Uzbeks, Kazakhs, Azerbaijanis, Ukrainians) under 45 years old ($\chi^2 = 4.342$; df = 1; p = 0.037). Among Belarusian recipients, no cases of rejection were observed with 0–1 MHC mismatches, while rejection occurred in 35.4% of cases with 2–4 mismatches (OR 9.44, CI 0.51–173.61). Similarly, in recipients of other nationalities, acute rejection did not develop with 0–1 mismatches, but occurred in 50.0% of cases with 2–4 mismatches (OR 11.00, CI 0.56–217.69). **Conclusion.** It has been reliably established that MHC class II mismatches, donor-recipient nationality differences, and recipient age under 45 years significantly increase the risk of acute rejection crisis in the postoperative period.

Keywords: heart transplantation, HLA typing, HLA mismatch, graft rejection.

INTRODUCTION

In organ transplantation, the recipient's immune system can recognize the donor organ as foreign due to differences in antigens, leading to a rejection response. This response can manifest as immediate-type hypersensitivity or delayed-type hypersensitivity. While optimal antigen matching between donor and recipient is the goal, in clinical practice, solid organ transplants are often carried out despite varying degrees of antigenic mismatch [1, 2].

As a result, antigen mismatches – regardless of the immune response pathway – increase the risk of transplant rejection. In the case of heart transplants, this rejection leads to graft dysfunction and progression of secondary heart failure (HF) [3].

Currently, there are no clear clinical signs that reliably indicate the onset of graft rejection. One diagnostic method capable of identifying structural changes in the myocardium is magnetic resonance imaging. However, the current gold standard in clinical practice remains endomyocardial biopsy. Despite its diagnostic accuracy, this technique is invasive and carries risks of serious complications, including hemopericardium, cardiac tamponade, pneumothorax, and infections. In some cases, these complications may result in fatal outcomes. These significant limitations underscore the urgent need for further research and the development of non-invasive approaches to improve the diagnosis and prediction of allograft rejection [2–5].

One of the key targets for modern non-invasive methods in predicting graft rejection is the assessment of human leukocyte antigens (HLA). These molecules are referred to as HLA because they were initially identified through antigenic differences observed in human white blood cells [4, 5]. HLAs are categorized into two main groups: major histocompatibility complex (MHC) an-

Corresponding author: Artem Tsyrkunov. Address: 110b, Rose Luxembourg str., Minsk, 220036, Republic of Belarus. Phone: +375 (29) 779-20-51. E-mail: cir.a@icloud.com

tigens and minor histocompatibility antigens (miHAs). miHAs, which are encoded by histocompatibility genes (HCG), play a relatively limited role in the immune response leading to transplant rejection. In contrast, antigens encoded by MHC loci are responsible for eliciting the most significant allograft rejection response [6].

MHC genes are indeed located on the short arm (6p) of chromosome 6. Their primary role is to present antigenic peptides on the surface of cells, allowing T-lymphocytes to identify and target cells that are either infected or have undergone changes [4, 7].

MHC structure:

1. MHC Class I molecules (HLA-A, HLA-B, and HLA-C) are expressed on the surface of all nucleated cells. Their primary role is to present endogenously derived antigens (e.g., viral or intracellular pathogenic peptides) to cytotoxic T-lymphocytes ($CD8^+$ T cells), thereby mediating a targeted cellular immune response against infected or abnormal cells.
2. MHC Class II molecules (HLA-DM, HLA-DO, HLA-DP, HLA-DQ, and HLA-DR) are expressed primarily on professional antigen-presenting cells, including dendritic cells, macrophages, and B lymphocytes. These molecules present exogenous antigens (e.g., bacterial proteins or environmental peptides) to helper T-lymphocytes ($CD4^+$ T cells), triggering humoral immune response and promoting activation of other immune effector cells.
3. MHC Class III encompasses a diverse group of molecules involved in broader aspects of immune regulation, such as components of the complement cascade and certain pro-inflammatory cytokines, including tumor necrosis factor (TNF) family members. Although Class III molecules in graft rejection is less significant, they play important functions in the regulation of inflammation and cellular immune activity [3, 4, 8, 9].

Structure of the HLA class I molecule:

– α-chain (heavy chain): encoded by HLA genes, has a molecular mass of 44–47 kDa.
– β2-microglobulin: a non-HLA encoded subunit with a molecular mass of 12 kDa.
– the α-chain consists of three domains: α1 and α2 form the peptide-binding groove, while the α3 domain is a highly conserved immunoglobulin-like structure that interacts with $CD8^+$ T-lymphocytes.
– It binds peptides that are 8–10 amino acids in length.
– Peptide anchoring is achieved through a network of hydrogen bonds between α-chain residues and the carboxyl terminus of the peptide.
– The groove accounts for the high polymorphism of HLA class I molecules, leading to variations in electrostatic charge, hydrophobicity, and shape, all of which influence peptide binding affinity [10–14].

Structure of the HLA class II molecule:

– α-chain: molecular mass of 32–34 kDa.
– β-chain: molecular mass of 29–32 kDa.
– Both chains are encoded by HLA genes and consist of two domains each.
– α2 and β2 domains: are highly conserved immunoglobulin-like structures that interact with $CD4^+$ T-lymphocytes.
– α1 and β1 domains: come together to form the peptide-binding groove.
– Unlike HLA class I, this groove is open at both ends, enabling the binding of longer peptides – typically 12–24 amino acids, though sometimes even longer.
– Peptides bind in an extended conformation, exposing about one-third of their surface area for interaction with T-cell receptors (TCRs).
– The terminus of the peptides are not rigidly anchored within the groove and may protrude beyond its boundaries [12, 15].

Class I and class II HLA molecules play a central role in T cell–mediated adaptive immune responses. During maturation in the thymus, T lymphocytes develop tolerance to self-HLA molecules, a process crucial for distinguishing self from non-self, even when peptides are bound within the HLA binding groove.

The antigen recognition process involves four key steps: peptide generation or uptake, typical for antigen-presenting cells; peptide processing and HLA binding to HLA molecules; transport to the cell surface; the final step is analysis, direct interaction with (TCRs). In this case, there is a dual recognition of the antigen and the HLA molecule. As mentioned above, a mismatch in HLA molecules disrupts this recognition process and is the primary trigger for T cell activation, involving both immunoregulatory $CD4^+$ T cells and cytotoxic $CD8^+$ T cells [3, 16].

The effector functions of $CD8^+$ and $CD4^+$ T-lymphocytes are different, as $CD8^+$ T-cells exhibit a cytotoxic activity, enabling them to directly destroy cells presenting foreign peptides in the context of HLA class I molecules. These target cells may include virus-infected cells, tumor cells, or allogeneic donor cells that express mismatched or foreign HLA molecules.

$CD4^+$ T-lymphocytes act as central regulators of immune function and are often referred to as “helper” cells. Their effector functions are diverse and depend on their subtype, with three major subsets playing critical roles: Th1 cells that secrete interferon gamma (IFN-γ), which promotes activation and proliferation of $CD8^+$ cytotoxic T cells and enhances macrophage activity; Th2 cells which produce interleukins IL-4 and those that produce IL-5, supporting B-lymphocyte proliferation and synthesis of IgG antibodies. The type of allograft rejection – T-cell-mediated rejection (mediated by $CD8^+$ T

cells) or antibody-mediated rejection (mediated by B cells and antibodies) – depends on both the pathway of alloantigen recognition and the duration of exposure to the donor tissue [3, 16].

Acute rejection (AR) of a donor organ is most commonly driven by cellular immune response. However, antibody-mediated rejection (AMR), can also play a pivotal role in graft failure.

Antibodies targeting histocompatibility antigens (HLA molecules) may be present prior to transplantation or develop postoperatively. Based on their antigen specificity, these antibodies are generally classified into two main categories: donor-specific antibodies (DSA) – these are directed specifically against the donor's HLA antigens; non-donor-specific antibodies (non-DSA) – they may arise from prior blood transfusions or pregnancies.

Two other anti-HLA antibodies merit special attention: natural anti-HLA antibodies, which may be present innately and infection-induced anti-HLA antibodies, which can be triggered by diseases.

Having outlined the mechanisms of action associated with HLA molecules and their critical role in the recognition and destruction of donor cells (as foreign to the recipient), it is important to highlight the two primary methods currently used to predict AR risk: HLA typing and the crossmatch test. HLA typing enables the identification of mismatches between donor and recipient HLA alleles, and its predictive value has been well-documented in the transplantation of solid organs such as the kidney, liver, and lungs [17–20]. The crossmatch test assesses the recipient's immunologic risk by detecting the presence of pre-formed antibodies against donor-specific antigens. However, these methods are not universally applicable and require further research and refinement, including integration with other methods [21].

Another significant risk factor in transplantation is the age of the recipient. Studies have shown that younger recipients are at higher risk of death from AR, cardiac allograft vasculopathy, and graft failure [22, 23].

Race can also be a contributing factor. HLA haplotypes are strongly associated with racial and ethnic background, adding complexity to achieving optimal donor–recipient matching. On average, HLA polymorphism is highest among African American populations and lowest among Caucasians, with Asian, Caucasian, and Hispanic groups exhibiting intermediate variability. This genetic diversity is reflected in clinical outcomes, as recipients of African American, Hispanic, Asian, and Caucasian descent show varying levels of predisposition to AR episodes [24].

Considering these demographic and immunogenetic factors enables the identification of patients at increased risk of rejection. This, in turn, supports the development of personalized monitoring strategies, optimization of immunosuppressive therapy targets post-transplant, and ultimately reducing transplant-related morbidity and mortality.

Objective: to investigate the impact of mismatches in MHC antigens (HLA), while accounting for recipient age and ethnicity, on the likelihood of developing AR. In addition, to evaluate the potential of HLA typing as a predictive tool for immunologic risk assessment during donor–recipient selection.

MATERIAL AND METHODS OF RESEARCH

A retrospective analysis was conducted using inpatient medical records and protocols of heart transplants performed from 2009 to 2023 at the Republican Scientific and Practical Center "Cardiology" ("Cardiology Center"). All patients included in the study underwent orthotopic heart transplantation, either via the classical biatrial technique or the bicaval technique.

HLA typing was performed for a total of 1,054 samples, comprising 527 recipient–donor pairs. Typing was conducted using both serological and molecular genetic methods (sequence-specific primers, SSP). Peripheral venous blood samples were collected from recipients by clinical personnel at Cardiology Center" and from donors at the respective institutions where the donor heart was procured.

The primary antigens selected for evaluation were those most commonly implicated in transplant immunogenicity, including MHC class I antigens (HLA-A, HLA-B) and MHC class II antigens (HLA-DRB1, HLA-DQB1). Typing for HLA-DQA1 was not conducted during the study period, as this antigen was not included in the standard transplantation protocol at our center. HLA-C and HLA-DRB3 were also excluded from analysis, based on literature suggesting limited relevance to transplant outcomes [25].

The following recipients were excluded from the study:

1) Individuals with incomplete HLA typing for HLA-A, HLA-B, HLA-DRB1, or HLA-DQB1;
2) Patients under 18 years of age;
3) Cases involving heart retransplantation;
4) Patients who underwent combined heart–lung transplantation;
5) Recipients who developed an AR crisis verified by endomyocardial biopsy within 7 days after reduction of immunosuppressive therapy due to an infectious complication;
6) Recipients for whom AR diagnosis was inconclusive due to critical clinical condition and subsequent in-hospital mortality.

The final analysis included 264 recipients and 264 matched donors. To ensure adequate sample sizes

for statistical analysis of key parameters, the study population was stratified as follows:

1) By overall mismatch level for each MHC class: subgroups were formed based on the number of mismatches – 0–1 and 2–4.
2) By mismatch in class II antigens (DRB1 and DQB1): subgroups were divided into those with 0 mismatches and those with 1–2 mismatches.
3) By recipient age: the cohort was divided into two subgroups – recipients <45 years of age and those ≥45.
4) By nationality: recipients were grouped into those of Belarusian nationality and those of other nationalities (Russian, Jewish, Georgian, Armenian, Uzbek, Kazakh, Azerbaijani, and Ukrainian).
5) By clinical outcome: two outcome categories were defined – recipients who experienced an AR crisis and those who did not.

Statistical data processing was done using the JAMOVI software package. The chi-square test (χ^2) was used to assess the statistical significance of differences between the groups studied. The odds ratio (OR) with a 95% confidence interval (CI) was calculated to evaluate the strength of associations.

RESULTS

Of the 264 recipients included in the final analysis, 207 (78.4%) were of Belarusian nationality, while 57 (21.6%) represented other nationalities.

Analysis revealed that for MHC class I, a mismatch of 0–1 with the donor was observed in only 5 recipients (1.9%), while 259 recipients (98.1%) had 2–4 mismatches.

For MHC class II, 33 recipients (12.5%) had 0–1 mismatches, whereas 231 recipients (87.5%) had 2–4 mismatches.

Regarding specific HLA class II antigens, 0 mismatches for HLA-DRB1 were found in 14 recipients (5.3%), and for HLA-DQB1, in 39 recipients (14.8%).

The remaining recipients – 250 (94.7%) for DRB1 and 225 (85.2%) for DQB1 – had 1–2 mismatches with their donors.

In the group of recipients of Belarusian nationality, there were 178 men (86.0%) and 29 women (14.0%). Median age of male recipients was 54.00 years (95% CI: 52.20–55.80), while median age of female recipients was 50.00 years (95% CI: 40.90–59.10).

Among recipients of other ethnicities, 50 were male (87.7%) and 7 female (12.3%). The median age of males in this group was 40.00 years (95% CI: 34.00–46.00), and for females, 49.00 years (95% CI: 31.60–66.40).

AR were documented in 64 out of 264 recipients (24.2%). Median age of patients who experienced AR was 47.00 years (95% CI: 41.20–52.80), compared to 53.50 years (95% CI: 52.10–54.90) among those who did not.

An analysis of the association between MHC class mismatches and AR incidence yielded the following results: mismatches in MHC class I did not significantly influence the occurrence of AR episodes ($\chi^2 = 0.0499$; df = 1; p = 0.823). In contrast, MHC class II mismatches were found to have a statistically significant impact, increasing the likelihood of AR ($\chi^2 = 6.790$; df = 1; p = 0.009). AR incidence rose from 6.1% in patients with 0–1 mismatches to 26.8% in those with 2–4 mismatches. The odds ratio (OR) for AR in the presence of MHC class II mismatches was 5.69 (95% CI: 1.32–24.50) (Figs. 1, 2).

An analysis of individual MHC class II antigens and their association with AR revealed that mismatches in HLA-DRB1 ($\chi^2 = 2.350$; df = 1; p = 0.125) and HLA-

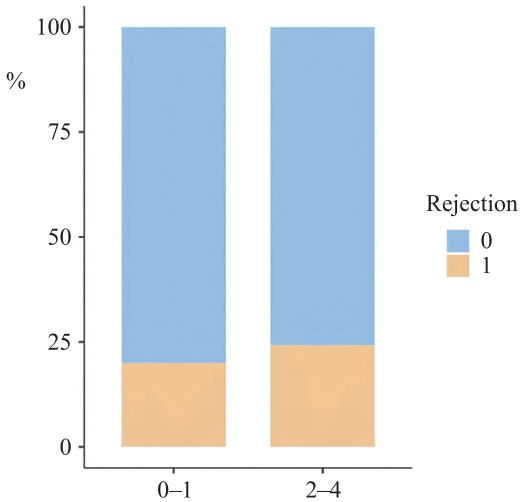

Fig. 1. Distribution of outcomes depending on the number of MHC class I mismatches

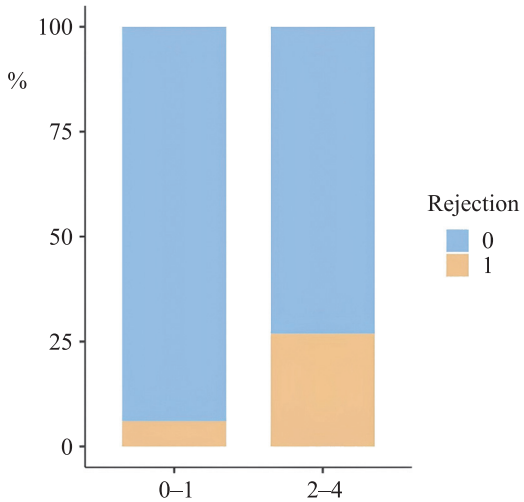

Fig. 2. Distribution of outcomes depending on the number of MHC class II mismatches

DQB1 (χ^2 = 3.250; df = 1; p = 0.071) did not reach statistical significance. However, graphical analysis demonstrated a clear trend toward increased rejection rates with the presence of mismatches: from 7.14% to 25.23% for HLA-DRB1 and from 12.81% to 25.22% for HLA-DQB1, respectively (Figs. 3 and 4).

An analysis of the influence of recipient nationality on the incidence of AR revealed a statistically significant difference (χ^2 = 4.660; df = 1; p = 0.031). Specifically, heart transplant from a Belarusian donor to a recipient of other nationality (Russian, Jewish, Georgian, Armenian, Uzbek, Kazakh, Azerbaijani, and Ukrainian) was associated with a 2.00-fold increased risk of developing an AR (95% CI: 1.06–3.79). The corresponding increase in incidence rose from 21.3% to 35.1% (Fig. 5).

When analyzing age as a risk factor for AR, it was found that recipients under 45 years of age experienced rejection in 34.8% of cases, which is 18.9% higher compared to recipients aged 45 and above. This difference was statistically significant (χ^2 = 8.200; df = 1; p = 0.004), with an OR of 2.30 (95% CI: 1.29–4.10) (Fig. 6).

When analyzing the combined effect of MHC class II mismatches and recipient age, a statistically significant association was observed in the subgroup of recipients under 45 years of age (χ^2 = 8.690; df = 1; p = 0.004). In this group, AR incidence was 0% with 0–1 mismatches, compared to 40.8% with 2–4 mismatches, yielding an OR of 18.69 (95% CI: 1.07–326.1). In contrast, no significant association between MHC class II mismatches and rejection was found in recipients aged 45 and older (Fig. 7).

When evaluating the combined influence of MHC class II antigen mismatches and recipient nationality, it was found that mismatches did not significantly affect AR incidence among Belarusian recipients (χ^2 = 3.560; df = 1; p = 0.059). Similarly, no statistically significant

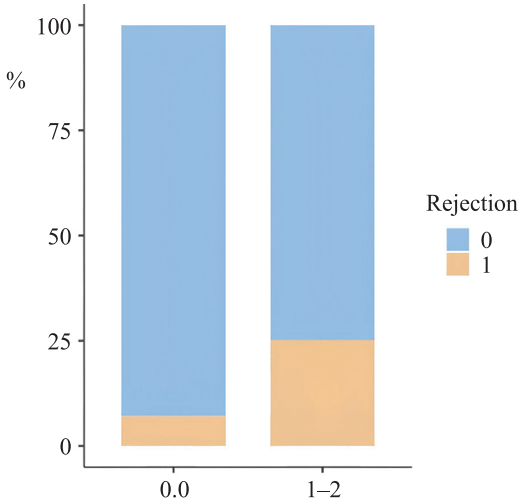

Fig. 3. Distribution of outcomes depending on HLA-DRB1 antigen mismatches

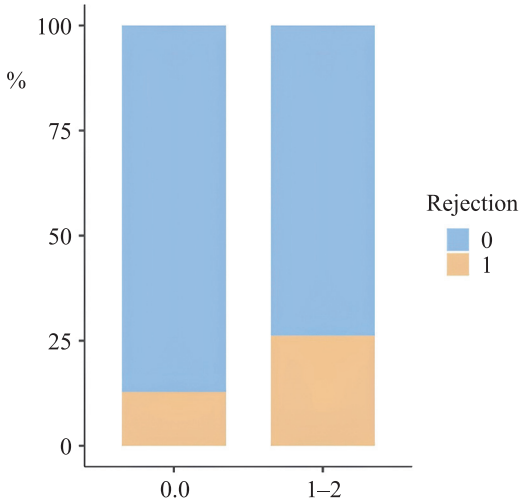

Fig. 4. Distribution of outcomes depending on HLA-DQB1 antigen mismatches

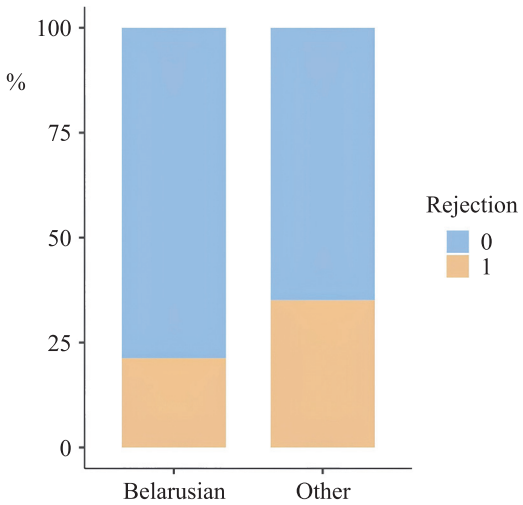

Fig. 5. Distribution of outcomes by nationality

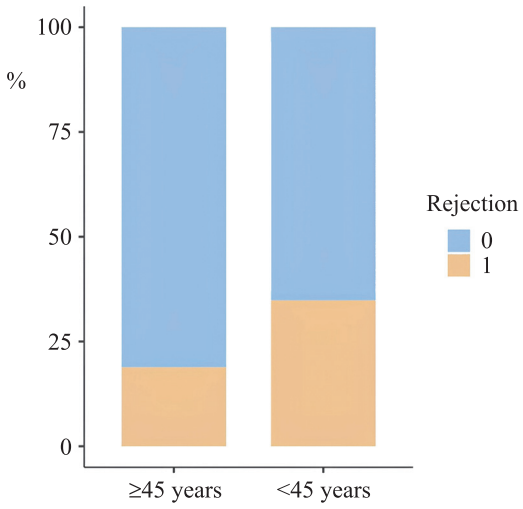

Fig. 6. Distribution of outcomes by age

difference was observed in the subgroup of recipients of other nationalities (χ^2 = 3.620; df = 1; p = 0.057). However, graphical analysis revealed a notable trend: in recipients of non-Belarusian nationality, the incidence of rejection increased from 0% to 39.2% in the presence of 2–4 mismatches, whereas among Belarusian recipients, the increase was from 7.4% to 23.3% (Fig. 8).

An analysis incorporating all three factors – MHC class II mismatches, recipient age, and nationality – revealed that mismatches significantly influenced the incidence of acute graft rejection in recipients under 45 years of age, both among those of Belarusian nationality (χ^2 = 4.068; df = 1; p = 0.044) and of other nationalities (χ^2 = 4.342; df = 1; p = 0.037). In Belarusian recipients under 45 years old, no cases of acute rejection were observed in the 0–1 mismatch subgroup, while the rejection rate increased to 35.4% with 2–4 mismatches (OR = 9.44; 95% CI: 0.51–173.61). Similarly, in recipients of other nationalities under 45, no rejection occurred with 0–1 mismatches, while the incidence reached 50.0% in the 2–4 mismatch group (OR = 11.00; 95% CI: 0.56–217.69) (Fig. 9).

When analyzing HLA-DRB1 antigen mismatches across all subgroups, no statistically significant associations with AR were observed. However, analysis of the HLA-DQB1 antigen revealed a significant association between mismatches and development of AR in the subgroup of recipients of other nationalities (χ^2 = 4.342; df = 1; p = 0.037), with an OR of 11.00 (95% CI: 0.56–217.69) (Figs. 10 and 11).

DISCUSSION

The results of our study demonstrate that recipients with a higher number of MHC class II mismatches (specifically HLA-DQB1 and HLA-DRB1), particularly in the range of 2–4 mismatches, are at an increased risk of

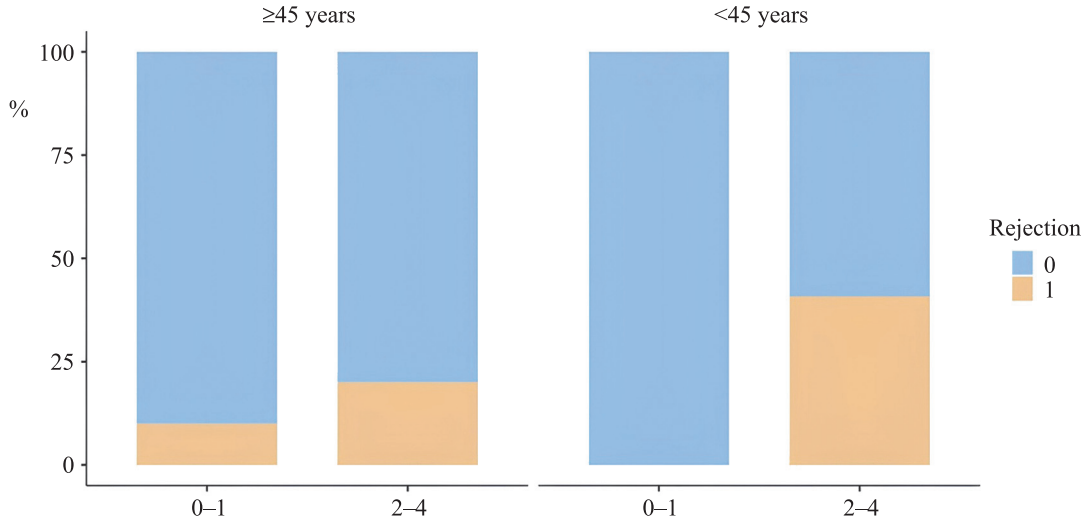

Fig. 7. Distribution of outcomes by MHC class II antigen mismatches and age

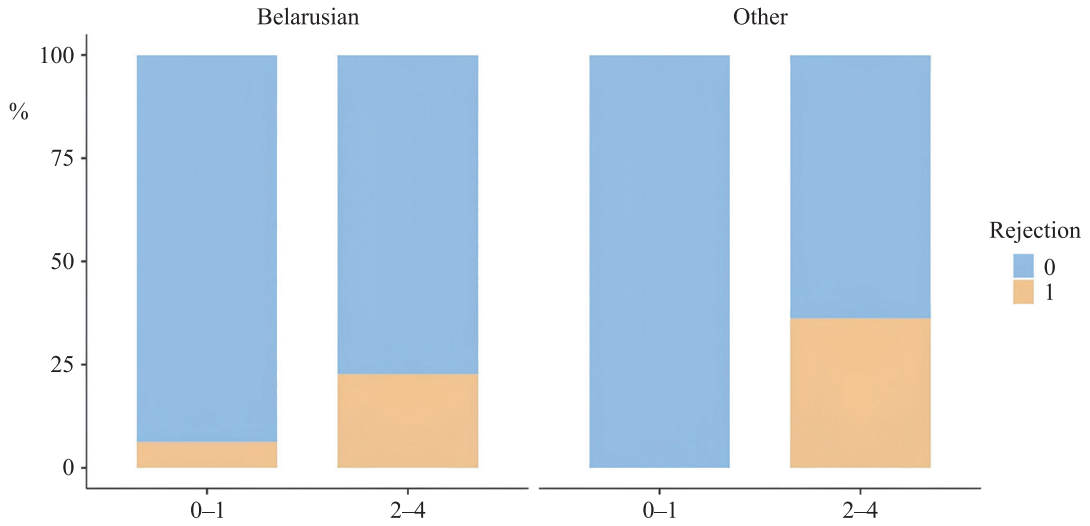

Fig. 8. Distribution of outcomes by MHC class II antigen mismatches and nationality

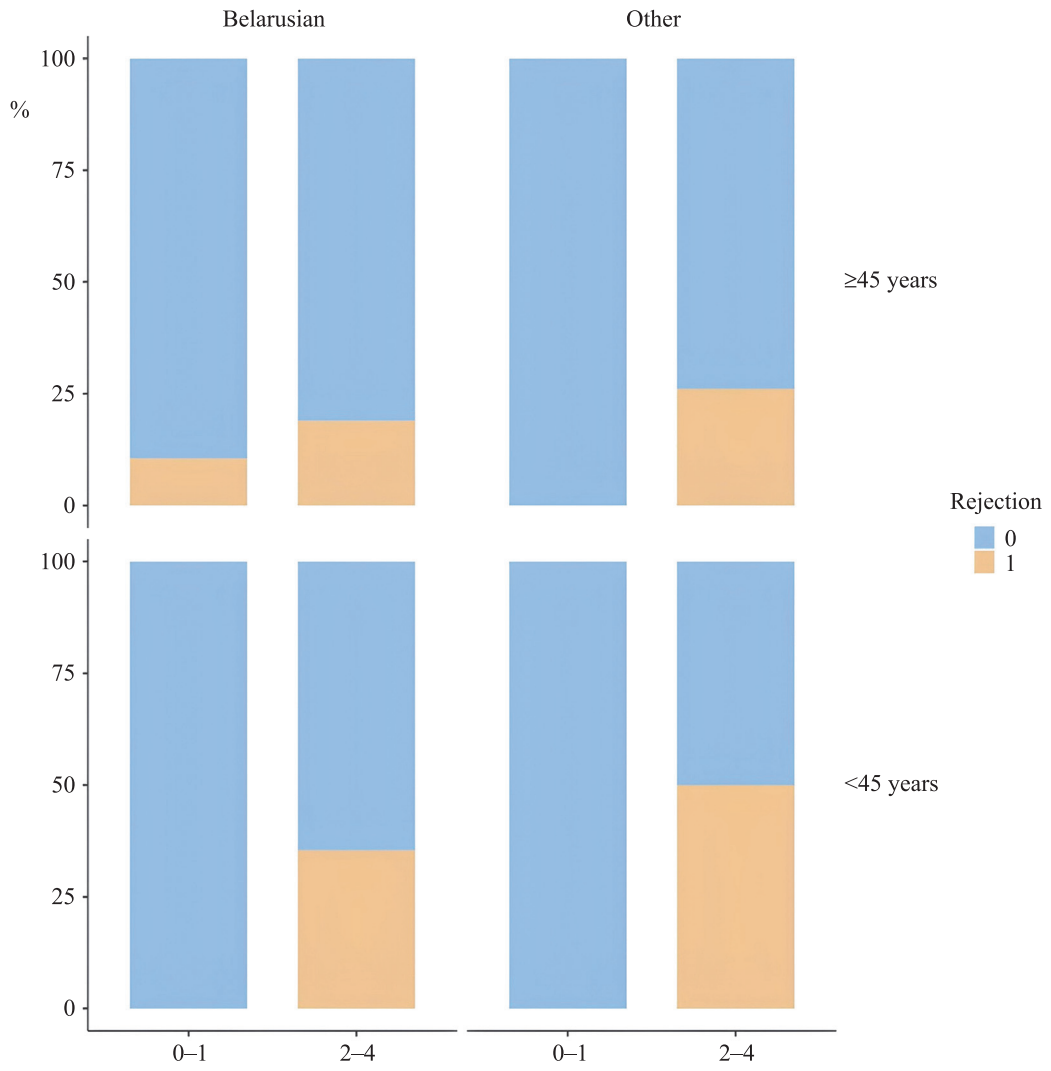

Fig. 9. Distribution of outcomes by MHC class II antigen mismatches, age and nationality

developing an AR in the postoperative period. In contrast, the role of MHC class I mismatches (HLA-A, HLA-B) in the onset of AR could not be conclusively confirmed.

Our findings are consistent with those reported by Johan Nilsson et al. in a 2019 publication in the Journal of the American Heart Association. That study showed that a high number of mismatches in HLA-A, HLA-B, and HLA-DR significantly reduced graft survival ($P < 0.001$). Conversely, the number of HLA-A/B/C mismatches was not associated with graft loss ($P = 0.584$), unlike mismatches in HLA-DR/DQ ($P = 0.025$). Specifically, recipients with more than four mismatched HLA-A/B/C alleles had an unadjusted OR for graft loss of 1.08 (95% CI: 0.99–1.19; $P = 0.099$), while those with four mismatched HLA-DR/DQ alleles had an OR of 1.13 (95% CI: 1.03–1.23; $P = 0.009$) [26].

A retrospective study conducted by Nitta et al. found that the number of HLA-DR mismatches was significantly associated with AR ($p = 0.029$). In their univariate analysis, having two HLA-DR mismatches was identified as the only independent risk factor for the development of AR episodes ($p = 0.017$). While our findings do not align with those of Nitta et al., this discrepancy may be attributed to the smaller sample size in our study, where the number of recipients with 0 HLA-DRB1 mismatches was limited. This issue warrants further investigation.

Regarding the HLA-DQB1 antigen, there is a lack of major studies investigating its impact on adult recipients. However, in 2024, Wright et al. published a study examining HLA-DQB1 mismatches in pediatric transplantation. Their results showed that recurrence-free survival at 5 years was higher in children with 0 DQB1 mismatches (68%) compared to those with 1 (62%) or 2 (63%) mismatches ($p = 0.08$ for both comparisons). Interestingly, rejection was most frequently observed in children with darker skin tones. In our study, recipients under 18 years of age were excluded due to specific study parameters, making direct comparison with the pediatric study less valid. Nevertheless, the findings by Wright et al., along with the limited adult-focused stu-

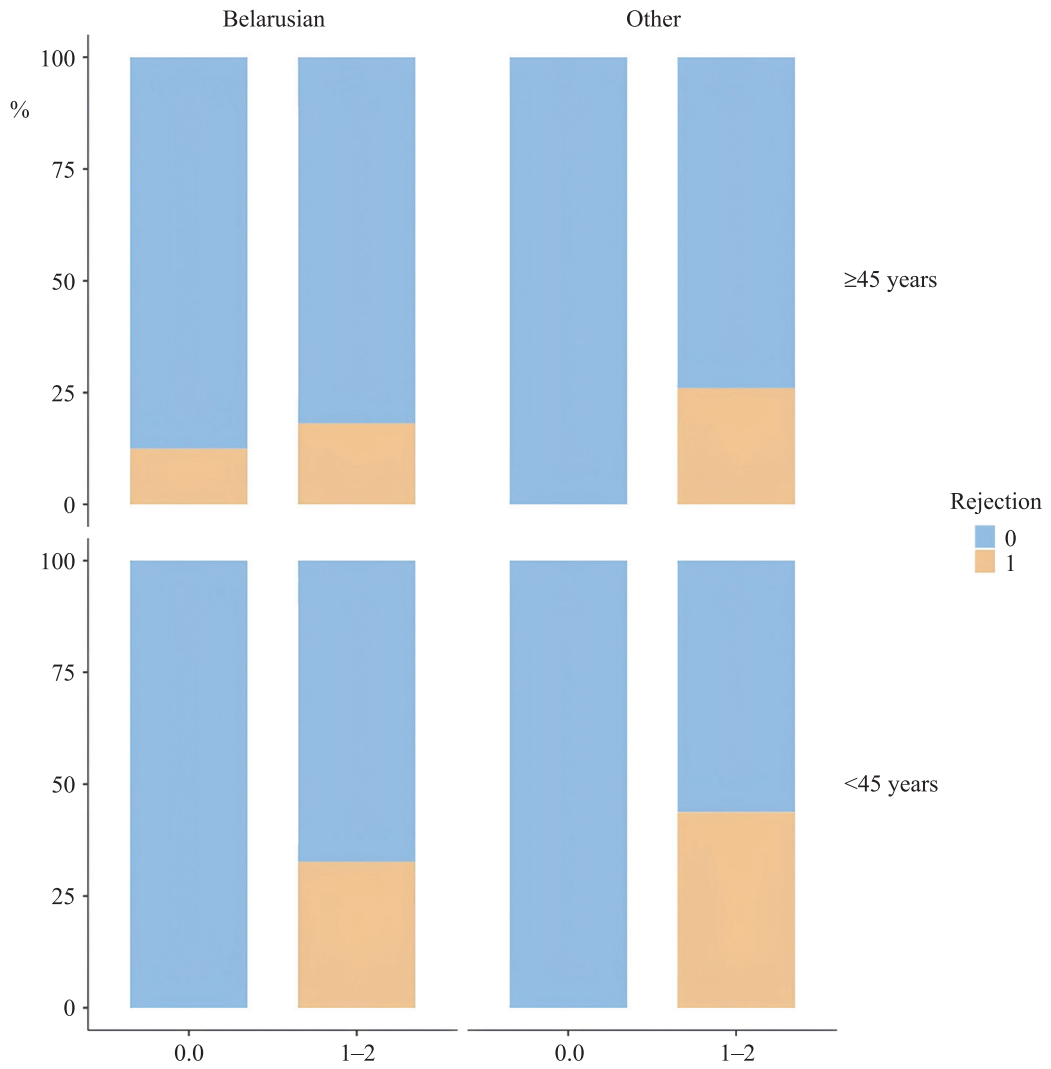

Fig. 10. Distribution of outcomes by HLA-DRB1 mismatches, age and nationality

dies, highlight the need for further investigation into the role of this antigen.

In our study, recipient age (<45 years) and nationality were identified as additional independent risk factors for heart transplant, each significantly increasing the odds of developing an AR – 2.00-fold (CI 95% 1.06 to 3.79) for nationality and 2.30-fold (CI 95% 1.29 to 4.10) for age. These findings are consistent with results from several international studies and systematic reviews [22–24].

When analyzing the combined influence of risk factors, with MHC class II mismatches as the primary factor and recipient age and nationality as secondary factors, we were able to reliably identify the groups at the highest risk for AR. Notably, when considering the combination of HLA-DQB1 mismatches, age, and nationality, a significant effect was observed in recipients of other nationalities under 45 years old. This highlights the importance of further research into the roles of both HLA-DRB1 and HLA-DQB1 antigens in predicting AR risk.

CONCLUSION

1) It was reliably established that MHC class II mismatches, donor-recipient nationality differences, and younger recipient age (<45 years) are all significant risk factors for AR following transplantation.
2) Two groups were identified as most at risk for AR: recipients of Belarusian nationality under 45 years old, and recipients of other nationalities younger than 45 years old. In the presence of 0–1 MHC class II incompatibility, the rejection rate was 0% in both groups. However, with 2–4 mismatches, the rejection rate increased to 35.40% for Belarusian recipients and 50.00% for recipients of other nationalities.
3) The HLA-DQB1 antigen was found to contribute most to the development of AR in non-Belarusian recipients.

The authors declare no conflict of interest.

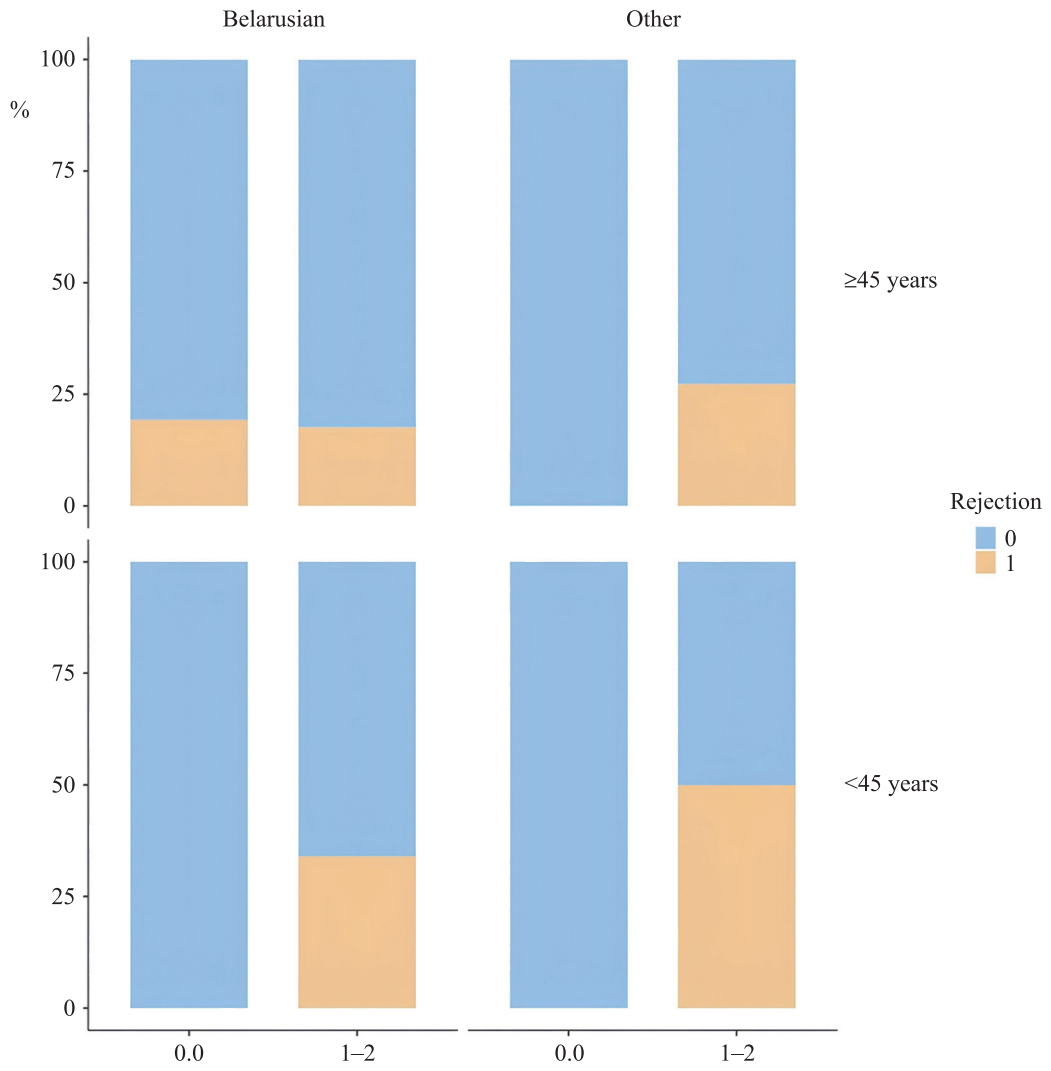

Fig. 11. Distribution of outcomes by HLA-DQB1 mismatches, age and nationality

REFERENCES

1. *Kolyubaeva SN, Myakoshina LA, Eliseeva MI, Glushakov RI*. HLA typing methods used for organ and tissue transplantation. *Russian Military Medical Academy Reports*. 2021; 40 (2): 21–32. [In Russ, English abstract]. doi: https://doi.org/10.17816/rmmar81197.
2. *Thatl LK, Kosmacheva ED, Kompaniets OG*. Humoral Rejection of the Transplanted Heart. *Difficult patient*. 2017; 15 (6–7): 14–18. [In Russ, English abstract].
3. *Marino J, Paster J, Benichou G.* Allorecognition by T Lymphocytes and Allograft Rejection. *Front Immunol*. 2016 Dec 14; 7: 582. doi: 10.3389/fimmu.2016.00582. eCollection 2016.
4. Immunobiology – The Immune System in Health and Disease (5th Ed.) / C.A. Janeway, P. Travers, M. Walport, M. Shlomchik (Eds.). New York: Garland Science, 2001; 910.
5. *Kumbala D, Zhang R.* Essential concept of transplant immunology for clinical practice. *World J Transplant*. 2013 Dec 24; 3 (4): 113–118. doi: 10.5500/wjt.v3.i4.113. PMCID: PMC3879520. PMID: 24392315.
6. *Oli AN, Babajide Rowaiye A, Adejumo SA, Anazodo FI, Ahmad R, Sinha S et al.* Classic and Current Opinions in Human Organ and Tissue Transplantation. *Cureus*. 2022 Nov 1; 14 (11): e30982. doi: 10.7759/cureus.30982. PMCID: PMC9624478. PMID: 36337306.
7. *Alelign T, Ahmed MM, Bobosha K, Tadesse Y, Howe R, Petros B*. Kidney Transplantation: The Challenge of Human Leukocyte Antigen and Its Therapeutic Strategies. *J Immunol Res*. 2018 Mar 5; 2018: 5986740. doi: 10.1155/2018/5986740. PMCID: PMC5859822. PMID: 29693023.
8. *Wieczorek M, Abualrous ET, Sticht J, Álvaro-Benito M, Stolzenberg S, Noé F, Freund C*. Major Histocompatibility Complex (MHC) Class I and MHC Class II Proteins: Conformational Plasticity in Antigen Presentation. *Front Immunol*. 2017 Mar 17; 8: 292. doi: 10.3389/fimmu.2017.00292. PMID: 28367149. PMCID: PMC5355494.
9. *Berger A*. Hla typing. *BMJ*. 2001 Jan 27; 322 (7280): 218. doi: 10.1136/bmj.322.7280.218. PMCID: PMC1119473. PMID: 11159622.
10. *Klein J, Sato A.* The HLA system. First of two parts. *N Engl J Med*. 2000 Sep 7; 343 (10): 702–709. doi: 10.1056/NEJM200009073431006.

11. *Richardson BC*. Role of DNA Methylation in the Regulation of Cell Function: Autoimmunity, Aging and Cancer. *J Nutr*. 2002 Aug; 132 (8 Suppl): 2401S–2405S. doi: 10.1093/jn/132.8.2401S. PMID: 12163700.
12. *Rammensee HG.* Chemistry of peptides associated with MHC class I and class II molecules. *Curr Opin Immunol*. 1995 Feb; 7 (1): 85–96. doi: 10.1016/0952-7915(95)80033-6. PMID: 7772286.
13. *Rammensee HG*. Peptides Made to Order. *Immunity*. 2006 Nov; 25 (5): 693–695. doi: 10.1016/j.immuni.2006.10.008. PMID: 17098199.
14. *Deres K, Beck W, Faath S, Jung G, Rammensee HG*. MHC/Peptide Binding Studies indicate Hierarchy of Anchor Residues. *Cell Immunol*. 1993 Oct 1; 151 (1): 158–167. doi: 10.1006/cimm.1993.1228. PMID: 8402926.
15. *Brown JH, Jardetzky TS, Gorga JC, Stern LJ, Urban RG, Strominger JL, Wiley DC*. Three-dimensional structure of the human class II histocompatibility antigen HLA-DR1. *Nature*. 1993 Jul 1; 364 (6432): 33–39. doi: 10.1038/364033a0. PMID: 8316295.
16. *Cantani A*. Pediatric Allergy, Asthma and Immunology. Berlin, Heidelberg: Springer, 2008; 1618. https://doi.org/10.1007/978-3-540-33395-1_1.
17. *Lim WH, Chapman JR, Coates PT, Lewis JR, Russ GR, Watson N et al*. HLA-DQ Mismatches and Rejection in Kidney Transplant Recipients. *Clin J Am Soc Nephrol*. 2016 May 6; 11 (5): 875–883. doi: 10.2215/CJN.11641115. Epub 2016 Mar 31. PMID: 27034399. PMCID: PMC4858494.
18. *Wiebe C, Kosmoliaptsis V, Pochinco D, Gibson IW, Ho J, Birk PE et al.* HLA-DR/DQ molecular mismatch: A prognostic biomarker for primary alloimmunity. *Am J Transplant*. 2019 Jun; 19 (6): 1708–1719. doi: 10.1111/ajt.15177. Epub 2018 Dec 15. PMID: 30414349. PMCID: PMC6563434.
19. *Peltz M, Edwards LB, Jessen ME, Torres F, Meyer DM*. HLA mismatches influence lung transplant recipient survival, bronchiolitis obliterans and rejection: implications for donor lung allocation. *J Heart Lung Transplant*. 2011 Apr; 30 (4): 426–434. doi: 10.1016/j.healun.2010.10.005. Epub 2010 Dec 8. PMID: 21145259.
20. *Kok G, Ilcken EF, Houwen RHJ, Lindemans CA, Nieuwenhuis EES, Spierings E, Fuchs SA*. The Effect of Genetic HLA Matching on Liver Transplantation Outcome: A Systematic Review and Meta-Analysis. *Ann Surg Open*. 2023 Sep 15; 4 (3): e334. doi: 10.1097/AS9.0000000000000334. eCollection 2023 Sep. PMID: 37746594. PMCID: PMC10513352.
21. *Althaf MM, El Kossi M, Jin JK, Sharma A, Halawa AM*. Human leukocyte antigen typing and crossmatch: A comprehensive review. *World J Transplant*. 2017 Dec 24; 7 (6): 339–348. doi: 10.5500/wjt.v7.i6.339. PMID: 29312863. PMCID: PMC5743871.
22. *Kobashigawa JA, Kirklin JK, Naftel DC, Bourge RC, Ventura HO, Mohanty PK et al.* Pretransplantation risk factors for acute rejection after heart transplantation: a multiinstitutional study. The Transplant Cardiologists Research Database Group. *J Heart Lung Transplant*. 1993 May-Jun; 12 (3): 355–366. PMID: 8329404.
23. *Wever-Pinzon O, Edwards LB, Taylor DO, Kfoury AG, Drakos SG, Selzman CH et al.* Association of recipient age and causes of heart transplant mortality: Implications for personalization of post-transplant management – An analysis of the International Society for Heart and Lung Transplantation Registry. *J Heart Lung Transplant*. 2017 Apr; 36 (4): 407–417. doi: 10.1016/j.healun.2016.08.008. Epub 2016 Aug 20. PMID: 27686602.
24. *Morris AA, Kransdorf EP, Coleman BL, Colvin M*. Racial and ethnic disparities in outcomes after heart transplantation: A systematic review of contributing factors and future directions to close the outcomes gap. *J Heart Lung Transplant*. 2016 Aug; 35 (8): 953–961. doi: 10.1016/j.healun.2016.01.1231. Epub 2016 Feb PMID: 27080415. PMCID: PMC6512959.
25. *Butts RJ, Savage AJ, Nietert PJ, Kavarana M, Moussa O, Burnette AL, Atz AM.* Effect of HLA-C and -DQ matching on Pediatric Heart Transplant Graft Survival. *J Heart Lung Transplant*. 2014 Dec; 33 (12): 1282–1287. doi: 10.1016/j.healun.2014.07.014. Epub 2014 Jul 2. doi: 10.1016/j.healun.2014.07.014. PMID: 25128416. PMCID: PMC4252914.
26. *Nilsson J, Ansari D, Ohlsson M, Höglund P, Liedberg AS, Smith JG et al.* Human Leukocyte Antigen-Based Risk Stratification in Heart Transplant Recipients – Implications for Targeted Surveillance. *J Am Heart Assoc*. 2019 Aug 6; 8 (15): e011124. doi: 10.1161/JAHA.118.011124. Epub 2019 Jul 24. PMID: 31339067. PMCID: PMC6761633.
27. *Nitta D, Kinugawa K, Imamura T, Iino J, Endo M, Amiya E et al.* Association of the Number of HLA-DR Mismatches With Early Post-transplant Acute Cellular Rejection Among Heart Transplantation Recipients: A Cohort Study in Japanese Population. *Transplant Proc*. 2017 Jan-Feb; 49 (1): 125–129. doi: 10.1016/j.transproceed.2016.11.001. PMID: 28104119.
28. *Wright LK, Gajarski RJ, Hayes E, Parekh H, Yester JW, Nandi D*. DQB1 antigen matching improves rejection-free survival in pediatric heart transplant recipients. *J Heart Lung Transplant*. 2024 May; 43 (5): 816–825. doi: 10.1016/j.healun.2024.01.008. PMID: 38232791.

The article was submitted to the journal on 9.12.2024

DOI: 10.15825/1995-1191-2025-2-81-88

BENCH STUDIES OF A SMALL AXIAL PUMP FOR IMPLANTATION IN PATIENTS WITH LOW ANTHROPOMETRY

A.S. Buchnev[1], A.P. Kuleshov[1], A.A. Drobyshev[1], V.A. Elenkin[1], G.A. Shevchenko[2], N.V. Grudinin[1]

[1] Shumakov National Medical Research Center of Transplantology and Artificial Organs, Moscow, Russian Federation

[2] Peoples' Friendship University of Russia named after Patrice Lumumba, Moscow, Russian Federation

Objective: to conduct bench tests and determine the working range of the pump speed for an implanted left ventricular bypass system aimed at diagnosing and treating patients with low anthropometric status. **Materials and methods.** The axial pump was investigated using a custom-developed hydrodynamic test bench simulating the cardiovascular system. The bench included systems for pressure and flow measurement and registration, along with software for processing both technical and biomedical parameters. **Results.** The operating range of the rotor speed for the STREAM CARDIO pump required to achieve a flow rate of 2.5 ± 0.5 L/min at a pressure drop of 80 ± 5 mm Hg is 8000 ± 1000 rpm, with a power consumption of 6.5 ± 1 W.

Keywords: heart failure, left ventricular bypass, hydrodynamic bench, pump flow rate, pump head, axial pump.

INTRODUCTION

Heart transplantation remains the gold standard treatment for patients with end-stage heart failure (HF) [1]. However, a critical shortage of organs continues to pose a major challenge. Despite efforts to expand donor eligibility, many patients die while waiting for a suitable heart [2].

Over the past decade, significant progress has been made in the use of mechanical circulatory support (MCS) systems for managing HF [3]. MCS, including first-, second-, and third-generation left ventricular assist devices (LVADs), is increasingly being adopted as a viable treatment option for end-stage HF [4–7].

First-generation devices include pneumatically driven systems such as the Thoratec (Thoratec Laboratories Corporation, USA) and EXCOR (Berlin Heart, Germany) ventricular assist devices, which are used in both adult and pediatric patients. However, these systems are associated with some limitations, including the extracorporeal placement of artificial ventricles and the bulky size of external actuators. Additionally, these devices had a limited lifespan and relatively low reliability [8].

Second-generation devices include low-pulsatile flow rotary pumps, such as the HeartAssist (MicroMed Cardiovascular, Houston), Jarvik 2000 FlowMaker (Jarvik Heart, Inc., New York), HeartMate II (Thoratec Corporation, Pleasanton, CA), AVK-N (Russia), and Stream Cardio (Dona-M, Russia). These systems are small in size and weight, silent, relatively inexpensive, have enhanced reliability and service life [9–11].

Third-generation devices consist of pumps equipped with electromagnetic drives. Notable systems in this category include the Incor axial pump (Berlin Heart AEG), HeartWare HVAD centrifugal pump (HeartWare, Inc., Miami Lakes, FL), HeartMate III (Thoratec Inc., Pleasanton, CA), EvaHeart LVAS (Sun Medical Technology Research Corporation, Nagano, Japan), and Terumo DuraHeart (Terumo Heart Inc., Ann Arbor, MI) [12–14].

In many cardiology centers, implanted MCS has become one of the primary treatment modalities for adult patients with end-stage chronic heart failure (CHF). However, in children and patients with small anthropometric measurements, the implantation of circulatory support systems is often constrained by limited body surface area, low body weight, and an insufficiently sized thoracic cavity to accommodate the device.

As Russian-made pediatric pump systems remain under development, and the HeartMate III is primarily used for patients with a low body mass index, we propose considering the use of the compact axial-flow pump Stream Cardio (LLC "DONA-M", Russia). Although originally designed for patients with a high body mass index, this device can also function effectively at reduced blood flow rates (2 ± 0.5 L/min).

The operational control of implanted MCS systems is typically based on maintaining a preset pump rotor speed (PS), which ensures the required blood flow to sustain vital organ function [15]. This RS is established intraoperatively and subsequently adjusted throughout the phases of postoperative care and patient rehabilitation [16].

Corresponding author: Alexander Buchnev. Address: 1, Shchukinskaya str., Moscow, 123182, Russian Federation. Phone: (926) 470-09-88. E-mail: labbts@mail.ru

Alternatively, rotor speed, pressure differential across the pump, blood flow, and power consumption can be estimated indirectly by analyzing the pump's flow-pressure curve (FPC) [17–20]. These FPC data can be obtained both during isolated pump operation and in conjunction with a ventricular assist device.

The present study presents bench testing of the Stream Cardio axial rotary pump, focusing on its flow-pressure, energy, and hemodynamic characteristics. These data help determine the optimal operating speed ranges of the pump for use in clinical settings, particularly for patients with low body mass index (BMI) requiring left ventricular bypass (LVB).

MATERIALS AND METHODS

Stream Cardio is a compact axial-flow blood pump with an outer diameter of 28 mm, a length of 60 mm, a weight of 120 grams, and operates at speeds between 5000 and 10000 rpm. It can deliver up to 10 liters of blood per minute and is powered by a control unit with a single rechargeable battery and AC adapter. Since 2020, it has been implanted in Russian patients either as a long-term support or for bridge-to-transplant use, effectively replacing left ventricular function in patients with HF. The device is implanted via the apex of the left ventricle, with its outlet connected to either the ascending or descending aorta.

The core component of the axial flow pump is the impeller with vanes, which generates rotational energy and imparts it to the blood, initiating and directing flow (Fig. 1). The impeller is mounted on bearings at both ends, ensuring stable rotation. Downstream of the impeller is a flow straightener – a stationary blade assembly oriented opposite to the direction of impeller rotation. This component induces a "reverse spinning" effect, which transforms the kinetic energy of the rotating blood into pressure-based potential energy [21].

The pump's DC motor stator is integrated directly into the pump casing, while permanent magnets are embedded within the impeller.

In the initial stage of the study, FPCs were obtained using a hydrodynamic bench setup to determine the operating range of pump speeds at low blood flow rates and axial pump power (Fig. 2).

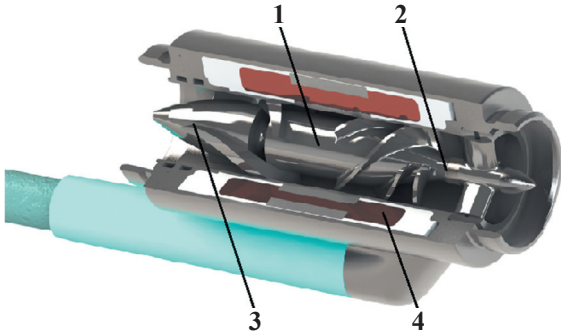

Fig. 1. 3D model of axial pump: 1, pump impeller; 2, bearing; 3, flow straightener; 4, electric motor stator

The hydrodynamic bench (HB) comprises a 400 mL CAPIOX reservoir (Terumo), 10 mm diameter Tygon tubing (Saint-Gobain, France), a variable hydraulic resistance, and integrated pressure and flow sensors. Pump inlet and outlet pressures of the HB were measured using Edwards pressure transducers (Life Sciences), while flow rates were recorded with a Transonic TS402 ultrasonic flow sensor (Transonic Systems Inc., USA) positioned on the bench outlet line.

Pressure and flow measurements were monitored via a multichannel Angioton module (Biosoft-M, Russia) and visualized in real-time using Pumpax software (Biosoft-M, Russia). The pump's rotor speed was adjusted systematically, and at each set speed, the corresponding pressure drop vs. flow rate curve was plotted by varying the inlet and outlet pressures.

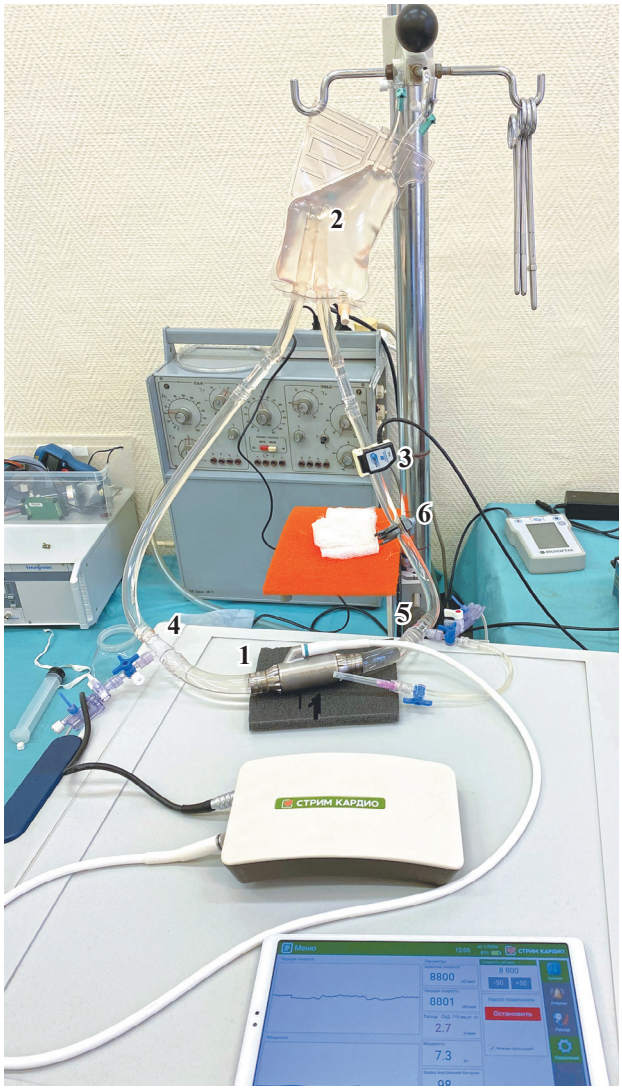

Fig. 2. Mock circulation loop. 1, axial pump; 2, tank; 3, fluid flow sensor; 4–5, pressure sensors at the pump inlet and outlet; 6, hydraulic resistance

In the second stage of the study, hemodynamic parameters of the axial flow pump at low blood flow conditions were evaluated within a LVB configuration, using a hydrodynamic bench designed to simulate the cardiovascular system (CVS) [22].

The CVS model incorporated key physiological characteristics, including arterial compliance (pliability/elasticity), inertia, total hydraulic resistance, a programmable heart ventricle simulator, replicating left ventricular contractility, including parameters such as heart rate, systole/diastole ratio, and corresponding pressure and flow profiles.

HF conditions were simulated by adjusting pressure in the artificial heart ventricle using the Sinus IS control system (Russia) and modifying peripheral resistances, while aortic capacitance remained unchanged. The system was initially set to reflect HF hemodynamics with the following baseline parameters: mean aortic flow 1 ± 0.3 L/min, mean arterial pressure (MAP) 65 ± 5 mmHg, mean left atrial pressure 20 ± 1 mmHg.

Following this, the pump was activated in LVB mode, leading to the restoration of hemodynamics flow rate 2.5 ± 1 L/min, MAP 80 ± 5 mm Hg, and mean atrial pressure 5 ± 1 mm Hg.

The obtained data were processed and summarized in Table.

RESULTS

The performance of the circulatory assist pump is inherently linked to cardiac hemodynamics. During each cardiac cycle, the contractility of the heart fluctuates in response to varying physiological conditions, particularly changes in preload and afterload, which lead to changes in pump parameters, namely pump power and fluid flow through the pump.

Fig. 4 presents the hydrodynamic parameters recorded on the HB across a range of pump speeds from 5000 to 10000 rpm.

Analysis of the obtained differential pressure and flow curves indicates that, to achieve a target flow rate of 2.5 ± 0.5 L/min, the rotational speed of the Stream Cardio axial flow pump must be maintained within the range of 8000 ± 1000 rpm. The Stream Cardio pump exhibits a relatively steep FPC, indicating that its output is less sensitive to variations in pressure differential.

The pressure difference across the pump can be approximated by the gradient between left ventricular pressure and aortic pressure. Consequently, the pump flow is inversely proportional to this pressure difference, as illustrated in Fig. 5.

This flow behavior is observed throughout each cardiac cycle: during diastole, as the pressure difference across the pump increases, flow rate decreases; conversely, during systole, when the pressure gradient narrows, flow rate increases.

Pump power – a function of the voltage and current supplied to the pump motor – serves as a direct indicator of mechanical load and system performance. Power output fluctuates in response to hemodynamic variations or pathophysiological changes. For instance, pump power

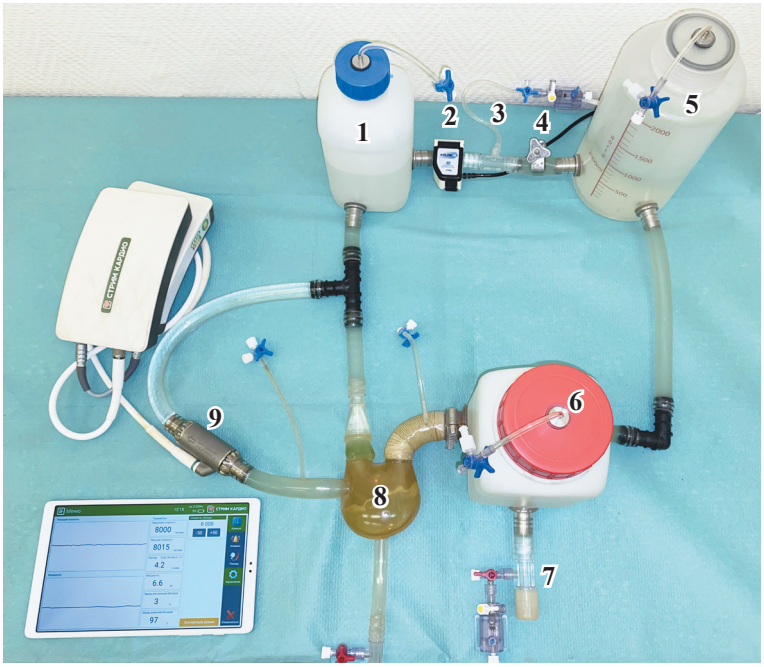

Fig. 3. Mock circulation loop. 1, arterial reservoir; 2, aortic flow sensor; 3, arterial pressure measurement sensor; 4, systemic hydraulic resistance; 5, venous reservoir; 6, reservoir simulating the "pulmonary veins, left atrium" system; 7, atrial pressure measurement sensor; 8, cardiac ventricle simulator simulating the left ventricle of the heart during a left ventricular bypass; 9, test pump

may rise in the presence of reduced blood viscosity or onset of rotor thrombosis, with such changes occurring either gradually or abruptly. Power also varies with preload and afterload conditions, and the sensitivity of this relationship is modulated by the pump's set rotational speed (see Fig. 6).

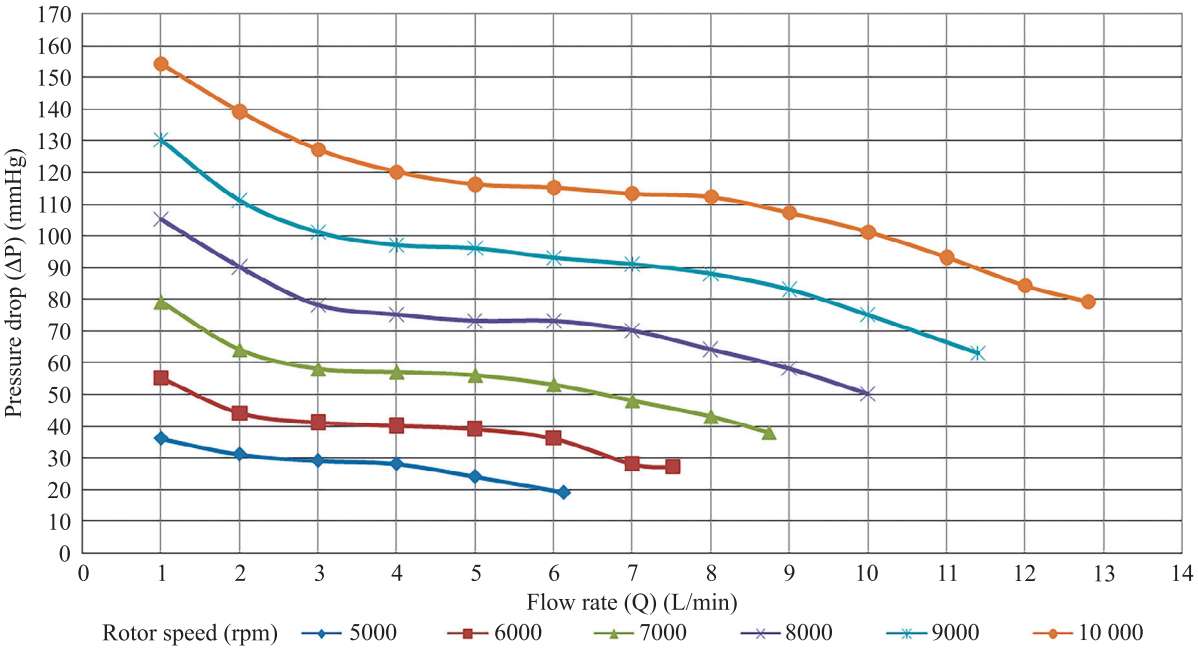

Fig. 4. Flow-pressure curve of the Stream Cardio left ventricular assist device

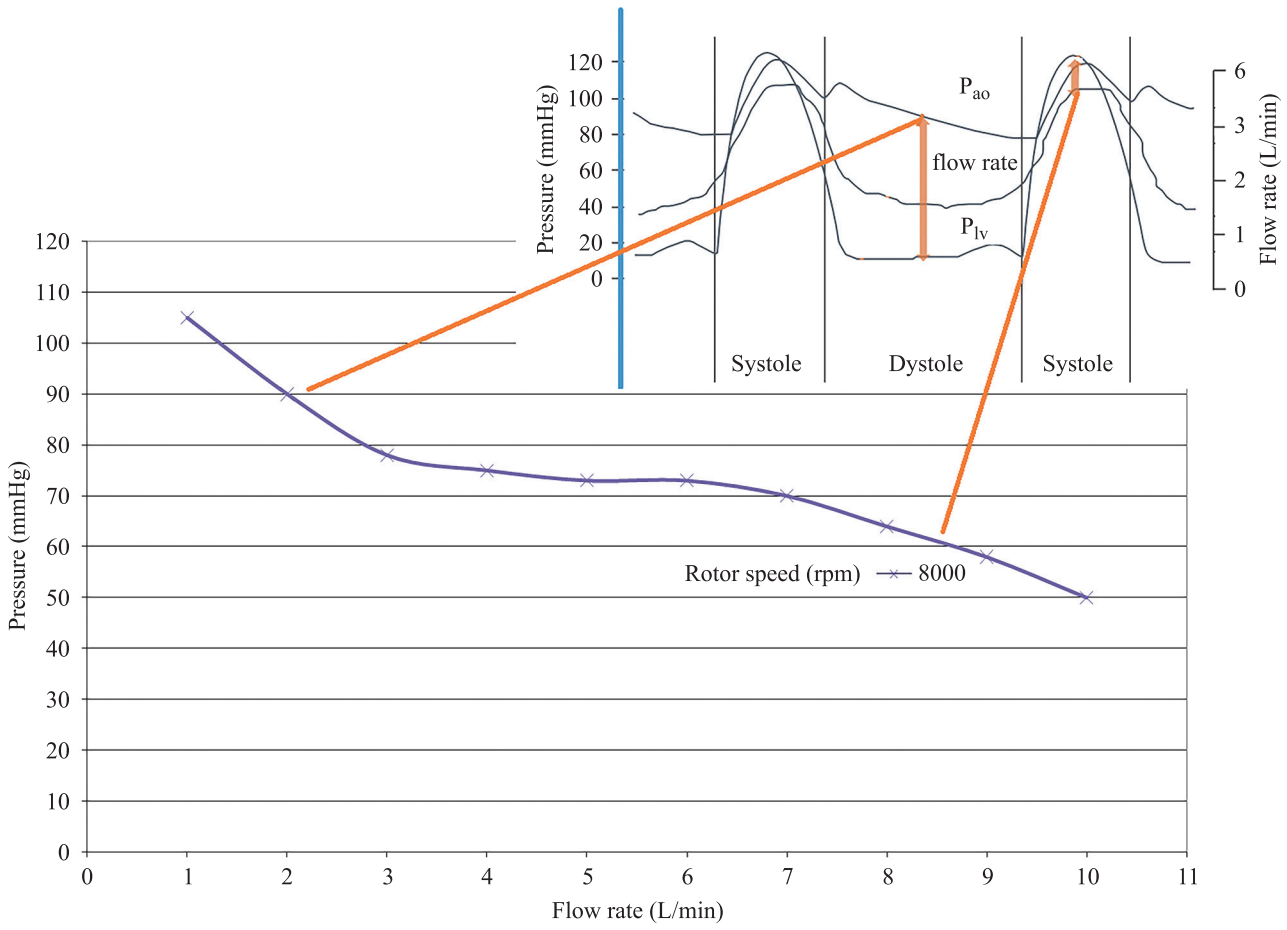

Fig. 5. Flow variation in the pump during cardiac cycle. P_{AO}, aortic pressure; P_{LV}, left ventricular pressure

The design constraints of the axial flow pump inherently limit its speed and flow rate. To achieve a target flow of 2.5 ± 0.5 L/min, the Stream Cardio pump requires a rotational speed of about 8000 ± 1000 rpm, with an associated power consumption of 6.5 ± 1 W.

This low power requirement is a key advantage, as it contributes to reduction in size and weight of critical system components – namely, the control unit and battery pack. Consequently, this enhances autonomous operation time, extending the period between battery replacements.

Fig. 7 presents the hemodynamic parameters of CVS under HF conditions and during Stream Cardio operation in LVB mode. Flow during LVB was provided by pump

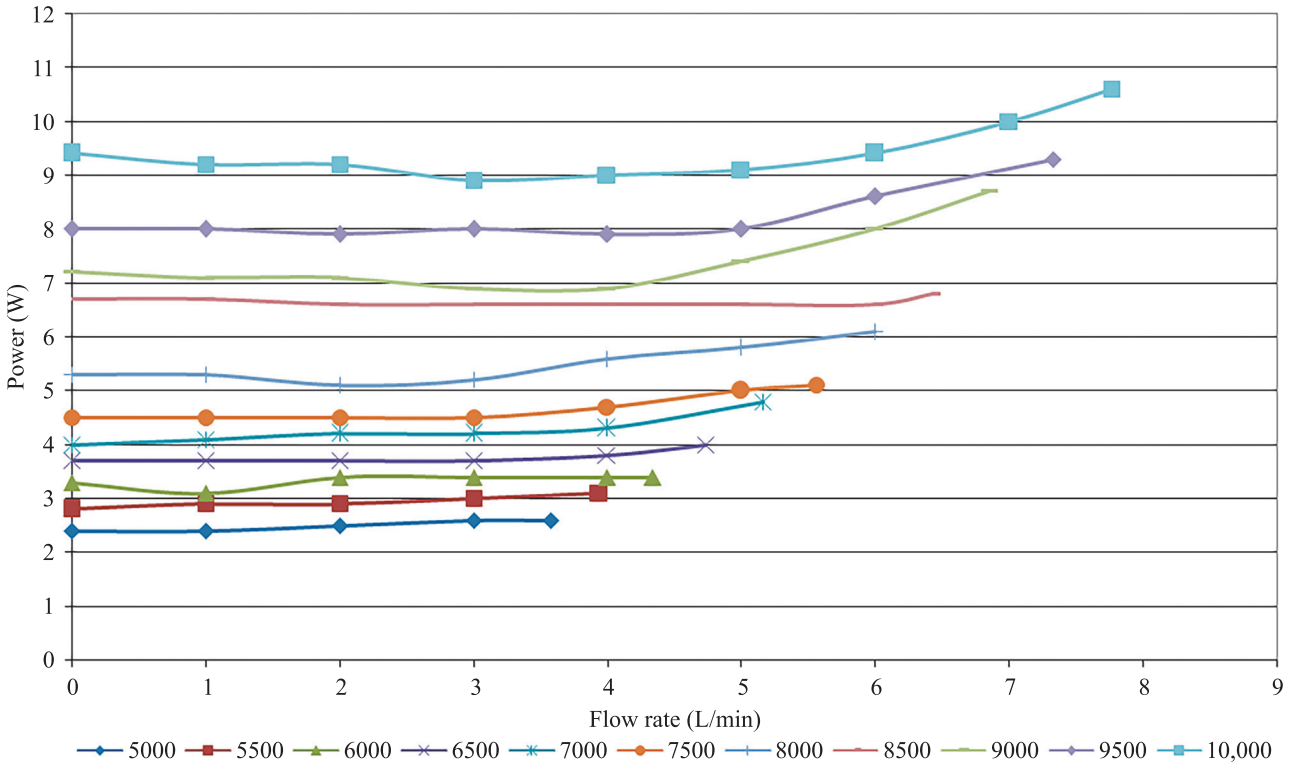

Fig. 6. Flow-power curve of the Stream Cardio ventricular assist device

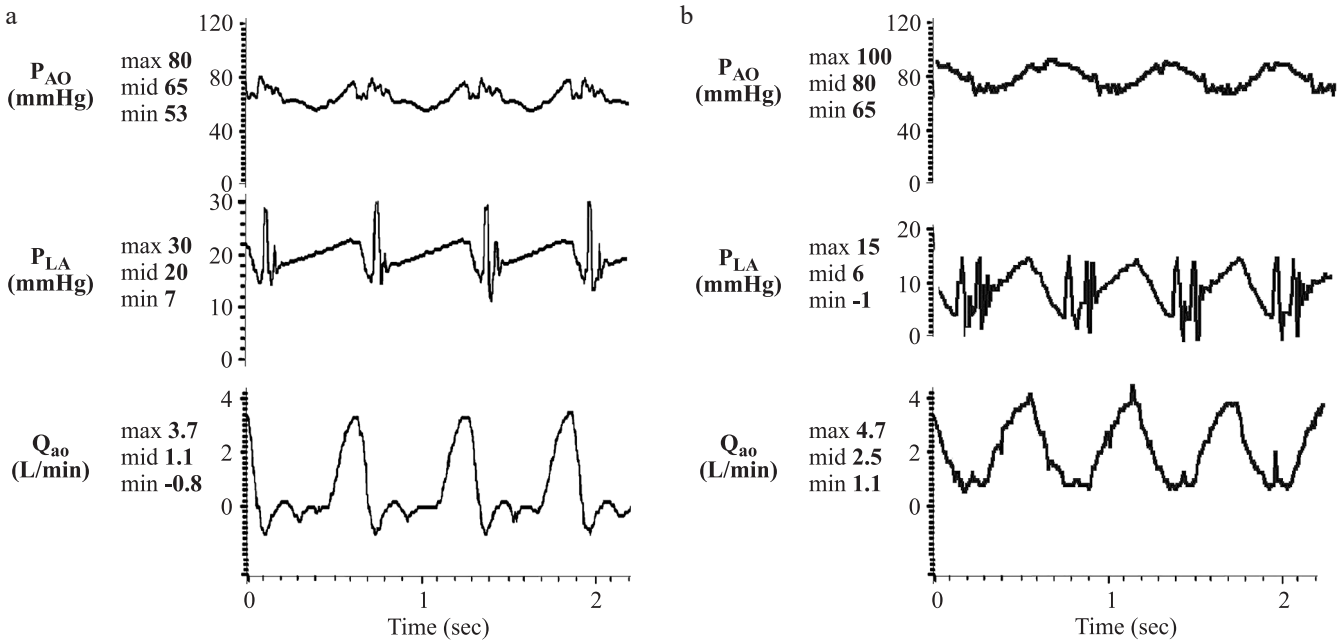

Fig. 7. Hemodynamic parameters of Stream Cardio under conditions of heart failure (a) and left ventricular bypass (b). P_{AO}, aortic pressure; P_{LA}, left atrial pressure; Q_{AO}, aortic flow

Table

Hemodynamic parameters of the Stream Cardio pump at different rotor speeds under conditions of left ventricular bypass

Rotor speed (rpm)	P_{AO} (mmHg)	P_{LA} (mmHg)	Q_{AO} (L/min)
6900	90/75/65	5	1.5
7300	91/75/61	4	2.0
7800	95/75/59	3	2.5
8100	95/75/60	5	3.0
7000	95/80/69	4	1.5
7500	95/80/70	4	2.0
8100	100/80/65	6	2.5
8400	100/80/64	4	3.0
7400	103/85/73	4	1.5
7900	102/85/71	5	2.0
8400	104/85/69	3	2.5
8700	105/85/71	4	3.0
7700	110/90/76	3	1.5
8100	107/90/75	4	2.0
8600	109/90/73	4	2.5
8900	110/90/73	3	3.0

Note. P_{AO}, aortic pressure; P_{LA}, mean left atrial pressure; Q_{ao}, aortic flow.

speed 8100 ± 50 rpm, MAP at 80 ± 2 mm Hg, and mean aortic flow of 2.5 ± 0.1 L/min.

Table presents the summarized results of key hemodynamic parameters, including various combinations of aortic flow and MAP, measured at specific pump speeds in the LVB configuration.

According to the data in Table, achieving a target flow rate of 2.5 ± 0.5 L/min at a pressure gradient of 80 ± 5 mmHg requires a pump speed of approximately 8000 ± 1000 rpm for the Stream Cardio device.

These experimentally derived values of pump speed under both hydrodynamic and hemodynamic testing conditions at defined MAP levels provide an indirect estimation of the blood flow needed to sustain vital organ function.

The *in vitro* data obtained on pump speed and power consumption of the Stream Cardio pump at low flow conditions offer valuable guidance for defining optimal operating modes during left ventricular bypass procedures, particularly in patients with low BMI. This enables precise adjustment of pump speed during both intraoperative support and the rehabilitation phase.

DISCUSSION

The Stream Cardio pump operates on a relatively steep FPC curve, which makes it less sensitive to changes in the pressure differential that are typical for axial flow pumps. Despite its compact size, the pump is capable of providing sufficient power to achieve a pressure drop of 80 ± 5 mm Hg at a flow rate of 2.5 ± 0.5 L/min.

In LVB mode, at a flow rate of 2.5 ± 0.5 L/min, the rotor speed of the Stream Cardio pump is set at 8000 ± 1000 rpm, which is similar to the rotor speed of the HeartMate II pump. The HeartMate II has been FDA approved since April 2008 and has been implanted over 27,000 times [23], including in four adolescent patients aged 12 to 15 years, with body surface areas ranging from 1.5 m^2 to 1.7 m^2 [24]. The primary goal of these pumps is to enhance systemic cardiac output and reduce ventricular loading throughout the cardiac cycle, while minimizing the risk of significant biological or hematologic complications. The hydrodynamic and hemodynamic characteristics of the Stream Cardio pump at low blood flow rates, combined with the encouraging clinical outcomes observed with the HeartMate II pump in adolescent patients, suggest that the Stream Cardio pump holds significant potential for clinical application in patients with small anthropometric indices, for accurate assessment, diagnosis and treatment of such patients during left ventricular bypass procedures.

CONCLUSION

In today's rapidly evolving medical landscape, it is crucial for the medical community to evaluate and integrate emerging technologies effectively. Programs aimed at supporting patients with drug-naive heart failure must consider a range of devices that can meet the diverse clinical needs and body sizes of patients. A more thorough understanding of the pressure-drop and flow relationship in LVADs will be instrumental in optimizing hemocompatibility and hydraulic efficiency during pump design.

Looking ahead, future research will focus on testing the Stream Cardio pump at low blood flow rates to evaluate potential blood element injury. Besides, a series of animal experiments will be conducted to assess and rule out thrombosis in the pump.

The authors declare no conflict of interest.

REFERENCES

1. *Hunt SA, Abraham WT, Chin MH, Feldman AM, Francis GS, Ganiats TG et al.* 2009 Focused update incorporated into the ACC/AHA 2005 Guidelines for the Diagnosis and Management of Heart Failure in Adults A Report of the American College of Cardiology Foundation/American Heart Association Task Force on Practice Guidelines Developed in Collaboration With the International Society for Heart and Lung Transplantation. *J Am Coll Cardiol*. 2009 Apr 14; 53 (15): e1–e90.
2. *Taylor DO, Stehlik J, Edwards LB, Aurora P, Christie JD, Dobbels F et al.* Registry of the International Society for Heart and Lung Transplantation: twenty-sixth official adult heart transplant report – 2009. *J Heart Lung Transplant*. 2009 Oct; 28 (10): 1007–1022.
3. *Slaughter MS, Pagani FD, Rogers JG, Miller LW, Sun B, Russell SD et al.* Clinical management of continuous-flow left ventricular assist devices in advanced heart fai-

lure. *J Heart Lung Transplant*. 2010 Apr; 29 (4 Suppl): S1–S39.
4. *Norman JC, Duncan JM, Frazier OH, Hallman GL, Ott DA, Reul GJ, Cooley DA.* Intracorporeal (abdominal) left ventricular assist devices or partial artificial hearts: A five-year clinical experience. *Arch Surg*. 1981 Nov; 116 (11): 1441–1445.
5. *Liotta D, Hall CW, Henly WS, Cooley DA, Crawford ES, Debakey ME*. Prolonged assisted circulation during and after cardiac or aortic surgery. prolonged partial left ventricular bypass by means of intracorporeal circulation. *Am J Cardiol*. 1963 Sep; 12: 399–405.
6. *DeBakey ME*. Left ventricular bypass pump for cardiac assistance. Clinical experience. *Am J Cardiol*. 1971 Jan; 27 (1): 3–11.
7. *DeBakey ME, Kennedy JH.* Mechanical circulatory support: current status. *Am J Cardiol*. 1971 Jan; 27 (1): 1–2.
8. *Oz MC, Rose EA, Levin HR*. Selection criteria for placement of left ventricular assist devices. *Am Heart J*. 1995 Jan; 129 (1): 173–177.
9. *Frazier OH, Rose EA, Macmanus Q, Burton NA, Lefrak EA, Poirier VL, Dasse KA.* Multicenter clinical evaluation of the HeartMate 1000 IP left ventricular assist device. *Ann Thorac Surg*. 1992 Jun; 53 (6): 1080–1090.
10. *Portner PM, Oyer PE, Pennington DG, Baumgartner WA, Griffith BP, Frist WR et al.* Implantable electrical left ventricular assist system: bridge to transplantation and the future. *Ann Thorac Surg*. 1989 Jan; 47 (1): 142–150.
11. *Gautier SV, Itkin GP, Shemakin SYu, Saitgareev RSh, Poptsov VN, Zakharevich VM et al*. The first experience in clinical application of domestic circulatory support device on basis of implantable axial pump for two stage heart transplantation. *Russian Journal of Transplantology and Artificial Organs*. 2013; 15 (3): 92–101. [In Russ, English abstract]. doi: 10.15825/1995-1191-2013-3-92-101.
12. *Rogers JG, Aaronson KD, Boyle AJ, Russell SD, Milano CA, Pagani FD et al.* Continuous flow left ventricular assist device improves functional capacity and quality of life of advanced heart failure patients. *J Am Coll Cardiol*. 2010 Apr 27; 55 (17): 1826–1834.
13. *Pagani FD, Miller LW, Russell SD, Aaronson KD, John R, Boyle AJ et al.* Extended mechanical circulatory support with a continuous-flow rotary left ventricular assist device. *J Am Coll Cardiol*. 2009 Jul 21; 54 (4): 312–321.
14. *Kirklin JK, Naftel DC, Kormos RL, Stevenson LW, Pagani FD, Miller MA et al*. Second INTERMACS annual report. More than 1,000 primary left ventricular assist device implants. *J Heart Lung Transplant*. 2010 Jan; 29 (1): 1–10.
15. *Stevenson LW, Kormos RL.* Mechanical cardiac support 2000: current applications and future trial design. *J Heart Lung Transpl*. 2001 Jan; 20 (1): 1–38.
16. *Itkin GP, Filatov IA, Dozorov KN, Adaskin AV*. Indirect methods of measuring flow rate and pressure drop of rotary blood pumps. *Russian Journal of Transplantology and Artificial Organs*. 2015; 17 (1): 97–102. [In Russ, English abstract]. doi: 10.15825/1995-1191-2015-1-97-102.
17. *Ayre PJ, Lowell NH, Woodard JC*. Non-invasive flow estimation in an implantable rotory pump: a study considering non-pulsatile and pulsatile flow. *Phyiol Meas*. 2003 Feb; 24 (1): 179–189.
18. *Funakibo A, Ahmed S, Sakuma I, Fukui Y.* Flow rate and pressure head estimation in a centrifugal blood pump. *Artif Organs*. 2002 Nov; 26 (11): 985–990.
19. *Giridharan GA, Skliar M*. Physiological Control of Blood Pumps Using Intrinsic Pump Parameters: a Computer Simulation Study. *Artif Organs*. 2006 Apr; 30 (4): 301–307.
20. *Schima H, Trubel W, Moritz A, Wieselthaler G, Stohr HG, Thoma H et al.* Noninvasive monitoring of rotary blood pumps: necessity, possibilities, and limitations. *Artif Organs*. 1992 Apr;16(2): 195–202.
21. *Itkin GP, Shemakin SJu, Shokhina EG, Burcev VI, Avramov PV, Volkova EA et al*. The first domestic implantable axial flow pump: results of experimental studies in calves. *Russian Journal of Transplantology and Artificial Organs*. 2013; 15 (3): 49–58. [In Russ, English abstract]. doi: 10.15825/1995-1191-2013-3-49-58.
22. *Itkin GP, Buchnev AS, Kuleshov AP, Drobyshev AA, Syrbu AI.* A hydrodynamic bench for testing pediatric circulatory support devices. *Biomedical Engineering*. 2022; 56 (1): 6–10. [In Russ, English abstract]. doi: 10.1007/s10527-022-10156-9.
23. *Maher TR, Butler KC, Poirier VL, Gernes DB*. HeartMate left ventricular assist devices: a multigeneration of implanted blood pumps. *Artif Organs*. 2001 May; 25 (5): 422–426.
24. *Owens WR, Bryant R 3rd, Dreyer WJ, Price JF, Morales DL.* Initial Clinical Experience with the HeartMate II Ventricular Assist System in a Pediatric Institution. *Artif Organs*. 2010 Jul; 34 (7): 600–603.

The article was submitted to the journal on 10.02.2025

DOI: 10.15825/1995-1191-2025-2-89-99

LONG-TERM MECHANICAL CIRCULATORY SUPPORT: EVOLUTION, PRESENT MILESTONES, AND FUTURE DIRECTIONS

R.Yu. Bangarov[2], T.A. Khalilulin[1], V.M. Zakharevich[1], Sh.R. Galeev[2], G.V. Nabiev[2]

[1] Shumakov National Medical Research Center of Transplantology and Artificial Organs, Moscow, Russian Federation

[2] Volzhsky Branch of Shumakov National Medical Research Center of Transplantology and Artificial Organs, Volzhsky, Russian Federation

Objective: to examine the historical evolution, current advancements, and future prospects of long-term mechanical circulatory support (LT-MCS) devices in the management of end-stage heart failure. **Materials and methods.** An analysis was conducted on clinical studies (MOMENTUM 3, INTERMACS, EUROMACS), historical records, and technological progress in the field of LT-MCS. The review covered three generations of devices: pulsatile pumps (first generation), axial-flow pumps (second generation), and centrifugal pumps with magnetic levitation (third generation). Key outcomes evaluated included survival rates, complication rates (thrombosis, infections, right ventricular failure), and developments within national technology. **Results.** The HeartMate III third-generation device has a 2-year survival rate of 82% with a pump thrombosis risk of less than 1%. However, complications remain, including driveline infections (10–15%), right ventricular failure (20–40%), and bleeding events (15–20%). Domestic systems (Stream Cardio) are comparable to second-generation devices but lag in terms of miniaturization and clinical trials. Emerging technologies like the Leviticus FiVAD wireless energy transfer system and the Carmat Aeson fully implantable artificial heart are opening up promising new directions for the future of mechanical circulatory support. **Conclusion.** Modern LT-MCS systems have emerged as a viable alternative to heart transplantation (HT), particularly for patients who are not candidates for HT. Key areas of ongoing development include device miniaturization, wireless energy transfer technologies, and integration of artificial intelligence. The future of LT-MCS will largely depend on overcoming current system limitations, notably the risks of infection and right ventricular failure.

Keywords: long-term mechanical circulatory support, heart failure, thrombosis, right ventricular failure, miniaturization, artificial intelligence.

INTRODUCTION

Heart failure (HF) remains one of the most pressing global health challenges. According to the World Health Organization (WHO), more than 26 million people worldwide are affected, with a five-year mortality rate exceeding 50% – a figure comparable to that of many oncologic diseases [1, 2]. While heart transplantation (HT) is considered the gold standard for treating end-stage chronic heart failure (CHF), its widespread application is severely limited by a critical organ shortage, with only slightly above 5,000 transplants performed globally each year [2, 3]. In this context, mechanical circulatory support (MCS) has emerged not merely as an alternative, but as an essential life-saving option, particularly for patients with refractory HF and cardiogenic shock.

Modern long-term mechanical circulatory support (LT-MCS) devices, such as HeartMate III and HeartWare HVAD, have demonstrated revolutionary clinical outcomes. According to the MOMENTUM 3 trial, the 1-year and 2-year survival rates following the implantation of this left ventricular assist device (LVAD) were 86.6% and 79%, respectively [4]. In the ELEVATE registry, the 2-year survival rate was even higher, reaching 83.4% [5] – a figure comparable to survival rates observed after HT [6, 7].

EVOLUTION OF MECHANICAL CIRCULATORY SUPPORT TECHNOLOGIES

As early as the first half of the 20th century, it became evident that even with the breakthroughs in cardiac surgery – particularly the advent of cardiopulmonary bypass – conservative therapies and traditional surgical interventions often failed to fully restore the heart's pumping function. This realization spurred an active search for methods of temporary or permanent MCS.

In 1952, Michael DeBakey proposed the concept of MCS, and in 1963, together with Domingo Liotta, successfully implanted the first mechanical pump for temporary left ventricular support – a key milestone in the development of MCS technologies [8]. Just six years later, in 1969, American cardiac surgeon Denton Cooley implanted the first total artificial heart (TAH) [8]. These

Corresponding author: Rizvan Bangarov. Address: 86, Generala Karbysheva str., Volzhsky, 404120, Russian Federation. Phone: (999) 625-87-50. E-mail: rizvan.bangarov@yandex.ru

groundbreaking achievements, combined with the persistent shortage of donor organs, catalyzed the emergence of MCS as a promising and technologically sophisticated approach to treating HF.

Today, a wide range of devices has been developed to support either the entire heart or individual ventricles. The evolution of MCS technologies is generally divided into three main generations, each characterized by revolutionary advances that have led to clinical outcomes for end-stage CHF comparable to those of HT.

First generation: pulsatile pumps

The development of first-generation MCS devices began in the 1960s. Initially, these systems were extracorporeal (e.g., Novacor, HeartMate XVE) and later evolved into fully implantable devices (e.g., Jarvik 7, SynCardia TAH), utilizing membrane chambers in which pressure differentials – created by external pneumatic or hydraulic actuators – enabled blood pumping [9, 10]. These devices mimicked the natural cardiac cycle by generating a pulsatile blood flow.

The primary purpose of first-generation devices was to serve as a "bridge to transplantation" (BTT), and the latest models of this era generally fulfilled this role effectively for durations ranging from weeks to several months. However, the were associated with a number of limitations.

Due to their heavy weight and reliance on external actuators, patient mobility was severely restricted, despite the devices' ability to achieve high cardiac outputs (up to 10 L/min). Their large size necessitated the creation of relatively large cavities for implantation, increasing the contact area between foreign materials and host tissues and thereby raising the risk of infectious complications. Additionally, the wide diameter of the percutaneous driveline (6–10 mm) further increased infection risks.

The design incorporated mechanical valves and was prone to blood stasis within the pump chambers, contributing to a high incidence of thromboembolic events (10–15%). Furthermore, mechanical wear and diaphragm fatigue significantly reduced the long-term reliability of these pumps, generally limiting their functional lifespan to 12–18 months [10–12].

Second generation: axial pumps

In response to the limitations of first-generation devices, a major breakthrough occurred in the field of MCS. Numerous studies demonstrated that, in most cases, prosthetic support of the left ventricle alone was sufficient to maintain effective cardiac output.

Second-generation devices – fully implantable LVADs such as the DeBakey VAD, HeartMate II, and Jarvik 2000 – were developed during the 1990s and 2000s. These devices operate based on the principle of continuous axial blood flow and represent a significant advancement over their predecessors in terms of both size and performance [11–14].

They weigh between 150 and 300 grams and measure less than 10 cm in length. Their compact axial rotor design efficiently unloads the left ventricle and provides continuous blood flow with outputs reaching up to 10 L/min. This ensures uninterrupted perfusion of vital organs and significantly reduces the risk of thrombus formation, thus making them applicable to a wider range of patients [7, 11–16].

A study by Miller et al. (2007) demonstrated a 75% survival rate at six months among patients implanted with the HeartMate II device, along with significant improvements in functional status and quality of life, further validating the efficacy of axial-flow pumps [17].

Thanks to several fundamental advantages over first-generation devices – including a longer service life of 5 to 7 years – second-generation pumps expanded the therapeutic scope of MCS from the initial "bridge to transplantation" (BTT) concept to include "bridge to recovery" (BTR) and "destination therapy" (DT) [7, 17–19]. Notably, the HeartMate II became the first implantable LVAD approved for lifelong implantation in 2010, and it remains one of the most widely used MCS devices worldwide.

However, continuous blood flow, while ensuring reliable organ perfusion, is non-physiological for the vascular endothelium. This unnatural flow pattern can lead to endothelial dysfunction, impair baroreceptor activity, disrupt blood pressure regulation, and contribute to the formation of arteriovenous malformations. As a result, bleeding complications, particularly in the gastrointestinal (GI) tract, are relatively common in patients supported by continuous-flow devices [20].

The presence of mechanical bearings in the design, axial nature of blood flow, and high rotor speed contribute to thrombus formation in 10–14% of cases within two years following implantation [21]. Additionally, right ventricular failure is a characteristic complication associated with second-generation devices. High pump output can cause malpositioning or rightward displacement of the interventricular septum (IVS), negatively impacting the septum's contribution to right ventricular (RV) stroke volume. This impairment can lead to significant RV dysfunction, necessitating either the implantation of a right ventricular assist device or proceeding to HT [13, 20–23, 36].

Third generation: centrifugal pumps with magnetic levitation

Although second-generation devices offered clear advantages over their predecessors, complications such as pump thrombosis and neurologic events continued to drive research toward further improvements in LVADs. Development and testing of third-generation pumps

began around 2012, involving approximately 10 different prototypes. This research culminated in a major breakthrough in the treatment of end-stage HF with the introduction of technologies that eliminated mechanical contact within the pump.

The pioneer among third-generation devices was the HeartMate III (Abbott), approved in 2017 [21, 24]. Its key innovation lies in the fully magnetically levitated (FML) rotor, suspended entirely by magnetic fields, thereby eliminating friction, reducing shear stress, and minimizing blood cell damage [4, 21]. This achievement was confirmed in the MOMENTUM 3 clinical trial, where the HeartMate III demonstrated unprecedented levels of safety [4, 21, 25, 26].

The third generation also included the Medtronic HVAD, which used fluid dynamic bearings. Despite its centrifugal flow and compact design, the HVAD's classification as a full third-generation device remained controversial. Although developed in the 2010s as an advanced model, the use of fluid bearings involving microcontacts contributed to a higher risk of thrombosis (12%) and stroke (15%), ultimately leading to its recall in 2021 [4, 21, 24, 28]. This experience underscored that the gold standard for third-generation LVADs is specifically full magnetic levitation.

Modern third-generation LVADs, such as the HeartMate III, rely on centrifugal flow combined with full magnetic levitation. In this system, a rotor suspended entirely by magnetic fields rotates at speeds of 5,500–6,000 rpm, producing blood flows of up to 10 liters per minute. The elimination of mechanical contact between pump components prevents hemolysis and thrombosis, contributing to an expected device lifespan of up to 10 years [4, 21, 27]. By contrast, the HVAD employed a hybrid suspension system, where passive magnetic levitation was combined with hydrodynamic bearings. Although a thin blood layer reduced friction, it did not completely eliminate mechanical contact [7, 28, 30].

According to the INTERMACS 2023 registry, third-generation devices now dominate clinical practice, with the HeartMate III representing approximately 85% of all implantations in the United States. The 2-year survival rate for patients supported by this device reaches 82%, approximately 6% higher than that achieved with earlier technologies and comparable to outcomes following HT [31–33]. In Europe, data from the EUROMACS 2022 report indicate a 1-year survival rate exceeding 80%, with thromboembolic events reduced to just 1–2% [34].

Among the clear advantages of the HeartMate III is its exceptional safety profile. Owing to the FML technology, the risk of pump thrombosis with HeartMate III is less than 1% – a significant improvement over earlier generations [4, 21, 26, 27, 32, 35]. The device's high durability, driven by the absence of mechanical wear, further positions third-generation LVADs a step above their predecessors. According to M.R. Mehra, HeartMate III does not require replacement for at least 5 years, providing strong justification for considering it a cornerstone in the evolution of destination therapy [37, 40].

Patient quality of life has also improved markedly. Studies have demonstrated that following implantation, patients experience sustained enhancements in functional capacity and overall well-being. Moreover, the reduction in operational noise – from approximately 40 dB in the HeartMate II to 25–30 dB in the HeartMate III – alongside the compact design of the device and its external components, enables greater patient mobility and promotes better social integration [4, 21, 40].

Despite the clear advantages of third-generation LVADs, these devices are not without limitations. While patients often experience marked improvements in physical activity, reduced dyspnea, and overall functional status, several challenges remain associated with long-term LVAD use.

Firstly, the need to continuously wear an external controller and power source can cause discomfort and restrict mobility, particularly in active patients. Secondly, although the risk of thrombosis has been significantly reduced compared to second-generation devices, the threat of ischemic and hemorrhagic complications – such as stroke and gastrointestinal bleeding – persists [4, 21, 26, 29, 35, 40]. For example, the ENDURANCE trial demonstrated a 29.7% stroke rate among patients with HVAD, which was notably higher than that observed in HeartMate II recipients [41].

Another persistent concern is infection at the driveline exit site. Despite advancements in materials and antimicrobial coatings, driveline infections remain one of the leading causes of hospitalization among LVAD patients, with an incidence of 10–15% [40, 43–45]. Furthermore, the anticoagulation therapy necessary to prevent thrombosis substantially increases the risk of major bleeding events (15–20%), necessitating continuous clinical monitoring [21, 27, 40].

Thus, although third-generation LVADs represent a major technological advancement, they are not a definitive solution to end-stage HF but rather an important bridge to transplantation or a means of long-term support.

Prospects of LT-MCS devices as a "bridge to recovery" (BTR)

The reverse myocardial remodeling observed in patients with end-stage HF following LVAD implantation has become a cornerstone argument supporting the BTR strategy. Mechanical left ventricular unloading leads to a significant reduction in ventricular volumes: end-diastolic volume (EDV) decreases by 20–30%, and myocardial wall thickness is reduced by 15–20%, contributing to partial restoration of normal cardiac geometry [46, 47]. For instance, in patients implanted with the HeartMa-

te III, left ventricular ejection fraction (LVEF) improved from an average of 15% to 35–40% in approximately 30% of cases, a result attributed to improved hemodynamics and a reduced neurohormonal load [21, 27, 40, 45].

The effectiveness of this process is closely linked to the technological generation of the LVAD used. First-generation devices (e.g., HeartMate XVE) employing pulsatile flow demonstrated reverse remodeling in only 10–15% of patients; however, complications such as thrombosis often negated these benefits [46, 48–50]. With the advent of second-generation axial flow pumps, the incidence of reverse remodeling improved to 25–30%. Nonetheless, a significant complication – *de novo* aortic regurgitation – emerged in about 40% of patients, compromising the durability of myocardial recovery [7, 15–20, 47].

A breakthrough was achieved with third-generation centrifugal pumps using full magnetic levitation technology. Devices like the HeartMate III enabled a 28–32% reduction in left ventricular volumes in 35–40% of patients, with a concomitant risk of pump thrombosis dropping to 1%, thereby offering a much more stable platform for ventricular recovery [7, 21, 27].

Despite significant progress, sustained long-term recovery of cardiac function following LVAD support remains relatively rare. Only 15–20% of patients maintain improved cardiac function for 1–2 years after device explantation. The success rate of LVAD removal with second-generation devices such as the HeartMate II was modest, approximately 12%. However, more recent data regarding the third-generation HeartMate III indicate higher myocardial recovery and retrieval rates, ranging from 18% to 22% [4, 7, 21, 27, 40, 50]. Importantly, younger patients without significant myocardial fibrosis demonstrate the highest likelihood of sustained myocardial recovery [32–34, 41–43, 45].

Thus, while third-generation LT-MCS devices not only extend survival but also foster myocardial recovery, the transition from a BTT paradigm to a true BTR strategy remains a major clinical and technological challenge. Achieving this transition will require solving issues related to the long-term durability of myocardial remodeling and improving the accessibility and affordability of advanced device technologies.

Development prospects: from miniaturization to bioartificial systems

The leading directions of innovation in MCS are focused on device miniaturization – including pediatric-specific solutions – the introduction of wireless power transmission technologies to reduce infectious risks, and development of fully implantable systems aimed at maximizing autonomy and patient safety [51].

First and foremost, the trend toward miniaturization is particularly crucial in pediatric practice. The use of bulky circulatory support systems in newborns and infants is severely limited by anatomical constraints and a heightened risk of complications. In response, recent years have seen the widespread adoption of compact devices with tailored hydrodynamic characteristics. A notable example is the Berlin Heart EXCOR Pediatric system, a pneumatic extracorporeal device featuring chamber volumes from 10 to 60 mL, widely utilized in patients weighing less than 20 kg. Parallel to this, implantable solutions are under active development, including the Jarvik Infant 2015 VAD and the Penn State Infant VAD, designed for children weighing as little as 4 kg. These devices are characterized by continuous blood flow, high reliability, and reduced thrombogenicity.

Particular attention is also being directed toward the PediaFlow VAD system, a magneto-hydrodynamic mini-pump with a thickness of less than 1 cm, capable of delivering effective circulatory support in newborns while minimizing hemolysis. Thus, the advancement of miniaturized VADs is significantly expanding the indications for long-term MCS in pediatric populations [54–56].

Currently, there is active advancement in the implementation of wireless energy transfer technologies, aimed primarily at eliminating percutaneous cables. This innovation significantly reduces the risk of infectious complications and improves both functional and aesthetic outcomes of therapy.

Among these systems, special attention is given to the Leviticus FiVAD, which employs the principle of coplanar energy transfer (CET) – allowing electromagnetic power transmission through the skin without physical contact with the external environment. A similar concept is realized in the experimental FREE-D system. Another notable development is the ICOMS Flowmaker (FineHeart, France) – a fully intraventricular, wireless LVAD synchronized with native heartbeats. This device integrates transcutaneous energy transfer (TET) with intelligent blood flow adaptation to physiological load, offering a new standard in circulatory support [57–61].

The next major milestone in LT-MCS technology has been the development of fully implantable mechanical support systems. A striking example is the aforementioned ICOMS Flowmaker, in which all components – including the controller, battery, and pump – are housed entirely within the body. The Leviticus FiVAD system is also capable of operating in a fully implantable mode, using an internal battery.

Total artificial heart (TAH) systems also deserve special mention, with the most innovative example being the CARMAT Aeson – a bioprosthetic heart that mimics the function of both ventricles, featuring pulsatile ejection and biocompatible materials. The device is fully implanted within the patient's thoracic cavity and utilizes a transcutaneous energy transfer (TET) system, thereby eliminating the need for external components. In addition to its advanced pump mechanism, CARMAT is equipped

with an autonomous blood flow adaptation system that responds dynamically to changes in the patient's physical activity. Clinical trials conducted within the framework of the European EFICAS program have demonstrated improved survival rates and enhanced quality of life in non-urgent transplant candidates [62–66].

By the end of 2024, the company had achieved 100 implantations of its device, with the number of surgeries doubling within just one year – a clear indication of growing medical confidence and renewed hope for thousands of patients facing an acute shortage of donor hearts [67].

The current trajectory of MCS development is profoundly multidisciplinary, combining advances in bioengineering, electronics, and materials science. Miniaturization is expanding the application of these technologies to pediatric populations, while wireless energy transmission significantly enhances safety and mobility. Fully implantable systems, meanwhile, are elevating circulatory support to an unprecedented level of autonomy. Together, these innovations are laying the groundwork for the next generation of devices capable of replacing or sustaining cardiac function with minimal disruption to patients' daily lives.

RUSSIAN INNOVATIONS IN THE FIELD OF MECHANICAL CIRCULATORY SUPPORT

Alongside global advancements in MCS systems, Russia has established its own scientific and technological base, marked by both historical achievements and current trends. Since the Soviet era, Russian innovations have demonstrated notable advancements in miniaturization, digital integration, and functional design, although they continue to face systemic challenges, particularly in terms of funding, clinical scalability, and integration into international research networks [7, 15, 16, 70–74].

Historical foundation: Poisk-10M

A landmark development in the Soviet Union's contribution to MCS technology was the creation of the Poisk-10M, an all-artificial heart designed in the 1980s under the leadership of Prof. Valery Shumakov. This pulsatile, pneumatic-type device, weighing approximately 900 grams and featuring a chamber volume of 60–80 mL, was intended to provide temporary heart replacement for patients awaiting transplantation. Its clinical application included 17 implantations, including 4 operations in Poland, underscoring early global interest in Soviet cardiovascular innovations. Preclinical testing on calves demonstrated survival periods of up to 102 days, validating the device's fundamental viability. However, the system's large size, susceptibility to mechanical wear, and the economic crisis of the 1990s ultimately led to the discontinuation of the project. Despite these limitations, the Poisk-10M laid the foundation for further research, proving the feasibility of two-stage HT [68–69, 76–79].

Evolution of technology: transition to axial flow pumps

The next stage in the development of Russian MCS systems was marked by a transition to axial flow pumps, aligning Russian innovations with the second and third generations of international MCS technologies. A pivotal point in this evolution was the initiation of clinical trials in 2012 for the AVK-N axial pump, a second-generation LVAD designed for long-term support of patients with end-stage HF. The AVK-N demonstrated technical and clinical performance comparable to international counterparts, such as the HeartMate II, while offering a key advantage – compatibility with domestically sourced materials. The device has been successfully applied in clinical practice under both BTT and DT strategies, showing outcomes similar to those of established Western models of its generation [70, 74–76, 80].

Among current domestic technologies, the most sophisticated innovation is arguably the Stream Cardio system – a universal axial-flow MCS device engineered to support both the left and right ventricles. The pump operates within a wide flow range of 3–7 L/min for the left ventricle and a pressure range of 20–60 mmHg for right ventricular support, making it adaptable for patients with a minimum body surface area (BSA) of 0.9 m^2. What sets Stream Cardio apart is its integration of digital technologies. The system includes wireless control via a mobile interface, autonomous power supply for up to 12–14 hours, real-time monitoring through a graphical interface and artificial intelligence (AI) algorithms capable of predicting complications. An additional innovation is its multimedia training module, which includes a surgical video archive, significantly enhancing surgeon training and system usability.

Despite these advancements, Stream Cardio has limitations. Notably, the high cost of disposable modules and the inapplicability for pediatric patients with a BSA <0.9 m^2 restrict its universal use [81–83].

Systemic challenges and prospects

A critical analysis of Russian MCS innovations reveals several structural challenges. One of the foremost barriers is the dependence on imported critical components, particularly rare-earth magnets and high-precision sensors. This reliance on foreign suppliers undermines the autonomy of production. Secondly, the limited scale and duration of clinical trials significantly delay the regulatory approval and broad clinical implementation of innovative devices. For instance, although the Stream Cardio system has already been introduced in select cardiac surgery centers, other promising developments – such as DON-3 – remain in the experimental phase. A third critical limitation is the technological gap between Russian and leading international MCS platforms. Devices such as the HeartMate III and Carmat demonstrate higher

reliability and miniaturization, corresponding to third to fifth generation of MCS systems.

Despite these constraints, Russian MCS projects have significant potential. The focus on biventricular support in Stream Cardio aligns with the global paradigm shift toward universal MCS systems. Digitalization, including AI integration and telemedicine capabilities, opens up opportunities for a personalized approach and reduced risk of complications.

Realizing this potential requires strategic investments in clinical research, localization of production of critical components and international certification.

Russian MCS developments have progressed from bulky pulsatile systems to compact, digital solutions, reflecting a gradual but evident convergence with global technological standards. Despite this progress, the future of Russian MCS devices hinges on elimination of systemic constraints – particularly those of a financial, technological, and regulatory nature. Projects such as Stream Cardio can strengthen Russia's position in the domestic market and also create prerequisites for technology export, which is especially important in the context of global competition in the field of medical innovations.

CONCLUSION

The increasing use of LT-MCS devices as destination therapy reflects a significant global shift in cardiology, driven by a persistent shortage of donor hearts and enhanced device reliability. Modern systems – such as the HeartMate III and advanced domestic technologies – have demonstrated long-term survival exceeding five years, making them a viable alternative to transplantation for patients who are not candidates for donor organs. The expansion of clinical indications, ongoing miniaturization of devices, and a marked reduction in complication rates (including right ventricular failure, thrombosis, and infection) collectively reinforce the growing role of LT-MCS as a definitive treatment option for end-stage HF.

These advances, however, represent only the initial phase of a new evolutionary wave in mechanical circulatory support systems. The industry's prospects lie in personalized therapy, integration of AI, and development of hybrid systems that combine mechanical support with myocardial regeneration. As M.R. Mehra, lead investigator of the MOMENTUM 3 trial, aptly stated, "We are on the cusp of an era where LVADs will become not just a temporary bridge, but a definitive treatment option for millions of patients." This vision underscores the transformative potential of current and emerging MCS technologies in addressing the global burden of HF.

The authors declare no conflict of interest.

REFERENCES

1. *Virani SS, Alonso A, Benjamin EJ, Bittencourt MS, Callaway CW, Carson AP et al.* Heart Disease and Stroke Statistics-2020 Update: A Report From the American Heart Association. *Circulation*. 2020 Mar 3; 141 (9): e139–e596. doi: 10.1161/CIR.0000000000000757.
2. *Lippi G, Sanchis-Gomar F.* Global epidemiology and future trends of heart failure. *AME Med J*. 2020; 5: 15. doi: 10.21037/amj.2020.03.03.
3. *Khush KK, Cherikh WS, Chambers DC, Harhay MO, Hayes D Jr, Hsich E et al.* The International Thoracic Organ Transplant Registry of the International Society for Heart and Lung Transplantation: thirty-sixth adult heart transplantation report – 2019; focus theme: donor and recipient size match. *J Heart Lung Transplant*. 2019 Oct; 38 (10): 1056–1066. doi: 10.1016/j.healun.2019.08.004.
4. *Goldstein DJ, Naka Y, Horstmanshof D, Ravichandran AK, Schroder J, Ransom J et al.* Association of clinical outcomes with left ventricular assist device use by bridge to transplant or destination therapy intent: the multicenter study of MagLev technology in patients undergoing mechanical circulatory support therapy with HeartMate 3 (MOMENTUM 3) randomized clinical trial. *JAMA Cardiol*. 2020 Apr 1; 5 (4): 411–419. doi: 10.1001/jamacardio.2019.5323.
5. *Pettit SJ.* HeartMate 3: real-world performance matches pivotal trial. *Eur Heart J*. 2020 Oct 14; 41 (39): 3810–3812. doi: 10.1093/eurheartj/ehaa642.
6. *Lund LH, Khush KK, Cherikh WS, Goldfarb S, Kucheryavaya AY, Levvey BJ et al.* The Registry of the International Society for Heart and Lung Transplantation: Thirty-fourth Adult Heart Transplantation Report-2017; Focus Theme: Allograft ischemic time. *J Heart Lung Transplant*. 2017 Oct; 36 (10): 1037–1046. doi: 10.1016/j.healun.2017.07.019.
7. *Khalilulin TA.* Dlitel'naya mekhanicheskaya podderzhka krovoobrashcheniya v lechenii potentsial'nykh retsipientov donorskogo serdtsa s kriticheskoy serdechnoy nedostatochnost'yu (kliniko-eksperimental'noe issledovanie): Dis. … d-ra med. nauk. M., 2019; 212.
8. *DeBakey ME.* Left ventricular bypass pump for cardiac assistance: clinical experience. *Am J Cardiol*. 1971 Jan; 27 (1): 3–11. doi: 10.1016/0002-9149(71)90076-2.
9. *Frazier OH, Rose EA, Macmanus Q, Burton NA, Lefrak EA, Poirier VL, Dasse KA.* Multicenter clinical evaluation of the HeartMate 1000 IP left ventricular assist device. *Ann Thorac Surg*. 1992 Jun; 53 (6): 1080–1090. doi: 10.1016/0003-4975(92)90393-i.
10. *Rose EA, Gelijns AC, Moskowitz AJ, Heitjan DF, Stevenson LW, Dembitsky W et al.* Long-term use of a left ventricular assist device for end-stage heart failure. *N Engl J Med*. 2001 Nov 15; 345 (20): 1435–1443. doi: 10.1056/NEJMoa012175.
11. *Rigatelli G, Santini F, Faggian G.* Past and present of cardiocirculatory assist devices: a comprehensive critical review. *J Geriatr Cardiol*. 2012 Dec; 9 (4): 389–400. doi: 10.3724/SP.J.1263.2012.05281.
12. *Itkin GP.* Ventricle assist device: past, present, and future nonpulsatile pumps. *Russian Journal of Transplantology and Artificial Organs*. 2009; 11 (3): 81–87. (In Russ.). https://doi.org/10.15825/1995-1191-2009-3-81-87.
13. *Pagani FD, Miller LW, Russell SD, Aaronson KD, John R, Boyle AJ et al.* Extended mechanical circulato-

ry support with a continuous-flow rotary left ventricular assist device. *J Am Coll Cardiol*. 2009 Jul 21; 54 (4): 312–321. doi: 10.1016/j.jacc.2009.03.055.
14. *Mankad AK, Tang DG, Clark WB, Flattery M, Harton S, Katlaps GJ et al.* Persistent anemia after implantation of the total artificial heart. *J Card Fail*. 2012 Jun; 18 (6): 433–438. doi: 10.1016/j.cardfail.2012.03.003.
15. *Itkin GP, Shokhina EG, Shemakin SYu, Poptsov VN, Shumakov DV, Gautier SV*. Features of long-term mechanical circulatory support with continuous-flow pump. *Russian Journal of Transplantology and Artificial Organs*. 2012; 14 (2): 110–115. (In Russ.). https://doi.org/10.15825/1995-1191-2012-2-110-115.
16. *Itkin GP, Selishchev SV.* Rotornye nasosy dlya iskusstvennogo i vspomogatel'nogo krovoobrashcheniya. Meditsinskaya tekhnika. 2010; 264 (6): 39–45.
17. *Miller LW, Pagani FD, Russell SD, John R, Boyle AJ, Aaronson KD et al.* Use of a continuous-flow device in patients awaiting heart transplantation. *N Engl J Med*. 2007 Aug 30; 357 (9): 885–896. doi: 10.1056/NEJMoa067758.
18. *Giridharan GA, Lee TJ, Ising M, Sobieski MA, Koenig SC, Gray LA, Slaughter MS.* Miniaturization of mechanical circulatory support systems. *Artif Organs*. 2012 Aug; 36 (8): 731–739. doi: 10.1111/j.1525-1594.2012.01523.x.
19. *Maher TR, Butler KC, Poirier VL, Gernes DB*. HeartMate left ventricular assist devices. A multigeneration of implanted blood pumps. *Artif Organs*. 2001 May; 25 (5): 422–426. doi: 10.1046/j.1525-1594.2001.06756.x.
20. *Williams ML, Trivedi JR, McCants KC, Prabhu SD, Birks EJ, Oliver L, Slaughter MS.* Heart transplant *vs* left ventricular assist device in heart transplant-eligible patients. *Ann Thorac Surg*. 2011 May; 91 (5): 1330–1333; discussion 1333–1334. doi: 10.1016/j.athoracsur.2011.01.062.
21. *Mehra MR, Uriel N, Naka Y, Cleveland JC Jr, Yuzefpolskaya M, Salerno CT et al.* A Fully Magnetically Levitated Left Ventricular Assist Device – Final Report. *N Engl J Med*. 2019 Apr 25; 380 (17): 1618–1627. doi: 10.1056/NEJMoa1900486.
22. *John R.* Current axial-flow devices – the HeartMate II and Jarvik 2000 left ventricular assist devices. *Semin Thorac Cardiovasc Surg*. 2008 Fall; 20 (3): 264–272. doi: 10.1053/j.semtcvs.2008.08.001.
23. *Slaughter MS, Rogers JG, Milano CA, Russell SD, Conte JV, Feldman D et al.* Advanced heart failure treated with continuous-flow left ventricular assist device. *N Engl J Med.* 2009 Dec 3; 361 (23): 2241–2251. doi: 10.1056/NEJMoa0909938.
24. *Rogers JG, Aaronson KD, Boyle AJ, Russell SD, Milano CA, Pagani FD et al.* Continuous flow left ventricular assist device improves functional capacity and quality of life of advanced heart failure patients. *J Am Coll Cardiol.* 2010 Apr 27; 55 (17): 1826–1834. doi: 10.1016/j.jacc.2009.12.052.
25. *Strueber M, O'Driscoll G, Jansz P, Khaghani A, Levy WC, Wieselthaler GM.* Multicenter evaluation of an intrapericardial left ventricular assist system. *J Am Coll Cardiol*. 2011 Mar 22; 57 (12): 1375–1382. doi: 10.1016/j.jacc.2010.10.040.
26. *Netuka I, Kvasnička T, Kvasnička J, Hrachovinová I, Ivák P, Mareček F et al.* Evaluation of von Willebrand factor with a fully magnetically levitated centrifugal continuous-flow left ventricular assist device in advanced heart failure. *J Heart Lung Transplant*. 2016 Jul; 35 (7): 860–867. doi: 10.1016/j.healun.2016.05.019.
27. *Mehra MR, Goldstein DJ, Cleveland JC, Cowger JA, Hall S, Salerno CT et al.* Five-Year Outcomes in Patients With Fully Magnetically Levitated *vs* Axial-Flow Left Ventricular Assist Devices in the MOMENTUM 3 Randomized Trial. *JAMA*. 2022 Sep 27; 328 (12): 1233–1242. doi: 10.1001/jama.2022.16197.
28. FDA alerts health care providers to stop new implants of certain ventricular assist device system. [Electronic resource]. Access mode: free. Date of access: 22.04.2025. https://www.fda.gov/news-events/press-announcements/fda-alerts-health-care-providers-stop-new-implants-certain-ventricular-assist-device-system.
29. *Gustafsson F, Shaw S, Lavee J, Saeed D, Pya Y, Krabatsch T et al.* Six-month outcomes after treatment of advanced heart failure with a full magnetically levitated continuous flow left ventricular assist device: report from the ELEVATE registry. *Eur Heart J*. 2018 Oct 1; 39 (37): 3454–3460. doi: 10.1093/eurheartj/ehy513.
30. *Teuteberg JJ, Slaughter MS, Rogers JG, McGee EC, Pagani FD, Gordon R et al.* The HVAD Left Ventricular Assist Device: Risk Factors for Neurological Events and Risk Mitigation Strategies. *JACC Heart Fail*. 2015 Oct; 3 (10): 818–828. doi: 10.1016/j.jchf.2015.05.011.
31. *Tedford RJ, Leacche M, Lorts A, Drakos SG, Pagani FD, Cowger J.* Durable Mechanical Circulatory Support: JACC Scientific Statement. *J Am Coll Cardiol*. 2023 Oct 3; 82 (14): 1464–1481. doi: 10.1016/j.jacc.2023.07.019.
32. *Chamogeorgakis T, Toumpoulis I, Bonios MJ, Lanfear D, Williams C, Koliopoulou A, Cowger J.* Treatment Strategies and Outcomes of Right Ventricular Failure Post Left Ventricular Assist Device Implantation: An INTERMACS Analysis. *ASAIO J*. 2024 Apr 1; 70 (4): 264–271. doi: 10.1097/MAT.0000000000002105.
33. *Jorde UP, Saeed O, Koehl D, Morris AA, Wood KL, Meyer DM et al.* The Society of Thoracic Surgeons Intermacs 2023 Annual Report: Focus on Magnetically Levitated Devices. *Ann Thorac Surg*. 2024 Jan; 117 (1): 33–44. doi: 10.1016/j.athoracsur.2023.11.004.
34. *De By TMMH, Schoenrath F, Veen KM, Mohacsi P, Stein J, Alkhamees KMM et al.* The European Registry for Patients with Mechanical Circulatory Support of the European Association for Cardio-Thoracic Surgery: third report. *Eur J Cardiothorac Surg*. 2022 Jun 15; 62 (1): ezac032. doi: 10.1093/ejcts/ezac032.
35. *Narang N, Raikhelkar J, Sayer G, Uriel N.* Hemodynamic Pump-Patient Interactions and Left Ventricular Assist Device Imaging. *Cardiol Clin.* 2018 Nov; 36 (4): 561–569. doi: 10.1016/j.ccl.2018.06.013.
36. *Alvarez J, Rao V.* HeartMate 3 – a "Step" in the right direction. *J Thorac Dis*. 2017 May; 9 (5): E457–E460. doi: 10.21037/jtd.2017.04.39.
37. *Melendo-Viu M, Dobarro D, Raposeiras Roubin S, Llamas Pernas C, Moliz Cordón C, Vazquez Lamas M et al.* Left Ventricular Assist Device as a Destination Thera-

py: Current Situation and the Importance of Patient Selection. *Life (Basel)*. 2023 Apr 21; 13 (4): 1065. doi: 10.3390/life13041065.
38. *Fernandez Valledor A, Rubinstein G, Moeller CM, Lorenzatti D, Rahman S, Lee C et al.* Durable left ventricular assist devices as a bridge to transplantation in The Old and The New World. *J Heart Lung Transplant*. 2024 Jun; 43 (6): 1010–1020. doi: 10.1016/j.healun.2024.01.019.
39. *Fernandez Valledor A, Moeller CM, Rubinstein G, Oren D, Rahman S, Baranowska J et al.* Durable left ventricular assist devices as a bridge to transplantation: what to expect along the way? *Expert Rev Med Devices*. 2024 Sep; 21 (9): 829–840. doi: 10.1080/17434440.2024.2393344.
40. *Jakovljevic DG, Yacoub MH, Schueler S, MacGowan GA, Velicki L, Seferovic PM et al.* Left Ventricular Assist Device as a Bridge to Recovery for Patients With Advanced Heart Failure. *J Am Coll Cardiol*. 2017 Apr 18; 69 (15): 1924–1933.
41. *Malone G, Abdelsayed G, Bligh F, Al Qattan F, Syed S, Varatharajullu P et al.* Advancements in left ventricular assist devices to prevent pump thrombosis and blood coagulopathy. *J Anat*. 2023 Jan; 242 (1): 29–49. doi: 10.1111/joa.13675.
42. *Meyer DM, Nayak A, Wood KL, Blumer V, Schettle S, Salerno C et al.* The Society of Thoracic Surgeons Intermacs 2024 Annual Report: Focus on Outcomes in Younger Patients. *Ann Thorac Surg*. 2025 Jan; 119 (1): 34–58. doi: 10.1016/j.athoracsur.2024.10.003.
43. *Aslam S, Cowger J, Shah P, Stosor V, Copeland H, Reed A et al.* The International Society for Heart and Lung Transplantation (ISHLT): 2024 infection definitions for durable and acute mechanical circulatory support devices. *J Heart Lung Transplant*. 2024 Jul; 43 (7): 1039–1050. doi: 10.1016/j.healun.2024.03.004.
44. *Chu VH, Bielick CG, Arnold CJ*. Cardiovascular Implantable Electronic Device Infections: A Contemporary Review. *Infect Dis Clin North Am*. 2024; 38 (2): 693–712.
45. *Kormos RL, Antonides CFJ, Goldstein DJ, Cowger JA, Starling RC, Kirklin JK et al.* Updated definitions of adverse events for trials and registries of mechanical circulatory support: A consensus statement of the mechanical circulatory support academic research consortium. *J Heart Lung Transplant*. 2020 Aug; 39 (8): 735–750. doi: 10.1016/j.healun.2020.03.010.
46. *Mancini DM, Beniaminovitz A, Levin H, Catanese K, Flannery M, DiTullio M et al.* Low incidence of myocardial recovery after left ventricular assist device implantation in patients with chronic heart failure. *Circulation*. 1998 Dec 1; 98 (22): 2383–2389. doi: 10.1161/01.cir.98.22.2383.
47. *Birks EJ, George RS, Firouzi A, Wright G, Bahrami T, Yacoub MH, Khaghani A.* Long-term outcomes of patients bridged to recovery versus patients bridged to transplantation. *J Thorac Cardiovasc Surg.* 2012 Jul; 144 (1): 190–196. doi: 10.1016/j.jtcvs.2012.03.021.
48. *Dandel M, Weng Y, Siniawski H, Potapov E, Drews T, Lehmkuhl HB et al.* Prediction of cardiac stability after weaning from left ventricular assist devices in patients with idiopathic dilated cardiomyopathy. *Circulation*. 2008 Sep 30; 118 (14 Suppl): S94–S105. doi: 10.1161/CIRCULATIONAHA.107.755983.
49. *Simon MA, Kormos RL, Murali S, Nair P, Heffernan M, Gorcsan J et al.* Myocardial recovery using ventricular assist devices: prevalence, clinical characteristics, and outcome. *Circulation*. 2005 Aug 30; 112 (9 Suppl): I32–I36. doi: 10.1161/CIRCULATIONAHA.104.524124.
50. *Wever-Pinzon O, Drakos SG, McKellar SH, Horne BD, Caine WT, Kfoury AG et al.* Cardiac Recovery During Long-Term Left Ventricular Assist Device Support. *J Am Coll Cardiol*. 2016 Oct 4; 68 (14): 1540–1553. doi: 10.1016/j.jacc.2016.07.743.
51. *Lodge AJ, Antunez AG, Jaquiss RDB*. Pediatric ventricular assist devices. *Progress in Pediatric Cardiology*. 2012; 33 (2): 169–176.
52. *Huber CH, Tozzi P, Hurni M, von Segesser LK*. No drive line, no seal, no bearing and no wear: magnetics for impeller suspension and flow assessment in a new VAD. *Interact Cardiovasc Thorac Surg.* 2004 Jun; 3 (2): 336–340. doi: 10.1016/j.icvts.2004.01.014.
53. *Lucke L, Bluvshtein V.* Safety considerations for wireless delivery of continuous power to implanted medical devices. *Annu Int Conf IEEE Eng Med Biol Soc.* 2014; 2014: 286–289. doi: 10.1109/EMBC.2014.6943585.
54. *Adachi I, Jaquiss RD.* Mechanical Circulatory Support in Children. *Curr Cardiol Rev.* 2016; 12 (2): 132–140. doi: 10.2174/1573403X12666151119165841.
55. *Greenberg JW, Perry T, Morales DLS*. Management of Mechanical Circulatory Support in Pediatric Heart Failure. *Management of Acute and Chronic Severe Heart Failure: Advances in Mechanical Circulatory Support*. Cham: Springer Nature Switzerland, 2025: 371–385. doi: 10.1007/978-3-031-74963-6_23.
56. *Amdani S, Conway J, George K, Martinez HR, Asante-Korang A, Goldberg CS et al.* Evaluation and Management of Chronic Heart Failure in Children and Adolescents With Congenital Heart Disease: A Scientific Statement From the American Heart Association. *Circulation*. 2024 Jul 9; 150 (2): e33–e50. doi: 10.1161/CIR.0000000000001245.
57. *Campi T, Cruciani S, Maradei F, Montalto A, Feliziani M*. Wireless Power Transmission for Left Ventricular Assist Devices: Advancements, Challenges, and Future Directions. *2024 IEEE Wireless Power Technology Conference and Expo (WPTCE)*. 2024: 505–508. doi: 10.1109/WPTCE59894.2024.10557316.
58. *Moore J, Castellanos S, Xu S, Wood B, Ren H, Tse ZTH.* Applications of Wireless Power Transfer in Medicine: State-of-the-Art Reviews. *Ann Biomed Eng*. 2019 Jan; 47 (1): 22–38. doi: 10.1007/s10439-018-02142-8.
59. *Alabsi A, Hawbani A, Wang X, Al-Dubai A, Hu J, Aziz SA et al.* Wireless power transfer technologies, applications, and future trends: A review. *IEEE Transactions on Sustainable Computing*. 2025 Jan-Feb; 10 (1): 1–17. doi: 10.1109/TSUSC.2024.3380607.
60. *Khalili HF, Kirchner J, Bartunik M, Werner S, Ebel N, Schubert DW et al.* Transcutaneous energy transfer system for cardiac-assist devices by use of inhomogeneous biocompatible core material. *IEEE Transactions on Magnetics*. 2021; 57 (12): 1–12.

61. *Knecht OM.* Transcutaneous Energy and Information Transfer for Left Ventricular Assist Devices: Diss. ETH No. 24719. Zurich, 2017; 363.
62. *Campi T, Cruciani S, Maradei F, Montalto A, Musumeci F, Feliziani M*. Thermal analysis of a transcutaneous energy transfer system for a left ventricular assist device. *IEEE Journal of Electromagnetics, RF and Microwaves in Medicine and Biology*. 2021; 6 (2): 253–259.
63. *Jordan A, Tchantchaleishvili V.* Recent progress in the field of artificial organs. *Artif Organs*. 2020 Dec; 44 (12): 1318–1319. doi: 10.1111/aor.13855.
64. *Han JJ.* Aeson – The Carmat total artificial heart is approved for enrollment in the United States. *Artif Organs*. 2021 May; 45 (5): 445–446. doi: 10.1111/aor.13959.
65. Recent progress in the field of Artificial Organs. *Artif Organs*. 2023; 47 (12): 1805–1806. doi: 10.1111/aor.14663.
66. *Peronino C.* Caractérisation de l'hémocompatibilité acquise du coeur artificiel total Aeson (Carmat, A-TAH): Thèse de doctorat. Discipline: Hématologie. Université Paris Cité, 2023; 227.
67. CARMAT franchit le cap des 100 implantations de son cœur artificiel total Aeson® / CARMAT – 10 février 2025. https://www.carmatsa.com/communique-de-presse/carmat-franchit-le-cap-des-100-implantations-de-son-coeur-artificiel-total-aeson/ (Date of access: 23.04.2025).
68. *Itkin GP.* Development of experimental and clinical approbation methodology of implantable axial pumps. *Transplantology: results and prospects*. Vol. VI. 2014 / Ed. by S.V. Gautier. M.–Tver: Triada, 2015: 138–143.
69. *Shumakov DV, Shemakyn SYu, Kozlov IL, Popzov VN, Kormer AYa, Romanov OV et al.* The fist experience of clinic application the implanting pump INCOR for the round about way of left ventricular in Russia. *Russian Journal of Transplantology and Artificial Organs*. 2007; 10 (1): 19–27.
70. *Gautier SV, Kuleshov AP, Efimov AE, Agapov II, Itkin GP*. Optimization of Implantable Axial Pump to Increase Efficiency of Mechanical Circulatory Support. *Russian Journal of Transplantology and Artificial Organs*. 2017; 19 (2): 61–68. (In Russ.). https://doi.org/10.15825/1995-1191-2017-2-61-68.
71. *Itkin GP, Dmitrieva OYu, Buchnev AS, Drobyshev AA, Kuleshov AP, Volkova AV, Halilulin TA*. Results of experimental studies of the children's axial pump "DON-3". *Russian Journal of Transplantology and Artificial Organs*. 2018; 20 (2): 61–68. https://doi.org/10.15825/1995-1191-2018-2-61-68.
72. *Dmitrieva OYu, Buchnev AS, Kuleshov AP, Drobyshev AA, Volkova EA, Itkin GP.* First experience of using a children's axial pump in an experiment. *Russian Journal of Transplantology and Artificial Organs*. 2017; 19 (S): 172.
73. *Gautier SV, Itkin GP, Shemakin SYu, Saitgareev RSh, Poptsov VN, Zakharevich VM et al*. The first experience in clinical application of domestic circulatory support device on basis of implantable axial pump for two stage heart transplantation. *Russian Journal of Transplantology and Artificial Organs*. 2013; 15 (3): 92–101. (In Russ.). https://doi.org/10.15825/1995-1191-2013-3-92-101.
74. *Gautier SV, Itkin GP, Shevchenko AO, Khalilulin TA, Kozlov VA*. Durable mechanical circulation support as an alternative to heart transplantation. *Russian Journal of Transplantology and Artificial Organs*. 2016; 18 (3): 128–136. (In Russ.). https://doi.org/10.15825/1995-1191-2016-3-128-136.
75. *Khalilulin TA, Zacharevich VM, Poptsov VN, Itkin GP, Shevchenko AO, Saitgareev RSh et al*. Special aspects of implantation of a heart pump support system AVK-N as a "bridge" to heart transplantation. *Russian Journal of Transplantology and Artificial Organs*. 2018; 20 (1): 13–22. https://doi.org/10.15825/1995-1191-2018-1-13-22.
76. *Itkin GP.* Mechanical circulatory support: problems, solutions and new directions. *Russian Journal of Transplantology and Artificial Organs*. 2014; 16 (3): 76–84. (In Russ.). https://doi.org/10.15825/1995-1191-2014-3-76-84.
77. *Hubutiya MSh, Kasakov EN, Kormer AYa*. Complications after heart transplantation. *Russian Journal of Transplantology and Artificial Organs*. 2005; 7 (3): 9–10.
78. *Shumakov VI.* Current status and advances in the field of transplantology and artificial organs in Russia. *Russian Journal of Transplantology and Artificial Organs*. 2006; 8 (4): 6–10.
79. *Tolpekin VE, Kilasev NB, Ignatova NV*. Current issues of artificial heart and ventricular bypass using blood pumps of membrane type. *Transplantologiya. The Russian Journal of Transplantation*. 2012; (1–2): 43–47. (In Russ.). https://doi.org/10.23873/2074-0506-2012-0-1-2-43-47.
80. *Chernyavskiy AM, Doronin DV, Fomichev AV, Karaskov AM.* The initial experience of implantation of the left ventricular assist device "Sputnik" at a cardiac surgery center. *Circulation pathology and cardiac surgery*. 2019; 23 (1): 26–32.
81. *Nevzorov AM, Khaustov AI, Itkin GP*. Experience of using domestic pumps for auxiliary blood circulation. *Russian Journal of Transplantology and Artificial Organs*. 2022; 24 (S): 150.
82. *Khubutia MS, Shemakin SY, Filatov IA, Nevzorov AM.* Universal complex for mechanical support of the pumping function of the left and right ventricles of the heart – "STREAM CARDIO". *Russian Journal of Transplantology and Artificial Organs*. 2019; 21 (S): 135–135.
83. BIOSOFT-M. STREAM CARDIO. [Electronic resource]. Date of access: 23.04.2025. https://biosoft-m.ru/produkty/strim-kardio/.

The article was submitted to the journal on 23.04.2025

DOI: 10.15825/1995-1191-2025-2-100-111

DEVELOPMENT AND EVALUATION OF BIODEGRADABLE SILK FIBROIN SCAFFOLDS

E.I. Podbolotova[1, 2], L.A. Kirsanova[1], E.G. Kuznetsova[1], N.V. Grudinin[1], A.R. Pashutin[1, 2], O.I. Agapova[1], A.E. Efimov[1], E.A. Nemets[1], Yu.B. Basok[1], I.I. Agapov[1]

[1] Shumakov National Medical Research Center of Transplantology and Artificial Organs, Moscow, Russian Federation

[2] Moscow Institute of Physics and Technology (National Research University), Dolgoprudny, Moscow Oblast, Russian Federation

Objective: to investigate the biodegradation of natural silk-based tissue scaffolds (NS-TS) under *in vitro* and *in vivo* conditions, assessing their potential for tissue engineering applications. **Materials and methods.** Two types of NS-TS, Fibroplen-Atlas and Fibroplen-Gas, along with their modified versions, were analyzed. *In vitro* biodegradation was assessed in Fenton's solution, while *in vivo* studies were conducted on rats, with histological and morphometric analysis of the implants at 4, 14, and 56 days post-implantation. **Results.** *In vitro* biodegradation studies showed that Fibroplen-Gas completely degraded in <15 days, whereas Fibroplen-Atlas persisted for up to 45 days. *In vivo* analysis showed gradual resorption of all scaffolds, with Fibroplen-Gas exhibiting more pronounced degradation. Histological examination revealed a macrophage response, formation of foreign-body giant cells, and signs of implant vascularization. Morphometry confirmed a reduction in filament cross-sectional area, particularly in modified samples. **Conclusion.** Modifications of NS-TS influence their biodegradation rate, inflammatory response, and vascularization.

Keywords: silk, biodegradation, tissue engineering.

INTRODUCTION

The development of biodegradable materials for wound treatment and tissue defect replacement is a key challenge in modern medicine and bioengineering. Traditional methods, such as using autologous grafts, present several limitations, including limited availability of donor material, risk of complications at donor site, potential graft rejection, and inability to fully restore the complex anatomy of damaged tissues [1, 2]. Effective tissue repair requires not only innovative techniques but also creation of new biomaterials that meet the specific requirements of clinical applications. Over recent decades, biomaterials, particularly those of natural origin, have garnered increasing attention due to their unique properties, such as biocompatibility, biodegradability, and the potential for modification to suit individual patient needs [3]. Among these biomaterials, silk has received special attention because of its outstanding physicochemical and biological properties, making it a promising foundation for the manufacture of medical devices [4].

Silk, obtained from the cocoons of Bombyx mori silkworms, is a natural protein polymer primarily composed of two key proteins: fibroin and sericin. Fibroin, in particular, possesses unique mechanical properties, such as high tensile strength and elasticity, making it highly attractive for medical applications [5, 6]. Silk is also noted for its high biocompatibility, which helps minimize the body's immune response, and its controlled biodegradability, a crucial factor for development of implantable materials designed for long-term use [7]. These properties make silk an ideal candidate for creating materials for tissue engineering and wound care [8].

In recent years, silk has been extensively researched as a foundation for the development of various medical devices. Notably, biodegradable materials based on silk fibroin have been developed for bone replacement [9, 10]. These materials, which incorporate silk fibroin, calcium phosphates, and other bioactive components, have shown promising biological performance and potential for use in bone engineering, particularly in bone defect repair. Silk is also being explored for the creation of scaffolds – three-dimensional structures that support cell growth and differentiation. Such scaffolds can be used to regenerate various tissues, including bone, cartilage, skin, nerve tissue [11–13], and even corneal tissue [14]. This approach represents a promising alternative to traditional tissue repair methods.

One of the key advantages of silk is its high flexibility in modifying its properties according to the specific requirements of a given application. By adjusting the processing conditions, it is possible to regulate the material's biodegradation rate, mechanical properties,

Corresponding author: Igor Agapov. Address: 1, Shchukinskaya str., Moscow, 123182, Russian Federation. Phone: (495) 231-60-42. E-mail: igor_agapov@mail.ru

and cell interaction, which opens up significant potential for creating personalized medical devices that can be tailored to the unique needs of individual patients [15, 16]. In addition, silk has low immunogenicity, reducing the risk of implant rejection and inflammation. This property is particularly crucial for the development of materials intended for long-term implantation [17, 18]. This makes silk especially valuable in the creation of products for treating chronic diseases and repairing damaged tissues.

Despite the clear advantages of silk, its use in medicine comes with several challenges. The production and processing of silk must be carefully controlled to ensure the stability of the material's properties and its safety for the patient. Even minor changes in the production process can significantly alter the mechanical, biological, and chemical properties of the material, necessitating stringent standards and additional research to confirm its effectiveness over the long term.

Thus, while silk shows considerable promise as a biomaterial, its application in medical technologies requires further investigation. The development of new methods for modifying and optimizing the properties of silk-based materials will open new opportunities for their successful integration into clinical practice and their use in various medical fields, including tissue engineering and tissue repair. This article explores the properties of tissue scaffolds made from natural silk, their potential for medical applications, and possible ways to to optimize their properties.

MATERIALS AND METHODS

Preparation of Fibroplen-Gas 0 and Fibroplen-Atlas 0 samples

For the fabrication of biodegradable fabric scaffolds, natural silk fabrics composed solely of silk fibers and free from extraneous impurities were used (EAC Declaration of Conformity, No. RU D-CN.PA09.B.91575/23, Tianjin Textile Industrial Supply And Sale Co., Ltd, China). Two types of silk fabrics with differing densities – 15 g/m^2 and 155 g/m^2 – were selected for this study. The preparation process for the fabric samples followed previously described protocols [19]. Initially, the fabrics were boiled in a sodium bicarbonate solution in a water bath for 40 minutes, followed by thorough rinsing in distilled water and a second boiling for 30 minutes. This cycle was repeated three times after which the scaffolds were air-dried at room temperature. The resulting samples were designated as "Fibroplen-Gas 0" (lower-density fabric) and "Fibroplen-Atlas 0" (higher-density fabric).

Preparation of modified Fibroplen-Gas 80 and Fibroplen-Atlas 80 samples

To obtain modified scaffold variants, the previously prepared Fibroplen-Gas 0 and Fibroplen-Atlas 0 samples were subjected to controlled degradation in a water-alcohol solution of calcium chloride, using a molar ratio of 1 : 2 : 8. Incubation was carried out at 46 °C for 352 minutes for Fibroplen-Gas 0 samples and 216 minutes for Fibroplen-Atlas 0 samples – corresponding to 80% of the total degradation time for each fabric type. Following incubation, the samples were thoroughly rinsed with distilled water and then air-dried at room temperature. The resulting samples are hereinafter designated as "Fibroplen-Gas 80" and "Fibroplen-Atlas 80", respectively.

In vitro biodegradation study

In vitro biodegradation of samples was evaluated in accordance with GOST 10993-13-2009 ("Assessment of biological effect of medical devices"). Samples were incubated in 40 mL of Fenton's reagent, composed of 100 μM $FeSO_4$ and 1 mM H_2O_2, at a temperature of 37 °C. The oxidative medium was renewed every 3 days. At the end of incubation, the samples were rinsed with 40 mL of distilled water, dried in a thermostat at 37 °C for 48 hours, and subsequently placed in a Binder VD-54 vacuum desiccator (Germany) at a residual pressure of 10–20 mmHg for 24 hours.

Biodegradation was assessed gravimetrically using a Sartorius CPA-225D analytical scale (Germany), by measuring the change in the sample mass before and after the incubation period.

In vivo biodegradation study

In vivo biodegradation experiment was carried out on male Wistar rats weighing 250–300 g, obtained from the Krolinfo laboratory animal nursery (Vysokovo, Orekhovo-Zuyevsky urban district, Russia). Prior to the experiment, the animals were acclimatized to the housing conditions for a period of 7 days. Throughout the study, the rats were kept isolated in single cages, they were provided with standard laboratory feed and had ad libitum access to water. Vivarium temperature was maintained at 22 ± 2 °C, relative humidity at 55–65%, and a 12-hour light/dark cycle.

Before surgery, general anesthesia was induced using Zoletil® 100 (Virbac, France) at a dose of 15 mg/kg body weight administered intramuscularly. For antiseptic preparation, a 0.05% chlorhexidine solution was applied to the skin in the interscapular region. To prevent mechanical irritation and minimize the risk of postoperative infection, the surgical site was shaved using electric clippers prior to intervention.

Following skin antisepsis, a subcutaneous pocket was created using sterile surgical scissors and a scalpel. A 1×1 cm silk scaffold sample was inserted into the prepared cavity and secured in place with four knotted sutures using Prolene 4/0 monofilament polypropylene surgical thread (Ethicon, USA). The sutures ensured close adherence of the implant to the surrounding subcutaneous tissue, thereby preventing displacement. After

implantation, the incision was closed using additional knotted sutures.

The experimental durations were set at 4, 14, and 56 days. Upon completion of each time point, the animals were euthanized. Following confirmation of biological death, the implanted materials along with surrounding tissue were explanted for subsequent histological examination.

Histological study

After explantation, tissue samples were fixed in 10% buffered formalin solution for at least 24 hours. Standard histological processing was performed, including dehydration through a graded ethanol series (50%, 60%, 70%, 80%, and 96%), paraffin embedding, and sectioning at a thickness of 5–6 μm using a RM2245 microtome (Leica, Germany).

Histological staining was performed using the following methods:

– Mayer's hematoxylin and eosin (BioVitrum, Russia) – to evaluate the overall tissue structure;
– Masson's trichrome stain (BioVitrum, Russia) – to detect total collagen.

The preparations were examined using an Eclipse 50i optical microscope (Nikon, Japan) equipped with a digital camera.

The histological evaluation focused on the following parameters:

– Cellular response (presence of macrophages, foreign-body giant cells, lymphocytes, and granulocytes);
– Vascularization (capillary formation);
– Formation of connective tissue capsules;
– Degree of material bioresorption.

Morphometric analysis

Morphometric evaluation of the filament cross-sectional area was conducted using ImageJ software (version 1.49v, National Institutes of Health, USA). For each filament type, 40 cross-sections with clearly defined contours and free from overlapping neighboring structures were selected for analysis.

Statistical data processing

Statistical analysis was performed using IBM SPSS Statistics version 26. Data distribution was assessed using the Kolmogorov–Smirnov test. The following statistical tests were applied:

– Mann–Whitney U test – for comparison between two independent groups;
– Kruskal–Wallis test – for comparison among three or more independent groups;
– Tukey's test – for post hoc multiple comparisons.

Differences were considered statistically significant at $p < 0.05$. For variables with non-normal distribution, data are presented as median (Me) and interquartile range (Q1–Q3).

RESULTS AND DISCUSSION

In vitro biodegradation studies

The Fibroplen-Atlas silk samples with different pretreatments showed varying rates of biodegradation (Table 1). For Fibroplen-Atlas 0 samples, slow degradation was observed on day 15, with a weight loss of 5%. By day 30, degradation accelerated, reaching a mass loss of 44%, and by day 45, the total weight loss amounted to 79%. In contrast, Fibroplen-Gas samples underwent complete degradation in less than 15 days. For each time point, five samples of each type were analyzed.

Table 1

Effect of pretreatment on silk degradation profile

	15 days	30 days / Δ 15–30 days	45 days / Δ 30–45 days
Fibroplen-Atlas 0	5%	44% / 39%	79% / 35%
Fibroplen-Atlas 80	5%	49% / 44%	86% / 37%
Fibroplen-Gas	All samples were completely degraded in less than 15 days		

The results obtained indicate that pretreatment of silk has an effect on its biodegradation *in vitro* biodegradation rate. Therefore, the choice of material treatment may play a critical role in developing materials with the required degradation rate for various biomedical applications.

In vivo biodegradation studies (morphologic analysis)

Implantation at day 4 (unmodified samples)

Fibroplen-Gas 0

On day 4 following implantation of the control Fibroplen-Gas 0 sample, histological examination revealed a large fragment of transverse striated muscle tissue, surrounded by a thin fibrous layer and loose connective tissue (Fig. 1, a). Within this area, implant fragments were identified as homogeneous filaments observed in both transverse and longitudinal sections. These filaments showed a delicate cream coloration with hematoxylin and eosin staining and appeared pale pink with Masson's trichrome stain.

A moderate cellular response to the implant was observed, characterized by the presence of macrophages, foreign-body giant cells (FBGCs), a few lymphocytes, and occasional granulocytes. Only faint signs of macrophage-mediated resorption of the implant material was noted. No signs of inflammation were detected in the surrounding muscle tissue. Overall, inflammatory response was mild and primarily lymphoid-macrophage in nature.

Fibroplen-Atlas 0

Fig. 1, b presents the histological image of the control sample "Fibroplen-Atlas 0", demonstrating a fragment

of transverse striated muscle tissue adjacent to a fibrous layer and loose connective tissue, within which the implant was identified. Surrounding the implant, there is loose connective tissue with pronounced hypercellularity, characterized by a high concentration of fibroblasts, histiocytes, and lymphocytes, as well as numerous full-blooded capillaries. This morphological pattern is indicative of active granulation tissue formation.

The content of FBGCs was very low, with only occasional individual cells detected. While granulocytes were generally scarce in the surrounding tissue, a localized area of intense cellular infiltration was identified, suggesting the presence of a residual acute inflammatory response. There were virtually no signs of bioresorption.

Implantation at day 14 (unmodified samples)

Fibroplen-Gas 0

The examined sample contains adipose tissue, within which the Fibroplen-Gas 0 implant was located (Fig. 2, a). The implant fragments were surrounded by thin connective tissue strands, interspersed with thin-walled, full-blood blood vessels, indicating ongoing processes of encapsulation and vascularization. Numerous macrophages and FBGCs were observed in close proximity to the implant strands, along with clear signs of bioresorption. In addition, few lymphocytes and occasional granulocytes were detected. The inflammatory response was predominantly macrophage-mediated.

Fibroplen-Atlas 0

The implant is surrounded by loose connective tissue along its perimeter (Fig. 2, b). In close proximity to the implant, thin connective tissue strands oriented parallel to its long axis were observed, which likely indicate early stages of capsule formation. Connective tissue fibers and thin-walled blood vessels were seen infiltrating the implant. Numerous macrophages, FBGCs, and epithelioid cells were present around the implant filaments.

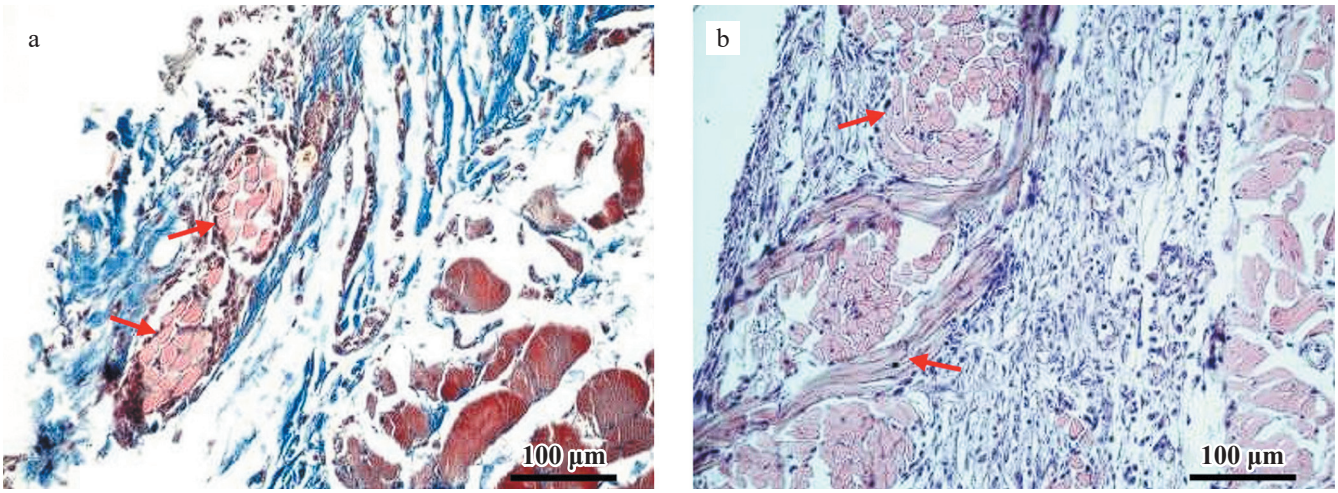

Fig. 1. Samples at 4 days post-implantation: a, Fibroplen-Gas 0, H&E stain; b, Fibroplen-Atlas 0, H&E stain. Arrows indicate implant fragments. 200×

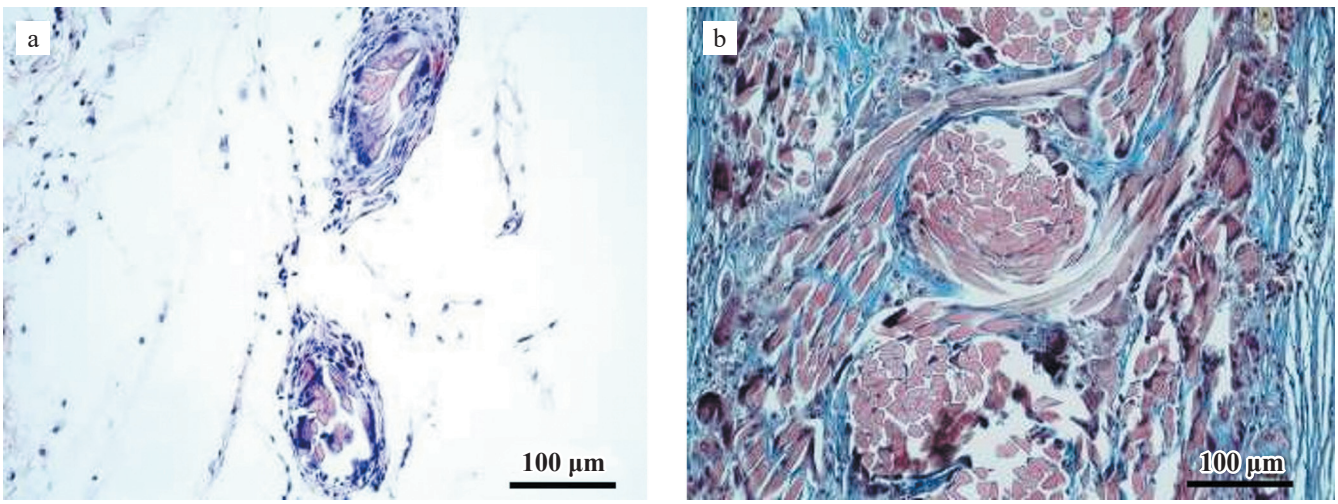

Fig. 2. Samples at 14 days post-implantation: a, Fibroplen-Gas 0, H&E stain; b, Fibroplen-Atlas 0, Masson's trichrome stain. 200×

However, signs of bioresorption were minimal, with the majority of the implant material remaining structurally intact. Overall, the inflammatory response was predominantly macrophage-mediated, with small admixture of lymphocytes and occasional granulocytes.

Implantation at day 56 (unmodified samples)

Fibroplen-Gas 0

The implant is embedded in a layer of loose connective tissue, adjacent to fragments of transverse striated muscle tissue (Fig. 3, a). A sustained macrophage response is evident, including the presence of FBGCs, accompanied by partial resorption of the implant material. Vascularization persists, with thin-walled capillaries noted in the surrounding tissue. A thin connective tissue capsule has formed along the implant perimeter, and in some areas, it is penetrated by capillaries. Besides, individual filaments of the implant are enveloped by collagen fibers. Compared to the 14-day observation period, both the signs of bioresorption and encapsulation of the implant threads appear more pronounced.

Fibroplen-Atlas 0

The implant is surrounded by loose connective and adipose tissue (Fig. 3, b). The inflammatory response remains mild and predominantly macrophage-mediated. FBGCs are scarce and primarily located in the peripheral zone of the implant adjacent to surrounding tissues. A substantial portion of the implant material appears structurally intact, showing minimal signs of resorption. Vascularization is evident, with full-blooded capillaries observed among the implant filaments. A thin connective tissue capsule has formed around the implant, with occasional capillary penetration. Besides, individual strands of the implant are encapsulated by collagen fibers.

Implantation at day 4 (modified samples)

Fibroplen-Gas 80

The histological profile is characterized by transverse striated muscle tissue adjacent to a broad layer of loose connective tissue exhibiting signs of inflammatory infiltration (Fig. 4, a). The infiltrate includes granulocytes, lymphocytes, mast cells, macrophages, numerous full-blooded capillaries, and fibroblasts – indicative of active granulation tissue formation. Single FBGCs are locally present. Notably, in comparison to the unmodified Fibroplen-Gas 0 samples at the same time point, inflammatory response in the modified samples is more pronounced and polymorphic, whereas the unmodified implants evoked a milder, predominantly lymphoid-macrophage reaction.

Fibroplen-Atlas 80

In the examined sample, the histological profile consists of transverse striated muscle tissue bordered by a thin fibrous layer and a layer of loose connective tissue. Along the boundary, numerous implant fragments are identified, primarily as transverse and, less frequently, longitudinal sections of filaments (Fig. 4, b). Inflammatory response is characterized by abundant macrophages, the presence of FBGCs, and lymphocytes. Granulocytes are sparse and predominantly localized within the lumens of capillaries in the loose connective tissue. Evidence of implant resorption is present, mediated by both FBGCs and individual macrophages infiltrating between implant threads. Thin-walled blood vessels containing erythrocytes are observed within the implant structure. The adjacent muscle tissue appears unaltered.

It should be noted that at the same observation period, unmodified Fibroplen-Atlas 0 samples displayed features of an incomplete acute inflammatory phase, while the

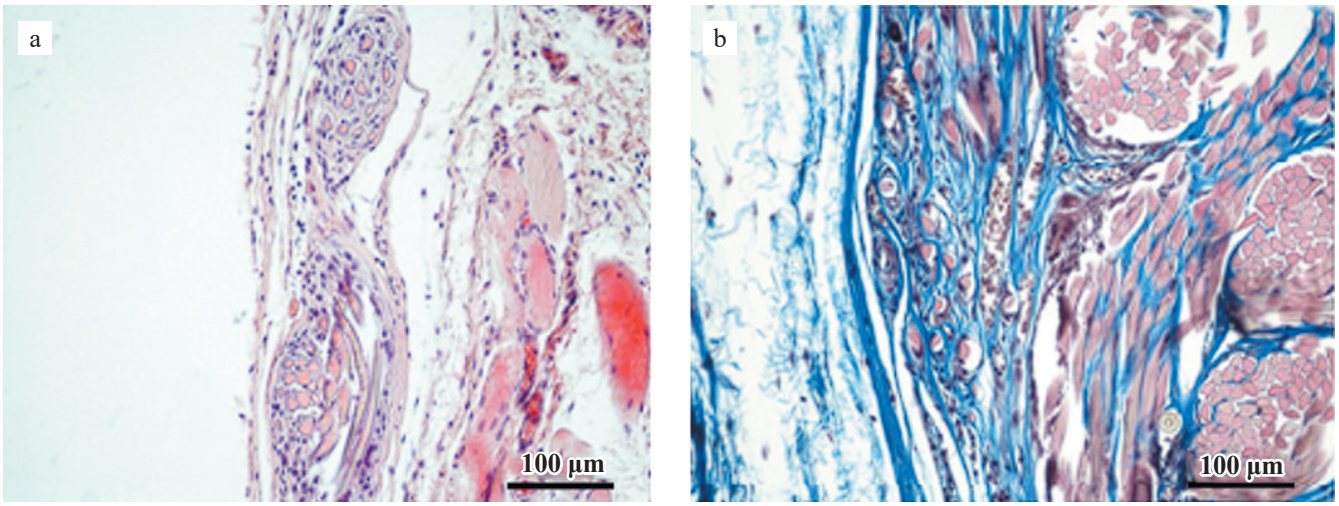

Fig. 3. Samples at 56 days post-implantation: a, Fibroplen-Gas 0, H&E stain; b, Fibroplen-Atlas 0, Masson's trichrome stain. 200×

response in Fibroplen-Atlas 80 samples shifted toward a more organized lymphoid-macrophage pattern.

The histological evaluation of the modified samples at the 4-day observation point revealed the following key features:

a) In Fibroplen-Gas 80 samples, characteristic signs of the acute phase of inflammatory response were observed, whereas the Fibroplen-Atlas 80 samples exhibited a predominantly lymphoid-macrophage type of inflammation.
b) All samples showed evidence of partial bioresorption of the implanted material. Notably, in the Fibroplen-Atlas 80 group, the implant exhibited good structural preservation, with the majority of the material remaining intact.
c) Signs of vascularization were identified only in one of the presented samples – Fibroplen-Atlas 80.
d) Fibroplen-Gas 80 samples exhibited moderate inflammation in the tissues surrounding the implant.

Implantation at day 14 (modified samples)

Fibroplen-Gas 80

In the examined specimen, the implant was surrounded by loose connective tissue (Fig. 5, a). A macrophage response to the implant was noted, accompanied by the formation of numerous FBGCs and partial resorption of the implant. The inflammatory infiltrate also contained single lymphocytes and granulocytes. Evidence of vascularization was noted within the implant, represented by the presence of isolated capillaries. Encapsulation was generally poorly developed; however, intensive ingrowth of connective tissue fibers into the implant structure was evident. The surrounding loose connective tissue showed no visible changes.

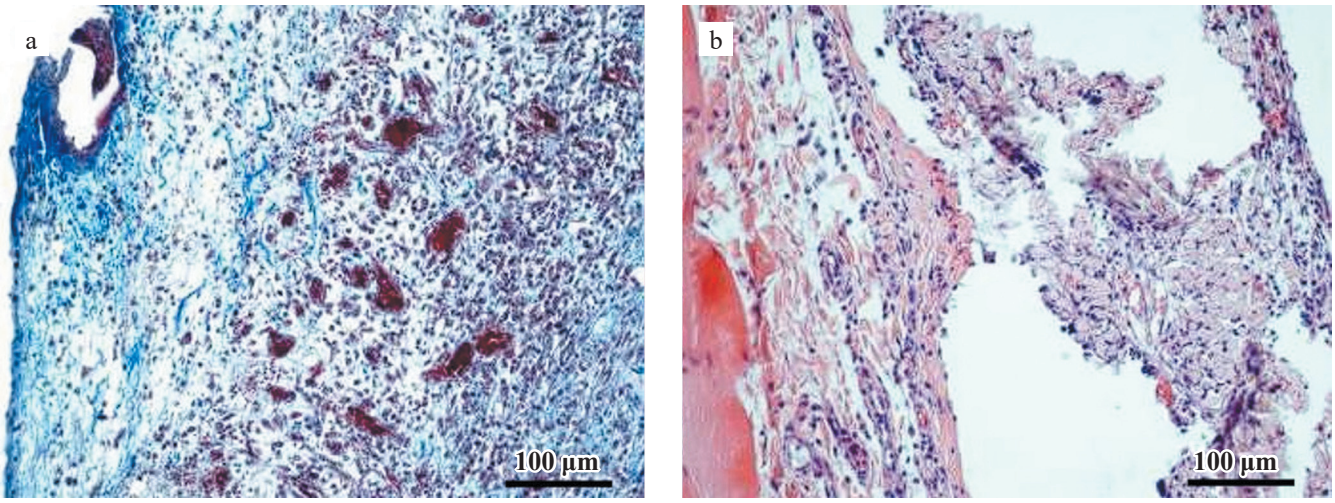

Fig. 4. Samples at 4 days post-implantation: a, Fibroplen-Gas 80, Masson's trichrome stain; b, Fibroplen-Atlas 80, H&E stain. 200×

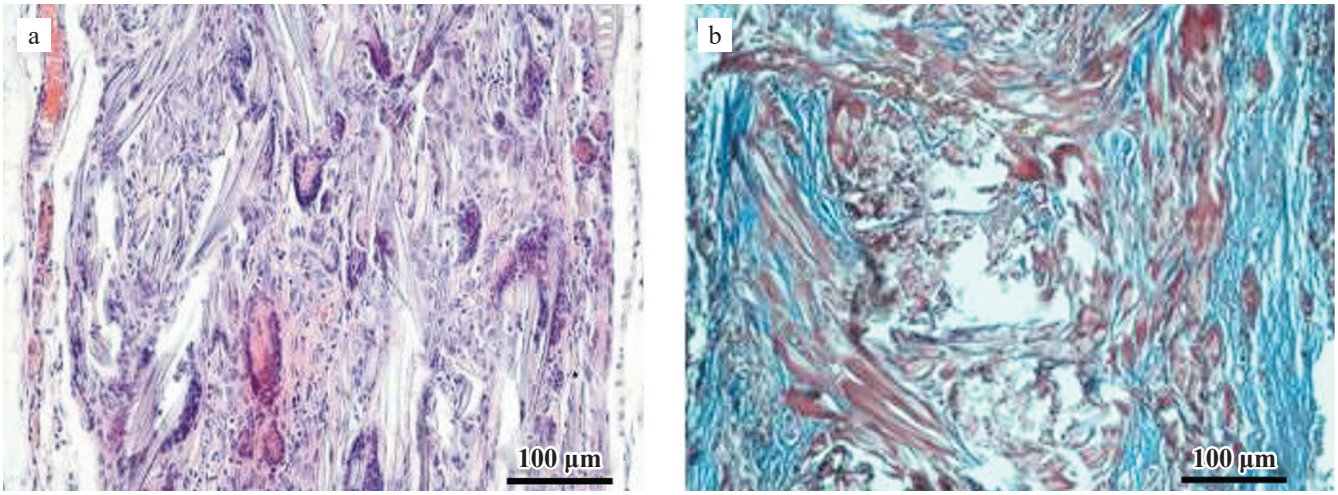

Fig. 5. Samples at 14 days post-implantation: a, Fibroplen-Gas 80, H&E stain; b, Fibroplen-Atlas 80, Masson's trichrome stain. 200×

Comparable results were observed in the unmodified Fibroplen-Gas 0 samples at the same time point. These included a predominantly macrophage-driven inflammatory response, ingrowth of connective tissue strands into the implant, as well as signs of bioresorption and vascularization.

Fibroplen-Atlas 80

The histological examination shows the implant surrounded by loose connective tissue (Fig. 5, b). A loose, unevenly thick connective tissue capsule is present around the implant's perimeter. A lymphoid-macrophage inflammatory response involving FBGCs is noted. Compared to Fibroplen-Gas 80 samples, a slightly higher number of lymphocytes is observed. Evidence of partial resorption of the implant is also present. Signs of vascularization and ingrowth of connective tissue strands into the implant are apparent. The adjacent loose connective tissue contains full-blooded capillaries, increased number of lymphocytes and macrophages (relative to previous samples), as well as isolated plasmocytes.

The overall morphologic picture is generally consistent with that observed in the experiment using unmodified Fibroplen-Atlas samples at the same time point. However, it should be noted that the degree of fibrosis, vascularization, and bioresorption is greater in the modified samples compared to their unmodified counterparts. In addition, differences were observed in the composition of the inflammatory infiltrate: specifically, a slightly higher number of lymphocytes was recorded in the modified samples, and the inflammatory response exhibited a more pronounced lymphoid-macrophage character.

The histological features observed in the modified Fibroplen-Gas 80 and Fibroplen-Atlas 80 samples at 14 days post-implantation can be summarized as follows:

a) A predominance of the gigantocellular component in the inflammatory infiltrate, most notably in the Fibroplen-Gas 80 sample.
b) Formation of a connective tissue capsule around the implant, with the least pronounced capsule observed in the Fibroplen-Gas 80 group.
c) Ingrowth of connective tissue fibers into the implant, partially replacing the original material.
d) Evidence of implant vascularization.
e) Partial resorption of implant material.

Implantation at day 56 (modified samples)

Fibroplen-Gas 80

In the examined specimen, the Fibroplen-Gas 80 implant was localized within a layer of loose connective tissue (Fig. 6, a). A macrophage-dominated inflammatory response was observed, with the presence of FBGCs and signs of ongoing resorption of the implant material. Vascularization within the implant was minimal, with only isolated capillaries identified. There was no formed connective tissue capsule encasing the implant; instead, encapsulation was limited to individual threads and/or fibers. The adjacent loose connective tissue showed no apparent changes.

It is worth noting that these findings partially resemble those seen in the control group (Fibroplen-Gas 0), particularly regarding the macrophage-driven inflammatory response and limited vascularization. However, unlike the modified samples, the control group showed the formation of a continuous encapsulating capsule around the implant, along with more pronounced signs of bioresorption.

Fibroplen-Atlas 80

The histological picture reveals the implant surrounded by loose connective tissue and a fragment of adjacent transverse striated muscle tissue (Fig. 6, b). A macrophage-dominated inflammatory response is evident, including the presence of FBGCs, accompanied by ongoing resorption of the implant material. Vascularization within the implant is minimal, with only isolated

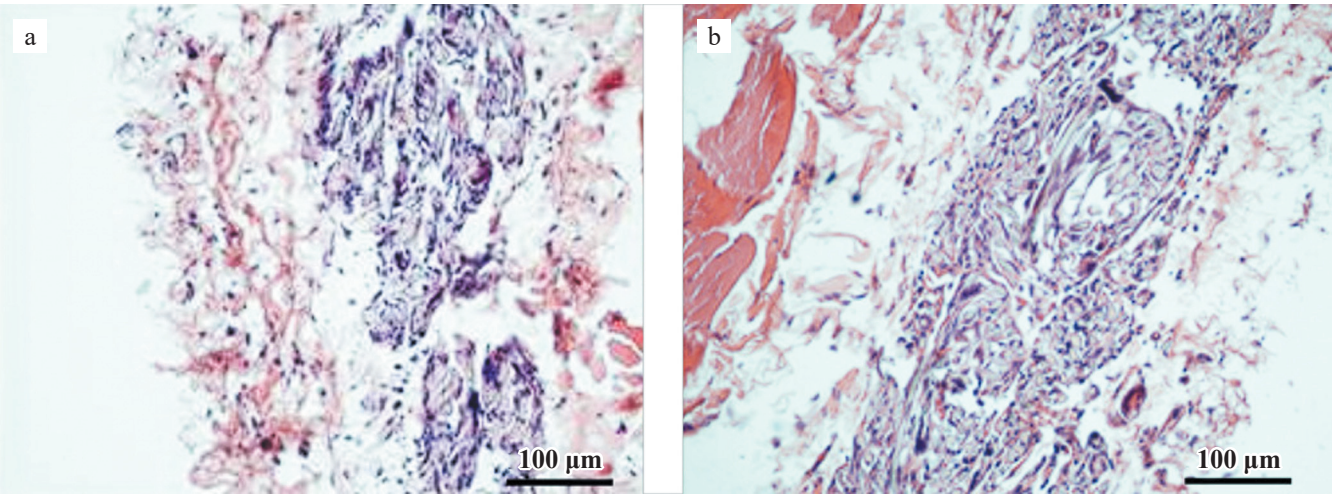

Fig. 6. Samples at 56 days post-implantation: a, Fibroplen-Gas 80, H&E stain; b, Fibroplen-Atlas 80, H&E stain. 200×

Table 2

Cross-sectional areas of Fibroplen-Gas and Fibroplen-Atlas filaments at different implantation dates

Description	Cross-sectional area, μm²			Statistical significance (p)
	4 days	14 days	56 days	
Fibroplen-Gas 0	132.5 (111.8–157.6)	86.3 (68.4–102.9)	56.7 (42.1–71.0)	$p_{4–14} < 0.05$*
				$p_{4–56} < 0.05$*
				$p_{14–56} < 0.05$*
Fibroplen-Gas 80	84.6 (60.6–102.9)	47.5 (25.5–66.8)	54.2 (41.0–71.5)	$p_{4–14} < 0.05$*
				$p_{4–56} < 0.05$*
				$p_{14–56} > 0.05$
Fibroplen-Atlas 0	121.8 (101.3–134.7)	111.3 (102.6–120.2)	97.5 (81.2–117.3)	$p_{4–14} > 0.05$
				$p_{4–56} < 0.05$*
				$p_{14–56} > 0.05$
Fibroplen-Atlas 80	48.1 (40.8–62.0)	44.4 (31.5–52.8)	31.6 (22.7–41.7)	$p_{4–14} > 0.05$
				$p_{4–56} > 0.05$*
				$p_{14–56} > 0.05$*

* sample differences are statistically significant at $p < 0.05$.

capillaries observed. No continuous connective tissue capsule around the implant; however, encapsulation of individual implant strands by collagen fibers is noted. No pathological alterations were identified in the tissue adjacent to the implant.

In the control samples (Fibroplen-Atlas 0) examined at the same time point, a similar macrophage response was observed, though it appeared less intense. Moreover, a greater portion of the implant material remained intact, showing no signs of bioresorption. Besides, a thin but continuous connective tissue capsule was observed around the implant in the control group.

The morphological study of Fibroplen-Gas and Fibroplen-Atlas samples with varying degrees of modification at 56 days post-implantation revealed the following:

a) A macrophage response to the implant, involving FBGCs and partial resorption of the material, persisted. However, compared to the previous observation period, the intensity of the cellular response was notably reduced.
b) Vascularization within the implant was minimal across all samples, though it was more pronounced in the Fibroplen-Atlas 80 group compared to Fibroplen-Gas 80.
c) No organized, restrictive fibrous capsule was observed around the perimeter of the implant.

Morphometric analysis of filament cross-sectional area

To assess the biodegradation of silk filaments in Fibroplen-Gas and Fibroplen-Atlas samples with varying levels of modification, the cross-sectional areas of the filaments were measured. The results are presented as medians and interquartile ranges (Q1–Q3) in Table 2.

The data obtained indicate that for the control Fibroplen-Gas 0 samples, the median values of filament cross-sectional areas significantly decreased ($p < 0.05$) throughout the study period. For Fibroplen-Gas 80 filaments, a significant reduction in the filament cross-sectional area occurred between 4 and 14 days of implantation. However, from 14 to 56 days of implantation, there was no significant change in the size of the filaments.

The table also reveals that in both Fibroplen-Atlas 0 and Fibroplen-Atlas 80 samples, there was a significant decrease in filament cross-sectional area between 4 and 56 days of implantation.

CONCLUSION

The conducted studies showed varying degrees of biodegradation of the Fibroplen-Gas and Fibroplen-Atlas silk materials in both *in vitro* and *in vivo* experiments.

In the *in vitro* studies, it was observed that Fibroplen-Gas silk samples underwent complete degradation in less than 15 days. In contrast, all Fibroplen-Atlas samples exhibited slow degradation in the early stages of the experiment. However, by 30 days of incubation in Fenton's solution, the rate of mass loss accelerated significantly, continuing at an increased pace until 45 days. The total mass loss reached 76–86%. Based on experimental data, it can be concluded that the choice of pretreatment method significantly influences the degradation rate *in vitro*, with Fibroplen-Gas samples showing a notably faster degradation compared to the Fibroplen-Atlas 0 samples.

As a result of the conducted morphological study, it was found that for the control Fibroplen-Gas 0 samples (implantation period of 4 days), the degree of inflammatory reaction was less pronounced and exhibited a lymphoid-macrophage character. This was in contrast to the modified samples, where signs of the acute phase of the inflammatory reaction were observed at the same experimental time point.

In the control Fibroplen-Atlas 0 samples, some signs of incomplete acute phase of the inflammatory process persisted. However, in the modified Fibroplen-Atlas 80

samples, inflammatory response was characterized as lymphoid-macrophagic at this stage.

In the control samples (Fibroplen-Atlas 0), bioresorption signs were weakly expressed and not clearly visible. In contrast, in the modified samples, particularly Fibroplen-Atlas 80, the first signs of bioresorption and vascularization were already evident at this observation period. At the 14-day observation period, the morphological study of all Fibroplen-Gas samples yielded similar results: inflammatory reaction was primarily macrophage-driven, with connective tissue strands detected within the implant. Signs of partial bioresorption and vascularization of the implant were also noted.

In contrast, at the same observation period for all Fibroplen-Atlas samples, the morphological picture shared common features: signs of bioresorption, vascularization of the implant, and growth of connective tissue fibers both on the surface and within the implant were noted. However, the degree of vascularization and fibrosis was more pronounced in the modified samples compared to the control (unmodified) samples. Additionally, some differences were observed in the inflammatory infiltrate composition. The Fibroplen-Atlas 80 samples showed a slightly higher lymphocyte content, and the reaction had a lymphoid-macrophage character. In comparison, the Fibroplen-Atlas 0 samples displayed a macrophage-driven inflammatory response.

At the 56-day observation period, histological examination of both unmodified and modified samples revealed the following features: in all samples, there was a continuation of the macrophage reaction to the implant, with the involvement of FBGCs and partial bioresorption of the material. The largest proportion of intact material was preserved in the Fibroplen-Atlas 0 sample. Compared to the 14-day period, the degree of cellular reaction was significantly reduced, most notably in the Fibroplen-Atlas 0 sample.

Vascularization was minimal across all samples, though it was more noticeable in the Fibroplen-Atlas samples. An organized restrictive connective tissue capsule around the perimeter of the implant was observed only in the Fibroplen-Atlas 0 and Fibroplen-Gas 0 samples. In all the samples, there were episodes of encapsulation of individual threads of the implant material by collagen fibers.

In the morphometric analysis of the histological samples, conducted using the ImageJ program, it was found that the cross-sectional areas of the Fibroplen-Gas 0 filaments significantly decreased throughout the study. For the Fibroplen-Gas 80 filaments, a significant decrease in cross-sectional area occurred from day 4 to day 14 of implantation. In the Fibroplen-Atlas 0 and Fibroplen-Atlas 80 samples, the filament areas significantly decreased from day 4 to day 56 of implantation. In the Fibroplen-Atlas 80 samples, a significant decrease in the cross-sectional area of the filaments was also noted from day 14 to day 56 of implantation.

FINDINGS

The following conclusions can be drawn based on the results of the conducted research:

1. Pretreatment influences the degradation rate *in vitro*. The degradation rate for modified Fibroplen-Atlas samples was higher compared to the unmodified samples. Notably, Fibroplen-Gas samples were completely degraded in less than 15 days.
2. Results of morphological study:
   a) Fibroplen-Atlas 0 samples had the largest proportion of intact material after 56 days.
   b) Signs of incomplete acute-phase inflammation were observed at the 4-day period in the Fibroplen-Gas 80 and Fibroplen-Atlas 0 samples. From the 14-day observation onward, inflammatory response in the Fibroplen-Atlas 80 sample was lymphoid-macrophage in character, while the Fibroplen-Gas and Fibroplen-Atlas 0 samples exhibited a macrophage-type reaction. By the 56-day observation period, all studied samples exhibited a macrophage-driven (predominantly gigantocellular) reaction.
   c) Partial bioresorption was observed as early as the 4-day period in the modified Fibroplen-Gas and Fibroplen-Atlas samples, involving FBGCs and single macrophages. In contrast, bioresorption was not visible in the unmodified samples at this time. Starting from day 14, bioresorption was noted in all the studied samples.
   d) Vascularization was only observed at the 4-day period in the Fibroplen-Atlas 80 sample. In all other samples, signs of vascularization were evident from the 14-day observation period onward.
   e) Signs of formation of a restrictive capsule along the perimeter of the implant were seen by the 14-day period in most of the samples. However, by day 56, a thin connective tissue capsule was observed only in the control samples Fibroplen-Atlas 0 and Fibroplen-Gas 0. All samples, regardless of modification, exhibited signs of fibrosis, including the growth of connective tissue fibers deep into the implant and episodes of encapsulation of individual implant threads by collagen fibers.
3. Morphometric analysis of histological specimens showed that the cross-sectional area of Fibroplen-Gas 0 filaments significantly decreased throughout the entire study period. For Fibroplen-Gas 80, a significant decrease was observed between days 4 and 14, with no further significant changes up to day 56. In contrast, both Fibroplen-Atlas 0 and Fibroplen-Atlas 80 samples showed a significant decrease in filament area from day 4 to day 56. Notably, in Fib-

roplen-Atlas 80, there was an additional significant reduction between days 14 and 56.

These findings confirm that modification of silk-based scaffolds enables targeted tuning of their biodegradation rate, inflammatory response, and vascularization profile. The ability to regulate these parameters provides valuable flexibility for tailoring biomaterials to specific clinical needs – such as wound healing and the development of biodegradable implants.

The authors declare no conflict of interest.

REFERENCES

1. *Dionigi B, Fauza DO*. Autologous approaches to tissue engineering. In: StemBook [Internet]. Cambridge (MA): Harvard Stem Cell Institute; 2008. 2012 Dec 10. doi: 10.3824/stembook.1.90.1.
2. *Williams D.* Challenges with the development of biomaterials for sustainable tissue engineering. *Front Bioeng Biotechnol*. 2019 May 31; 7: 127. doi: 10.3389/fbioe.2019.00127.
3. *Sevastianov VI, Basok YuB, Baranova NV, Belova AD, Grigoriev AM, Kholodenko IV et al.* Biomimetics of Extracellular Matrices for Cell and Tissue Engineered Medical Products / Eds. V. Sevastianov and Yu. Basok. Cambridge Scholars Publishing; 2023.
4. *Sahoo JK, Hasturk O, Falcucci T, Kaplan DL.* Silk chemistry and biomedical material designs. *Nat Rev Chem*. 2023 May; 7 (5): 302–318. doi: 10.1038/s41570-023-00486-x.
5. *Kamalathevan P, Ooi PS, Loo YL.* Silk-based biomaterials in cutaneous wound healing: A systematic review. *Adv Skin Wound Care*. 2018 Dec; 31 (12): 565–573. doi: 10.1097/01.ASW.0000546233.35130.a9.
6. *Kundu B, Rajkhowa R, Kundu SC, Wang X.* Silk fibroin biomaterials for tissue regenerations. *Adv Drug Deliv Rev*. 2013 Apr; 65 (4): 457–470. doi: 10.1016/j.addr.2012.09.043.
7. *Cao Y, Wang B.* Biodegradation of silk biomaterials. *Int J Mol Sci*. 2009 Mar 31; 10 (4): 1514–1524. doi: 10.3390/ijms10041514. PMID: 19468322; PMCID: PMC2680630.
8. *Vidya M, Rajagopal S.* Silk fibroin: A promising tool for wound healing and skin regeneration. *Int J Polym Sci*. 2021 Oct; 2021 (6): 1–10. doi: 10.1155/2021/9069924.
9. *Sofia S, McCarthy MB, Gronowicz G, Kaplan DL.* Functionalized silk-based biomaterials for bone formation. *J Biomed Mater Res*. 2001 Jan; 54 (1): 139–148. doi: 10.1002/1097-4636(200101)54:1<139::AID-JBM17>3.0.CO;2-7.
10. *Klimentyev AA, Naboka VA.* Biological characteristics of the biodegradable material for bone repair. *Medicine: theory and practice*. 2021; 3: 6–9. [In Russ, English abstract].
11. *Kotliarova MS, Arkhipova AYu, Moysenovich AM, Kulikov DA, Molochkov AV, Moysenovich MM.* Trehmernye poristye skaffoldy na osnove fibroina shelka dlya vosstanovleniya kostnoy tkani. *Genes & Cells*. 2017; 12 (3): 131–132. [In Russ]. doi: 10.23868/gc120968.
12. *Liu Q, Huang J, Shao H, Song L, Zhang Y*. Dual-factor loaded functional silk fibroin scaffolds for peripheral nerve regeneration with the aid of neovascularization. *RSC Adv*. 2016; 6 7683–7691. doi: 10.1039/C5RA22054H.
13. *Safonova L, Bobrova M, Efimov A, Davydova L, Tenchurin T, Bogush V et al*. Silk Fibroin/Spidroin Electrospun Scaffolds for Full-Thickness Skin Wound Healing in Rats. *Pharmaceutics*. 2021 Oct 15; 13 (10): 1704. doi: 10.3390/pharmaceutics13101704.
14. *Gavrilova NA, Borzenok SA, Revishchin AV, Tishchenko OE, Ostrovkiy DS, Bobrova MM et al.* The effect of biodegradable silk fibroin-based scaffolds containing glial cell line-derived neurotrophic factor (GDNF) on the corneal regeneration process. *Int J Biol Macromol*. 2021 Aug 31; 185: 264–276. doi: 10.1016/j.ijbiomac.2021.06.040.
15. *Aigner TB, DeSimone E, Scheibel T.* Biomedical applications of recombinant silk-based materials. *Adv Mater*. 2018 May; 30 (19): e1704636. doi: 10.1002/adma.201704636.
16. *Murphy AR, Kaplan DL*. Biomedical applications of chemically-modified silk fibroin. *J Mater Chem*. 2009 Jun 23; 19 (36): 6443–6450. doi: 10.1039/b905802h.
17. *Kolesnikov AYu, Prokudina ES, Senokosova EA, Arnt AA, Antonova LV, Mironov AV et al.* Results of long-term patency and lifetime visualization of vascular patches from silk fibroin. *Clinical and Experimental Surgery. Petrovsky Journal*. 2023: 11 (3): 68–75. [In Russ, English abstract]. https://doi.org/10.33029/2308-1198-2023-11-3-68-75.
18. *Perrone GS, Leisk GG, Lo TJ, Moreau JE, Haas DS, Papenburg BJ et al.* The use of silk-based devices for fracture fixation. *Nat Commun*. 2014 Mar 4; 5: 3385. doi: 10.1038/ncomms4385. PMID: 24594992.
19. *Agapov II, Agapova OI, Efimov AE, Sokolov DYu, Bobrova MM, Safonova LA.* Sposob polucheniya biodegradiruemykh skaffoldov na osnove tkaney iz natural'nogo shelka. Patent na izobretenie RU2653428 S1, 08.05.2018.

The article was submitted to the journal on 17.02.2025

DOI: 10.15825/1995-1191-2025-2-112-126

THE USE OF AUTOLOGOUS BIOMATERIALS IN COMBINATION WITH BIOCOMPATIBLE MATRICES FOR RESTORATION OF BONE TISSUE DEFECTS (LITERATURE REVIEW)

D.V. Bulgin[1], I.S. Bazarov[2], V.V. Khominets[2], A.L. Kovtun[3], D.A. Ivanov[4], E.Yu. Radomskaya[1], A.A. Shiryaev[5], D.A. Zaichikov[6]

[1] Kurchatov Institute, Moscow, Russian Federation
[2] Kirov Military Medical Academy, St. Petersburg, Russian Federation
[3] Russian Foundation for Advanced Research Projects, Moscow, Russian Federation
[4] Sirius University of Science and Technology, Sirius, Russian Federation
[5] Sechenov University, Moscow, Russian Federation
[6] State Research and Test Institute for Military Medicine, St. Petersburg, Russian Federation

Bone defect repair is an interdisciplinary research field encompassing surgical orthopedics, regenerative medicine, tissue engineering, immunology (*addressing biocompatibility challenges*), materials science and technology (*including additive manufacturing, porosity, and mechanical strength*), and nanotechnology for developing biocompatible matrices that enhance bone regeneration. This literature review highlights recent advancements in bone tissue engineering, focusing on the application of autologous biomaterials in combination with biocompatible matrices to improve bone regeneration outcomes.

Keywords: bone tissue defects, bone marrow, peripheral blood, adipose tissue, autologous biomaterials, biocompatible matrices.

INTRODUCTION

Bone has the unique ability to fully restore its integrity after damage without fibrous tissue formation, retaining its original shape, size, and mechanical strength [1, 2]. Age-related pathology, immunodeficiency states, large areas of damage, and infectious complications can significantly reduce the regenerative potential of bone tissue. In such cases, bone restoration requires specialized methods and surgical techniques, along with a prolonged postoperative rehabilitation period [3]. Bone grafting (using autografts, allografts, and xenografts), along with biocompatible matrices (natural or synthetic) and metal/polymer implants, are currently standard approaches in surgical orthopedics for bone defect repair [3, 4]. Worldwide, approximately 2 million bone grafting procedures are performed annually, making bone tissue the second most frequently transplanted tissue after blood transfusion. Bone autografting is widely regarded as the gold standard for bone defect replacement [5]. However, this procedure has significant limitations, especially when dealing with large or multiple bone defects: limited donor site availability, increased surgical time & anesthesia requirements, and postoperative pain at the donor site [6]. An alternative strategy to traditional bone grafting is the application of regenerative medicine technologies, which use autologous cells and tissues combined with tissue engineering methods [7, 8]. This review explores the potential sources of autologous biomaterials that can be harvested in a hospital setting – bone tissue, bone marrow, peripheral blood, and adipose tissue – and examines their integration with biocompatible matrices to create *in situ* tissue-engineered constructs for bone defect replacement [7, 9].

TISSUE-ENGINEERED BONE CONSTRUCTS

The use of tissue-engineered constructs based on autologous biomaterials in combination with biocompatible matrices can serve as both a supplement to standard techniques and an independent method for bone defect replacement [9, 10].

A tissue-engineered construct for bone defect replacement is a triad that integrates three essential components for stimulating osteogenesis and new bone tissue formation: biocompatible matrix, growth factors, osteogenic cell populations (Fig. 1) [1, 9].

To fully restore bone tissue at the defect site, a tissue-engineered construct must exhibit the following key characteristics [1, 9]:

1. Osteoinduction – growth factor-mediated recruitment, proliferation, and differentiation of mesenchymal stem cells (MSCs) into osteogenic cell lines.

Corresponding author: Dmitry Bulgin. Address: 177, Akademika Lapina str., Veseloye, Adler city district, Sochi, Krasnodar Krai, 354376, Russian Federation.
Phone: (862) 243-24-07. E-mail: bulgin@primatologia.ru

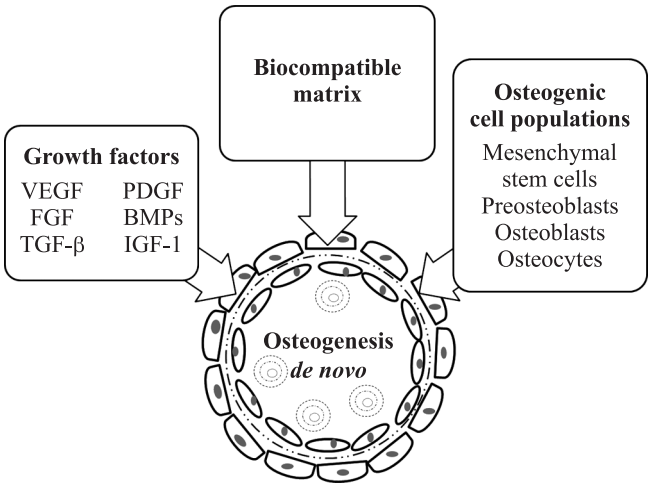

Fig. 1. Bone tissue engineering triad optimal for *de novo* bone formation

2. Osteogenesis – the process of *de novo* bone formation by osteogenic cells.
3. Osteoconduction – the ability to support bone formation across the entire construct surface by providing mechanical support for cell attachment and migration.
4. Osteointegration – the ability to bind seamlessly to adjacent bone without triggering aseptic inflammation or fibrous tissue formation.

AUTOLOGOUS BIOMATERIALS OBTAINED IN A CLINICAL HOSPITAL SETTING

Bone tissue

Bone tissue for autotransplantation is typically harvested from the iliac crest, long tubular bones, skull bones, or mandible [11]. Trabecular bone is known for its ideal osteoconductive characteristics and contains MSCs with high osteogenic potential [12]. The large surface area, due to its spongy structure, ensures high metabolic activity, facilitating the exchange of nutrients, biomolecules, and gases. This structural advantage enables rapid revascularization of the graft, typically occurring within 48 hours [13]. A cortical bone graft exhibits lower osteoconductive, osteoinductive, and osteogenic properties, but it compensates for this with higher mechanical strength [14]. A dense matrix in cortical bone grafts slows down revascularization, extending the process up to two months [15]. Vascularized bone grafts are among the most effective methods for bone defect replacement [16]. The material for transplantation in the form of a bone flap is typically harvested from the fibula, distal metaepiphysis of the femur, or distal metaepiphysis of the radius. The survival rate of these grafts is close to 100% [17, 18]. The difficulty of routine application of vascularized bone grafts arises from the need for microsurgical techniques, which require an operating microscope and special instruments [19, 20], as well as the duration of the operation and the high traumatization of the donor site [21].

Bone marrow

Numerous studies and clinical trials have demonstrated the safety and efficacy of using autologous bone marrow (BM) aspirate as a component of tissue-engineered constructs for bone tissue defect replacement [22]. BM-derived MSCs (BM-MSCs) have been shown to stimulate bone tissue regeneration [23]. BM-MSCs secrete growth factors that regulate chemotaxis, differentiation, proliferation, and secretory activity of bone cells, ultimately controlling physiological remodeling and healing of bone defects [24]. Thus, Bone marrow aspirate is an accessible and abundant source of cells that can be used in self-donor technologies for bone defect replacement [25].

Peripheral blood

Peripheral (venous) blood (PB) is used to isolate platelet-rich plasma (PRP) [26, 27]. PRP is rich in growth factors that can accelerate bone tissue regeneration [28, 29].

According to the classification proposed in 2009, platelet concentrates are divided into four main types based on their biological properties and mechanisms of action, which are determined by the concentration of platelets, leukocytes, and fibrin and, therefore, have different indications for clinical use. These types are:
– pure platelet-rich plasma (P-PRP);
– leukocyte- and platelet-rich plasma (L-PRP);
– pure platelet-rich fibrin (P-PRF);
– leukocyte- and platelet-rich fibrin (L-PRF) [30].

Pure platelet-rich plasma

In clinical practice, P-PRP can be used as either a liquid (injectable) form or a gel (fibrin glue) directly applied to the injury site [31]. Platelet lysate (PL) is derived from P-PRP through a process that involves successive cycles of freezing at –80 °C and rapid thawing at +37 °C. This process causes the destruction of platelet α-granules, which results in the release of numerous growth factors [32]. PL contains all known components found in human venous blood, promotes proliferation and migration of stem and progenitor cells due to the high content of platelet-derived growth factor (PDGF), epidermal growth factor (EGF), fibroblast growth factor (FGF), transforming growth factor-beta 1 (TGF-β1), vascular endothelial growth factor (VEGF), and several other and other bioactive substances (stromal cell factor-1/SDF-1, thrombospondin, P-selectin) [33]. PL has been shown to significantly enhance the proliferative activity of MSCs) and promote their differentiation into osteoblasts. The angiogenic factors released from PL stimulate the formation of new blood vessels [34]. PL can be stored at low temperatures for long periods

(up to 9 months), with full retention of its activity after thawing [35].

Leukocyte- and platelet-rich plasma

L-PRP, like P-PRP, can be prepared in either liquid form or as a gel [36]. L-PRP is widely used in cardiac surgery, operative gynecology, reconstructive surgery [37], traumatology and orthopedics, and sports medicine [38]. L-PRP has been shown to possess antibacterial properties, which can significantly accelerate wound healing [40]. Experimental studies, both *in vitro* and *in vivo*, have demonstrated that L-PRP promotes angiogenesis and osteogenesis at the site of bone tissue damage [41].

Pure platelet-rich fibrin

P-PRF is a fibrin-based biomaterial derived from whole blood without the addition of anticoagulants [42]. P-PRF has a dense consistency, and consists of two visible parts: yellow portion (main body with fibrin) and red portion (red blood cells) [43]. P-PRF contains numerous fibrin strands and is an ideal matrix for promoting the growth and differentiation of osteoblasts osteoblasts, fibroblasts and endothelial cells (Fig. 2) [44].

Concentrated P-PRF (C-PRF) exhibits a high osteogenic potential. C-PRF is an advanced form of P-PRF; the resulting fibrin clot is significantly larger, denser, and richer in growth factors compared to P-PRF [45].

Leukocyte- and platelet-rich fibrin

L-PRF has unique biological and mechanical properties, characterized by a dense fibrin network, enmeshed with platelets and leukocytes, which allows it to be used as a carrier for other cell types [46]. The L-PRF clot, when compressed between two layers of sterile gauze, forms a strong and resilient membrane that can be immediately used intraoperatively as a barrier membrane in bone defect repair [47, 48].

The combined use of PRP and various biocompatible matrices offers a safe, simple, and effective alternative to traditional autologous bone grafts in bone defect repair [49].

Adipose tissue

Adipose tissue is primarily composed of mature adipocytes making up over 90% of its volume, and a smaller heterogeneous fraction of cells collectively known as the stromal-vascular fraction (SVF) [50, 51]. The SVF contains various cell populations including preadipocytes, fibroblasts, immunocompetent cells, vascular smooth muscle cells, endothelial cells, and adipose tissue-derived MSCs (AD-MSCs) [52]. AD-MSCs secrete growth factors like FGF-2, VEGF, IGF-1, TGF-β1, PDGF, and BMP-2, which allows using these cells for *in situ* bone repair [53]. The safety and efficacy of AD-MSCs for bone tissue defect repair have been validated through numerous preclinical studies and clinical trials [54, 55].

EXAMPLES OF COMBINATION OF AUTOLOGOUS BIOMATERIALS WITH BIOCOMPATIBLE MATRICES FOR RESTORING BONE TISSUE DEFECTS (ANIMAL MODELS, CLINICAL USE)

Preclinical studies using animal models (*in vivo*) (Table 1) are essential for validating the effectiveness of bone tissue defect repair methods based on tissue engineering technologies [56].

An ideal animal model should closely mimic human physiology, biology, and biomechanics [88, 89]. Numerous studies have shown that small laboratory animals like mice, rats, and rabbits present challenges in adequately modeling extensive bone defects and their restoration in humans [89]. These models only partially reflect the diversity of processes involved in bone tissue

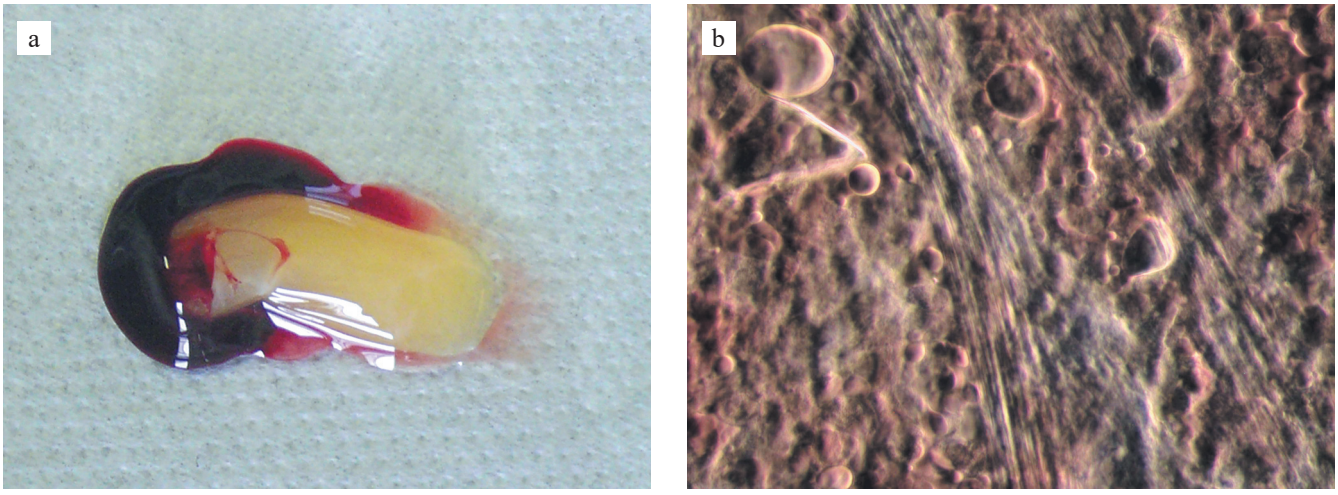

Fig. 2. Structure of fibrin clot (P-PRF): a, yellow part – main body with fibrin, red part – erythrocytes; b, microphotograph of fibrin filaments in the main body, hanging drop method, phase-contrast microscopy of native material, 100× magnification. Photographs from the authors's personal archive

regeneration in humans, making them less suitable for translational medicine research [56]. The advantage of large animals is that their immune systems are more similar to that of humans, which is particularly important when studying the role of immune factors in bone regeneration [90]. Large animals have a body mass and bone structure comparable to humans, allowing for the creation of large bone defects, the fixation of implants or prostheses, and the performance of surgical interventions that closely mimic real clinical conditions for bone integrity restoration in humans [91].

Currently, some methods for restoring damaged bone tissue using autologous biomaterials in combination with various biocompatible matrices are being introduced into clinical practice (Fig. 3) [92, 93].

The clinical results obtained confirm the efficacy of these methods, but scientific publications on this topic are limited to reports of single cases or cases with small groups of patients (Table 2) [93].

PROSPECTS FOR THE USE OF SKELETAL BONES IN COMBAT-RELATED TRAUMATIC INJURY

The enormous kinetic energy of modern munitions causes multiple extensive tissue and organ damage [115]. Studies indicate that limb injuries in approximately 75% of the wounded are the result of mine blast wounds (Fig. 4) [116].

Bone injuries in such wounds are characterized by multiple comminuted fractures, often with the formation of extensive defects (Fig. 5) [116, 118].

Treating military personnel with combat injuries, especially those involving skeletal bones, is a critical and urgent task for the military medical service of the Russian Armed Forces [115, 119, 120]. The Ilizarov compression-distraction osteosynthesis method has traditionally been the only effective treatment for extensive bone defects [121]. However, Russian researchers have proposed an innovative alternative involving intramedullary osteosynthesis using transplantation combined

Table 1

Preclinical *in vivo* animal models of bone defects

Animal models	Anatomical localization of bone defects – composition of tissue-engineered construct – animal count
Rat	cranial vault – BM-MSCs (*xenogeneic, human) + poly-L-lactic acid (PLLA) – 9 individuals [57] cranial vault – BM-MSCs + chitosan + alginate + hydroxyapatite (Hap) – 6 individuals [58]. cranial vault – BM-MSCs + β-tricalcium phosphate (β-TCP) – 9 individuals [59] cranial vault – BM-MSCs + alginate + PLLA – 8 individuals [60] cranial vault – BM-MSCs (*xenogeneic, murine) + PRP + polyvinyl alcohol (PVA) + chitosan + silk fibroin + polycaprolactone (PCL) + β-TCF – 12 individuals [61] cranial vault – BM-MSCs + nano-HAp (nHAp) + gelatin – 5 individuals [62] femur – BM-MSCs (*allogeneic, rat) + (70% PLA + 30% PCL) – 8 individuals [63]
Rabbit	femur – BM-MSCs + PRF + biphasic calcium phosphate (BCP/80% β-TCP + 20% HAp) – 6 individuals [64] femur – PRF + DPC (40% β-TCP and 60% HAp) – 6 individuals [65] radius – BM-MSCs (*allogeneic, rabbit) + PRF + BCP (40% β-TCP + 60% HAp) + PVA – 9 individuals [66] radius – BM-MSCs + PLA + HAp – 9 individuals [67]
Sheep	tibia – BM-MSCs (*allogeneic, sheep) + PCL + HAp – 8 individuals [68] tibia – BM-MSCs + HAp – 4 individuals [69] tibia – BM-MSCs + (20% PLLA + 80% PCL) – 4 individuals [70] tibia – BM-MSCs (*allogeneic, sheep) + PCL – 8 individuals [71] tibia – PRP + PCL + β-TCP – 8 individuals [72] mandible – L-PRF + PLGA – 6 individuals [73] femur – carbon nanotubes + HAp + LPRF – 4 individuals [74] femur – AD-MSCs + β-TCP – 4 individuals (castrated rams) [75] metatarsus – AD-MSCs + autologous bone + nHAp – 6 individuals [76]
Goat	tibia – BM-MSCs + β-TCP – 6 individuals [77]
Pig	mandible – AD-MSCs (*allogeneic, porcine) + β-TCP + PLGA – 7 individuals [78] femur – PRF + BCP (40% β-TCP + 60% HAp) – 4 individuals [79] tibia – BM-MSCs + PRP + α-TCP – 8 individuals [80] tibia – AD-MSCs (*xenogeneic, human) + TCP – 1 individual [81]
Dog	femur – PRP + BCP (40% β-TCP + 60% HAp) – 8 individuals [82] mandible – AD-MSCs + PCL + β-TCP – 3 individuals [83] mandible – BM-MSCs + PCL + β-TCP – 3 individuals [83]
Monkey	femur – BM-MSCs + β-TCP – 7 individuals [84]

* – use of xenogeneic and allogeneic biomaterial as an alternative source. BM-MSCs, bone marrow-derived mesenchymal stem cell; nano-HAp or nHAp, nano-hydroxyapatite; PRF, pure platelet-rich fibrin; P-PRF, pure platelet-rich fibrin; L-PRF, leucocyte and platelet-rich fibrin; PRP, platelet-rich plasma; PLGA, poly(lactic-co-glycolic acid); AD-MSCs, adipose-derived mesenchymal stem cells.

with the transplantation of autologous bone tissue and a collagen-based biocompatible matrix. This approach enables the successful reconstruction of bone defects up to 12 cm in length and offers significant improvements

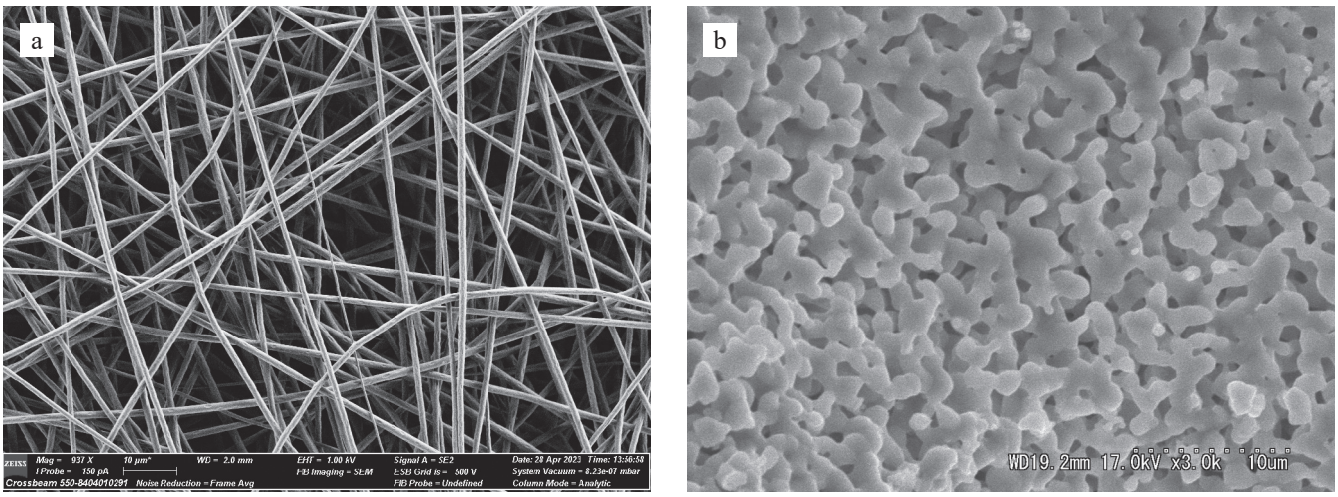

Fig. 3. SEM micrographs of some of the most commonly used biocompatible porous matrices in clinical practice. a, porous polylactide (PLA) matrix, obtained by electrospinning with the formation of a system of open and interconnected pores (average fiber diameter 800 nm, average pore diameter in the fiber 70 nm); b, matrix based on β-TCP, β-TCP granules contain multiple micropores with sizes ranging from 100 to 400 μm, total matrix porosity 75%

Table 2

Use of autologous biomaterials in combination with biocompatible matrices in clinical practice

Anatomical localization of bone defects	Composition of tissue-engineered construct	Patient count	Literature source
Cranial vault	Autologous bone + AD-MSCs + P-PRP (gel)	1	[94]
	AD-MSCs + β-TCP	2	[95]
	BM-MSCs (*allogeneic, donor) + β-TCP + PLLA mesh membrane	3	[96]
Maxilla	Autologous bone + BCP (40% β-TCP + 60% HAp)	27	[97]
	AD-MSCs + β-TCP	1	[98]
	BM-MSCs + β-TCP	3	[99]
	AD-MSCs + PRF + *Allogeneic bone	1	[100]
	AD-MSCs + carbonate apatite (CO_3Ap)	10	[101]
Mandible	AD-MSCs + β-TCP	23	[102]
	BM-MSCs + BCP (80% β-TCP + 20% HAp)	11	[103]
	Autologous bone + L-PRF	22	[104]
Mandible and maxilla	PRF + bioactive glass 45S5 (45% SiO_2, 24.5% Na_2O, 24.5% CaO, 6% P_2O_5)	20	[105]
Humerus	BM-MSCs + β-TCP + collagen sponge	1	[106]
Femur	BM-MSCs + β-TCP	9	[107]
Femur and tibia	Personalized 3D printed tubular mesh structures consisting of PCL (80%) + β-TCP (20%) filled with autologous bone in combination with HAp (40%) + calcium sulfate (60%) + gentamicin sulfate.	4	[108]
	Autologous bone + bioactive glass S53P4 (53% SiO_2, 23% NaO, 20% CaO, 4% P_2O_5)	13	[109]
Tibia	BM-MSCs + β-TCP	16	[110]
	Autologous bone + β-TCP	1	[111]
	Autologous bone + P-PRF (fibrin clot)	1	[112]
Bone defects of various localizations	Bone marrow aspirate + HAp (27 patients) Bone marrow aspirate + collagen sponge (12 patients)	39	[113]
	BM-MSCs + β-TCP	42	[114]

* – use as an alternative source of allogeneic biomaterial. BM-MSCs, bone marrow-derived mesenchymal stem cell; HAp, тфтщhydroxyapatite; PRF, pure platelet-rich fibrin; P-PRF, pure platelet-rich fibrin; L-PRF, leucocyte and platelet-rich fibrin; P-PRP, pure platelet-rich plasma; AD-MSCs, adipose-derived mesenchymal stem cells.

in both anatomical and functional outcomes, while also reducing the incidence of complications compared to the classical Ilizarov technique [9].The induced membrane (IM) method, proposed by French orthopedic surgeon Alain-Charles Masquelet in 2000 (Masquelet method), has become widespread and is actively used in clinical practice [122]. Bone defect repair using this method is performed in two stages. In the first stage, a cylindrical spacer made of polymethylmethacrylate is implanted into the defect site. This spacer mechanically isolates the defect from surrounding tissues, preserves a cavity for the subsequent placement of osteogenic biomaterials, and prevents fibrous tissue formation. Outside, a capsule of granulation tissue (the result of reaction to the foreign body) is formed around the spacer – this is the IM, which contains numerous collagen fibers, blood vessels, osteoprogenitor cells, immune cells (macrophages, lymphocytes), multinucleated foreign-body giant cells, osteoclasts. In the second stage, the spacer is removed, and the encapsulated space is filled with autologous bone graft or a biocompatible matrix. Within this space delimited by IM, revascularization of the graft and new bone formation occur [123]. The average interval between the two stages is approximately 22 months, while bone regeneration at the graft site typically takes 8–10 months. This technique allows for the restoration of bone defects ranging from 4 to 25 cm in length [124, 125].

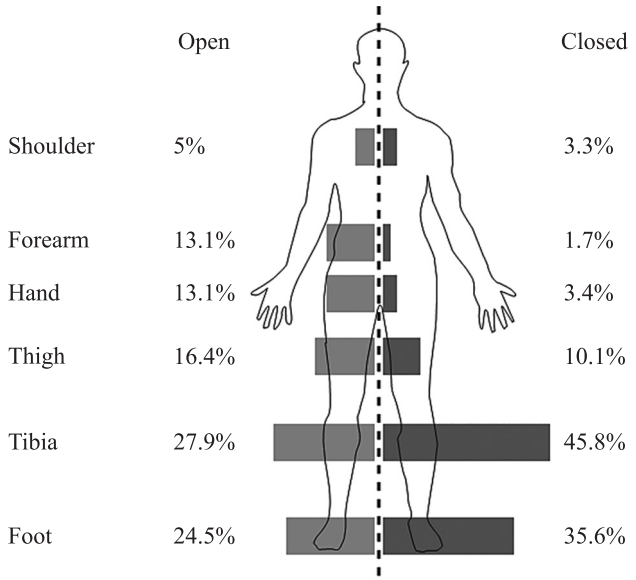

Fig. 4. Anatomical localization of skeletal injuries in an explosion [117]

The IM technique does not require complex equipment or advanced microsurgical skills, as is necessary with vascularized bone grafts. Its relative simplicity makes it especially valuable in military orthopedic surgery, particularly in scenarios involving active combat and limited medical resources [125].

It should be noted that there is no universal method that would be suitable for all wounded patients with bone defects. Each case requires an individualized treatment approach tailored to the specific clinical circumstances [126]. Servicemen with combat-related skeletal injuries represent a valuable human resource for our country's

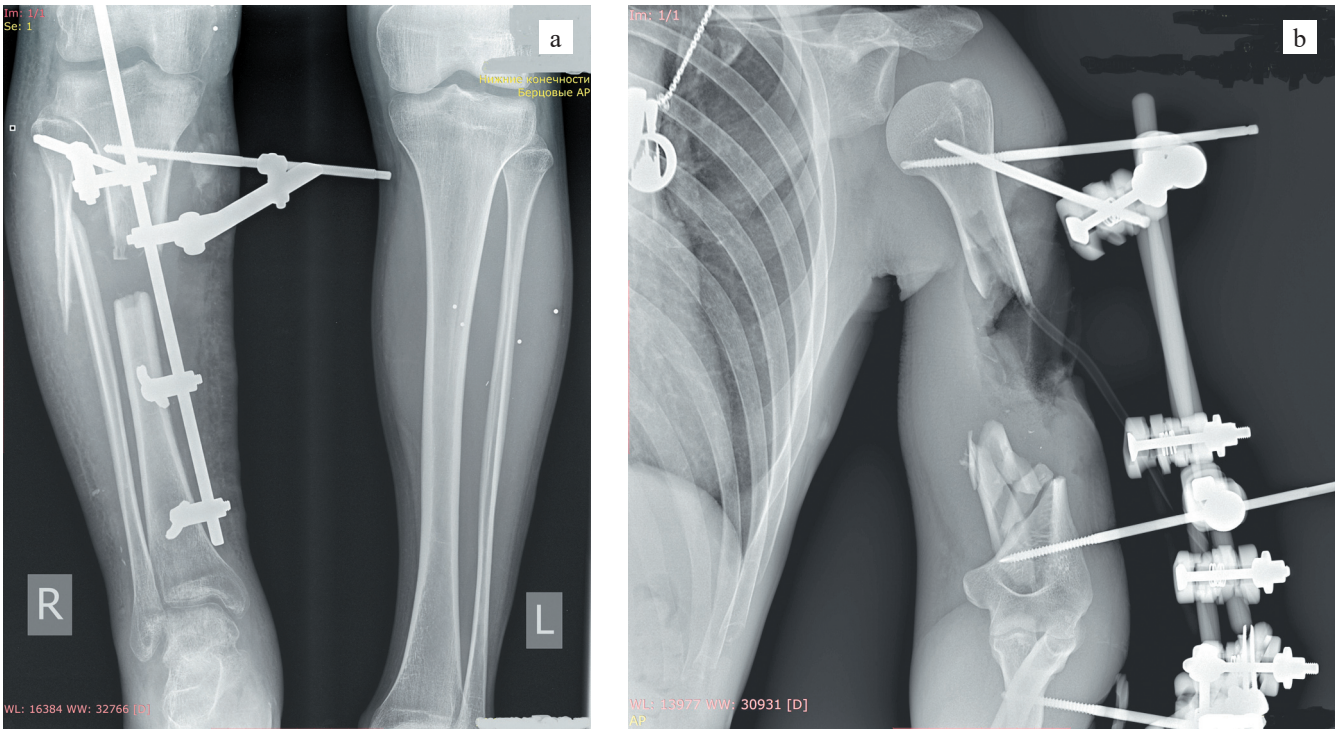

Fig. 5. Bone defects in mine blast injuries: a, right diaphyseal tibial defect, fracture of the right fibula in the upper third with displacement of the fragments, fixed with an external fixation device (EFD); b, soft tissue defect and left humerus defect in the middle third, fixed with an EFD device. Photographs from the authors's personal archive

Armed Forces. Successful treatment and rehabilitation of these individuals enable the return of experienced and battle-tested soldiers to active duty [127].

CONCLUSION

Methods utilizing autologous biomaterials with minimal *ex vivo* manipulation, combined with biocompatible matrices, have demonstrated effectiveness in restoring bone tissue defects across various fields, including orthopedics, traumatology, and dentistry. However, despite significant scientific and technical advancements and promising preclinical research, few of these approaches have transitioned into routine clinical practice. This gap between extensive research and real-world application highlights key challenges, including the scalability and cost-effectiveness of biocompatible matrices, as well as the need for standardized protocols for autologous biomaterial production.

The work was carried out within the framework of the State assignment National Research Centre "Kurchatov Institute" and Supported by the Ministry of Science and Higher Education of the Russian Federation (Agreement 075-10-2021-093).

The authors declare no conflict of interest.

REFERENCES

1. *Winkler T, Sass FA, Duda GN, Schmidt-Bleek K.* A review of biomaterials in bone defect healing, remaining shortcomings and future opportunities for bone tissue engineering: The unsolved challenge. *Bone Joint Res*. 2018 May 5; 7 (3): 232–243. doi: 10.1302/2046-3758.73.BJR-2017-0270.R1. PMID: 29922441.
2. *Ansari M*. Bone tissue regeneration: biology, strategies and interface studies. *Prog Biomater*. 2019 Dec; 8 (4): 223–237. doi: 10.1007/s40204-019-00125-z. PMID: 31768895.
3. *Giannoudis PV, Krettek C, Lowenberg DW, Tosounidis T, Borrelli J Jr.* Fracture Healing Adjuncts-The World's Perspective on What Works. *J Orthop Trauma*. 2018 Mar; 32 Suppl 1: S43–S47. doi: 10.1097/BOT.0000000000001127. PMID: 29461403.
4. *Perez JR, Kouroupis D, Li DJ, Best TM, Kaplan L, Correa D.* Tissue Engineering and Cell-Based Therapies for Fractures and Bone Defects. *Front Bioeng Biotechnol*. 2018 Jul 31; 6: 105. doi: 10.3389/fbioe.2018.00105. PMID: 30109228.
5. *Schmidt AH.* Autologous bone graft: Is it still the gold standard? *Injury.* 2021 Jun; 52 Suppl 2: S18–S22. doi: 10.1016/j.injury.2021.01.043. PMID: 33563416.
6. *Baldwin P, Li DJ, Auston DA, Mir HS, Yoon RS, Koval KJ.* Autograft, Allograft, and Bone Graft Substitutes: Clinical Evidence and Indications for Use in the Setting of Orthopaedic Trauma Surgery. *J Orthop Trauma*. 2019 Apr; 33 (4): 203–213. doi: 10.1097/BOT.0000000000001420.
7. *Kryukov E, Brizhan' L, Khominets V, Davydov D, Chirva Yu, Sevastianov V et al.* Clinical use of scaffold-technology to manage extensive bone defects. *Genij Ortopedii.* 2019; 25 (1): 49–57. doi: 10.18019/1028-4427-2019-25-1-49-57.
8. *Laubach M, Hildebrand F, Suresh S, Wagels M, Kobbe P, Gilbert F et al.* The Concept of Scaffold-Guided Bone Regeneration for the Treatment of Long Bone Defects: Current Clinical Application and Future Perspective. *J Funct Biomater*. 2023 Jun 27; 14 (7): 341. doi: 10.3390/jfb14070341. PMID: 37504836.
9. *Korel' AV, Kuznecov SB.* Tkaneinzhenernye strategii dlya vosstanovleniya defektov kostnoj tkani. Sovremennoe sostoyanie voprosa. *Mezhdunarodnyj zhurnal prikladnyh i fundamental'nyh issledovanij.* 2019; 4: 228–234.
10. *Bulgin DV, Kovtun AL, Reshetov IV, Radomskaya EYu.* Prospects for fabrication of artificial human tissues and organs based on 3D bioprinting. *Russian Journal of Transplantology and Artificial Organs*. 2023; 25 (2): 63–81. doi: 10.15825/1995-1191-2023-2-63-81.
11. *Kamal M, Gremse F, Rosenhain S, Bartella AK, Hölzle F, Kessler P, Lethaus B.* Comparison of Bone Grafts From Various Donor Sites in Human Bone Specimens. *J Craniofac Surg.* 2018 Sep; 29 (6): 1661–1665. doi: 10.1097/SCS.0000000000004586. PMID: 29762319.
12. *Tuli R, Tuli S, Nandi S, Wang ML, Alexander PG, Haleem-Smith H et al*. Characterization of multipotential mesenchymal progenitor cells derived from human trabecular bone. *Stem Cells.* 2003; 21 (6): 681–693. doi: 10.1634/stemcells.21-6-681. PMID: 14595128.
13. *Sagi HC, Young ML, Gerstenfeld L, Einhorn TA, Tornetta P.* Qualitative and quantitative differences between bone graft obtained from the medullary canal (with a Reamer/Irrigator/Aspirator) and the iliac crest of the same patient. *J Bone Joint Surg Am*. 2012 Dec 5; 94 (23): 2128–2135. doi: 10.2106/JBJS.L.00159. PMID: 23224383.
14. *Wang W, Yeung KWK.* Bone grafts and biomaterials substitutes for bone defect repair: A review. *Bioact Mater*. 2017 Jun 7; 2 (4): 224–247. doi: 10.1016/j.bioactmat.2017.05.007. PMID: 29744432.
15. *Dimitriou R, Jones E, McGonagle D, Giannoudis PV.* Bone regeneration: current concepts and future directions. *BMC Med*. 2011 May 31; 9: 66. doi: 10.1186/1741-7015-9-66. PMID: 21627784.
16. *Shapovalov VM, Gubochkin NG, Mikityuk SI.* Formation of vascularized bone grafts and their use for treatment of pseudoarthroses and bone defects. *Grekov's Bulletin of Surgery.* 2013; 172 (4): 063–067. (In Russ.). doi: 10.24884/0042-4625-2013-172-4-063-067.
17. *Asmus A, Vogel K, Vogel A, Eichenauer F, Kim S, Eisenschenk A.* Gefäßgestieltes Beckenkammtransplantat zur Behandlung der Femurkopfnekrose [Pedicled vascularized iliac bone graft for treatment of osteonecrosis of the femoral head]. *Oper Orthop Traumatol*. 2020 Apr; 32 (2): 127–138. doi: 10.1007/s00064-020-00650-2. PMID: 32052100.
18. *Quintero JI, Childs D, Moreno R.* The medial femoral condyle free flap: An excellent option for difficult cases: case series. *SAGE Open Med Case Rep*. 2020 Jun 29; 8: 2050313X20933763. doi: 10.1177/2050313X20933763. PMID: 32647579.

19. *Pape HC, Evans A, Kobbe P.* Autologous bone graft: properties and techniques. *J Orthop Trauma*. 2010 Mar; 24 Suppl 1: S36–S40. doi: 10.1097/BOT.0b013e3181cec4a1. PMID: 20182233.
20. *Petrella G, Tosi D, Pantaleoni F, Adani R.* Vascularized bone grafts for post-traumatic defects in the upper extremity. *Arch Plast Surg*. 2021 Jan; 48 (1): 84–90. doi: 10.5999/aps.2020.00969. PMID: 33503750.
21. *Nevedrov AV, Shibayev EYu, Kalenskiy VO, Zadneprovskiy NN, Shishkin VB, Sharifullin FA et al.* Experience of using vascularized bone grafts to treat nonunion fractures and limb bone defects. *Transplantologiya. The Russian Journal of Transplantation.* 2019; 11 (1): 9–20. doi: 10.23873/2074-0506-2019-11-1-9-20.
22. *Verboket R, Leiblein M, Seebach C, Nau C, Janko M, Bellen M et al.* Autologous cell-based therapy for treatment of large bone defects: from bench to bedside. *Eur J Trauma Emerg Surg*. 2018 Oct; 44 (5): 649–665. doi: 10.1007/s00068-018-0906-y. PMID: 29352347.
23. *Venkataiah VS, Yahata Y, Kitagawa A, Inagaki M, Kakiuchi Y, Nakano M et al*. Clinical Applications of Cell-Scaffold Constructs for Bone Regeneration Therapy. *Cells*. 2021 Oct 8; 10 (10): 2687. doi: 10.3390/cells10102687. PMID: 34685667.
24. *Baron M, Drohat P, Crawford B, Hornicek FJ, Best TM, Kouroupis D.* Mesenchymal Stem/Stromal Cells: Immunomodulatory and Bone Regeneration Potential after Tumor Excision in Osteosarcoma Patients. *Bioengineering (Basel)*. 2023 Oct 13; 10 (10): 1187. doi: 10.3390/bioengineering10101187. PMID: 37892917.
25. *Mavrogenis AF, Karampikas V, Zikopoulos A, Sioutis S, Mastrokalos D, Koulalis D et al.* Orthobiologics: a review. *Int Orthop*. 2023 Jul; 47 (7): 1645–1662. doi: 10.1007/s00264-023-05803-z. PMID: 37071148.
26. *Bochkova TV, Gantsev ShKh.* The application of autoplasma, enriched with platelets in various fields of medicine. *Bashkortostan Medical Journal*. 2019; 14 (5): 61–67. (In Russ.).
27. *Foster TE, Puskas BL, Mandelbaum BR, Gerhardt MB, Rodeo SA.* Platelet-rich plasma: from basic science to clinical applications. *Am J Sports Med*. 2009 Nov; 37 (11): 2259–2272. doi: 10.1177/0363546509349921. PMID: 19875361.
28. *Blazhenko AN, Rodin IA, Ponkina ON, Mukhanov ML, Samoilova AS, Verevkin AA et al.* The effect of A-PRP-therapy on reparative regeneration of bone tissue with acute bone fractures of the limbs. *Innovative Medicine of Kuban.* 2019; (3): 32–38. (In Russ.). doi: 10.35401/2500-0268-2019-15-3-32-38.
29. *Bacevich BM, Smith RDJ, Reihl AM, Mazzocca AD, Hutchinson ID.* Advances with Platelet-Rich Plasma for Bone Healing. *Biologics.* 2024 Jan 25; 18: 29–59. doi: 10.2147/BTT.S290341. PMID: 382991.
30. *Dohan Ehrenfest DM, Rasmusson L, Albrektsson T.* Classification of platelet concentrates: from pure platelet-rich plasma (P-PRP) to leucocyte- and platelet-rich fibrin (L-PRF). *Trends Biotechnol*. 2009 Mar; 27 (3): 158–167. doi: 10.1016/j.tibtech.2008.11.009. PMID: 19187989.
31. *Chou TM, Chang HP, Wang JC.* Autologous platelet concentrates in maxillofacial regenerative therapy. *Kaohsiung J Med Sci*. 2020 May; 36 (5): 305–310. doi: 10.1002/kjm2.12192. PMID: 32052598.
32. *Shanskii YD, Sergeeva NS, Sviridova IK, Kirakozov MS, Kirsanova VA, Akhmedova SA et al.* Human platelet lysate as a promising growth-stimulating additive for culturing of stem cells and other cell types. *Bull Exp Biol Med*. 2013 Nov; 156 (1): 146–151. doi: 10.1007/s10517-013-2298-7. PMID: 24319712.
33. Lizat trombocitov cheloveka kak rostovaya dobavka dlya kul'tivirovaniya razlichnyh tipov kletok. [Dissertation]. M., 2016; 15.
34. *Fayn AM, Vaza AYu, Gnetetskiy SF, Skuratovskaya KI, Bondarev VB, Bogolyubskiy YuA et al.* Available methods to enhance regenerative potential of plastic materials for bone defects replacement in orthopedics. Part 2. Use of autologous human platelet lysate. *Transplantologiya. The Russian Journal of Transplantation.* 2022; 14 (2): 184–194. doi: 10.23873/2074-0506-2022-14-2-184-194.
35. *Da Fonseca L, Santos GS, Huber SC, Setti TM, Setti T, Lana JF*. Human platelet lysate – A potent (and overlooked) orthobiologic. *J Clin Orthop Trauma*. 2021 Jul 28; 21: 101534. doi: 10.1016/j.jcot.2021.101534. PMID: 34386346.
36. *Everts PA, Hoffmann J, Weibrich G, Mahoney CB, Schönberger JP, van Zundert A, Knape JT.* Differences in platelet growth factor release and leucocyte kinetics during autologous platelet gel formation. *Transfus Med*. 2006 Oct; 16 (5): 363–368. doi: 10.1111/j.1365-3148.2006.00708.x. PMID: 16999760.
37. *Everts PA, Hoogbergen MM, Weber TA, Devilee RJ, van Monftort G, de Hingh IH*. Is the use of autologous platelet-rich plasma gels in gynecologic, cardiac, and general, reconstructive surgery beneficial? *Curr Pharm Biotechnol*. 2012 Jun; 13 (7): 1163–1172. doi: 10.2174/138920112800624346. PMID: 21740375.
38. *Yuan T, Guo SC, Han P, Zhang CQ, Zeng BF.* Applications of leukocyte- and platelet-rich plasma (L-PRP) in trauma surgery. *Curr Pharm Biotechnol*. 2012 Jun; 13 (7): 1173–1184. doi: 10.2174/138920112800624445. PMID: 21740374.
39. *Kobayashi Y, Saita Y, Nishio H, Ikeda H, Takazawa Y, Nagao M et al*. Leukocyte concentration and composition in platelet-rich plasma (PRP) influences the growth factor and protease concentrations. *J Orthop Sci*. 2016 Sep; 21 (5): 683–689. doi: 10.1016/j.jos.2016.07.009. PMID: 27503185.
40. *Bielecki T, Dohan Ehrenfest DM, Everts PA, Wiczkowski A.* The role of leukocytes from L-PRP/L-PRF in wound healing and immune defense: new perspectives. *Curr Pharm Biotechnol*. 2012 Jun; 13 (7): 1153–1162. doi: 10.2174/138920112800624373. PMID: 21740376.
41. *Yin WJ, Xu HT, Sheng JG, An ZQ, Guo SC, Xie XT, Zhang CQ.* Advantages of Pure Platelet-Rich Plasma Compared with Leukocyte- and Platelet-Rich Plasma in Treating Rabbit Knee Osteoarthritis. *Med Sci Monit*. 2016 Apr 17; 22: 1280–1290. doi: 10.12659/msm.898218. PMID: 27086145.
42. *Dohan DM, Choukroun J, Diss A, Dohan SL, Dohan AJ, Mouhyi J, Gogly B*. Platelet-rich fibrin (PRF): a second-generation platelet concentrate. Part I: technological

concepts and evolution. *Oral Surg Oral Med Oral Pathol Oral Radiol Endod*. 2006 Mar; 101 (3): e37–e44. doi: 10.1016/j.tripleo.2005.07.008. PMID: 16504849.

43. *De Lima Barbosa R, Stellet Lourenço E, de Azevedo dos Santos JV, Rodrigues Santiago Rocha N, Mourão CF, Alves GG.* The Effects of Platelet-Rich Fibrin in the Behavior of Mineralizing Cells Related to Bone Tissue Regeneration – A Scoping Review of *In Vitro* Evidence. *J Funct Biomater*. 2023 Oct 9; 14 (10): 503. doi: 10.3390/jfb14100503.
44. *Wang X, Zhang Y, Choukroun J, Ghanaati S, Miron RJ.* Effects of an injectable platelet-rich fibrin on osteoblast behavior and bone tissue formation in comparison to platelet-rich plasma. *Platelets*. 2018 Jan; 29 (1): 48–55. doi: 10.1080/09537104.2017.1293807. PMID: 28351189.
45. *Rochira A, Siculella L, Damiano F, Palermo A, Ferrante F, Carluccio MA et al.* Concentrated Growth Factors (CGF) Induce Osteogenic Differentiation in Human Bone Marrow Stem Cells. *Biology (Basel)*. 2020 Oct 30; 9 (11): 370. doi: 10.3390/biology9110370. PMID: 33143015.
46. *Khorshidi H, Raoofi S, Bagheri R, Banihashemi H.* Comparison of the Mechanical Properties of Early Leukocyte- and Platelet-Rich Fibrin versus PRGF/Endoret Membranes. *Int J Dent*. 2016; 2016: 1849207. doi: 10.1155/2016/1849207. PMID: 26880919.
47. *Yu P, Zhai Z, Jin X, Yang X, Qi Z.* Clinical Application of Platelet-Rich Fibrin in Plastic and Reconstructive Surgery: A Systematic Review. *Aesthetic Plast Surg*. 2018 Apr; 42 (2): 511–519. doi: 10.1007/s00266-018-1087-0. PMID: 29396591.
48. *Castro AB, Meschi N, Temmerman A, Pinto N, Lambrechts P, Teughels W, Quirynen M.* Regenerative potential of leucocyte- and platelet-rich fibrin. Part B: sinus floor elevation, alveolar ridge preservation and implant therapy. A systematic review. *J Clin Periodontol*. 2017 Feb; 44 (2): 225–234. doi: 10.1111/jcpe.12658. PMID: 27891638.
49. *Jia K, You J, Zhu Y, Li M, Chen S, Ren S et al.* Platelet-rich fibrin as an autologous biomaterial for bone regeneration: mechanisms, applications, optimization. *Front Bioeng Biotechnol*. 2024 Apr 16; 12: 1286035. doi: 10.3389/fbioe.2024.1286035. PMID: 38689760.
50. *Al-Ghadban S, Artiles M, Bunnell BA.* Adipose Stem Cells in Regenerative Medicine: Looking Forward. *Front Bioeng Biotechnol*. 2022 Jan 13; 9: 837464. doi: 10.3389/fbioe.2021.837464. PMID: 35096804.
51. *Gorkun AA, Revokatova DP, Zurina IM, Nikishin DA, Bikmulina PY, Timashev PS et al.* The Duo of Osteogenic and Angiogenic Differentiation in ADSC-Derived Spheroids. *Front Cell Dev Biol*. 2021 Apr 9; 9: 572727. doi: 10.3389/fcell.2021.572727. PMID: 33898413.
52. *Mizuno H, Tobita M, Uysal AC.* Concise review: Adipose-derived stem cells as a novel tool for future regenerative medicine. *Stem Cells.* 2012 May; 30 (5): 804–810. doi: 10.1002/stem.1076. PMID: 22415904.
53. *Paduano F, Marrelli M, Amantea M, Rengo C, Rengo S, Goldberg M et al.* Adipose Tissue as a Strategic Source of Mesenchymal Stem Cells in Bone Regeneration: A Topical Review on the Most Promising Craniomaxillofacial Applications. *Int J Mol Sci*. 2017 Oct 13; 18 (10): 2140. doi: 10.3390/ijms18102140. PMID: 29027958.
54. *Storti G, Scioli MG, Kim BS, Orlandi A, Cervelli V.* Adipose-Derived Stem Cells in Bone Tissue Engineering: Useful Tools with New Applications. *Stem Cells Int*. 2019 Nov 6; 2019: 3673857. doi: 10.1155/2019/3673857. PMID: 31781238.
55. *Labusca L.* Adipose tissue in bone regeneration – stem cell source and beyond. *World J Stem Cells*. 2022 Jun 26; 14 (6): 372–392. doi: 10.4252/wjsc.v14.i6.372. PMID: 35949397.
56. *Ferguson JC, Tangl S, Barnewitz D, Genzel A, Heimel P, Hruschka V et al.* A large animal model for standardized testing of bone regeneration strategies. *BMC Vet Res*. 2018 Nov 6; 14 (1): 330. doi: 10.1186/s12917-018-1648-0. PMID: 30400796.
57. *Baba S, Inoue T, Hashimoto Y, Kimura D, Ueda M, Sakai K et al.* Effectiveness of scaffolds with pre-seeded mesenchymal stem cells in bone regeneration – Assessment of osteogenic ability of scaffolds implanted under the periosteum of the cranial bone of rats. *Dent Mater J*. 2010 Nov;29(6): 673–681. doi: 10.4012/dmj.2009-123. PMID: 21099156.
58. *He X, Liu Y, Yuan X, Lu L.* Enhanced healing of rat calvarial defects with MSCs loaded on BMP-2 releasing chitosan/alginate/hydroxyapatite scaffolds. *PLoS One*. 2014 Aug 1; 9 (8): e104061. doi: 10.1371/journal.pone.0104061. PMID: 25084008.
59. *Del Rosario C, Rodríguez-Évora M, Reyes R, Delgado A, Évora C.* BMP-2, PDGF-BB, and bone marrow mesenchymal cells in a macroporous β-TCP scaffold for critical-size bone defect repair in rats. *Biomed Mater*. 2015 Jul 23; 10 (4): 045008. doi: 10.1088/1748-6041/10/4/045008. PMID: 26201844.
60. *Kong Y, Zhao Y, Li D, Shen H, Yan M.* Dual delivery of encapsulated BM-MSCs and BMP-2 improves osteogenic differentiation and new bone formation. *J Biomed Mater Res A*. 2019 Oct; 107 (10): 2282–2295. doi: 10.1002/jbm.a.36737. PMID: 31152570.
61. *Cheng G, Ma X, Li J, Cheng Y, Cao Y, Wang Z et al.* Incorporating platelet-rich plasma into coaxial electrospun nanofibers for bone tissue engineering. *Int J Pharm*. 2018 Aug 25; 547 (1–2): 656–666. doi: 10.1016/j.ijpharm.2018.06.020. PMID: 29886100.
62. *Li X, Zhang R, Tan X, Li B, Liu Y, Wang X.* Synthesis and Evaluation of BMMSC-seeded BMP-6/nHAG/GMS Scaffolds for Bone Regeneration. *Int J Med Sci*. 2019 Jun 10; 16 (7): 1007–1017. doi: 10.7150/ijms.31966. PMID: 31341414.
63. *Hara K, Hellem E, Yamada S, Sariibrahimoglu K, Mølster A, Gjerdet NR et al.* Efficacy of treating segmental bone defects through endochondral ossification: 3D printed designs and bone metabolic activities. *Mater Today Bio*. 2022 Mar 7; 14: 100237. doi: 10.1016/j.mtbio.2022.100237. PMID: 35280332.
64. *Ng MH, Duski S, Tan KK, Yusof MR, Low KC, Rose IM et al.* Repair of segmental load-bearing bone defect by autologous mesenchymal stem cells and plasma-derived fibrin impregnated ceramic block results in early reco-

very of limb function. *Biomed Res Int.* 2014; 2014: 345910. doi: 10.1155/2014/345910. PMID: 25165699.

65. *Wong CC, Yeh YY, Chen CH, Manga YB, Jheng PR, Lu CX, Chuang EY.* Effectiveness of treating segmental bone defects with a synergistic co-delivery approach with platelet-rich fibrin and tricalcium phosphate. *Mater Sci Eng C Mater Biol Appl*. 2021 Oct; 129: 112364. doi: 10.1016/j.msec.2021.112364. PMID: 34579883.
66. *Song Y, Lin K, He S, Wang C, Zhang S, Li D et al.* Nano-biphasic calcium phosphate/polyvinyl alcohol composites with enhanced bioactivity for bone repair via low-temperature three-dimensional printing and loading with platelet-rich fibrin. *Int J Nanomedicine*. 2018 Jan 25; 13: 505–523. doi: 10.2147/IJN.S152105. PMID: 29416332.
67. *Liu Z, Ge Y, Zhang L, Wang Y, Guo C, Feng K et al.* The effect of induced membranes combined with enhanced bone marrow and 3D PLA-HA on repairing long bone defects *in vivo*. *J Tissue Eng Regen Med*. 2020 Oct; 14 (10): 1403–1414. doi: 10.1002/term.3106. Epub 2020 Aug 2. PMID: 32666697.
68. *Berner A, Henkel J, Woodruff MA, Steck R, Nerlich M, Schuetz MA, Hutmacher DW.* Delayed minimally invasive injection of allogenic bone marrow stromal cell sheets regenerates large bone defects in an ovine preclinical animal model. *Stem Cells Transl Med*. 2015 May; 4 (5): 503–512. doi: 10.5966/sctm.2014-0244. PMID: 25834121.
69. *Kengelbach-Weigand A, Thielen C, Bäuerle T, Götzl R, Gerber T, Körner C et al.* Personalized medicine for reconstruction of critical-size bone defects – a translational approach with customizable vascularized bone tissue. *NPJ Regen Med*. 2021 Aug 19; 6 (1): 49. doi: 10.1038/s41536-021-00158-8. PMID: 34413320.
70. *Smith JO, Tayton ER, Khan F, Aarvold A, Cook RB, Goodship A et al.* Large animal *in vivo* evaluation of a binary blend polymer scaffold for skeletal tissue-engineering strategies; translational issues. *J Tissue Eng Regen Med*. 2017 Apr; 11 (4): 1065–1076. doi: 10.1002/term.2007. PMID: 25690518.
71. *Black C, Kanczler JM, de Andrés MC, White LJ, Savi FM, Bas O et al.* Characterisation and evaluation of the regenerative capacity of Stro-4+ enriched bone marrow mesenchymal stromal cells using bovine extracellular matrix hydrogel and a novel biocompatible melt electro-written medical-grade polycaprolactone scaffold. *Biomaterials.* 2020 Jul; 247: 119998. doi: 10.1016/j.biomaterials.2020.119998. PMID: 32251928.
72. *Henkel J, Medeiros Savi F, Berner A, Fountain S, Saifzadeh S, Steck R et al*. Scaffold-guided bone regeneration in large volume tibial segmental defects. *Bone.* 2021 Dec; 153: 116163. doi: 10.1016/j.bone.2021.116163. PMID: 34461285.
73. *Witek L, Tian H, Tovar N, Torroni A, Neiva R, Gil LF, Coelho PG.* The effect of platelet-rich fibrin exudate addition to porous poly(lactic-co-glycolic acid) scaffold in bone healing: An *in vivo* study. *J Biomed Mater Res B Appl Biomater*. 2020 May; 108 (4): 1304–1310. doi: 10.1002/jbm.b.34478. PMID: 31429195.
74. *Bastami F, Noori-Kooshki MH, Semyari H, Tabrizi R, Abrishamchian A, Mashhadi-Abbas F et al.* Multi-walled carbon nanotube/hydroxyapatite nanocomposite with leukocyte- and platelet-rich fibrin for bone regeneration in sheep model. *Oral Maxillofac Surg*. 2022 Mar; 26 (1): 63–72. doi: 10.1007/s10006-020-00933-9. PMID: 33852090.
75. *Szivek JA, Gonzales DA, Wojtanowski AM, Martinez MA, Smith JL.* Mesenchymal stem cell seeded, biomimetic 3D printed scaffolds induce complete bridging of femoral critical sized defects. *J Biomed Mater Res B Appl Biomater*. 2019 Feb; 107 (2): 242–252. doi: 10.1002/jbm.b.34115. PMID: 29569331.
76. *Pappa EI, Barbagianni MS, Georgiou SG, Athanasiou LV, Psalla D, Vekios D et al.* The Use of Stromal Vascular Fraction in Long Bone Defect Healing in Sheep. *Animals (Basel).* 2023 Sep 9; 13 (18): 2871. doi: 10.3390/ani13182871. PMID: 37760271.
77. *Chu W, Gan Y, Zhuang Y, Wang X, Zhao J, Tang T, Dai K.* Mesenchymal stem cells and porous β-tricalcium phosphate composites prepared through stem cell screen-enrich-combine(-biomaterials) circulating system for the repair of critical size bone defects in goat tibia. *Stem Cell Res Ther*. 2018 Jun 13; 9 (1): 157. doi: 10.1186/s13287-018-0906-1. PMID: 29895312.
78. *Probst FA, Fliefel R, Burian E, Probst M, Eddicks M, Cornelsen M et al.* Bone regeneration of minipig mandibular defect by adipose derived mesenchymal stem cells seeded tri-calcium phosphate- poly(D,L-lactide-co-glycolide) scaffolds. *Sci Rep*. 2020 Feb 6; 10 (1): 2062. doi: 10.1038/s41598-020-59038-8. PMID: 32029875.
79. *Wong KW, Chen YS, Lin CL.* Evaluation optimum ratio of synthetic bone graft material and platelet rich fibrin mixture in a metal 3D printed implant to enhance bone regeneration. *J Orthop Surg Res*. 2024 May 16; 19 (1): 299. doi: 10.1186/s13018-024-04784-y. PMID: 38755635.
80. *Hakimi M, Grassmann JP, Betsch M, Schneppendahl J, Gehrmann S, Hakimi AR et al.* The composite of bone marrow concentrate and PRP as an alternative to autologous bone grafting. *PLoS One*. 2014 Jun 20; 9 (6): e100143. doi: 10.1371/journal.pone.0100143. PMID: 24950251.
81. *Lin CC, Lin SC, Chiang CC, Chang MC, Lee OK.* Reconstruction of Bone Defect Combined with Massive Loss of Periosteum Using Injectable Human Mesenchymal Stem Cells in Biocompatible Ceramic Scaffolds in a Porcine Animal Model. *Stem Cells Int*. 2019 Nov 23; 2019: 6832952. doi: 10.1155/2019/6832952. PMID: 31871469.
82. *Balaguer T, Fellah BH, Boukhechba F, Traverson M, Mouska X, Ambrosetti D et al.* Combination of blood and biphasic calcium phosphate microparticles for the reconstruction of large bone defects in dog: A pilot study. *J Biomed Mater Res A*. 2018 Jul; 106 (7): 1842–1850. doi: 10.1002/jbm.a.36384. PMID: 29573560.
83. *Lee JW, Chu SG, Kim HT, Choi KY, Oh EJ, Shim JH et al.* Osteogenesis of Adipose-Derived and Bone Marrow Stem Cells with Polycaprolactone/Tricalcium Phosphate and Three-Dimensional Printing Technology in a Dog Model of Maxillary Bone Defects. *Polymers (Basel).* 2017 Sep 15; 9 (9): 450. doi: 10.3390/polym9090450. PMID: 30965755.

84. *Masaoka T, Yoshii T, Yuasa M, Yamada T, Taniyama T, Torigoe I et al.* Bone Defect Regeneration by a Combination of a β-Tricalcium Phosphate Scaffold and Bone Marrow Stromal Cells in a Non-Human Primate Model. *Open Biomed Eng J*. 2016 Mar 18; 10: 2–11. doi: 10.2174/1874120701610010002. PMID: 27073583.
85. *Houdebine LM.* Transgenic animal models in biomedical research. *Methods Mol Biol.* 2007; 360: 163–202. doi: 10.1385/1-59745-165-7:163. PMID: 17172731.
86. *Muschler GF, Raut VP, Patterson TE, Wenke JC, Hollinger JO.* The design and use of animal models for translational research in bone tissue engineering and regenerative medicine. *Tissue Eng Part B Rev*. 2010 Feb; 16 (1): 123–145. doi: 10.1089/ten.TEB.2009.0658. PMID: 19891542.
87. *Muschler GF, Nakamoto C, Griffith LG.* Engineering principles of clinical cell-based tissue engineering. *J Bone Joint Surg Am*. 2004 Jul; 86 (7): 1541–1558. doi: 10.2106/00004623-200407000-00029. PMID: 15252108.
88. *Gabriele Sommer N, Hahn D, Okutan B, Marek R, Weinberg AM*. Animal Models in Orthopedic Research: The Proper Animal Model to Answer Fundamental Questions on Bone Healing Depending on Pathology and Implant Material [Internet]. *Animal Models in Medicine and Biology.* IntechOpen; 2020. doi: 10.5772/intechopen.89137.
89. *Taguchi T, Lopez MJ.* An overview of *de novo* bone generation in animal models. *J Orthop Res*. 2021 Jan; 39 (1): 7–21. doi: 10.1002/jor.24852. PMID: 32910496.
90. *Cibelli J, Emborg ME, Prockop DJ, Roberts M, Schatten G, Rao M et al.* Strategies for improving animal models for regenerative medicine. *Cell Stem Cell*. 2013 Mar 7; 12 (3): 271–274. doi: 10.1016/j.stem.2013.01.004. PMID: 23472868.
91. *Cardoso MN, Souza AF de, De Zoppa AL do V.* Large animals as experimental models of critical size bone defects studies: a protocol for a systematic review. *Research, Society and Development.* 2023; 12 (5): p.e10912541509. doi: 10.33448/rsd-v12i5.41509.
92. *Stamnitz S, Klimczak A.* Mesenchymal Stem Cells, Bioactive Factors, and Scaffolds in Bone Repair: From Research Perspectives to Clinical Practice. *Cells.* 2021 Jul 29; 10 (8): 1925. doi: 10.3390/cells10081925. PMID: 34440694.
93. *Schulze F, Lang A, Schoon J, Wassilew GI, Reichert J.* Scaffold Guided Bone Regeneration for the Treatment of Large Segmental Defects in Long Bones. *Biomedicines.* 2023 Jan 24; 11 (2): 325. doi: 10.3390/biomedicines11020325. PMID: 36830862.
94. *Lendeckel S, Jödicke A, Christophis P, Heidinger K, Wolff J, Fraser JK et al*. Autologous stem cells (adipose) and fibrin glue used to treat widespread traumatic calvarial defects: case report. *J Craniomaxillofac Surg*. 2004 Dec; 32 (6): 370–373. doi: 10.1016/j.jcms.2004.06.002. PMID: 15555520.
95. *Thesleff T, Lehtimäki K, Niskakangas T, Mannerström B, Miettinen S, Suuronen R, Öhman J.* Cranioplasty with adipose-derived stem cells and biomaterial: a novel method for cranial reconstruction. *Neurosurgery.* 2011 Jun; 68 (6): 1535–1540. doi: 10.1227/NEU.0b013e31820ee24e. PMID: 21336223.
96. *Morrison DA, Kop AM, Nilasaroya A, Sturm M, Shaw K, Honeybul S.* Cranial reconstruction using allogeneic mesenchymal stromal cells: A phase 1 first-in-human trial. *J Tissue Eng Regen Med*. 2018 Feb; 12 (2): 341–348. doi: 10.1002/term.2459. PMID: 28488350.
97. *Artzi Z, Weinreb M, Carmeli G, Lev-Dor R, Dard M, Nemcovsky CE*. Histomorphometric assessment of bone formation in sinus augmentation utilizing a combination of autogenous and hydroxyapatite/biphasic tricalcium phosphate graft materials: at 6 and 9 months in humans. *Clin Oral Implants Res*. 2008 Jul; 19 (7): 686–692. doi: 10.1111/j.1600-0501.2008.01539.x. PMID: 18492077.
98. *Mesimäki K, Lindroos B, Törnwall J, Mauno J, Lindqvist C, Kontio R et al.* Novel maxillary reconstruction with ectopic bone formation by GMP adipose stem cells. *Int J Oral Maxillofac Surg*. 2009 Mar; 38 (3): 201–209. doi: 10.1016/j.ijom.2009.01.001. PMID: 19168327.
99. *Bulgin D, Hodzic E.* Autologous bone marrow-derived mononuclear cells combined with β-TCP for maxillary bone augmentation in implantation procedures. *J Craniofac Surg*. 2012 Nov; 23 (6): 1728–1732. doi: 10.1097/SCS.0b013e31826cf177. PMID: 23147336.
100. *Solakoglu Ö, Götz W, Kiessling MC, Alt C, Schmitz C, Alt EU.* Improved guided bone regeneration by combined application of unmodified, fresh autologous adipose derived regenerative cells and plasma rich in growth factors: A first-in-human case report and literature review. *World J Stem Cells*. 2019 Feb 26; 11 (2): 124–146. doi: 10.4252/wjsc.v11.i2.124. PMID: 30842809.
101. *Kizu Y, Ishii R, Matsumoto N, Saito I.* Retrospective study on the effect of adipose stem cell transplantation on jaw bone regeneration. *Int J Implant Dent*. 2024 Feb 5; 10 (1): 3. doi: 10.1186/s40729-024-00523-4. PMID: 38315258.
102. *Sándor GK.* Tissue engineering of bone: Clinical observations with adipose-derived stem cells, resorbable scaffolds, and growth factors. *Ann Maxillofac Surg*. 2012 Jan; 2 (1): 8–11. doi: 10.4103/2231-0746.95308. PMID: 23483030.
103. *Gjerde C, Mustafa K, Hellem S, Rojewski M, Gjengedal H, Yassin MA et al.* Cell therapy induced regeneration of severely atrophied mandibular bone in a clinical trial. *Stem Cell Res Ther*. 2018 Aug 9; 9 (1): 213. doi: 10.1186/s13287-018-0951-9. PMID: 30092840.
104. *Paolantonio M, Di Tullio M, Giraudi M, Romano L, Secondi L, Paolantonio G et al.* Periodontal regeneration by leukocyte and platelet-rich fibrin with autogenous bone graft versus enamel matrix derivative with autogenous bone graft in the treatment of periodontal intrabony defects: A randomized non-inferiority trial. *J Periodontol*. 2020 Dec; 91 (12): 1595–1608. doi: 10.1002/JPER.19-0533. PMID: 32294244.
105. *Bodhare GH, Kolte AP, Kolte RA, Shirke PY.* Clinical and radiographic evaluation and comparison of bioactive bone alloplast morsels when used alone and in combination with platelet-rich fibrin in the treatment of periodontal intrabony defects-A randomized controlled trial. *J Periodontol*. 2019 Jun; 90 (6): 584–594. doi: 10.1002/JPER.18-0416. PMID: 30488952.

106. *Bulgin D, Irha E, Hodzic E, Nemec B.* Autologous bone marrow derived mononuclear cells combined with β-tricalcium phosphate and absorbable atelocollagen for a treatment of aneurysmal bone cyst of the humerus in child. *J Biomater Appl*. 2013 Sep; 28 (3): 343–353. doi: 10.1177/0885328212451047. PMID: 22693044.
107. *Šponer P, Filip S, Kučera T, Brtková J, Urban K, Palička V et al.* Utilizing Autologous Multipotent Mesenchymal Stromal Cells and β-Tricalcium Phosphate Scaffold in Human Bone Defects: A Prospective, Controlled Feasibility Trial. *Biomed Res Int.* 2016; 2016: 2076061. doi: 10.1155/2016/2076061. PMID: 27144159.
108. *Laubach M, Suresh S, Herath B, Wille ML, Delbrück H, Alabdulrahman H et al*. Clinical translation of a patient-specific scaffold-guided bone regeneration concept in four cases with large long bone defects. *J Orthop Translat*. 2022 Jun 16; 34: 73–84. doi: 10.1016/j.jot.2022.04.004. PMID: 35782964.
109. *Findeisen S, Gräfe N, Schwilk M, Ferbert T, Helbig L, Haubruck P et al.* Use of Autologous Bone Graft with Bioactive Glass as a Bone Substitute in the Treatment of Large-Sized Bone Defects of the Femur and Tibia. *J Pers Med*. 2023 Nov 24; 13 (12): 1644. doi: 10.3390/jpm13121644. PMID: 38138871.
110. *Chu W, Wang X, Gan Y, Zhuang Y, Shi D, Liu F et al.* Screen-enrich-combine circulating system to prepare MSC/β-TCP for bone repair in fractures with depressed tibial plateau. *Regen Med*. 2019 Jun; 14 (6): 555–569. doi: 10.2217/rme-2018-0047. PMID: 31115268.
111. *Aoki K, Ideta H, Komatsu Y, Tanaka A, Kito M, Okamoto M et al.* Bone-Regeneration Therapy Using Biodegradable Scaffolds: Calcium Phosphate Bioceramics and Biodegradable Polymers. *Bioengineering (Basel).* 2024 Feb 13; 11 (2): 180. doi: 10.3390/bioengineering11020180. PMID: 38391666.
112. *Stanciugelu SI, Patrascu JM Jr, Florescu S, Marian C.* Sticky Bone as a New Type of Autologous Bone Grafting in Schatzker Type II Tibial Plateau Fracture Case Report. *Life (Basel).* 2024 Aug 21; 14 (8): 1042. doi: 10.3390/life14081042. PMID: 39202784.
113. *Jäger M, Herten M, Fochtmann U, Fischer J, Hernigou P, Zilkens C et al.* Bridging the gap: bone marrow aspiration concentrate reduces autologous bone grafting in osseous defects. *J Orthop Res*. 2011 Feb; 29 (2): 173–180. doi: 10.1002/jor.21230. PMID: 20740672.
114. *Zhuang Y, Gan Y, Shi D, Zhao J, Tang T, Dai K.* A novel cytotherapy device for rapid screening, enriching and combining mesenchymal stem cells into a biomaterial for promoting bone regeneration. *Sci Rep*. 2017 Nov 13; 7 (1): 15463. doi: 10.1038/s41598-017-15451-0.
115. *Polushin YuS.* Blast Injuries (Lecture). *Messenger of anesthesiology and resuscitation.* 2022; 19 (6): 6–17. (In Russ.). doi: 10.21292/2078-5658-2022-19-6-6-17.
116. *Perez KG, Eskridge SL, Clouser MC, McCabe CT, Galarneau MR*. A Focus on Non-Amputation Combat Extremity Injury: 2001–2018. *Mil Med*. 2022 May 3; 187 (5–6): e638–e643. doi: 10.1093/milmed/usab143. PMID: 33939807.
117. *Ramasamy A, Hill AM, Masouros S, Gibb I, Bull AM, Clasper JC.* Blast-related fracture patterns: a forensic biomechanical approach. *J R Soc Interface*. 2011 May 6; 8 (58): 689–698. doi: 10.1098/rsif.2010.0476. PMID: 21123255.
118. *Stewart L, Shaikh F, Bradley W, Lu D, Blyth DM, Petfield JL et al.* Combat-Related Extremity Wounds: Injury Factors Predicting Early Onset Infections. *Mil Med*. 2019 Mar 1; 184 (Suppl 1): 83–91. doi: 10.1093/milmed/usy336. PMID: 30901441.
119. *Khominets VV, Shchukin AV, Mikhailov SV, Foos IV.* Features of consecutive osteosynthesis in treatment of patients with gunshot fractures of long bones of the extremities. *Polytrauma*. 2017; 3: 12–22.
120. *Seliverstov PA, Shapkin YuG.* Application of damage control tactics in combat injuries of limbs at the advanced stages of medical evacuation in modern war settings (literature review). *Medico-Biological and Socio-Psychological Problems of Safety in Emergency Situations*. 2023; (1): 42–52. (In Russ.). doi: 10.25016/2541-7487-2023-0-1-42-52.
121. *Gubin AV, Borzunov DY, Marchenkova LO, Malkova TA, Smirnova IL.* Contribution of G.A. Ilizarov to bone reconstruction: historical achievements and state of the art. *Strategies Trauma Limb Reconstr*. 2016 Nov; 11 (3): 145–152. doi: 10.1007/s11751-016-0261-7. PMID: 27432154.
122. *Masquelet AC, Fitoussi F, Begue T, Muller GP.* Reconstruction des os longs par membrane induite et autogreffe spongieuse [Reconstruction of the long bones by the induced membrane and spongy autograft]. *Ann Chir Plast Esthet*. 2000 Jun; 45 (3): 346–353. French. PMID: 10929461.
123. *Masquelet AC.* Induced Membrane Technique: Pearls and Pitfalls. *J Orthop Trauma*. 2017 Oct; 31 Suppl 5: S36–S38. doi: 10.1097/BOT.0000000000000979. PMID: 28938390.
124. *Mathieu L, Bilichtin E, Durand M, de l'Escalopier N, Murison JC, Collombet JM, Rigal S.* Masquelet technique for open tibia fractures in a military setting. *Eur J Trauma Emerg Surg*. 2020 Oct; 46 (5): 1099–1105. doi: 10.1007/s00068-019-01217-y. PMID: 31451864.
125. *Mathieu L, Mourtialon R, Durand M, de Rousiers A, de l'Escalopier N, Collombet JM*. Masquelet technique in military practice: specificities and future directions for combat-related bone defect reconstruction. *Mil Med Res*. 2022 Sep 2; 9 (1): 48. doi: 10.1186/s40779-022-00411-1. PMID: 36050805.
126. *Grün W, Hansen EJJ, Andreassen GS, Clarke-Jenssen J, Madsen JE.* Functional outcomes and health-related quality of life after reconstruction of segmental bone loss in femur and tibia using the induced membrane technique. *Arch Orthop Trauma Surg*. 2023 Aug; 143 (8): 4587–4596. doi: 10.1007/s00402-022-04714-9. PMID: 36460763.
127. *Khominets VV, Shchukin AV, Tkachenko MV, Ivanov VS, Goldobin AN.* The experience with treatment of a serviceman with gunshot fracture dislocation of the proximal humerus. *Polytrauma*. 2022; 3: 55–61. doi: 10.24412/1819-1495-2022-3-55-61.

The article was submitted to the journal on 9.07.2024

DOI: 10.15825/1995-1191-2025-2-127-138

PRECLINICAL EVALUATION OF TISSUE-ENGINEERED VASCULAR GRAFTS WITH BIODEGRADABLE COMPONENTS: ASSESSING THE EFFECTIVENESS OF ANIMAL MODELS FROM RATS TO PRIMATES

L.V. Antonova, E.A. Senokosova, A.V. Mironov, A.R. Shabaev, E.S. Sardin, V.G. Matveeva, E.O. Krivkina, M.Yu. Khanova, E.A. Torgunakova, L.S. Barbarash

Research Institute for Complex Issues of Cardiovascular Diseases, Kemerovo, Russian Federation

Currently, there are no highly effective small-diameter (≤4 mm) grafts on the market for cardiovascular surgery. Tissue-engineered, functionally active vascular grafts with prolonged resorption and regeneration capacity have the potential to serve as alternatives to traditional arterial grafts. These bioengineered grafts could eliminate the need for repeated surgical interventions to replace failed grafts. The accuracy of assessing the risks of failure in biodegradable small-diameter vascular grafts (SDVGs) during preclinical trials is highly dependent on the choice of animal model. This article presents the results of comprehensive preclinical trials conducted on an SDVG developed at the Research Institute for Complex Issues of Cardiovascular Diseases. Based on these findings, the study evaluates the effectiveness and feasibility of different animal models for testing biodegradable SDVGs.

Keywords: tissue engineering, small-diameter vascular graft, preclinical trials.

INTRODUCTION

At present, the field of application of artificial substitutes for some parts of organs and systems of the human body has a trend towards serious growth with the medical devices market expanding annually. However, the use of synthetic materials is associated with various complications, which the global scientific and medical community continues to address through ongoing research and innovation [1].

Despite the extensive availability of products for cardiovascular surgery, effective small-diameter (≤4 mm) vascular grafts (SDVGs) have yet to be developed [2]. Meanwhile, the annual demand for SDVGs in the Russian Federation alone is estimated at approximately 80,000, driven by the high number of surgical interventions on small-caliber arteries [3].

Tissue-engineered, functionally active vascular grafts (VGs) with prolonged resorption and regenerative potential offer a promising alternative to synthetic vascular prostheses. These grafts could eliminate the need for repeated surgeries to replace failed vascular implants. The integration of tissue engineering into the development of medical devices is increasingly relevant, as its approaches are designed to closely mimic the biocompatibility of native tissues, enhancing their long-term clinical success [4, 5].

There are two widely adopted approaches to fabricating tissue-engineered VGs [6]. The first involves creating a cell-populated prosthesis *in vitro* under simulated blood flow conditions, ideally using the patient's own cells and proteins [7–9]. The second approach focuses on *in vivo* vascular graft development, utilizing a functionally active, highly porous scaffold that guides the recruitment and differentiation of vascular cells toward the formation of fully functional vascular tissue [10–12]. Ideally, this scaffold should be completely resorbed over time [13, 14].

Various bioactive components are incorporated into VGs to enhance their functionality and promote full remodeling, with proteins exhibiting high proangiogenic activity being particularly favored [1, 15]. Understanding the synergy of interactions between these bioactive components is crucial to the success of the prosthesis.

SDVGs are classified as high-risk medical devices, falling into the third class (Class III) [16]. Consequently, they must meet the highest standards of biocompatibility and long-term effectiveness. Once *in vitro* testing demonstrates that the product meets the necessary safety and biocompatibility requirements, the next step involves preclinical testing using animal models. These preclinical trials are essential, as they provide insights into the prosthesis's performance in the complex environment of a living organism. The reliability of preclinical re-

Corresponding author: Larisa Antonova. Address: 6, Bul'var im. Akademika L.S. Barbarasha, Kemerovo, 650002, Russian Federation. Phone: (999) 648-50-41. E-mail: antonova.la@mail.ru

sults in predicting the success of a prosthesis is heavily influenced by the choice of the animal model used in these tests.

A biodegradable SDVG with a prolonged resorption period was developed at the Research Institute for Complex Issues of Cardiovascular Diseases. The prosthesis incorporates proangiogenic factors – VEGF, bFGF, and SDF-1α – layer by layer into its wall during the electrospinning process. VEGF plays a key role in vascularization by activating and supporting endothelial cell migration, proliferation, survival, and differentiation. It also enhances nitric oxide production and increases vascular permeability [17]. Basic fibroblast growth factor (bFGF) promotes endothelial and smooth muscle cell migration, proliferation, and survival, ultimately contributing to the maturation of blood vessels [18]. SDF-1α acts as a chemoattractant for endothelial cells, stimulates the formation of long and branched capillary networks, and enhances the migration of bone marrow-derived mesenchymal stem cells, which can differentiate into smooth muscle cells within the vascular wall [19, 20].

After extensive *in vitro* testing and confirmation of the' biocompatibility, functional efficacy, and acceptable physical, mechanical, and structural properties of the prostheses, we proceeded to the stage of preclinical trials on laboratory animals. Preclinical testing is crucial, as it allows for the assessment of biocompatibility and effectiveness of the developed prosthesis within a living organism.

However, highly contradictory results were observed across different animal models. This inconsistency highlighted the need to reassess not only the fabrication technology of the prosthesis but also the choice of the most appropriate animal model for final preclinical evaluations.

EFFECTIVENESS OF THE RAT MODEL IN PRECLINICAL TESTING OF SMALL-DIAMETER VASCULAR GRAFTS

The rat model is one of the most widely used and accessible options for preclinical testing of SDVGs. Implantation is typically performed in the abdominal aorta, particularly for prostheses with a diameter of 2 mm or less, making it the standard approach for evaluating SDVGs [21–23].

In our study, VGs composed of polycaprolactone and polyhydroxybutyrate/valerate, incorporating proangiogenic factors, were implanted into the abdominal aorta of rats for 12 months. The prostheses had a diameter ranging from 1.5 to 2 mm. Remarkably, the patency rate after 12 months was nearly 100%, even in the absence of postoperative antiplatelet therapy (Fig. 1) [24–26].

Cell population within the porous walls of the biodegradable prosthesis after implantation into the vascular system occurred naturally through implant remodeling, ultimately forming a three-layered vascular tissue structure resembling that of a native vessel wall [25, 26]. However, in the control group (grafts without proangiogenic factors), moderate chronic granulomatous inflammation was observed in some cases.

A well-documented characteristic of rats is their rapid endothelialization, along with the technical limitation of

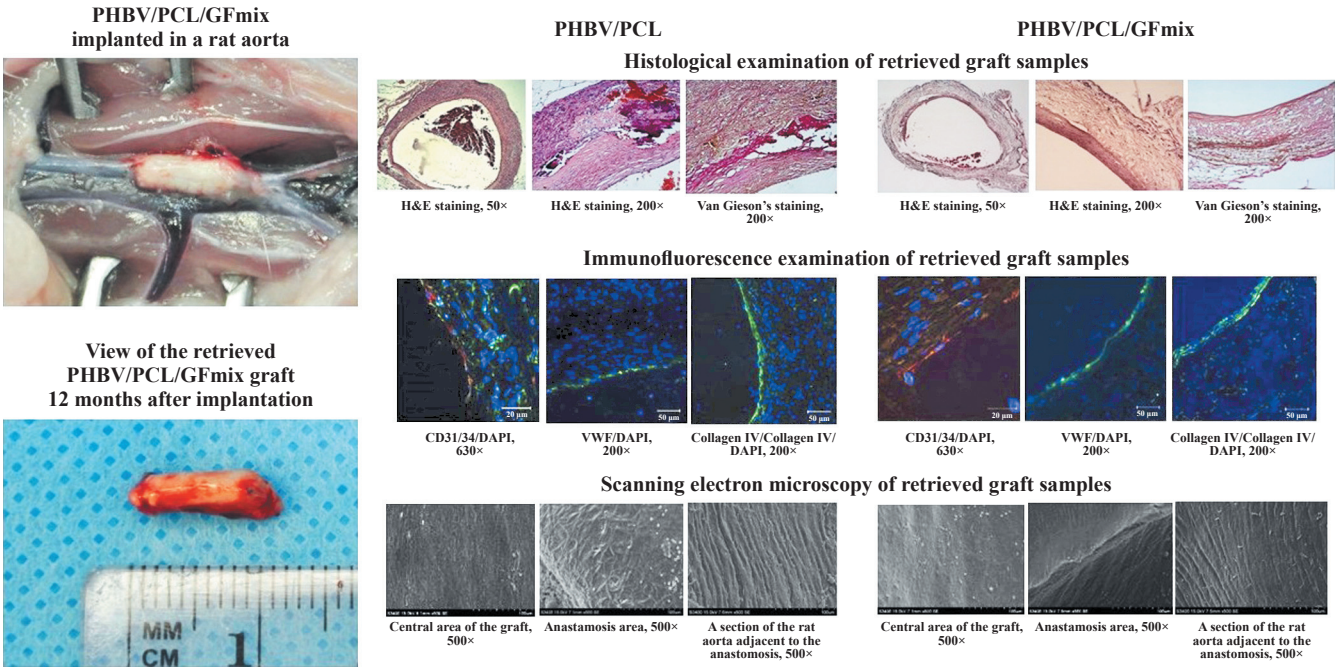

Fig. 1. Results of morphological study of PHBV|PCL vascular grafts with and without a proangiogenic factor complex (GFmix) implanted in rat aorta for 12 months [26]

implanting prostheses longer than 1 cm. This combination often results in a favorable long-term outcome regardless of the prosthesis material used [27]. Consequently, preclinical testing in a rat model has limitations – it does not fully reveal all potential risks of prosthesis failure nor reliably predict the efficacy of the device in human applications.

That said, the rat model remains a valuable tool for assessing the risk of vascular graft calcification (Fig. 2) [24].

The extent of calcification observed in VGs serves as an indirect indicator of their functional integrity. Comparative analysis of calcification in our developed grafts provided indirect evidence that incorporating a complex of proangiogenic factors helped synchronize tissue formation, prevent cell apoptosis, and significantly reduce prosthesis wall calcification. This reduction in calcification contributes to the long-term effectiveness of prostheses, provided their patency is maintained (Fig. 2).

It was also revealed that the presence and controlled release of proangiogenic factors in biodegradable VGs were found to lower the incidence of both granulomatous inflammation and prosthesis calcification [24]. In the rat model, it was discovered that in the absence of blood flow, such as in thrombosed biodegradable prostheses, no wall calcification occurred. This finding suggests that blood, as a biologically aggressive medium, and pulsatile flow play a crucial role in triggering calcification mechanisms in patent VGs [24].

These promising results encouraged further preclinical testing of the VGs on large laboratory animal models.

EFFECTIVENESS OF THE SHEEP MODEL IN PRECLINICAL TESTING OF SMALL-DIAMETER VASCULAR GRAFTS

The sheep model was chosen as a large laboratory animal model for testing biodegradable SDVGs. Sheep are widely recognized as an optimal model for assessing vascular graft growth, patency, endothelialization, thromboresistance, and postimplantation imaging. One key advantage of using sheep is that they reach their maximum size relatively quickly and do not continue to grow, making them particularly suitable for long-term graft implantation. The anatomical structure of sheep provides practical benefits for surgical procedures. Their long neck and easily accessible carotid artery facilitate the implantation of longer prostheses. Furthermore, sheep are known for their increased tendency toward thrombosis and vascular calcification, making them an ideal choice for worst-case modeling [28–30]. These characteristics enable the most rigorous *in vivo* testing of VGs for assessment of their potential degeneration.

The results obtained from the two animal models (rats and sheep) were so divergent and unexpected that it became necessary to significantly modify the prosthesis manufacturing technology. In addition, a thorough investigation of the hemostasiology profile of sheep was required, comparing it with that of patients with cardiovascular pathology to optimize pre-, intra-, and postoperative anticoagulant and antiplatelet therapy.

In pilot studies using sheep, a high incidence of early postoperative thrombosis was observed in 4-mm-diameter PHBV/PCL/GFmix biodegradable VGs implanted in the carotid artery. The primary cause of thrombosis was linked to the porosity of the inner prosthesis surface, which was confirmed through ultrasound and angiographic assessments of prosthesis patency immediately after blood flow initiation. These imaging studies clearly captured the moment of thrombus formation, characterized by rapid imbibition of the prosthesis walls with blood components, thickening of the walls, and subsequent rapid narrowing of the prosthesis lumen along its entire length (Fig. 3).

This finding necessitated enhancing the thromboresistance of the prostheses, which was achieved by developing a hydrogel-based antithrombotic drug coating for PHBV/PCL/GFmix prostheses. This coating effectively protected the graft surface from thrombosis for up to 20 days post-implantation [31].

Additionally, investigations were conducted to determine the specific aspects of sheep hemostasis that contributed to their pronounced thrombogenic response [32]. It was discovered that sheep platelets exhibited an increased response to adenosine diphosphate (ADP) induction but showed minimal reactivity to adrenaline.

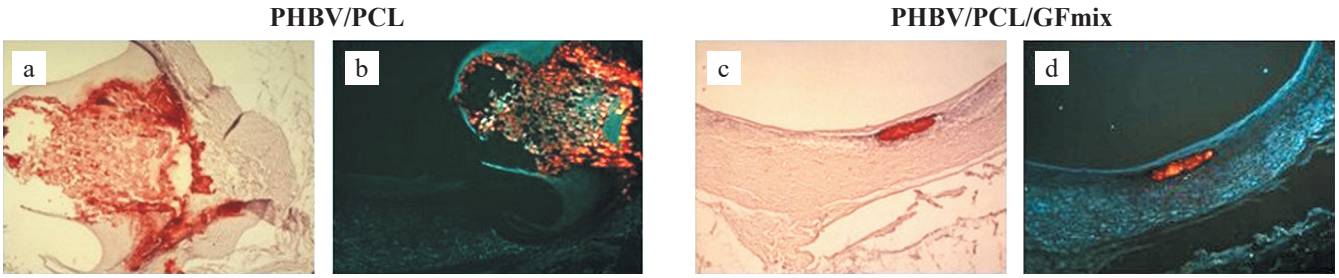

Fig. 2. Light (a) and fluorescence (b) microscopy of slices of PHBV/PCL and PHBV/PCL/GFmix vascular grafts retrieved: staining with alizarin red S (bright red color of Ca crystals) and Dapi (blue color of cell nuclei), 100×

The coagulation system of sheep was characterized by increased activity of prothrombin complex and a shortened thrombin time, while activated partial thromboplastin time (aPTT) and fibrinogen levels were comparable. Meanwhile, sheep exhibited a significant reduction in the activity of both the antiserum and fibrinolytic systems compared to coronary heart disease (CHD) patients. Evaluation of clot formation dynamics in animals revealed a faster initiation phase and higher clot density compared to patients [32]. Based on these findings, we adjusted the pre-, intra-, and postoperative antiplatelet and anticoagulant therapy as follows: preoperative phase – a single loading dose of clopidogrel administered the day before surgery; intraoperative phase – шntravenous administration of unfractionated heparin before carotid artery clamping and anastomosis, followed by an additional dose after blood flow restoration; postoperative phase (for 30 days post-implantation, provided the prostheses remained patent) – subcutaneous administration of low-molecular-weight heparin, following the manufacturer's dosage guidelines, oral administration of clopidogrel at a standard dosage, in accordance with the manufacturer's instructions. Nevertheless, the addition of an atrombogenic drug coating to the prostheses, combined with the adjusted anticoagulant therapy, improved vascular graft patency rates from 0% to 50% after 18 months of implantation in the carotid arteries of sheep [33]. However, this patency rate remains unconvincing for clinicians. A 50% thrombosis rate limits the potential clinical applicability of these prostheses, despite the fact that vascular surgery itself in sheep has been shown to induce thrombosis, as evidenced by previous studies on autoarterial implantation of the sheep carotid artery [34].

Given the high thrombotic tendency observed in sheep, it became crucial to investigate the patency outcomes of widely used synthetic VGs implanted in sheep carotid arteries.

To investigate this further, six animals underwent implantation of synthetic Gore-Tex® VGs (4 mm in diameter) into their carotid arteries – prostheses that are widely and successfully used in clinical practice. However, all Gore-Tex® grafts thrombosed within 24 hours of implantation. Despite the immediate loss of patency, it was decided to retrieve the thrombosed prostheses after 6 months to assess the response of surrounding tissues and potential calcific formation.

It was revealed that after 6 months, the walls of the thrombosed Gore-Tex® grafts exhibited massive calcification, despite the absence of blood flow. This calcification is presumed to result from insufficient biocompatibility of the material, which may have triggered a pathological reaction in the surrounding tissues. The

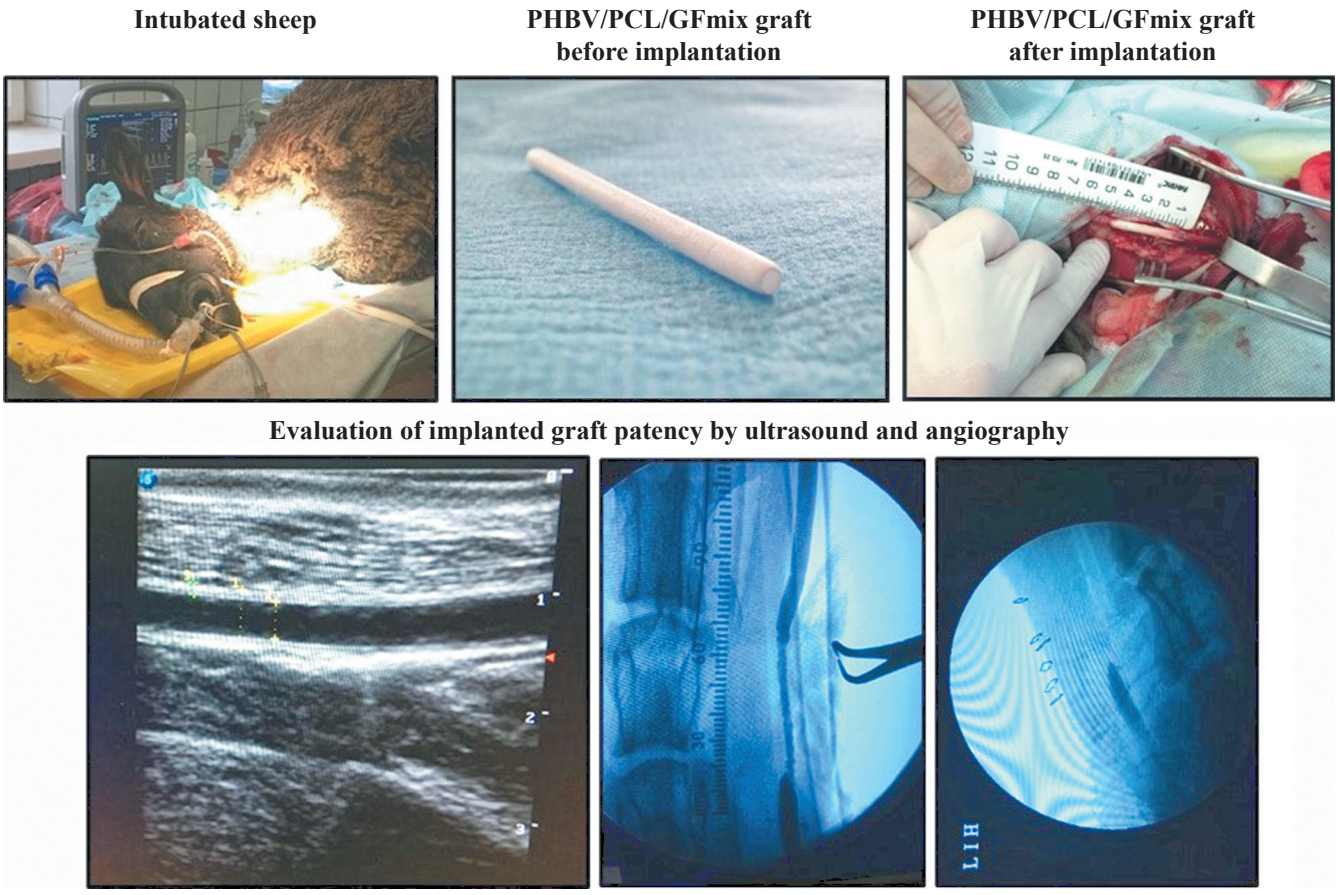

Fig. 3. Pilot preclinical trials of PHBV/PCL/GFmix vascular grafts in a sheep model

response likely involved apoptosis and the death of monocytic-macrophage and fibroblastic cells capable of penetrating the prosthesis wall from the adventitia side during the remodeling process [33, 35]. Despite the known aggressiveness of the sheep model regarding calcification, the drug-coated PHBV/PCL/GFmix grafts we developed exhibited minimal calcification. Only one retrieved patent graft showed small calcium deposits 1.5 years post-implantation, with a composition consistent with mature calcifications found in biological tissues [33, 35].

The second unexpected finding was the extremely rapid resorption of the polymeric scaffold, leading to aneurysm formation in all patent grafts. The onset of aneurysm development was observed as early as 1.5 months post-implantation, reaching its peak at 6 months, when the diameter of the VGs expanded from 4.0 mm to 2.2 cm. This dilation remained unchanged for the remainder of the 18-month implantation period [33, 35].

Morphological analysis of the retrieved prosthesis samples confirmed complete endothelialization of the inner surface, formation of new vascular tissue (neointima and adventitia) replacing the resorbed tubular scaffold, and minimal wall calcification. However, a critical limitation was identified – the absence of elastic fibers and true smooth muscle cells within the remodeled prosthesis walls (Fig. 4) [33, 35].

It should be noted that major publications on the testing of biodegradable SDVGs in sheep models have emerged since 2020. These studies have also reported early aneurysm formation in the walls of prostheses made from biodegradable polymers such as polycaprolactone, polylactide, and thermoplastic polyurethane [36, 37].

However, some authors have presented very impressive results, demonstrating the successful implantation of 4-mm biodegradable vascular grafts reinforced with a nitinol microframework into the coronary arteries of sheep. The incorporation of this microframework effectively prevented aneurysm formation [38].

Thus, the sheep model revealed an additional risk of prosthesis failure – early aneurysm formation – caused by accelerated resorption of biodegradable prosthetic frameworks. This resorption rate was significantly higher than that observed in the rat model. Moreover, the absence of elastin and true smooth muscle cells, combined with the rapid degradation of the polymeric framework, underscored the urgent need to modify the vascular graft fabrication process to incorporate aneurysmal protection.

To address this challenge, we explored three distinct approaches to prevent aneurysmal expansion of biodegradable vascular prosthesis walls:

1. Reinforcement of the outer contour of the prosthesis with extruded polymer spiral.
2. Creation of a reinforcing layer of polymer – synthetic elastomer with a low rate of bioresorption – on the outer surface of the prosthesis by electrospinning.
3. Introduction of synthetic elastomer with low biosorption rate into the tubular biodegradable framework

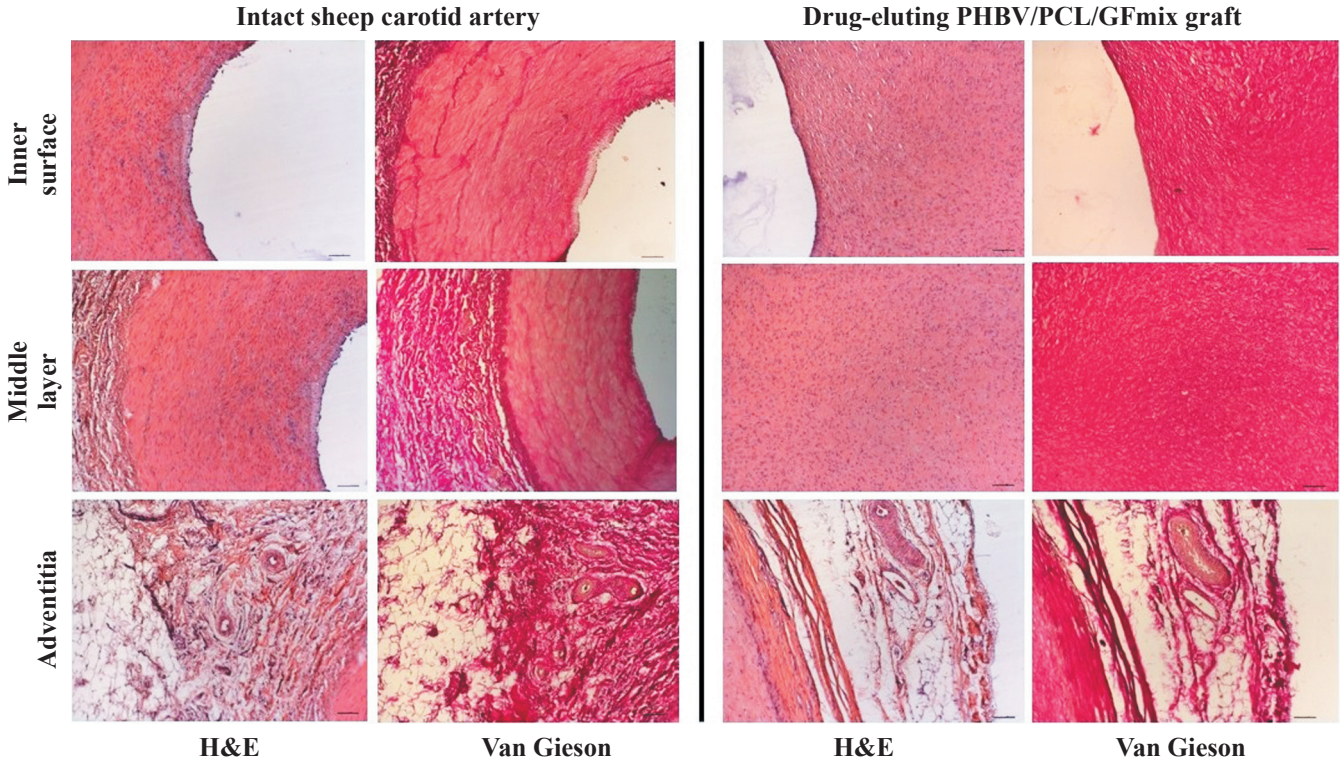

Fig. 4. Comparative histological picture of sheep carotid artery and drug-eluting PHBV/PCL/GFmix vascular graft at 18 months of implantation into a sheep carotid artery. Scale bar 100 μm

in the process of vascular prosthesis fabrication by electrospinning.

The first approach led to excessive weight gain and impaired surgical handling, making anastomosis more challenging. The second approach failed to establish a strong bond between the biodegradable prosthesis framework and the synthetic polymer outer layer, resulting in prosthesis delamination both before and during implantation, which triggered thrombosis. Therefore, the third approach – integrating a synthetic elastomer into the main polymer framework during electrospinning – proved to be the most effective. This method produced a cohesive, structurally stable prosthesis while preserving functional activity through controlled release of incorporated proangiogenic factors, and complete remodeling potential via the porous structure and partial biodegradation of the polymeric framework.

EFFECTIVENESS OF A PRIMATE MODEL IN PRECLINICAL TRIALS OF SMALL-DIAMETER VASCULAR GRAFTS

A primate model was selected for the final preclinical trials, as it closely resembles humans and provides the most reliable assessment of potential risks associated with biodegradable vascular grafts. Baboons were chosen as the largest primates available for experimental use from Russian research nurseries.

The similarities between baboons and humans in terms of metabolism, diet, body structure, and blood coagulation function were expected to minimize the species-specific limitations encountered in the sheep model. A thorough review of literature on vascular anatomy and structure of baboons was conducted [39, 40].

As a result, the femoral artery was identified as the optimal implantation site for <4 mm grafts. This selection minimized the risk of global limb ischemia in the event of graft thrombosis.

It is important to note that in adult male baboons aged 9 to 17 years and weighing 18 to 38 kg, femoral artery diameters do not exceed 3.2 mm. To ensure optimal graft performance, baboons were preselected, and ultrasound measurements were conducted to determine the diameter of each femoral artery.

To minimize the risk of thrombosis due to graft/artery diameter mismatch, custom-fabricated VGs were designed for each baboon, ensuring an exact fit with the native artery during implantation.

VGs with diameters of 3.0–3.5 mm and lengths of 3.0–4.5 cm were implanted into the femoral arteries of 6 adult male baboons for a period of 6 months (Fig. 5). The pre-, intra-, and postoperative antiplatelet therapy regimen mirrored that used in the sheep model.

No delamination of the prosthetic walls was observed during implantation or after 6 months. Ultrasound assessments confirmed a final prosthesis patency rate of 83.3%. Early thrombosis occurred in one case, attributed to concomitant pathology (excessive body weight twice the age norm, respiratory insufficiency, and arrhythmia).

Histological and immunofluorescence analyses of retrieved graft samples demonstrated complete endothelization of the internal surface, a neointima without signs of hyperplasia, and a neoadventitia containing all typical structural elements. Additionally, cell migration into the prosthesis walls was observed (Fig. 6). There were no signs of inflammation or calcification.

A significant advantage was the interchangeability of staining with human fluorescent antibodies for im-

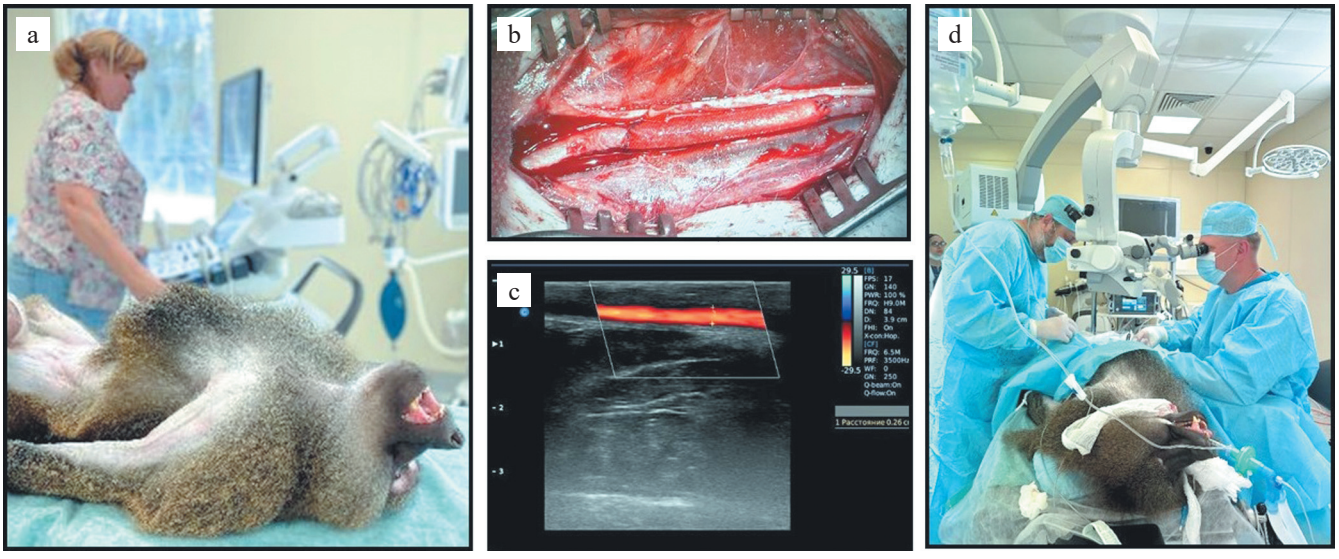

Fig. 5. Preclinical trials of small-diameter vascular grafts on a primate model: a, ultrasound assessment of femoral artery diameter; b, view of the implanted vascular graft in the femoral artery of a baboon; c, ultrasound confirmation of implanted graft patency; d, vascular graft implantation procedure

munofluorescence studies of retrieved prosthetic specimens. This proved highly convenient, as primate-specific primary antibodies are scarcely available on the market. The compatibility of human-specific antibodies with primate antibodies allowed for a more comprehensive morphological analysis, leveraging the broader range of available human antibody panels compared to those for other animal models.

All baboons in the experiment were adult, age-matched males. Given that the average lifespan of baboons in the wild is around 30 years – but significantly lower in captivity – the experimental group already exhibited a premorbid background typical for age-matched individuals.

For instance, thrombosis of one prosthesis occurred in a 15-year-old male with obesity, arrhythmia, and respiratory failure. In addition, the oldest baboon (17 years old) exhibited hypertrophy of the femoral artery wall throughout and a discontinuous endothelial layer.

When comparing the quality of endothelization in the vascular graft implanted in this baboon with that of its intact contralateral femoral artery, it was found that the graft exhibited superior endothelization. This finding indirectly confirmed the efficacy and activity of the proangiogenic factors incorporated into the prosthesis (Fig. 7).

CONCLUSION

1. The accuracy of identifying failure risks in biodegradable SDVGs during preclinical testing is highly dependent on the choice of the animal model.
2. The rat model does not accurately predict long-term patency of VGs due to its rapid endothelialization, inability to implant long prostheses into the rat aorta, and its incompatibility with human physiology. However, it remains useful for evaluating the calcification potential of VGs.
3. The sheep model exhibits an excessively high susceptibility to thrombosis, necessitating modifications in the manufacturing process to enhance the thromboresistance of the medical device. Consequently, the hemocompatibility of the device may be tailored more to the hemostasiologic profile of a laboratory animal rather than humans. However, a significant advantage of this model is its ability to reveal the accelerated biodegradation of polymers, which led to aneurysm formation throughout the entire length of the prosthesis. Moreover, according to various literature sources, polymers used in VGs should not undergo resorption before three years. In addition, the sheep model is highly prone to calcification, making the low calcification rates observed in the developed prostheses an indicator of their biocompatibility.

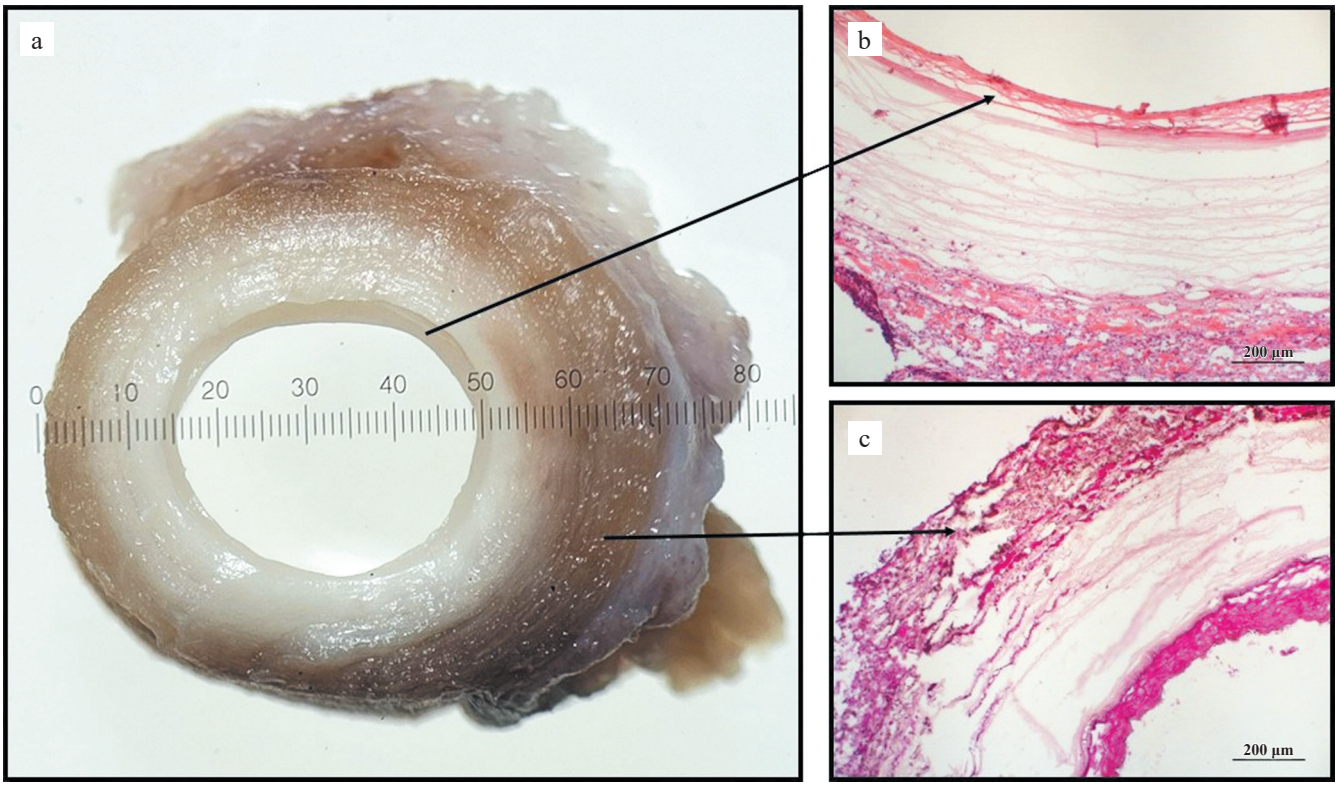

Fig. 6. Results of morphological analysis of small-diameter vascular grafts at 6 months post-implantation in the femoral arteries of baboons: a, spectroscopy of a cross-section of the retrieved graft (10×); b, hematoxylin-eosin staining (100×); c, Van Gieson's staining (100×)

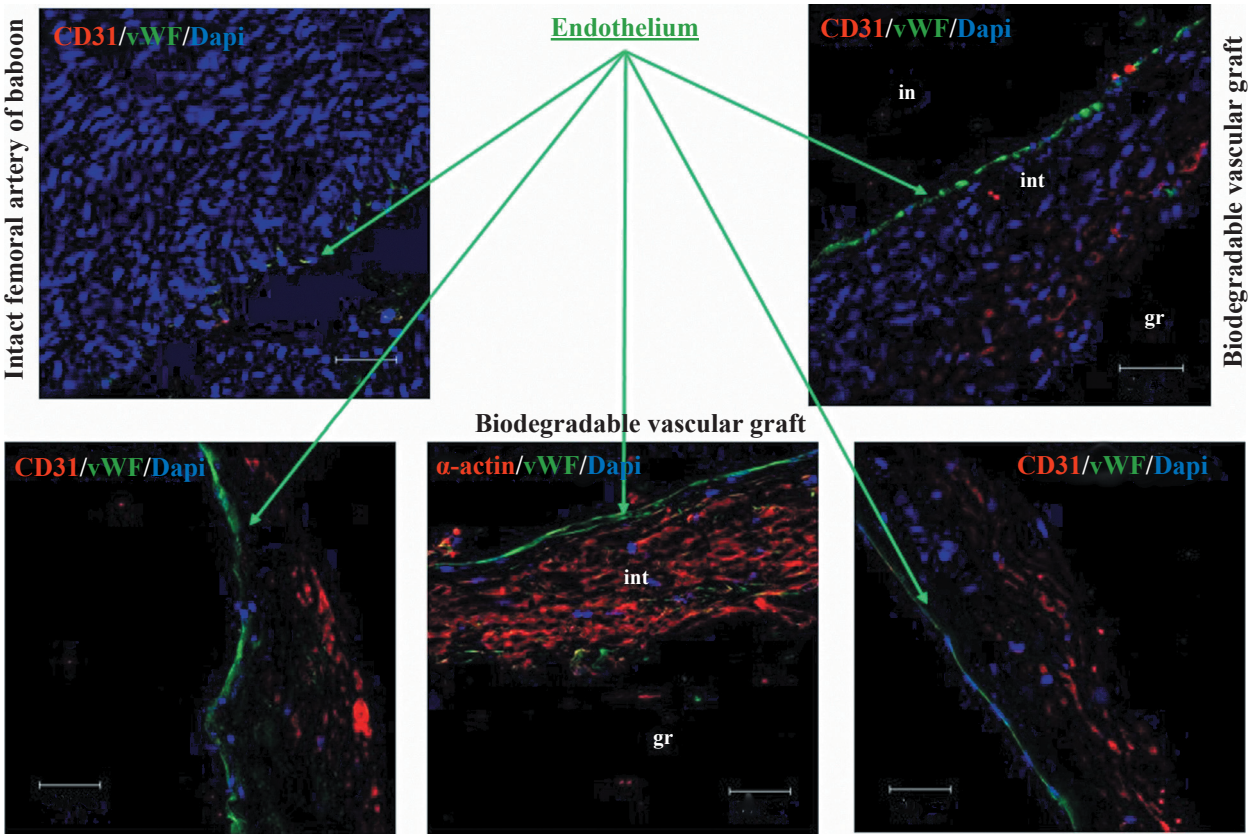

Fig. 7. Immunofluorescence results of a retrieved small-diameter vascular graft and a contralateral intact femoral artery of a baboon. Scale bar 50 μm

4. The primate model proved to be the most balanced for preclinical testing, providing an accurate assessment of both long-term patency and graft remodeling. It also demonstrated appropriate sensitivity to intra- and postoperative antiplatelet therapy. When using age-matched animals with a premorbid background similar to that of elderly patients with cardiovascular pathology, the evaluation of VGs occurs under conditions that closely resemble future human clinical trials. The identity of specific human antibodies with primate antibodies significantly enhances the depth of morphological analysis of retrieved prosthesis samples.

This research was conducted as part of the fundamental theme of the Research Institute for Complex Issues of Cardiovascular Diseases, No. 0419-2022-0001: "Molecular, cellular, and biomechanical mechanisms of the pathogenesis of cardiovascular diseases in the development of new treatment methods for cardiovascular diseases, based on personalized pharmacotherapy, introduction of minimally invasive medical devices, biomaterials, and tissue-engineered implants".

The authors declare no conflict of interest.

REFERENCES

1. *Nelson RA, Rhee EK, Alaeddine M, Nikkhah M.* Advances in Biomaterials for Promoting Vascularization. *Curr Stem Cell Rep*. 2022; 8: 184–196. doi: 10.1007/s40778-022-00217-w.
2. *Naegeli KM, Kural MH, Li Yu, Wang J, Hugentobler EA, Niklason LE.* Bioengineering Human Tissues and the Future of Vascular Replacement. *Circ Res*. 2022 Jun 24; 131 (1): 109–126. doi: 10.1161/CIRCRESAHA.121.319984.
3. *Bokeriya LA, Milievskaya EB, Pryanishnikov VV, Yurlov IA, Kudzoeva ZF.* Serdechno-sosudistaya khirurgiya – 2021. Bolezni i vrozhdennye anomalii sistemy krovoobrashcheniya. M: NMITs SSKh im. A.N. Bakuleva, 2022; 310.
4. *Malektaj H, Nour S, Imani R, Siadati MH.* Angiogenesis induction as a key step in cardiac tissue Regeneration: From angiogenic agents to biomaterials. *Int J Pharm*. 2023 Aug 25; 643: 123233. doi: 10.1016/j.ijpharm.2023.123233.
5. *Watanabe T, Sassi S, Ulziibayar A, Hama R, Kitsuka T, Shinoka T.* The Application of Porous Scaffolds for Cardiovascular Tissues. *Bioengineering (Basel).* 2023 Feb 10; 10 (2): 236. doi: 10.3390/bioengineering10020236.
6. *Tan W, Boodagh P, Selvakumar PP, Keyser S.* Strategies to counteract adverse remodeling of vascular graft: A 3D view of current graft innovations. *Front Bioeng Biotechnol*. 2023 Jan 10; 10: 1097334. doi: 10.3389/fbioe.2022.1097334.

7. *Robotti F, Franco D, Bänninger L, Wyler J, Starck CT, Falk V et al*. The influence of surface micro-structure on endothelialization under supraphysiological wall shear stress. *Biomaterials*. 2014 Oct; 35 (30): 8479–8486. doi: 10.1016/j.biomaterials.2014.06.046.
8. *Cai Q, Liao W, Xue F, Wang X, Zhou W, Li Y, Zeng W*. Selection of different endothelialization modes and different seed cells for tissue-engineered vascular graft. *Bioact Mater*. 2021 Feb 6; 6 (8): 2557–2568. doi: 10.1016/j.bioactmat.2020.12.021.
9. *Kojima T, Nakamura T, Saito J, Hidaka Yu, Akimoto T, Inoue H et al*. Hydrostatic pressure under hypoxia facilitates fabrication of tissue-engineered vascular grafts derived from human vascular smooth muscle cells *in vitro*. *Acta Biomater*. 2023 Nov; 171: 209–222. doi: 10.1016/j.actbio.2023.09.041.
10. *Stowell CET, Wang Ya*. Quickening: Translational design of resorbable synthetic vascular grafts. *Biomaterials*. 2018 Aug; 173: 71–86. doi: 10.1016/j.biomaterials.2018.05.006.
11. *Tang Y, Yin L, Gao S, Long X, Du Z, Zhou Y et al*. A small-diameter vascular graft immobilized peptides for capturing endothelial colony-forming cells. *Front Bioeng Biotechnol*. 2023 Apr 10; 11: 1154986. doi: 10.3389/fbioe.2023.1154986.
12. *Zulkifli MZA, Nordin D, Shaari N, Kamarudin SK*. Overview of Electrospinning for Tissue Engineering Applications. *Polymers (Basel)*. 2023 May 23; 15 (11): 2418. doi: 10.3390/polym15112418.
13. *Kim JY, Kim JI, Park CH, Kim CS*. Design of a modified electrospinning for the in-situ fabrication of 3D cotton-like collagen fiber bundle mimetic scaffold. *Materials Letters*. 2019 Feb 1; 236: 521–525. doi: 10.1016/j.matlet.2018.10.087.
14. *Di Francesco D, Pigliafreddo A, Casarella S, Di Nunno L, Mantovani D, Boccafoschi F*. Biological Materials for Tissue-Engineered Vascular Grafts: Overview of Recent Advancements. *Biomolecules*. 2023 Sep 14; 13 (9): 1389. doi: 10.3390/biom13091389.
15. *Xie X, Wu Q, Liu Y, Chen C, Chen Z, Xie C et al*. Vascular endothelial growth factor attenuates neointimal hyperplasia of decellularized smalldiameter vascular grafts by modulating the local inflammatory response. *Front Bioeng Biotechnol*. 2022 Dec 20; 10: 1066266. doi: 10.3389/fbioe.2022.1066266.
16. Prikaz Ministerstva zdravookhraneniya Rossiyskoy Federatsii ot 6 iyunya 2012 g. № 4n, g. Moskva "Ob utverzhdenii nomenklaturnoy klassifikatsii meditsinskikh izdeliy". Registratsionnyy № 24852. Zaregistrirovan v Minyuste RF 9 iyulya 2012 g. Data podpisaniya: 06.06.2012. Opublikovan: 23.10.2012. Vstupaet v silu: 04.11.2012.
17. *Thanigaimani S, Kichenadasse G, Mangoni AA*. The emerging role of vascular endothelial growth factor (VEGF) in vascular homeostasis: Lessons from recent trials with anti-VEGF drugs. *Curr Vasc Pharmacol*. 2011 May; 9 (3): 358–380. doi: 10.2174/157016111795495503.
18. *Yang X, Liaw L, Prudovsky I, Brooks PC, Vary C, Oxburgh L, Friesel R*. Fibroblast growth factor signaling in the vasculature. *Curr Atheroscler Rep*. 2015 Jun; 17 (6): 509. doi: 10.1007/s11883-015-0509-6.
19. *Salcedo R, Oppenheim JJ*. Role of chemokines in angiogenesis: CXCL12/SDF-1 and CXCR4 interaction, a key regulator of endothelial cell responses. *Microcirculation*. 2003 Jun; 10 (3–4): 359–370. doi: 10.1038/sj.mn.7800200.
20. *Schober A*. Chemokines in vascular dysfunction and remodeling. *Arterioscler Thromb Vasc Biol*. 2008 Nov; 28 (11): 1950–1959. doi: 10.1161/ATVBAHA.107.161224.
21. *Zhu M, Wu Y, Li W, Dong X, Chang H, Wang K et al*. Biodegradable and elastomeric vascular grafts enable vascular remodeling. *Biomaterials*. 2018 Nov; 183: 306–318. doi: 10.1016/j.biomaterials.2018.08.063.
22. *Wu P, Wang L, Li W, Zhang Y, Wu Y, Zhi D et al*. Construction of vascular graft with circumferentially oriented microchannels for improving artery regeneration. *Biomaterials*. 2020 Mar 4; 242: 119922. doi: 10.1016/j.biomaterials.2020.119922.
23. *Navarro RS, Jiang L, Ouyang Y, Luo J, Liu Z, Yang Y et al*. Biomimetic tubular scaffold with heparin conjugation for rapid degradation in *in situ* regeneration of a small diameter neoartery. *Biomaterials*. 2021 Jul; 274: 120874. doi: 10.1016/j.biomaterials.2021.120874.
24. *Antonova LV, Sevostyanova VV, Mironov AV, Krivkina EO, Velikanova EA, Matveeva VG et al*. *In situ* vascular tissue remodeling using biodegradable tubular scaffolds with incorporated growth factors and chemoattractant molecules. *Complex Issues of Cardiovascular Diseases*. 2018; 7 (2): 25–36. (In Russ.). doi: 10.17802/2306-1278-2018-7-2-25-36.
25. *Antonova L, Kutikhin A, Sevostianova V, Velikanova E, Matveeva V, Glushkova T et al*. bFGF and SDF-1α Improve *In Vivo* Performance of VEGF-Incorporating Small-Diameter Vascular Grafts. *Pharmaceuticals (Basel)*. 2021 Mar 28; 4 (4): 302. doi: 10.3390/ph14040302.
26. *Antonova LV, Barbarash OL, Barbarash LS*. Tissue-Engineered Constructions for the Needs of Cardiovascular Surgery: Possibilities of Personalization and Prospects for Use (Problem Article). *Annals of the Russian Academy of Medical Sciences*. 2023; 78 (2): 141–150. [In Russ, English abstract]. doi: 10.15690/vramn7578.
27. *Hao D, Fan Y, Xiao W, Liu R, Pivetti C, Walimbe T et al*. Rapid endothelialization of small diameter vascular grafts by a bioactive integrin-binding ligand specifically targeting endothelial progenitor cells and endothelial cells. *Acta Biomater*. 2020 May; 108: 178–193. doi: 10.1016/j.actbio.2020.03.005.
28. *Liu RH, Ong CS, Fukunishi T, Ong K, Hibino N*. Review of vascular graft studies in large animal models. *Tissue Eng Part B Rev*. 2018 Apr; 24 (2): 133–143. doi: 10.1089/ten.TEB.2017.0350.
29. *Swartz DD, Andreadis ST*. Animal models for vascular tissue-engineering. *Curr Opin Biotechnol*. 2013 Oct; 24 (5): 916–925. doi: 10.1016/j.copbio.2013.05.005.

30. *Thomas LV, Lekshmi V, Nair PD*. Tissue engineered vascular grafts – preclinical aspects. *Int J Cardiol*. 2013 Aug 20; 167 (4): 1091–1100. doi: 10.1016/j.ijcard.2012.09.069.
31. Patent № 2702239 RF. Tekhnologiya izgotovleniya funktsional'no aktivnykh biodegradiruemykh sosudistykh protezov malogo diametra s lekarstvennym pokrytiem / Antonova L.V., Sevost'yanova V.V., Rezvova M.A., Krivkina E.O., Kudryavtseva Yu.A., Barbarash O.L., Barbarash L.S.; zayavitel' i pravoobladatel' Federal'noe gosudarstvennoe byudzhetnoe nauchnoe uchrezhdenie "Nauch.-issled. in-t kompleksnykh problem serdechno-sosudistykh zabolevaniy" – № 2019119912; zayavl. 25.06.2019; zaregistr. 07.10.2019. – 1 s.
32. *Gruzdeva OV, Bychkova EE, Penskaya TYu, Kuzmina AA, Antonova LV, Barbarash LS*. Comparative Analysis of the Hemostasiological Profile in Sheep and Patients with Cardiovascular Pathology as the Basis for Predicting Thrombotic Risks During Preclinical Tests of Vascular Prostheses. *Sovremennye tehnologii v medicine*. 2021; 13 (1): 52–58. [In Russ, English abstract]. doi: 10.17691/stm2021.13.1.06.
33. *Antonova LV, Krivkina EO, Khanova MYu, Velikanova EA, Matveeva VG, Mironov AV et al*. Results of preclinical trials in a sheep model of biodegradable small-diameter vascular grafts. *Russian Journal of Transplantology and Artificial Organs*. 2022; 24 (3): 80–93. [In Russ, English abstract]. doi: 10.15825/1995-1191-2022-3-80-93.
34. *Antonova LV, Mironov AV, Yuzhalin AE, Krivkina EO, Shabaev AR, Rezvova MA et al*. A brief report on an implantation of small-caliber biodegradable vascular grafts in a carotid artery of the sheep. *Pharmaceuticals (Basel)*. 2020 May 21; 13 (5): 101. doi: 10.3390/ph13050101.
35. *Antonova LV, Krivkina EO, Sevostianova VV, Mironov AV, Rezvova MA, Shabaev AR et al*. Tissue-engineered carotid artery interposition grafts demonstrate high primary patency and promote vascular tissue regeneration in the ovine model. *Polymers (Basel)*. 2021 Aug 8; 13 (16): 2637. doi: 10.3390/polym13162637.
36. *Wang C, Li Z, Zhang L, Sun W, Zhou J*. Long-term results of triple-layered small diameter vascular grafts in sheep carotid arteries. *Med Eng Phys*. 2020 Nov; 85: 1–6. doi: 10.1016/j.medengphy.2020.09.007.
37. *Matsuzaki Yu, Iwaki R, Reinhardt JW, Chang Yu-C, Miyamoto S, Kelly J et al*. The effect of pore diameter on neo-tissue formation in electrospun biodegradable tissue-engineered arterial grafts in a large animal model. *Acta Biomater*. 2020 Oct 1; 115: 176–184. doi: 10.1016/j.actbio.2020.08.011.
38. *Ono M, Kageyama S, O'Leary N, El-Kurdi MS, Reinöhl J, Solien E et al*. 1-Year Patency of Biorestorative Polymeric Coronary Artery Bypass Grafts in an Ovine Model. *JACC Basic Transl Sci*. 2023 Nov 9; 8 (1): 19–34. doi: 10.1016/j.jacbts.2022.06.021.
39. *Dyl L, Topol M*. The femoral artery and its branches in the baboon Papio Anubis. *Folia Morphol (Warsz).* 2007 Nov; 66 (4): 291–295.
40. *Chai D, Cuneo S, Falconer H, Mwenda JM, D'Hooghe T*. Olive baboon (Papio anubis anubis) as a model for intrauterine research. *J Med Primatol*. 2007 Dec; 36 (6): 365–369. doi: 10.1111/j.1600-0684.2006.00204.x.

The article was submitted to the journal on 17.09.2024

DOI: 10.15825/1995-1191-2025-2-139-147

IMPACT OF PANCREATIC CELL-ENGINEERED CONSTRUCTS ON THE ISLET APPARATUS IN RECIPIENT RATS WITH TYPE I DIABETES MELLITUS

N.V. Baranova[1], L.A. Kirsanova[1], G.N. Bubentsova[1], A.S. Ponomareva[1], A.O. Nikolskaya[1], Yu.B. Basok[1], V.I. Sevastianov[1, 2]

[1] Shumakov National Medical Research Center of Transplantology and Artificial Organs, Moscow, Russian Federation

[2] Institute of Biomedical Research and Technology, Moscow, Russian Federation

Current research focuses on exploring strategies to stimulate the regenerative capacity of pancreatic beta cells as a potential therapeutic approach for diabetes mellitus (DM). **Objective:** this study aims to perform a comparative histological analysis of the islet apparatus in rats with streptozotocin (STZ)-induced DM following the implantation of a pancreatic cell-engineered construct (PCEC). The PCEC consists of isolated allogeneic islets of Langerhans embedded within a scaffold derived from decellularized human pancreatic fragments. **Materials and methods.** The pancreases of rats from the control group (n = 4; untreated type 1 DM – T1DM), experimental group 1 (n = 4; intraperitoneal injection of pancreatic islets), and experimental group 2 (n = 4; intraperitoneal injection of PCEC) underwent histological analysis. Immunohistochemical staining for insulin and glucagon was performed using specific antibodies and an imaging system. **Results.** In the pancreatic islets of the control group, insulin-immunopositive beta cells were either absent or detected as isolated cells, with alpha cells predominating. In the pancreases of experimental group 1 rats, beta cells were observed in most islets and within the surrounding exocrine parenchyma, albeit in low numbers (1–2 per field of view), while alpha cells remained the dominant population. A significant increase in insulin-positive cells was observed in the pancreas of rats in experimental group 2, along with a reduction in glucagon-positive cell numbers. **Conclusion.** Morphological examination of the pancreatic islet apparatus in the experimental animals revealed that implantation of the PCEC had a beneficial effect on restoration of the recipient's pool of functionally active beta cells, serving as a trigger for the regenerative process.

Keywords: diabetes mellitus, pancreas, pancreatic islets, regeneration.

INTRODUCTION

Restoring insulin-producing β-cells lost in type 1 diabetes mellitus (T1DM) is a major challenge. The regenerative capacity of pancreatic islet is inherently limited [1]. Consequently, current research efforts are increasingly focused on strategies aimed at stimulating β-cell formation from alternative pancreatic cell populations [2], as well as generating β-cells from stem cells of various origins [3].

Presently, considerable attention is being directed toward understanding the mechanisms of β-cell regeneration within the pancreas and elucidating the molecular pathways involved in this process. The insights gained from such studies may facilitate the development of novel, effective, and safe therapeutic approaches for the treatment of diabetes mellitus (DM) [4, 5].

Restoration of the β-cell pool involves several mechanisms, including limited β-cell proliferation, hypertrophy, and transdifferentiation of other pancreatic cell types such as ductal epithelial cells, acinar cells, and other insulocytes [5–8]. Recent research shows that various pancreatic cells possess significant plasticity, meaning they can change their identity and adopt characteristics of other cell types within the pancreas [5]. In murine models, when β-cells are injured or destroyed, a small percentage of glucagon-producing α-cells and somatostatin-producing δ-cells can begin to express insulin [9].

Remedi et al. further revealed that multiple pancreatic cell types, including ductal cells, centroacinar cells, α-cells [10], and δ-cells [11], can transdifferentiate into functional β-cells, thereby compensating for impaired insulin secretion, a key factor in maintaining normoglycemia. The regeneration process involving ductal cells appears to mimic key aspects of embryonic β-cell differentiation, underscoring the plasticity of pancreatic tissue [12, 13]. Supporting this, W.-C. Li et al. demonstrated that β-cell regeneration can dedifferentiate to a precursor-like state, and then redifferentiate through specific signaling pathways that parallel those active during embryonic development [14].

Corresponding author: Natalia Baranova. Address: 1, Shchukinskaya str., Moscow, 123182, Russian Federation. Phone: (917) 568-98-22. E-mail: barnats@yandex.ru

Given that acinar cells constitute the most abundant cell population in the pancreas, they have emerged as a promising source for generating new β-cells [15–19]. In a landmark study, Q. Zhou et al. demonstrated that differentiated acinar cells in adult mice possess the capacity to transdifferentiate into β-cells phenotypically similar to endogenous islet insulin-producing cells, capable of expressing insulin and alleviating hyperglycemia [20].

The concept of restoring lost cell populations by stimulating intrinsic adaptive plasticity *in situ* presents a compelling therapeutic avenue for the treatment of degenerative diseases [21]. However, it remains unclear whether human pancreatic cells exhibit a comparable degree of plasticity, particularly under diabetic conditions. This uncertainty stems from potential differences in the signaling pathways and molecular mediators – such as glucose levels, hormones, and growth factors – that govern β-cell regeneration in humans compared to animal models [9].

One of the strategies for cell replacement therapy in patients with T1DM is pancreatic islet transplantation. This approach not only ensures physiological insulin delivery but may also exert a stimulatory effect on endogenous β-cell regeneration. Jörns et al. support the concept that long-term normoglycemia maintained by insulin-producing grafts provides an optimal environment for β-cell regeneration and replication within the pancreas [22]. This regenerative stimulation is likely mediated by the paracrine effects of transplanted endocrine cells, which secrete bioactive polypeptides such as C-peptide and amylin, each with distinct physiological roles [23]. Supporting this concept, studies have shown that islet transplantation following partial pancreatectomy in mice enhances the regeneration and preservation of endogenous β-cells, resulting in increased β-cell mass and improved glycemic stability [24].

Previously, we showed a more pronounced reduction in glycemia levels in T1DM rats following intraperitoneal administration of a pancreatic cell-engineered construct (PCEC). This construct was based on isolated allogeneic islets of Langerhans and a scaffold derived from decellularized human pancreatic tissue fragments [25]. Morphological changes in the pancreas indicative of β-cell regeneration were also observed.

The objective of the present study was to conduct a comparative histological analysis of the islet apparatus between control and experimental animal groups.

MATERIALS AND METHODS

Composition of pancreatic cell-engineered construct (PCEC)

The PCEC was composed of two main components: viable insulin-producing rat pancreatic islets (PIs), cultured for 24 hours under standard conditions (37 °C, 5% CO_2), and a tissue-specific, fine-dispersed scaffold derived from decellularized human pancreatic fragments (dHPF scaffold) [26–28].

Each PCEC sample contained 2000 islets immobilized within 10.0 ± 0.1 mg of sterile dHPF scaffold, suspended in 100 μL of Hanks' balanced salt solution.

Islet viability within the PCEC was assessed using vital fluorescent dyes – acridine orange and propidium iodide (AO/PI) (PanEco, Russia).

The prepared PCEC samples were administered intraperitoneally to rats with streptozotocin (STZ)-induced T1DM using a 23G syringe needle.

In vivo experiment design

A T1DM model was induced in male Wistar rats (300–380 g) by fractional intraperitoneal administration of STZ (Biorbyt, India) at a dose of 15 mg/kg/day every 5 days. To confirm the stability of the T1DM model and exclude spontaneous reversion, glycemia levels were assessed 14 days after the final STZ dose. Only animals with fasting blood glucose levels exceeding 20.0 mmol/L were included in subsequent experiments.

The selected diabetic rats (n = 12) were randomly allocated into three groups: control group (n = 4; no treatment), experimental group 1 (n = 4; received intraperitoneal injection of 2000 isolated PIs) and experimental group 2 (n = 4; intraperitoneal injection of PCEC).

Fasting capillary blood glucose levels were measured weekly for 10 weeks. At the end of the experimental period, animals were euthanized, and pancreatic tissue was harvested for morphological and histological analysis.

Histologic study

A histologic examination of the pancreas was performed in control and experimental groups to identify morphological features of the islet apparatus. The excised pancreas samples were fixed in 10% buffered formalin for 24 hours. Dehydration was carried out using a graded ethanol series (50%, 60%, 70%, 80%, 95%), followed by sequential incubation in a mixture of ethanol and chloroform, pure chloroform, and a chloroform-paraffin mixture at +37 °C. Tissues were embedded in paraffin (Paraplast® X-tra™, Leica, Germany), and 4–5 μm sections were prepared using a rotary microtome (RM2245, Leica, Germany).

The paraffin sections were stained with hematoxylin and eosin. To identify the main islet cell types, immunohistochemical (IHC) staining for insulin and glucagon was performed using specific primary anti-insulin antibody (Abcam, UK) and anti-glucagon antibody (Merck, Germany). Visualization of immunoreactivity was carried out using the Rabbit Specific HRP/DAB (ABC) Detection IHC kit (Abcam, UK) according to the manufacturer's protocol.

RESULTS

Pancreatic cell-engineered construct (PCEC)

PCEC was formed immediately prior to intraperitoneal administration in rats with experimentally induced T1DM. PIs, pre-cultured for 24 hours, exhibited adhesive properties, attaching effectively to the surface of the decellularized pancreatic scaffold (Fig. 1, a). Only a few isolated islets remained free-floating in the culture medium.

Viability of the islets within PCEC was assessed using acridine orange and propidium iodide (AO/PI) vital staining. The staining results confirmed high islet viability within the construct, which was found to be 95 ± 2% (Fig. 1, b).

Comparative evaluation of functional efficiency of PCEC and PIs in rats with streptozotocin-induced diabetes mellitus

The study showed that intraperitoneal administration of PCEC in rats of experimental group 2 led to a significant reduction in blood glucose levels – by an average of 19.5 ± 3.9 mmol/L (from 25.8 ± 5.1 mmol/L to 6.3 ± 2.7 mmol/L). By week 10 of observation, glycemia levels were reduced to less than half of their baseline values.

In contrast, administration of a suspension of PIs in rats from experimental group 1 resulted in a mean glucose reduction of 14.8 ± 3.4 mmol/L (from 28.2 ± 4.2 mmol/L to 13.4 ± 2.6 mmol/L). However, this glycemic control was transient, lasting approximately 7 weeks, after which glucose levels began to rise and, in some cases, approached baseline values.

Thus, the administration of PCEC in T1DM rats demonstrated a more pronounced and sustained hypoglycemic effect compared to administration of a suspension of PIs alone [25, 29].

Morphologic changes in the islet apparatus of diabetic rats after intraperitoneal injection of pancreatic islets or PCEC

In **healthy rats**, the pancreas is characterized by diffuse structure with well-defined lobularity of the exocrine parenchyma interspersed with discrete PIs. These islets typically appear as spherical or oval clusters with sharply defined borders. Within the islets, insulocyte cells are arranged uniformly and display pale, fine-granular cytoplasm and rounded nuclei containing one to two prominent nucleoli (Fig. 2, a). The main endocrine cell types in rat islets exhibit a distinct spatial distribution: insulin-positive β-cells are primarily located in the central zone of the islet (Fig. 2, b), while glucagon-positive α-cells are arranged along the periphery, forming the characteristic “mantle” structure (Fig. 2, c).

The administration of STZ, which selectively targets insulin-producing β-cells in pancreatic islets, led to notable morphological alterations in the islet architecture. In pancreatic tissue samples from **control group rats** (10 weeks post-induction without treatment), islets appeared irregular in shape, with uneven contours and small protrusions extending into the surrounding exocrine parenchyma (Fig. 3, a). The cytotoxic effect of STZ culminated in β-cell death, predominantly affecting the central zone of the islets. This was evidenced by the presence of hypertrophied cells, necrotic cells exhibiting karyolysis, vacuolated cells, and areas of cellular debris. Additionally, islet cytoarchitecture was disrupted, with regions of hypercellularity emerging – these areas displayed a strong immunopositive signal for glucagon (Fig. 3, c). The observed hypercellularity likely reflected compensatory α-cell proliferation triggered by chronic

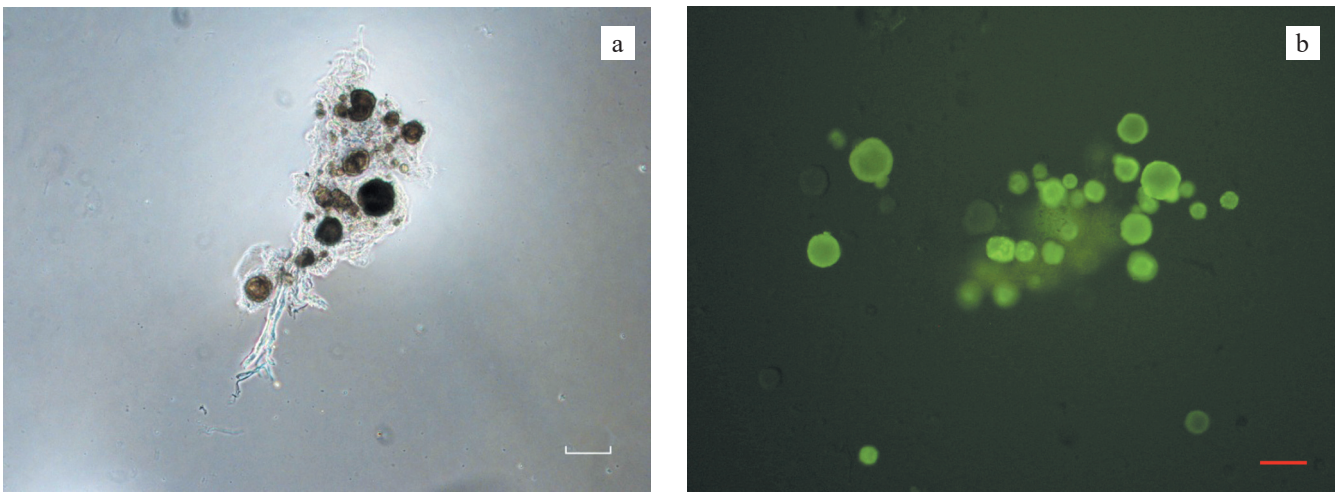

Fig. 1. Pancreatic cell-engineered construct (PCEC) composed of rat Pancreatic islets and a tissue-specific scaffold derived from decellularized human pancreas (DHP scaffold). (a) Inverted phase-contrast microscopy; (b) Acridine Orange/Propidium Iodide (AO/PI) fluorescence staining. Scale bar: 100 μm

hyperglycemia and altered paracrine signaling due to β-cell loss. Consequently, α-cells became the dominant islet population. In contrast, insulin-positive cells were absent in most islets or detected only as isolated cells (Fig. 3, b).

By the end of the 10-week experiment, histological examination of the pancreatic tissue in rats from experimental group 1 (injected with PIs) revealed no substantial morphological improvement compared to the control group. The islets retained an irregular shape and contours, with evident vacuolized and necrotic cells, as well as zones of hypercellularity (Fig. 4, a). IHC staining demonstrated the presence of β-cells, albeit in very small numbers (typically 1–2 cells per field of view), both within the islets and occasionally in the surrounding exocrine parenchyma (Fig. 4, b). However, the limited number of these cells likely rendered them insufficient to significantly impact glycemic regulation. Notably, α-cells continued to represent the predominant islet population (Fig. 4, c). These findings suggest that the observed reduction in blood glucose levels in this group was primarily mediated by the exogenous insulin secreted by the transplanted islets rather than endogenous β-cell regeneration.

Intraperitoneal injection of PCEC induced certain morphological changes in the islet apparatus of **rats in experimental group 2**. In addition to islets exhibiting hypercellularity and necrotic alterations, distinctive is-

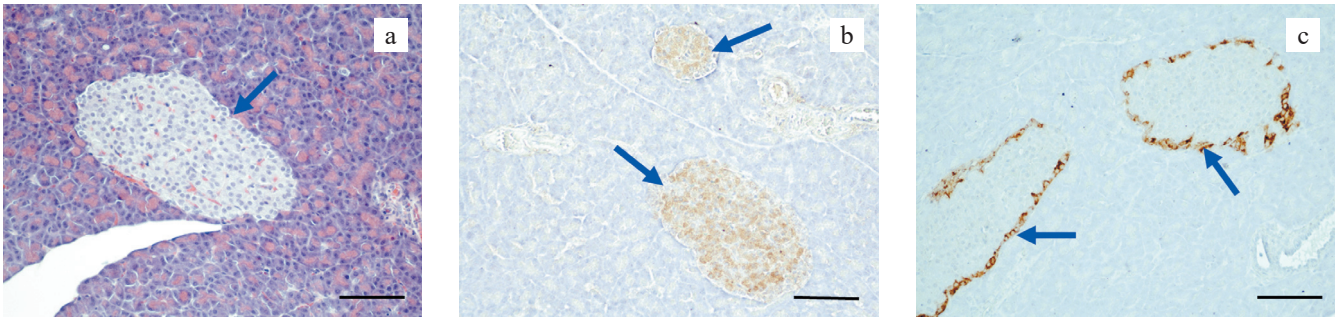

Fig. 2. Histological appearance of the pancreas in a healthy rat. (a) Hematoxylin and eosin (H&E) staining; (b) Immunohistochemical (IHC) staining for insulin; (c) IHC staining for glucagon. Blue arrows indicate pancreatic islets. Scale bar: 100 μm

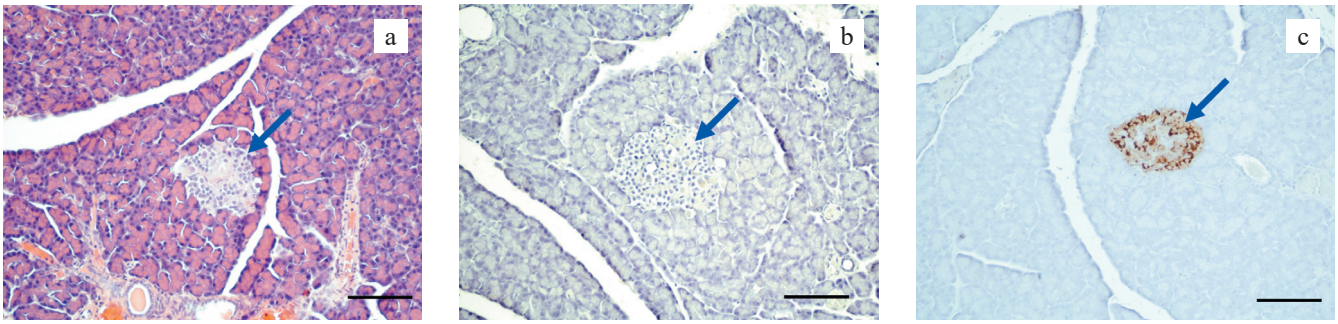

Fig. 3. Histological appearance of the pancreas in a control group rat with experimental T1DM (10 weeks without treatment). (a) Hematoxylin and eosin (H&E) staining; (b) Immunohistochemical (IHC) staining for insulin; (c) IHC staining for glucagon. Blue arrows indicate pancreatic islets. Scale bar: 100 μm

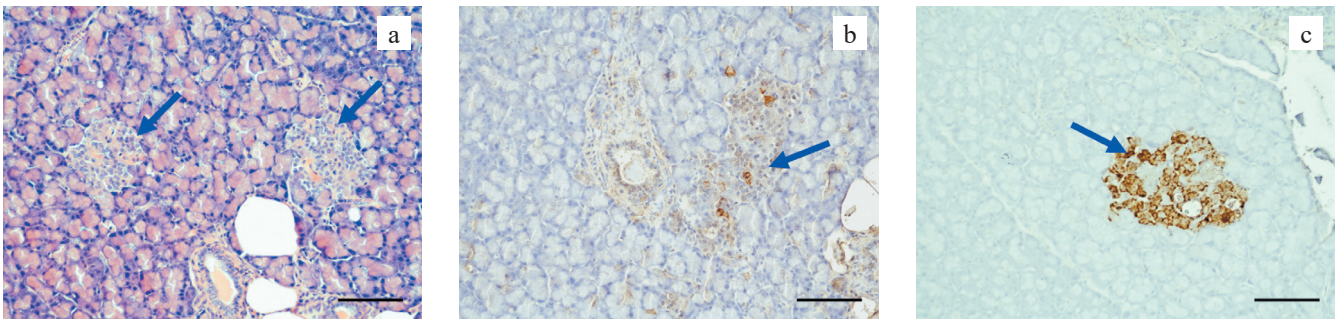

Fig. 4. Histological appearance of the pancreas in a rat from experimental group 1 with experimental T1DM after intraperitoneal injection of pancreatic islets (10 weeks post-treatment). (a) Hematoxylin and eosin (H&E) staining; (b) Immunohistochemical (IHC) staining for insulin; (c) IHC staining for glucagon. Blue arrows indicate pancreatic islets. Scale bar: 100 μm

lets with irregular morphology and branching structures extending into the adjacent exocrine parenchyma were observed in half of the animals (n = 2) (Fig. 5, a). These atypical islets lacked zones of hypercellularity and displayed a relatively uniform distribution of insulocytes (Fig. 5, b). A marked increase in the number of insulin-

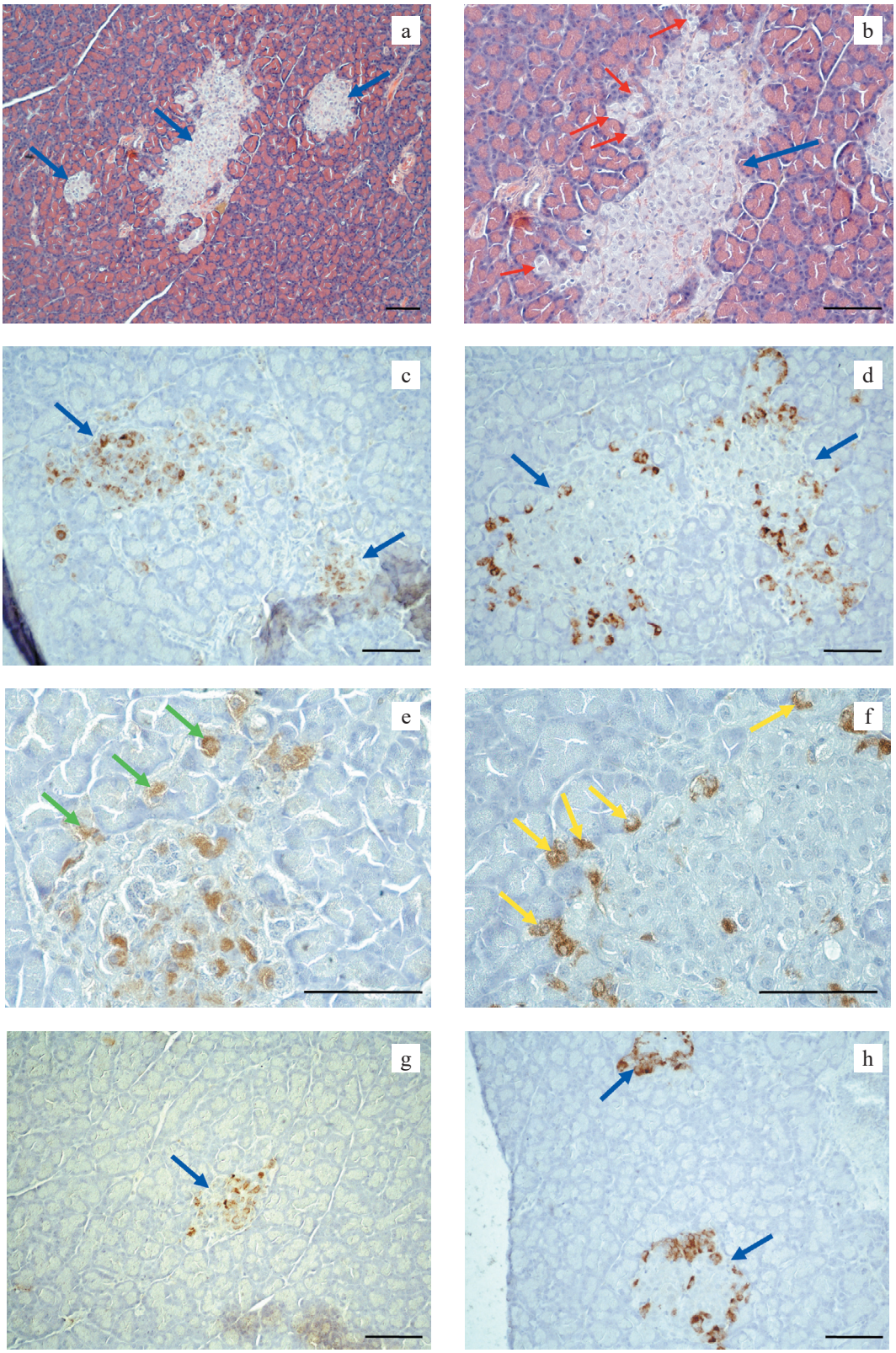

Fig. 5. Histological appearance of the pancreas in rats from experimental group 2 with T1DM after intraperitoneal injection of pancreatic cell-engineered construct (10 weeks post-treatment). (a, b) Hematoxylin and eosin (H&E) staining; (c, e, g) Immunohistochemical (IHC) staining for insulin; (d, f, h) IHC staining for glucagon. Blue arrows indicate pancreatic islets; green arrows indicate insulin-positive cells in the acinus; yellow arrows indicate glucagon-positive cells in the acinus; red arrows indicate acino-insular complexes. Scale bar: 100 μm

immunopositive β-cells was detected in these islets, reaching several dozen per islet – substantially exceeding the levels observed in control specimens (Fig. 5, c). Glucagon-positive α-cells no longer constituted the dominant islet cell population (Fig. 5, d).

At the same time, light-colored cells with no apical-basal polarity, fine-grained cytoplasm and large, well-structured nucleus were detected in the neighboring acinus, directly in the lining. Their number ranged from one to several per acinus. IHC staining revealed that a subset of these cells expressed either insulin (Fig. 5, e) or glucagon (Fig. 5, f), hormones characteristic of β- and α-cells, respectively.

It is noteworthy that the described structures, known as acino-insular complexes (Fig. 5, b), are typically observed in the developing pancreas of certain animal species during intrauterine life and are considered to play a significant role in the ontogeny of the islet apparatus [30–32]. Standard-shaped islets in other animals (n = 2) from experimental group 2 also showed a more prominent replenishment of insulin-positive β-cells compared to those receiving only PIs suspensions (Fig. 5, f). Concurrently, a reduction in the number of glucagon-positive α-cells was observed relative to the control group (Fig. 5, g). Such islets were observed in other rats (n = 2) of experimental group 2.

These findings suggest that the observed replenishment of the β-cell population likely resulted from induced reprogramming and transdifferentiation processes involving both acinar epithelial cells and certain islet-resident insulocytes. This regenerative activity may represent a compensatory mechanism. We believe that the most significant reduction in glycemia observed in the experiment was due not only to the sustained insulin secretion from the implanted PCECs, but also to endogenous insulin production by the regenerated population of the recipient's own β-cells.

Thus, our findings support the current understanding of pancreatic cell plasticity, suggesting that β-cell regeneration can occur not only from other insulocyte types but also from the exocrine components of the pancreas [7, 21, 33]. These results highlight the relevance of further research to explore and elucidate this regenerative potential.

Partial restoration of the endogenous β-cell pool was observed following the intraperitoneal implantation of a pancreatic tissue-engineered construct composed of floating islet-like cultures derived from the PIs of newborn rabbits and a collagen-containing hydrogel [34].

Identifying and harnessing factors that induce β-cell regenerative capacity could provide novel therapeutic avenues for diabetes treatment. However, further investigation is needed to elucidate the mechanisms, regulatory pathways, and specific cell types involved in β-cell regeneration under both physiological and pathological conditions [21].

CONCLUSION

Based on the presented data, it can be concluded that PCEC implantation in rats with STZ-induced T1DM not only compensates for lost β-cell function and exerts a direct antidiabetic effect, but also serves as a catalyst for regenerative processes, potentially restoring the recipient's insulinocyte pool.

Therefore, the use of PCEC for stimulating β-cell regeneration represents a promising therapeutic strategy in the treatment of diabetes characterized by β-cell deficiency.

The authors declare no conflict of interest.

REFERENCES

1. *Wang KL, Tao M, Wei TJ, Wei R.* Pancreatic β cell regeneration induced by clinical and preclinical agents. *World J Stem Cells.* 2021 Jan 26; 13 (1): 64–77. doi: 10.4252/wjsc.v13.i1.64.
2. *Zhong F, Jiang Y.* Endogenous Pancreatic β Cell Regeneration: A Potential Strategy for the Recovery of β Cell Deficiency in Diabetes. *Front Endocrinol (Lausanne)*. 2019 Feb 20; 10: 101. doi: 10.3389/fendo.2019.00101.
3. *Hogrebe NJ, Maxwell KG, Augsornworawat P, Millman JR.* Generation of insulin-producing pancreatic β cells from multiple human stem cell lines. *Nat Protoc.* 2021 Sep; 16 (9): 4109–4143. doi: 10.1038/s41596-021-00560-y.
4. *Spears E, Serafimidis I, Powers AC, Gavalas A*. Debates in Pancreatic Beta Cell Biology: Proliferation Versus Progenitor Differentiation and Transdifferentiation in Restoring β Cell Mass. *Front Endocrinol (Lausanne*). 2021 Aug 6; 12: 722250. doi: 10.3389/fendo.2021.722250.
5. *Pylaev TE, Smyshlyaeva IV, Popyhova EB.* Regeneration of β-cells of the islet apparatus of the pancreas. Literature review. *Diabetes mellitus*. 2022; 25 (4): 395–404. (In Russ.). doi: 10.14341/DM12872.
6. *Lu J, Jaafer R, Bonnavion R, Bertolino P, Zhang CX.* Transdifferentiation of pancreatic α-cells into insulin-secreting cells: From experimental models to underlying mechanisms. *World J Diabetes*. 2014 Dec 15; 5 (6): 847–853. doi: 10.4239/wjd.v5.i6.847.
7. *Aguayo-Mazzucato C, Bonner-Weir S.* Pancreatic β Cell Regeneration as a Possible Therapy for Diabetes. *Cell Metab*. 2018 Jan 9; 27 (1): 57–67. doi: 10.1016/j.cmet.2017.08.007.
8. *Courtney M, Gjernes E, Druelle N, Ravaud C, Vieira A, Ben-Othman N et al.* The inactivation of Arx in pancreatic alpha-cells triggers their neogenesis and conversion into functional beta-like cells. *PLoS Genet*. 2013 Oct; 9 (10): e1003934. doi: 10.1371/journal.pgen.1003934.
9. *Furuyama K, Chera S, van Gurp L, Oropeza D, Ghila L, Damond N et al.* Diabetes Relief in Mice by Glucose-Sensing Insulin-Secreting Human α-Cells. *Nature.* 2019 Mar; 567 (7746): 43–48. doi: 10.1038/s41586-019-0942-8.
10. *Thorel F, Népote V, Avril I, Kohno K, Desgraz R, Chera S, Herrera PL.* Conversion of adult pancreatic alpha-

cells to beta-cells after extreme beta-cell loss. *Nature*. 2010 Apr 22; 464 (7292): 1149–1154. doi: 10.1038/nature08894.
11. *Remedi MS, Emfinger C.* Pancreatic β-cell identity in diabetes. *Diabetes Obes Metab.* 2016 Sep; 18 Suppl 1 (Suppl 1): 110–116. doi: 10.1111/dom.12727.
12. *Bonner-Weir S, Toschi E, Inada A, Reitz P, Fonseca SY, Aye T, Sharma A.* The pancreatic ductal epithelium serves as a potential pool of progenitor cells. *Pediatr Diabetes*. 2004; 5 (Suppl 2): 16–22. doi: 10.1111/j.1399-543X.2004.00075.x.
13. *Bonner-Weir S, Inada A, Yatoh S, Li WC, Aye T, Toschi E, Sharma A.* Transdifferentiation of pancreatic ductal cells to endocrine beta-cells. *Biochem Soc Trans*. 2008 Jun; 36 (Pt 3): 353–356. doi: 10.1042/BST0360353.
14. *Li W-C, Rukstalis JM, Nishimura W, Tchipashvili V, Habener JF, Sharma A, Bonner-Weir S.* Activation of pancreatic-duct-derived progenitor cells during pancreas regeneration in adult rats. *J Cell Sci.* 2010 Aug 15; 123 (Pt 16): 2792–2802. doi: 10.1242/jcs.065268.
15. *Bouwens L.* Transdifferentiation versus stem cell hypothesis for the regeneration of islet beta-cells in the pancreas. *Microsc Res Tech.* 1998 Nov 15; 43 (4): 332–336. doi: 10.1002/(SICI)1097-0029(19981115)43:4<332::AID-JEMT7>3.0.CO;2-1.
16. *Kim HS, Lee MK*. β-Cell regeneration through the transdifferentiation of pancreatic cells: Pancreatic progenitor cells in the pancreas. *J Diabetes Investig*. 2016 May; 7 (3): 286–296. doi: 10.1111/jdi.12475.
17. *Baeyens L, Lemper M, Leuckx G, De Groef S, Bonfanti P, Stange G et al.* Transient cytokine treatment induces acinar cell reprogramming and regenerates functional beta cell mass in diabetic mice. *Nat Biotechnol.* 2014 Jan; 32 (1): 76–83. doi: 10.1038/nbt.2747.
18. *Miyazaki S, Tashiro F, Miyazaki J.* Transgenic Expression of a Single Transcription Factor Pdx1 Induces Transdifferentiation of Pancreatic Acinar Cells to Endocrine Cells in Adult Mice. *PLoS One.* 2016 Aug 15; 11 (8): e0161190. doi: 10.1371/journal.pone.0161190.
19. *Baeyens L, De Breuck S, Lardon J, Mfopou JK, Rooman I, Bouwens L*. *In vitro* generation of insulin-producing beta cells from adult exocrine pancreatic cells. *Diabetologia*. 2005 Jan; 48 (1): 49–57. doi: 10.1007/s00125-004-1606-1.
20. *Zhou Q, Brown J, Kanarek A, Rajagopal J, Melton DA*. *In vivo* reprogramming of adult pancreatic exocrine cells to beta-cells. *Nature.* 2008 Oct 2; 455 (7213): 627–632. doi: 10.1038/nature07314.
21. *Docherty FM, Sussel L.* Islet Regeneration: Endogenous and Exogenous Approaches. *Int J Mol Sci*. 2021 Mar 24; 22 (7): 3306. doi: 10.3390/ijms22073306.
22. *Jörns A, Klempnauer J, Tiedge M, Lenzen S.* Recovery of pancreatic beta cells in response to long-term normoglycemia after pancreas or islet transplantation in severely streptozotocin diabetic adult rats. *Pancreas.* 2001 Aug; 23 (2): 186–196. doi: 10.1097/00006676-200108000-00009.
23. *Mikhailichenko VYu, Stolyarov SS*. Effect tranplantation of pancreas islet cell cultures at alloxan diabetes at rats in experiment. *International Journal of Applied and fundamental research*. 2015; 9 (4): 670–672.
24. *Jung HS, Ahn YR, Oh SH, Kim YS, No H, Lee MK, Kim KW.* Enhancement of beta-cell regeneration by islet transplantation after partial pancreatectomy in mice. *Transplantation.* 2009 Aug 15; 88 (3): 354–359. doi: 10.1097/TP.0b013e3181b07a02.
25. *Baranova NV, Ponomareva AS, Kirsanova LA, Nikolskaya AO, Bubentsova GN, Basok YuB, Sevastianov VI.* Functional efficiency of pancreatic cell-engineered construct in an animal experimental model for type I diabetes. *Russian Journal of Transplantology and Artificial Organs*. 2024; 26 (2): 94–104. [In Russ, English abstract]. doi: 10.15825/1995-1191-2024-2-94-104.
26. *Ponomareva AS, Kirsanova LA, Baranova NV, Surguchenko VA, Bubentsova GN, Basok YuB et al.* Decellularization of donor pancreatic fragment to obtain a tissue-specific matrix scaffold. *Russian Journal of Transplantology and Artificial Organs*. 2020; 22 (1): 123–133. [In Russ, English abstract]. doi: 10.15825/1995-1191-2020-1-123-133.
27. *Sevastianov VI, Basok YB.* Biomimetics of Extracellular Matrices for Cell and Tissue Engineered Medical Products. Newcastle upon Tyne, UK: Cambridge Scholars Publishing, 2023; 339.
28. *Sevastianov VI, Ponomareva AS, Baranova NV, Kirsanova LA, Basok YuB, Nemets EA et al.* Decellularization of Human Pancreatic Fragments with Pronounced Signs of Structural Changes. *Int J Mol Sci.* 2023 Dec 21; 24 (1): 119. doi: 10.3390/ijms24010119.
29. *Sevastianov VI, Ponomareva AS, Baranova NV, Belova AD, Kirsanova LA, Nikolskaya AO et al.* A Tissue-Engineered Construct Based on a Decellularized Scaffold and the Islets of Langerhans: A Streptozotocin-Induced Diabetic Model. *Life (Basel)*. 2024 Nov 19; 14 (11): 1505. doi: 10.3390/life14111505.
30. *Sanchez A, Lawzewitsch J.* Histological study of endocrine pancreas: cell differentiation process in Langerhans islets of bovine fetus and adult bovines. *Commun Biol*. 1985; 5 (3): 345–365.
31. *Riadinskaia NI, Siraziev RZ.* [Histological and histochemical characteristics of pancreas of deer at the Altay]. *Tsitologiia.* 2008; 50 (8): 719–724. [In Russ]. PMID: 18822792.
32. *Kirsanova LA, Bliumkin VN.* [Some characteristics of the histological structure of the fetal bovine pancreas]. *Biull Eksp Biol Med*. 1990 Sep; 110 (9): 330–332. [In Russ]. PMID: 2268733.
33. *Skaletskaya GN, Skaletskiy NN, Kirsanova LA, Bubentsova GN, Volkova EA, Sevastyanov VI.* Experimental implantation of tissue-engineering pancreatic construct. *Russian Journal of Transplantology and Artificial Organs*. 2019; 21 (2): 104–111. [In Russ, English abstract]. doi: 10.15825/1995-1191-2019-2-104-111.

The article was submitted to the journal on 14.03.2025

DOI: 10.15825/1995-1191-2025-2-148-162

MODERN STRATEGIES FOR THE PREVENTION AND TREATMENT OF POST-BURN SCARS (A SYSTEMATIC REVIEW)

A.S. Umnikov, I.I. Glazko, E.I. Balakin, A.S. Samoilov, V.I. Pustovoit
Burnazyan Federal Medical and Biophysical Center, Moscow, Russian Federation

Despite advancements in modern reconstructive surgery, preventing the formation of thick scar tissue that impairs limb function or causes cosmetic defects remains a critical challenge. Equally important is the effective correction of existing scars to optimize both functional and aesthetic outcomes. Severe functional impairment of the upper limbs can result in disability. A combination of surgical and nonsurgical interventions is essential to enhance functionality while minimizing the risk of scar recurrence. Platelet-rich plasma injections, stem cell therapy, adipose tissue transplantation, and a combination of negative pressure wound therapy (NPWT) with traditional flap reconstruction and other transplantation methods are gaining popularity in modern reconstructive surgery. NPWT plays a crucial role in preparing the wound bed for subsequent tissue reconstruction and serves as an effective alternative to traditional dressings. The vacuum created over the wound after closure with a skin autograft helps prevent inflammation at the graft base, reduces excessive granulation tissue formation, and minimizes the risk of rough scar development in the long term. The mechanisms of formation of hypertrophic scar and keloids have not yet been completely understood. However, research indicates that bone marrow-derived cells, including fibrocytes and keratinocyte-like cells, contribute to the inflammatory cell infiltrate during wound healing, and can play a role in cutaneous fibrosis, especially in cases of impaired healing. Several pathophysiological and biochemical processes involved in the repair of extensive and deep wounds have been established. Additionally, the role of keratinocytes within hair follicle bulbs in promoting epithelialization of post-burn wound surfaces, particularly in areas with preserved skin appendages, has been recognized. Studies indicate that stromal-vascular fraction of adipose tissue plays a positive role in various stages of wound healing, including keloid and hypertrophic scar formation. Adipose-derived stem cells can be used in combination with hydrogel. The hydrogel base of dressings maintains a moist environment in both burn wounds and wound surfaces following tangential or radical excision of burn scab. This promotes faster wound healing, reduces the risk of scar hyperplasia, and enhances the sustained release and effectiveness of medications applied to the hydrogel base. Prompt surgical intervention, including early excision and grafting, along with modern treatment methods in the early postoperative period for deep burns, can significantly reduce the risk of hypertrophic and keloid scar formation.

Keywords: burns, scars, cell technologies, biomedical cell products.

INTRODUCTION

Advancements in surgical techniques, resuscitation protocols, and the overall management of deep burns have led to significant improvements in survival rate of patients with acute thermal injuries. However, it should be emphasized that research into the long-term functional outcomes for burn survivors remains an ongoing area of study.

Patients with severe post-burn scarring, particularly in the upper extremities, often experience a substantial reduction in functional capacity [1].

The type of surgical intervention significantly impacts the likelihood of contracture development. In this context, the preference for reconstructive surgery aims to improve limb function and reduce the risk of contracture recurrence [2]. Ongoing research focuses on improving long-term surgical outcomes by integrating time-tested technologies with established surgical techniques. dermal tissue substitutes and platelet-rich plasma (PRP) are gaining traction as promising regenerative therapies for tissue repair and functional restoration.

The application of autologous PRP therapy, stem cells, adipose tissue autotransplantation, negative pressure wound therapy (NPWT), traditional flap reconstruction, and other transplantation techniques is becoming increasingly common in burn treatment. Dermal scaffolds and split-thickness skin grafts (STSG) are among the options that enhance skin quality, flexibility, and overall patient quality of life.

NPWT plays a crucial role in improving graft fixation by minimizing displacement and reducing the risk of complications. It also stimulates granulation tissue formation, accelerates revascularization, and supports successful graft integration into the wound bed. NPWT has been shown to effectively enhance the engraftment of both split-thickness and full-thickness skin grafts

Corresponding author: Evgenii Balakin. Address: 46/8, Zhivopisnaya str., 123098, Moscow, Russian Federation.
Phone: (499) 190-96-77. E-mail: evgbalakin@yandex.ru

(FTSGs) [3–7]. This technique provides an almost ideal interface between the graft and the recipient site [8, 9], preventing the accumulation of seromas and hematomas, as well as the onset of infections – key contributors to graft loss during the early postoperative period [10].

Acellular dermal matrix (ADM) is a single-layer dermal component composed of bovine collagen and hydrolyzed elastin. This material transforms into a highly viable neoderm, both functionally and morphologically, facilitating adhesion between the skin epidermis and underlying bone tissue [11]. A one-stage ADM grafting procedure, combined with overlapping skin grafts of varying thicknesses (STSG), has been reported in clinical practice. After a few weeks following surgery, an ADM integrates into the recipient's tissue, developing vascular and nerve connections, effectively functioning as the patient's own tissue. This unique characteristic of ADM contributes to complete assimilation of the graft. The minimally invasive procedure has yielded results that are either excellent or comparable to those achieved with more complex skin or skin-fascial flaps, without resulting in donor site morbidity [1, 11].

PRP is an autologous blood-derived product where plasma, rich in platelets, growth factors, and cytokines, is concentrated. Since the 1970s, PRP has been used for tissue repair [12]. PRP injections, stem cell injections, and NPWT all promote tissue regeneration and enhance integration within the recipient skin area.

According to Karakol and Bozkurt [1], the combined use of surgical techniques with advanced approaches – such as ADM, PRP therapy, and NPWT for wound management – has been shown to be effective in achieving both functional and aesthetic outcomes for patients suffering from severe burn contractures.

In each of the aforementioned therapeutic approaches and disease prevention strategies, biotechnologies play a central role, with a focus on stimulating the body's natural recovery processes. The research methods discussed for both autologous and xenobiomaterials can be applied in the development and implementation of biomedical cellular products aimed at preventing post-burn scars. This direction holds significant promise and is supported by scientific justification and potential.

RESEARCH METHODS

A literature review was conducted using specialized scientific databases, including MEDLINE, Google Scholar, EMBASE, and PubMed. The efficiency in selecting relevant scientific papers was enhanced by using targeted keywords and phrases in search queries, such as "burns," "scars," "post-burn scars," and "post-burn scar prevention techniques". The inclusion criteria for publications in the review involved an initial screening of titles and abstracts to assess their relevance to the research topic. Additionally, a supplementary search method was employed, where the reference lists of the selected papers were reviewed to identify other significant sources. The final step involved a comprehensive full-text analysis and systematic evaluation of the chosen studies, enabling the extraction of key information for incorporation into the preparation of this research article.

An information search using the outlined strategy yielded a dataset of 2,335 scientific articles. During the initial screening, in which irrelevant materials were excluded, the number of articles was reduced to 238. A subsequent detailed full-text analysis identified 152 articles that did not meet the established criteria. Consequently, the final selection consisted of 86 articles that fully met the search parameters.

RESULTS

Factors causing hypertrophic and keloid scars

While research continues, the exact biological mechanisms behind the formation of hypertrophic and keloid scars are not fully understood. However, studies by Curran and Ghahary have identified a link between delayed re-epithelialization and enhanced extracellular matrix production. Recent research indicates that bone marrow-derived cells, especially fibrocytes and keratinocyte-like cells (KLCs), may contribute to the inflammatory infiltrate during wound healing [13, 14]. These findings underscore the potential role of these cells in the re-epithelialization process and their critical role in stimulating skin fibrosis when healing is impaired [14, 15].

Fibrocytes and KLCs are products of transdifferentiation from $CD14^+$ adherent monocytes, a specific subset of mononuclear stem cells found in peripheral blood [15, 16]. This process allows $CD14^+$ monocytes to transform not only into myofibroblasts [17], but also into osteoblasts, skeletal myoblasts, chondrocytes, adipocytes [18], and cardiomyocytes [19], depending on the surrounding environmental conditions. This discovery highlights the remarkable plasticity and potential of peripheral blood monocytes in regenerative processes and tissue repair. Fibrocytes were first described in 1994 by Richard Bucala and colleagues [16], who identified a large number of adhesive, fibroblast-like, spindle-shaped cells that infiltrated wound cavities shortly after implantation, serving as a model for tissue reparative reactions *in vivo*. These cells, which exhibit adhesive properties and the ability to migrate to sites of tissue damage, exhibit unique characteristics, including expression of collagens I and III, vimentin, and CD34. These markers suggest their multipotent stem cell potential and their ability to differentiate into various mesenchymal cell types depending on local conditions [16]. Over time, as fibrocytes mature, a loss of CD34 expression is observed, which may serve as a marker of their differentiation into mature cellular forms during tissue repair and regeneration [20].

Transformation of $CD14^+$ monocytes into fibrocytes *in vitro* can be induced by cultivating them in a specialized fibroblast culture medium [13, 21].

In vivo, fibrocytes can be found in areas of injured tissue by day 4 after injury, appearing simultaneously with the influx of inflammatory cells. Fibrocyte migration is believed to be driven by the activation of CCR7 chemokine receptors on their surface, enabling them to interact with chemokines present in lymphoid tissues. Accumulation of fibrocytes in the wound area continues until the day 9 or 10 after injury [22, 23].

Exposure of $CD14^+$ monocytes to a specialized keratinocyte-enriched culture medium or to bone morphogenic protein-4 (BMP-4) can initiate their transdifferentiation into KLCs after about 7 days in culture [14, 24]. These KLCs morphologically resemble native keratinocytes, characterized by enlarged elliptical nuclei, and express specific keratinocyte markers such as stratifin, keratin-5, and 14-3-3σ protein [14, 15]. While "keratinocyte-like cells" was coined by the research teams of Curran and Ghahary, other labs refer to them as bone marrow-derived keratinocyte precursors, obtained through transdifferentiation protocols from various stem cell populations.

Curran and Ghahary's research demonstrated that, in addition to the previously understood pathway from $CD14^+$ monocytes, KLCs can also be directly derived from $CD34^+$ bone marrow cells, bypassing the need for $CD14^+$ intermediates [17, 24, 25]. Identifying keratinocyte-like differentiation involves two key indicators: checking for the expression of keratin-14, and the absence of CD45, a marker specific to hematopoietic lineage cells.

The recruitment of mononuclear cells, including $CD14^+$ monocytes, from peripheral blood to sites of tissue injury is mediated by fibroblast-derived chemokines and cytokines like CXCL5 and fibroblast growth factor beta [26]. Resident keratinocytes also actively contribute to directed migration of mesenchymal stem cells (MSCs) by releasing the secondary lymphoid chemokine (CCL21), which interacts with CCR7 receptors on these stem cells, enhancing their movement [24].

While fibrocytes constitute a small fraction (about 0.5%) of circulating leukocytes, they can make up a significant portion (up to 10%) of cells within subcutaneous implantation chambers in mice, highlighting their crucial role in tissue healing and regeneration [16]. Fibrocytes can also act as antigen-presenting cells by expressing class II MHC molecules, costimulatory molecules (CD80, CD86), and adhesion molecules (CD11a, CD54, CD58) [27], unlike mature fibroblasts that require interferon-γ stimulation to achieve similar levels of antigen expression. The transdifferentiation of $CD14^+$ monocytes into dendritic-related (DR) fibrocytes appears to be dependent on the presence of $CD14^+$ cells and can be induced by conditioned medium, even in their absence. However, this process is inhibited by antibodies against transforming growth factor-β1 (TGF-β1), underscoring the pivotal role of TGF-β1 in promoting this transdifferentiation [29]. In burn patients, elevated serum levels of TGF-β1 are correlated with a higher number of fibrocytes observed in their peripheral blood mononuclear cell (PBMC) cultures compared to healthy controls [29].

The plasticity of fibrocytes is evidenced by their ability to adapt fibrogenic activity in response to environmental cues. These cells play an active role in the regulating and transmiting genetic information, producing substantial amounts of mRNA required for the synthesis of key fibrogenic growth factors, particularly platelet-derived growth factor A (PDGF-A) and transforming growth factor-β1 (TGF-β1). Beyond their role in fibrogenesis, fibrocytes contribute to hematopoiesis and immune responses by producing mRNA for macrophage colony-stimulating factors (M-CSF) and proinflammatory mediators like macrophage inflammatory protein-1α (MIP-1α) and related chemokines [22]. Even at low levels, interleukin-1α (IL-1α) and tumor necrosis factor-α (TNF-α) cytokines play a crucial role in maintaining a regulated inflammatory response.

Fibrocytes, derived from PBMCs, can influence fibroproliferative activity by modulating matrix metalloproteinase-1 (MMP-1) expression, even in the absence of TGF-β signaling [14, 15, 27]. This suggests that they may not always contribute to pathological scar formation but can also participate in matrix remodeling under certain conditions. Collectively, these findings support the hypothesis that fibrocytes, when activated at an injury site, transform functionally and collaborate with other cell types to perform diverse roles in tissue repair and remodeling.

To test this hypothesis, Medina and Ghahary [13] injected bone marrow-derived stem and progenitor cells into rat inguinal fascial-fat flaps. Some of these flaps treated to inhibit TGF-β signaling using an antibody targeting the TGF-β type II receptor, aiming to induce immunological resistance to the transplanted cells. Flaps with mock cells and untreated bone marrow exhibited increased density, weight, and stronger fibrotic adhesion compared to flaps treated with a TGF-β antagonist. Histological analysis further revealed that flaps treated with synthetic or bone marrow-derived cells exhibited significantly higher collagen deposition compared to those treated with a TGF-β inhibitor. The collagen architecture in the TGF-β-exposed group closely resembled that of native fascial-fatty tissue harvested from the contralateral thigh of the rat.

Evidence suggests that an overpopulation of fibrocytes in the wound bed can lead to excessive tissue repair and fibrotic outcomes like hypertrophic scarring and keloid formation [13, 16, 30]. Fibrocytes, which migrate to injury sites alongside inflammatory cells, are highly responsive to the local inflammatory environment, influencing their function. *In vitro* studies show that interleukin-1β (IL-1β), a key mediator in tissue re-

generation, suppresses the synthesis of type I collagen [31]. Concurrently, IL-1β, stimulates the production of various pro-inflammatory and pro-fibrotic cytokines, including macrophage inflammatory protein-1α (MIP-1α), MIP-1β, monocyte chemoattractant protein-1 (MCP-1), interleukin-8 (IL-8), oncogene-related growth factor-α, interleukin-6 (IL-6), macrophage colony-stimulating factors, TGF-β1, and TNF-α. These mediators further amplify the inflammatory response and may contribute to dysregulated wound healing and fibrosis.

Patients with extensive burns exhibit increased fibrocyte differentiation compared to non-injured individuals, which contributes to the sustained presence of these cells at the injury site and perpetuates the inflammatory response [32]. This prolonged inflammation, a characteristic of severe burn injuries, promotes greater fibrocyte differentiation and retention within the wound area. In PBMC cultures, burn patients exhibit a higher proportion of collagen-producing fibrocytes compared to healthy controls [29]. Moreover, inflammatory microenvironment significantly impacts fibrocytes, altering their morphology and gene expression, which in turn influences their behavior and function [16, 22]. Leukocyte-specific protein 1 (LSP-1), a protein highly expressed in fibrocytes and associated with type I procollagen, has been identified as a reliable biomarker for detecting and characterizing fibrocytes [33]. Elevated LSP-1 expression in fibrocytes suggests an adhesive phenotype, differentiating them from surrounding leukocytes in inflamed tissue, and persistent inflammation promotes fibrotic activity, with fibrocytes abundant in hypertrophic scar tissue after burns compared to non-hypertrophic scar tissue (Fig. 1) [33].

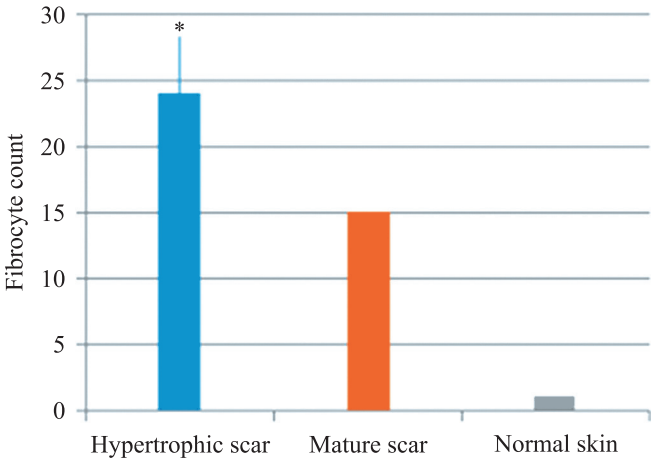

Fig. 1. Fibrocyte count (immunofluorescence staining) in cryosections of a hypertrophic scar, mature scar, and normal skin collected from 10 burn patients. The number of double-labeled fibrocytes per high-power field (HPF) in the dermis was compared using one-way analysis of variance (ANOVA). (* $P < 0.5$)

Consequently, unchecked expansion of fibrocytes contributes significantly to hypertrophic scar development and persistence by differentiating into collagen-producing fibroblasts and stimulating collagen synthesis in resident fibroblasts through paracrine signaling [19, 33].

In a wound scenario, PBMC (specifically $CD34^+$ cells) migrate to the injury site and are stimulated to differentiate into KLCs through interaction with the chemokine ligand CCL27, which attracts skin T-cells and whose activation occurs in the tissue affected by the wound, as well as through binding to the CCR10 receptor [25].

Bone marrow-derived keratinocyte precursors ($CD34^-$ cells) migrate to injury sites, in part, via interaction with the chemokine CCL21, which is typically expressed in secondary lymphoid tissues [24, 25]. In parallel, $CD14^+$ monocytes have also demonstrated the capacity to transdifferentiate into KLCs when exposed to a specialized microenvironment enriched with keratinocyte-specific factors [23, 24]. The cellular environment conditioned by these KLCs influences dermal fibroblast activity through the secretion of exosomes, which in turn enhance the production of matrix proteins. This environment promotes increased synthesis of matrix metalloproteinase-1 (MMP-1) compared to that observed in fibroblasts cultured with keratinocyte-conditioned medium alone (Fig. 2) [15].

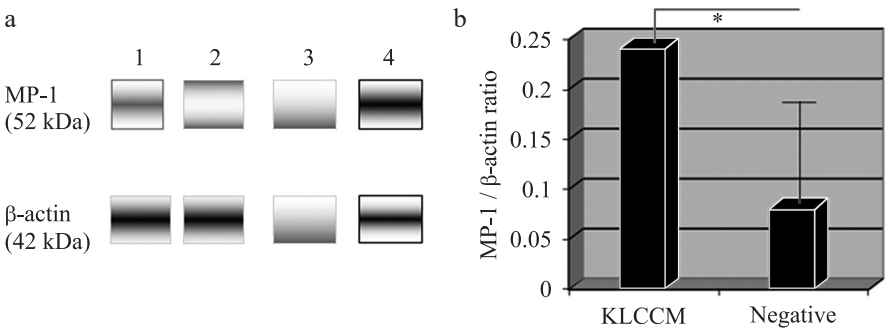

Fig. 2. Matrix metalloproteinase-1 (MP-1) expression in dermal fibroblasts treated with keratinocyte-like cell (KLC)-conditioned medium. a, showed MP-1 expression in dermal fibroblasts after 24 hours in each case: 1 = KLC-conditioned medium from day 28 of cell transdifferentiation, 2 = Dulbecco's modified Eagle medium + 2% fetal bovine serum (FBS; negative control), 3 = blank, 4 = dermal fibroblasts treated with recombinant stratifin (positive control); b, densitometric analysis of MP-1/β-actin ratio. (n = 4)

It was found that decreased levels of 14-3-3 proteins under these conditions lead to a decrease in the described effect, indicating the critical role of these proteins in modulating the antifibrotic response when interacting with dermal fibroblasts [15]. In addition, it has been found that keratinocytes from hair follicles are able to migrate to wound areas, actively contributing to re-epithelialization, especially between days 2 and 4 after injury [11]. These data are supported by the observation that wounds where hair follicles have been destroyed heal significantly slower, confirming the crucial role of keratinocytes within follicles in the healing process [34].

Recent advancements show that bone marrow, peripheral blood, and umbilical cord blood sources are increasingly used in local skin wound treatments, particularly for accelerating healing and converting chronic wounds to acute ones [35–37]. These materials stimulate the healing response by modulating cellular activity, including fibrocytes and KLCs, which are specialized subsets of stem cells derived from these sources. This stimulation leads to the chemotaxis of PBMCs to the injury site, where chemokines in the wound bed activate the transdifferentiation of $CD14^+$ mononuclear cells into fibrocytes or KLCs. The outcome of this transdifferentiation is heavily influenced by the local environment, which can fluctuate, particularly in burn wounds with varying depth and lesion area. Although the precise mechanisms remain incompletely understood, it is known that these cell subpopulations are more prominent in hypertrophic scars than in normotrophic scars, suggesting they may play a role in modulating fibrosis in affected tissues. Further research is needed to fully determine the role of these cells in wound healing.

Application of stromal-vascular fraction of adipose tissue

One of the emerging trends in the treatment of burns, post-burn scars, and other complex wounds is the use of adipose tissue. Adipose-derived stem cells (ADSCs) are increasingly used for regenerative purposes. These cells possess the ability to differentiate into various tissue types, including adipose, bone, cartilage, and muscle, with potential for even broader tissue differentiation. ADSCs are also rich sources of regenerative and metabolic factors, secreting growth factors like epidermal growth factor (EGF), TGF-β, hepatocyte growth factor (HGF), platelet-derived growth factor (PDGF), and basic fibroblast growth factor (bFGF). Adipose tissue, harvested via liposuction, can be processed using physical or chemical methods to separate its components (like stromal vascular fraction) either at the point of care or in a lab [38–44].

The Coleman technique is widely burn in the treatment of burn injuries, involving cyclic injections at intervals of two to four weeks until the wound is completely healed or a specific medical procedure, such as wound closure, skin grafting, or skin flap placement, is performed. For ongoing scar management, injections are administered under the scar every three months, following the Coleman's procedure [45–48].

Fat grafting, used as an adjunct in treating acute and subacute burn wounds, and chronic vascular wounds (e.g., venous insufficiency or diabetic arterial disease), harnesses the regenerative and metabolic properties of fat tissue to enhance vascularization and accelerate tissue regeneration. When used in repeated sessions (15–21 days apart), autologous fat grafting can promote healing and aid in wound recovery [48–50].

The primary goals of burn scar therapy are to reduce tissue hypertrophy (fibrosis), decrease scar thickness, and increase scar elasticity. Therapeutic techniques aim not only to improve the appearance of the affected area but also to address functional impairments caused by excessive fibrotic activity. These methods are also widely applied in treating fibrosis that arises in the joint area after trauma or surgery, as well as in preventing the formation of adhesions following tendon surgeries [51–54].

For open wounds, injections are typically administered under general anesthesia at intervals of 15 to 21 days. In patients with hypertrophic scars after burn healing or keloids of any origin, repeated injections (up to four injections in total) are administered at intervals of 8 to 12 weeks.

Fat is most commonly harvested from the abdomen, thighs, or lateral surfaces of the upper buttocks, with shaving of the pubic area or proximal thigh performed in the operating room if necessary just before the procedure. For liposuction cannula insertion, puncture incisions are typically made along the midline in the suprapubic crease, medial to the femoral artery pulse, in the inguinal crease, or along the mid-axillary line, extending towards the superior border of the iliac spin

While previously viewed as a passive energy storage and insulation tissue, contemporary science recognizes adipose tissue as a significant endocrine organ, playing a crucial role in regulating various physiological processes. Adipose tissue contains a diverse range of cellular components, offering promising opportunities in regenerative medicine. Adipose tissue, while primarily composed of adipocytes (one-third of the tissue's volume), also contains a complex stromal-vascular fraction (SVF) including preadipocytes, fibroblasts, MSCs, endothelial cells, and immune cells, forming a complex network [47]. The enzymatic breakdown of adipose tissue yields a cellular precipitate, the SVF, containing a heterogeneous population of progenitor cells.

The International Federation of Adipose Therapy and Science (IFATS) and the International Society for Cellular Therapy (ISCT) have defined the cellular composition of adipose tissue's SVF as a mixture of cells including stromal cells (15–30%), endothelial cells (10–20%), lymphocytes (10–15%), granulocytes (10–15%), monocytes

(5–15%), pericytes (3–5%), and stem and progenitor cells (<0.1%) [55]. This diverse cellular population of adipose tissue-derived SVF has garnered significant interest for its potential therapeutic applications in regenerative medicine. More specifically, MSCs within the SVF, also known as adipose-derived stem cells (ASCs), have been identified as a key cell type responsible for the therapeutic effects of SVF. *In vitro* studies demonstrate that ASCs enhance human skin fibroblast proliferation, migration, and collagen production through both direct cell-to-cell contact and paracrine signaling [56]. However, it remains to be determined whether these beneficial effects can be harnessed for the development of effective therapies for chronic and non-healing wounds.

Adipose tissue is classically categorized into two types: white adipose tissue (WAT) and brown adipose tissue (BAT) [57]. WAT primarily functions in energy storage, storing triglycerides, and providing thermal insulation and physical cushioning for the body. In contrast, BAT is specialized for energy dissipation by generating heat [58]. WAT is the dominant form of adipose tissue in humans, while BAT is less abundant, typically found in specific areas such as the supraclavicular, periadrenal, and paravertebral regions of the body [47].

Fibroblasts at the dermis-hypodermis interface play a crucial role in wound healing due to their unique characteristics, differing from adipogenic stem cells derived from adipose tissue and fibroblasts from the papillary and reticular dermis. These cells contribute to tissue repair in distinct ways. While adipose tissue plays a role in regeneration, obesity significantly impairs natural healing processes. This is primarily due to alterations in adipose tissue metabolism, including hypertrophy and hyperplasia of adipocytes, making them less functional [58]. These changes disrupt angiogenesis, as the rate of new vessel formation becomes mismatched with the increased demand from the growing adipocytes, resulting in hypoxia and delayed healing [59]. Moreover, obesity is linked to reduced adiponectin levels, a cytokine produced by fat cells, and this reduction can complicate tissue regeneration [42].

Adiponectin, a key mediator, plays an essential role in skin damage repair by promoting the growth and migration of keratinocytes in a concentration-dependent manner, as observed in mouse cell cultures. This effect occurs through activation of the extracellular signal-regulated kinase (ERK) pathway, as confirmed by various studies [60]. These findings highlight the importance of understanding the role of adiponectin in skin repair mechanisms, which is crucial for developing more effective treatments aimed at minimizing side effects and complications.

Table summarizes the paracrine factors produced by adipose tissue stem cells that stimulate the functional activities of dermal fibroblasts.

While research into the regenerative potential of adipose stem cells is ongoing, pioneers of autologous adipose tissue transfer have demonstrated the significant therapeutic potential of this technique. Adipose tissue transplantation has shown promise in improving both the appearance and function of scars, particularly in areas with abnormal healing and scarring. Concurrent laboratory studies using *in vitro* cultures suggest that adipose-derived stem cells (ASCs) play a crucial role in the therapeutic effects observed.

Application of hydrogel dressings in the treatment of burn wounds and scars

In burn treatment, ASCs are often combined with hydrogels containing hyaluronic acid, Aloe vera extract, and other beneficial components. Skin repair is typically sufficient when the intensity of the injury is within the skin's regenerative capacity. The healing process involves three main interrelated phases: the inflammation, proliferation, and extracellular matrix (ECM) reconstruction [66]. However, when the damage surpasses the skin's regenerative threshold, the healing process becomes more complicated. The final stage, which is particularly crucial, involves fibroblast activation, collagen

Table

Regulation of dermal fibroblast activity by adipocyte stem cell secretion: significance for effective wound healing

Stimulatory effect of ASC secretion on dermal fibroblast function	Paracrine factors secreted by ASCs	References
Increased proliferation	Fibroblast growth factor (FGF-2)	[37, 59, 60]
	Hepatocyte growth Factor (HGF)	[61]
	Exosomes	[62, 63]
	Microvesicles	[64]
Increased migration	FGF-2	[4, 37]
	Exosomes	[4, 62, 63]
	Microvesicles	[64]
Matrix remodeling (increased production of collagen I and III, TGFβ, FGF2 and MMP1)	Adiponectin	[65]
	Exosomes	[62, 63]

deposition, and new blood vessel formation. In response to critical injuries, macrophages release cytokines like fibroblast growth factor-2 (FGF-2), transforming growth factor-β (TGF-β), and insulin-like growth factor, which subsequently stimulate fibroblast migration, proliferation, and intensive collagen production. The formed collagen undergoes further reconstruction for up to two years. In addition, the regeneration process involves a complex interplay of a variety of components, including cellular elements, growth factors, cytokines, and ECM. An imbalance in this process can lead to uncontrolled repair and hypertrophic scarring.

Hypertrophic scars, resulting from increased fibroblast proliferation and excessive collagen production, are characterized by a range of properties that distinguish them from healthy skin. These include visible thickening, loss of elasticity, a firm texture upon palpation, and a color change to an abnormal purple-red hue. In the early stages (4–8 weeks), these scars are often accompanied by intense pain and itching. Over time, they gradually mature, transforming into atrophic scars over a period of weeks to two years, which can significantly impact both the physical and psychological well-being of patients. In industrialized countries, approximately 4 million individuals suffer from hypertrophic scarring annually, with the numbers in developing countries reaching up to 5 million, highlighting the need for effective treatment methods. Contemporary treatments for hypertrophic scars include surgery, laser therapy, and drug treatments, but challenges persist with large scars, where complete wound healing after surgical intervention or closing skin defects can be difficult, limiting easy suture closure [68].

Alongside other leading techniques, carbon dioxide laser therapy is widely employed in burn treatment centers alongside other leading techniques to address hypertrophic scars. This method effectively induces fibroblast apoptosis and eliminates excess collagen, making it a highly targeted and efficient treatment. In addition, corticosteroids are commonly used to enhance therapeutic outcomes in scar management [69, 70].

Beyond the direct application of medications to the affected area, scar healing can also be facilitated through the use of drugs incorporated into hydrogels. Hydrogels are an innovative type of wound dressing that has gained popularity due to their exceptional ability to absorb moisture and deliver pharmacological agents directly to the wound site. Hiwatashi et al. developed collagen-gelatin matrices saturated with basic fibroblast growth factor, demonstrating the ability to reduce the accumulation of dense collagen and having a positive therapeutic effect on vocal cord scars [71]. Le Wang et al. created a PCL/gelatin scaffold by electrospinning, saturated with small molecule inhibitors of TGF-β1 signaling, which inhibits the growth of fibroblasts, the main cells contributing to scar formation, and effectively prevents hypertrophic scars in wound healing [70]. Bu et al. successfully developed a nanoliposomal gel with 5-aminolevulinic acid applied by photodynamic delivery, which changes the structure of collagen fibers and accelerates the apoptosis of fibroblasts in scar tissue [71]. The introduction of skin grafts and their substitutes has had an encouraging effect on the healing process, but also comes with potential difficulties in the field of dermal restoration, for example, increasing the size of the graft correlates with the duration of re-epithelialization, which may promote scar formation [72]. This suggests the need to develop new strategies for the prevention of hypertrophic scars characterized by minimal side effects.

Papain, a cysteine protease derived from the immature milk of Carica papaya, is known for its high enzymatic activity, excellent heat stability, and safety profile, making it widely used in medical applications [73]. This proteolytic enzyme plays a crucial role in preventing the formation of granulation tissue (GR) during wound healing by affecting various cell types involved in tissue regeneration. Papain exerts anti-inflammatory, antibacterial, and antioxidant functions while also degrading proteins and collagen [73–75].

For example, papain strongly inhibits the angiogenic effects induced by vascular endothelial growth factor (VEGF) in human umbilical vein endothelial cells (HUVECs) by blocking AKT, MEK1/2, and SAPK/JNK phosphorylation. Moreover, papain is known to degrade proteins involved in tight junctions, including ZO-1, claudin-4, and occludin, in keratinocytes [76]. It has also been observed that papain effectively suppresses monocyte activation, particularly that induced by monocyte-derived pro-inflammatory cytokines (MPAs), by inhibiting the MAPK and PI3K/Akt signaling pathways [77]. Even papain pretreatment at a concentration of 10 mg/mL also inhibits T-lymphocyte activation induced by islet allografts [78].

Papain actively suppresses the expression of TGF-β1 protein and the phosphorylation of Smad-3, key components of the TGF-β signaling pathway. This suppression effectively controls cell proliferation, cell-cell interactions, and ECM remodeling by modulating the TGF-β/Smad signaling cascade. It also contributes to reducing collagen and keratin formation in the dermal layer [79]. In scar tissue compared to healthy skin, elevated NF-κB p65 protein levels contribute to excessive fibroblast activity, leading to uncontrolled collagen production and abnormal ECM accumulation. Papain significantly lowers NF-κB p65 levels, thereby promoting the healing of hyperplastic scars by regulating the NF-κB pathway. However, topical papain application *in vivo* faces challenges due to difficulties in maintaining consistent contact with the wound, potentially limiting its therapeutic benefits.

Hydrogels offer a promising alternative for pharmaceutical delivery, enabling precise and controlled release of active ingredients. Chitosan, a natural bio-

polymer derived from chitin through deacetylation, is widely used in this context due to its biocompatibility, non-toxicity, and biodegradability. This polysaccharide is known for its enhanced bioactivity, stability *in vivo*, and affordability, and it is obtained from renewable natural sources. As a result, it has extensive applications in the medical field, particularly in the development of hydrogels for various therapeutic purposes when combined with other natural or synthetic polymers [80]. For instance, hydrogels containing poly (γ-glutamic acid) and chito-oligosaccharide, enriched with the enzyme papain (G/C/P hydrogels), show potential in regulating skin repair and preventing formation of hypertrophic scars.

Hydrogels are increasingly used for local and transdermal drug delivery of bioactive molecules, as well as effective wound dressings because of their ability to create an optimal microenvironment that promotes cell growth and differentiation [80]. Specifically, chitosan-based hydrogels have demonstrated unique therapeutic properties: they activate macrophages and gradually degrade to release N-acetyl-β-D-glucosamine. This metabolite stimulates fibroblast proliferation, promotes angiogenesis, normalizes collagen deposition, and enhances natural hyaluronic acid synthesis at the wound site, thereby accelerating healing and reducing scar formation [81, 82].

Furthermore, hydrogel bases are widely used to prolong the therapeutic effects of the drugs they deliver. This property is particularly valuable in applications like hydrogel-based antibacterial dressings for burn treatment, enabling controlled, sustained release of antimicrobial agents directly into the wound, improving efficacy and reducing dressing changes [83].

An innovative, multifunctional macroporous antimicrobial hydrogel has been developed to combat bacterial infections and promote skin regeneration by modulating cytokine production from the body's own stem cells. This advanced hydrogel is created using a cryogenic gelation technique, forming a hyaluronic acid-based cryogel with a macroporous architecture. The surface of the cryogel is then functionalized via dopamine oxidative polymerization, enabling the immobilization of the antimicrobial peptide DP7, resulting in the DA7CG construct. Placenta-derived MSCs are subsequently introduced into this cryogel (DA7CG@C).

The DA7CG@C hydrogel, according to *in vitro* and clinical trial data, exhibits stage-specific actions during wound healing, with DP7, during the inflammatory phase, suppressing infection and modulating the inflammatory response. In the proliferation phase, the presence of placenta-derived MSCs supports the regeneration of skin, vasculature, and hair follicles. In the remodeling phase, DP7 enhances paracrine secretion of stem cells, facilitating extracellular matrix remodeling and promoting scar-free healing.

Due to its multifunctional properties, this hydrogel presents a promising alternative to traditional dressings for the treatment of burn wounds [84].

Hydrogel dressings provide optimal wound hydration for both burn injuries and wounds following the removal of necrotic burn tissue via tangential or full-thickness excision. This moist environment facilitates accelerated re-epithelialization and significantly reduces the risk of hypertrophic scar formation [84].

Despite their proven efficacy in wound management, hydrogel dressings may not be suitable during certain healing phases. Their limited absorbency makes them unsuitable for wounds with heavy exudate, as they can reduce effectiveness. Furthermore, a common challenge with hydrogel drug delivery systems is the rapid release of incorporated drugs, with a large portion of the active compounds being released within the first few hours post-application. This can increase the risk of local toxicity and reduce sustained therapeutic efficacy. In contrast, advanced hydrogels and xerogels incorporating nanocomponents offer enhanced wound healing potential. Their mesoporous architecture enables better control over the release of bioactive substances, making them potentially more preferable in certain clinical scenarios [8].

In modern wound care, two primary types of hydrogel dressings are used, each with distinct structural and functional characteristics. The first type comprises hydrogels with a stable three-dimensional macroscopic structure formed through molecular cross-linking. These dressings typically appear as elastic, transparent sheets of variable thickness. They maintain their structural integrity during exudate absorption, although they may swell as fluid is absorbed. This swelling continues until the gel reaches its saturation point, achieving equilibrium with the wound microenvironment.

The second type includes amorphous hydrogels, which lack a fixed structure and adapt dynamically to the wound surface upon contact with moisture. These hydrogels fill all irregularities and contours of the wound bed, conforming to its shape. As they absorb increasing volumes of exudate, their viscosity decreases, eventually transforming into a more fluid-like solution that becomes fully integrated into the wound environment. The most advanced developments in this field are third-generation hydrogel dressings, which provide an optimal moisture environment for wound healing. These dressings actively absorb exudate while preventing fluid accumulation through their evaporative properties. In addition, they promote the formation of a natural protective protein layer – rich in endogenously produced growth factors – on the wound surface, a critical factor in accelerating tissue regeneration [47, 85].

Silicone-based formulations, particularly siloxane polymers, are a widely recommended, non-invasive first-line treatment for preventing and treating hypertrophic

and keloid scars. These agents are considered among the most effective nonsurgical interventions available, with their efficacy well supported by extensive scientific research [86].

CONCLUSION

The formation of hypertrophic and keloid scars following deep burns and severe skin trauma remains a complex and not fully understood process. Emerging evidence suggests that bone marrow-derived cells, like fibrocytes and keratinocyte-like cells, may contribute significantly to skin regeneration and potentially to the development of fibrotic responses during aberrant wound healing. Recent research has identified specific pathophysiological and biochemical mechanisms that become activated in tissues during the healing of extensive and deep wounds. In particular, hair follicle keratinocytes have been shown to play a critical role in promoting epithelialization of wound surfaces following burn injuries.

In the early post-injury phase, negative pressure wound therapy (NPWT) has been shown to significantly reduce infection risk, promote granulation tissue, and prepare the injury site for reconstruction, whether through autologous skin grafting or transplantation of composite tissue flaps. Incorporating pharmacological agents into hydrogel dressings at specific stages of healing creates a microenvironment that promotes tissue regeneration. This therapeutic approach supports repair in both open wounds and beneath the "living protective layer" formed by repositioned skin flaps.

Adipose tissue has emerged as a promising therapy for burn wound healing, scar reduction, and complex wound management. The therapeutic efficacy of adipose-derived stromal-vascular fraction (SVF) has been validated through numerous animal studies and is increasingly used clinically.

Adipose-derived SVF is a heterogeneous mix of cells capable of differentiating into various tissues including adipose, bone, cartilage, and muscle. These cells also play a vital role in tissue repair and metabolic regulation, primarily through secretion of growth factors. Recognized as one of the body's highly active endocrine organs, adipose tissue is a readily available source of regenerative cells, with wide-ranging applications in both regenerative medicine and aesthetic dermatology. Unlike mesenchymal stem cells, the clinical use of SVF is already supported by an established regulatory framework and is facilitated by relatively simple and accessible extraction and processing methods. Burnazyan Federal Medical and Biophysical Center is actively developing innovative methods for targeted delivery of regenerative cells to injury sites, including intra-articular injections. A key focus of this research is the long-term preservation of cell functionality through the use of hydrogels and other high-viscosity carriers with enhanced adhesive properties. This integrated approach holds significant promise for advancing the development of next-generation biomedical cell-based therapies specifically tailored for burn treatment.

The accumulated medical knowledge and clinical experience enable the integrated treatment of patients with burns and wounds, including the restoration of skin defects. Optimizing the healing process and enhancing the quality of scar tissue formation, along with preventing scar contractures in areas near joints, ultimately contributes to improved long-term quality of life for the burn victims.

The authors declare no conflict of interest.

REFERENCES

1. *Karakol P, Bozkurt M.* Recent strategic approach in post-burn extremity scars and contractures. *J Plast Surg Hand Surg*. 2021 Jun; 55 (3): 153–161.
2. *Askari M, Cohen MJ, Grossman PH, Kulber DA.* The use of acellular dermal matrix in release of burn contracture scars in the hand. *Plast Reconstr Surg*. 2011 Apr; 127 (4): 1593–1599.
3. *Blackburn JH 2nd, Boemi L, Hall WW, Jeffords K, Hauck RM, Banducci DR, Graham WP 3rd.* Negative-pressure dressings as a bolster for skin grafts. *Ann Plast Surg*. 1998 May; 40 (5): 453–457.
4. *Hanasono MM, Skoracki RJ.* Securing skin grafts to microvascular free flaps using the vacuum-assisted closure (VAC) device. *Ann Plast Surg*. 2007 May; 58 (5): 573–576.
5. *Scherer LA, Shiver S, Chang M, Meredith JW, Owings JT.* The vacuum assisted closure device: a method of securing skin grafts and improving graft survival. *Arch Surg*. 2002 Aug; 137 (8): 930–933; discussion 933–934.
6. *Stone PA, Hass SM, Flaherty SK, DeLuca JA, Lucente FC, Kusminsky RE.* Vacuum-assisted fascial closure for patients with abdominal trauma. *J Trauma*. 2004 Nov; 57 (5): 1082–1086.
7. *Tang AT, Okri SK, Haw MP*. Vacuum-assisted closure to treat deep sternal wound infection following cardiac surgery. *J Wound Care*. 2000 May; 9 (5): 229–230.
8. *Nakayama Y, Iino T, Soeda S.* A new method for the dressing of free skin grafts. *Plast Reconstr Surg*. 1990 Dec; 86 (6): 1216–1219.
9. *Stokes TH, Follmar KE, Silverstein AD, Weizer AZ, Donatucci CF, Anderson EE, Erdmann D.* Use of negative-pressure dressings and split-thickness skin grafts following penile shaft reduction and reduction scrotoplasty in the management of penoscrotal elephantiasis. *Ann Plast Surg*. 2006 Jun; 56 (6): 649–653.
10. *Landau AG, Hudson DA, Adams K, Geldenhuys S, Pienaar C.* Full-thickness skin grafts: maximizing graft take using negative pressure dressings to prepare the graft bed. *Ann Plast Surg*. 2008 Jun; 60 (6): 661–666.
11. *Gáspár K, Erdei I, Péter Z, Dezsö B, Hunyadi J, Juhász I.* Role of acellular dermal matrix allograft in minimal invasive coverage of deep burn wound with bone exposed – case report and histological evaluation. *Int Wound J*. 2006 Mar; 3 (1): 51–58.

12. *Alser OH, Goutos I*. The evidence behind the use of platelet-rich plasma (PRP) in scar management: a literature review. *Scars Burn Heal*. 2018 Nov 18; 4: 2059513118808773.
13. *Medina A, Ghahary A.* Fibrocytes can be reprogrammed to promote tissue remodeling capacity of dermal fibroblasts. *Mol Cell Biochem*. 2010 Nov; 344 (1–2): 11–21.
14. *Medina A, Brown E, Carr N, Ghahary A.* Circulating monocytes have the capacity to be transdifferentiated into keratinocyte-like cells. *Wound Repair Regen*. 2009 Mar-Apr; 17 (2): 268–277.
15. *Medina A, Ghahary A.* Transdifferentiated circulating monocytes release exosomes containing 14-3-3 proteins with matrix metalloproteinase-1 stimulating effect for dermal fibroblasts. *Wound Repair Regen*. 2010 Mar-Apr; 18 (2): 245–253.
16. *Bucala R, Spiegel LA, Chesney J, Hogan M, Cerami A.* Circulating fibrocytes define a new leukocyte subpopulation that mediates tissue repair. *Mol Med*. 1994 Nov; 1 (1): 71–81.
17. *Jabs A, Moncada GA, Nichols CE, Waller EK, Wilcox JN.* Peripheral blood mononuclear cells acquire myofibroblast characteristics in granulation tissue. *J Vasc Res*. 2005 Mar-Apr; 42 (2): 174–180.
18. *Kuwana M, Okazaki Y, Kodama H, Izumi K, Yasuoka H, Ogawa Y et al.* Human circulating $CD14^+$ monocytes as a source of progenitors that exhibit mesenchymal cell differentiation. *J Leukoc Biol*. 2003 Nov; 74 (5): 833–845.
19. *Kodama H, Inoue T, Watanabe R, Yasuoka H, Kawakami Y, Ogawa S et al.* Cardiomyogenic potential of mesenchymal progenitors derived from human circulating $CD14^+$ monocytes. *Stem Cells Dev*. 2005 Dec; 14 (6): 676–686.
20. *Bellini A, Mattoli S.* The role of the fibrocyte, a bone marrow-derived mesenchymal progenitor, in reactive and reparative fibroses. *Lab Invest*. 2007 Sep; 87 (9): 858–870.
21. *Quan TE, Cowper S, Wu SP, Bockenstedt LK, Bucala R.* Circulating fibrocytes: collagen-secreting cells of the peripheral blood. *Int J Biochem Cell Biol*. 2004 Apr; 36 (4): 598–606.
22. *Abe R, Donnelly SC, Peng T, Bucala R, Metz CN.* Peripheral blood fibrocytes: differentiation pathway and migration to wound sites. *J Immunol*. 2001 Jun 15; 166 (12): 7556–7562.
23. *Kao HK, Chen B, Murphy GF, Li Q, Orgill DP, Guo L.* Peripheral blood fibrocytes: enhancement of wound healing by cell proliferation, re-epithelialization, contraction, and angiogenesis. *Ann Surg*. 2011 Dec; 254 (6): 1066–1074.
24. *Sasaki M, Abe R, Fujita Y, Ando S, Inokuma D, Shimizu H.* Mesenchymal stem cells are recruited into wounded skin and contribute to wound repair by transdifferentiation into multiple skin cell type. *J Immunol*. 2008 Feb 15; 180 (4): 2581–2587.
25. *Inokuma D, Abe R, Fujita Y, Sasaki M, Shibaki A, Nakamura H et al.* CTACK/CCL27 accelerates skin regeneration via accumulation of bone marrow-derived keratinocytes. *Stem Cells*. 2006 Dec; 24 (12): 2810–2816.
26. *Nedeau AE, Bauer RJ, Gallagher K, Chen H, Liu ZJ, Velazquez OC.* A CXCL5- and bFGF-dependent effect of PDGF-B-activated fibroblasts in promoting trafficking and differentiation of bone marrow-derived mesenchymal stem cells. *Exp Cell Res*. 2008 Jul 1; 314 (11–12): 2176–2186.
27. *Chesney J, Bacher M, Bender A, Bucala R.* The peripheral blood fibrocyte is a potent antigen-presenting cell capable of priming naive T cells *in situ*. *Proc Natl Acad Sci USA*. 1997 Jun 10; 94 (12): 6307–6312.
28. *Geppert TD, Lipsky PE*. Antigen presentation by interferon-gamma-treated endothelial cells and fibroblasts: differential ability to function as antigen-presenting cells despite comparable Ia expression. *J Immunol*. 1985 Dec; 135 (6): 3750–3762.
29. *Yang L, Scott PG, Giuffre J, Shankowsky HA, Ghahary A, Tredget EE.* Peripheral blood fibrocytes from burn patients: identification and quantification of fibrocytes in adherent cells cultured from peripheral blood mononuclear cells. *Lab Invest*. 2002 Sep; 82 (9): 1183–1192.
30. *Chesney J, Bucala R.* Peripheral blood fibrocytes: mesenchymal precursor cells and the pathogenesis of fibrosis. *Curr Rheumatol Rep*. 2000 Dec; 2 (6): 501–505.
31. *Yang L, Scott PG, Dodd C, Medina A, Jiao H, Shankowsky HA et al.* Identification of fibrocytes in postburn hypertrophic scar. *Wound Repair Regen*. 2005 Jul-Aug; 13 (4): 398–404.
32. *Chesney J, Metz C, Stavitsky AB, Bacher M, Bucala R.* Regulated production of type I collagen and inflammatory cytokines by peripheral blood fibrocytes. *J Immunol*. 1998 Jan 1; 160 (1): 419–425.
33. *Langton AK, Herrick SE, Headon DJ.* An extended epidermal response heals cutaneous wounds in the absence of a hair follicle stem cell contribution. *J Invest Dermatol*. 2008 May; 128 (5): 1311–1318. doi: 10.1038/sj.jid.5701178.
34. *Fathke C, Wilson L, Hutter J, Kapoor V, Smith A, Hocking A, Isik F.* Contribution of bone marrow-derived cells to skin: collagen deposition and wound repair. *Stem Cells*. 2004; 22 (5): 812–822.
35. *Han SK, Yoon TH, Lee DG, Lee MA, Kim WK.* Potential of human bone marrow stromal cells to accelerate wound healing *in vitro*. *Ann Plast Surg*. 2005 Oct; 55 (4): 414–419.
36. *Burd A, Ahmed K, Lam S, Ayyappan T, Huang L.* Stem cell strategies in burns care. *Burns*. 2007 May; 33 (3): 282–291.
37. *Park SR, Kim JW, Jun HS, Roh JY, Lee HY, Hong IS.* Stem Cell Secretome and Its Effect on Cellular Mechanisms Relevant to Wound Healing. *Mol Ther*. 2018 Feb 7; 26 (2): 606–617.
38. *Zuk PA, Zhu M, Mizuno H, Huang J, Futrell JW, Katz AJ et al.* Multilineage cells from human adipose tissue: implications for cell-based therapies. *Tissue Eng*. 2001 Apr; 7 (2): 211–228.
39. *Zuk PA, Zhu M, Ashjian P, De Ugarte DA, Huang JI, Mizuno H et al.* Human adipose tissue is a source of multipotent stem cells. *Mol Biol Cell*. 2002 Dec; 13 (12): 4279–4295.

40. *Fujimura J, Ogawa R, Mizuno H, Fukunaga Y, Suzuki H.* Neural differentiation of adipose-derived stem cells isolated from GFP transgenic mice. *Biochem Biophys Res Commun*. 2005 Jul 22; 333 (1): 116–121.
41. *Dominici M, Le Blanc K, Mueller I, Slaper-Cortenbach I, Marini F, Krause D et al*. Minimal criteria for defining multipotent mesenchymal stromal cells. The International Society for Cellular Therapy position statement. *Cytotherapy*. 2006; 8 (4): 315–317.
42. *Gimble JM, Katz AJ, Bunnell BA*. Adipose-derived stem cells for regenerative medicine. *Circ Res*. 2007 May 11; 100 (9): 1249–1260.
43. *Akita S, Akino K, Hirano A, Ohtsuru A, Yamashita S.* Noncultured autologous adipose-derived stem cells therapy for chronic radiation injury. *Stem Cells Int*. 2010 Dec 1; 2010: 532704.
44. *Brown SA, Levi B, Lequex C, Wong VW, Mojallal A, Longaker MT.* Basic science review on adipose tissue for clinicians. *Plast Reconstr Surg*. 2010 Dec; 126 (6): 1936–1946.
45. *Coleman SR*. Long-term survival of fat transplants: controlled demonstrations. *Aesthetic Plast Surg*. 1995 Sep-Oct; 19 (5): 421–425.
46. *Coleman SR.* Structural fat grafts: the ideal filler? *Clin Plast Surg*. 2001 Jan; 28 (1): 111–119.
47. *Kim WS, Park BS, Sung JH, Yang JM, Park SB, Kwak SJ, Park JS.* Wound healing effect of adipose-derived stem cells: a critical role of secretory factors on human dermal fibroblasts. *J Dermatol Sci*. 2007 Oct; 48 (1): 15–24.
48. *Lolli P, Malleo G, Rigotti G*. Treatment of chronic anal fissures and associated stenosis by autologous adipose tissue transplant: a pilot study. *Dis Colon Rectum*. 2010 Apr; 53 (4): 460–466.
49. *Bene MD, Pozzi MR, Rovati L, Mazzola I, Erba G, Bonomi S.* Autologous fat grafting for scleroderma-induced digital ulcers. An effective technique in patients with systemic sclerosis. *Handchir Mikrochir Plast Chir*. 2014 Aug; 46 (4): 242–247.
50. *Viard R, Bouguila J, Voulliaume D, Comparin JP, Dionyssopoulos A, Foyatier JL.* [Fat grafting in facial burns sequelae]. *Ann Chir Plast Esthet*. 2012 Jun; 57 (3): 217–229.
51. *Sultan SM, Barr JS, Butala P, Davidson EH, Weinstein AL, Knobel D et al.* Fat grafting accelerates revascularisation and decreases fibrosis following thermal injury. *J Plast Reconstr Aesthet Surg*. 2012 Feb; 65 (2): 219–227.
52. *Carpaneda CA, Ribeiro MT*. Study of the histologic alterations and viability of the adipose graft in humans. *Aesthetic Plast Surg*. 1993 Winter; 17 (1): 43–47.
53. *Sarantopoulos CN, Banyard DA, Ziegler ME, Sun B, Shaterian A, Widgerow AD.* Elucidating the Preadipocyte and Its Role in Adipocyte Formation: a Comprehensive Review. *Stem Cell Rev Rep*. 2018 Feb; 14 (1): 27–42.
54. *Bourin P, Bunnell BA, Casteilla L, Dominici M, Katz AJ, March KL et al*. Stromal cells from the adipose tissue-derived stromal vascular fraction and culture expanded adipose tissue-derived stromal/stem cells: a joint statement of the International Federation for Adipose Therapeutics and Science (IFATS) and the International Society for Cellular Therapy (ISCT). *Cytotherapy*. 2013 Jun; 15 (6): 641–648.
55. *Lee YH, Mottillo EP, Granneman JG*. Adipose tissue plasticity from WAT to BAT and in between. *Biochim Biophys Acta*. 2014 Mar; 1842 (3): 358–369.
56. *Saely CH, Geiger K, Drexel H*. Brown versus white adipose tissue: a mini-review. *Gerontology*. 2012; 58 (1): 15–23.
57. *Pierpont YN, Dinh TP, Salas RE, Johnson EL, Wright TG, Robson MC, Payne WG.* Obesity and surgical wound healing: a current review. *ISRN Obes*. 2014 Feb 20; 2014: 638936.
58. *Shibata S, Tada Y, Asano Y, Hau CS, Kato T, Saeki H et al.* Adiponectin regulates cutaneous wound healing by promoting keratinocyte proliferation and migration via the ERK signaling pathway. *J Immunol*. 2012 Sep 15; 189 (6): 3231–3241.
59. *Hu L, Wang J, Zhou X, Xiong Z, Zhao J, Yu R et al.* Exosomes derived from human adipose mensenchymal stem cells accelerates cutaneous wound healing via optimizing the characteristics of fibroblasts. *Sci Rep*. 2016 Sep 12; 6: 32993.
60. *Makino T, Jinnin M, Muchemwa FC, Fukushima S, Kogushi-Nishi H, Moriya C et al.* Basic fibroblast growth factor stimulates the proliferation of human dermal fibroblasts via the ERK1/2 and JNK pathways. *Br J Dermatol*. 2010 Apr; 162 (4): 717–723.
61. *Zhang W, Bai X, Zhao B, Li Y, Zhang Y, Li Z et al.* Cell-free therapy based on adipose tissue stem cell-derived exosomes promotes wound healing via the PI3K/Akt signaling pathway. *Exp Cell Res*. 2018 Sep 15; 370 (2): 333–342.
62. *Ren S, Chen J, Duscher D, Liu Y, Guo G, Kang Y et al.* Microvesicles from human adipose stem cells promote wound healing by optimizing cellular functions via AKT and ERK signaling pathways. *Stem Cell Res Ther*. 2019 Jan 31; 10 (1): 47. doi: 10.1186/s13287-019-1152-x.
63. *Ezure T, Amano S.* Adiponectin and leptin up-regulate extracellular matrix production by dermal fibroblasts. *Biofactors*. 2007; 31 (3–4): 229–236.
64. *Palmieri B, Vadalà M, Laurino C*. Nutrition in wound healing: investigation of the molecular mechanisms, a narrative review. *J Wound Care*. 2019 Oct 2; 28 (10): 683–693.
65. *Profyris C, Tziotzios C, Do Vale I*. Cutaneous scarring: Pathophysiology, molecular mechanisms, and scar reduction therapeutics Part I. The molecular basis of scar formation. *J Am Acad Dermatol*. 2012 Jan; 66 (1): 1–10; quiz 11–12.
66. *Ogawa R.* The most current algorithms for the treatment and prevention of hypertrophic scars and keloids. *Plast Reconstr Surg*. 2010 Feb; 125 (2): 557–568.
67. *Amini Nik S, Ebrahim RP, Van Dam K, Cassiman JJ, Tejpar S.* TGF-beta modulates beta-Catenin stability and signaling in mesenchymal proliferations. *Exp Cell Res*. 2007 Aug 1; 313 (13): 2887–2895.
68. *Widelitz RB*. Wnt signaling in skin organogenesis. *Organogenesis*. 2008 Apr; 4 (2): 123–133.
69. *Hiwatashi N, Hirano S, Mizuta M, Kobayashi T, Kawai Y, Kanemaru SI et al.* The efficacy of a novel colla-

gen-gelatin scaffold with basic fibroblast growth factor for the treatment of vocal fold scar. *J Tissue Eng Regen Med*. 2017 May; 11 (5): 1598–1609.
70. *Wang L, Yang J, Ran B, Yang X, Zheng W, Long Y, Jiang X.* Small Molecular TGF-β1-Inhibitor-Loaded Electrospun Fibrous Scaffolds for Preventing Hypertrophic Scars. *ACS Appl Mater Interfaces*. 2017 Sep 27; 9 (38): 32545–32553.
71. *Bu Y, Zhang L, Sun G, Sun F, Liu J, Yang F et al*. Tetra-PEG Based Hydrogel Sealants for *In Vivo* Visceral Hemostasis. *Adv Mater*. 2019 Jul; 31 (28): e1901580.
72. *Shahrokhi S, Arno A, Jeschke MG*. The use of dermal substitutes in burn surgery: acute phase. *Wound Repair Regen*. 2014 Jan-Feb; 22 (1): 14–22.
73. *Atacan K, Özacar M, Özacar M.* Investigation of antibacterial properties of novel papain immobilized on tannic acid modified Ag/$CuFe_2O_4$ magnetic nanoparticles. *Int J Biol Macromol*. 2018 Apr 1; 109: 720–731.
74. *Lawrence JW, Mason ST, Schomer K, Klein MB.* Epidemiology and impact of scarring after burn injury: a systematic review of the literature. *J Burn Care Res*. 2012 Jan-Feb; 33 (1): 136–146.
75. *Bock O, Schmid-Ott G, Malewski P, Mrowietz U.* Quality of life of patients with keloid and hypertrophic scarring. *Arch Dermatol Res*. 2006 Apr; 297 (10): 433–438. doi: 10.1007/s00403-006-0651-7.
76. *Fei X, Yuan W, Zhao Y, Wang H, Bai S, Huang Q.* Papain Ameliorates the MPAs Formation-Mediated Activation of Monocytes by Inhibiting Cox-2 Expression via Regulating the MAPKs and PI3K/Akt Signal Pathway. *Biomed Res Int*. 2018 Oct 16; 2018: 3632084. doi: 10.1155/2018/3632084.
77. *Stremnitzer C, Manzano-Szalai K, Willensdorfer A, Starkl P, Pieper M, König P et al.* Papain Degrades Tight Junction Proteins of Human Keratinocytes *In Vitro* and Sensitizes C57BL/6 Mice via the Skin Independent of its Enzymatic Activity or TLR4 Activation. *J Invest Dermatol*. 2015 Jul; 135 (7): 1790–1800.
78. *Kumano K, Nishinakamura H, Mera T, Itoh T, Takahashi H, Fujiwara T, Kodama S.* Pretreatment of donor islets with papain improves allograft survival without systemic immunosuppression in mice. *Islets*. 2016 Sep 2; 8 (5): 145–155.
79. *Leask A, Abraham DJ*. TGF-beta signaling and the fibrotic response. *FASEB J*. 2004 May; 18 (7): 816–827.
80. *Yang K, Han Q, Chen B, Zheng Y, Zhang K, Li Q, Wang J.* Antimicrobial hydrogels: promising materials for medical application. *Int J Nanomedicine*. 2018 Apr 12; 13: 2217–2263.
81. *Yuan N, Shao K, Huang S, Chen C.* Chitosan, alginate, hyaluronic acid and other novel multifunctional hydrogel dressings for wound healing: A review. *Int J Biol Macromol*. 2023 Jun 15; 240: 124321.
82. *Hudek M, Kubiak-Ossowska K, Johnston K, Ferro VA, Mulheran PA.* Chitin and Chitosan Binding to the α-Chitin Crystal: A Molecular Dynamics Study. *ACS Omega*. 2023 Jan 10; 8 (3): 3470–3477.
83. *Zaitsev SY, Savina AA, Zaitsev IS.* Biochemical aspects of lipase immobilization at polysaccharides for biotechnology. *Adv Colloid Interface Sci*. 2019 Oct; 272: 102016.
84. *Shang NS, Cui BH, Wang C, Gao H, Xu B, Zhao R, Huo R.* A prospective randomized controlled study of the application effect of hydrogel dressings on deep partial-thickness burn wounds after dermabrasion and tangential excision. *Zhonghua Shao Shang Za Zhi*. 2021 Nov 20; 37 (11): 1085–1089.
85. *Wang S, Wu S, Yang Y, Zhang J, Wang Y, Zhang R, Yang L.* Versatile Hydrogel Dressings That Dynamically Regulate the Healing of Infected Deep Burn Wounds. *Adv Healthc Mater*. 2023 Dec; 12 (30): e2301224.
86. *Mustoe TA*. Evolution of silicone therapy and mechanism of action in scar management. *Aesthetic Plast Surg*. 2008 Jan; 32 (1): 82–92.

The article was submitted to the journal on 25.09.2024

DOI: 10.15825/1995-1191-2025-2-163-170

LYMPHOCYTIC RNA STIMULATES PHYSIOLOGICAL REGENERATION AND ENHANCES MICROCIRCULATION IN THE THYROID GLAND

N.V. Tishevskaya, E.S. Golovneva, R.V. Takhaviev
South Ural State Medical University, Chelyabinsk, Russian Federation

Objective: to investigate the regulatory effects of exogenous lymphocyte RNA on thyroid gland regeneration. **Materials and methods.** The study was conducted on 18 male Wistar rats (310–350 g), divided into three groups (n = 6 per group). Group 1 – intact rats; group 2 – control rats (subjected to 6 weeks of physical activity), group 3 – experimental rats (subjected to 6 weeks of physical activity + RNA injection). Total RNA, isolated from the spleen of a 30-day-old pig, was administered four times at a dose of 30 μg/100 g body weight, once per week. Follicular epithelium and vascular structures were analyzed using morphometry, VEGF content was quantified via immunohistochemistry with specific antibodies, and thyroid microvascular function was assessed using laser flowmetry. **Results.** Following RNA administration, the relative thyroid gland mass increased by 16%, the follicular epithelium area expanded 1.5-fold, and the vasculature area doubled. Additionally, VEGF content increased 2.5-fold compared to intact rats, while microcirculation intensity rose by 64%, and vascular resistance decreased by 21%. **Conclusion.** Administration of morphogenetically active total RNA under conditions of increased oxygen demand promotes regenerative hypertrophy of the glandular epithelium and enhances microcirculation in the thyroid gland.

Keywords: RNA, regeneration, microcirculation, thyroid gland.

INTRODUCTION

Regenerative thyroidology focuses on the ability of thyroid tissue to renew itself and recover after injury or resection, and experimental evidence demonstrating the induction of thyrocyte proliferation and differentiation *in vitro*. However, the underlying mechanisms of thyroid regeneration remain poorly understood. In murine models, a distinct cluster of cells expressing the transcription factor NKX2-1 – a key regulator of thyroid growth, development, and functional maintenance – has been identified within the thyroid gland [1]. These NKX2-1-positive cells are assumed to represent precursor populations that, through differentiation and maturation, give rise to the follicular architecture of the thyroid [2]. Notably, thyroid tissue retains a lifelong potential for hypertrophic and hyperplastic regeneration, a process that may be activated in response to increased thyroid-stimulating hormone secretion from the adenohypophysis during physiological stress or intense physical activity [3, 4]. During physical activity, the body enters a distinct hormonal state in which the thyroid gland enhances the secretion and release of thyroxine and triiodothyronine into the bloodstream. This increased hormonal output leads to a reduction in the colloid content within thyroid follicles. It has been shown that after a single session of intensive physical exercise, there is a rapid decrease in follicle size. Moreover, with sustained daily physical training over a 35-day period, adaptive and compensatory responses are reinitiated within the thyroid gland. These changes are characterized by a marked increase in the proliferative activity of the thyroid epithelium [5].

In mammals, tissue growth and development are regulated, in part, by tissue-specific clones of T-lymphocytes. Early studies identified T cells within the lymph nodes of Wistar rats that began to proliferate robustly upon contact with thyrocytes or after addition of rat thyroglobulin to the culture medium [6]. Cloning of these thyroid-specific T-lymphocytes revealed that all clones exhibited a $CD4^+CD8^-$ phenotype. Of the 23 T-cell clones analyzed, 7 showed selective proliferation in the presence of thyrocytes alone, while the remainder proliferated in response to both thyrocytes and thymic cells [7]. Further investigations of T-lymphocytes isolated directly from the thyroid gland identified the presence of both $CD4^+$ T-helper cells and $CD8^+$ cytotoxic T cells, all expressing αβ T-cell receptors [8]. $CD4^+$ T-helper cells were found to localize predominantly in the centers of thyroid lymphoid follicles, whereas $CD8^+$ T cells were primarily distributed along the follicular periphery [9]. Under physiological conditions, both $CD4^+$ T-helper cells and cytotoxic T lymphocytes contribute to thyrocyte hyperplasia and proliferation through production of tumor necrosis factor-alpha (TNF-α). In experimental models, mice lacking T-helper cells exhibited signs of thyroid

Corresponding author: Natalya Tishevskaya. Address: 64, Vorovskogo str., Chelyabinsk, 454092, Russian Federation. Phone: (351) 232-74-67. E-mail: natalya-tishevskaya@yandex.ru

fibrosis when exposed to the activity of cytotoxic T lymphocytes alone [10].

To date, compelling evidence has shown that not only lymphoid cells themselves, but also total RNA isolated from these cells, can stimulate tissue regeneration and enhance cell–cell interactions in rapidly renewing tissues. For example, erythroid cells and bone marrow macrophages are known to actively form new erythroblastic islets, not only in response to erythropoietin and macrophage colony-stimulating factor [11], but also following the administration of exogenous lymphocytic RNA in experimental animals [12]. Based on this, the present study aimed to explore the regulatory role of morphogenetically active exogenous RNA on cellular processes in a slowly renewing secretory organ – the thyroid gland – under conditions of enhanced tissue respiration induced by regular physical exercise.

MATERIALS AND METHODS

The study was conducted on 18 male Wistar rats weighing 310–350 g. All experimental procedures adhered to the principles of humane treatment outlined in the European Union Directive 86/609/EEC, the Declaration of Helsinki, and the Order of the Ministry of Health of the Russian Federation No. 199N dated April 1, 2016, "On the Approval of the Rules of Good Laboratory Practice". Animals were housed in standard cages (n = 6 per cage) with ad libitum access to food and water, maintained at an ambient temperature of +24 ± 2 °C in accordance with sanitary regulations SP 2.2.1.3218.

The animals received a daily diet of specialized pelleted feed that met international standards for nutrient, vitamin, and mineral content, in accordance with GOST R 50258-92 ("Complete feeds for laboratory animals"). All procedures involving potential pain or distress were performed under general anesthesia, and euthanasia was carried out in a designated room, separate from the animal housing area, using ether anesthesia followed by cervical dislocation.

The experimental animals were randomly divided into 3 groups, with 6 rats per group: Group 1 consisted of intact (non-exercised, untreated) rats; Group 2 included control rats subjected to a 6-week exercise protocol; Group 3 consisted of rats undergoing the same 6-week exercise regimen and receiving additional injections of total RNA.

The training regimen involved swimming exercises performed in a 200-liter tank filled with water to a depth of 0.5 meters, maintained at a temperature of +22–23 °C. The rats swam 3 times per week, with the duration of each session gradually increasing from 30 minutes to 55 minutes, in 5-minute increments each week.

Lymphocytes, the source of morphogenetically active RNA, were isolated from the spleen of a 30-day-old piglet. The tissue was homogenized in a glass homogenizer, filtered through a capron mesh, and subjected to 3 rounds of centrifugation in sterile 0.9% NaCl solution to collect the cells. Total RNA was extracted using the guanidine thiocyanate–phenol–chloroform method. RNA concentration was determined spectrophotometrically by measuring optical density at 260 nm. The extracted RNA was lyophilized and stored in sterile vials at +5 °C. Stability tests confirmed that the RNA quantity remained unchanged after lyophilization.

Before injection, lyophilized RNA was dissolved in sterile 0.9% NaCl, filtered using sterile syringe filters with a pore size of 0.22 μm, and administered intraperitoneally. Each rat in Group 3 received a total of four injections, administered once weekly, at a dose of 30 μg RNA per 100 g body weight in a total volume of 0.5 mL per injection.

Six weeks after the start of the experiment, the microcirculatory status of the thyroid gland was assessed in all animals using laser Doppler flowmetry with the LAKK-OP analyzer (NPO "LAZMA", Russia). The procedure was performed under general anesthesia (Zoletil, 10 mg/kg, intramuscularly; VIRBAC, France). After careful dissection of the skin and adjacent tissues, the device's sensor was placed directly on the thyroid tissue and securely fixed to the lateral skin margins using adhesive tape.

The Doppler flowmetry data were analyzed using proprietary software from NPO "LAZMA", focusing on the following parameters: microcirculation Index – the arithmetic mean value of perfusion, expressed in perfusion units (p.u.); shunt coefficient (Sc) calculated as: Sc = An/Am, where An – is the largest amplitude of perfusion fluctuations in the neurogenic range (p.u.), Am – is the largest amplitude of perfusion fluctuations in the myogenic range (p.u.); the resistance coefficient of the microcirculatory channel was calculated using the formula: Rc = (AHF + ACF)/σ where is the amplitude of fast (respiratory) fluxmotion waves (p.u.), ACF is the amplitude of cardiac (pulse) fluxmotion waves (p.u.), σ is the standard deviation of the amplitude of blood flow fluctuations from the mean microcirculation index. The amplitude-frequency spectra of perfusion oscillations were assessed within specific frequency ranges:

- Endothelial oscillations (A(E)): 0.007–0.017 Hz
- Neurogenic oscillations (A(H)): 0.023–0.046 Hz
- Myogenic oscillations (A(M)): 0.06–0.15 Hz
- Respiratory rhythm (A(D)): 0.21–0.6 Hz
- Cardiac rhythm (A(C)): 0.7–1.6 Hz

The amplitudes were then normalized to the standard deviation (σ) and mean microcirculation index (M), enabling the assessment of the functional contribution of each regulatory mechanism to modulation of microcirculatory flow. The following normalized parameters were calculated:

- Endothelial activity (E) = A(E)/3σ
- Neurogenic activity (H) = A(H)/3σ
- Myogenic activity (M) = A(M)/3σ
- Respiratory rhythm (D) = A(D)/3σ

– Cardiac rhythm (C) = A(C)/3σ

These normalized parameters were automatically computed by the system after identifying the maximum amplitude (Amax) within the corresponding frequency range [13].

After measurement of microcirculation parameters, the animals were euthanized. Thyroid tissue samples were fixed in 10% neutral buffered formalin. Standard histological processing was performed, including paraffin embedding, sectioning, and staining with hematoxylin and eosin.

Histological evaluation was conducted using a LEICA DMRXA microscope (Germany) equipped with a LEICA DFC 290 digital video camera and connected to a personal computer. Microstructural images were captured in *TIFF format within the RGB color space. Quantitative analysis was performed using the licensed ImageScope-M image analysis software (Russia), measuring the following parameters: total follicle area, follicular and vascular lumen area, thyrocyte nuclear area, epithelial height, and vascular wall thickness. The relative vascular area was calculated as the percentage ratio of vessel area to total tissue section area.

Vascular endothelial growth factor (VEGF) expression was assessed immunohistochemically using specific anti-VEGF antibodies (Biorbyt, USA) and a biotin-streptavidin-peroxidase detection system (DakoCytomation, Denmark). Integral VEGF index was calculated as the product of the stained area (relative) and staining intensity (scored), with results expressed in arbitrary units.

Data were analyzed using licensed versions of Microsoft Excel 2020 and PAST software (version 4.03). The nonparametric Mann–Whitney U test was applied to evaluate significance of differences between groups. Comparative analysis of morphometric data sets was performed using Wald's sequential probability ratio test [14]. Results are presented as arithmetic mean ± standard error of mean (M ± m). A p-value of ≤0.05 was considered statistically significant.

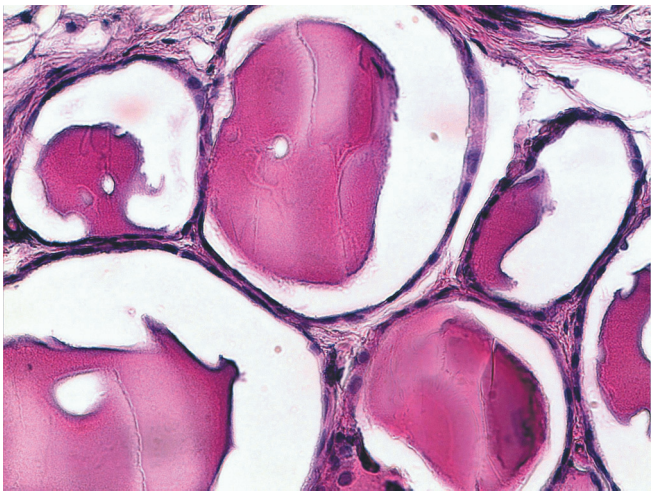

Fig. 1. Follicular apparatus of the thyroid gland. Group 1 (intact rats). H&E stain; 400×; oil immersion

RESULTS

Histological analysis of thyroid tissue in rats from Group 2 (Fig. 2), which underwent regular physical exercise, revealed a reduction in follicle size, decreased colloid content, and morphological changes in the follicular epithelium, which adopted a cuboidal shape compared to the intact animals (Fig. 1). In Group 3 animals, which were exposed to the same physical exercise regimen but also received total RNA (Fig. 3), a similar decrease in follicle size and colloid volume was observed. However, the follicular epithelium exhibited a highly prismatic structure with pronounced papillary proliferation. This histological pattern is recognized as indicative of enhanced hormone-producing activity of the thyroid gland [15]. These findings suggest that total RNA administration enhanced the functional activity

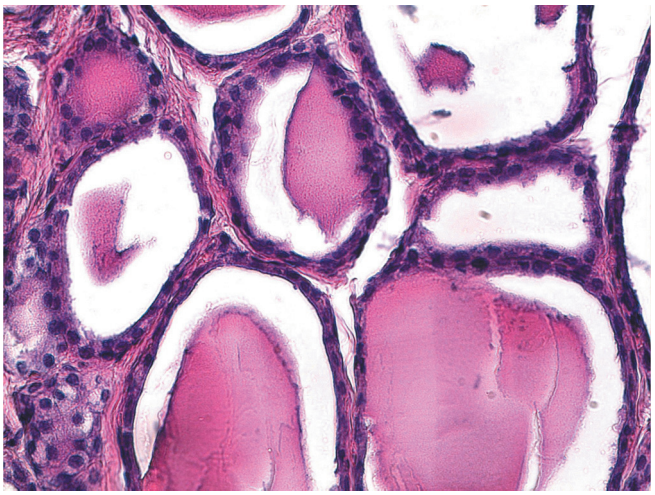

Fig. 2. Follicular apparatus of the thyroid gland. Group 2 (physical activity). H&E stain; 400×; oil immersion

Fig. 3. Follicular apparatus of the thyroid gland. Group 3 (physical activity + RNA). H&E stain; 400×; oil immersion

of the glandular epithelium, thereby supporting an adequate supply of thyroid hormones required to meet the increased physiological demands associated with regular physical exertion.

Morphometric analysis revealed that, in the control group rats subjected to several days of physical activity, thyroid gland mass did not differ significantly from that of intact animals (Table 1). However, in rats exposed to the same physical activity regimen but additionally administered lymphocytic RNA, both the absolute and relative mass of the thyroid gland were increased compared to the intact group. Specifically, the relative gland mass in group 3 was 16.7% higher than in group 1 and 15% higher than in group 2. A marked and statistically significant increase in the area occupied by follicular epithelium cells was also observed in group 3 – 1.5 times greater than in intact animals and 1.4 times greater than in the control group. These structural alterations were corroborated by morphometric findings: epithelial cell height in group 3 animals was 33% greater, while the follicular cavity area was 39% less compared to intact rats.

Morphometric analysis of arterioles and venules in the thyroid tissue revealed a pronounced reorganization of the microcirculatory bed in response to exogenous RNA administration. In group 3 animals, a significant increase in the thickness of arteriole and venule walls was observed compared to both intact rats and the control group. Additionally, the relative area of the vascular bed was doubled. This expansion of the microcirculatory network likely resulted from the formation of new capillaries, as the luminal area of arterioles and venules remained unchanged. Supporting the evidence of angiogenic activation, a marked elevation in VEGF content was detected in the thyroid tissue gland of animals subjected to prolonged physical exercise. While VEGF levels in group 2 animals increased by 1.9-fold relative to intact controls, group 3 rats, which received exogenous RNA in conjunction with regular physical activity, exhibited a 2.5-fold increase in VEGF content.

Previous studies have demonstrated that the angioprotective effects of lymphoid cells may be attributed to their elevated expression of hypoxia-inducible factor 1-alpha (HIF-1α), a key regulator that promotes VEGF synthesis under hypoxic conditions [16]. A dual role of T-lymphocytes in regulating angiogenesis and cell proliferation has been documented in renal tissue [17]. It was shown that T-lymphocytes migrating to areas of tissue injury exerted a pronounced proangiogenic and proregenerative effect during reparative regeneration. Conversely, in conditions leading to fibrosis, their role shifted toward a predominantly proinflammatory profile. These findings highlight the remarkable functional plasticity of T-cells in morphogenetic processes, a capacity that remains both underrecognized and poorly explored in the context of tissue regeneration.

Using laser Doppler flowmetry combined with spectral amplitude-frequency wavelet analysis of blood flow oscillations in microvessels, we assessed the functional changes in the thyroid microcirculatory bed induced by morphogenetically active exogenous RNA (Table 2). Regular physical activity in rats of group 2 led to a 38% increase in the microcirculation index compared to intact controls. Notably, administration of exogenous RNA in rats subjected to identical physical exertion (group 3) resulted in a 64% increase in this index. The vascular shunt coefficient within the microcirculatory network remained stable across groups. However, a 21% decrease in the resistance coefficient was observed in group 3 animals, indicating improved vascular wall elasticity. This suggests optimal blood supply to the follicular apparatus of the thyroid gland in animals that received total RNA.

Changes in the normalized parameters of amplitude-spectral analysis (Fig. 4) further indicated enhanced engagement of both local and systemic regulatory me-

Table 1

Thyroid morphometry

Indicators	Intact rats (group 1), n = 6	Physical activity (Swimming)	
		Control (group 2), n = 6	RNA injection (group 3), n = 6
Absolute thyroid mass (g)	0.245 ± 0.009	0.255 ± 0.009	0.286 ± 0.012*
Relative thyroid mass (μg/g)	0.74 ± 0.03	0.75 ± 0.05	0.86 ± 0.04*▲
Follicular epithelium area (μm^2)	1242.1 ± 56.6	1358.4 ± 44.3	1871.7 ± 40.5*▲
Follicular epithelium height (μm)	7.6 ± 0.4	8.9 ± 0.6	10.1 ± 0.3*▲
Follicle cavity area (μm^2)	3645.5 ± 99.8	3162.2 ± 31.4*	2236 ± 22.2*▲
Thyrocyte nuclei area (μm^2)	13.2 ± 0.7	13.1 ± 0.6	12.7 ± 0.7
Arteriole wall thickness (μm)	7.6 ± 0.3	7.9 ± 0.3	8.7 ± 0.3*▲
Arteriole lumen area (μm^2)	121.3 ± 18.8	123.3 ± 14.6	127.8 ± 16.2
Venule wall thickness (μm)	4.2 ± 0.1	4.4 ± 0.3	5.1 ± 0.2*
Venule lumen area (μm^2)	218.2 ± 16.5	193.2 ± 13.7	191.9 ± 11.9
Relative vasculature area (%)	4.2 ± 0.2	4.8 ± 0.3	8.4 ± 0.2*▲
Vascular endothelial growth factor (c.u.)	4.7 ± 0.2	8.9 ± 0.2*	11.9 ± 0.5*▲

Notes: * – differences between groups 2, 3 and group 1 ($p < 0.05$); ▲ – differences between group 2 and group 3 ($p < 0.05$).

chanisms in the thyroid microvasculature of rats that received exogenous RNA. It is well established that rhythmic variability of microvascular blood flow is influenced by several active regulatory components – myogenic (M), neurogenic (N), and endothelial (E) – as well as passive components associated with cardiac (C) and respiratory (D) rhythms. The spectral characteristics of these oscillatory processes not only permitted quantification of the contribution of each of the regulatory mechanisms but also allowed identification of specific features in the adaptive responses of the thyroid microcirculatory network. Notably, during physical exercise, the myogenic component remained largely unchanged, suggesting a stable muscle tone in thyroid precapillaries, which play a critical role in modulating nutrient blood flow. At the same time, the endothelial component – reflecting the influence of vasodilatory substances such as nitric oxide, ADP, and VEGF, as well as passive effects from respiratory and pulse wave modulation – was significantly elevated in the thyroid microcirculatory bed following prolonged physical exercise. In animals that underwent physical activity and received injections of morphogenetically active RNA (group 3), the endothelial component was four times higher than in the control group. Additionally, the cardiac and respiratory components were elevated by twofold and threefold, respectively, compared to rats in the control group.

It is known that stable adaptation and maintenance of structural and hemodynamic homeostasis in microvascular networks at a new functional level are achieved through the coordinated and balanced involvement of all regulatory mechanisms. This is characterized by a uniform increase in amplitude parameters without the dominance of oscillations in any frequency range [18, 19]. Such a regulatory pattern is referred to as multichannel or multistable regulation. In the present study, exogenous RNA administration in combination with regular physical activity resulted in the development of a clearly defined multistable variant of microvascular blood flow regulation.

Table 2

Amplitude-spectral analysis of the thyroid microvasculature (standard indicators)

Indicators	Intact rats (group 1), n = 6	Physical activity (Swimming)	
		Control (group 2), n = 6	RNA injection (group 3), n = 6
Microcirculation index (p.u.)	14.3 ± 0.9	19.8 ± 0.7*	23.5 ± 0.3*▲
Shunt coefficient in the microvasculature (c.u.)	0.87 ± 0.04	1.0 ± 0.04	1.05 ± 0.12
Microcirculatory resistance coefficient (c.u.)	0.88 ± 0.01	0.9 ± 0.01	0.69 ± 0.02*▲

Notes: * – differences between groups 2, 3 and group 1 ($p < 0.05$); ▲ – differences between group 2 and group 3 ($p < 0.05$).

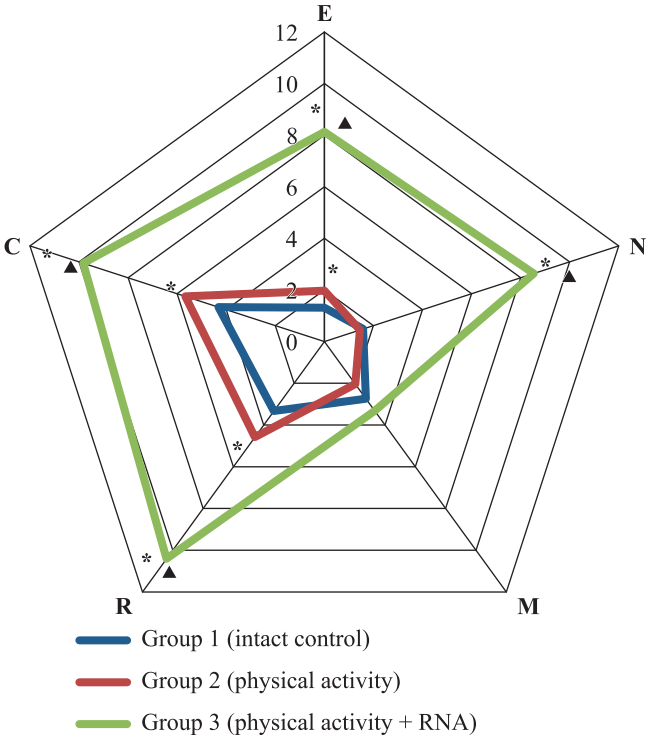

Fig. 4. Amplitude-spectral analysis of the thyroid microvasculature (normalized indicators): endothelial component (E), neurogenic component (N), myogenic component (M), respiratory component (R), cardiac component (C). * – differences between groups 2, 3 and group 1 ($p < 0.05$); ▲ – differences between group 2 and group 3 ($p < 0.05$)

CONCLUSION

The administration of morphogenetically active total RNA, under conditions of increased oxygen demand, induces regenerative hypertrophy of the thyroid glandular epithelium and enhances microcirculation within the organ. This results in a significant increase in both the absolute and relative mass of the thyroid gland, as well as in the size of thyrocytes, the number of capillaries, and the intensity of blood flow in the microcirculatory channel. Exogenous RNA also leads to marked changes in the regulatory parameters of tissue blood flow in the thyroid gland during periods of intensified functional activity. These changes are associated with a notable reduction in vascular wall stiffness and an improved adaptive capacity of the microcirculatory network in the thyroid gland of rats in group 3.

The authors declare no conflict of interest.

REFERENCES

1. *Kusakabe T, Kawaguchi A, Hoshi N, Kawaguchi R, Hoshi S, Kimura S.* Thyroid-specific enhancer-binding protein/NKX2.1 is required for the maintenance of ordered architecture and function of the differentiated thyroid. *Mol Endocrinol.* 2006 Aug; 20 (8): 1796–1809. doi: 10.1210/me.2005-0327.
2. *Iwadate M, Takizawa Y, Shirai YT, Kimura S.* An *in vivo* model for thyroid regeneration and folliculogenesis. *Lab Invest.* 2018 Sep; 98 (9): 1126–1132. doi: 10.1038/s41374-018-0068-x.
3. *Ozaki T, Matsubara T, Seo D, Okamoto M, Nagashima K, Sasaki Y et al.* Thyroid regeneration: characterization of clear cells after partial thyroidectomy. *Endocrinology.* 2012 May; 153 (5): 2514–2525. doi: 10.1210/en.2011-1365.
4. *Dumont J, Lamy F, Roger P, Maenhaut C.* Physiological and pathological regulation of thyroid cell proliferation and differentiation by thyrotropin and others. *Physiol Rev.* 1992 Jul; 72 (3): 667–697. doi: 10.1152/physrev.1992.72.3.667.
5. *Krishtop VV, Rumyantseva TA, Nikonorova VG.* Peculiarities of thyroid morphology in cerebral hypoperfusion in the complex with short-term exercise in rats with different results in the Morris labyrinth. *Journal of Volgograd State Medical University.* 2021; 78 (2): 103–107. doi: 10.19163/1994-9480-2021-2(78)-103-107.
6. *Kimura H, Davies TF.* Thyroid-specific T cells in the normal Wistar rat. I. Characterization of lymph node T cell reactivity to syngeneic thyroid cells and thyroglobulin. *Clin Immunol Immunopathol.* 1991 Feb; 58 (2): 181–194. doi: 10.1016/0090-1229(91)90135-w.
7. *Kimura H, Davies TF.* Thyroid-specific T cells in the normal Wistar rat. II. T cell clones interact with cloned Wistar rat thyroid cells and provide direct evidence for autoantigen presentation by thyroid epithelial cells. *Clin Immunol Immunopathol.* 1991 Feb; 58 (2): 195–206. doi: 10.1016/0090-1229(91)90136-x.
8. *Sugihara S, Fujiwara H, Shearer GM.* Autoimmune thyroiditis induced in mice depleted of particular T cell subsets. Characterization of thyroiditis-inducing T cell lines and clones derived from thyroid lesions. *J Immunol.* 1993 Jan 15; 150 (2): 683–694.
9. *Zha B, Huang X, Lin J, Liu J, Hou Y, Wu G.* Distribution of lymphocyte subpopulations in thyroid glands of human autoimmune thyroid disease. *J Clin Lab Anal.* 2014 May; 28 (3): 249–254. doi: 10.1002/jcla.21674.
10. *Yu S, Fang Y, Sharav T, Sharp GC, Braley-Mullen H.* CD8+ T cells induce thyroid epithelial cell hyperplasia and fibrosis. *J Immunol.* 2011 Feb 15; 186 (4): 2655–2662. doi: 10.4049/jimmunol.1002884.
11. *Tishevskaya NV, Shevyakov SA, Zakharov YuM.* Vliyaniye eritropoetina i makrofagal'nogo koloniyestimuliruyushchego faktora na proliferativnuyu aktivnost' eritroidnykh kletok v kul'turakh eritroblasticheskikh ostrovkov. *Meditsinskiy akademicheskiy zhurnal.* 2003; 3 (3): 67–72. [In Russ.].
12. *Gevorkyan NM, Tishevskaya NV, Bolotov AA.* Effect of preliminary administration of total RNA of bone marrow cells on the dynamics of erythropoiesis recovery in rats after acute gamma irradiation. *Bull Exp Biol Med*. 2016 Sep; 161 (5): 670–673. [In Russ., English abstract]. doi: 10.1007/s10517-016-3494-z.
13. *Krupatkin AI, Sidorov VV.* Funkcional'naya diagnostika sostoyaniya mikrocirkulyatorno-tkanevyh sistem. Kolebaniya, informaciya, nelinejnost'. Rukovodstvo dlya vrachej. Moscow: URSS, 2016; 496. [In Russ.].
14. *Tishevskaya NV, Bolotov AA, Zakharov YuM.* Matematicheskoye modelirovaniye mezhkletochnykh vzaimodeystviy v kul'ture eritroblasticheskikh ostrovkov. *Meditsinskiy akademicheskiy zhurnal.* 2005; 5 (4): 50–59. [In Russ.].
15. *Kirillov YuB, Chumachenko AP, Aristarkhov VG, Potapov AA, Panteleyev IV.* Rapid morphometric method for assessment of thyroid functional activity. *Problems of Endocrinology.* 1994; 40 (4): 19–21. [In Russ.] doi: 10.14341/probl12135.
16. *Lin Y, Tang Y, Wang F.* The Protective effect of HIF-1α in T lymphocytes on cardiac damage in diabetic mice. *Ann Clin Lab Sci.* 2016 Winter; 46 (1): 32–43.
17. *Do Valle Duraes F, Lafont A, Beibel M, Martin K, Darribat K, Cuttat R et al.* Immune cell landscaping reveals a protective role for regulatory T cells during kidney injury and fibrosis. *JCI Insight.* 2020 Feb 13; 5 (3): e130651. doi: 10.1172/jci.insight.130651.
18. *Hu HF, Hsiu H, Sung CJ, Lee CH.* Combining laser-Doppler flowmetry measurements with spectral analysis to study different microcirculatory effects in human prediabetic and diabetic subjects. *Lasers Med Sci.* 2017 Feb; 32 (2): 327. doi: 10.1007/s10103-016-2117-2.
19. *Sun PC, Kuo CD, Wei SH, Lin HD.* Microvascular reactivity using laser Doppler measurement in type 2 diabetes with subclinical atherosclerosis. *Lasers Med Sci*. 2023 Feb 28; 38 (1): 80. doi: 10.1007/s10103-023-03737-x.

The article was submitted to the journal on 11.10.2024

DOI: 10.15825/1995-1191-2025-2-171-178

MOLECULAR DIAGNOSTICS OF CARDIAC ALLOGRAFT REJECTION: DEVELOPMENT PATHWAYS AND FUTURE CLINICAL PROSPECTS

D.A. Velikiy[1], S.O. Sharapchenko[1], A.O. Shevchenko[1–3], O.P. Shevchenko[1, 2]

[1] Shumakov National Medical Research Center of Transplantology and Artificial Organs, Moscow, Russian Federation

[2] Sechenov University, Moscow, Russian Federation

[3] Pirogov Russian National Research Medical University, Moscow, Russian Federation

Recent advances in molecular diagnostics have opened new avenues for integrating genetic and epigenetic biomarkers into clinical practice. Areas such as gene expression profiling, extracellular DNA quantification, and microRNA expression analysis have seen significant development in recent years. The diagnostic value of molecular genetic biomarkers has been demonstrated across a range of pathological conditions. Emerging clinical data now support the use of molecular diagnostics to detect post-transplant complications in recipients of solid organ transplants. In heart transplant recipients, a comprehensive assessment that includes molecular genetics, epigenetic, and clinical parameters is essential for personalized selection of immunosuppressive therapy and for prevention of graft dysfunction and vasculopathy. This review highlights the current state of molecular diagnostics in cardiac allograft rejection and explores its potential for clinical application.

Keywords: heart transplantation, gene expression profiling, extracellular DNA, miRNA, graft rejection, personalization.

INTRODUCTION

A heart transplant (HT) is generally considered the only definitive treatment option for patients with end-stage chronic heart failure that does not respond to medication. In 2023, 388 HTs were performed in the Russian Federation [1]. While advances in surgical techniques, postoperative care, and immunosuppressive protocols have significantly improved patient outcomes, the 5-year survival rate is still around 72%, and the median survival for those who survive the first year is about 13 years [2].

Acute graft rejection, both T cell-mediated rejection (TCMR) or antibody-mediated rejection (AMR), is a major hurdle to long-term survival after HT. Both types of rejection crises are directly linked to an increased risk of graft dysfunction and the development of cardiac allograft vasculopathy (CAV) [3]. To prevent TCMR, lifelong immunosuppressive therapy is required for all transplant recipients, guided by standard treatment protocols. However, a mismatch between standard drug dosages and individual patient needs can lead to adverse outcomes – insufficient dosing may result in graft rejection, while overdosing increases the risk of infections and drug toxicity.

The integration of non-invasive molecular diagnostic methods in post-transplant monitoring holds promise for enabling personalized immunosuppressive therapy, tailored to the individual characteristics of each patient. This approach may significantly reduce the incidence of post-transplant complications and prolong the heart graft function.

Posttranslational biomarkers, such as cardiac troponins T and I and brain natriuretic peptides (BNP and NT-proBNP), have shown their diagnostic value in a variety of cardiovascular diseases. Cardiac troponins, in particular, are recognized as highly sensitive and specific indicators of myocardial injury.

However, multiple studies have demonstrated that cardiac troponins lack diagnostic effectiveness in detecting acute transplant rejection in HT recipients [4]. Similarly, natriuretic peptides, including BNP and NT-proBNP, have also been found to possess insufficient sensitivity and specificity for reliable detection of post-transplant complications in this patient population [5].

In recent years, molecular genetic methods have emerged as promising tools for the diagnosis of various pathological conditions, offering the potential. Among these methods, gene expression profiling, extracellular DNA (exDNA) quantification, and microRNA (miRNA) expression analysis have shown particular diagnostic relevance.

Gene expression profiling allows identifying genes with altered expression patterns in specific disease states. Several studies have delineated distinct gene signatures associated with the development of cancers and immune-mediated disorders [6, 7]. Meanwhile, exDNA, which

Corresponding author: Dmitriy Velikiy. Address: 1, Shchukinskaya str., Moscow, 123182, Russian Federation. Phone: (499) 193-87-62. E-mail: dim_vel@mail.ru

results from cellular damage and apoptosis, can be found in various body fluids including plasma, serum, urine, cerebrospinal fluid, and saliva. Elevated levels of exDNA have been reported in patients with cardiovascular conditions, including arterial hypertension, myocardial infarction, and heart failure [8].

Among the diverse group of circulating non-coding RNAs, miRNAs have gained significant attention due to their ability to regulate gene expression. Altered expression profiles of specific miRNAs have been linked to numerous diseases. Certain circulating miRNAs are elevated in the plasma of patients with coronary artery disease and acute coronary syndrome, distinguishing compared to healthy individuals [9].

The aim of this review is to examine recent advances in molecular diagnostic methods for the detection of acute transplant rejection in HT recipients, with a focus on their diagnostic effectiveness and clinical applicability.

GENE EXPRESSION PROFILING

Gene expression profiling (GEP) refers to the simultaneous measurement of the activity of a large number of genes in biological samples like blood, tissue, or cell cultures [10]. GEP of peripheral blood leukocytes can be used as a noninvasive diagnostic tool for detecting acute rejection episodes, particularly in the months following HT [11].

In a study by Horwitz et al., it was first demonstrated that GEP could be effectively used to diagnose transplant rejection in HT recipients, with results showing a strong correlation with endomyocardial biopsy findings [12]. Building on this discovery, a composite GEP test was developed, which analyzes the expression of 20 specific genes to estimate the risk of acute TCMR. This risk is quantified on a scale from 0 to 40, where a score of 34 or higher is associated with a low probability of rejection [13, 14].

This diagnostic tool is notable for its high negative predictive value (NPV >90%), making it a reliable noninvasive method to rule out acute TCMR in HT patients. However, the test has certain limitations, including a low positive predictive value (about 10%) and inability to detect acute AMR [15].

In a study by Shannon et al., a panel of nine mRNA transcripts was developed using high-throughput transcriptomic analysis to diagnose acute cellular rejection in HT recipients. A key advantage of this test is its high sensitivity in the early post-transplant period, with reliable detection as early as 55 days after transplantation [16].

GEP analysis of peripheral blood mononuclear cells and endomyocardial biopsy samples allowed us to identify gene signatures associated with AMR. These include four distinct gene sets involved in endothelial function, macrophage activity, natural killer (NK) cell activation, and interferon-γ signaling. These profiles have shown diagnostic value in identifying AMR in HT recipients [17, 18].

An emerging area of interest is the analysis of mitochondrial gene expression during transplant rejection. Tarazón et al. sequenced 112 mitochondrial-related genes in a cohort of 40 HT patients and found that expression of several mitochondrial genes was significantly elevated during episodes of acute TCMR [19]. This aligns with earlier studies suggesting that mitochondrial gene expression is upregulated during immune activation, implicating these genes not only as biomarkers but also as potential mediators of rejection [20, 21].

EXTRACELLULAR DNA

Extracellular DNA (cfDNA, cell-free DNA) is released into the bloodstream during cell apoptosis and necrosis and is a promising biomarker of organ injury [22]. In solid organ transplantation, graft injury resulting from acute TCMR or AMR leads to the release of donor-derived cell-free DNA (dd-cfDNA) into the recipient's blood [23].

Early detection methods for dd-cfDNA relied on genetic differences between donor and recipient, such as sex mismatch, human leukocyte antigen (HLA) differences, and single nucleotide polymorphisms (SNPs) [24, 25]. Later, digital droplet polymerase chain reaction (PCR) [26] and whole-genome sequencing [27] were used for more precise quantification of dd-cfDNA.

De Vlaminck I. et al. demonstrated a significant rise in dd-cfDNA levels in the blood of HT recipients during acute rejection episodes, with levels decreasing following appropriate treatment. In addition, dd-cfDNA levels increased even prior to the appearance of characteristic morphological changes in endomyocardial biopsy, indicating its potential for early detection of rejection and timely adjustment of immunosuppressive therapy [28].

A prospective multicenter study established a threshold value of 0.2% for the ratio of dd-cfDNA to total recipient cfDNA. This threshold enabled the differentiation between patients with and without acute rejection, achieving a specificity of 80%, sensitivity of 44%, and a negative predictive value of 97.1% [23].

A study by Agbor-Enoh et al. demonstrated that elevated levels of dd-cfDNA in cardiac transplant recipients correlate with the severity of both TCMR and AMR, as well as with the extent of echocardiographic changes. The authors noted that the proportion of circulating dd-cfDNA was significantly higher in patients with acute AMR compared to those with acute TCMR of the heart graft [27].

Moreover, recent findings have shown increased dd-cfDNA levels in recipients without signs of acute rejection and with verified graft vasculopathy [29].

Beyond its diagnostic value in detecting acute and chronic rejection, elevated dd-cfDNA has also been associated with the formation of donor-specific antibodies

(DSA), suggesting that subclinical graft injury may predispose to DSA formation, revealing a potential unique risk factor for sensitization [30].

MIRNAS

MicroRNAs (miRNAs, miR) are short (19–25 nucleotides), single-stranded, non-coding RNA molecules. The human genome encodes about 2,200 distinct miRs. MiRs can suppress protein synthesis by blocking translation of matrix RNA into proteins or accelerating their degradation. Because each miRNA typically controls multiple transcripts, they operate in interconnected "miR networks" that modulate entire biological pathways. Many miRs are organ- and tissue-specific, and their circulating levels are stable. These features make circulating miRNAs attractive non-invasive biomarkers for tracking post-transplant complications in solid-organ recipients [31].

Nováková T. et al. examined 11 miRNAs in biopsy samples and found that miR-144, miR-589, and miR-182 were significantly dysregulated in patients with verified acute TCMR compared with those without rejection [32].

In our previous studies, plasma levels of miR-101 and miR-27 were strong predictors of acute TCMR. Expression below the preset threshold conferred a relative risk (RR) of 1.77 ± 0.16 for miR-101 (95% CI 1.30–2.42; p = 0.0003) and RR = 1.59 ± 0.18 for miR-27 (95% CI 1.11–2.26; p = 0.011) [33].

Elevated plasma levels of miR-27 and miR-339 were associated with post-transplant myocardial fibrosis, with RR of 1.50 ± 0.16 (95% CI 1.10–2.04; p = 0.009) and 1.31 ± 0.13 (95% CI 1.02–1.69; p = 0.036), respectively [34].

Combining miRNA profiling with protein biomarkers such as ST2 and galectin-3 markedly enhanced overall diagnostic performance [35].

Analysis of 26 circulating microRNAs in HT recipients has shown that serum miR-144 levels rise in parallel with episodes of acute cellular rejection, including mild rejection graded 1R by the 2004 ISHLT criteria [36]. Diagnostic performance improves further when miR-144 is combined with miR-652, outperforming either marker alone for identifying acute cellular rejection [37].

Recent studies showing successful targeted inhibition of specific microRNAs suggest that these molecules could become therapeutic targets for slowing or preventing graft pathology in solid-organ transplant recipients.

In a porcine model of ischemia–reperfusion injury, Hinkel R. et al. demonstrated that intracoronary delivery of an antimiR-21 oligonucleotide markedly improved cardiac function while attenuating myocardial fibrosis and hypertrophy. RNA-sequencing and histological analyses confirmed lowered miR-21 expression and a reduced macrophage and fibroblast burden within the injured myocardium [38].

In a murine HT model, Lu J. et al. used an anti-miR-146a oligonucleotide to silence miR-146a. This intervention boosted autophagy in regulatory T cells, thereby strengthening their suppression of $CD4^+$ T cells and dendritic cells and, collectively, significantly ameliorated acute allograft rejection [39].

OTHER DIRECTIONS

Anti-HLA antibodies

Major histocompatibility complex molecules HLA class I (A, B and C) are expressed on all nucleated cells, while class II molecules (DPA1, DPB1, DQA1, DQB1, DRA, and DRB1) are primarily found on antigen-presenting cells, B cells, and endothelial cells. Among these, HLA-A, HLA-B, and HLA-DR are the most relevant for donor-recipient matching in organ transplantation.

Prior organ transplants, blood transfusions, implantation of circulatory assist devices, or pregnancy can lead to the formation of anti-HLA antibodies. The presence and level of these antibodies in transplant candidates are commonly assessed using panel-reactive antibody (PRA) testing. Elevated pre-transplant PRA levels are associated with an increased risk of adverse transplant outcomes [40].

The study by Sciaccaluga C. et al. evaluated the prognostic value of anti-HLA antibody detection in relation to acute graft rejection and graft vasculopathy in HT recipients. It was found that the presence of circulating anti-HLA antibodies was associated with early, mild graft dysfunction – even in the absence of verified antibody-mediated rejection or verified graft vasculopathy [41].

Donor-specific antibodies

Donor-specific antibodies (DSAs) are proteins produced by the recipient's immune system that specifically recognize and bind to donor antigens, triggering complement activation and leading to graft injury. The *de novo* formation of DSAs following heart transplantation is considered a major risk factor for the onset of antibody-mediated rejection (AMR) and is associated with poor clinical outcomes. Circulating DSAs are frequently detected in heart recipients experiencing AMR, with higher antibody titers correlating with more severe forms of rejection [42].

Moreno J.D. et al. showed elevated titers of antibodies against angiotensin II type 1 receptor (AT1R-Ab) in HT recipients with graft dysfunction. The study suggests that combining standard immunosuppressive therapy with angiotensin receptor blockers may enhance treatment efficacy in cases of AMR [43].

In the early post-transplant period, the presence of anti-endothelial cell antibodies (AECAs) has been associated with an increased risk of acute allograft rejection in cardiac recipients. Furthermore, studies have shown a correlation between the presence of antibodies targeting endothelial cytoskeletal proteins – such as vimentin,

actin, and tubulin – and a heightened risk of rejection episodes. Notably, HT recipients with diagnosed graft vasculopathy within the first five years post-transplantation exhibited significantly elevated anti-vimentin antibody titers [44].

Extracellular vesicles

Extracellular vesicles (EVs) are small (typically up to 1000 nm), spherical, membrane-bound particles released into the extracellular environment, facilitating intercellular communication under both physiological and pathological conditions – including immune activation and inflammation. Due to their presence in various biological fluids and their cargo of nucleic acids, proteins, and lipids that mirror the molecular state of their parent cells, EVs have emerged as promising noninvasive biomarkers [45].

A study by Castellani C. et al. showed a significant increase in EV levels, along with a decrease in their diameter in HT recipients with acute TCMR and AMR compared to patients without signs of rejection. The authors identified specific surface markers on EVs that were characteristic of different types of rejection. For acute TCMR, markers included CD3, CD2, ROR1, SSEA-4, HLA-I, and CD41b, while EVs associated with AMR expressed HLA-II, CD326, CD19, CD25, CD20, ROR1, SSEA-4, HLA-I, and CD41b [46].

In a study by Hu R.W. et al., donor-derived extracellular vesicles were isolated from the blood of heart recipients using antibodies targeting donor HLA class I molecules. The study found that during episodes of acute AMR, these donor EVs exhibited surface expression of the complement protein C4d – a hallmark of antibody-mediated injury. Expression of C4d on donor EVs subsided following successful treatment of the rejection episode [47].

Another study analyzed the concentration of EVs expressing tetraspanin, platelet, and endothelial markers in the plasma of HT recipients in the long-term post-transplant period (more than three years). It was found that the level of $CD90^{+}$ microvesicles was significantly higher in recipients without signs of acute rejection compared to those with biopsy-confirmed evidence of transplant rejection [48].

CONCLUSION

In recent years, numerous studies have demonstrated the effectiveness of novel molecular diagnostic approaches in verifying and predicting rejection episodes in HT recipients. These methods include the assessment of genomic, transcriptomic, and proteomic biomarkers. Implementation of such molecular diagnostics holds the potential to significantly improve long-term outcomes by enabling early detection of post-transplant complications [49].

However, despite the growing body of research in the field of noninvasive diagnostics for HT rejection, only a limited number of molecular tests have been integrated into clinical practice. This is largely due to the absence of standardized protocols and methodological limitations, such as small patient cohorts. To ensure the reproducibility, standardization, and clinical relevance of these diagnostic tools, large-scale, randomized multicenter studies are needed [50].

The study of molecular diagnostic methods for HT rejection not only enhances diagnostic accuracy and reduces reliance on invasive procedures, but also deepens our understanding of the regulatory mechanisms involved in acute TCMR and AMR. This, in turn, may pave the way for the development of novel therapeutic strategies [51].

Based on these findings, the creation of multimodal diagnostic panels appears particularly promising. These panels could integrate multiple noninvasive techniques – such as gene expression profiling, measurement of donor-derived cell-free DNA, and circulating microRNAs – to improve the detection of post-transplant complications in heart recipients [52]. Furthermore, the personalized selection of immunosuppressive therapy based on a combination of molecular-genetic, epigenetic, and clinical parameters has the potential to significantly enhance both the duration and quality of life in HT patients.

The authors declare no conflict of interest.

REFERENCES

1. *Gautier SV.* Transplantologiya: itogi i perspektivy. Tom XV. 2023 god. M.–Tver': Triada, 2024; 320.
2. *Singh TP, Cherikh WS, Hsich E, Lewis A, Perch M, Kian S et al.* Graft survival in primary thoracic organ transplant recipients: A special report from the International Thoracic Organ Transplant Registry of the International Society for Heart and Lung Transplantation. *J Heart Lung Transplant*. 2023 Oct; 42 (10): 1321–1333. doi: 10.1016/j.healun.2023.07.017.
3. *Wu MY, Ali Khawaja RD, Vargas D.* Heart Transplantation: Indications, Surgical Techniques, and Complications. *Radiol Clin North Am*. 2023 Sep; 61 (5): 847–859. doi: 10.1016/j.rcl.2023.04.011.
4. *Fitzsimons SJ, Evans JDW, Rassl DM, Lee KK, Strachan FE, Parameshwar J et al*. High-sensitivity Cardiac Troponin Is Not Associated With Acute Cellular Rejection After Heart Transplantation. *Transplantation*. 2022 May 1; 106 (5): 1024–1030. doi: 10.1097/TP.0000000000003876.
5. *Zhu V, Perry LA, Plummer M, Segal R, Smith J, Liu Z.* Diagnostic accuracy of brain natriuretic peptide and N-terminal-pro brain natriuretic peptide to detect complications of cardiac transplantation in adults: A systematic review and meta-analysis. *Transplant Rev (Orlando)*. 2023 Jul; 37 (3): 100774. doi: 10.1016/j.trre.2023.100774.
6. *Suspitsin EN, Raupov RK, Kuchinskaya EM, Kostik MM.* Analysis of interferon type I signature for differential diagnosis of diseases of the immune system (review of literature). *Klinicheskaya Laboratornaya Diagnostika (Russian Clinical Laboratory Diagnostics)*. 2021; 66

(5): 279–284. (in Russ.). https://doi.org/10.51620/0869-2084-2021-66-5-279-284.
7. *Mihajlov AM, Karavaj MF, Sivcov VA, Kurnikova MA*. Mashinnoe obuchenie dlya diagnostiki zabolevanij po polnomu profilyu ekspressii genov. *Avtomatika i telemekhanika*. 2023; (7): 83–92.
8. *Alieva AM, Teplova NV, Kislyakov VA, Valiev RK, Rahaev AM, Saryev MN et al*. Vnekletochnaya DNK i serdechno-sosudistye zabolevaniya. *RMZh*. 2022; 5: 26–29.
9. *Stonogina DA, Zhelankin AV, Vasiliev SV, Generozov EV, Akselrod AS*. Diagnostic capabilities of circulating microRNA profiles in patients with acute coronary syndrome and stable coronary artery disease. *Russian Journal of Cardiology and Cardiovascular Surgery*. 2024; 17 (2): 125–132. (In Russ.). https://doi.org/10.17116/kardio202417021125.
10. *Villaseñor-Altamirano AB, Balderas-Martínez YI, Medina-Rivera A.* Chapter 8 – Review of gene expression using microarray and RNA-seq. *Rigor and Reproducibility in Genetics and Genomics: Peer-reviewed, Published, Cited (Translational and Applied Genomics).* Eds: D.F. Dluzen, M.H.M. Schmidt. Academic Press, 2024: 159–187. https://doi.org/10.1016/B978-0-12-817218-6.00008-5.
11. *Kobashigawa J, Patel J, Azarbal B, Kittleson M, Chang D, Czer L et al.* Randomized pilot trial of gene expression profiling versus heart biopsy in the first year after heart transplant: early invasive monitoring attenuation through gene expression trial. *Circ Heart Fail*. 2015 May; 8 (3): 557–564. https://doi.org/10.1161/CIRCHEARTFAILURE.114.001658.
12. *Horwitz PA, Tsai EJ, Putt ME, Gilmore JM, Lepore JJ, Parmacek MS et al.* Detection of cardiac allograft rejection and response to immunosuppressive therapy with peripheral blood gene expression. *Circulation*. 2004 Dec 21; 110 (25): 3815–3821.
13. *Deng MC, Eisen HJ, Mehra MR, Billingham M, Marboe CC, Berry G et al.* Noninvasive discrimination of rejection in cardiac allograft recipients using gene expression profiling. *Am J Transplant*. 2006 Jan; 6 (1): 150–160.
14. *Fang KC.* Clinical utilities of peripheral blood gene expression profiling in the management of cardiac transplant patients. *J Immunotoxicol.* 2007 Jul; 4 (3): 209–217.
15. *Deng MC.* The AlloMap™ genomic biomarker story: 10 years after. *Clin Transplant*. 2017 Mar; 31 (3): e12900. https://doi.org/10.1111/ctr.12900.
16. *Shannon CP, Hollander Z, Dai DLY, Chen V, Assadian S, Lam KK et al.* HEARTBiT: A transcriptomic signature for excluding acute cellular rejection in adult heart allograft patients. *Can J Cardiol*. 2020 Aug; 36 (8): 1217–1227.
17. *Loupy A, van Huyen JPD, Hidalgo L, Reeve J, Racapé M, Aubert O et al.* Gene expression profiling for the identification and classification of antibody-mediated heart rejection. *Circulation*. 2017 Mar 7; 135 (10): 917–935. https://doi.org/10.1161/CIRCULATIONAHA.116.022907.
18. *Afzali B, Chapman E, Racapé M, Adam B, Bruneval P, Gil F et al.* Molecular assess ment of microcirculation injury in formalin-fixed human cardiac allograft biopsies with antibody-mediated rejection. *Am J Transplant.* 2017 Feb; 17 (2): 496–505. https://doi.org/10.1111/ ajt.13956.
19. *Tarazon E, Perez-Carrillo L, Garcia-Bolufer P, Triviño JC, Feijóo-Bandín S, Lago F et al.* Circulating mitochondrial genes detect acute cardiac allograft rejection: role of the mitochondrial calcium uniporter complex. *Am J Transplant*. 2021 Jun; 21 (6): 2056–2066.
20. *Deuse T, Hu X, Agbor-Enoh S, Koch M, Spitzer MH, Gravina A et al. De novo* mutations in mitochondrial DNA of iPSCs produce immunogenic neoepitopes in mice and humans. *Nat Biotechnol*. 2019 Oct; 37 (10): 1137–1144.
21. *Shah P, Valantine HA, Agbor-Enoh S.* Transcriptomics in transplantation: more than just biomarkers of allograft rejection. *Am J Transplant*. 2021 Jun; 21 (6): 2000–2001.
22. *Lo YMD, Han DSC, Jiang P, Chiu RWK.* Epigenetics, fragmentomics, and topology of cell-free DNA in liquid biopsies. *Science*. 2021 Apr 9; 372 (6538): eaaw3616. doi: 10.1126/science.aaw3616.
23. *Khush KK, Patel J, Pinney S, Kao A, Alharethi R, DePasquale E et al*. Noninvasive detection of graft injury after heart transplant using donor-derived cell-free DNA: A prospective multicenter study. *Am J Transplant*. 2019 Oct; 19 (10): 2889–2899. doi: 10.1111/ajt.15339.
24. *Snyder TM, Khush KK, Valantine HA, Quake SR.* Universal noninvasive detection of solid organ transplant rejection. *Proc Natl Acad Sci USA*. 2011 Apr 12; 108 (15): 6229–6234. doi: 10.1073/pnas.1013924108.
25. *Sorbini M, Togliatto GM, Simonato E, Boffini M, Cappuccio M, Gambella A et al*. HLA-DRB1 mismatch-based identification of donor-derived cell free DNA (dd-cfDNA) as a marker of rejection in heart transplant recipients: A single-institution pilot study. *J Heart Lung Transplant*. 2021 Aug; 40 (8): 794–804. doi: 10.1016/j.healun.2021.05.001.
26. *Knüttgen F, Beck J, Dittrich M, Oellerich M, Zittermann A, Schulz U et al*. Graft-derived Cell-free DNA as a Noninvasive Biomarker of Cardiac Allograft Rejection: A Cohort Study on Clinical Validity and Confounding Factors. *Transplantation*. 2022 Mar 1; 106 (3): 615–622. doi: 10.1097/TP.0000000000003725.
27. *Agbor-Enoh S, Shah P, Tunc I, Hsu S, Russell S, Feller E et al*. Cell-Free DNA to Detect Heart Allograft Acute Rejection. *Circulation*. 2021 Mar 23; 143 (12): 1184–1197. doi: 10.1161/CIRCULATIONAHA.120.049098.
28. *De Vlaminck I, Valantine HA, Snyder TM, Strehl C, Cohen G, Luikart H et al*. Circulating cell-free DNA enables noninvasive diagnosis of heart transplant rejection. *Sci Transl Med*. 2014 Jun 18; 6 (241): 241ra77. doi: 10.1126/scitranslmed.3007803.
29. *Holzhauser L, Clerkin KJ, Fujino T, Alenghat FJ, Raikhelkar J, Kim G et al*. Donor-derived cell-free DNA is associated with cardiac allograft vasculopathy. *Clin Transplant*. 2021 Mar; 35 (3): e14206. doi: 10.1111/ctr.14206.
30. *DePasquale EC, Kobashigawa J, Hall S, Wolf-Doty T, Teuteberg J, Khush KK.* Donor derived cell free DNA as a risk factor for initiating de-novo donor specific antibo-

dies in heart transplantation. *J Heart Lung Transplant.* 2021 Apr; 40 (4): S217–S218.
31. *Shah P, Bristow MR, Port JD*. MicroRNAs in Heart Failure, Cardiac Transplantation, and Myocardial Recovery: Biomarkers with Therapeutic Potential. *Curr Heart Fail Rep*. 2017 Dec; 14 (6): 454–464. doi: 10.1007/s11897-017-0362-8.
32. *Nováková T, Macháčková T, Novák J, Hude P, Godava J, Žampachová V et al*. Identification of a Diagnostic Set of Endomyocardial Biopsy microRNAs for Acute Cellular Rejection Diagnostics in Patients after Heart Transplantation Using Next-Generation Sequencing. *Cells*. 2019 Nov 6; 8 (11): 1400. doi: 10.3390/cells8111400.
33. *Velikiy DA, Gichkun OE, Sharapchenko SO, Mozheiko NP, Kurabekova RM, Shevchenko OP*. Diagnostic value of miRNA-101 and miRNA-27 in acute heart transplant rejection. *Russian Journal of Transplantology and Artificial Organs*. 2020; 22 (4): 20–26. (In Russ.). https://doi.org/10.15825/1995-1191-2020-4-20-26.
34. *Shevchenko OP, Velikiy DA, Sharapchenko SO, Gichkun OE, Marchenko AV, Ulybysheva AA et al*. Diagnostic value of microRNA-27 and -339 in heart transplant recipients with myocardial fibrosis. *Russian Journal of Transplantology and Artificial Organs*. 2021; 23 (3): 73–81. (In Russ.). https://doi.org/10.15825/1995-1191-2021-3-73-81.
35. *Shevchenko O, Sharapchenko S, Gichkun O, Velikiy D, Mozheiko N, Makarova L et al*. Diagnostic value of microRNA-27, microRNA-101 and ST2 for heart transplant acute rejection. *Clinica Chimica Acta*. 2022; 530: S452.
36. *Pérez-Carrillo L, Sánchez-Lázaro I, Triviño JC, Feijóo-Bandín S, Lago F, González-Juanatey JR et al*. Diagnostic value of serum miR-144-3p for the detection of acute cellular rejection in heart transplant patients. *J Heart Lung Transplant*. 2022 Feb; 41 (2): 137–147. doi: 10.1016/j.healun.2021.10.004.
37. *Pérez-Carrillo L, Sánchez-Lázaro I, Triviño JC, Feijóo-Bandín S, Lago F, González-Juanatey JR et al*. Combining Serum miR-144-3p and miR-652-3p as Potential Biomarkers for the Early Diagnosis and Stratification of Acute Cellular Rejection in Heart Transplantation Patients. *Transplantation*. 2023 Sep 1; 107 (9): 2064–2072. doi: 10.1097/TP.0000000000004622.
38. *Hinkel R, Ramanujam D, Kaczmarek V, Howe A, Klett K, Beck C et al*. AntimiR-21 Prevents Myocardial Dysfunction in a Pig Model of Ischemia/Reperfusion Injury. *J Am Coll Cardiol*. 2020 Apr 21; 75 (15): 1788–1800. doi: 10.1016/j.jacc.2020.02.041.
39. *Lu J, Liu Y, Wang W, Li P, Qi F.* Knockdown of miR-146a in regulatory T cells suppresses heart transplantation rejection in mice by increasing autophagy. *Transpl Immunol*. 2021 Apr; 65: 101372. doi: 10.1016/j.trim.2021.101372.
40. *Gavroy B, Timmermans T, Van Caenegem O, Mastrobuoni S, Jacquet L, Latinne D, Poncelet AJ.* Significance of HLA-matching and anti-HLA antibodies in heart transplant patients receiving induction therapy? *Transpl Immunol*. 2022 Dec; 75: 101706. doi: 10.1016/j.trim.2022.101706.
41. *Sciaccaluga C, Natali BM, Righini FM, Sorini Dini C, Landra F, Mandoli GE et al*. Heart transplantation and anti-HLA antibodY: myocardial dysfunction and prognosis – HeartLAy study. *ESC Heart Fail*. 2023 Oct; 10 (5): 2853–2864. doi: 10.1002/ehf2.14442.
42. *Kobashigawa J, Colvin M, Potena L, Dragun D, Crespo-Leiro MG, Delgado JF et al*. The management of antibodies in heart transplantation: An ISHLT consensus document. *J Heart Lung Transplant*. 2018 May; 37 (5): 537–547. doi: 10.1016/j.healun.2018.01.1291.
43. *Moreno JD, Verma AK, Kopecky BJ, Dehner C, Kostelecky N, Vader JM et al*. Angiotensin II Type 1 Receptor Antibody-mediated Rejection Following Orthotopic Heart Transplant: A Single-center Experience. *Transplantation*. 2022 Feb 1; 106 (2): 373–380. doi: 10.1097/TP.0000000000003712.
44. *Nair N.* Vascular rejection in cardiac allograft vasculopathy: Impact on graft survival. *Front Cardiovasc Med*. 2022 Aug 4; 9: 919036. doi: 10.3389/fcvm.2022.919036.
45. *Giarraputo A, Barison I, Fedrigo M, Burrello J, Castellani C, Tona F et al*. A Changing Paradigm in Heart Transplantation: An Integrative Approach for Invasive and Non-Invasive Allograft Rejection Monitoring. *Biomolecules*. 2021 Feb 1; 11 (2): 201. doi: 10.3390/biom11020201.
46. *Castellani C, Burrello J, Fedrigo M, Burrello A, Bolis S, Di Silvestre D et al*. Circulating extracellular vesicles as non-invasive biomarker of rejection in heart transplant. *J Heart Lung Transplant*. 2020 Oct; 39 (10): 1136–1148. doi: 10.1016/j.healun.2020.06.011.
47. *Hu RW, Korutla L, Reddy S, Harmon J, Zielinski PD, Bueker A et al*. Circulating Donor Heart Exosome Profiling Enables Noninvasive Detection of Antibody-mediated Rejection. *Transplant Direct*. 2020 Oct 19; 6 (11): e615. doi: 10.1097/TXD.0000000000001057.
48. *Korneva LO, Osipova MA, Borcova MA, Musaeva BB, Simonenko MA, Akino AD et al*. Uroven' nekotoryh mikrovezikul u pacientov s ottorzheniem serdechnogo transplantata. *Rossijskij kardiologicheskij zhurnal*. 2024; 29 (S8): 307.
49. *Qian X, Shah P, Agbor-Enoh S*. Noninvasive biomarkers in heart transplant: 2020–2021 year in review. *Curr Opin Organ Transplant*. 2022 Feb 1; 27 (1): 7–14. doi: 10.1097/MOT.0000000000000945.
50. *Khachatoorian Y, Khachadourian V, Chang E, Sernas ER, Reed EF, Deng M et al*. Noninvasive biomarkers for prediction and diagnosis of heart transplantation rejection. *Transplant Rev (Orlando)*. 2021 Jan; 35 (1): 100590. doi: 10.1016/j.trre.2020.100590.
51. *Benck L, Sato T, Kobashigawa J.* Molecular Diagnosis of Rejection in Heart Transplantation. *Circ J*. 2022 Jun 24; 86 (7): 1061–1067. doi: 10.1253/circj.CJ-21-0591.
52. *Holzhauser L, DeFilippis EM, Nikolova A, Byku M, Contreras JP, De Marco T et al*. The End of Endomyocardial Biopsy?: A Practical Guide for Noninvasive Heart Transplant Rejection Surveillance. *JACC Heart Fail*. 2023 Mar; 11 (3): 263–276. doi: 10.1016/j.jchf.2022.11.002.

The article was submitted to the journal on 12.03.2025

DOI: 10.15825/1995-1191-2025-2-179-188

ASSOCIATION OF PLASMA TGF-β1 LEVELS WITH POLYMORPHIC LOCI AND *TGFB1* HAPLOTYPES RS1800469 AND RS1800470 IN PEDIATRIC LIVER TRANSPLANT RECIPIENTS

R.M. Kurabekova[1], O.M. Tsirulnikova[1, 2], O.E. Gichkun[1, 2], I.E. Pashkova[1], O.P. Shevchenko[1, 2]

[1] Shumakov National Medical Research Center of Transplantology and Artificial Organs, Moscow, Russian Federation

[2] Sechenov University, Moscow, Russian Federation

Objective: to investigate the association between plasma TGF-β1 levels in pediatric liver transplant (LT) recipients, both pre- and post-transplantation, and the polymorphic alleles and haplotypes at rs1800469 and rs1800470 loci of the *TGFB1* gene. **Materials and methods.** The study cohort comprised 135 pediatric LT recipients, aged 3 to 98.4 months (mean age 8.2 years, median 8 months). The control group consisted of 77 healthy individuals, aged 30.3 ± 5.2 years. Plasma TGF-β1 levels were quantified using ELISA. Genomic DNA from participants was analyzed for the polymorphic loci rs1800469 and rs1800470 of the *TGFB1* gene using real-time polymerase chain reaction PCR with TaqMan probes. **Results.** Blood TGF-β1 level in pediatric LT recipients pre-transplant was 4.6 (1.1–9.5) ng/mL. One month post-transplant, cytokine level increased to 6.3 (1.7–15.0) ng/mL (p = 0.008), and after one year, it rose further to 7.0 (1.9–13.5) ng/mL (p = 0.0001). Healthy adults had significantly higher TGF-β1 levels, with a median of 11.7 (6.4–16.9) ng/mL (p = 0.0000), compared to pediatric recipients. The distribution frequencies of the rs1800469 and rs1800470 polymorphic alleles in pediatric LT recipients did not significantly differ from those in healthy individuals. However, the occurrence of rare haplotypes (T-T and C-C) was significantly higher in pediatric recipients. Before transplantation and 1 month after the procedure, TGF-β1 levels in pediatric recipients were not associated with the carriage of the studied alleles or haplotypes. However, at 1-year post-transplant, higher TGF-β1 levels in pediatric recipients were significantly associated with the major alleles (C/C + C/T) of rs1800469 and the rs1800470 T/T genotype, as well as with the T-T haplotype. In healthy individuals, TGF-β1 levels were not influenced by the rs1800469 and rs1800470 alleles individually, but high cytokine levels were associated with the C-C haplotype. **Conclusion.** In pediatric LT recipients, elevated TGF-β1 levels at 1-year post-transplant are associated with the presence of the major alleles C (rs1800469) and T (rs1800470), as well as the T-T haplotype of the *TGFB1* gene. This suggests that these polymorphic loci may influence the development of post-transplant complications and could potentially serve as biomarkers for predicting clinical outcomes in LT.

Keywords: single nucleotide polymorphism, profibrogenic cytokine, congenital liver diseases, biliary atresia and hypoplasia/

INTRODUCTION

Liver transplantation is generally considered the only effective treatment for young children with end-stage liver failure, whether caused by congenital or acquired liver diseases. Overall posttransplant survival currently exceeds 85% at 5 years [1, 2]. To further improve treatment outcomes, it is crucial to enhance the prediction and diagnosis of post-transplant complications, which can be achieved through the use of minimally invasive molecular genetic markers.

One promising candidate is transforming growth factor β1 (TGF-β1), a multifunctional cytokine with immunosuppressive and profibrogenic properties. The level of TGF-β1 has been associated with graft dysfunction, infectious complications, and variations in the immunosuppression regimen in pediatric liver transplant (LT) recipients, making it a potential biomarker for monitoring the clinical status of these patients [3–5].

TGF-β1 is synthesized in almost all tissues, and its effects vary depending on its concentration and the cell type involved. Low levels of TGF-β1 are believed to promote inflammation, whereas high levels can lead to tissue fibrosis [6, 7]. Regulation of this cytokine is influenced by multiple factors and interactions, including the cellular TGF-β signaling pathway, which comprises a family of ligands and their transmembrane receptors and interacts with other cellular pathways such as SMAD

Corresponding author: Rivada Kurabekova. Address: 1, Shchukinskaya str., Moscow, 123182, Russian Federation. Phone: (499) 190-53-41. E-mail: kourabr@yandex.ru

and Notch [8, 9]. Additionally, TGF-β1 secretion may be influenced by polymorphisms in the *TGFB1* gene. To date, eight single nucleotide polymorphisms (SNPs) have been identified that may affect TGF-β1 production and have been associated with various diseases, including liver diseases [10, 11].

A review of the literature suggests that two polymorphic loci, rs1800469 and rs1800470, are of particular significance in liver diseases [12–16]. The rs1800469 polymorphism involves a cytosine-to-thymine substitution (–509C>T) in the promoter region of the *TGFB1* gene, while the rs1800470 variant results from a thymine-to-cytosine substitution (+869T>C), leading to an amino acid change from leucine to proline in the TGF-β1 protein [17, 18].

To date, there is no definitive consensus regarding the effect of these loci on TGF-β1 production. It is suggested that the –509C>T substitution may either increase TGF-β1 levels or have no significant effect, while the +869T>C substitution is generally believed to enhance its secretion [19, 20]. *In vitro* experiments using HeLa cell cultures infected with various vectors showed increased TGF-β1 production when cells were infected with a construct carrying the minor C allele of rs1800470 [20]. However, it is known that regulation of TGF-β1 secretion in cancer cells differs substantially from that in normal cells [6–9].

Studies investigating the association between *TGFB1* genetic polymorphisms and plasma TGF-β1 levels in patients with liver disease have predominantly focused on adults with cirrhosis secondary to chronic hepatitis B or C infections and hepatic steatosis [21–24]. Plasma TGF-β1 concentrations in patients with liver disease are generally higher than in healthy individuals; however, findings regarding the relationship between TGF-β1 levels and specific polymorphic alleles have been inconsistent. For example, Mohy et al. [22], de Brito et al. [23], and Felicidade et al. [24] reported that elevated TGF-β1 levels were associated with the minor homozygous TT genotype of rs1800469, whereas Wang et al. [21] found that higher TGF-β1 levels correlated with the major alleles C (rs1800469) and T (rs1800470).

In young children with terminal liver failure caused by congenital or acquired liver diseases, TGF-β1 levels differ from those observed in healthy children and may correlate with the severity of liver fibrosis [3–5, 25]. However, no data are currently available regarding the extent to which blood cytokine levels are influenced by *TGFB1* gene polymorphisms. Our previous studies showed that distribution of the polymorphic alleles rs1800469, rs1800470, and rs1800471 of the *TGFB1* gene in young children with liver diseases did not differ significantly from that in healthy controls. However, the frequency of rare haplotypes at these loci was significantly higher in the group of pediatric patients listed for LT [26].

The aim of the present study was to assess the association between plasma TGF-β1 levels in pediatric LT candidates, both before and after transplantation, and the carriage of polymorphic alleles and haplotypes at the rs1800469 and rs1800470 loci of the *TGFB1* gene.

MATERIALS AND METHODS

The study included 135 children (59 boys and 76 girls) who underwent LT, aged between 3 and 98.4 months (mean age: 8.2 months; median: 8 months).

To evaluate the association between blood TGF-β1 levels and TGFB1 gene polymorphisms in healthy individuals, a comparison group consisting of 77 healthy adults (35 boys and 42 girls) with a mean age of 30.3 ± 5.2 years was used. Although cytokine levels are generally considered to be independent of age, the limited number of studies addressing this relationship report ambiguous results [3–5].

The indication for LT in the children was the end stage of liver disease resulting from various conditions, including biliary atresia (n = 74), biliary hypoplasia (n = 10), Alagille syndrome (n = 9), Caroli's disease (n = 10), and Byler's disease (n = 6). Additionally, 26 children had other rare liver disorders such as Crigler–Najjar syndrome, von Gierke disease, alpha-1 antitrypsin deficiency, tyrosinemia, fulminant hepatitis, autoimmune hepatitis, cryptogenic cirrhosis, and others.

Following transplantation, recipients received immunosuppressive therapy consisting of two or three agents: tacrolimus, mycophenolate, and corticosteroids. Examination and treatment protocols adhered to the clinical guidelines of the Russian Transplant Society and the protocols established by the Shumakov National Medical Research Center of Transplantology and Artificial Organs.

TGF-β1 levels in blood plasma was measured by quantitative enzyme-linked immunosorbent assay (ELISA) with a reagent kit from Bender MedSystems (Austria), following the manufacturer's instructions. Optical density was measured in microplate wells using a Zenyth 340r spectrophotometer (Biochrom Anthos, UK) at a wavelength of 450 nm. Cytokine levels were assessed at three time points: before transplantation, one month after transplantation, and one year after transplantation.

Polymorphic loci rs1800469 and rs1800470 of the TGFB1 gene were identified in genomic DNA using real-time polymerase chain reaction (PCR) with TaqMan probes (Applied Biosystems, USA) on a CFX96™ real-time PCR system (Bio-Rad, USA), following the manufacturer's instructions. The TaqMan probes used

for genotyping were C_8708473_10 for rs1800469 and C_22272997_10 for rs1800470. Genomic DNA was extracted from venous blood samples using the QIAamp DNA Blood Mini Kit (Qiagen, Germany) and the QIAcube™ automated analyzer (Qiagen, Germany), in accordance with the manufacturers' protocols.

Data were collected and initially processed using Microsoft Excel. Statistical analyses were performed using the STATISTICA software package (StatSoft Inc., USA). Quantitative variables are presented as mean ± standard deviation for parametric data, or as median and interquartile range (Q1–Q3) for nonparametric variables (with range excluding outliers shown in the graphs). Comparisons between two dependent groups were conducted using the Wilcoxon signed-rank test, while comparisons between two independent groups employed the Mann–Whitney U test. For comparisons among multiple independent groups, the Kruskal–Wallis test was used. Genotype and haplotype frequencies were analyzed using Fisher's exact test (p-value) via the SNPstats software. Differences were considered statistically significant at a p-value <0.05.

The study was approved by the Local Ethics Committee, Shumakov National Medical Research Center of Transplantology and Artificial Organs. Informed consent was obtained from all participants or their legal guardians and documented in the patients' medical records.

RESULTS

The median plasma TGF-β1 levels in pediatric LT recipients prior to transplantation was 4.6 ng/mL (interquartile range [IQR]: 1.1–9.5 ng/mL). One month after transplantation, the median TGF-β1 level significantly increased to 6.3 ng/mL (IQR: 1.7–15.0 ng/mL; p = 0.008). One year after transplantation, plasma TGF-β1 levels remained significantly higher compared to pre-transplant levels, reaching 7.0 ng/mL (IQR: 1.9–13.5 ng/mL; p = 0.0001) (Fig. 1).

The results of DNA genotyping for polymorphic alleles rs1800469 and rs1800470 of the TGFB1 gene in pediatric LT recipients are presented in Fig. 2, showing the distribution frequencies of different genotypes.

The frequency of occurrence of these SNP alleles in pediatric recipients did not differ significantly from that observed in healthy controls. In healthy adults, the genotype frequencies were as follows: for rs1800469 – 40% C/C, 44% C/T, and 16% T/T; for rs1800470 – 43% T/T, 40% T/C, and 17% C/C. Notably, plasma TGF-β1 level in healthy adults was 11.7 ng/mL (IQR: 6.4–16.9 ng/mL), which was significantly higher than the levels observed in pediatric liver recipients both before and after transplantation (p = 0.0000).

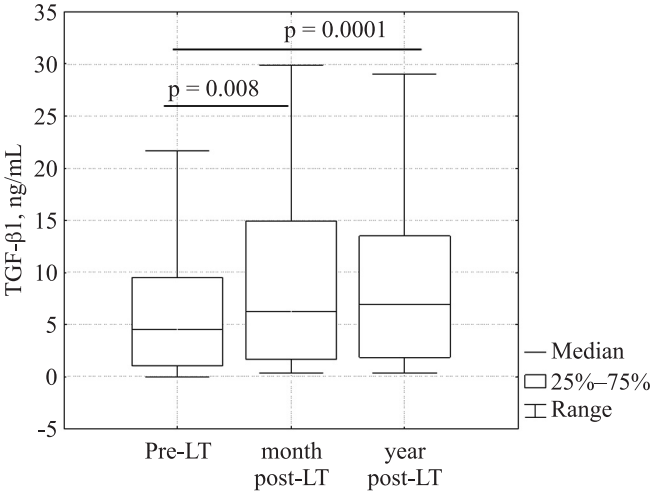

Fig. 1. Plasma TGF-β1 levels in pediatric liver transplant recipients measured before transplantation, one month after, and one year after transplantation

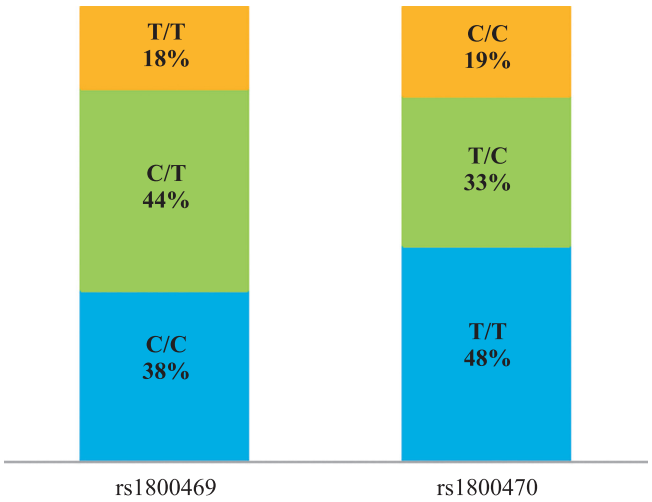

Fig. 2. Frequencies of polymorphic variants rs1800469 and rs1800470 of the TGFB1 gene in pediatric liver recipients

A comparative analysis of plasma TGF-β1 levels was conducted in pediatric recipients and healthy individuals across different genotypes of the rs1800469 polymorphism, considering the main genetic models of allelic interaction: codominant, dominant, recessive, and over dominant models. In pediatric recipients, TGF-β1 levels were assessed at three time points: before liver transplantation, one month post-transplant, and one year post-transplant. The results are illustrated in Fig. 3, using box plots showing the median, interquartile ranges (2nd–3rd quartiles), and the data range excluding outliers.

The results showed that plasma TGF-β1 levels in pediatric liver transplant recipients (PLTRs) with different genotypes of the rs1800469 polymorphic locus of the TGFB1 gene did not differ significantly either before or one month after LT. However, one year after transplantation, under the recessive model of allelic interaction,

carriers of the homozygous minor allele (T/T genotype) exhibited significantly lower TGF-β1 levels compared to carriers of the C/T and C/C genotypes (p = 0.045). In healthy individuals, TGF-β1 levels were found to be independent of the rs1800469 genotype (p > 0.05 in all comparisons).

Similarly, the TGF-β1 content in PLTRs with different genotypes of another TGFB1 polymorphism, rs1800470, was analyzed based on models of allelic gene interaction. The results are presented in Fig. 4.

Fig. 4 shows that TGF-β1 levels in the blood of PLTRs with different rs1800470 genotypes did not differ significantly before or one month after LT, similar to the findings for rs1800469. However, one year after transplantation, under the dominant model of allelic interaction, carriers of the homozygous major allele (T/T genotype) exhibited significantly higher TGF-β1 levels compared to carriers of the T/C and C/C genotypes (p = 0.039). In healthy individuals, TGF-β1 levels were independent of the rs1800470 genotype (p > 0.05 in all comparisons).

Fig. 5 presents the frequencies of haplotypes formed by the rs1800469 and rs1800470 polymorphic variants in PLTRs and healthy adult subjects

In both PLTRs and healthy adults, four haplotype variants were identified, with the most common being the C-T haplotype, which consists of the major alleles of both polymorphic loci. The second most frequent haplotype in healthy individuals was T-C, containing two minor alleles. The frequencies of the most common haplotypes did not differ significantly between recipients and healthy individuals. However, the occurrence of the T-T and C-C haplotypes was significantly higher in PLTRs compared to healthy adults (p = 0.007 and p = 0.021, respectively).

The results of the comparative analysis of TGF-β1 levels based on carriage of different haplotypes of the rs1800469 and rs1800470 polymorphic alleles in pediatric recipients and healthy adults are presented in Fig. 6.

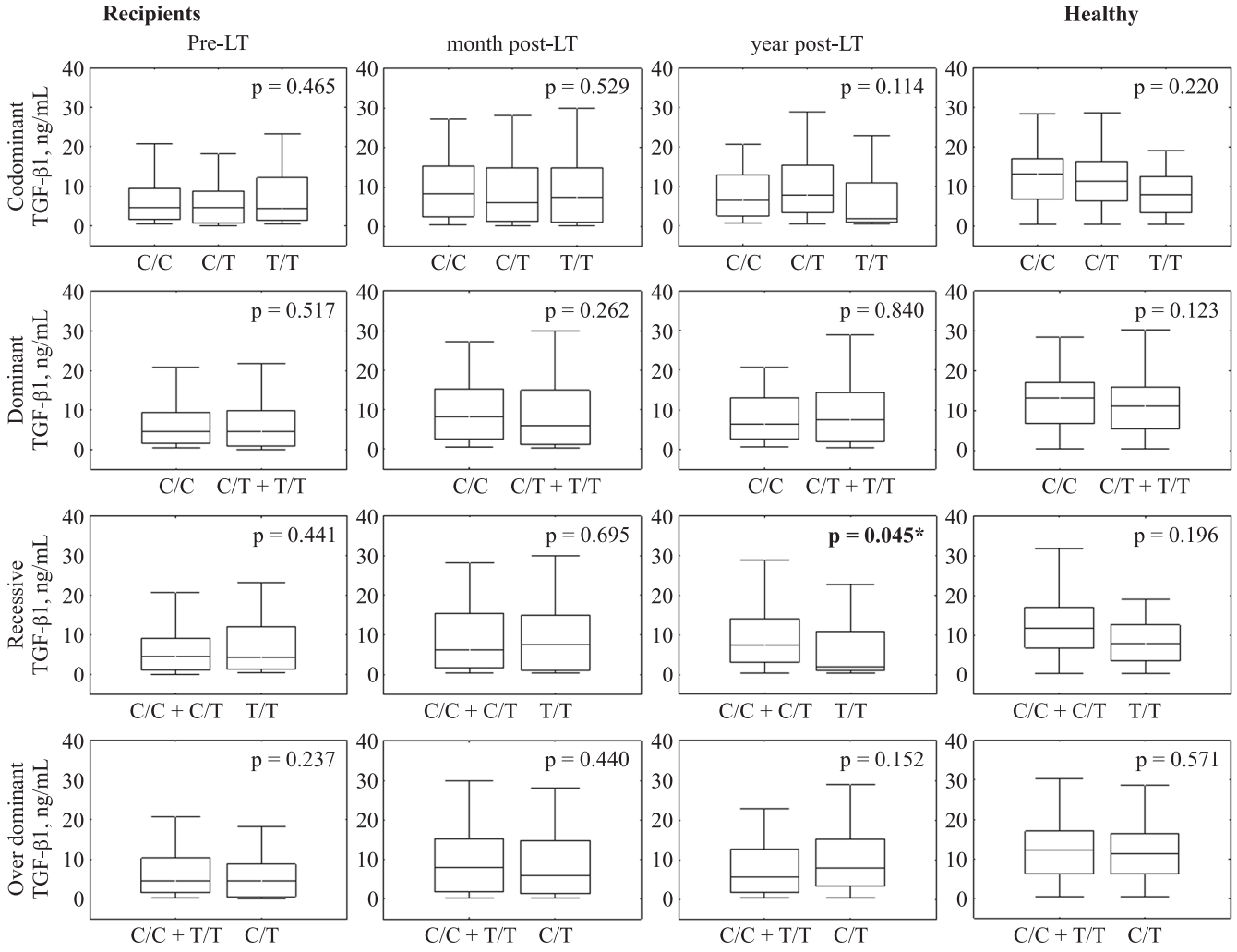

Fig. 3. Comparison of plasma TGF-β1 levels in pediatric liver transplant recipients measured before transplantation, one month after, and one year after transplantation, and in healthy adults, stratified by genotypes of the rs1800469 polymorphic allele of the TGFB1 gene, analyzed using allelic interaction models. p < 0.05

The results showed that TGF-β1 levels in the blood of PLTRs carrying different haplotypes did not differ significantly before LT or one month after LT. However, one year after LT, recipients carrying the haplotype consisting of two minor alleles (T-C) showed the lowest cytokine levels, which were significantly lower compared to recipients carrying the haplotype composed of a minor and a major allele (T-T) ($p = 0.019$).

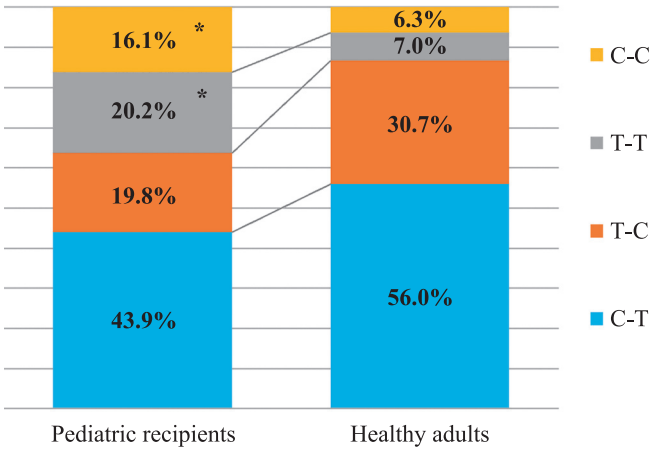

Fig. 5. Haplotype frequencies of the rs1800469 and rs1800470 polymorphic variants of the TGFB1 gene in pediatric liver transplant recipients and healthy adults. $p < 0.05$

In contrast, among healthy individuals, the lowest TGF-β1 levels were observed in carriers of the T-T haplotype, while the highest levels were found in carriers of the C-C haplotype ($p = 0.03$).

DISCUSSION

In PLTRs, TGF-β1 levels can vary significantly depending on the underlying disease etiology, degree of liver fibrosis, presence of post-transplant complications, immunosuppressive therapy regimen, and other factors [3–5]. However, the causal mechanisms underlying this variability remain poorly understood. In this study, we evaluated the extent to which plasma TGF-β1 levels may be associated with carriage of polymorphic loci and hap-

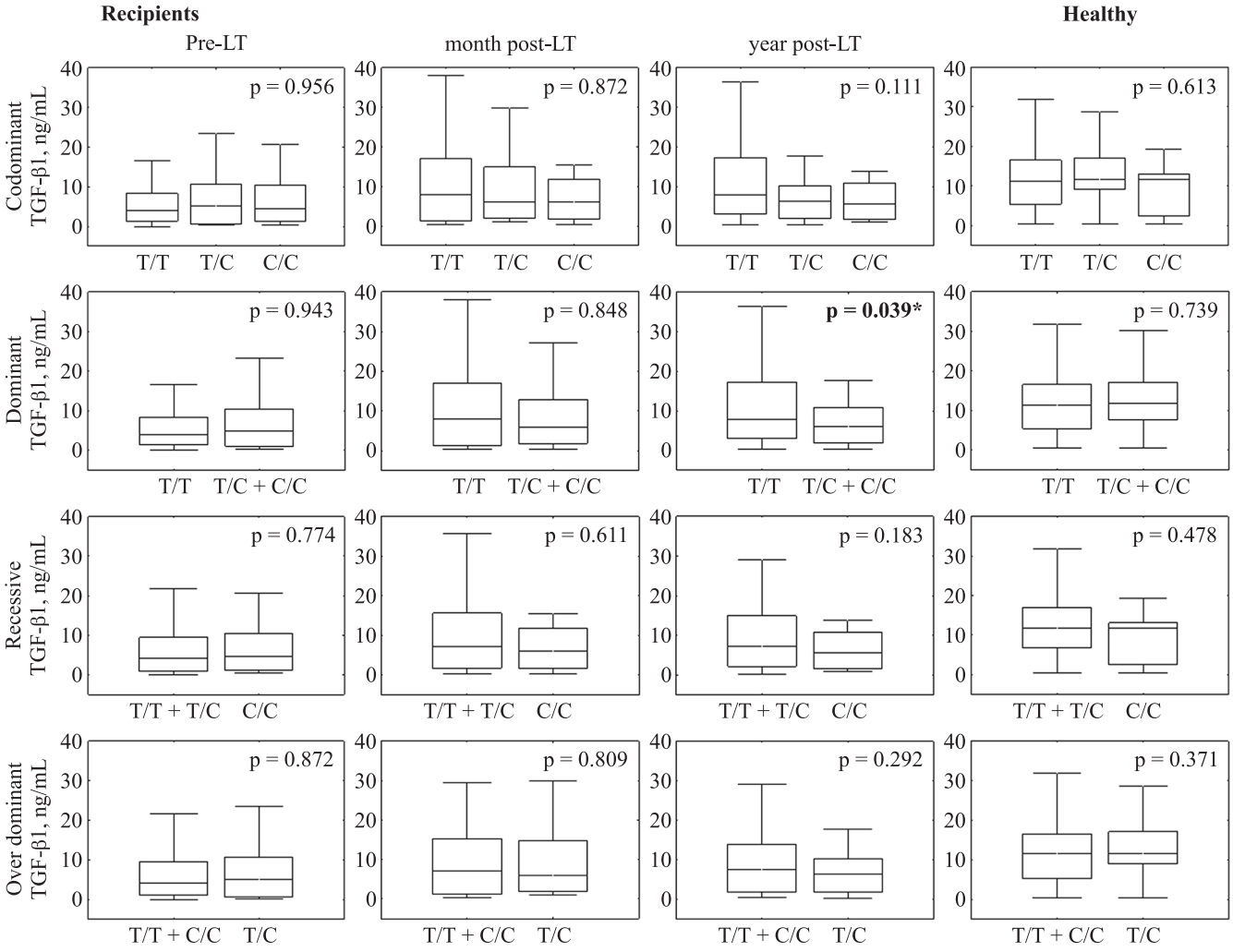

Fig. 4. Comparison of plasma TGF-β1 levels in pediatric liver transplant (LT) recipients measured before transplantation, one month after, and one year after transplantation, and in healthy adults, stratified by genotypes of the rs1800470 polymorphic allele of the TGFB1 gene, analyzed using allelic interaction models. $p < 0.05$

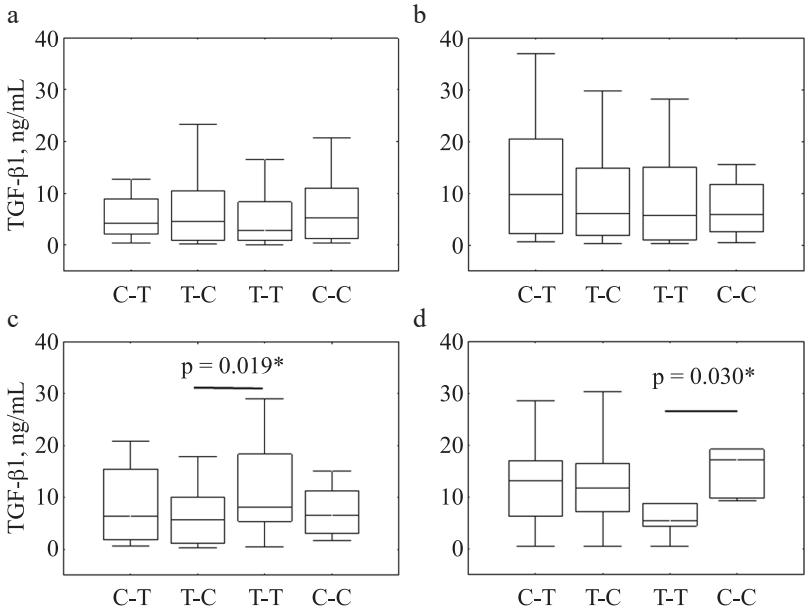

Fig. 6. TGF-β1 levels in pediatric liver recipients measured before (a), one month (b), and one year (c) after liver transplantation, as well as in healthy adults (d), stratified by haplotypes of the rs1800469–rs1800470 polymorphic variants of the TGFB1 gene. $p < 0.05$

lotypes (rs1800469 and rs1800470) of the TGFB1 gene in PLTRs.

LT was associated with a significant increase in TGF-β1 levels in pediatric recipients; however, cytokine concentrations did not reach those observed in healthy adults or, as shown previously, in healthy children of the same age group [5]. The distribution of the rs1800469 and rs1800470 polymorphic loci and their most common haplotypes (C-T and T-C) did not differ significantly between PLTRs and healthy individuals. In contrast, the rare haplotypes T-T and C-C were significantly more frequent among PLTRs than among healthy controls, corroborating previous findings [26] and suggesting a potential association between these rare haplotypes and the development of liver disease in PLTRs.

Comparison of TGF-β1 blood levels in PLTRs carrying different genotypes of the studied polymorphic loci and their haplotypes revealed no significant differences before or one month after LT. However, one year after LT, significant associations were observed: for rs1800469, carriage of the major allele (C/C + C/T) was associated with higher TGF-β1 levels, whereas carriers of the homozygous minor genotype (T/T) exhibited lower cytokine levels. Similarly, for rs1800470, the homozygous major genotype (T/T) was associated with higher, and carriage of the minor allele (T/C + C/C) with lower TGF-β1 levels.

Among pediatric recipients, carriers of the T-T haplotype (combining the minor allele of rs1800469 and the major allele of rs1800470) had higher TGF-β1 levels, while carriers of the T-C haplotype (both minor alleles) exhibited the lowest cytokine levels.

In healthy individuals, TGF-β1 levels did not differ significantly based on the individual carriage of rs1800469 or rs1800470 genotypes. However, differences emerged when rare haplotypes were analyzed: the C-C haplotype (major allele of rs1800469 and minor allele of rs1800470) was associated with higher, and the T-T haplotype with lower TGF-β1 levels – the opposite pattern compared to pediatric recipients.

These findings suggest that the T allele of rs1800469 may reduce, while the C allele of rs1800470 may enhance TGF-β1 production. The opposing effects of these polymorphisms may explain the relatively higher frequency of the T-C haplotype among healthy individuals, where the influence of the two variants appears to compensate each other, resulting in normal cytokine levels comparable to those associated with the major alleles.

The absence of differences in TGF-β1 levels in recipients before or one month after surgery can be attributed to the disruption of normal regulatory processes during these periods, which may be influenced by disease-related complications or drug therapies. It is also possible that, one year post-surgery, the patients' condition stabilizes, leading to partial normalization of TGF-β1 production regulation, despite the ongoing influence of immunosuppressive therapy. In healthy adults, cytokine regulation may differ significantly from that in pediatric recipients. For example, under normal conditions, TGF-β1 is produced by liver stellate cells at a basal le-

vel, with production increasing in response to activating factors [28].

Thus, our findings suggest that blood TGF-β1 levels in PLTRs may be influenced by the carriage of specific loci and haplotypes of the *TGFB1* gene, namely rs1800469 and rs1800470.

As mentioned in the introduction, no other studies have specifically examined the association between TGF-β1 levels and TGFB1 genetic polymorphism in PLTRs. When compared to data from adults with liver disease, our findings align with those of Chinese researchers [21] but differ from results observed in Brazilian and Egyptian populations [22–24]. Additionally, there are studies that did not find a significant association between cytokine levels and its gene polymorphism [12].

Interestingly, studies investigating the relationship between TGF-β1 levels and TGFB1 genetic polymorphism in other diseases also present mixed results. These studies can be divided into two groups: one group associates higher cytokine levels with the major alleles (C rs1800469 or T rs1800470) in diseases such as human papillomavirus infection [31], systemic lupus erythematosus [32], gastric adenocarcinoma [33], and rheumatoid arthritis [34], while the other group finds higher levels associated with the minor alleles (T rs1800469 and C rs1800470) in conditions like breast cancer [20, 29] and coronary artery ectasia [30].

The contradictory findings in these studies can be attributed to the pleiotropic nature of TGF-β1 cytokine, its complex regulation, variations in experimental designs, or differences in the ethnic backgrounds of the study populations. However, given the significant number of studies that have found an association between protein levels and gene polymorphisms, and the consistent division of results into two opposing trends (with high TGF-β1 levels being associated either with major or minor alleles), it is reasonable to assume that such an association exists. Yet, depending on various factors, this association could be either direct or inverse.

One such factor could be the stage of disease progression when TGF-β1 levels are measured. For example, cytokine levels may fluctuate significantly depending on the severity of liver fibrosis [5, 23]. An initially low or high cytokine production, which may contribute to the disease pathogenesis, could either increase or decrease over time, potentially reflecting the progression of the disease rather than causing it. Therefore, while the studies reviewed suggest an association between TGF-β1 levels and its gene polymorphism, they do not conclusively answer the question of causal relationships.

The retrospective nature of this study, its reliance on the case-control method, and the genetic heterogeneity of the sample may present certain limitations to the conclusions drawn. Most phenotypic traits are influenced by numerous genetic loci, making it challenging to isolate the contribution of a single locus. Additionally, the haplotype occurrence analysis performed in this study is approximate, as precise haplotype determination for heterozygous variants requires sequencing. Further research is necessary to confirm the findings presented here.

Despite these limitations, the results of this study suggest a potential association between blood TGF-β1 levels and carriage of polymorphic loci and haplotypes rs1800469 and rs1800470 of the TGFB1 gene. As a critical regulator of fibrosis and immune response, TGF-β1 may play a significant role in the regulation of protein levels in PLTRs. These findings open up new avenues for understanding protein regulation and may position the studied variants as potential prognostic markers for complications in PLTRs.

CONCLUSION

Elevated TGF-β1 levels in the blood of PLTRs one year after LT are associated with carriage of the major alleles – C rs1800469 and T rs1800470, as well as the T-T haplotype of the TGFB1 gene. This finding suggests that these polymorphic loci may influence the development of post-transplant complications, highlighting their potential use as predictive markers for transplant outcomes.

The authors declare no conflict of interest.

REFERENCES

1. *Gautier SV, Tsiroulnikova OM, Moysyuk YG, Akhaladze DG, Tsiroulnikova IE, Silina OV et al.* Liver transplantation in children: six-year experience analysis. *Russian Journal of Transplantology and Artificial Organs*. 2014; 16 (3): 54–62. (In Russ.). https://doi.org/10.15825/1995-1191-2014-3-54-62.
2. *Baumann U, Karam V, Adam R, Fondevila C, Dhawan A, Sokal E et al*. Prognosis of Children Undergoing Liver Transplantation: A 30-Year European Study. *Pediatrics.* 2022 Oct 1; 150 (4): e2022057424. doi: 10.1542/peds.2022-057424.
3. *Hussein MH, Hashimoto T, AbdEl-Hamid Daoud G, Kato T, Hibi M, Tomishige H et al*. Pediatric patients receiving ABO-incompatible living related liver transplantation exhibit higher serum transforming growth factor-beta1, interferon-gamma and interleukin-2 levels. *Pediatr Surg Int.* 2011 Mar; 27 (3): 263–268. doi: 10.1007/s00383-010-2784-1.
4. *Briem-Richter A, Leuschner A, Krieger T, Grabhorn E, Fischer L, Nashan B et al*. Peripheral blood biomarkers for the characterization of alloimmune reactivity after pediatric liver transplantation. *Pediatr Transplant.* 2013 Dec; 17 (8): 757–764. doi: 10.1111/petr.12161.

5. *Kurabekova R, Tsirulnikova O, Pashkova I, Gichkun O, Mozheyko N, Gautier S, Shevchenko O*. Transforming growth factor beta 1 levels in the blood of pediatric liver recipients: Clinical and biochemical correlations. *Pediatr Transplant.* 2020 May; 24 (3): e13693. doi: 10.1111/petr.13693.
6. *Leask A, Abraham DJ*. TGF-beta signaling and the fibrotic response. *FASEB J.* 2004 May; 18 (7): 816–827. doi: 10.1096/fj.03-1273rev.
7. *Kajdaniuk D, Marek B, Borgiel-Marek H, Kos-Kudla B*. Transforming growth factor β1 (TGFβ1) in physiology and pathology. *Endokrynol Pol.* 2013; 64 (5): 384–396. doi: 10.5603/EP.2013.0022.
8. *Braczkowski MJ, Kufel KM, Kulińska J, Czyż D, Dittmann A, Wiertelak M et al.* Pleiotropic Action of TGF-Beta in Physiological and Pathological Liver Conditions. *Biomedicines*. 2024 Apr 22; 12 (4): 925. doi: 10.3390/biomedicines12040925.
9. *Bakalenko N, Kuznetsova E, Malashicheva A*. The Complex Interplay of TGF-β and Notch Signaling in the Pathogenesis of Fibrosis. *Int J Mol Sci.* 2024 Oct 8; 25 (19): 10803. doi: 10.3390/ijms251910803.
10. *Martelossi Cebinelli GC, Paiva Trugilo K, Badaró Garcia S, Brajão de Oliveira K*. TGF-β1 functional polymorphisms: a review. *Eur Cytokine Netw.* 2016 Nov 1; 27 (4): 81–89. doi: 10.1684/ecn.2016.0382.
11. *Fang J, Liu ZW, Han QY*. [Polymorphism of codon25 in signal peptide region of transforming growth factor beta 1 and its association with chronic hepatitis C virus infection]. *Zhonghua Gan Zang Bing Za Zhi.* 2008 Aug; 16 (8): 586–589.
12. *Punia V, Agrawal N, Bharti A, Mittal S, Chaudhary D, Mathur A et al*. Association of TGF-β1 Polymorphism and TGF-β1 Levels With Chronic Hepatitis C and Cirrhosis: A Systematic Review and Meta-Analysis. *Cureus.* 2023 Jun 29; 15 (6): e41157. doi: 10.7759/cureus.41157. eCollection. 2023 Jun.
13. *Liu K, Liu X, Gu S, Sun Q, Wang Y, Meng J, Xu Z*. Association between *TGFB1* genetic polymorphisms and chronic allograft dysfunction: a systematic review and meta-analysis. *Oncotarget.* 2017 Jul 24; 8 (37): 62463–62469. doi: 10.18632/oncotarget.19516.
14. *Ge YZ, Wu R, Lu TZ, Jia RP, Li MH, Gao XF et al*. Combined effects of *TGFB1* +869 T/C and +915 G/C polymorphisms on acute rejection risk in solid organ transplant recipients: a systematic review and meta-analysis. *PLoS One.* 2014 Apr 4; 9 (4): e93938. doi: 10.1371/journal.pone.0093938.
15. *Guo P, Liu S, Sun X, Xu L*. Association of TGF-β1 polymorphisms and chronic hepatitis C infection: a Meta-analysis. *BMC Infect Dis.* 2019 Aug 30; 19 (1): 758. doi: 10.1186/s12879-019-4390-8.
16. *Wu XD, Zeng K, Gong CS, Chen J, Chen YQ*. Transforming growth factor-β genetic polymorphisms on development of liver cirrhosis in a meta-analysis. *Mol Biol Rep.* 2013 Jan; 40 (1): 535–543. doi: 10.1007/s11033-012-2090-1.
17. *Ncbi.nlm.nih.gov* [Internet]. The National Center for Biotechnology Information. Bethesda: National Library of Medicine; [cited. 2024 June 17]. Available from: [https://www.ncbi.nlm.nih.gov/snp/?term=TGFB1].
18. *Shah R, Rahaman B, Hurley CK, Posch PE*. Allelic diversity in the TGFB1 regulatory region: characterization of novel functional single nucleotide polymorphisms. *Hum Genet.* 2006 Mar; 119 (1–2): 61–74. doi: 10.1007/s00439-005-0112-y.
19. *Grainger DJ, Heathcote K, Chiano M, Snieder H, Kemp PR, Metcalfe JC et al*. Genetic control of the circulating concentration of transforming growth factor type beta1. *Hum Mol Genet.* 1999 Jan; 8 (1): 93–97. doi: 10.1093/hmg/8.1.93.
20. *Dunning AM, Ellis PD, McBride S, Kirschenlohr HL, Healey CS, Kemp PR et al*. A transforming growth factor-beta1 signal peptide variant increases secretion *in vitro* and is associated with increased incidence of invasive breast cancer. *Cancer Res.* 2003 May 15; 63 (10): 2610–2615.
21. *Wang H, Mengsteab S, Tag CG, Gao CF, Hellerbrand C, Lammert F et al*. Transforming growth factor-beta1 gene polymorphisms are associated with progression of liver fibrosis in Caucasians with chronic hepatitis C infection. *World J Gastroenterol.* 2005 Apr 7; 11 (13): 1929–1936. doi: 10.3748/wjg.v11.i13.1929.
22. *Mohy A, Fouad A*. Role of transforming growth factor-β1 in serum and –509C>T promoter gene polymorphism in development of liver cirrhosis in Egyptian patients. *Meta Gene.* 2014 Sep 9; 2: 631–637. doi: 10.1016/j.mgene.2014.08.002.
23. *De Brito WB, Queiroz MAF, da Silva Graça Amoras E, Lima SS, da Silva Conde SRS, Dos Santos EJM et al*. The TGFB1 –509C/T polymorphism and elevated TGF-β1 levels are associated with chronic hepatitis C and cirrhosis. *Immunobiology.* 2020 Sep; 225 (5): 152002. doi: 10.1016/j.imbio.2020.152002.
24. *Felicidade I, Bocchi M, Ramos MRZ, Carlos LO, Wagner NRF, Campos ACL et al*. Transforming growth factor beta 1 (TGFβ1) plasmatic levels and haplotype structures in obesity: a role for TGFβ1 in steatosis development. *Mol Biol Rep.* 2021 Sep; 48 (9): 6401–6411. doi: 10.1007/s11033-021-06640-2.
25. *Rosensweig JN, Omori M, Page K, Potter CJ, Perlman EJ, Thorgeirsson SS, Schwarz KB*. Transforming growth factor-beta1 in plasma and liver of children with liver disease. *Pediatr Res.* 1998 Sep; 44 (3): 402–409. doi: 10.1203/00006450-199809000-00023.
26. *Kurabekova RM, Gichkun OE, Tsirulnikova OM, Pashkova IE, Fomina VA, Shevchenko OP, Gautier SV*. Analysis of the Association between the Tgfb1 Gene Haplotype and Liver Diseases in Children. *Acta Naturae.* 2023 Jul-Sep; 15 (3): 75–81. doi: 10.32607/actanaturae.19425.
27. *Solé X, Guinó E, Valls J, Iniesta R, Moreno V*. SNPStats: a web tool for the analysis of association studies. *Bioinformatics.* 2006 Aug 1; 22 (15): 1928–1929. doi: 10.1093/bioinformatics/btl268.

28. *Morikawa M, Derynck R, Miyazono K*. TGF-β and the TGF-β Family: Context-Dependent Roles in Cell and Tissue Physiology. *Cold Spring Harb Perspect Biol.* 2016 May 2; 8 (5): a021873. doi: 10.1101/cshperspect.a021873.
29. *Vitiello GAF, Guembarovski RL, Hirata BKB, Amarante MK, de Oliveira CEC, de Oliveira KB et al*. Transforming growth factor beta 1 (TGFβ1) polymorphisms and haplotype structures have dual roles in breast cancer pathogenesis. *J Cancer Res Clin Oncol.* 2018 Apr; 144 (4): 645–655. doi: 10.1007/s00432-018-2585-9.
30. *Ser ÖS, Çetinkal G, Kiliçarslan O, Dalgıç Y, Batit S, Keskin K et al*. The comparison of serum TGF-beta levels and associated polymorphisms in patients with coronary artery ectasia and normal coronary artery. *Egypt Heart J.* 2021 Mar 31; 73 (1): 32. doi: 10.1186/s43044-021-00153-w.
31. *Trugilo KP, Cebinelli GCM, Pereira É R, Okuyama NCM, Cezar-Dos-Santos F, Castilha EP et al*. Haplotype Structures and Protein Levels of TGFB1 in HPV Infection and Cervical Lesion: A Case-Control Study. *Cells.* 2022 Dec 25; 12 (1): 84. doi: 10.3390/cells12010084.
32. *Stadtlober NP, Flauzino T, Santos L, Iriyoda TMV, Costa NT, Lozovoy MAB et al*. *TGFB1* +869T>C (rs1800470) variant is independently associated with susceptibility, laboratory activity, and TGF-β1 in patients with systemic lupus erythematosus. *Autoimmunity.* 2021 Dec; 54 (8): 569–575. doi: 10.1080/08916934.2021.1975680.
33. *Juarez I, Gutierrez A, Vaquero-Yuste C, Molanes-López EM, López A, Lasa I et al*. TGFB1 polymorphisms and TGF-β1 plasma levels identify gastric adenocarcinoma patients with lower survival rate and disseminated disease. *J Cell Mol Med.* 2021 Jan; 25 (2): 774–783. doi: 10.1111/jcmm.16131.
34. *Iriyoda TMV, Flauzino T, Costa NT, Lozovoy MAB, Reiche EMV, Simão ANC*. TGFB1 (rs1800470 and rs1800469) variants are independently associated with disease activity and autoantibodies in rheumatoid arthritis patients. *Clin Exp Med.* 2022 Feb; 22 (1): 37–45. doi: 10.1007/s10238-021-00725-9.

The article was submitted to the journal on 17.03.2025

DOI: 10.15825/1995-1191-2025-2-189-211

COMBINED SEQUENTIAL *EX VIVO* PERFUSION OF LIVER GRAFTS FROM EXPANDED CRITERIA DONORS: A CONTEMPORARY PERSPECTIVE

M.A. Boldyrev[1], *N.V. Grudinin*[1], *V.K. Bogdanov*[1], *A.R. Monakhov*[1, 2], *C.V. Gautier*[1, 2]

[1] Shumakov National Medical Research Center of Transplantology and Artificial Organs, Moscow, Russian Federation

[2] Sechenov University, Moscow, Russian Federation

Despite significant advancements in the field of liver transplantation (LT) over the last 30 years, the gold standard for allograft preservation – static cold storage with pharmacological agents – has remained largely unchanged. The growing disparity between demand for liver transplants and shortage of donor livers, along with a high waiting list mortality rate (potentially up to 20%), has forced transplant teams to broaden donor eligibility criteria. This expansion, however, has inevitably impacted both the immediate and long-term LT outcomes. Dynamic preservation of liver allografts has shown consistently positive outcomes, particularly among expanded criteria donors, including those classified as high-risk donors" Over the past decade, several perfusion techniques, integrating various temperature conditions, have been developed and are under active investigation. A significant advancement in this area is the emergence of combined sequential *ex vivo* machine perfusion, which integrates multiple perfusion strategies. This approach leverages the strengths of each method while mitigating their individual limitations. This paper reviews current experience with combined sequential *ex vivo* perfusion of liver grafts, providing a concise overview of the key stages encompassed within this protocol.

Keywords: ex vivo perfusion, liver perfusion, liver transplantation.

INTRODUCTION

Liver transplantation, a definitive treatment for various end-stage and focal liver diseases, has evolved significantly since its inception, becoming a routine procedure in many medical centers. While the expansion of liver transplant (LT) indications has allowed more patients to be treated, it also results in a growing pool of potential recipients on the waiting list each year [1, 2]. However, the relatively static donor pool limits the availability of liver transplants, prompting the global transplant community to broaden the criteria for liver allograft suitability, despite potential risks associated with such a step [3–5].

MP (MP) has emerged as a leading strategy for improving LT outcomes, particularly when using organs from expanded criteria donors (ECDs). Beyond conditioning and direct "recovery-rehabilitation" of the organ – notably of mitochondrial function – after a period of cold ischemia during hypothermic oxygenated perfusion (HOPE), MP significantly increases the number of usable organs by enabling *ex vivo* viability testing of both hepatocellular and cholangiocellular components during the normothermic machine perfusion (NMP) phase. However, NMP's protective capacity against ischemia-reperfusion-conservation injury remains relatively modest compared to HOPE [6–8]. Controlled oxygenated rewarming (COR) further optimizes graft preservation by minimizing "rewarming injury" [9] when transitioning from hypothermic to physiological perfusion conditions. The combination of all three MP approaches maximizes the protective and predictive capabilities of the method by harnessing the strengths of each. For example, combined perfusion protocols have achieved excellent outcomes with grafts from donation after circulatory death (DCD) – the highest-risk group – historically associated with poorer outcomes compared to donation after brain death (DBD), largely due to an initial period of warm ischemia.

STATIC COLD STORAGE

Static cold storage (SCS), due to its simplicity and affordability, has been the gold standard for solid organ preservation in transplantation for decades [10–12]. However, the use of isolated SCS in ECDs leads to severe ischemia-reperfusion-preservation injury (IRPI) affecting various components of the liver allograft [13, 14]. Hepatocellular injury manifests as graft dysfunction or primary nonfunction, driven by extensive hepatocyte dysfunction and necrosis [15, 16]. Early allograft dysfunction (EAD) can occur in up to 53.6% of recipients and significantly impacts transplant outcomes: analysis of 1,950 liver transplants showed that 1-year and 5-year graft survival rates were markedly lower in recipients

Corresponding author: Mikhail Boldyrev. Address: 1, Shchukinskaya str., Moscow, 123182, Russian Federation. Phone: (961) 974-59-55. E-mail address: comex.ksb@gmail.com

with EAD compared to those without (84.1% *vs* 92.7% and 73.4% *vs* 83.9%, respectively), as were patient survival rates (86.8% *vs* 95.2% and 67.9% *vs* 79.6%; $p < 0.01$) [17, 18].

The most significant consequence of biliary IRPI is the development of diffuse fibrosis and ischemic non-anastomotic strictures, a condition termed non-anastomotic ischemic cholangiopathy (NAIC), which adversely affects graft survival, recipient quality of life, and overall treatment costs, including the need for retransplantation [19, 20]. In a 29-year analysis of asystolic donor experience by the University of Wisconsin group, a significantly higher rate of biliary complications was observed among recipients of non-heart-beating (NHB) donor grafts (51% *vs* 33.4% in the DBD group; $p < 0.01$), as well as a markedly higher risk of retransplantation due to ischemic cholangiopathy (13.9% *vs* 0.2% in the DBD group; $p < 0.01$).

A cost analysis by Jay et al. revealed a 53% increase in treatment costs at 1 year for patients who developed NAIC ($p < 0.01$), and a 107% increase ($p < 0.001$) if retransplantation was required due to disease progression [21]. LT recipients generally experience a higher incidence of NAIC when receiving grafts from DCD donors compared to those from DBD donors (44% *vs* 1.6%, $p < 0.001$).

The aforementioned complications reach their peak when using DCD allografts, primarily due to the unavoidable period of primary warm ischemia. This significantly limits the utilization of marginal allografts unless supplemented by additional protective strategies.

MP, being a long-established organ preservation technique, has consistently demonstrated excellent outcomes in high-risk allograft cases, achieving outcomes comparable to transplants from optimal donors [22, 23].

HYPOTHERMIC OXYGENATED PERFUSION

HOPE facilitates the restoration of electron flow through the mitochondrial electron transport chain (ETC), promoting ATP resynthesis while simultaneously minimizing consumption under hypothermic conditions. It actively clears ischemic metabolites such as succinate and NAD+, thereby preventing excessive formation of reactive oxygen species during subsequent rewarming and averting damage to critical ETC components, particularly complex I [24–26].

HOPE helps maintain cellular energy by effectively reprogramming mitochondria, the cell's energy hubs, to function under extremely low metabolic conditions. This "reprogramming" allows cells to thrive even when their energy production is 10–15 times lower than during typical SCS.

HOPE offers the advantage of relative technical simplicity: a short-term session (1–2 hours) conducted at the end of SCS – the so-called end-ischemic or back-to-base approach – is sufficient to achieve meaningful graft protection [24]. The perfusate used is typically a standard preservation solution (used routinely in SCS) or a modified variant such as the University of Wisconsin-Belzer Machine Perfusion Solution (UW-Belzer MPS), actively oxygenated to achieve a partial oxygen pressure (pO_2) of 400–600 mmHg under hypothermic conditions (8–12 °C) [25]. The standard HOPE protocol is detailed in Table 3. This technique does not require the addition of oxygen carriers to the perfusate, and the use of hypothermic temperatures reduces the risk of rewarming injury in the event of device malfunction.

Perfusion can also be initiated directly at the donor site (upfront approach); however, this method is limited by the need for specialized portable perfusion devices. Moreover, the absence of active oxygenation in many such systems often results in suboptimal oxygen delivery to the allograft [25]. Nonetheless, several studies have shown promising outcomes with this approach. For instance, Guarrera et al. reported a statistically significant reduction in biliary complications (4 *vs* 13 cases, $p = 0.016$) and shorter hospital stays (3.64 ± 10.9 *vs* 20.14 ± 11.12 days, $p = 0.001$) in the perfusion group compared to standard preservation [27, 28]. Results from the PILOT study indicated a significant reduction in the risk of irreversible graft dysfunction (IQR 3.4% [2.4–6.5] *vs* 4.5% [2.9–9.4], $p = 0.024$). However, differences between the MP and SCS groups in rates of primary nonfunction (0% *vs* 2.2%, $p = 0.10$) and biliary complications (6.3% *vs* 16.4%, $p = 0.18$) did not reach statistical significance [29].

HOPE can significantly enhance LT outcomes when using grafts from ECDs, especially those from DCD donors (Table 1), enabling the use of allografts from both optimal and marginal donors, particularly NHB donors. One of the largest randomized trials conducted by the Groningen group confirmed the strong protective capacity of a brief end-ischemic dual HOPE (D-HOPE) session: NAIC occurred in only 6% of the HOPE group versus 18% in the control group (OR 0.36; 95% CI, 0.14–0.94; $p = 0.03$). Similarly, EAD was observed in 26% of the D-HOPE group compared to 40% in the control group (OR 0.61; 95% CI, 0.39–0.96) [30]. However, the specific additional benefit of D-HOPE over single HOPE (mono-HOPE) during the hypothermic phase of MP remains under investigation [31, 32]. For example, Koch et al., in an analysis of 183 liver transplants preserved with either mono-HOPE ($n = 90$) or D-HOPE ($n = 93$), reported no significant difference in the incidence of NAIC (10.96% *vs* 8.22%, $p = 0.574$) or graft survival (91.2% *vs* 93.3%, $p = 0.893$) between the two groups [31].

NORMOTHERMIC MACHINE PERFUSION

Normothermic machine perfusion (NMP) is a more technically demanding and complex method of liver allograft preservation. Operating at normal body temperature (36–37 °C), NMP maintains the organ in a near-normal

metabolic state, necessitating precise and continuous monitoring of perfusion parameters. Any technical failure during this process may result in significant graft injury and potentially require a return to SCS [33, 34]. The standard NMP protocol is summarized in Table 3. This procedure requires the use of an oxygen-carrying perfusate, most commonly red blood cell (RBC) concentrates, due to their hemoglobin content. However, the limited organ availability, along with their unsuitability for hypothermic conditions due to increased membrane fragility and cold-induced agglutination, has prompted efforts to develop alternatives.

In this context, hemoglobin-based oxygen carriers (HBOCs) have emerged as a promising substitute. Van Leeuwen et al. reported comparable graft preservation outcomes between HBOC- and RBC-based perfusates (Table 1). A key advantage of HBOCs is their versatility: unlike RBCs, they are compatible across all MP phases – HOPE, COR, and NMP – allowing for seamless, uninterrupted perfusion protocols without the need to change the perfusate [35].

Conducting NMP sessions in both "upfront" and "end-ischemic" modes results in IRPI, although typically to a lesser degree than observed in the recipient organism, due to the absence of the effector component of the recipient's immune response [36–38]. In the VITTAL study, Mergental et al. reported a 18.2% incidence of NAIC, which was comparable to controls ($p = 0.063$), and a 31.8% incidence of EAD, which was higher than in controls ($n = 4$, $p = 0.034$) [33]. Similarly, Nasralla et al., in their analysis of 220 liver transplants, found no statistically significant differences between the NMP and SCS groups regarding biliary complications, including NAIC, despite a 74% reduction in the incidence of EAD in the NMP group ($p < 0.001$) [39]. These findings support the notion that NMP has limited protective capacity against IRPI.

Nevertheless, as a standalone technique, NMP remains an effective method for preserving liver grafts obtained from ECDs, showing superior outcomes compared to SCS, as confirmed by multiple studies (Table 1), though generally less effective than HOPE [6]. A key advantage of NMP – beyond organ reconditioning – is the ability to assess liver graft viability prior to transplantation. This pre-implantation assessment enables the rejection of organs that would likely result in severe post-transplant complications, such as ischemic cholangiopathy, EAD, or primary non-function (PNF) [40].

On the other hand, considering the largely subjective nature of macroscopic organ assessment by transplant surgeons, the ability to reassess initially "rejected" organs based on objective viability criteria offers a promising opportunity to significantly expand the donor pool. This is especially relevant in light of projections indicating that by 2030, only 44% of liver allografts will be utilized – down from 78% in 2010 – which would translate to approximately 2,230 fewer liver transplants annually [41]. Viability assessment thus emerges as a key strategy to address the growing gap between organ demand and availability. Notably, several studies have included grafts that had been declined by all transplant centers, yet achieved successful transplantation in 30% to 91% of these cases [33, 40], resulting in a donor organ utilization increase of 20% or more.

CONTROLLED OXYGENATED REWARMING (COR)

One of the critical challenges of static cold preservation of liver allografts – besides the accumulation of anaerobic metabolic byproducts and subsequent oxidative damage during warm reperfusion – is the so-called "rewarming injury". This injury is associated with the rapid rise in graft temperature to physiological levels (36–37 °C) [9, 42–44]. The underlying pathophysiology involves a progressive loss of mitochondrial transmembrane potential during cold ischemia. Upon rewarming – either in the recipient or during NMP – this dysfunction manifests as severe mitochondrial injury due to the massive opening of mitochondrial permeability transition pores, calcium ion leakage, apoptosis, free radical formation, and disintegration of the mitochondrial respiratory chain. Collectively, these processes are recognized as key components of ischemia-reperfusion-conservation injury. Interestingly, such thermal damage is not observed in isolated hepatocyte cultures preserved at temperatures above 16 °C [9, 43].

A potential solution to rewarming injury has been proposed by a group of researchers from University Hospital Essen. To minimize thermal damage, they advocate for a brief session of highly oxygenated MP with a gradual increase in temperature to 20 °C, performed in an "end-ischemic" format. The standard COR protocol is detailed in Table 3. In the first clinical validation of this approach, Hoyer et al. evaluated 6 LT recipients and reported a statistically significant reduction in peak transaminase levels – used as surrogate markers of IRPI – in the COR group (AST 563.5 *vs* 1204 U/L, $p = 0.023$) compared to a control group that underwent SCS ($n = 106$). Improvements in coagulation parameters were also observed, with a lower international normalized ratio (INR) in the COR group (1.48 *vs* 1.86, $p = 0.07$), reflecting better synthetic liver function postoperatively. Furthermore, the incidence of EAD and PNF was lower in the COR group (0% *vs* 35.9%, $p = 0.07$ and 0% *vs* 2.8%, $p = 0.68$, respectively). Graft survival in the COR group was 100%, compared to 80.9% in the SCS group ($p = 0.24$) [9, 43]. However, not all outcome differences reached statistical significance.

A subsequent randomized controlled trial involving 40 LT recipients, randomized to receive either COR ($n = 20$) or SCS ($n = 20$) for graft preservation, further

supported the potential benefits of COR. Improved graft function was demonstrated by a higher 13C-methacetin clearance (LiMAx test, 294 ± 106 *vs* 187 ± 121 ng/kg/hour, p = 0.006) and increased synthesis of coagulation factor V on postoperative day 1 (103 ± 34 *vs* 66 ± 26, p = 0.001) [45]. However, the study did not meet its primary endpoint, as the difference in peak AST levels between the groups was not statistically significant (767 ± 1157 *vs* 1371 ± 2871 U/L, p = 0.273).

In summary, COR shows promise as a supplementary MP strategy for liver graft preservation. Nonetheless, its clinical efficacy requires confirmation through larger-scale studies and direct comparisons with other established techniques such as HOPE.

Despite the current absence of established practice for assessing allograft viability at the COR stage – owing to its inherently end-ischemic application – Hoyer et al. reported a strong correlation between AST levels measured at 120 minutes of COR perfusion at 20 °C and peak AST levels observed in the postoperative period. The coefficient of determination was $R^2 = 0.90$, $p < 0.001$). In comparison, similar correlations observed during HOPE were associated with lower predictive accuracy ($R^2 = 0.73$) [46].

COMBINED SEQUENTIAL MACHINE PERFUSION

With the development and introduction of HOPE and NMP into routine clinical practice, several researchers have attempted to compare the two techniques [6]. The results of a meta-analysis of 7 randomized trials and 1017 patients included demonstrate a statistically significant reduction in the incidence of EAD with both HOPE and NMP (NMP *vs* SCS, OR 0.50, 95% CI 0.30–0.86, p = 0.01, I2 = 39%; HOPE *vs* SCS: OR 0.48, 95% CI 0.35–0.65, p < 0.00001, I2 = 5%). At the same time, a greater protective potential of HOPE has been noted, consisting of a reduction in serious complications (Clavien–Dindo >IIIb, HOPE *vs* SCS: OR 0.76, 95% CI 0.63–0.93, p = 0.006, I2 = 0%), retransplantation rate (HOPE *vs* SCS: OR 0.21, 95% CI 0.04–0.96, p = 0.04; I2 = 0%) and graft loss (HOPE *vs* SCS: OR 0.40, 95% CI 0.17–0.95, p = 0.04; I2 = 0%). Both techniques also had a positive effect on the incidence of biliary complications and non-anastomotic strictures. Over time, the view on the use of MP has changed toward the use of combined protocols that include sequential HOPE and NMP [35, 47]. At the D-HOPE stage, the previously described reconditioning of mitochondria of the liver allograft is performed, which allows approaching the period of warm reperfusion in an optimal energetic and metabolic state. Thus, in an experimental study, Boteon et al. report a 1.8-fold increase in ATP levels during HOPE and decreased expression of markers of oxidative stress and inflammation (p = 0.008 and p = 0.02) during the NMP stage in the combined perfusion group compared to isolated NMP, with 100% of organs achieving viability criteria in the combined perfusion group compared to 40% in the isolated perfusion group [48].

In more recent studies, the combined perfusion protocol has evolved to incorporate the COR stage as a transitional link between hypothermic and normothermic perfusion phases. By enabling a gradual, stepwise rewarming of the organ under conditions of high oxygenation, COR mitigates the abrupt thermal shift associated with direct transitions from hypothermic to normothermic perfusion. Although definitive clinical evidence demonstrating the superiority of this integrated approach is still lacking, the strong pathophysiological rationale and promising outcomes observed with isolated COR have led several researchers to adopt it as part of their combined perfusion strategies [35, 49]. Following the COR phase, D-HOPE is succeeded by NMP, allowing not only continued graft reconditioning through restoration and maintenance of ATP reserves but also real-time assessment of organ viability under near-physiological conditions. Once the graft meets established viability criteria – identical to those used in isolated NMP – it is deemed suitable for transplantation and can be successfully implanted into the recipient [49–51].

The choice of perfusate in the combined perfusion protocol warrants careful reconsideration. The use of oxygen carrier-free perfusate during the normothermic phase is inadequate due to the high metabolic demand of the liver graft and the limited oxygen-carrying capacity of such solutions. Conversely, the most commonly employed perfusate in NMP – based on red cell mass – is unsuitable for hypothermic conditions due to increased fragility of erythrocyte membranes, a heightened risk of hemolysis, and cold-induced RBC agglutination. According to van Leeuwen et al. [35], two primary strategies have been proposed to address this limitation. The first involves replacing the perfusate following the HOPE phase with a RBC-based solution and initiating the subsequent perfusion at a starting temperature of 20 °C. This approach avoids erythrocyte damage while enabling effective oxygen delivery during the COR and NMP phases. Importantly, the perfusate exchange typically requires no more than 20–30 minutes and does not significantly affect overall perfusion outcomes. The second approach employs HBOCs throughout all stages of the combined perfusion protocol. This method has demonstrated safety and efficacy in comparison to both RBC-based perfusates during NMP and conventional UW-MPS during HOPE [35, 49, 50]. However, the clinical application of HBOCs remains limited, primarily due to the absence of regulatory approvals for use in perfusion preservation in the United States and European Union. Nevertheless, given the constrained availability of donor red cell mass, HBOC-based perfusion is a promising area for future research.

The main outcomes of the combined MP protocol are presented in Table 1. It is important to note the relatively small number of studies, the limited patient cohorts, and the near-complete absence of direct comparisons between combined and isolated protocols, which currently makes it difficult to draw definitive conclusions about the advantages of combined perfusion. However, several ongoing clinical trials – particularly the DHOPE-COR-NMP study led by the Groningen group – are expected to provide deeper insights into the potential benefits of integrating multiple perfusion techniques [52].

Table 1

Outcomes of hypothermic oxygenated perfusion (HOPE) and normothermic machine perfusion (NMP) in liver transplantation (Adapted from Jakubauskas et al. [66] and Banker et al. [8], with additions)

Research	Comparison groups	Donation type	Study design	Number of patients	Duration of machine perfusion	Perfusion system and perfusate	Effects observed
1	2	3	4	5	6	7	8
HMP and HOPE, including dual-HOPE (D-HOPE)							
Guarrera et al. [27] 2010	HMP and SCS	Brain-dead donors	Prospective cohort study, case-matched 1 : 1	20 and 20	4.3 ± 0.9 hours	Modified Medtronic PBS (Vasosol)	1. No statistically significant difference: early allograft dysfunction (EAD), primary non-function (PNF), survival 2. In HMP group: significant reduction in length of hospital stay, decreased peak levels of AST, ALT, and total bilirubin, as well as improved renal function (significantly lower serum creatinine levels)
Henry et al. [67] 2012	HMP and SCS	Not indicated	Prospective cohort study, case-matched 1 : 1	18 and 15	4.2 ± 0.9 hours	Modified Medtronic PBS (Vasosol)	In HMP group: decreased expression of proinflammatory cytokines, activation of adhesion molecules, along with reduced ultrastructural damage to the allograft
Guarrera et al. [68] 2015	HMP and SCS	Donation after brain death (DBD)	Prospective non-randomized, case-matched 1 : 1	31 and 30	3.8 ± 0.9 hours	Modified Medtronic PBS (Vasosol)	1. Equal number of EAD, 1-year recipient survival 2. In NMR group: lower incidence of biliary complications within the first year post-transplant 3. Significant reduction in length of stay in the hospital
Dutkowski et al. [69] 2015	HOPE and SCS	Donation after circulatory death (DCD) and DBD	Multicenter study, case-matched analysis 1 : 1	25 and 50	2.2 hours	Liver Assist device, UW gluconate solution (KPS-1)	In HOPE group: significant reduction in peak ALT levels, lower incidence of cholangiopathies and biliary complications, and improved 1-year graft survival
Van Rijn et al. [70] 2017	D-HOPE and SCS	DCD	Non-randomized study, case-matched 1 : 2	10 and 20	2.1 (2.1–2.3) hours	Liver Assist device, UW gluconate solution (Belzer MPS) and glutathione 3 mmol/L	In D-HOPE group: 1. Decreased peak levels of ALT, gamma-glutamyl transferase, alkaline phosphate, total bilirubin at 30 days post-transplant, along with an 11-fold increase in ATP levels 2. ALT and bilirubin at 1 week post-transplant are two times lower
Patrono et al. [71] 2019	D-HOPE and SCS	DBD	Non-randomized study, case-matched 1 : 2	25 and 50	3.1 ± 0.8 hours	Liver Assist device, UW-MP solution (Belzer MPS)	Acute renal injury stage 2–3 and severe postreperfusion syndrome are significantly lower in the D-HOPE group

Continuation of Table 1

1	2	3	4	5	6	7	8
Schlegel et al. [72] 2019	HOPE and SCS	DCD and DBD	Prospective study, case-matched 1 : 1 : 1 (HOPE-DCD and SCS-DCD and brain-dead SCS donor	50 and 50	2 (1.6–2.4) hours	Liver Assist device, UW gluconate solution (Belzer MPS)	Significant increase in graft survival in the HOPE-DCD group compared to the DCD-SCS group
Ravaioli et al. [73] 2020	HOPE and SCS	DBD	Non-randomized study, case-matched 1 : 3	10 and 30	2.2 (1–3.5) hours	Center-developed perfusion device, UW-MP solution (Belzer MPS)	Mean AST at postoperative day 7 significantly lower in the HOPE group
Rayar et al. [74]	HOPE and SCS	DBD	Non-randomized study, case-matched 1 : 3	25 and 69	2 (1.3–4.2) hours	Liver Assist device, UW-MP solution (Belzer MPS)	Mean leant of stay in the hospital and in ICU significantly lower in the HOPE group
Van Rijn et al. [30] 2021	D-HOPE and SCS	DCD	Multicenter prospective randomized controlled clinical study	78 and 78	2.2 (2–2.5) hours	Liver Assist device, UW gluconate solution (Belzer MPS) and glutathione 3 mmol/L	In HOPE group: significant reduction in symptomatic non-anastomotic stricture (NAS), EAD, incidence of postreperfusion syndrome
Czigany et al. [75] 2021	HOPE and SCS	DBD	Prospective, randomized controlled study	23 and 23	–	Liver Assist device, UW gluconate solution (Belzer MPS)	In HOPE group: decreased peak ALT levels, along with shorter ICU stays and overall hospitalization time
NMP							
Ravikumar et al. [76] 2016	NMP and SCS	DCD and DBD	Non-randomized study, case-matched 1 : 2	20 and 40	9.3 (3.5–18.5) hours	OrganOx metra, colloidal solution (Gelofusine)	1. Similar 30-day patient and graft survival 2. Significant reduction in peak AST levels within the first 7 days in the NMP
Selzner et al. [77] 2016	NMP and SCS	DCD and DBD	Pilot study, case-matched 1 : 3	10 and 30	8 (5.7–9.7) hours	OrganOx metra, dextran-based perfusate (Steen solution), red cell mass (RCM), albumin	1. Similar 30-day recipient and graft survival 2. No cases of graft loss 3. Similar postoperative graft function, hospitalization duration, and ICU stay between groups
Bral et al. [78]	NMP and SCS	DCD and DBD	Non-randomized study, case-matched 1 : 2	9 and 27 (intention-to-treat 10 and 30)	11.5 (3.3–22.5) hours	OrganOx metra, perfusate based on erythrocyte-RCM and colloidal solution	1. Similar 30-day and 6-month graft and patient survival 2. Hospitalization and ICU stays significantly longer in the NMP group 3. Similar postoperative graft function
Nasralla et al. [39] 2018	NMP and SCS	DCD and DBD	Multicenter, randomized controlled study, case-matched 1 : 2	120 and 101	9.1 (6.2–11.8) hours	OrganOx metra, colloidal solution (Gelofusine), RCM	1. In NMP group: lower incidence of EAD, less organ injury (by 50%, based on peak transaminase levels), lower rate of postreperfusion syndrome 2. Increased number of allografts transplanted 3. Similar 1-year recipient and graft survival
Ghinolfi et al. [28] 2019	NMP and SCS	DBD donors aged >70 years	Single-center controlled study	121 and 101	4.2 (3.3–4.7) hours	Liver Assist, colloidal solution (Gelofusine), albumin, RCM	Similar 6-month patient and graft survival Similar complication rates and length of hospitalization in both groups Less organ injury in the NMP group according to histological analysis

Continuation of Table 1

1	2	3	4	5	6	7	8
Mergental et al. [33, 79] 2020, 2024 – the VITTAL trial	NMP	DCD and DBD	Single-center, non-randomized study, case-matched 1 : 2	31	587 (450–705) minutes	OrganOx metra, colloidal solution (Gelofusine), RCM	1. 71% of organs (n = 22) reached viability criteria and were successfully transplanted 2. 90-day graft survival was 100% 3. Ischemic strictures requiring retransplantation occurred in 18% of patients (n = 4, mean follow-up 542 days), comparable to 2.3% (n = 1) in the control group (p = 0.063) 4. No cases of PNF 5. EAD in 31.8% of cases (n = 7), more frequent than in the control group (n = 4, p = 0.034) 6. 1-year graft and recipient survival of 86.4% and 100% (comparable to control group: 86.4% and 95.5%) 7. 5-year graft and recipient survival: 72% and 82% 8. All deceased recipients had a functioning graft
Liu et al. [80] 2020	NMP and SCS	DCD and DBD	Non-randomized study, case-matched 1 : 4	21 and 84	5 ± 1.1 hours	Custom-built perfusion device; perfusate composed of fresh frozen plasma, RCM, and albumin.	Frequency of EAD, peak ALT and AST levels significantly lower in NMP group
Quintini et al. [81] 2022	NMP of liver allografts declined by other transplant centers	DCD and DBD	Non-randomized clinical study	21	3.49–10.29 hours	Custom-built perfusion device	Ability to rehabilitate and successfully transplant 15 of 21 organs initially deemed unsuitable
Markmann et al. [82] 2022	NMP and SCS	DCD and DBD	Prospective randomized study	153 and 147	2.0–5.5 hours	Transmedics Organ Care Systems, albumin-based perfusate (Steen solution), RCM	1. In NMP group: reduced incidence of EAD, ischemic biliary complications 2. Decreased intensity of ischemia-reperfusion-preservation injury (according to histologic study) 3. Increased number of utilized organs from DCD donors in the group where NMP was used
Combined *ex-vivo* machine perfusion protocols							
Boteon et al. [48] 2018	NMP and HOPE-NMP	DCD and DBD	Prospective cohort study, case-matched 1 : 1 (pilot study)	5 and 5	6 hours NMP (NMP group). 2 hours HOPE and 4 hours NMP (HOPE-NMP group)	Liver Assist device, perfusate: hemoglobin-based oxygen carrier (HBOC) with albumin (for NMP); UW-MP solution (Belzer MPS) for HOPE	*Birmingham (Mergental, 2016) criteria were used to assess allograft viability at the NMP stage (see Table 2)* 1. 60% (n = 3) in the NMP group and 100% (n = 6) in the HOPE-NMP group were deemed viable and successfully transplanted 2. In the combined perfusion group: statistically reduced expression of oxidative stress markers (4-hydroxynonenal, CD14), inflammatory markers (CD11b, VCAM)

Continuation of Table 1

1	2	3	4	5	6	7	8
de Vries et al. [49] 2019	DHOPE-COR-NMP	DCD	Prospective single-center	7	283–517 minutes	Liver Assist device, perfusate: HBOC with albumin used throughout all perfusion stages	*The Groningen (van Leeuwen, 2019) criteria were used to assess allograft viability at the NMP stage (see Table 2)* 1. 5 out of 7 liver grafts used 2. No cases of EAD 3. No cases of PNF 4. 3-month graft and recipient survival – 100%
van Leeuwen et al. [58] 2019	DHOPE-COR-NMP	DCD	Prospective (stage 1), retrospective cohort study (stage 2)	16	Total perfusion time is not specified. Standard protocol: 1 hour D-HOPE, 1 hour COR, 150 minutes NMP. If the graft is deemed viable, prolong perfusion until ready for implantation. Total preservation time: 868 (IQR 805–924) min	Liver Assist device, perfusate: HBOC with albumin used throughout all perfusion stages	*The Groningen (van Leeuwen, 2019) criteria were used to assess allograft viability at the NMP stage (see Table 2)* 1. 69% of organs (n = 11) were deemed viable and were transplanted 2. Recipient and graft survival at 3, 6, and 12 months was 100% 3. 1 case (9%) of ischemic cholangiopathy (4 months post-transplant) 4. No cases of PNF 6. Transplant activity increased by 20% following implementation of the protocol
van Leeuwen et al. [35] 2022	DHOPE-COR-NMP	DCD and DBD (2%, n = 1)	Prospective observational cohort study	54	Total perfusion time is not specified. Standard protocol: 1 hour D-HOPE, 1 hour COR, 150 minutes NMP. If the graft is deemed viable, prolong perfusion until ready for implantation	Liver Assist device, perfusate: HBOC with albumin (n = 12) used for all perfusion stages; or UW-MPS for HOPE and red blood cell mass with albumin for COR-NMP stages (n = 22)	*The Groningen (van Leeuwen, 2019) criteria were used to assess allograft viability at the NMP stage (see Table 2)* 1. 63% of organs (n = 34) were deemed viable and successfully transplanted 2. 1-year survival rates were 100% for recipients and 94% for grafts 3. Non-anastomotic cholangiopathy developed in 3% of cases (n = 1) 4. Comparable results when using HBOC and RCM in the perfusate 5. No cases of PNF 6. Two retransplantations for reasons unrelated to perfusion (venous outflow obstruction and chronic rejection)
Liu et al. [82] 2023	HOPE-NMP	DCD and DBD	Prospective, observational, single-center	17	1–2 hours at NOPE stage and 4–9 hours at NMP stage	Perfusion device: center-developed custom perfusion system. UW-MPS (HOPE stage) and RCM-based perfusate (NMP stage)	*The Quintini et al. (2022) criteria was used to assess allograft viability at the NMP stage (see Table 2)* 1. 76.5% of organs (n = 13) were deemed viable and successfully transplanted 2. Graft and recipient survival rates were 100% (follow-up period 6–13 months) 3. EAD occurred in 5 patients (35%) 4. Non-anastomotic ischemic cholangiopathy developed in 2 patients (15%) 5. No statistically significant differences in post-transplant outcomes when compared to the retrospective NMP group without HOPE

End of Table 1

1	2	3	4	5	6	7	8
Thorne et al. [83] 2023	DHOPE-COR-NMP	DCD	Prospective, observational, single-center	55	Total perfusion time not specified. Standard protocol: 1 hour D-HOPE, 1 hour COR, 150 minutes NMP. If the graft is deemed viable, prolong perfusion until ready for implantation	Liver Assist device, RCM- and albumin-based perfusate (for NMP and COR stages), UW-MP solution (Belzer MPS) (for D-HOPE)	*The Groningen (van Leeuwen, 2019) criteria were used to assess allograft viability at the NMP stage (see Table 2)* 1. 70% of allografts (n = 35) were deemed viable and successfully transplanted 2. Recipient and graft survival (death-censored): 97% and 94%, respectively 3. Two retransplantations were required (due to chronic rejection and hepatic artery thrombosis) 4. One patient death occurred (due to interstitial lung disease) 5. One case of ischemic cholangiopathy was reported
Magistri et al. [84] 2025	D-HOPE – NMP	DCD and DBD	Retrospective, observational, single-center	33	90 minutes D-HOPE NMP time: 427 (260–559) in the viable allograft group and 240 (120–375) in the non-viable allograft group	Liver Assist device, PerLife (Aferetica) RCM-based perfusate (NMP)	*The "traffic light" criteria developed by the Groningen group were used to assess allograft viability at the NMP stage, modified (by excluding biliary tree viability assessment due to logistical and laboratory limitations) in the center (see Table 4)* 1. 48.5% (n = 16) of grafts were deemed viable and successfully transplanted 2. One case of EAD (with the patient surviving 30 months post-transplant) and one case of PNF (resulting in death on postoperative day 46)

Note: HMP, hypothermic machine perfusion; SCS, static cold storage; HOPE, hypothermic oxygenated perfusion; D-HOPE, dual hypothermic oxygenated perfusion; NMP, normothermic machine perfusion; COR, controlled oxygenated rewarming; AST, Aspartate Transaminase; ALT, Alanine Transaminase.

VIABILITY ASSESSMENT

Assessment of liver allograft viability is a critical aspect of machine perfusion: identifying and discarding non-viable allografts during preservation can prevent most complications associated with transplanting a non-viable organ. The main methods used for viability assessment are summarized in Table 2.

The ability to evaluate viability during hypothermic perfusion is considerably limited due to the considerably reduced allograft metabolism. Although several studies have described correlations between various perfusate parameters (such as glucose, lactate, AST, and ALT) during HOPE and post-transplant outcomes [53], the only validated marker for viability assessment is the measurement of flavin mononucleotide (FMN, a component of mitochondrial complex I) levels in the perfusate at 30 minutes of perfusion [31, 72].

A multicenter, cross-national study analyzing 473 HOPE/D-HOPE perfusate samples confirmed the strong predictive value of FMN levels for graft loss (due to NAIC or PNF), showing ROC values between 0.7733 and 0.8418 depending on the determination method ($p < 0.0001$), for NAIC (ROC 0.7456–0.7686, $p < 0.0001$), and for the risk of acute kidney injury (ROC 0.7616–0.7144, $p < 0.0001$ and $p < 0.0014$) [54].

However, FMN assessment requires mass spectrometry or fluorometry, necessitating specialized equipment and limiting the widespread adoption of this method. The role of FMN measurement in combined perfusion protocols remains undefined. Of particular interest is the combined perfusion protocol developed at the Zurich clinic, where a decision to proceed with or abandon subsequent NMP is guided by FMN levels: NMP is withheld for severely damaged allografts with high FMN values, whereas optimal allografts with elevated FMN levels proceed to NMP. [55].

A comprehensive and detailed assessment of organ viability becomes possible during the normothermic perfusion stage. As previously mentioned, by recreating near-physiological conditions during normothermic perfusion, it is feasible to evaluate key metabolic parameters and identify signs of dysfunction or injury, which may indicate organ non-viability or future graft dysfunction.

Table 2

Assessment of liver graft viability during hypothermic oxygenated perfusion (HOPE) and normothermic machine perfusion (NMP): current criteria and practical outcomes (adapted from Groen et al. [56] and Jeddou et al. [40], with additions). Criteria related to cholangiocellular viability are italicized in the NMP section

Study	Number of organs / salvage rate (%) *Use of initially rejected organs*	DCD / DBD	Viability criteria	Perfusion device	Perfusate base	Outcomes
1	2	3	4	5	6	7
HOPE, D-HOPE						
Eden et al. [85] (2023)	Perfused: not indicated Transplanted: 158	Not indicated	Flavin mononucleotide (FMN) at 30 minutes HOPE (<6000 A.U.) NADH at 30 minutes HOPE (<8000 A.U.)	ECOPS, Liver Assist, VitaSmart	UW-MPS (Belzer MPS)	1-year graft survival: 89% Primary non-function (PNF): 7 cases Ischemic cholangiopathy (IC): 11 cases Anastomotic strictures (AS): 53 cases Biliary congestion (BC): 9 cases
Patrono et al. [53] (2020)	Perfused: 50 Transplanted: 50 100% utilization rate	0/50	Perfusate during HOPE: lactate, AST, ALT, LDH, glucose, pH	Liver Assist device	UW-MPS (Belzer MPS)	Graft loss: 1 case Early allograft dysfunction (EAD): 13 cases
Schlegel et al. [26] (2020)	Perfused: 50 Transplanted: 50 100% utilization rate	32/18	Perfusate, liver parenchyma and mitochondria during HOPE: FMN at 30 minutes (<8000 A.U.) NADH (<10000 A.U.)	Liver Assist device	UW-MPS (Belzer MPS)	Graft loss (unspecified causes): 7 cases
Muller et al. [86] (2019)	Perfused: 54 Transplanted: 54 Utilization rate: 100%	35/19	FMN at 30 minutes HOPE	Liver Assist device	UW-MPS (Belzer MPS)	Graft loss: 7 cases PNF: 4 cases IC: 1 case
NMP						
Olumba et al. [87] (2023)	Perfused: 22 Transplanted: 16 Utilization rate: 72.7%	10/12	Within the first 2 Hours of NMP: – Perfusate lactate <2.2 mmol/L – Hepatic artery (HA) flow >100 mL/min and portal vein (PV) flow >500 mL/min *Plus at least two of the following*: – Evidence of glucose metabolism – Perfusate pH >7.25, with sodium bicarbonate requirement <70 mL – Evidence of bile production – Perfusate AST <10,000 U/L and ALT <7,000 U/L – Homogeneous parenchymal perfusion and soft allograft consistency	OrganOx metra device	Red cell mass (RCM)	PNF: none Graft-related death: none Non-anastomotic stricture (NAS): none
van Leeuwen et al. [35] (2022)	Perfused: 54 Transplanted: 34 Utilization rate: 63%	53/1	After 2.5 hours of NMP : – Perfusate lactate <1.7 mmol/L – Perfusate pH 7.35–7.45 without repeated bicarbonate administration – Bile output >10 mL, with >4 mL in the last hour – Bile pH >7.45 – ΔpH (bile – perfusate) >0.10 – Δ bicarbonate (bile – perfusate) >5.0 – Δ glucose (bile – perfusate) <–5.0	Liver assist device	Cases 1–8: hemoglobin-based oxygen carrier (HBOC), Cases 19–54: RCM	1-year graft survival: 94% NAS: 1 case AS: 12 cases Bile leaks: 4 cases

Continuation of Table 2

1	2	3	4	5	6	7
Seidita et al. [88] (2022)	Perfused: 19 Transplanted: 17	3/16	– Normalization or ≥50% reduction of lactate by the end of perfusion – Perfusate pH >7.3 without repeated sodium bicarbonate infusions – Evidence of bile production – HA and PV flows	Not indicated	RCM, fresh frozen plasma	1-year graft survival: 94% EAD: 1 case
Quintini et al. [80] (2022)	Perfused: 21 Transplanted: 15 Utilization rate: 71%	13/8	Within 6 hours of NMP – at least two of the following criteria: – Perfusate lactate <4.5 mmol/L or 60% reduction from peak value within the first 4 hours – Bile output >2 mL/hour – Stable perfusion flows: HA >0.05 mL/min/g and PV >0.4 mL/min/g – Homogeneous parenchymal perfusion and soft allograft consistency	OrganOx metra device	RCM	EAD: 7 cases Ischemic strictures: 1 case (due to biliary wall obstruction) PNF: none
Zhang et al. [89] (2020)	Perfused: 4 Transplanted: 4 (retrospective) Utilization rate: 100%	3/1	Within the first 4 hours of NMP: – Perfusate lactate <2.5 mmol/L – Evidence of bile production – Stable HA and PV perfusion flows (>150 mL/min and >500 mL/min) – Perfusate pH >7.3 without a need for repeated sodium bicarbonate infusions	Liver Assist device	RCM leukoreduced, washed red blood cells	6-month graft survival: 100% EAD: 1 case 1 AS PNF or NAS: none
Reiling et al. [90] (2020)	Perfused: 10 Transplanted: 10 Utilization rate: 100%	5/5	After 4 hours of NMP: – Perfusate lactate <2 mmol/L within the first 2 hours – Glucose metabolism trending downward within 4 hours – Physiologic perfusate pH without need for continuous sodium bicarbonate infusion – Stable HA and PV flows – Homogeneous parenchymal perfusion and soft allograft consistency – Evidence of bile production	OrganOx metra device	RCM	6-month graft survival: 100% EAD: 5 cases AS: 1 case Bile leaks: 1 case (originating from the biliary anastomosis) PNF or NAS: none
Mergental et al. [33, 78] – the modified **Birmingham criteria** (2020–2024)	Perfused: 31 Transplanted: 22 Utilization rate: 71%	14/17	Within the first 4 hours of NMP: – Perfusate lactate ≤2.5 mmol/L *Plus at least two of the following criteria:* – Evidence of bile production – Perfusate pH ≥7.3 without a need for repeated sodium bicarbonate injections – Evidence of glucose metabolism – Stable PV and HA perfusion flows (≥150 mL/min and ≥500 mL/min, respectively) – Homogeneous parenchymal perfusion and soft allograft consistency	OrganOx metra device	RCM	1-year graft survival: 86.4% EAD: 7 cases NAS (requiring retransplantation): 4 cases AS: 2 cases PNF: none
Cardini et al. [91] (2020)	Perfused: 34 Transplanted: 25 Utilization rate: 73%	4/30	After 2 hours of NMP – Rapid decrease and sustained low lactate levels during the first 2 hours of perfusion – Continued bile production, bile pH – Maintenance of physiologic perfusate pH without the need for continuous sodium bicarbonate infusion – "Danger signals": Exceptionally high and rapidly rising levels of AST, ALT, LDH	OrganOx metra device	RCM	20-month graft survival: 88% AS: 7 cases Bile leaks: 3 cases PNF or NAS: none

Continuation of Table 2

1	2	3	4	5	6	7
van Leeuwen et al. [58] (2019) – the **Groningen criteria**	Perfused: 16 Transplanted: 11 Utilization rate: 69%	16/0	After 2.5 hours NMP: – Lactate clearance to <1.7 mmol/L – Perfusate pH between 7.35–7.45, without repeated sodium bicarbonate infusions – Total bile production >10 mL, with at least 4 mL produced in the last hour – *Bile pH >7.45*	Liver Assist Device	HBOC	PNF: none NAS: 1 case
Bral et al. [92] (2019)	Perfused: 46 Transplanted: 43 Utilization rate: 93%	10/33	– Lactate level at the start of perfusion – Lactate clearance – Need for pH correction with sodium bicarbonate – Hourly bile production	OrganOx metra device	RCM	3-month graft survival: 100% EAD: 11 cases NAS: 2 cases AS: 6 cases
Modified Groningen criteria	Preclinical study: 23 Clinical study: 4/6 Utilization rate: 66%	6/0	After 2.5 hours of NMP: – Lactate clearance to <1.7 mmol/L – Perfusate pH between 7.35–7.45, without repeated sodium bicarbonate infusions – Total bile production >10 mL – *Bile pH >7.48*	Liver assist device	HBOC	PNF or NAS: none
Ceresa et al. [93] (2019)	Perfused: 34 Transplanted: 31 Utilization rate: 91%	8/23	Within the first 4 hours of NMP: – Lactate clearance – Glucose metabolism – Maintenance of pH without repeated sodium bicarbonate infusions – Evidence of bile production – Perfusate transaminase levels – HA and PV perfusion flows	OrganOx metra device	RCM	PNF or NAS: none
De Vries et al. [49] (2019)	Perfused: 7 Transplanted: 5 Utilization rate: 71%	7/0	After 2.5 hours of NMP: – Lactate clearance to <1.7 mmol/L – Perfusate pH between 7.35–7.45, without repeated sodium bicarbonate infusions – Bile output >10 mL total – *Bile pH >7.45*	Liver Assist Device	HBOC	PNF: none NAS: 1 case
Watson et al. [94] – the **Cambridge-criteria** (2018)	Perfused: 47 Transplanted: 22 Utilization rate: 47%	35/12	Within the first 2 hours of perfusion: – Maximal decrease in lactate level ≥4.4 mmol/L/kg/hour – ALT at 2 hours: <600 U/L – Perfusate pH >7.2, while sodium bicarbonate requirement ≤30 mmol/L – *Maximal bile pH >7.5* – *Bile glucose: ≤3 mmol/L, or at least 10 mmol/L lower than perfusate glucose* – Decrease in glucose levels after 2 hours of perfusion, or perfusate glucose <10 mmol/L with further decrease following administration of 2.5 g of glucose – ALT perfusate <6000 U/L	OrganOx Metra device	RCM leukoreduced, washed red blood cells	PNF: 1 case NAS: 4 cases EAD: 1 case
Watson et al. [84] (2017)	Perfused: 12 Transplanted: 12 Utilization rate: 100%	9/3	– Lactate clearance – Perfusate glucose level – Maintenance of pH without repeated sodium bicarbonate infusions – Perfusate transaminase levels	OrganOx metra device	RCM	PNF: 1 case NAS: 3 cases

End of Table 2

1	2	3	4	5	6	7
Birmingham criteria	Perfused: 6 Transplanted: 5 Utilization rate: 83%	4/1	Within the first 3 hours of NMP: Lactate clearance <2.5 mmol/L OR bile production plus at least two of the following criteria: – Perfusate pH >7.3 without repeated sodium bicarbonate injections – Perfusion flow >150 mL/min for HA and >500 mL/min for PV – Homogeneous parenchymal perfusion and soft allograft consistency	1–5 allografts: Liver assist device 6 allografts: OrganOx Metra device	RCM	PNF or NAS: none Transplant related complications: none

Note: HMP, hypothermic machine perfusion; SCS, static cold storage; HOPE, hypothermic oxygenated perfusion; D-HOPE, dual hypothermic oxygenated perfusion; NMP, normothermic machine perfusion; AST, Aspartate Transaminase; ALT, Alanine Transaminase; LDH, lactate dehydrogenase.

Table 3

Recommended perfusion protocols for hypothermic oxygenated perfusion (HOPE), normothermic machine perfusion (NMP), and controlled oxygenated rewarming (COR)

Parameter	HOPE [20, 63, 40]	NMP [23, 28, 40]	COR [9, 42, 46]
Perfusate temperature (°C)	8–10	36–38	8–10 °C (start) 12 °C (30 min) 16 °C (45 min) 20 °C (60 min) Sustained perfusion at 20 °C for functional assessment for up to 90 minutes, then flush with 1 L of preservative solution to reduce the temperature to 4–16 °C before implantation
Oxygenation level (pO_2, mmHg)	400–600	90–200	500
Flow – hepatic artery (mL/min)	40–70	>150–300	Not indicated
Flow – portal vein (mL/min)	300–400 (≤500)	>500	Not indicated
Pressure – hepatic artery (mmHg)	20–25	60–70	25
Pressure – portal vein (mmHg)	3–5	10–13	4

Research groups worldwide have long employed various combinations of parameters to assess the viability of both the hepatocellular and cholangiocellular compartments of the allograft [40, 56]. The main viability criteria currently used by different centers are summarized in Table 2.

A universal marker of hepatocellular viability is the measurement of perfusate lactate levels and their dynamics over the course of perfusion. Notably, current trends favor assessing the trend of lactate clearance rather than relying on absolute lactate values at fixed time points. Relying solely on static thresholds may lead to unnecessary rejection of potentially viable allografts. For example, in their study, Panconesi et al. demonstrated that when applying a lactate clearance criterion at 6 hours of NMP, only 13 (6.1%) out of 213 allografts were classified as non-viable. However, when the same cohort was evaluated using viability criteria from other centers, 14.6% of grafts would have been deemed non-viable based on the Groningen criteria and 11.2% based on the Brisbane criteria. The authors also highlighted comparable results among so-called "lactate-high" allografts [57].

An interesting observation was reported by Mergental et al.: in three allografts, lactate levels, although initially reaching the target threshold of less than 2.5 mmol/L, began to rise after 2 hours of perfusion. Two of these organs were subsequently classified as non-viable based on elevated lactate levels, while the third was transplanted due to a hepatectomy having already been performed. Notably, the recipient of this graft was alive at the time of reporting, despite experiencing EAD (ALT 2,074 U/L and AST 3,031 U/L) [33]. This case illustrates that, while lactate clearance is a key marker of viability, the criteria for interpreting lactate dynamics still require further refinement.

Assessment of bile parameters provides valuable insight into the viability of the biliary tree. It is important to distinguish that bile production primarily reflects hepatocyte function, whereas bile composition is determined by the activity of the biliary epithelium. Under normal conditions, cholangiocytes reabsorb glucose from bile and secrete bicarbonate anions into the ductal lumen, forming a protective layer known as the "bicarbonate umbrella" along the bile ducts [49]. Elevated bile glucose

Table 4

The Groningen group liver transplant viability criteria (van Leeuwen, 2022), based on the "traffic light" system. The criteria are divided into green, yellow, and red zones. In the yellow zone, the liver is borderline viable, meaning the organ might still be used depending on other indicators. In the green zone, the liver is considered optimal for transplantation with high viability, and the organ is ready for use. The red zone signifies that the liver does not meet essential viability criteria and is considered unsuitable for transplantation

	Parameter	Green zone (viable)	Yellow zone (borderline)	Red zone (unviable)
Hepatocellular link	Bile production (mL)	≥10 total (≥4 mL in the last hour)	5–10	<5
	Perfusate lactate (mmol/L)	<1.7	1.7–4	>4
	Perfusate pH	7.35–7.45	7.25–7.35	<7.25
Cholangiocellular link	Bile pH	>7.45	7.40–7.45	<7.40
	ΔpH (bile – perfusate)	>0.10	0.05–0.10	<0.05
	ΔHCO_3^- (mmol/L)	>5.0	3.0–5.0	<3.0
	ΔGlucose (bile – perfusate) (mmol/L)	<–5.0	–3.0…–5.0	>–3.0

and lactate levels, alongside decreased pH and bicarbonate concentrations, indicate biliary epithelial damage and a high risk of subsequent ischemic complications. Similar to lactate assessment, viability evaluation should focus not on absolute parameter values but rather on their relationship to corresponding perfusate parameters. For instance, van Leeuwen et al. reported a case in which a patient developed NAIC four months after liver transplantation, despite the bile pH reaching the cholangiocellular viability threshold (bile pH 7.45) [58].

In a retrospective analysis, the authors noted that the perfusate pH was 7.46. This finding led them to modify their viability criteria to include the calculation of the pH difference between bile and perfusate (Table 4). In several protocols, bile composition was not assessed, which, for example, resulted in cholangiopathy and the need for retransplantation in 4 recipients in the VITTAL study [33, 59]. Retrospective analysis further showed that 3 cases of non-anastomotic biliary strictures occurred in recipients of asystolic donor livers, where the bile was characterized by a low pH (<7.65) and low bicarbonate concentration (<25 mmol/L) [33]. In their study, Mateon et al. highlighted the critical role of bile analysis in preventing biliary complications. Based on perfusion analysis of 23 allografts and subsequent histological evaluation of bile ducts, the authors concluded that bile bicarbonate levels >18 mmol/L ($p = 0.002$), bile pH >7.48 ($p = 0.019$), bile glucose <16 mmol/L ($p = 0.013$), and a bile-to-perfusate glucose ratio <0.67 ($p = 0.013$) were associated with reduced bile duct injury. The use of these parameters as criteria for cholangiocellular viability could help prevent NAIC [60].

ISCHEMIC-FREE IMPLANTATION

A critical concern with normothermic preservation methods has been the need for re-cooling the organ via SCS following the completion of NMP. This re-cooling process results in repeated IRPI, which theoretically could exacerbate organ damage. Various strategies have been proposed to mitigate this risk by avoiding re-cooling altogether ("non-recooling"), allowing implantation of the allograft during ongoing NMP [61, 62]. However, the limited available data – based on small sample sizes ($n = 1$ and $n = 7$) and the lack of statistically significant differences between standard implantation and non-recooling groups ($p = 0.462$) – do not support a definitive recommendation for either approach. These findings may also suggest that the impact of re-cooling on overall preservation-related injury is relatively minor.

CONCLUSION

Despite its relatively recent introduction into routine clinical practice, MP of liver transplants is steadily emerging as the preferred method for preserving allografts from ECDs. According to UNOS data from 2016 to 2023, of 52,626 deceased liver donors, only 1,799 (3.5%) underwent MP. However, the use of MP has increased markedly, from 0.3% in 2016 to 15.5% in 2023 [63].

The currently available outcomes show that perfusion preservation of high-risk liver grafts yields results comparable to those achieved with standard-risk organs, significantly expanding the donor pool without a corresponding increase in complications or a decline in graft and recipient survival. For instance, in the United States, half of all allografts from DCD donors in 2023 were preserved using MP, demonstrating improved graft survival rates (HR 0.50, 95% CI 0.35–0.70, $p < 0.001$) [63, 64].

Nevertheless, most current studies evaluating MP are limited by relatively small sample sizes and lower levels of evidence. Future research is focused on multicenter randomized controlled trials, which are expected to establish perfusion preservation as the new gold standard for marginal allografts.

Choosing the optimal perfusion method for each specific allograft remains a pressing challenge. In most centers, the choice is restricted to a single type of MP,

meaning that comparisons are typically made between one perfusion modality and SCS, with few studies directly comparing different perfusion techniques.

The "upfront" use of MP, initiated at the donor site, has not demonstrated clear benefits over standard cold ischemia protocols and remains a complex, logistically demanding process. HOPE and D-HOPE, in contrast, are relatively easy to implement, safe, and have demonstrated excellent outcomes across multiple studies, including randomized controlled trials. While viability assessment during hypothermic perfusion has been advanced by the introduction of FMN measurement in the perfusate, the role of this biomarker within the broader context of perfusion preservation remains to be fully determined.

NMP alone does not offer sufficient protection against IRPI, but it enables detailed viability assessment. Importantly, studies comparing upfront and end-ischemic NMP approaches have not demonstrated significant differences in outcomes [65].

Controlled oxygenated rewarming (COR), although less widely adopted, is a physiologically sound method. When used in an end-ischemic setting, COR has been associated with improved LT outcomes, although the supporting evidence is limited by small sample sizes and single-center study designs.

Viability assessment during NMP stage has become the focus of extensive research within the field of MP. Emerging evidence suggests that the path toward establishing "ideal" viability criteria lies not in relying on isolated absolute values of individual parameters, but rather in evaluating the dynamics of their changes and the relationships between them – for example, comparing bile pH and glucose levels relative to those of the perfusate. Importantly, evaluation of cholangiocellular viability must be an integral part of viability assessment to reduce the risk of biliary complications. There is a clear need for the development of standardized, universal viability criteria, a goal that can only be achieved through large-scale, multicenter collaborative studies.

By combining the main perfusion techniques, the individual limitations of each method are effectively counterbalanced, making combined machine perfusion an especially promising approach for organ preservation. The excellent outcomes achieved with the DHOPE-COR-NMP protocol offer significant potential for further research, particularly in the use of marginal allografts. Integrating sequential MP into protocols for prolonged perfusion (lasting more than 12–24 hours) aimed at organ rehabilitation may further expand the donor pool by enabling the transplantation of initially severely damaged organs that demonstrate viability after several days of perfusion [55]. The transplant community eagerly awaits more data on the indications, broader applications, and long-term outcomes of combined perfusion strategies.

The authors declare no conflict of interest.

REFERENCES

1. *Kwong AJ, Kim WR, Lake JR, Schladt DP, Schnellinger EM, Gauntt K et al*. OPTN/SRTR 2022 Annual Data Report: Liver. *Am J Transplant*. 2024 Feb; 24 (2S1): S176–S265. doi: 10.1016/j.ajt.2024.01.014. PMID: 38431359.
2. *Terrault NA, Francoz C, Berenguer M, Charlton M, Heimbach J*. Liver Transplantation 2023: Status Report, Current and Future Challenges. *Clin Gastroenterol Hepatol*. 2023 Jul; 21 (8): 2150–2166. doi: 10.1016/j.cgh.2023.04.005. Epub 2023 Apr 20. PMID: 37084928.
3. *Moein M, Bahreini A, Razavi A, Badie S, Coyle S, Abedini M et al*. A Review of Long-Term Outcomes of Liver Transplantation Using Extended Criteria Donors in the United States. *J Surg Res*. 2025 Feb; 306: 561–569. doi: 10.1016/j.jss.2024.12.055. Epub 2025 Jan 31. PMID: 39892300.
4. *Goldaracena N, Cullen JM, Kim DS, Ekser B, Halazun KJ*. Expanding the donor pool for liver transplantation with marginal donors. *Int J Surg*. 2020 Oct; 82S: 30–35. doi: 10.1016/j.ijsu.2020.05.024. Epub 2020 May 15. PMID: 32422385.
5. *Briceño J, Marchal T, Padillo J, Solórzano G, Pera C*. Influence of marginal donors on liver preservation injury. *Transplantation*. 2002 Aug 27; 74 (4): 522–526. doi: 10.1097/00007890-200208270-00015. PMID: 12352912.
6. *Parente A, Tirotta F, Pini A, Eden J, Dondossola D, Manzia TM et al*. Machine perfusion techniques for liver transplantation – A meta-analysis of the first seven randomized-controlled trials. *J Hepatol*. 2023 Nov; 79 (5): 1201–1213. doi: 10.1016/j.jhep.2023.05.027. Epub 2023 Jun 9. PMID: 37302578.
7. *Mugaanyi J, Dai L, Lu C, Mao S, Huang J, Lu C*. A Meta-Analysis and Systematic Review of Normothermic and Hypothermic Machine Perfusion in Liver Transplantation. *J Clin Med*. 2022 Dec 28; 12 (1): 235. doi: 10.3390/jcm12010235. PMID: 36615037; PMCID: PMC9820958.
8. *Banker A, Bhatt N, Rao PS, Agrawal P, Shah M, Nayak M, Mohanka R*. A Review of Machine Perfusion Strategies in Liver Transplantation. *J Clin Exp Hepatol*. 2023 Mar-Apr; 13 (2): 335–349. doi: 10.1016/j.jceh.2022.08.001. Epub 2022 Aug 10. PMID: 36950485; PMCID: PMC10025749.
9. *Hoyer DP, Mathé Z, Gallinat A, Canbay AC, Treckmann JW, Rauen U et al*. Controlled Oxygenated Rewarming of Cold Stored Livers Prior to Transplantation: First Clinical Application of a New Concept. *Transplantation*. 2016 Jan; 100 (1): 147–152. doi: 10.1097/TP.0000000000000915. PMID: 26479280.
10. *Clavien PA, Harvey PR, Strasberg SM*. Preservation and reperfusion injuries in liver allografts. An overview and synthesis of current studies. *Transplantation*. 1992 May; 53 (5): 957–978. doi: 10.1097/00007890-199205000-00001. PMID: 1585489.
11. *Feng S.* Donor intervention and organ preservation: where is the science and what are the obstacles? *Am J Trans-*

plant. 2010 May; 10 (5): 1155–1162. doi: 10.1111/j.1600-6143.2010.03100.x. PMID: 20420628.
12. *Maathuis MH, Leuvenink HG, Ploeg RJ*. Perspectives in organ preservation. *Transplantation*. 2007 May 27; 83 (10): 1289–1298. doi: 10.1097/01.tp.0000265586.66475.cc. PMID: 17519776.
13. *Ito T, Naini BV, Markovic D, Aziz A, Younan S, Lu M et al*. Ischemia-reperfusion injury and its relationship with early allograft dysfunction in liver transplant patients. *Am J Transplant*. 2021 Feb; 21 (2): 614–625. doi: 10.1111/ajt.16219. Epub 2020 Sep 10. PMID: 32713098.
14. *Ghinolfi D, Melandro F, Torri F, Martinelli C, Cappello V, Babboni S et al*. Extended criteria grafts and emerging therapeutics strategy in liver transplantation. The unstable balance between damage and repair. *Transplant Rev (Orlando)*. 2021 Dec; 35 (4): 100639. doi: 10.1016/j.trre.2021.100639. Epub 2021 Jul 16. PMID: 34303259.
15. *Hartog H, Hann A, Perera MTPR*. Primary Nonfunction of the Liver Allograft. *Transplantation*. 2022 Jan 1; 106 (1): 117–128. doi: 10.1097/TP.0000000000003682. PMID: 33982912.
16. *Agopian VG, Harlander-Locke MP, Markovic D, Dumronggittigule W, Xia V, Kaldas FM et al*. Evaluation of Early Allograft Function Using the Liver Graft Assessment Following Transplantation Risk Score Model. *JAMA Surg*. 2018 May 1; 153 (5): 436–444. doi: 10.1001/jamasurg.2017.5040. Erratum in: *JAMA Surg*. 2018 May 1; 153 (5): 498. doi: 10.1001/jamasurg.2018.1209. PMID: 29261831; PMCID: PMC6584313.
17. *Lee DD, Croome KP, Shalev JA, Musto KR, Sharma M, Keaveny AP, Taner CB.* Early allograft dysfunction after liver transplantation: an intermediate outcome measure for targeted improvements. *Ann Hepatol*. 2016 Jan-Feb; 15 (1): 53–60. doi: 10.5604/16652681.1184212. PMID: 26626641.
18. *Wiemann BA, Beetz O, Weigle CA, Tessmer P, Störzer S, Kleine-Döpke D et al*. Early Allograft Dysfunction after liver transplantation-definition, incidence and relevance in a single-centre analysis. *Langenbecks Arch Surg*. 2025 Feb 19; 410 (1): 76. doi: 10.1007/s00423-025-03633-8. PMID: 39969574; PMCID: PMC11839853.
19. *Mourad MM, Algarni A, Liossis C, Bramhall SR*. Aetiology and risk factors of ischaemic cholangiopathy after liver transplantation. *World J Gastroenterol*. 2014 May 28; 20 (20): 6159–6169. doi: 10.3748/wjg.v20.i20.6159. PMID: 24876737; PMCID: PMC4033454.
20. *Fasullo M, Ghazaleh S, Sayeh W, Vachhani R, Chkhikvadze T, Gonda T et al*. Prognostic Factors for Non-anastomotic Biliary Strictures Following Adult Liver Transplantation: A Systematic Review and Meta-Analysis. *Dig Dis Sci*. 2023 Jun; 68 (6): 2683–2694. doi: 10.1007/s10620-023-07861-0. Epub 2023 Feb 9. PMID: 36757492.
21. *Jay CL, Lyuksemburg V, Ladner DP, Wang E, Caicedo JC, Holl JL et al*. Ischemic cholangiopathy after controlled donation after cardiac death liver transplantation: a meta-analysis. *Ann Surg*. 2011 Feb; 253 (2): 259–264. doi: 10.1097/SLA.0b013e318204e658. PMID: 21245668.
22. *Viana P, Castillo-Flores S, Mora MMR, Cabral TDD, Martins PN, Kueht M 2nd, Faria I.* Normothermic Machine Perfusion vs. Static Cold Storage in Liver Transplantation: A Systematic Review and Meta-Analysis. *Artif Organs*. 2025 Jan 30. doi: 10.1111/aor.14960. Online ahead of print. PMID: 39887468.
23. *Tingle SJ, Dobbins JJ, Thompson ER, Figueiredo RS, Mahendran B, Pandanaboyana S, Wilson C*. Machine perfusion in liver transplantation. *Cochrane Database Syst Rev*. 2023 Sep 12; 9 (9): CD014685. doi: 10.1002/14651858.CD014685.pub2. PMID: 37698189; PMCID: PMC10496129.
24. *Grąt M, Morawski M, Zhylko A, Rykowski P, Krasnodębski M, Wyporski A et al*. Routine End-ischemic Hypothermic Oxygenated Machine Perfusion in Liver Transplantation From Donors After Brain Death: A Randomized Controlled Trial. *Ann Surg*. 2023 Nov 1; 278 (5): 662–668. doi: 10.1097/SLA.0000000000006055. Epub 2023 Jul 27. PMID: 37497636.
25. *Schlegel A, Kron P, Dutkowski P*. Hypothermic Oxygenated Liver Perfusion: Basic Mechanisms and Clinical Application. *Curr Transplant Rep*. 2015; 2 (1): 52–62. doi: 10.1007/s40472-014-0046-1. PMID: 26097802; PMCID: PMC4469295.
26. *Schlegel A, Muller X, Mueller M, Stepanova A, Kron P, de Rougemont O et al*. Hypothermic oxygenated perfusion protects from mitochondrial injury before liver transplantation. *EBioMedicine*. 2020 Oct; 60: 103014. doi: 10.1016/j.ebiom.2020.103014. Epub 2020 Sep 24. PMID: 32979838; PMCID: PMC7519249.
27. *Guarrera JV, Henry SD, Samstein B, Odeh-Ramadan R, Kinkhabwala M, Goldstein MJ et al*. Hypothermic machine preservation in human liver transplantation: the first clinical series. *Am J Transplant*. 2010 Feb; 10 (2): 372–381. doi: 10.1111/j.1600-6143.2009.02932.x. Epub 2009 Dec 2. PMID: 19958323.
28. *Ghinolfi D, Rreka E, De Tata V, Franzini M, Pezzati D, Fierabracci V et al*. Pilot, Open, Randomized, Prospective Trial for Normothermic Machine Perfusion Evaluation in Liver Transplantation From Older Donors. *Liver Transpl*. 2019 Mar; 25 (3): 436–449. doi: 10.1002/lt.25362. PMID: 30362649.
29. Panayot*ova GG, Lunsford KE, Quillin RC 3rd, Rana A, Agopian VG, Lee-Riddle GS et al*. Portable hypothermic oxygenated machine perfusion for organ preservation in liver transplantation: A randomized, open-label, clinical trial. *Hepatology*. 2024 May 1; 79 (5): 1033–1047. doi: 10.1097/HEP.0000000000000715. Epub 2023 Dec 13. PMID: 38090880; PMCID: PMC11019979.
30. *Van Rijn R, Schurink IJ, de Vries Y, van den Berg AP, Cortes Cerisuelo M, Darwish Murad S et al*. Hypothermic Machine Perfusion in Liver Transplantation – A Randomized Trial. *N Engl J Med*. 2021 Apr 15; 384 (15): 1391–1401. doi: 10.1056/NEJMoa2031532. Epub 2021 Feb 24. PMID: 33626248.
31. *Koch DT, Tamai M, Schirren M, Drefs M, Jacobi S, Lange CM et al*. Mono-HOPE Versus Dual-HOPE in Liver Transplantation: A Propensity Score-Matched Evaluation of Early Graft Outcome. *Transpl Int*. 2025 Feb 5; 38:

13891. doi: 10.3389/ti.2025.13891. PMID: 39974599; PMCID: PMC11835512.

32. *De Vries Y, Brüggenwirth IMA, Karangwa SA, von Meijenfeldt FA, van Leeuwen OB, Burlage LC et al*. Dual Versus Single Oxygenated Hypothermic Machine Perfusion of Porcine Livers: Impact on Hepatobiliary and Endothelial Cell Injury. *Transplant Direct*. 2021 Aug 5; 7 (9): e741. doi: 10.1097/TXD.0000000000001184. PMID: 34386578; PMCID: PMC8354629.
33. *Mergental H, Laing RW, Kirkham AJ, Perera MTPR, Boteon YL, Attard J et al*. Transplantation of discarded livers following viability testing with normothermic machine perfusion. *Nat Commun*. 2020 Jun 16; 11 (1): 2939. doi: 10.1038/s41467-020-16251-3. PMID: 32546694; PMCID: PMC7298000.
34. *Chapman WC, Barbas AS, D'Alessandro AM, Vianna R, Kubal CA, Abt P et al*. Normothermic Machine Perfusion of Donor Livers for Transplantation in the United States: A Randomized Controlled Trial. *Ann Surg*. 2023 Nov 1; 278 (5): e912–e921. doi: 10.1097/SLA.0000000000005934. Epub 2023 Jun 26. PMID: 37389552.
35. *Van Leeuwen OB, Bodewes SB, Lantinga VA, Haring MPD, Thorne AM, Brüggenwirth IMA et al*. Sequential hypothermic and normothermic machine perfusion enables safe transplantation of high-risk donor livers. *Am J Transplant*. 2022 Jun; 22 (6): 1658–1670. doi: 10.1111/ajt.17022. Epub 2022 Apr 18. PMID: 35286759; PMCID: PMC9325426.
36. *Patrono D, De Carlis R, Gambella A, Farnesi F, Podestà A, Lauterio A et al*. Viability assessment and transplantation of fatty liver grafts using end-ischemic normothermic machine perfusion. *Liver Transpl*. 2023 May 1; 29 (5): 508–520. doi: 10.1002/lt.26574. Epub 2022 Oct 10. PMID: 36117430; PMCID: PMC10106107.
37. *Caballero-Marcos A, Rodríguez-Bachiller L, Baroja-Mazo A, Morales Á, Fernández-Cáceres P, Fernández-Martínez M et al*. Dynamics of Ischemia/Reperfusion Injury Markers During Normothermic Liver Machine Perfusion. *Transplant Direct*. 2024 Nov 14; 10 (12): e1728. doi: 10.1097/TXD.0000000000001728. PMID: 39553741; PMCID: PMC11567704.
38. *Ceresa CDL, Nasralla D, Pollok JM, Friend PJ*. Machine perfusion of the liver: applications in transplantation and beyond. *Nat Rev Gastroenterol Hepatol*. 2022 Mar; 19 (3): 199–209. doi: 10.1038/s41575-021-00557-8. Epub 2022 Jan 7. PMID: 34997204.
39. *Nasralla D, Coussios CC, Mergental H, Akhtar MZ, Butler AJ, Ceresa CDL et al*. A randomized trial of normothermic preservation in liver transplantation. *Nature*. 2018 May; 557 (7703): 50–56. doi: 10.1038/s41586-018-0047-9. Epub 2018 Apr 18. PMID: 29670285.
40. *Jeddou H, Tzedakis S, Chaouch MA, Sulpice L, Samson M, Boudjema K*. Viability Assessment During Normothermic Machine Liver Perfusion: A Literature Review. *Liver Int*. 2025 Feb; 45 (2): e16244. doi: 10.1111/liv.16244. PMID: 39821671; PMCID: PMC11740183.
41. *Orman ES, Mayorga ME, Wheeler SB, Townsley RM, Toro-Diaz HH, Hayashi PH, Barritt AS 4th*. Declining liver graft quality threatens the future of liver transplantation in the United States. *Liver Transpl*. 2015 Aug; 21 (8): 1040–1050. doi: 10.1002/lt.24160. PMID: 25939487; PMCID: PMC4566853.
42. *Hoyer DP, Paul A, Luer S, Reis H, Efferz P, Minor T*. End-ischemic reconditioning of liver allografts: Controlling the rewarming. *Liver Transpl*. 2016 Sep; 22 (9): 1223–1230. doi: 10.1002/lt.24515. PMID: 27398813.
43. *von Horn C, Baba HA, Hannaert P, Hauet T, Leuvenink H, Paul A et al*. Controlled oxygenated rewarming up to normothermia for pretransplant reconditioning of liver grafts. *Clin Transplant*. 2017 Nov; 31 (11). doi: 10.1111/ctr.13101. Epub 2017 Sep 19. PMID: 28871615.
44. *Minor T, Efferz P, Fox M, Wohlschlaeger J, Lüer B*. Controlled oxygenated rewarming of cold stored liver grafts by thermally graduated machine perfusion prior to reperfusion. *Am J Transplant*. 2013 Jun; 13 (6): 1450–1460. doi: 10.1111/ajt.12235. Epub 2013 Apr 25. PMID: 23617781.
45. *Minor T, von Horn C, Zlatev H, Saner F, Grawe M, Lüer B et al*. Controlled oxygenated rewarming as novel end-ischemic therapy for cold stored liver grafts. A randomized controlled trial. *Clin Transl Sci*. 2022 Dec; 15 (12): 2918–2927. doi: 10.1111/cts.13409. Epub 2022 Oct 17. PMID: 36251938; PMCID: PMC9747115.
46. *Hoyer DP, Paul A, Minor T*. Prediction of Hepatocellular Preservation Injury Immediately Before Human Liver Transplantation by Controlled Oxygenated Rewarming. *Transplant Direct*. 2016 Dec 12; 3 (1): e122. doi: 10.1097/TXD.0000000000000636. PMID: 28349122; PMCID: PMC5361565.
47. *Jeddou H, Tzedakis S, Boudjema K*. Biliary tract viability assessment and sequential hypothermic-normothermic perfusion in liver transplantation. *Hepatobiliary Surg Nutr*. 2024 Jun 1; 13 (3): 505–508. doi: 10.21037/hbsn-24-144. Epub 2024 May 23. PMID: 38911200; PMCID: PMC11190507.
48. *Boteon YL, Laing RW, Schlegel A, Wallace L, Smith A, Attard J et al*. Combined Hypothermic and Normothermic Machine Perfusion Improves Functional Recovery of Extended Criteria Donor Livers. *Liver Transpl*. 2018 Dec; 24 (12): 1699–1715. doi: 10.1002/lt.25315. PMID: 30058119; PMCID: PMC6588092.
49. *De Vries Y, Matton APM, Nijsten MWN, Werner MJM, van den Berg AP, de Boer MT et al*. Pretransplant sequential hypo- and normothermic machine perfusion of suboptimal livers donated after circulatory death using a hemoglobin-based oxygen carrier perfusion solution. *Am J Transplant*. 2019 Apr; 19 (4): 1202–1211. doi: 10.1111/ajt.15228. Epub 2019 Jan 23. PMID: 30588774; PMCID: PMC6590255.
50. *Goumard C, Savier E, Danion J, Pelissie J, Legallais C, Scatton O*. Cold-to-warm machine perfusion of the liver: a novel circuit for an uninterrupted combined perfusion protocol. *HPB (Oxford)*. 2020 Jun; 22 (6): 927–933. doi: 10.1016/j.hpb.2020.04.001. Epub 2020 May 12. PMID: 32409166.
51. *Patrono D, De Stefano N, Rigo F, Cussa D, Romagnoli R.* Some like it hot. Utility and mechanisms of ex-situ

normothermic machine perfusion of the liver. *EJT*. 2023; 1: 92–112. https://doi.org/10.57603/EJT-012.

52. *De Vries Y, Berendsen TA, Fujiyoshi M, van den Berg AP, Blokzijl H, de Boer MT et al*. Transplantation of high-risk donor livers after resuscitation and viability assessment using a combined protocol of oxygenated hypothermic, rewarming and normothermic machine perfusion: study protocol for a prospective, single-arm study (DHOPE-COR-NMP trial). *BMJ Open*. 2019 Aug 15; 9 (8): e028596. doi: 10.1136/bmjopen-2018-028596. PMID: 31420387; PMCID: PMC6701560.
53. *Patrono D, Catalano G, Rizza G, Lavorato N, Berchialla P, Gambella A et al*. Perfusate Analysis During Dual Hypothermic Oxygenated Machine Perfusion of Liver Grafts: Correlations With Donor Factors and Early Outcomes. *Transplantation*. 2020 Sep; 104 (9): 1929–1942. doi: 10.1097/TP.0000000000003398. PMID: 32769628.
54. *Eden J, Thorne AM, Bodewes SB, Patrono D, Roggio D, Breuer E et al*. Assessment of liver graft quality during hypothermic oxygenated perfusion: The first international validation study. *J Hepatol*. 2025 Mar; 82 (3): 523–534. doi: 10.1016/j.jhep.2024.08.030. Epub 2024 Sep 7. PMID: 39251091; PMCID: PMC11830552.
55. *Sousa Da Silva RX, Weber A, Dutkowski P, Clavien PA*. Machine perfusion in liver transplantation. *Hepatology*. 2022 Nov; 76 (5): 1531–1549. doi: 10.1002/hep.32546. Epub 2022 May 17. PMID: 35488496.
56. *Groen PC, van Leeuwen OB, de Jonge J, Porte RJ*. Viability assessment of the liver during ex-situ machine perfusion prior to transplantation. *Curr Opin Organ Transplant*. 2024 Aug 1; 29 (4): 239–247. doi: 10.1097/MOT.0000000000001152. Epub 2024 May 17. PMID: 38764406; PMCID: PMC11224566.
57. *Panconesi R, Shanmugarajah K, Satish S, Zhang M, Wehrle C, Jiao C et al*. Rethinking Lactate's Role as a Post-Transplant Outcome Predictor During Normothermic Machine Perfusion: Science or Speculation? *Am J Transplant*. 2025 Jan; 25 (1 Suppl 1): S126.
58. *Van Leeuwen OB, de Vries Y, Fujiyoshi M, Nijsten MWN, Ubbink R, Pelgrim GJ et al*. Transplantation of High-risk Donor Livers After *Ex Situ* Resuscitation and Assessment Using Combined Hypo- and Normothermic Machine Perfusion: A Prospective Clinical Trial. *Ann Surg*. 2019 Nov; 270 (5): 906–914. doi: 10.1097/SLA.0000000000003540. PMID: 31633615.
59. *Matton APM, de Vries Y, Burlage LC, van Rijn R, Fujiyoshi M, de Meijer VE et al*. Biliary Bicarbonate, pH, and Glucose Are Suitable Biomarkers of Biliary Viability During *Ex Situ* Normothermic Machine Perfusion of Human Donor Livers. *Transplantation*. 2019 Jul; 103 (7): 1405–1413. doi: 10.1097/TP.0000000000002500. PMID: 30395120; PMCID: PMC6613725.
60. *Chen Z, Hong X, Huang S, Wang T, Ma Y, Guo Y et al*. Continuous Normothermic Machine Perfusion for Renovation of Extended Criteria Donor Livers Without Recooling in Liver Transplantation: A Pilot Experience. *Front Surg*. 2021 May 24; 8: 638090. doi: 10.3389/fsurg.2021.638090. PMID: 34109206; PMCID: PMC8180843.
61. *Chen Z, Wang T, Chen C, Zhao Q, Ma Y, Guo Y et al*. Transplantation of Extended Criteria Donor Livers Following Continuous Normothermic Machine Perfusion Without Recooling. *Transplantation*. 2022 Jun 1; 106 (6): 1193–1200. doi: 10.1097/TP.0000000000003945. Epub 2022 Sep 7. PMID: 34495016; PMCID: PMC9128617.
62. *Ju W, Chen Z, Zhao Q, Zhang Y, Huang C, Wang L et al*. Non-re-cooling implantation of marginal liver graft after machine perfusion: report of a case. *Ann Transl Med*. 2020 Nov; 8 (21): 1465. doi: 10.21037/atm-20-2774. PMID: 33313210; PMCID: PMC7723619.
63. *Zhou AL, Akbar AF, Ruck JM, Weeks SR, Wesson R, Ottmann SE et al*. Use of *Ex Situ* Machine Perfusion for Liver Transplantation: The National Experience. *Transplantation*. 2024 Dec 26. doi: 10.1097/TP.0000000000005290. Epub ahead of print. PMID: 39724135.
64. *Dutkowski P, Guarrera JV, de Jonge J, Martins PN, Porte RJ, Clavien PA*. Evolving Trends in Machine Perfusion for Liver Transplantation. *Gastroenterology*. 2019 May; 156 (6): 1542–1547. doi: 10.1053/j.gastro.2018.12.037. Epub 2019 Jan 18. PMID: 30660724.
65. *Jakubauskas M, Jakubauskiene L, Leber B, Strupas K, Stiegler P, Schemmer P.* Machine Perfusion in Liver Transplantation: A Systematic Review and Meta-Analysis. *Visc Med*. 2022 Aug; 38 (4): 243–254. doi: 10.1159/000519788. Epub 2021 Nov 8. PMID: 36160822; PMCID: PMC9421699.
66. *Henry SD, Nachber E, Tulipan J, Stone J, Bae C, Reznik L et al*. Hypothermic machine preservation reduces molecular markers of ischemia/reperfusion injury in human liver transplantation. *Am J Transplant*. 2012 Sep; 12 (9): 2477–2486. doi: 10.1111/j.1600-6143.2012.04086.x. Epub 2012 May 17. PMID: 22594953.
67. *Guarrera JV, Henry SD, Samstein B, Reznik E, Musat C, Lukose TI et al*. Hypothermic machine preservation facilitates successful transplantation of "orphan" extended criteria donor livers. *Am J Transplant*. 2015 Jan; 15 (1): 161–169. doi: 10.1111/ajt.12958. Epub 2014 Dec 17. PMID: 25521639.
68. *Dutkowski P, Polak WG, Muiesan P, Schlegel A, Verhoeven CJ, Scalera I et al*. First Comparison of Hypothermic Oxygenated PErfusion Versus Static Cold Storage of Human Donation After Cardiac Death Liver Transplants: An International-matched Case Analysis. *Ann Surg*. 2015 Nov; 262 (5): 764–770; discussion 770–771. doi: 10.1097/SLA.0000000000001473. PMID: 26583664.
69. *Van Rijn R, Karimian N, Matton APM, Burlage LC, Westerkamp AC, van den Berg AP et al*. Dual hypothermic oxygenated machine perfusion in liver transplants donated after circulatory death. *Br J Surg*. 2017 Jun; 104 (7): 907–917. doi: 10.1002/bjs.10515. Epub 2017 Apr 10. PMID: 28394402; PMCID: PMC5484999.
70. *Patrono D, Surra A, Catalano G, Rizza G, Berchialla P, Martini S et al*. Hypothermic Oxygenated Machine Perfusion of Liver Grafts from Brain-Dead Donors. *Sci Rep*. 2019 Jun 27; 9 (1): 9337. doi: 10.1038/s41598-019-45843-3. PMID: 31249370; PMCID: PMC6597580.

71. *Schlegel A, Muller X, Kalisvaart M, Muellhaupt B, Perera MTPR, Isaac JR et al*. Outcomes of DCD liver transplantation using organs treated by hypothermic oxygenated perfusion before implantation. *J Hepatol*. 2019 Jan; 70 (1): 50–57. doi: 10.1016/j.jhep.2018.10.005. Epub 2018 Oct 18. PMID: 30342115.
72. *Ravaioli M, De Pace V, Angeletti A, Comai G, Vasuri F, Baldassarre M et al*. Hypothermic Oxygenated New Machine Perfusion System in Liver and Kidney Transplantation of Extended Criteria Donors: First Italian Clinical Trial. *Sci Rep*. 2020 Apr 8; 10 (1): 6063. doi: 10.1038/s41598-020-62979-9. Erratum in: Sci Rep. 2020 Sep 1; 10 (1): 14658. doi: 10.1038/s41598-020-70620-y. PMID: 32269237; PMCID: PMC7142134.
73. *Rayar M, Beaurepaire JM, Bajeux E, Hamonic S, Renard T, Locher C et al*. Hypothermic Oxygenated Perfusion Improves Extended Criteria Donor Liver Graft Function and Reduces Duration of Hospitalization Without Extra Cost: The PERPHO Study. *Liver Transpl*. 2021 Feb; 27 (3): 349–362. doi: 10.1002/lt.25955. PMID: 33237618.
74. *Czigany Z, Pratschke J, Froněk J, Guba M, Schöning W, Raptis DA et al*. Hypothermic Oxygenated Machine Perfusion Reduces Early Allograft Injury and Improves Post-transplant Outcomes in Extended Criteria Donation Liver Transplantation From Donation After Brain Death: Results From a Multicenter Randomized Controlled Trial (HOPE ECD-DBD). *Ann Surg*. 2021 Nov 1; 274 (5): 705–712. doi: 10.1097/SLA.0000000000005110. PMID: 34334635
75. *Ravikumar R, Jassem W, Mergental H, Heaton N, Mirza D, Perera MT et al*. Liver Transplantation After *Ex Vivo* Normothermic Machine Preservation: A Phase 1 (First-in-Man) Clinical Trial. *Am J Transplant*. 2016 Jun; 16 (6): 1779–1787. doi: 10.1111/ajt.13708. Epub 2016 Mar 7. PMID: 26752191.
76. *Selzner M, Goldaracena N, Echeverri J, Kaths JM, Linares I, Selzner N et al*. Normothermic *ex vivo* liver perfusion using steen solution as perfusate for human liver transplantation: First North American results. *Liver Transpl*. 2016 Nov; 22 (11): 1501–1508. doi: 10.1002/lt.24499. PMID: 27339754.
77. *Bral M, Gala-Lopez B, Bigam D, Kneteman N, Malcolm A, Livingstone S et al*. Preliminary Single-Center Canadian Experience of Human Normothermic *Ex Vivo* Liver Perfusion: Results of a Clinical Trial. *Am J Transplant*. 2017 Apr; 17 (4): 1071–1080. doi: 10.1111/ajt.14049. Epub 2016 Dec 9. PMID: 27639262.
78. *Mergental H, Laing RW, Kirkham AJ, Clarke G, Boteon YL, Barton D et al*. Discarded livers tested by normothermic machine perfusion in the VITTAL trial: Secondary end points and 5-year outcomes. *Liver Transpl*. 2024 Jan 1; 30 (1): 30–45. doi: 10.1097/LVT.0000000000000270. Epub 2023 Dec 15. PMID: 38109282.
79. *Liu Q, Hassan A, Pezzati D, Soliman B, Lomaglio L, Grady P et al*. *Ex Situ* Liver Machine Perfusion: The Impact of Fresh Frozen Plasma. *Liver Transpl*. 2020 Feb; 26 (2): 215–226. doi: 10.1002/lt.25668. PMID: 31642164.
80. *Quintini C, Del Prete L, Simioni A, Del Angel L, Diago Uso T, D'Amico G et al*. Transplantation of declined livers after normothermic perfusion. *Surgery*. 2022 Mar; 171 (3): 747–756. doi: 10.1016/j.surg.2021.10.056. Epub 2022 Jan 19. PMID: 35065791.
81. *Markmann JF, Vagefi PA, MacConmara MP*. Normothermic Machine Perfusion Increases Donor Liver Use. *JAMA Surg*. 2022 Aug 1; 157 (8): 742–743. doi: 10.1001/jamasurg.2022.1424. PMID: 35507357.
82. *Liu Q, Del Prete L, Ali K, Grady P, Bilancini M, Etterling J et al*. Sequential hypothermic and normothermic perfusion preservation and transplantation of expanded criteria donor livers. *Surgery*. 2023 Mar; 173 (3): 846–854. doi: 10.1016/j.surg.2022.07.035. Epub 2022 Oct 24. PMID: 36302699.
83. *Thorne AM, Wolters JC, Lascaris B, Bodewes SB, Lantinga VA, van Leeuwen OB et al*. Bile proteome reveals biliary regeneration during normothermic preservation of human donor livers. *Nat Commun*. 2023 Nov 30; 14 (1): 7880. doi: 10.1038/s41467-023-43368-y. PMID: 38036513; PMCID: PMC10689461.
84. *Magistri P, Zamboni S, Catellani B, Guidetti C, Esposito G, Caracciolo D et al*. Sequential Hypothermic and Normothermic Machine Perfusion of Extended Criteria Donors in Liver Transplantation: A Single-Center Preliminary Experience. *Artif Organs*. 2025 Feb 19. doi: 10.1111/aor.14936. Epub ahead of print. PMID: 39969150.
85. *Eden J, Breuer E, Birrer D, Müller M, Pfister M, Mayr H et al*. Screening for mitochondrial function before use-routine liver assessment during hypothermic oxygenated perfusion impacts liver utilization. *EBioMedicine*. 2023 Dec; 98: 104857. doi: 10.1016/j.ebiom.2023.104857. Epub 2023 Oct 31. PMID: 37918219; PMCID: PMC10641151.
86. *Muller X, Schlegel A, Kron P, Eshmuminov D, Würdinger M, Meierhofer D et al*. Novel Real-time Prediction of Liver Graft Function During Hypothermic Oxygenated Machine Perfusion Before Liver Transplantation. *Ann Surg*. 2019 Nov; 270 (5): 783–790. doi: 10.1097/SLA.0000000000003513. PMID: 31592808.
87. *Olumba FC, Zhou F, Park Y, Chapman WC; RESTORE Investigators Group.* Normothermic Machine Perfusion for Declined Livers: A Strategy to Rescue Marginal Livers for Transplantation. *J Am Coll Surg*. 2023 Apr 1; 236 (4): 614–625. doi: 10.1097/XCS.0000000000000555. Epub 2023 Jan 11. PMID: 36728302.
88. *Seidita A, Longo R, Di Francesco F, Tropea A, Calamia S, Panarello G et al*. The use of normothermic machine perfusion to rescue liver allografts from expanded criteria donors. *Updates Surg*. 2022 Feb; 74 (1): 193–202. doi: 10.1007/s13304-021-01169-2. Epub 2021 Sep 20. PMID: 34542843.
89. *Zhang Z, Ju W, Tang Y, Wang L, Zhu C, Gao N et al*. First Preliminary Experience with Preservation of Liver Grafts from Extended-Criteria Donors by Normothermic Machine Perfusion in Asia. *Ann Transplant*. 2020 Apr 21; 25: e921529. doi: 10.12659/AOT.921529. PMID: 32312947; PMCID: PMC7193227.

90. *Reiling J, Butler N, Simpson A, Hodgkinson P, Campbell C, Lockwood D et al*. Assessment and Transplantation of Orphan Donor Livers: A Back-to-Base Approach to Normothermic Machine Perfusion. *Liver Transpl*. 2020 Dec; 26 (12): 1618–1628. doi: 10.1002/lt.25850. Epub 2020 Sep 15. PMID: 32682340.
91. *Cardini B, Oberhuber R, Fodor M, Hautz T, Margreiter C, Resch T et al*. Clinical Implementation of Prolonged Liver Preservation and Monitoring Through Normothermic Machine Perfusion in Liver Transplantation. *Transplantation*. 2020 Sep; 104 (9): 1917–1928. doi: 10.1097/TP.0000000000003296. PMID: 32371845.
92. *Bral M, Dajani K, Leon Izquierdo D, Bigam D, Kneteman N, Ceresa CDL et al*. A Back-to-Base Experience of Human Normothermic *Ex Situ* Liver Perfusion: Does the Chill Kill? *Liver Transpl*. 2019 Jun; 25 (6): 848–858. doi: 10.1002/lt.25464. PMID: 30938039.
93. *Ceresa CDL, Nasralla D, Watson CJE, Butler AJ, Coussios CC, Crick K et al*. Transient Cold Storage Prior to Normothermic Liver Perfusion May Facilitate Adoption of a Novel Technology. *Liver Transpl*. 2019 Oct; 25 (10): 1503–1513. doi: 10.1002/lt.25584. Epub 2019 Jul 18. PMID: 31206217.
94. *Watson CJE, Kosmoliaptsis V, Pley C, Randle L, Fear C, Crick K et al*. Observations on the *ex situ* perfusion of livers for transplantation. *Am J Transplant*. 2018 Aug; 18 (8): 2005–2020. doi: 10.1111/ajt.14687. Epub 2018 Mar 14. PMID: 29419931; PMCID: PMC6099221.
95. *Watson CJE, Kosmoliaptsis V, Randle LV, Gimson AE, Brais R, Klinck JR et al*. Normothermic Perfusion in the Assessment and Preservation of Declined Livers Before Transplantation: Hyperoxia and Vasoplegia-Important Lessons From the First 12 Cases. *Transplantation*. 2017 May; 101 (5): 1084–1098. doi: 10.1097/TP.0000000000001661. PMID: 28437389; PMCID: PMC5642347.

The article was submitted to the journal on 8.04.2025

INSTRUCTIONS TO AUTHORS

Articles should contain original information that has not been previously published and is not considered for publication in other editions. Fee for publication of manuscripts will not be charged.

The manuscript should be presented in Microsoft Word format A4, 1.5 spacing, and Times New Roman font size 12. Submit your article to the online submission system in accordance with the instructions on the journal's website https://journal.transpl.ru.

Structure of the article

The Title page should include:

- Initials (first name and patronymic) of the authors of the article should be specified before their respective last names.
- Author names (list the author's initials before listing his or her last name as when registering for ORCID, or Open Researcher and Contributor ID – a non-proprietary alphanumeric code that uniquely identifies scientific authors).
- Full official name of the institution, city and country.
- If authors from different institutions participated in writing of the manuscript, it is necessary to correlate those with the names of the authors by adding a digital index uppercase after last name, and right before the name of the institution.

Information about the authors

For each author fully specify the last and the first name, patronymic and position in the relevant department/institution.

For correspondence

Fully specify the last and the first name, patronymic of the author, who will be holding correspondence, address (including postal code), telephone, fax number, e-mail.

Abstract

Each article must be accompanied by an abstract. The amount of text for the abstract of the original article should be of no more than 300 words, for a literature review, clinical observation – no more than 200 words. The abstract must fully comply with the content of the work. The abstract should not use abbreviations without prior expansion.

Abstract of ***the original article*** should contain the following sections: ***Objective***, ***Materials and methods***, ***Results***, ***Conclusion***. The abstract should present the most important results of the research.

Do not write: "*A comparative analysis of the sensitivity and specificity was conducted …*"

Should write: "*The sensitivity was ... % and ...%, p = , specificity, respectively ...% and ...%, p =* ".

Keywords

At the end of the abstract keywords must be given. To select the keywords a thesaurus of U.S. National Library of Medicine should be used – Medical Subject Headings (MeSH) at http://www.ncbi.nlm.nih.gov/mesh.

Conflict of interest

The author should inform the editor about the factual or potential conflict of interest have included the information about such conflict into the respective section of an article.

If there is no conflict of interest, the author should say so in the form like the following: "Author declares unawareness of the conflict of interest".

This information is supposed to be placed before the article text.

Text of article

Original article should include the following sections:

- Introduction
- Materials and methods
- Results
- Discussion
- Conclusion
- References

Review article should include an analysis of the literature with the presentation of modern sources (mainly in the last 5 years).

Clinical observation should be well illustrated (to reflect the essence of the problem) and include discussion with the use of literature data.

References in the text are indicated by number in square brackets: [1], [2, 5], [14–18] and ***in the references section are presented in order of their appearance in the text.*** All values given in the article should be expressed or duplicated in **SI** units.

References

The author is solely responsible for the accuracy of the data included in the references section of the article. References to unpublished papers or papers in print works are not allowed.

References are presented on a separate page.

The names of journals can be contracted in accordance with an embodiment of reduction adopted by the specific journal.

If the article quoted has DOI (a digital object identifier) or/and PMID (Pub Med identifier) they must be specified after the description of the article. To compile descriptions in References section NLM bibliographic reference citation standard is used – U.S. National Library of Medicine (http://www.nlm.nih.gov/bsd/uniform_requirements.html). If the number of authors does not exceed 6, the bibliographic description includes all the authors. If the number of authors is more, only the first six authors should be indicated and then add et al.

Requirements for tables and figures

Tables should be placed into the text; they should have numbered heading and clearly labeled graphs, convenient and simple to read. Table's data must comply with the numbers in the text, but should not duplicate the information therein. Table references in the text are required.

Illustrations and drawings should be submitted in electronic format (JPEG or TIFF format with a resolution of at least 300 dpi and no smaller than 6 × 9 cm), in a volume of close to 1 MB. Drawings must include all copyright symbols – arrows, numbers, signs, etc. Figure captions should be submitted in a separate file with the extension *.doc. First, the name is given, then all arithmetic and alphabetical symbols (lettering) are explained.

Articles should be addressed
to the Russian Journal of Transplantology and Artificial Organs website:
https://journal.transpl.ru/vtio
E-mail: vestniktranspl@gmail.com

Издание зарегистрировано в Госкомпечати РФ, № 018616 от 23.03.99 г.

Подписано к печати 18.06.25.

Тираж 1000 экз.

ООО «Издательство «Триада».
ИД № 06059 от 16.10.01 г.
170034, г. Тверь, пр. Чайковского, 9, оф. 514,
тел.: +7 (915) 730-10-37, +7 (910) 647-49-85
E-mail: triadatver@yandex.ru
http://www.triada.tver.ru

Заказ 24092